Aus dem Institut für Molekulare und Klinische Immunologie
der Medizinischen Fakultät
der Otto-von-Guericke Universität Magdeburg

Regulation of lymphocyte development and activation

Habilitationsschrift
Zur Erlangung des akademischen Grades
Dr. habil.
(doctor habilitatus)
an der Medizinischen Fakultät
der Otto-von-Guericke Universität Magdeburg

Vorgelegt von Luca Simeoni
Aus Valmontone, Rom, Italien
Magdeburg 2012

Table of Contents

List of Abbreviations

ADAP (adhesion and degranulation promoting adapter protein)

ANAs (antinuclear antibodies)

AP1 (activator protein 1)

APC (antigen presenting cell)

BCR (B-cell receptor)

BLNK (B-cell linker)

BM (bone marrow)

Cbp (Csk-binding protein)

CLP (common lymphoid progenitor)

CMP (common myeloid progenitor)

CTLA-4 (cytotoxic T-lymphocyte antigen 4)

DAG (diacylglyecerol)

DN (double negative)

DP (double positive)

EAE (experimental autoimmune encephalomyelitis)

Erk (extracellular-signal regulated kinase)

FO (follicular)

GADS (Grb2-related adaptor downstream of Shc)

GEF (guanine nucleotide exchange factor)

GEMs (glycosphingolipid-enriched microdomains)

Grb2 (growth factor receptor-bound protein 2)

HSC (hematopoietic stem cell)

IFNγ (interferon-gamma)

IL-# (interleukin-#)

ITAM (immunoreceptor tyrosine-based activation motif)

ITIM (immunoreceptor tyrosine-based inhibitory motif)

LAB (linker for activation of B cells)

LAT (linker for activation of T cells)

LAX (linker for activation of X cells)

Lck (lymphocyte-specific protein tyrosine kinase)

LIME (Lck-interacting membrane protein)

mAb (monoclonal antibody)

MAPK (mitogen-activated protein kinase)

MHC (major histocompatibility complex)

MZ (marginal zone)

NFAT (nuclear factor of activated T cells)

NFκB (nuclear factor kappa B)

NK (natural killer)

NTAL (non-T-cell activation linker)

PAG (phosphoprotein associated with GEMs)

PAMP (pathogen-associated molecular pattern)

PAS (periodic acid-Schiff)

PH (pleckstrin homology)

PHA (Phytohaemagglutinin A)

PI3K (phosphatidylinositol 3-kinase)

PIP_2 (phosphoinositol-4,5-bisphosphate)

PKB (protein kinase B)

PLCγ (phospholipase C gamma)

PRR (pattern recognition receptor)

PTB (phosphotyrosine binding)

Rag (recombination activating gene)

Ras (rat sarcoma)

RasGRP (Ras guanyl nucleotide-releasing protein)

RNAi (RNA interference)

SH (src homology)

SHP-2 (SH2-domain-containing protein tyrosine phosphatase)

siRNA (small interfering RNA)

SIT (SHP-2-interacting transmembrane adaptor protein)

SKAP-55 (Src kinase-associated phosphoprotein of 55 kDa)

SKAP-HOM (Src kinase-associated phosphoprotein of 55 kDa homologue)

SLAP (Src-like adaptor protein)

SLP-76 (SH2 domain containing leukocyte protein of 76kDa)

Sos (son of sevenless)

SP (single positive)

TBSM (tyrosine-based signalling motif)

TCR (T-cell receptor)

Th (T helper)

Treg (regulatory T cell)

TRAP (transmembrane adaptor protein)

TRIM (T-cell receptor interacting molecule)

ZAP-70 (zeta-chain associated protein of 70 kDa)

Abstract

T and B lymphocytes are crucial in the immune response to infections. T cells are organized in highly specialized subsets displaying distinct functions. Helper T cells are well-known orchestrators of the adaptive immune response, as they provide help to another group of T cells, referred to as cytotoxic, which recognize and eliminate virus-infected or tumor cells. Moreover, helper T cells also support antibody production by B cells. T and B lymphocyte are characterized by the expression of a particular receptor which is able to recognize antigen, referred to as TCR (T-cell receptor) and BCR (B-cell receptor), respectively. The antigen receptor is not only mandatory for the recognition of pathogens and the initiation of the immune response, but it is also essential for lymphocyte development and homeostasis. The question how a single receptor can interpret different signals and translate them into specific cellular outcomes has fascinated many researchers. It is now clear that the antigen receptor is endowed with different sets of molecules, which adjust the intensity of the signal, control its duration, and regulate its localization. Quantitative and qualitative differences in the nature of the signal will activate a different set of genes and will ultimately result in the appropriate cellular response. Defects in signal transduction may lead to unwanted responses which result in autoimmunity or immunodeficiency. Thus, the study of how signaling via antigen receptors is initiated, propagated, coordinated, and translated into a cellular response is important for the understanding not only of physiological processes, but also of the molecular mechanisms underlying human diseases.

My work focuses on how signaling via the antigen receptor is regulated, integrated, and translated into a cellular response. I have investigated with particular emphasis the function of transmembrane adaptor molecules in T and B cells. By using knockout mice, we have successfully demonstrated that TRAPs (Transmembrane Adaptor Proteins) are indeed important modulators of signals that regulate lymphocyte development, activation and homeostasis. Our study on SIT (SHP-2-interacting transmembrane adaptor protein) has revealed that SIT is required for setting the signaling threshold during thymocyte selection. We have further shown that SIT is a negative regulator of TCR-mediated signaling which inhibits the phosphorylation of TCRζ and ZAP-70 (zeta-chain-associated protein of 70 kDa). Moreover, we have also found that SIT regulates tolerance, thus preventing autoimmunity. Finally, we showed that SIT, LAX (linker for activation of X cells), and TRIM (T-cell receptor interacting molecule) possess redundant functions. By generating double-knockout

mice, we have demonstrated that SIT and LAX cooperatively regulate $CD4^+$ T-cell activation and prevent autoimmunity, while SIT together with TRIM controls T-cell fate.

More recently, my focus has shifted from the characterization of TRAPs to the analysis of how signaling networks are regulated in primary human T cells. In fact, I believe that it is a necessary goal for the future to characterize how signaling networks work during physiological responses and how they are integrated with upstream inputs and parallel signaling pathways in human T cells. This is important for truly understanding of the molecular events that trigger not only cellular responses, but also diseases.

We have analyzed how the Ras-Erk cascade is regulated in primary human T lymphocytes. Based on studies performed in cell lines, it has been postulated that Erk activation depends on the cooperative action of RasGRP1 and Grb2/Sos. Using RNAi approaches in primary cells, we found that TCR-mediated Erk activation requires RasGRP1, but not Grb2/Sos. Thus, conversely to the current model, our data demonstrate that Sos and Grb2 do not link the TCR to Ras-Erk activation in primary T cells. However, when we analyzed Erk activation downstream of the IL-2R, we found that Grb2/Sos are required to activate Erk. Collectively, our data suggest that RasGRP1 and Grb2/Sos function as insulators of signals leading to Ras activation induced by different stimuli rather than to cooperate downstream of the TCR. Our aim is to further investigate biochemical mechanisms underlying T-cell activation not only in normal processes (i.e. infections), but also in pathological modifications occurring in human diseases i.e. cancer, autoimmunity and chronic inflammation.

Zusammenfassung

T- und B-Lymphozyten sind Schlüsselzellen der spezifischen Immunantwort gegen Krankheitserreger. T-Lymphozyten koordinieren die spezifische Immunantwort und erkennen und zerstören virusinfizierte Zellen. Demgegenüber stehen B-Zellen, die für die humorale Immunantwort zuständig sind und Antikörper bilden, welche Antigene binden und eliminieren. T- und B-Lymphozyten stammen von unreifen Vorläuferzellen des Knochenmarks ab. B-Zellen reifen vollständig im Knochenmark aus, wohingegen die Vorläuferzellen der T-Zellen in den Thymus einwandern und dort ihre Entwicklung abschließen. Die Reifung der Lymphozyten ist ein komplexer schrittweiser Prozess, während dem sie Selektionsprozesse durchlaufen, die für eine Prüfung der Funktionalität der Zellen notwendig sind. T- und B-Lymphozyten besitzen an ihrer Oberfläche Antigenrezeptoren (TCR auf T- und BCR auf B-Zellen). Diese sind verantwortlich für die Antigen-Erkennung, die Auslösung der Immunantwort als auch für die Reifung der Lymphozyten. Darüber hinaus spielen Antigenrezeptoren auch eine wichtige Rolle bei der Lymphozytenhomöostase.

Eine zentrale Frage, die Immunologen immer noch fasziniert, ist: Wie entstehen aus dem Signal eines einzigen Rezeptors verschiedene zelluläre Antworten? In den letzten Jahren ist klar geworden, dass der Antigenrezeptor mit unterschiedlichen regulatorischen Molekülen zusammenarbeitet, welche die Intensität und die Dauer des Signals beeinflussen und dessen Lokalisierung kontrollieren. Quantitäts- und Qualitätsunterschiede in der Art des Signals werden im Zellkern durch die Aktivierung verschiedener Gene interpretiert, die schlussendlich die passende zelluläre Entscheidung fällen. Fehler in der Regulation der Antigenrezeptor-Signalübertragung können unerwünschte zelluläre Antworten auslösen, die in Autoimmunerkrankungen oder Immundefiziten resultieren. Deshalb ist die Erforschung, wie die Antigenrezeptor-Signalübertragung initiiert, weitergeleitet, koordiniert und letztendlich interpretiert wird, wichtig; nicht nur um die Grundlagen physiologischer Prozesse zu verstehen, sondern auch für das Verständnis der molekularen Mechanismen, die Krankheiten zu Grunde liegen.

In den letzten Jahren habe ich mich mit den Fragen beschäftigt, wie die Antigenrezeptor-Signalübertragung während der Lymphozytenentwicklung, -aktivierung und -homöostase reguliert wird und wie zelluläre Entscheidungen getroffen werden. Insbesondere, habe ich die Funktion der non-raft-assoziierten transmembranösen Adaptorproteine (TRAPs) in T- und B-Lymphozyten untersucht. Mittels Knockout-Mausmodellen habe ich mit meiner

Arbeitsgruppe demonstriert, dass TRAPs wichtige Modulatoren der Antigenrezeptor-Signalübertragung sind und dadurch die Entwicklung, Aktivierung und Homöostase von Lymphozyten regulieren. Unsere Arbeit über das transmembranöse Adaptorprotein SIT (SHP-2-interacting transmembrane adaptor protein) hat ergeben, dass SIT für die T-Zellentwicklung nötig ist und dass SIT die Signalschwelle des TCR senkt. Die Stärke des Signals spielt bei der Thymozytenentwicklung die entscheidende Rolle um festzulegen wie die Zelle auf einen spezifischen Liganden reagiert. SIT-defiziente Thymozyten zeigen einen hyperaktiven Phänotyp, erkennbar durch erhöhte CD69 und CD5 Expression. Daraus folgt, dass die Selektionsprozesse im Thymus der $SIT^{-/-}$-Mäuse verändert sind und, wie an Hand TCR-transgener Mausmodelle gezeigt, die positive Selektion in negative Selektion umgewandelt wird. $SIT^{-/-}$-Mäuse zeigen auch eine defekte T-Zell-Homöostase. Mittels adoptiven Transfers von T-Zellen in lymphopenische Empfänger-Mäuse haben wir gezeigt, dass SIT die homöostatische Proliferation hemmt. Schlussendlich demonstrieren unsere Studien auch, dass SIT eine wichtige Rolle bei der Aufrechterhaltung der Selbsttoleranz spielt. Tatsächlich sind SIT-defiziente Mäuse anfälliger für die Entwicklung experimenteller und spontaner Autoimmunerkrankungen im Vergleich zum Wildtyp. Darüber hinaus haben wir mittels RNAi in peripheren T-Zellen gezeigt, dass SIT ein negativer Regulator der TCR-vermittelten Signaltransduktion ist, welcher die Phosphorylierung von TCRζ und ZAP-70 (zeta-chain-associated protein of 70 kDa) inhibiert.

Zusätzlich haben wir untersucht, ob SIT mit anderen transmembranösen Adaptorproteinen eine redundante Funktion aufweist. Zu Beginn haben wir getestet, ob SIT und TRIM (T-cell receptor interacting molecule) funktionell überlappen. SIT und TRIM besitzen eine sehr ähnliche molekulare Struktur und sind beide in Thymozyten sehr stark exprimiert. Durch Generierung von SIT/TRIM Doppel-Knockout (DKO) Mäusen konnten wir feststellen, dass SIT und TRIM gemeinsam die Thymozytendifferenzierung regulieren. Die Selektionprozesse im Thymus von DKO-Mäusen sind komplett gestört. Tatsächlich wird die Non-Selektion in positive Selektion und die positive Selektion in negative Selektion umgewandelt. Anschließend haben wir getestet, ob SIT funktionell mit dem Adaptorprotein LAX (linker for activation of X cells) überlappt. Im Gegensatz zu SIT und TRIM haben wir festgestellt, dass SIT und LAX gemeinsam die Funktion peripherer T- und B-Zellen regulieren. SIT/LAX-DKO-Mäuse zeigen eine erhöhte Anzahl aktivierter $CD4^{+}$-T-Zellen sowie der B1-Zellen, eine Subpopulation der B-Lymphozyten die den größten Teil des IgM produzieren. B-Zellen, in denen SIT und LAX ausgeknockt wurde, proliferieren stärker als Wildtyp B-Zellen. Als Konsequenz ist auch die humorale Immunantwort in SIT/LAX-DKO-Mäusen verstärkt. Die

Veränderung der Funktion von T- und B-Zellen resultiert letztendlich in der spontanen Entwicklung einer Glomerulonephritis Autoimmunerkrankung in SIT/LAX-DKO-Mäusen. Zusammenfassend konnten wir demonstrieren, dass die non-raft-assoziierten transmembranösen Adaptorproteine SIT, TRIM und LAX eine wichtige Rolle bei der Lymphozytendifferentierung, -aktivierung und -homöostase spielen.

In den letzten Jahren habe ich meine Studien auf die Analyse der TCR-vermittelten Signalnetzwerke in peripheren menschlichen T-Zellen fokussiert. Ich glaube, dass es für die Zukunft notwendig sein wird, die detaillierte Funktionsweise von Signaltransduktionskaskaden zu bestimmen und ebenso zu charakterisieren, wie Signalmodule mit vorgeschalteten Inputs und parallelen Signaltransduktionswegen Informationen integrieren. Die Nutzung primärer humaner T-Zellen als experimentelles System sind von Vorteil, da sich manche menschliche biologische Prozesse oder Krankheiten in Tiermodellen oder Zelllinien nur teilweise widerspiegeln. Als ersten Aspekt haben wir untersucht, wie die Aktivierung der Ras-Erk Signalkaskade in peripheren humanen T-Zellen reguliert wird. Andere Arbeitsgruppen haben gezeigt, dass die TCR-vermittelte Aktivierung von Ras-Erk von der kooperativen Aktion zweier Aktivatoren abhängt, nämlich RasGRP1 und Grb2/Sos. Dieses Modell basiert auf Ergebnissen aus Zelllinien, deshalb ist noch nicht bekannt, ob bei primären T-Zellen sowohl RasGRP1 als auch Grb2/Sos notwendig sind, um Ras-Erk zu aktivieren. Vermittels RNAi haben wir demonstriert, dass die TCR-vermittelte Aktivierung von Ras-Erk in peripheren T-Zellen nur von RasGRP1, aber nicht von Grb2/Sos abhängt. Darüber hinaus haben wir gezeigt, dass Grb2/Sos, aber nicht RasGRP1 eine wichtige Rolle bei der IL-2-vermittelten Ras-Erk-Aktivierung spielt. Zusammengefasst veranschaulichen unsere Daten, dass RasGRP1 und Grb2/Sos keine kooperative Aktion bei der Aktivierung von Ras-Erk „downstream“ des TCR vermitteln. Beide Moleküle funktionieren unabhängig voneinander „downstream“ von wichtigen Rezeptoren der T-Zellen (TCR und IL-2R), die die Aktivierung und Proliferation von T-Zellen regulieren und damit eine effiziente Immunantwort erlauben. Dies unterstützt unsere Ansicht, dass sich primäre T-Zellen durch Zelllinien nur ungenügend repräsentiert lassen. Daher ist es unser Ziel die weitere Untersuchung der TCR-vermittelten Signalübertragung in primären T-Zellen während physiologischer bzw. pathologischer Prozesse wie Krebs, Autoimmunität und chronischen Entzündungen durchzuführen.

1. An introduction to the immune system

The constant selection pressure of microbes on multicellular organisms has led to the evolution of an orchestra of defense mechanisms, known as the immune system. Over the past several decades it has become clear that the immune system is a very complex network of proteins, cells, tissues, and organs that work together to protect the body not only against infectious agents (i.e. virus, bacteria, fungi, and parasites) and foreign substances (i.e. toxins) that can cause tissue damage and diseases, but also against tumor cells. Physical and chemical barriers, which include the skin, mucous membranes, tears, earwax, and stomach acid, are considered the first line of defense of the body. When pathogens eventually overcome the physico-chemical barriers, the immune system operates throughout the body to eliminate invaders. There are certain sites within the body where the immune system is organized into specific structures where the immune response (i.e. the reaction of the immune system against invaders) is initiated. These are called secondary lymphoid organs (e.g. lymph nodes, spleen, mucosa-associated lymphoid tissue). There are also primary lymphoid organs (i.e. bone marrow and thymus), which are the sites where the cells of the immune system are generated.

The immune system can be subdivided into two parts: the innate or non-specific and the adaptive, which is also referred to as acquired or specific immunity. Innate immunity is phylogenetically older than acquired immunity. The two branches of the immune system are composed of both cellular (i.e. neutrophils, macrophages, eosinophils, dendritic cells, and NK cells for the innate; T and B lymphocytes for the adaptive immune system) and humoral components (e.g. proteins of the complement for the innate and antibodies for the adaptive immunity). Each of these two branches of the immune system protects the body from pathogen attacks and possesses particular mechanisms of action. First, the components of the innate immune response are constitutively present in the body and are ready to be mobilized within minutes upon infection. Therefore, innate immunity is the first line of defense against invading organisms. Conversely, adaptive immunity needs to be induced and, hence, it acts as a second line of defense. The innate system recognizes pathogen-associated molecular patterns (PAMPs) present on bacteria, fungi, parasites and viruses (e.g. components of bacterial cellular walls, peculiar modifications of DNA and RNA, or viral double-stranded RNA). Thus, innate immunity is not specific and reacts equally well against a variety of organisms. In contrast, the adaptive immune system is antigen specific. This means that it reacts only to the specific microorganism causing an infection. Finally, once that the pathogen has been eradicated, the non-specific immune response ceases and the innate defense

mechanisms return to their previous state, without being altered by the infection. Conversely, the specific response develops 'memory'. In other words, when the same pathogen is encountered for a second time, the specific response will be faster and more effective. Despite the fact that the two arms of the immune system have distinct mechanisms of actions, they are not separated, but rather integrated by cytokines and hormones into a complex multilayered network. One of the most representative examples of a crosstalk between the adaptive and the innate immune system is antigen presentation. In fact, T cells initiate the adaptive immune response only when parts of the pathogens (antigens) are presented by antigen presenting cells (APCs), such as dendritic cells and macrophages, which belong to the innate immune system.

One of the most distinguishing features between the innate and adaptive immune system is the nature of the receptors that immune cells use to recognize pathogens. The innate immune system employs pattern recognition receptors (PRRs), which are encoded by separate genes and recognize groups of related molecules characteristic of microbes (the above mentioned PAMPs). In contrast, cells of the adaptive immune system, such as B and T lymphocytes, are endowed with a unique repertoire of diverse receptors (the B-cell receptor, BCR, and the T-cell receptor, TCR, respectively), which are generated de novo in each individual by the random recombination of gene segments. The repertoire of adaptive immune receptors has the possibility to recognize a numberless variety of antigens and is generated during the development of T and B cells in the primary lymphoid organs. During development, the antigen receptor repertoire is further selected for specificity to antigens and for lack of reactivity against self molecules.

The BCR and the TCR can be structurally divided in two modules: (i) an extracellular unit that recognizes and binds antigens and (ii) cytoplasmic subunits possessing signal-transducing capability. Signals emanating from these receptors are crucial not only for the activation and differentiation of T and B cells (and hence for the immune response), but are also necessary for their development and homeostasis.

2. Development of the immune system

All immune cells are derived from a common precursor, called the pluripotent hematopoietic stem cell (HSC) that reside in the bone marrow. HSCs differentiate into two intermediate stem cells: (i) the common myeloid progenitor (CMP), which is the precursor for the cells of the

innate immune system, such as granulocytes, macrophages, mast cells, and dendritic cells, and (ii) the common lymphoid progenitor (CLP), which can differentiate into lymphocytes, the key cells of the adaptive immune system.

Here, I will focus on the development of lymphocytes as these cells are the subject of my investigations. As mentioned above, lymphocytes originate from common lymphoid progenitors in the bone marrow. Cells destined to become B lymphocytes continue maturation in this organ, whereas precursors of T cells exit the bone marrow and enter the thymus, where they become irreversibly committed toward development in the T-cell lineage by the action of the master differentiation gene Notch1 (Radtke et al., 1999).

2.1. T-cell development

The development of T cells proceeds through discrete stages (Figure 1) (for a review see Starr et al., 2003). Early T-lymphocyte precursors are defined as double negative (DN or $CD4^-CD8^-$) since they do not express either CD4 or CD8. DN thymocytes can be further subdivided into four distinct developmental stages defined by the expression of CD44 and CD25 (IL2Rα). DN1 thymocytes ($CD44^+CD25^-$) are still pluripotential and can give rise to T, B, and NK cells. DN1 cells mature into DN2 cells ($CD44^+CD25^+$) possessing a more limited differentiation potential. DN2 further differentiate into DN3 thymocytes ($CD44^-CD25^+$), which are committed thymocytes that have undergone rearrangements of the gene segments coding for the TCR. These cells also express additional molecules characteristic of the T-cell lineage such as the CD3/TCRζ chains, Lck, ZAP-70, LAT, SLP-76 and others. However, DN3 thymocytes do not possess a functional αβTCR instead they express a complex called the pre-TCR. The TCR and the pre-TCR share many similarities (Figure 2). They both include CD3 εγ and εδ heterodimers, a TCR ζζ homodimer, and a fully rearranged TCRβ chain. Nevertheless, the pre-TCR does not contain the TCRα chain, but rather a surrogate chain called pTα.

The pre-TCR dictates the fate of developing DN3 thymocytes. In fact, mice lacking CD3 chains or TCRβ expression show a developmental arrest at the DN3 stage. The pre-TCR does not have a known ligand and appears to signal in a ligand-independent fashion. Signaling via the pre-TCR controls the transition from the DN3 to the DN4 stage ($CD44^-CD25^-$). During this process, known as "β-selection" (Figure 1), DN3 cells are rescued from apoptosis, proliferate, and stop recombination of the other TCRβ locus (allelic exclusion), thus ensuring that only one functional TCRβ is expressed on the surface of each T cell. The importance of

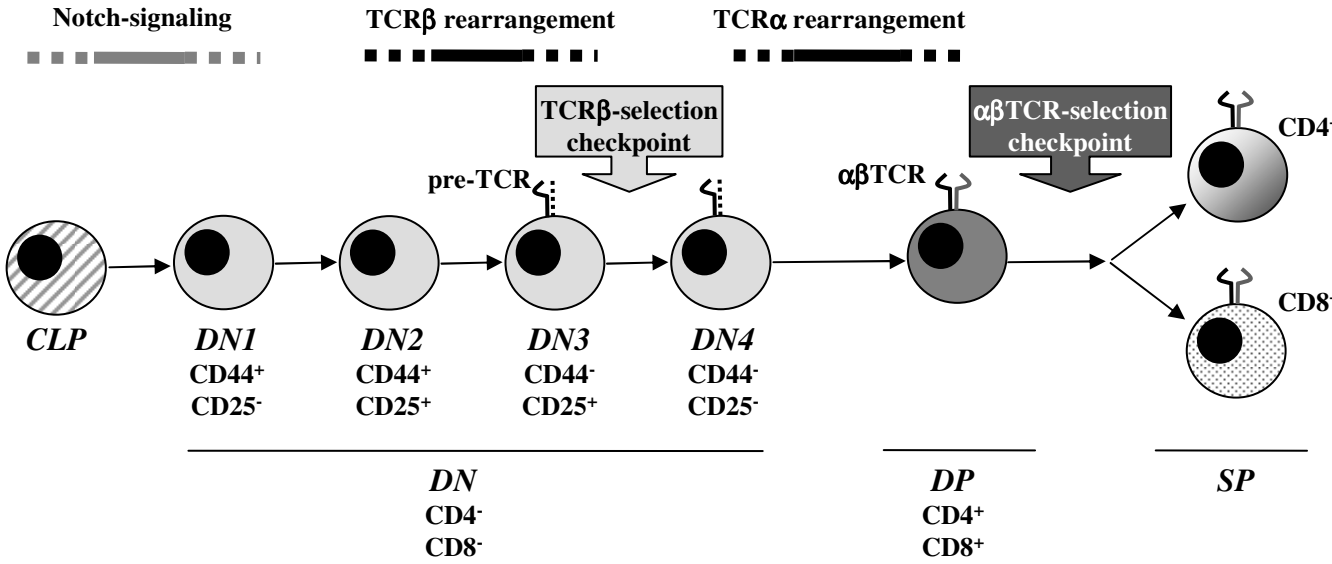

Figure 1. Schematic representation of T-cell development in the thymus.
Upon entering the thymus, lymphoid precursor cells undergo commitment to the T-cell lineage by the action of Notch. Early T-cell precursors express neither CD4 nor CD8 and are called double negative (DN) cells. The DN stage can be subdivided further into four discrete stages (DN1–4) by the expression of CD44 and CD25. DN2 thymocytes start to rearrange the TCRβ gene. DN3 cells express the pre-TCR which is required for successful transition to the DN4 stage (TCRβ-selection checkpoint). At DN4, thymocytes enter division and start to express the CD4 and CD8 genes, thus becoming double positive (DP) cells. DP thymocytes initiate the rearrangement of TCRα and hence replace the pre-TCR with the mature αβTCR. Finally, DP thymocytes undergo positive and negative selection (αβTCR selection). Positive selection results in the differentiation into $CD4^+$ or $CD8^+$ single positive (SP), whereas negative selection culminates with the elimination of the autoreactive clones by apoptosis.

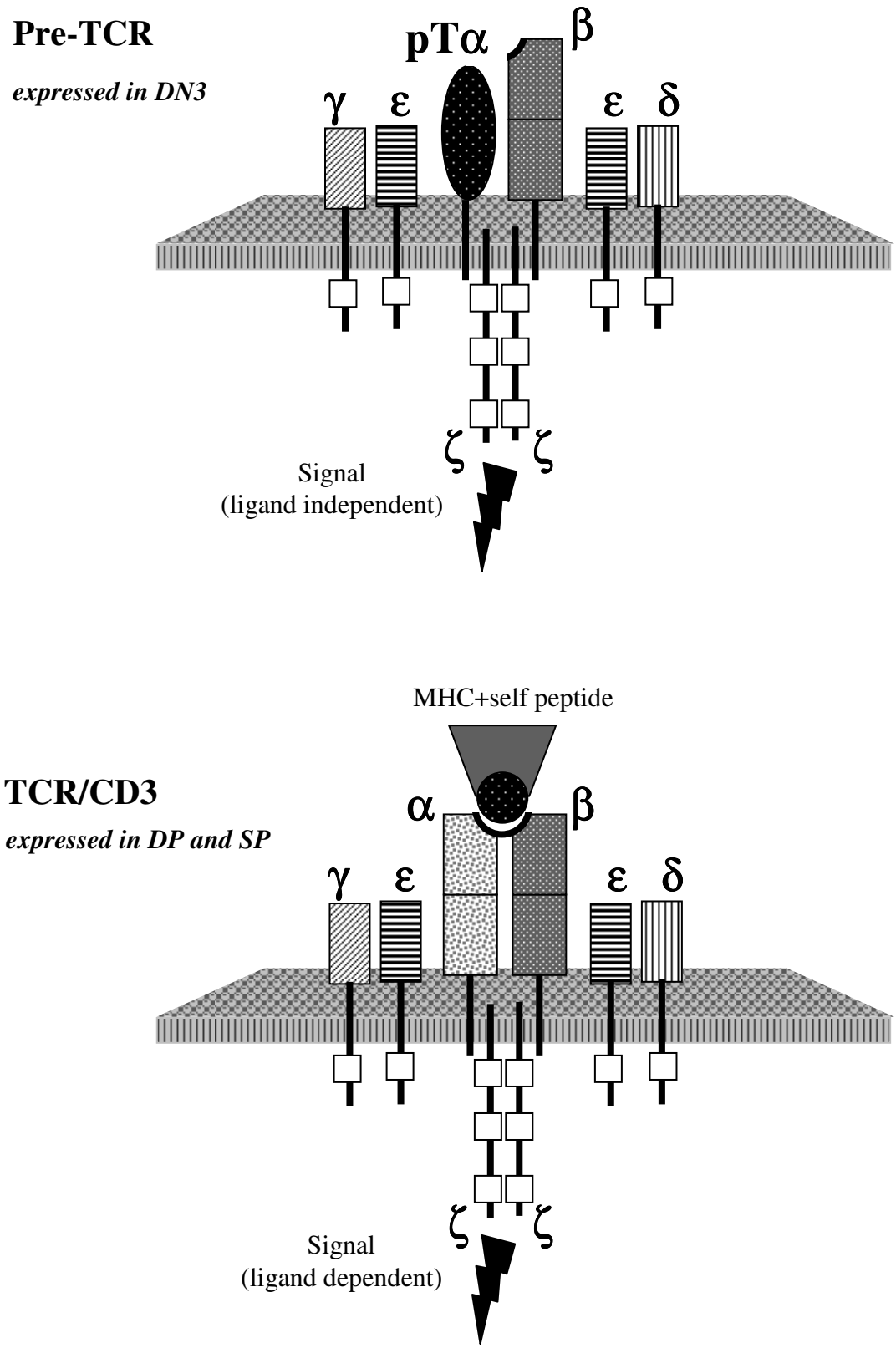

Figure 2. Structure of the pre-TCR and the αβTCR.
A schematic structure of the pre-TCR (left) and the αβTCR (right) is shown. The pre-TCR complex is composed of a TCRβ chain paired with surrogate preTα, two CD3ε chains, one dimerizing with a CD3γ chain, the other with a CD3δ chain, and a TCRζ homodimer. The pre-TCR and the αβTCR are very similar. The only difference is that the αβTCR express a TCRα chain instead of the surrogate preTα. ITAMs are indicated with white boxes.

pre-TCR-mediated signaling in DN3 development has been highlighted in $LAT^{-/-}$ or $SLP\text{-}76^{-/-}$ mice (Pivniouk and Geha, 2000). In these mice the pre-TCR is uncoupled from the activation of downstream signaling pathways and hence thymic development is arrested at the DN3 stage. At the end of β-selection, thymocytes further mature from DN4 to the double positive (DP) stage. During this transition, DN4 cells upregulate the coreceptors CD4 and CD8 and start to recombine the TCRα locus.

At the DP stage, thymocytes express a fully assembled αβTCR and undergo a second major developmental checkpoint (TCR αβ selection, see Figure 1). At this stage, the fate of DP thymocytes is determined by the avidity/affinity of the αβTCR for MHC/self-peptides (Figure 3). Thymocytes expressing a non-functional αβTCR complex that does not bind self-peptide/MHC complexes or that is unable to signal are rapidly eliminated (non-selection). About 90% of DP thymocytes die during this process, which is known as “death by neglect”. On the other hand, DP thymocytes that express a functional αβTCR undergo either positive or negative selection. This process is dictated by the affinity of the TCR for MHC+self peptide complexes (Figure 3). If DP thymocytes carry TCRs with intermediate affinities they will undergo positive selection. This means that thymocytes will complete the differentiation program and become mature T cells. If DP thymocytes bear TCRs with strong affinity for self peptides they will undergo negative selection, a process required to eliminate thymocytes expressing self reactive TCRs.

At the end of thymic selection, only about 5% of thymocytes complete maturation to become $CD4^+$ or $CD8^+$ T cell. Thymic selection ensures the generation of a normal TCR repertoire showing strong reactivity against pathogenic peptides, but lacking overt reactivity against self proteins. For this reason this process is also known as central tolerance. However, thymic selection is not completely safe and some potentially autoreactive T cells do escape negative selection and migrate into the periphery. Therefore, the body possesses a second layer of safety mechanisms, called peripheral tolerance, which prevents the activation of autoreactive T cells in the periphery. These mechanisms include the induction of anergy (i.e. refractory state), immunoregulation (e.g. inhibition of activation by regulatory T cells), expression of antigens in organs which are not accessible to T cells (immune privilege), and others.

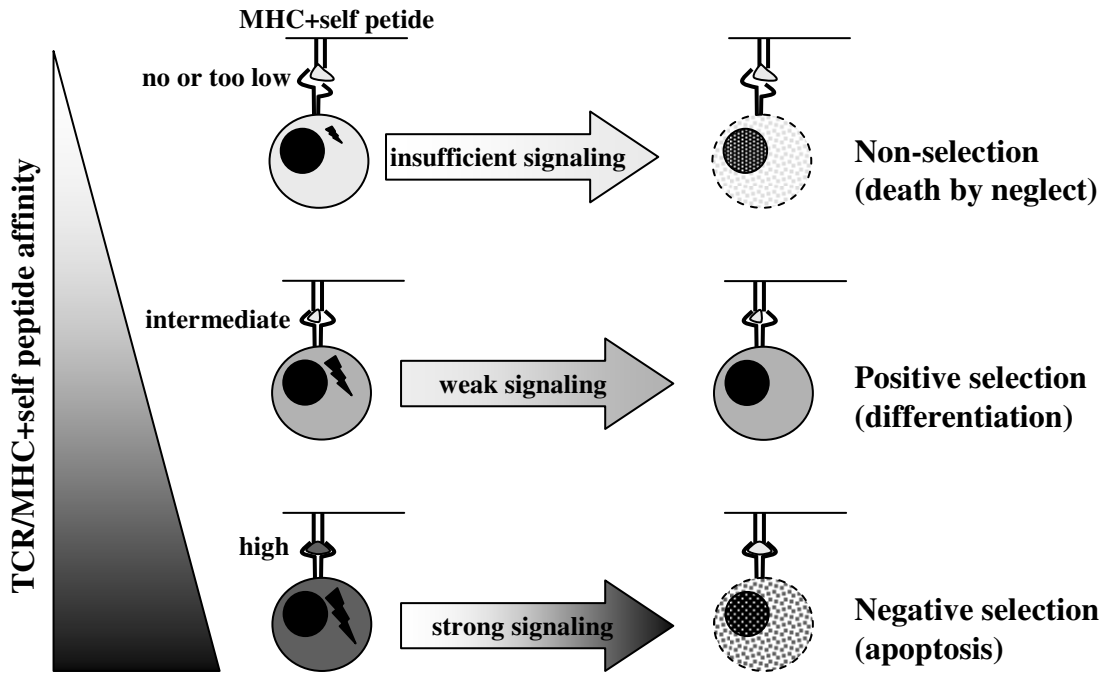

Figure 3. Relationship between TCR affinity, signaling potential, and the outcome of thymic selection.

Upon TCR/MHC+self peptide interactions, DP thymocytes undergo selection processes. TCRs that fail to recognize ligand generate signals of insufficient strength which are unable to induce selection and thymocytes die of neglect. Intermediate-strength signals lead to positive selection, which will result in the maturation of DP cells into $CD4^+$ or $CD8^+$ single positive T cells. Conversely, strong signals lead to deletion of autoreactive DP thymocytes.

2.2. B-cell development

B cells develop in the bone marrow from a common lymphoid progenitor. Similar to T-cell development, the development of B lymphocytes also occurs through a multistep process, which includes the ordered expression of different genes (Figure 4) (LeBien and Tedder, 2008). The earliest B lineage-committed progenitors are referred to as pro-B cells, which can be distinguished by the expression of B220 and CD43. These cells show recombination at the heavy chain locus. Once the immunoglobulin heavy chain genes are successfully rearranged and a heavy chain is expressed at the plasma membrane together with both the surrogate light chains and the signaling components Igα/β (forming the pre-BCR), pro-B cells undergo proliferation and clonal expansion. At this stage, pro-B cells are called large pre-B cells. Subsequently, large pre-B cells stop proliferating and start to rearrange the light chain locus. These cells are known as small pre-B cells.

Similar to the pre-TCR, also the expression of the pre-BCR is crucial for the differentiation of B cells. In fact, gene knockout mice that fail to express the pre-BCR display a developmental block at the pro-B cell stage (Martensson et al., 2010). Once functional light chains have been successfully synthesized and paired with the μ heavy chains, small pre-B cells develop into surface IgM^{+} immature B cells. At this stage, immature B cells undergo negative selection and die if they bind to self antigens in the bone marrow. Conversely, if immature B cells do not bind self antigen, then they start to express the δ chain and will display both IgM and IgD at the plasma membrane. These cells are called transitional 1 B cells and migrate from the BM to the secondary lymphoid organs. Transitional 1 (T1) B cells, are IgM^{hi} and IgD^{lo} and further differentiate into transitional 2 ($IgM^{hi}IgD^{hi}$) in the spleen. Finally, these cells develop into mature B cells ($IgM^{lo}IgD^{hi}$).

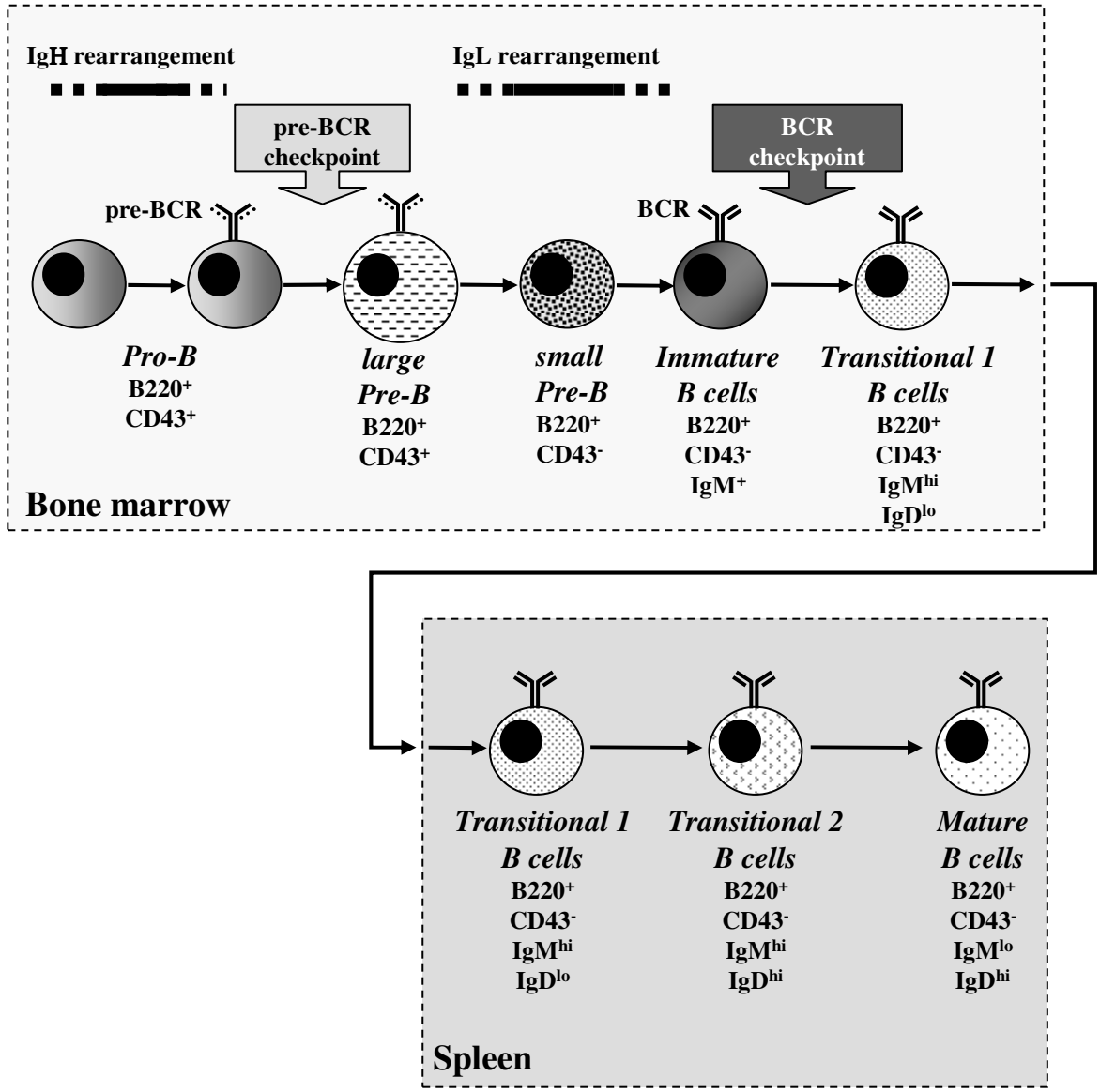

Figure 4. Schematic representation of B-cell development.
The development of B cells begins in the bone marrow and completes in the spleen. The stages of B-cell maturation can be defined by the expression of surface markers. Early B-cell precursors (pro-B) consist of cells that are negative for cell-surface immunoglobulin (IgM), but positive for the B-cell-lineage marker B220 and CD43. Pro-B cells switch on the expression of the Rag genes, which are responsible for the rearrangement of the *Igμ* locus (IgH). This in turn results in the expression of the Igμ heavy chain, which associates with the surrogate light chain (SLC) to form the pre-B-cell receptor (pre-BCR). Signaling through the pre-BCR promotes a proliferative burst and proliferating pro-B cells are defined as large pre-B cells. Successively, large pre-B cells stop proliferating and switch on the expression of the light chain (IgL) (small pre-B cells). Finally, B-cell precursors express the BCR, which will control the next stages of B-cell development.

3. Subpopulations of peripheral lymphocytes

Peripheral lymphocytes are not a homogeneous population, but rather exist in multiple subsets. Here, I shall briefly describe T- and B-cell subpopulations.

3.1. T-cell subsets

Peripheral T cells are subdivided into two distinct groups one expressing the αβ TCR (αβ T cells) and the other bearing the γδ TCR (γδ T cells).

αβ T cells, which represent the majority of T lymphocytes, can be further subdivided in $CD4^+$ and $CD8^+$ T lymphocytes. These two subpopulations are functionally distinct. Whereas $CD4^+$ T cells coordinate the adaptive immune response and are, therefore, called T-helper cells, $CD8^+$ T cells display cytotoxic activity and are able to kill virus-infected or tumor cells.

$CD4^+$ T cells orchestrate the adaptive immune response and perform their helper function mainly by secreting a variety of cytokines. T-helper cells are divided into T-helper (Th) subsets, which are defined according to the cytokines they secrete (Zhu and Paul, 2008). A growing number of Th subsets have been identified: Th1 cells, which produce IL-12, IL-18, and IFNγ support cell-mediated immune responses; Th2 cells, which secrete IL-4, IL-5, and IL-13 coordinate humoral immune responses; Th9 cells, which produce IL-9 may play a role against helminth infection; Th17, which secrete IL-17 have an anti-microbial function and are also implicated in the pathogenesis of many autoimmune diseases. Beside the Th types, $CD4^+$ T cells also include another important subset called regulatory T cells (Tregs). Tregs are characterized by the expression of the transcription factor Foxp3 and CD25 and play a pivotal role in peripheral tolerance.

Conversely to αβ T cells, γδ T lymphocytes represent a small subset of the T-cell pool which usually does not express the coreceptors CD4 or CD8 (for a Review see Bonneville et al.,2010). γδ T cells develop in the thymus at the DN2-DN3 stage. In the periphery, they are particularly abundant in the gut mucosa and in the skin. Their function is still largely unknown and antigen recognition by γδ T cells is very unique as it does not require MHC class I or class II molecules. The γδTCR repertoire is very limited and γδTCRs appear to recognize conserved molecules, similarly to pattern recognition receptors (the receptors of the cells of the innate immunity). γδ T cells appear to function as non-classical T cells and can contribute to both adaptive and innate immunity. In addition to a strong cytotoxic activity, γδ

T cells have also regulatory functions and produce large amounts of proinflammatory cytokines such as IFNγ and IL-17.

3.2. B-cell subsets

Mature B cells are divided into (i) follicular (FO) B cells (also called conventional or B-2 cells), which represent the majority of the mature B cells in the secondary lymphoid organs and (ii) marginal zone (MZ) B cells (for a review see LeBien and Tedder, 2008). These two B-cell subsets are functionally distinct. In fact, whereas FO B cells take part in both T-cell dependent and T-cell independent immune responses, MZ B cells play an important role in T-independent immune responses.

An additional B-cell subset called B-1 cells has been identified. In adult mice, B-1 cells are found mainly in the peritoneal and pleural cavity. On the basis of the expression of surface markers, B-1 cells can be defined as $CD5^{+}CD23^{+}CD43^{+}IgM^{hi}IgD^{lo}$. The origin of B-1 cells remains still unknown. One hypothesis proposes that B-1 cells and conventional B cells originate from distinct precursors. Conversely, a second model postulates that both B-1 and conventional B cells derive from a common precursor (Figure 5). According to this hypothesis, the strength of BCR signaling in B-cell precursors will dictate the developmental outcome. If the signal via the BCR is strong, B-cell precursors will develop into B-1 cells. Conversely, if the BCR signaling is more moderate, B cells will differentiate into conventional B cells. This hypothesis is based on the observation that genetically engineered mutant mice lacking important positive regulators of BCR-mediated signaling display a strong reduction in B-1 cell numbers. On the contrary, mice lacking negative regulators (e.g. CD22 or SHP-1) show an increase in B-1 cell numbers (Figure 5). This hypothesis is also corroborated by our recent data. In fact, we found that mice lacking both SIT and LAX, two inhibitory transmembrane adaptor proteins, display increased B-1-cell numbers (App.19 and sections 6.1., 6.3., and 6.4.).

From a functional point of view, B-1 cells are responsible for the production of most of the non-immune serum IgM (natural antibodies) and contribute substantially to the production of IgA and IgG3. Similar to MZ B cells, B-1 cells are important during T-independent immune responses.

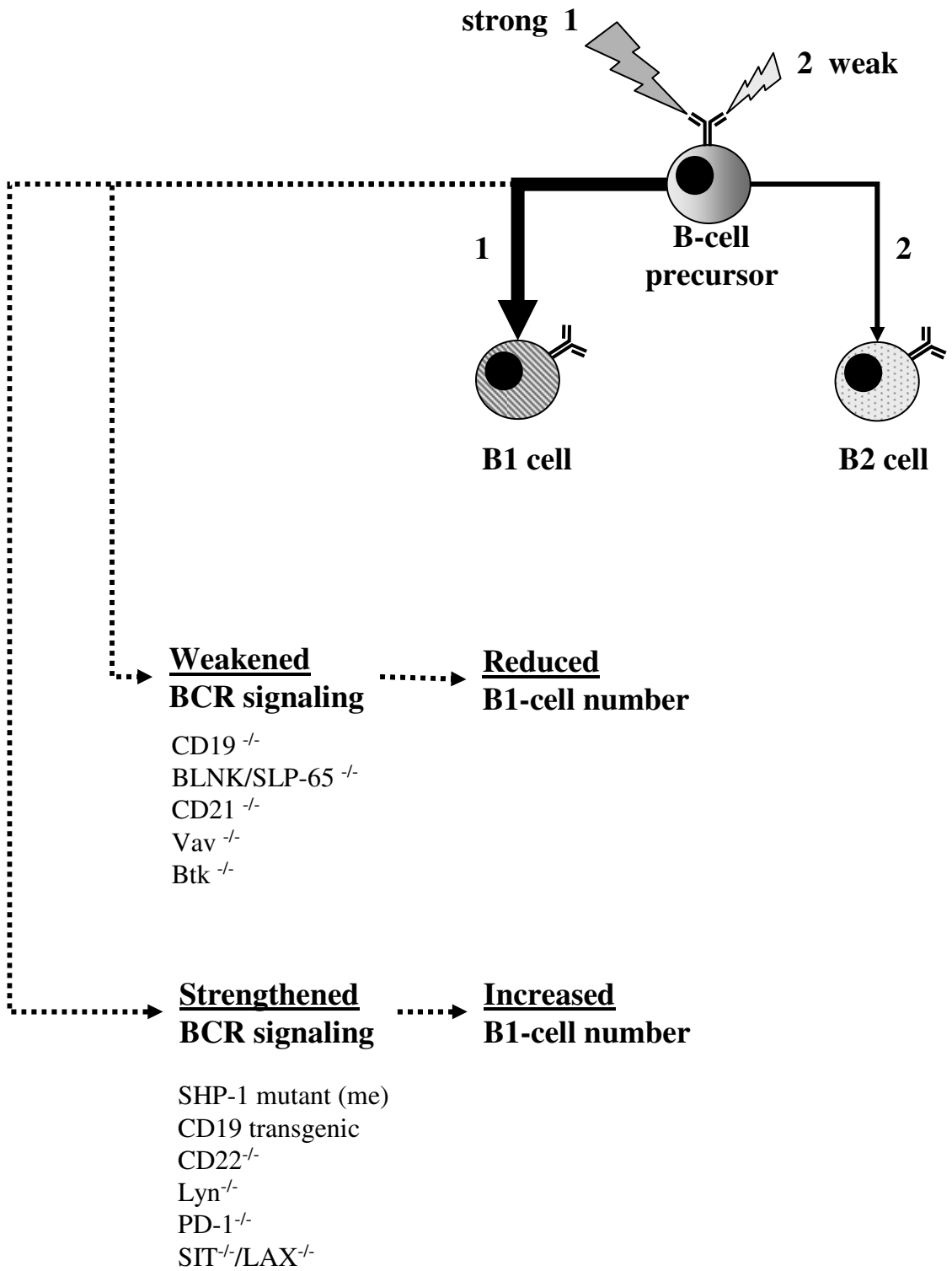

Figure 5. Development of B1 cells.
B-cell precursors can potentially differentiate into either conventional (B2) or B1 cells. The strength of the BCR-mediated signaling dictate the developmental outcome. Weak BCR signaling will support B2-cell development. Conversely, a stronger signaling via the BCR will result in the development of B1 cells. As demonstrated in many mouse models, alterations of the BCR signaling strength will in turn affect B1 cell development (Hardy and Hayakawa, 2001; App.19).

4. Lymphocyte homeostasis

T and B lymphocytes are the key players of the adaptive immune response. Therefore, the preservation of the size of the peripheral lymphocyte pool throughout life is a precondition for an effective immunity. Different strategies are used by the body to regulate the number of peripheral lymphocytes. These include expansion of mature cells, cell death, and the regulation of cell production. Together these processes are referred to as homeostasis (for a review see Grossman et al., 2004).

The homeostasis of different lymphocyte subsets appears to be independently regulated. In fact, T cells are found in normal numbers in B-cell deficient mice and vice versa. Similarly, naïve T cells cannot be replaced by expanding memory T cells and the peripheral memory pool cannot be displaced by an enhanced generation of new cells in the thymus. The fact that lymphocytes possess independent homeostatic control is a prerequisite (i) to safeguard a diverse repertoire of the antigen receptors and (ii) to preserve immunological memory against previously encountered pathogens.

Here, I would like to further focus on how homeostasis of naïve T cells is regulated. In young individuals, the pool of naïve peripheral T cells is initially generated through the continuous emigration of SP thymocytes into the blood stream. Successively, the number of naïve T cells in the periphery is kept constant by the balance between loss (i.e. death or gradual differentiation in the memory compartment after antigen encounter) and replacement (i.e. by the thymic output). In adults, as thymic output diminishes, naïve T-cell numbers are maintained by survival signals (i.e. MHC/self peptides and IL-7) (Figure 6A) and, when clones are lost, by antigen-independent cell divisions of the remaining T-cell clones (homeostatic proliferation) (Figure 6B).

One of the major achievements in our understanding of how homeostasis is regulated was the discovery that cytokines (e.g. IL-7 for naïve T cells) and TCR/MHC+self peptide interactions deliver homeostatic signals. The primary function of cytokines and self peptides/MHC molecules is to support T-cell survival (Figure 6A), as their absence results in T-cell loss. However, these homeostatic signals can also trigger proliferation under conditions in which the size of the T-cell pool is reduced (lymphopenia) (Figure 6B). Under lymphopenic conditions, residual T cells proliferate in the attempt to repopulate the void. Lymphopenia may occur after chemotherapy, during viral infections, or in patients suffering from

immunodeficiency. Under particular circumstances, however, lymphopenia may also provide the basis for the development of autoimmunity (Figure 6B). This may occur when T-cell depletion persists or is progressively repeated, or when lymphopenia arises concomitantly with an inflammation. In this scenario, T cells may be overstimulated or the T-cell repertoire may be skewed to a one enriched in self-reactive clones. In this regard, we found that SIT-deficient mice develop autoimmunity along with an enhanced homeostatic expansion (Posevitz et al., 2008/App.11; Arndt et al., 2011/App.16).

Homeostasis has been extensively studied in different experimental models. One of the most well-established methods to study homeostatic expansion is the adoptive transfer of T cells into lymphopenic recipients. Sublethally irradiated mice or Rag1/Rag2-deficient mice are frequently used as recipients. Studies employing these models have revealed that the strength of TCR signaling is a crucial determinant for homeostatic expansion. T cells expressing TCRs with higher affinity display homeostatic advantage over T cells carrying TCRs with lower affinity. Our studies have further empathized the importance of modulators of TCR signaling in the regulation of T-cell homeostasis (Posevitz et al., 2008/App.11). We have shown that mice lacking SIT, a transmembrane adaptor that inhibits TCR-mediated signaling, showed an enhanced lymphopenia-induced homeostatic expansion. One observation of our study was that the loss of SIT enables HY TCR transgenic T cells to undergo homeostatic proliferation. This is a striking effect as HY TCR transgenic T cells, due to the very low affinity of the TCR, are unable to undergo homeostatic proliferation in lymphopenic hosts.

An important issue that has been recently addressed is whether homeostatic TCR signals inducing survival are qualitatively different from those inducing expansion (Seddon and Zamoyska, 2003). It appears that Lck and Fyn, the most proximal signaling molecules in the TCR signaling cascade, are key discriminators between T-cell survival and expansion. In fact, whereas the expression of Lck is not required for the survival of naïve T cells, Lck expression is absolutely mandatory for TCR signals that induce homeostatic proliferation upon lymphopenia. Conversely, Fyn plays no role in lymphopenia-induced homeostatic expansion, but rather it mediates T-cell survival.

In addition to TCR signals, also cytokines (especially IL-7) play a crucial role in T-cell homeostasis (Fry and Mackall, 2005). Studies utilizing IL-7Rα deficient mice or blocking antibodies have shown that IL7Rα-mediated signaling is essential for the homeostatic proliferation and the survival of naïve T cells.

A)

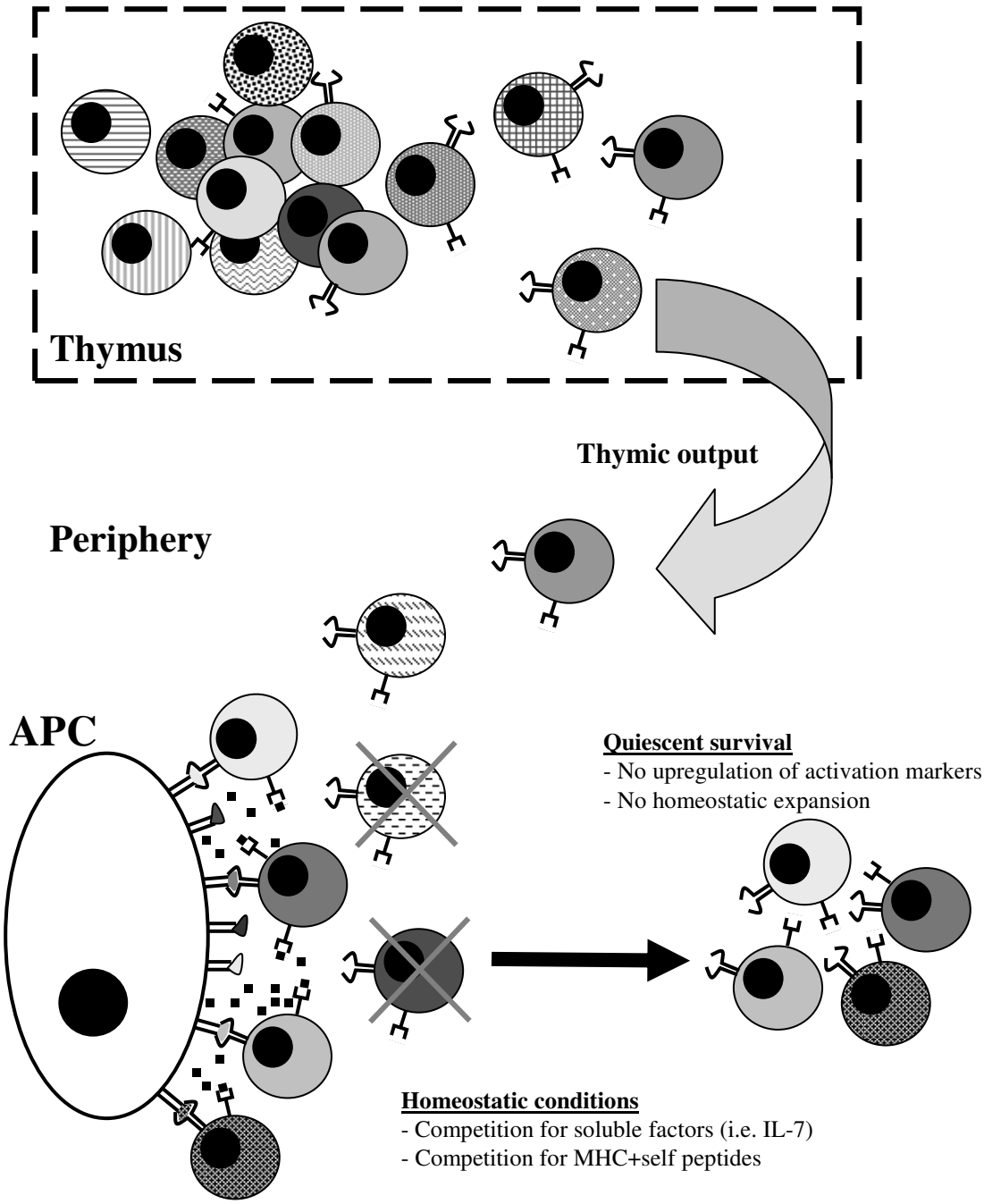

Figure 6A. Regulation of T-cell homeostasis under normal conditions.
Selection processes in the thymus generate T cells with a broad spectrum of affinities for self peptides. After emigrating into the periphery, these cells are kept alive (quiescent survival) by continuous signals generated upon TCR/MHC+self petides and by soluble factors (i.e. IL-7). Competition for soluble factors and MHC+self peptides limits the size of the peripheral T-cell pool and avoid uncontrolled homeostatic expansion (modified from Theofilopoulos et al., 2001).

B)

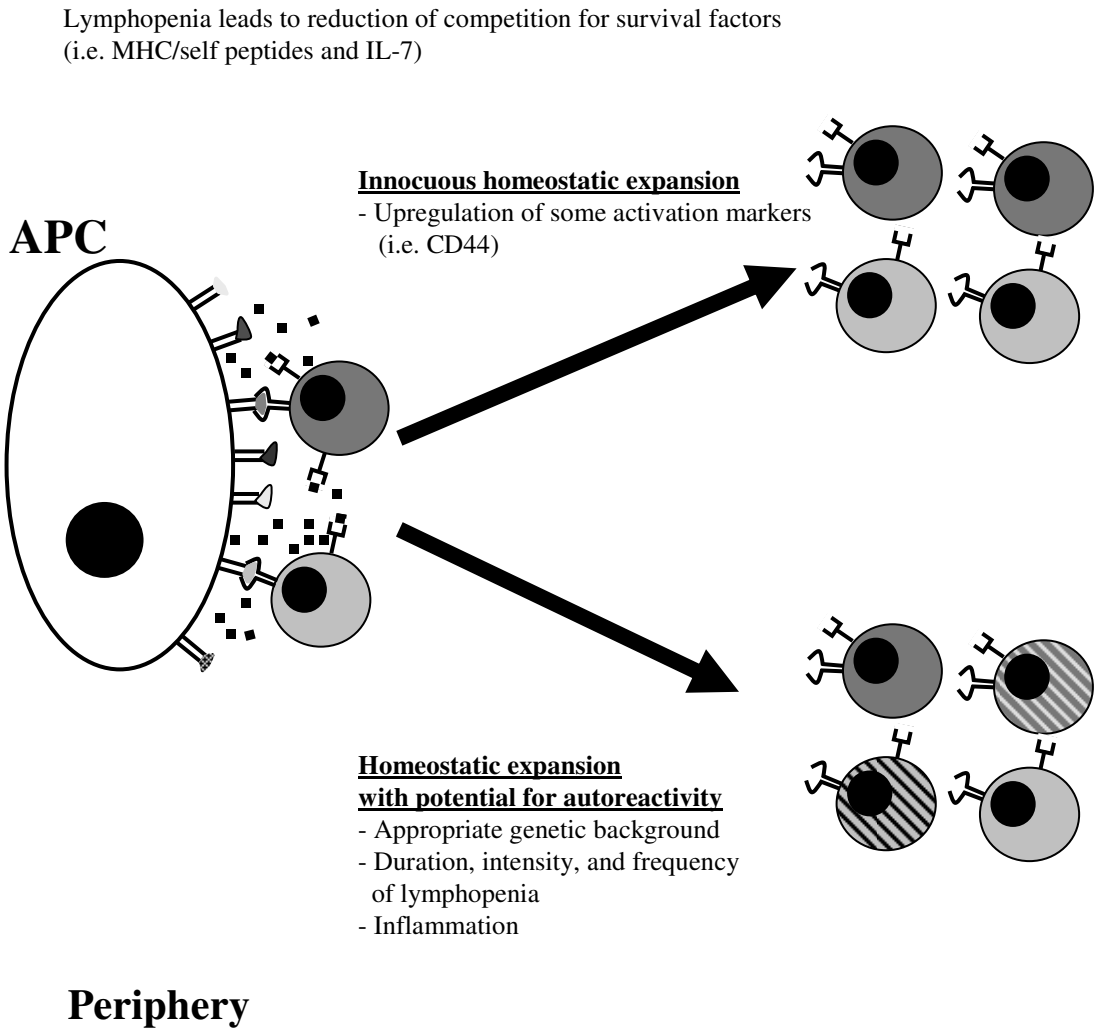

Figure 6B. Regulation of T-cell homeostasis under lymphopenic condition.
Reduction of T-cell numbers increases the availability of stimulatory signals (i.e. MHC+peptides and cytokines) resulting in homeostatic expansion. Lymphopenia-induced homeostatic proliferation is usually an innocuous process, and expanding T cells express some activation/memory markers without acquiring effector functions. However, when other pathological conditions are met (e.g. recurrence of lymphopenia, inflammation, etc,), T cells may become over reactive and the T-cell repertoire may be skewed. This may lead to the development of autoimmune diseases (modified from Theofilopoulos et al., 2001).

In summary, the homeostasis of naïve T cells depends on signals mediated by both TCR/MHC+self pepdide and IL7/IL7R interactions. It is the availability of these factors that limits the size of the different lymphocyte subpopulations. The relative contribution of the two signaling pathways to the activation of the homeostatic program has not yet clearly determined and may depend on both the characteristics of individual T-cell clones and the environmental conditions (e.g. the degree of the lymphopenia).

T cells undergoing homeostatic expansion do not upregulate activation markers such as CD69 or CD25 and keep the expression of the naive T-cell marker CD62L. Therefore, they are clearly distinguishable from activated T cells. Nevertheless, they upregulate memory markers such as CD44 and CD122, and also their functional responses resemble those of memory cells. Thus, T cells undergoing homeostatic proliferation are also referred as to memory-like T cells.

5. TCR-mediated signaling: an overview

As discussed above, signals transduced via the TCR are crucial for the development, the activation, and homeostasis of T cells. Therefore, in this section, I will discuss how TCR-mediated signaling is initiated, regulated, and propagated to the nucleus, where the cellular program is ultimately executed.

One of the first events induced upon TCR ligation is the aggregation of the receptors. Subsequently, Lck and Fyn, two members of the Src family of tyrosine kinases, come into play. The question of how the signaling cascade is initiated by Src kinases has fascinated many researchers. To date, however, a clear answer to this question is still missing and several models have been postulated. The current tenet suggests that Src kinases are activated upon TCR triggering. In turn, Lck and Fyn phosphorylate a variety of downstream molecules, thus allowing propagation of the signal to the nucleus. However, a recently proposed model has challenged this view (Nika et al., 2010). According to the studies of Nika et al., a pool of Lck, the Src kinase playing a major role in TCR signaling, is constitutively active. Therefore, the initiation of signaling does not require *de novo* activation of Lck, but rather the redistribution of the active pool of Lck to the TCR and other signaling molecules at the plasma membrane.

Nevertheless, Src-family tyrosine kinases are crucial for the propagation of the signal as they phosphorylate the two tyrosine residues of the ITAMs (immunoreceptor tyrosine-based activation motifs) located within the cytoplasmic tails of the antigen receptor-associated subunits (i.e. CD3 γ, δ, ε, and ζ in T cells). Fully phosphorylated ITAMs provide binding sites for ZAP-70, a protein tyrosine kinase with two tandem SH2 domains, which propagates the signal further. Recruitment of ZAP-70 to the ITAMs results in its phosphorylation and subsequent activation by Lck. Activated ZAP-70 in turn phosphorylates two adaptor proteins LAT and SLP-76, which form the backbone of a signaling complex that activates multiple downstream signaling pathways (e.g. MAPK, NFAT, NFkB etc.) leading to T-cell activation and proliferation (Smith-Garvin et al., 2009). T cells also possess a number of counter regulating mechanisms that fine-tune and shutdown signaling (Acuto et al., 2008; Linnemann et al., 2009/App.14; Marinari et al., 2003/App.3).

A central question in TCR-mediated signaling seeks to understand how the TCR produces diverse cellular outcomes (e.g. proliferation, differentiation, or apoptosis) in response to different stimuli by activating a limited number of signaling modules. During the last decades efforts have been made in order to answer this question and several hypotheses have been formulated. Recent progress emphasizes that variations in the magnitude or in the duration of activation of signaling cascades determine the specificity of the signaling output and of the consequent cellular outcome (Ebisuya et al., 2005). In the following subsections, I shall discuss two current models for signal discrimination.

5.1 Regulation of TCR-mediated signaling: signal amplification at the proximal level

The TCR/CD3 complex has an unique configuration compared to other antigen receptors as it contains ten ITAMs. As mentioned above, ITAMs are critical for the initiation of signaling following ligand engagement. It has been additionally proposed that ITAMs could also provide quantitative and/or qualitative contributions to the specific cellular response (Love and Hayes, 2010). In fact, the high number of ITAMs in the TCR signaling machinery can allow the generation of different signaling degrees, ranging from weak to strong, depending on the number of phosphorylated ITAMs and hence on available ZAP-70 molecules. Differences in the signal amplitude will be then translated into the nucleus, where diverse sets of responding genes will be activated, which will in turn dictate the specific cellular response.

A large body of evidence indicates that the ITAM-mediated signal amplification plays a critical role in T-cell development. ITAMs appear to be important at both the DN to DP and

the DP to SP transitions, as well as for the αβ/γδ T lineage choice. In fact, the attenuation of the γδTCR signaling potential by reducing the number of ζ ITAMs results in the diversion from the γδ to the αβ T-cell lineage. Additional studies have revealed that TCR$\zeta^{-/-}$ mice transgenically reconstituted with ζ chains lacking one or more ITAMs have a defect in thymic development (Love et al., 2000; Watanabe et al., 2000). Interestingly, the severity of the developmental defect is in close correlation with the number of inactivated ITAMs. Both positive and negative selection are affected in these mice (Figure 7). Positive selection is reduced or diverted to non-selection, whereas negative selection is converted to positive selection (Shores et al., 1997; Yamazaki et al., 1997). These alterations may potentially lead to the generation of autoreactive T cells. In summary, these data demonstrate that amplification of the TCR signal at a very proximal level determines the right signal intensity for the specific developmental outcome.

We have further explored how the TCR-mediated signaling is regulated during T-cell development. In particular, we have analyzed the function of the two transmembrane adaptor molecules SIT and TRIM. It has been shown that TRIM is an integral component of the TCR/CD3 complex (Bruyns et al., 1998; Kirchgessner et al., 2001). Similarly, SIT was identified as a protein co-immunoprecipitating with CD3ε (Marie-Cardine et al., 1999). Thus, both SIT and TRIM are physically located at the plasma membrane either as a part of or in close proximity to the TCR and hence may be involved in the regulation of TCR-mediated signaling. Indeed, we have demonstrated that SIT and TRIM function as suppressors of signal amplification and regulate thymic selection (Simeoni et al., 2005a/App.5; Koelsch et al., 2008/App.13). By generating SIT and TRIM single or double knockout mice, we found that the loss of SIT and TRIM converts non selection into positive selection (Figure 7). Using TCR transgenic models (i.e. HY and P14), we found that the loss of SIT alone is sufficient to induce a more efficient positive selection and a partial shift to negative selection, whereas the loss of both SIT and TRIM results in a complete conversion from positive to negative selection (Figure 7). Interestingly, the effects of SIT/TRIM double-deficiency on thymocyte development are opposite to those observed in mice carrying mutations in the TCR-associated ζ chain. On the basis of these observations, we propose a model whereby signal amplification by multiple ITAMs within the TCR/CD3 complex appears to be counter regulated by an inhibitory system based on several TBSMs within transmembrane adaptors (Koelsch et al., 2008/App.13).

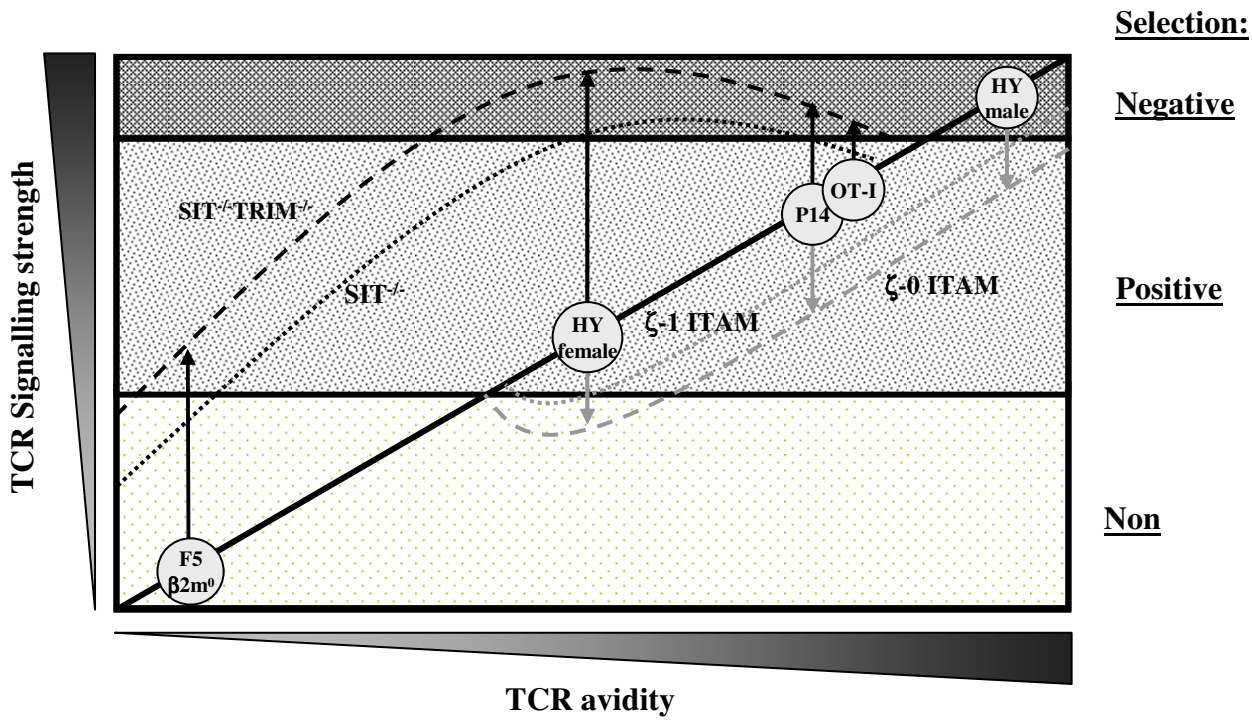

Figure 7. Model of thymic selection outcomes.
The model shows the effects of altering signal intensity on the selection of thymocytes expressing TCRs with increasing affinity/avidity for the ligand. The effects of SIT (black dotted line) or SIT and TRIM (black dashed line) deletions on selection outcomes are compared with those obtained by TCR-ζ mutants carrying only 1 ITAM (gray dotted line) or no ITAMs (gray dashed line) (from Koelsch et al., 2008/App.13)

5.2 Regulation of TCR-mediated signaling: signal amplification at the level of Ras

The Ras-Erk cascade is essential for cell-fate decisions in many cell types including T lymphocytes (Yasuda and Kurosaki, 2008). In T cells it is the magnitude of Erk activity that appears to be involved in cell-fate specification triggered via the TCR (Daniels et al., 2006; Prasad et al., 2009). For example, it was shown that strong Erk activation at the plasma membrane induces apoptosis (negative selection), whereas moderate Erk activation in intracellular compartments induces differentiation (positive selection) of immature T cells. A similar mechanism of Erk activation exists also in mature peripheral T cells. In fact, we have previously shown that in OT-I T cells strong Erk activation correlates with apoptosis, whereas, weak Erk activity corresponds with proliferation (Wang et al., 2008/App.12). More recently, we have shown that the duration of Erk activation may also play a role in cell-fate decisions in human T cells. In fact, transient Erk activation correlates with an unresponsive, anergic-like state, whereas sustained Erk activity corresponds with proliferation (App.18).

Upon ligation of the TCR, the activation of the Erk cascade is thought to occur through the action of two distinct GEFs, RasGRP1 and Sos1 (Figure 8A) (Roose and Weiss, 2000). RasGRP1 is activated by DAG, which is produced by PLCγ1 upon cleavage of PIP_2. PLCγ1 is activated upon binding to phosphorylated LAT, a transmembrane adaptor protein crucial for T-cell activation (Wange, 2000). Phosphorylated LAT also recruits the GADS/SLP-76 complex, which binds and further activates PLCγ1 by recruiting the tyrosine kinase Itk. Additionally, phosphorylated LAT is also required to recruit the Grb2/Sos complex to the plasma membrane. Thus, LAT may activate Ras via two distinct pathways: (i) PLCγ1-DAG-RasGRP1 and (ii) Grb2-Sos (Figure 8A) (Roose and Weiss, 2000).

A key finding on Ras-Erk regulation in T cells came from recent studies based on lymphoid cells, thymocytes and *in silico* simulations showing that Ras activation is further controlled by an unusual interplay between RasGRP1 and Sos (Das et al., 2009; Roose et al., 2007). These studies proposed that, upon initial receptor triggering, Ras is exclusively activated via RasGRP1 (Figure 8A). Once a certain threshold of Ras activation has been reached, RasGTP (active Ras) will prime Sos, thus triggering a feedback loop that results in the full activation of the Ras-Erk cascade. This mechanism relies on an allosteric pocket found in Sos crystal structure that is specific for RasGTP (Margarit et al., 2003). In fact, it has been shown that upon loading of the allosteric pocket of Sos with RasGTP, the GEF activity of Sos is significantly enhanced.

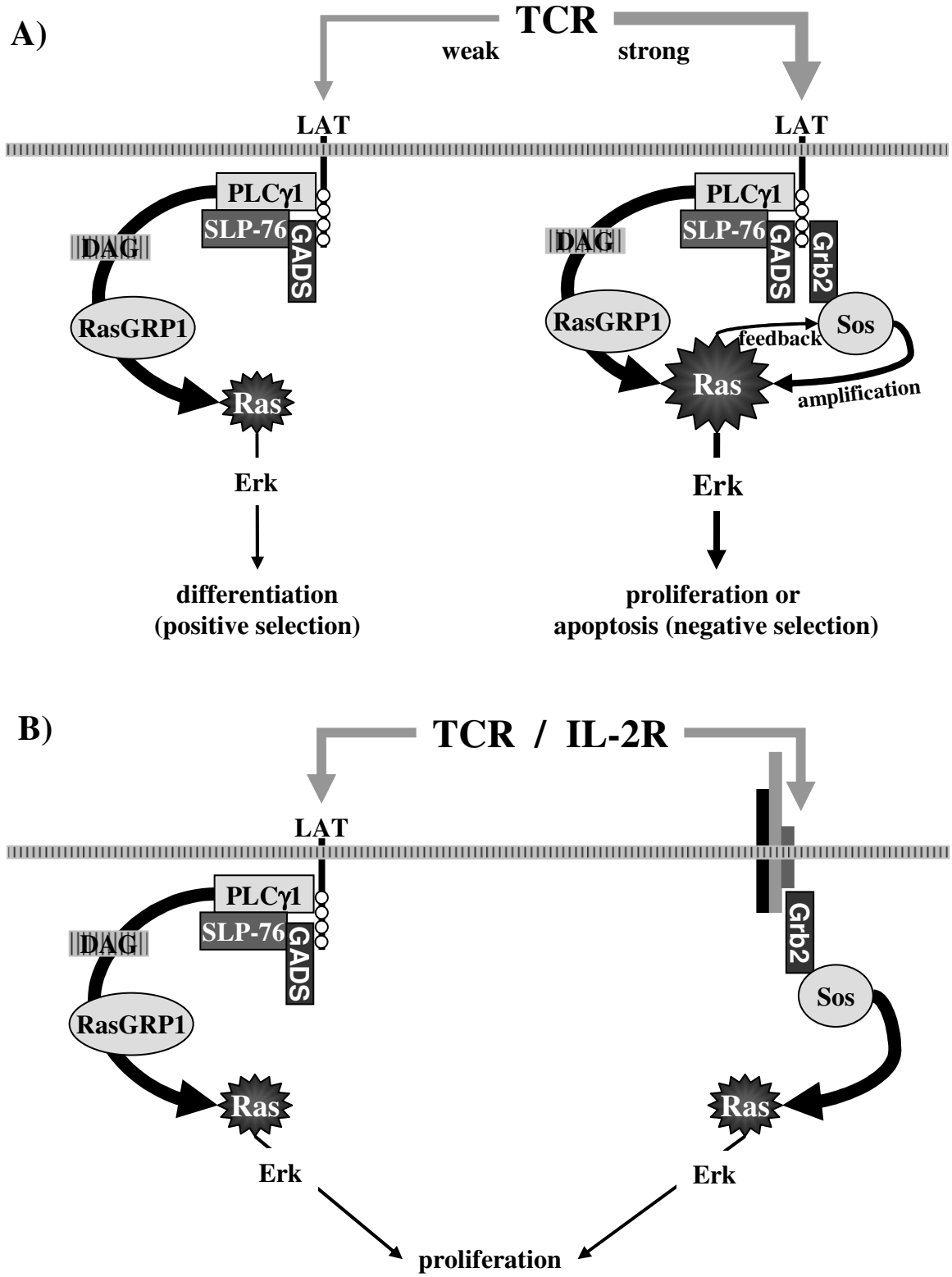

Figure 8. Models of Ras-Erk activation in T cells.
A) Model proposed by Das et al. 2009. Weak TCR ligands induce only a partial phosphorylation of LAT, which in turn activates Ras only via RasGRP1 (left), whereas strong ligands induces full LAT phosphorylation that will result in Ras activation through the coordinated action of RasGRP1 and Sos1 (right). The different strength of Erk activation will in turn regulate the cellular outcome. B) Alternative Ras-Erk activation model (Warnecke et al., 2012/App.17). TCR- and IL2-mediated pathways activate Ras-Erk by utilizing two independent mechanism, one involving RasGRP1, the other Grb2/Sos.

Thus, the current model postulates that the coordinated action of RasGRP1 and Sos1 regulates the magnitude of Ras-Erk activation (Figure 8A). Consequently, the magnitude of the Ras-Erk signaling is interpreted by the cells through the activation of a network of immediate-early genes, thus allowing the generation of the appropriate response.

However, it has not yet been demonstrated whether this model for TCR-mediated Ras-Erk activation is also valid in primary T cells. Given the central role of Erk activation in cell-fate specification processes induced by TCR triggering, we have further assessed the validity of this model in primary human T cells (Warnecke et al., 2012/App.17). Initially, we suppressed Grb2/Sos1 and RasGRP1 expression using siRNA. We found that, in primary T cells, neither the suppression of Sos1 nor Grb2 impairs TCR-mediated Erk activation. Conversely, suppression of RasGRP1 confirmed that RasGRP1 is the major activator of Ras-Erk in primary T cells. However, when we assessed the contribution of Grb2/Sos and RasGRP to Erk activation downstream of the IL-2 receptor, which is also required for T-cell activation, we found that only Grb2/Sos are required for IL2-mediated Erk activation. Consistent with previously published data (Priatel et al., 2010), we found that the downregulation of RasGRP1 did not affect IL-2-mediated Erk activation. Thus, RasGRP1 and Grb2/Sos do not function as integrators of signals to Ras downstream of the TCR, but rather they appear to function as insulators of signals that lead to Ras activation induced by different stimuli (Figure 8B).

6. Adaptor molecules

A major step in our understanding of lymphocyte development and activation has been achieved through the functional characterization of a group of molecules called adaptor proteins (Simeoni et al., 2005b; Simeoni et al., 2008). Adaptors function as linkers between the antigen receptor, which senses changes in the extracellular environment, and the cytoplasmic effectors, which transmit the signal to the nucleus. These proteins are involved in the regulation of many signaling cascades and can be divided into two main groups: TRansmembrane Adaptor Proteins (TRAPs), which are integral transmembrane proteins such as LAT, TRIM, SIT, PAG/Cbp, NTAL/LAB (Brdicka et al., 2002/App.2), LIME (Brdickova et al., 2003/App.4), and LAX (for a review see Lindquist et al., 2003; Horejsi et al., 2004) and Cytoplasmic Adaptor Proteins (CAPs) such as Grb2, Gads, SLP-76, ADAP, SKAP-55,

SKAP-HOM (Togni et al., 2005/App.6) etc., localized within the cytoplasm (for a review see Simeoni et al., 2004; Simeoni et al., 2005b).

Adaptor molecules are proteins that exhibit no intrinsic enzymatic or transcriptional activities. However, they possess a variety of signaling domains including Src-homology 2 and 3 domains (referred to as SH2 and SH3 domains respectively), phosphotyrosine binding (PTB) domains, pleckstrin homology (PH) domains, and many others (Simeoni et al., 2004). They also possess tyrosine-based signaling motifs (TBSMs), which interacts with SH2 or PTB domains. It is by virtue of their modular structure that adaptors couple proximal biochemical events initiated by ligation of the TCR to distal signaling pathways. Adaptors also play an important role in inside-out signaling and link the TCR to integrin activation (Horn et al., 2009/App.15).

The function of TRAPs is to ensure the proper positioning of signaling elements at the plasma membrane (Simeoni et al., 2005b). Upon antigen receptor stimulation, protein tyrosine kinases phosphorylate key tyrosine residues within TBSMs, which is the predominant signaling motif characterizing this group of adaptors. Tyrosine phosphorylation creates binding motifs that recruit signaling molecules containing SH2 or PTB domains to the plasma membrane. The group of transmembrane adaptors can be further subdivided into TRAPs that are raft-associated (LAT, PAG, LIME, and NTAL/LAB) and those that are not (SIT, TRIM, and LAX) (see Figure 9).

A large body of work derived from different laboratories supports the idea that LAT is an essential TRAP in T cells (Wange, 2000). In fact, LAT-deficient cell lines have a severe defect in the activation of important signaling cascades including Ca^{2+} and Ras. To specifically address the role of LAT *in vivo*, LAT-knockout and -knockin mice were generated (for a review see Malissen et al., 2005). The characterization of LAT-knockout mice has clearly demonstrated that LAT is essential for T-cell development, as $LAT^{-/-}$ mice display a developmental block at the DN3 stage.

In contrast to LAT, which is clearly crucial for T-cell functions, the other TRAPs such as LAX, NTAL, and SIT rather appear to function as signal attenuators, and thus participate in the fine-tuning of antigen receptor-mediated signaling. Recent data suggest that LAX (Zhu et al., 2005; App.19), NTAL (Zhu et al., 2006a), and SIT (Posevitz et al., 2008/App.11) regulate lymphocyte homeostasis and peripheral tolerance. Despite intense scrutiny, the *in vivo* function of other TRAPs, such as PAG (Dobenecker et al., 2005; Xu et al., 2005), TRIM

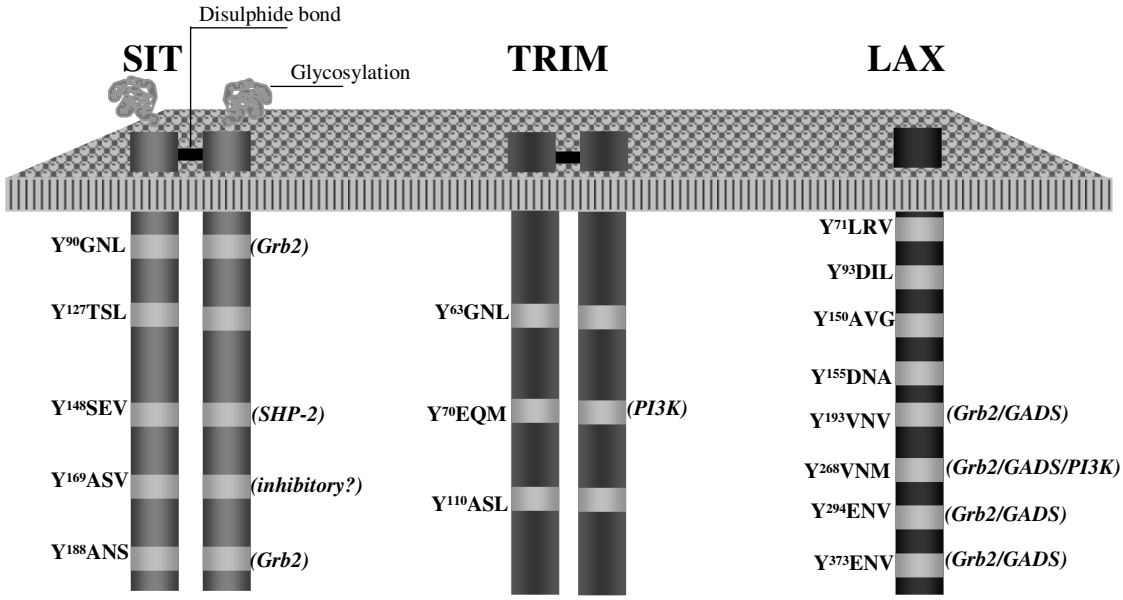

Mw:	30-40 kDa (monomer)	30 kDa (monomer)	70 kDa
Ex:	Thymocytes T cells B cells Plasma cells	Thymocytes	T cells B cells Mast cells

Figure 9. The three non-raft transmembrane adaptor proteins. SIT (SHP2-interacting transmembrane adaptor protein), TRIM (T-cell-receptor-interacting molecule), and LAX (linker for activation of X cells, where X denotes an as yet unidentified cell) are the TRAPs that do not localize to lipid rafts. All have short extracellular domains, typical transmembrane α-helices and long cytoplasmic tails that contains several potential phosphorylation sites known as tyrosine-based signaling motifs (TBSMs) ( ). The primary sequences (four amino acids beginning with Y) of TBSMs are shown. Upon immunoreceptor ligation, TBSMs are phosphorylated and thus function as binding sites for the SH2-domain-containing molecules (indicated in parenthesis). Mw, molecular weight; Ex, tissue expression.

(Kolsch et al., 2006/App.8), and LIME (Gregoire et al., 2007/App.10) remains still elusive. Here, I will primarily focus upon the non raft-associated transmembrane adaptors SIT, TRIM and LAX.

6.1. SIT (SHP-2-Interacting Transmembrane adaptor protein)

SIT has the typical structural organization of TRAPs, which consists of a short extracellular domain (18 aa), a single segment of hydrophobic amino acids representing the transmembrane region (20 aa), and a long cytoplasmic tail (136 aa) (Figure 9). However, SIT is a unique molecule among TRAPs, as (i) it is one of two expressed at the plasma membrane as a disulfide linked homodimer (this property is shared with TRIM) and (ii) it is heavily glycosylated on a single asparagine residue (N^{26}) in the extracellular domain. This glycosylation accounts for approximately 20 kDa of the molecular weight and may represent a binding site for an extracellular ligand, which, however, has yet to be identified.

The cytoplasmic domain of SIT is characterized by the presence of five TBSMs: Y^{90}GNL, Y^{127}TSL, Y^{148}SEV, Y^{169}ASV, and Y^{188}ANS respectively (Figure 9). Upon TCR stimulation, these TBSMs can be phosphorylated by the coordinated action of both Src and Syk families tyrosine kinases. Tyrosine Y^{90} (YGNL) and Y^{169} (YASV) are strongly phosphorylated, whereas residues Y^{127} (YTSL), Y^{148} (YTSL), and Y^{188} (YANS) represent only minor phosphorylation sites. It has been shown that SIT binds the tyrosine phosphatase SHP-2 and the tyrosine kinase Csk through the phosphorylated Y^{148}SEV and Y^{169}ASV motifs, respectively (Marie-Cardine et al., 1999; Pfrepper et al., 2001/App.1). Additionally, SIT also binds the adaptor protein Grb2 via phosphorylated tyrosines Y^{90}GNL and Y^{188}ANS (Figure 9). By acting as a scaffold, SIT may influence T-cell activation by recruiting signaling molecules to the plasma membrane. Previous experiments performed in the Jurkat T-cell line demonstrated that SIT is indeed involved in the regulation of TCR-mediated signaling (Marie-Cardine et al., 1999). Overexpression of full length SIT exerted a strong inhibitory effect on the TCR- and PHA-mediated transcriptional activity of NFAT. As reported above, SIT binds the inhibitory molecule SHP-2 via Y^{148}SEV, which is an immunoreceptor tyrosine-based inhibition motif (ITIM) and hence may inhibit T-cell activation via SHP-2. However, a SIT-mutant containing an amino acid substitution (Y to F) in the ITIM still inhibited TCR-mediated NFAT activation, despite the fact that the SHP-2 binding to SIT was largely lost. These results indicate that the binding of SHP-2 to SIT is not required for negative regulation of TCR signaling. Additional experiments revealed that the Y^{169}ASV motif mediates the

inhibition of TCR-induced NFAT activation. Pulldown assays performed on pervanadate treated T cells initially suggested that the tyrosine kinase Csk binds to the YASV motif and thus might mediate the inhibitory effect of SIT on TCR signaling (Pfrepper et al., 2001/App.1). Csk is the major negative regulator of Src protein tyrosine kinases that inhibits TCR-mediated signaling by several mechanisms (Marinari et al., 2003/App.3). However, so far we could not show an association between SIT and Csk in human or mouse T-cells under more physiological conditions of stimulation (e.g. CD3 mAb instead of pervanadate).

Recently, we have re-addressed the question of how SIT regulates TCR-mediated signaling by using RNAi (Arndt et al., 2011/App.16). We have found that suppression of SIT expression by siRNA in both Jurkat and primary T cells enhances proximal TCR signaling, thus confirming our initial hypothesis that SIT is a negative regulator. A more detailed analysis revealed that the loss of SIT also resulted in an enhanced TCRζ phosphorylation and ZAP-70 association. Collectively, these data suggest that SIT negatively regulates proximal TCR signaling at the level of TCRζ/ZAP-70. We propose that SIT influences the activation of signaling molecules, such as Lck, located in the apical part of the TCR signaling cascade. However, how SIT regulates TCR-mediated signaling requires further investigations.

SIT is strongly expressed in thymocytes. Additionally, SIT is abundant in peripheral T cells and is also expressed in B cells and in plasma cells, albeit at a much lower level. This expression pattern suggests that SIT may play a role in T-cell development and function. In fact, the analysis of thymic development in $SIT^{-/-}$ mice demonstrated that SIT inhibits selection processes, as the loss of SIT converted positive to negative selection in class-I-restricted HY and P14 TCR transgenic mice (Simeoni et al., 2005a/App.5). Moreover, SIT-deficient thymocytes are hyperactivated and overexpress the activation markers CD5 and of CD69, a similar phenotype to that observed in thymocytes from mice lacking negative regulatory cytosolic adaptors such as c-Cbl or SLAP (Naramura et al., 1998; Sosinowski et al., 2001).

Similarly to thymocytes, also SIT-deficient peripheral T cells are hyperactivated as they proliferate stronger to CD3 stimulation compared to wild-type cells and also produce more cytokines (Simeoni et al., 2005a/App.5). Moreover, in aged SIT-deficient mice T cells spontaneously activate and upregulate CD69 and CD40L (App.19). Collectively, these data emphasize the role of SIT as a negative regulator of TCR-mediated signaling and T-cell activation.

As SIT appears to be an inhibitor of T-cell activation, we have investigated whether SIT is required for the immune response. We tested different infection models including *Listeria* and *Toxoplasma* and also standard immunizations with T-dependent and T-independent antigens. However, in none of the conditions tested did it appear that the loss of SIT impaired the immune responses. We next investigated other processes that depend on TCR signals and found that SIT regulates T-cell homeostasis (see section 4) (Posevitz et al., 2008/App.11). SIT-deficient mice display an accumulation of $CD8^+$. T cells expressing high level of CD44, CD122, and CD62L, but normal levels of CD25 and CD69. These cells phenotypically resemble memory-like T cells, which are believed to be cells undergoing homeostatic proliferation. When we performed adoptive transfer experiments into lymphopenic hosts, we indeed found that SIT-deficient naïve $CD8^+$ T cells expand more vigorously than their wild type counterparts and acquire a memory-like phenotype. In addition SIT also appears to regulate the homeostasis of $\gamma\delta TCR^+$ lymphocytes, as $SIT^{-/-}$ mice displayed a marked increase in the absolute numbers of this T-cell subset in lymph nodes, spleen, Payer's patches, and bone marrow (Simeoni et al., 2005a/App.5).

Collectively, the data suggest that SIT negatively regulates both thymic selection and peripheral T-cell homeostasis. As both processes are regulated through signals triggered by low affinity self peptide/MHC complexes, it is likely that SIT is an important component of the machinery that translates low-affinity stimuli into a cellular outcome.

Alterations in T-cell development and homeostasis may compromise both central and peripheral tolerance and hence may enhance the susceptibility to develop autoimmune diseases. When we explored this possibility, we found that SIT-deficient mice spontaneously develop pathological features of a Lupus-like syndrome, which include anti-nuclear antibodies (ANAs) in the serum, an increase in glomerular size and cellularity, thickening of capillary walls, an augmented mesengial matrix with PAS-positive deposits, and proteinurea (App.19). Moreover, SIT-deficient mice were also more susceptible to the induction of experimental autoimmune encephalomyelitis (EAE) (Simeoni et al., 2005a/App.5), a prototypical T cell-mediated autoimmune disease. In summary, the data demonstrate that SIT is an important negative regulator of T-cell activation that controls thymic selection, inhibits homeostatic proliferation, and limits autoimmunity.

6.2. TRIM (T-cell Receptor Interacting Molecule)

TRIM was initially isolated as a molecule that specifically associated with the TCR/CD3 complex (Bruyns et al., 1998; Kirchgessner et al., 2001). The protein is structurally organized as follow: (i) it has a 8 amino acid extracellular domain, (ii) a 19 amino acid transmembrane region and (iii) a 159 amino acid cytoplasmic tail (Figure 9). The interaction between TRIM and the TCR complex occurs preferentially with the TCRζ chain and most of cellular TRIM is associated with the TCR/CD3 complex at the plasma membrane. From a functional point of view, this close association seems to be required to regulate TCR expression. In fact, overexpression of TRIM increased the levels of the TCR/CD3 complex on the cell surface by inhibiting spontaneous TCR internalization (Kirchgessner et al., 2001).

More recently, it has been shown that TRIM is also important for regulating the expression of CTLA-4 (Valk et al., 2006), a potent inhibitor of T-cell activation. Indeed, TRIM associates with CTLA-4 and leads to enhanced CTLA-4 surface expression in T cells. Collectively, the available data suggest that TRIM functions as a chaperone in modulating both TCR/CD3 and CTLA-4 expression.

Similarly to SIT, TRIM is expressed in T cells as a disulfide-linked homodimer (Figure 9). Three TBSMs (Y^{63}GNL, Y^{79}EQM, Y^{110}ASL) are located within the cytoplasmic tail of TRIM. Upon TCR-induced phosphorylation, tyrosine Y^{79}, which is located within a YxxM consensus motif, interacts with the p85 regulatory subunit of PI3K. The phosphorylation of TRIM appears to be mediated only by Src family tyrosine kinases, such as Lck and Fyn, and not by members of the Syk family. Overexpression of TRIM in Jurkat T cells resulted in a two fold elevation of calcium mobilization upon TCR stimulation. However, this phenomenon likely represents a consequence of higher TCR expression on the cell surface and not an effect of TRIM on TCR-mediated signaling (Kirchgessner et al., 2001). Indeed, overexpression of a TRIM mutant carrying Y to F substitutions in the TBSMs was still able to enhance calcium flux and to inhibit TCR internalization similarly to wild type TRIM. Transfection of TRIM in DC27.10 hybridoma T cells or peripheral blood lymphocytes enhanced the inhibitory effect of CTLA-4 on anti-CD3 mediated proliferation and IL-2 production (Valk et al., 2006). However, also these results reflect the regulatory activity of TRIM on CTLA-4 expression rather than a direct effect of TRIM on TCR-mediated signaling. Thus, it remains still unclear whether TRIM may also function as a signaling molecule during T-cell activation.

Despite the fact that TRIM has been shown to regulate TCR/CD3 expression and to facilitate CTLA-4 transport to the plasma membrane, TRIM-deficient mice possess normal TCR/CD3 and CTLA-4 levels (Kolsch et al., 2006/App.8). Additionally, $TRIM^{-/-}$ mice also do not show defects in T-cell development even though TRIM is strongly expressed in $CD4^{+}CD8^{+}$ thymocytes. Moreover, immune functions are unaffected in TRIM-deficient mice. The lack of an evident phenotype in $TRIM^{-/-}$ mice could indicate that loss of TRIM has been compensated by other transmembrane adaptors. In fact, we have found that together SIT and TRIM regulate thymic development (see section 5.1.).

6.3. LAX (Linker for Activation of X cells, where X indicates "to be defined")

LAX is another non-raft associated transmembrane adaptor expressed in T cells, B cells, monocytes, and bone marrow-derived mast cells. It contains eight tyrosine residues within its cytoplasmic domain (Zhu et al., 2002; Zhu et al., 2006b). Upon BCR and TCR stimulation, LAX is rapidly tyrosine phosphorylated. The four membrane distal residues (Y^{193}, Y^{268}, Y^{294}, Y^{373}) associate with Grb2, GADS, and PI3K (Figure 9).

LAX was identified as a LAT-like molecule. In fact, similarly to LAT, LAX binds the cytosolic adaptors Grb2 and GADS via its distal TBSMs. Moreover, LAX and LAT both become phosphorylated by Src- and Syk-family tyrosine kinases after T-cell activation. However, despite the structure similarity to LAT, LAX has no palmitoylation motif and is not localized to the lipid rafts. The functional difference between LAX and LAT was shown in experiments where LAX was expressed in LAT-deficient cells. In fact, LAX failed to reconstitute TCR-mediated signaling in LAT-deficient cells. Overexpression experiments in the Jurkat T-cell line finally demonstrated that LAX is a negative regulator of antigen receptor signaling rather than a positive one. The molecular mechanisms of this phenomenon are yet to be defined. However, it has been suggested that LAX may inhibit T-cell activation via the cytosolic adaptor ALX, a negative regulator of T-cell activation (Perchonock et al., 2006; Shapiro et al., 2008). Alternatively, it is conceivable that LAX acts by sequestering Grb2, GADS, or even PI3K away from the lipid rafts where they are required to link the TCR to downstream signaling pathways.

The generation and characterization of LAX-deficient mice confirmed that LAX is also a negative regulator in lymphocyte signaling *in vivo*. Indeed, $LAX^{-/-}$ T or B lymphocytes showed enhanced tyrosine phosphorylation and calcium flux upon BCR or TCR stimulation (Zhu et al., 2005). Analysis of the PI3K and MAPK pathways revealed that LAX-deficient

lymphocytes display also enhanced PKB, Erk, and p38 activation. Collectively, these data indicate that $LAX^{-/-}$ T and B cells are hyperresponsive. However, it appears as if the loss of LAX does not directly increase lymphocyte proliferation, but rather inhibits cell death.

Despite the fact that LAX-deficient lymphocytes are hyperresponsive to BCR- or TCR-mediated stimulation, $LAX^{-/-}$ mice display only modest alterations of immune function *in vivo* (Zhu et al., 2005). However, we have found that aged $LAX^{-/-}$ mice develop a mild Lupus-like disease (App.19). Thus, LAX may regulate signals required to limit autoimmunity.

6.4. Non-raft TRAPs: a group of molecules with redundant function

The lack of an evident phenotype in the immune system of TRIM-deficient mice and the modest phenotype observed in SIT- and LAX-deficient mice could indicate that there is a high degree of redundancy among the non-raft TRAPs. To explore the possibility, we have generated SIT/TRIM and SIT/LAX double-deficient mice.

The idea that SIT and TRIM could have redundant function is further supported by several structural similarities. First, SIT and TRIM are both homodimeric proteins located outside of the lipid rafts. Second, SIT shares two TBSMs with TRIM, YGNL and YASV/L whose order with respect to the membrane is conserved (see Figure 9). As reported above, these two motifs represent the major regulatory sites within the SIT cytoplasmic tail. Finally, both are strongly expressed in thymocytes.

The generation of SIT/TRIM double-deficient mice revealed that SIT and TRIM are indeed redundant and negatively regulate TCR-mediated signals in the thymus (Koelsch et al., 2008/App.13). $CD4^{+}CD8^{+}$ thymocytes from SIT/TRIM double-deficient mice show a more activated phenotype than $SIT^{-/-}$ mice, as they strongly upregulate TCRβ, CD5, and CD69. Moreover, thymic development is severely altered in these mice (see section 5.1.). Thus, SIT and TRIM together regulate the fate of developing thymocytes (Figure 7).

The characterization of SIT/LAX double-deficient mice showed that SIT and LAX together negatively regulate immune functions at different levels (App.19). First, SIT/LAX double-deficient mice show increased number of B1 cells, a particular B-cell subset associated with autoimmune diseases and also with malignant transformation (Kantor and Herzenberg, 1993; Kasaian and Casali, 1993), and activated $CD4^{+}$ T cells. Moreover, basal immunoglobulin levels and the titer of ANAs are increased in the double-knockout as compared with LAX or SIT single-mutant mice. Finally, aged SIT/LAX double-deficient mice develop

gromerulonephritis at a higher frequency as compared to $SIT^{-/-}$ mice. Collectively, the data suggest that SIT and LAX appear to restrain cellular and humoral responses that lead to autoimmunity.

Concluding remarks

Signaling via the TCR is a highly organized and tightly regulated process that is crucial for an immune response. Defects in signal transduction may lead to either T-cell hyperresponsiveness or impaired T-cell activation, which results in autoimmunity or immunodeficiency, respectively. Thus, the study of how TCR signaling is initiated, propagated, coordinated, and translated into a cellular response is important for the understanding not only of physiological processes, but also of the molecular mechanisms underlying human disease.

However, most of our knowledge on TCR-mediated signaling is based on data obtained from T-cell lines, hybridoma, and lymphoblasts. The extensive use of such a variety of different cellular systems has often led to conflicting results and to the identification of pathways that may not be active in resting primary T cells (see section 5.2.). Additionally, the use of several non-physiological stimuli (e.g. phorbol esters, cross-linked CD3, or anti-TCR antibodies) to analyze signaling events upon TCR engagement has also contributed to the generation of data that may not reflect physiological conditions (App.18). Finally, also the data generated using a variety of animal models have not taken into account the possible differences in the signaling mechanisms between human and mouse T cells.

Therefore, one of the major goals for the future is to understand how TCR-mediated signaling is regulated in primary human T cells under conditions mimicking physiological stimulation. One of the major problems is that antigen-specific stimulation can only be employed to trigger T cells expressing a transgenic TCR, hence this applies only to murine models. Thus, the availability of a method that mimics antigen-specific systems is of particular importance to study primary human T-cells, which cannot be stimulated on a large scale by antigen-specific systems. We have recently started to characterize which of the currently available systems to stimulate human T cells more closely reproduces physiological stimulation (App.18). We found that CD3xCD28 agonistic mAbs immobilized on beads mimics signaling induced by antigen-specific (physiologic) systems and also induce a functional outcome

(proliferation). Conversely to immobilized antibodies, antibodies applied in solution induce a transient signal and an abortive response. We further show that TCR activation kinetics and feedback regulation under proliferation-inducing conditions (immobilized mAbs) are markedly different from those leading to unresponsiveness (soluble mAbs). Thus, we concluded that immobilized mAbs are better suited than soluble mAbs for signaling studies. We believe that, by further employing immobilized mAbs, it may be possible to reveal new mechanistic insights into the regulation of TCR signaling in primary human T cells, which may additionally have important implications for understanding the molecular mechanisms of human diseases. This will also be helpful for the generation of maps of the TCR signaling network and will contribute to developing dynamic models (Saez-Rodriguez et al., 2007/App.9; Klamt et al., 2006/App.7).

Although antibody-coated beads represent an attractive and easy to use system, they clearly have limitations. Microbeads have rigid surfaces and lack the fluidity of biological membranes, whereby the analysis of the combined effects of different receptors is limited. Therefore, it will be necessary for the future to develop new stimulation methods that are better suited to mimic physiological cell-cell interactions.

With regard to the future of transmembrane adaptor molecules, it will be important to assess whether functional redundancy might apply to all TRAPs. In fact, the structural similarities between LAX and TRIM (both molecules are capable of binding PI3K and are strongly expressed in $CD4^+$ T cells) or between NTAL and LAX (which both carry several Grb2-binding site and both are expressed in B cells and mast cells) are suggestive of the existence of sophisticated and redundant mechanisms that regulate antigen receptor-mediated signaling. Interestingly, it has been published that aged NTAL-deficient mice show hyperactivation of $CD4^+$ T cells, possess anti-nuclear antibodies, and develop a lupus-like autoimmune disease (Zhu et al., 2006a). This phenotype strikingly resembles the alterations of the immune system that we observe in the SIT/LAX double-deficient mice. It will now be important to assess whether SIT/LAX/NTAL-triple deficient mice show an even more aggravated autoimmune phenotype. Similarly, the generation of additional double or triple knockout mice will help to assess how TRAPs control the intricate signal transduction network within immune cells.

Recently, two new members have been added to the family of transmembrane adaptors. Grb2-binding adaptor protein transmembrane (GAPT), which is expressed in B cells and myeloid cells (Liu and Zhang, 2008) and proline rich 7 (PRR7), which is readily upregulated in activated human peripheral blood lymphocytes (Hrdinka et al., 2011). The function of these

new TRAPs has not yet been completely clarified. Whereas GAPT appears to be involved in B-cell activation, PRR7 seems to inhibit TCR-mediated signaling and induce apoptosis in the Jurkat T-cell line.

A long-lasting question regarding TRAPs is whether B cells possess a LAT-like molecule that links the BCR to downstream signaling pathway. This question has been raised as T and B cells express many homologous signaling molecules and utilize conserved pathways to transduce signals from their respective antigen receptors. As mentioned above, LAT and SLP-76 are indispensable for the activation of NFAT, AP1, and NFκB upon TCR triggering. B cells are known to express only SLP-65, also referred as to BLNK, which is a cytosolic homolog of SLP-76 (Yablonski and Weiss, 2001), but they do not express a LAT-like molecule, which recruit SLP-65 to the plasma membrane. Therefore, how the BCR is linked to the activation of downstream signaling cascades still remains unknown. It was though that NTAL/LAB, which together with LAT arise from a duplication of a primordial gene, was the long searched LAT-like molecule in B cells (Brdicka et al., 2002/App.2; Janssen et al., 2003). Indeed, one of the name given to this TRAP is LAB (linker for activation of B cells) alluding to its desired function in BCR-mediated signaling (Janssen et al., 2003). However, further studies have clearly shown that NTAL/LAB is functionally different from LAT, as it functions as a negative regulator of antigen-receptor mediated signaling (Zhu et al., 2006a). Also LIME (Brdickova et al., 2003/App.4) and LAX, two other TRAPs, have been proposed to be LAT-like molecules (Ahn et al., 2006; Zhu et al., 2002). However, also in these cases *in vivo* studies clearly demonstrated that BCR-mediated signaling is not significantly affected in both $LIME^{-/-}$ and $LAX^{-/-}$ mice (Gregoire et al., 2007/App.10; Zhu et al., 2005). Thus, it will be important to understand how the BCR is linked to the activation of the transcriptional program leading to humoral immune responses. This may be important for the development of specific clinical therapeutics which would allow the manipulation of immune responses.

The role of TRAPs in human diseases has now just begun to be investigated. The fact that different TRAPs knockout mice develop autoimmunity is suggestive of their potential role in regulating tolerance. Recent studies have shown that TRAPs are differently expressed in leukemic cells (Svec et al., 2005; Svojgr et al., 2009; Svojgr et al., 2012; Tedoldi et al., 2006). However, whether TRAPs play a role in cancer or rather represent markers for the diagnosis and the identification of lymphoma cells requires further study.

References

Acuto, O., Di Bartolo, V., and Micheli, F. (2008). Tailoring T-cell receptor signals by proximal negative feedback mechanisms. Nat Rev Immunol *8*, 699-712.

Ahn, E., Lee, H., and Yun, Y. (2006). LIME acts as a transmembrane adapter mediating BCR-dependent B-cell activation. Blood *107*, 1521-1527.

Arndt, B., Krieger, T., Kalinski, T., Thielitz, A., Reinhold, D., Roessner, A., Schraven, B., and Simeoni, L. (2011). The Transmembrane Adaptor Protein SIT Inhibits TCR-Mediated Signaling. PLoS One *6*, e23761.

Bonneville, M., O'Brien, R.L., and Born, W.K. (2010). Gammadelta T cell effector functions: a blend of innate programming and acquired plasticity. Nat Rev Immunol *10*, 467-478.

Brdicka, T., Imrich, M., Angelisova, P., Brdickova, N., Horvath, O., Spicka, J., Hilgert, I., Luskova, P., Draber, P., Novak, P.*, et al.* (2002). Non-T cell activation linker (NTAL): a transmembrane adaptor protein involved in immunoreceptor signaling. J Exp Med *196*, 1617-1626.

Brdickova, N., Brdicka, T., Angelisova, P., Horvath, O., Spicka, J., Hilgert, I., Paces, J., Simeoni, L., Kliche, S., Merten, C.*, et al.* (2003). LIME: a new membrane Raft-associated adaptor protein involved in CD4 and CD8 coreceptor signaling. J Exp Med *198*, 1453-1462.

Bruyns, E., Marie-Cardine, A., Kirchgessner, H., Sagolla, K., Shevchenko, A., Mann, M., Autschbach, F., Bensussan, A., Meuer, S., and Schraven, B. (1998). T cell receptor (TCR) interacting molecule (TRIM), a novel disulfide-linked dimer associated with the TCR-CD3-zeta complex, recruits intracellular signaling proteins to the plasma membrane. J Exp Med *188*, 561-575.

Daniels, M.A., Teixeiro, E., Gill, J., Hausmann, B., Roubaty, D., Holmberg, K., Werlen, G., Hollander, G.A., Gascoigne, N.R., and Palmer, E. (2006). Thymic selection threshold defined by compartmentalization of Ras/MAPK signalling. Nature *444*, 724-729.

Das, J., Ho, M., Zikherman, J., Govern, C., Yang, M., Weiss, A., Chakraborty, A.K., and Roose, J.P. (2009). Digital signaling and hysteresis characterize ras activation in lymphoid cells. Cell *136*, 337-351.

Dobenecker, M.W., Schmedt, C., Okada, M., and Tarakhovsky, A. (2005). The ubiquitously expressed Csk adaptor protein Cbp is dispensable for embryogenesis and T-cell development and function. Mol Cell Biol *25*, 10533-10542.

Ebisuya, M., Kondoh, K., and Nishida, E. (2005). The duration, magnitude and compartmentalization of ERK MAP kinase activity: mechanisms for providing signaling specificity. J Cell Sci *118*, 2997-3002.

Fry, T.J., and Mackall, C.L. (2005). The many faces of IL-7: from lymphopoiesis to peripheral T cell maintenance. J Immunol *174*, 6571-6576.

Gregoire, C., Simova, S., Wang, Y., Sansoni, A., Richelme, S., Schmidt-Giese, A., Simeoni, L., Angelisova, P., Reinhold, D., Schraven, B.*, et al.* (2007). Deletion of the LIME adaptor protein minimally affects T and B cell development and function. Eur J Immunol *37*, 3259-3269.

Grossman, Z., Min, B., Meier-Schellersheim, M., and Paul, W.E. (2004). Concomitant regulation of T-cell activation and homeostasis. Nat Rev Immunol *4*, 387-395.

Hardy, R.R., and Hayakawa, K. (2001). B cell development pathways. Annu Rev Immunol *19*, 595-621.

Horejsi, V., Zhang, W., and Schraven, B. (2004). Transmembrane adaptor proteins: organizers of immunoreceptor signalling. Nat Rev Immunol *4*, 603-616.

Horn, J., Wang, X., Reichardt, P., Stradal, T.E., Warnecke, N., Simeoni, L., Gunzer, M., Yablonski, D., Schraven, B., and Kliche, S. (2009). Src homology 2-domain containing leukocyte-specific phosphoprotein of 76 kDa is mandatory for TCR-mediated inside-out signaling, but dispensable for CXCR4-mediated LFA-1 activation, adhesion, and migration of T cells. J Immunol *183*, 5756-5767.

Hrdinka, M., Draber, P., Stepanek, O., Ormsby, T., Otahal, P., Angelisova, P., Brdicka, T., Paces, J., Horejsi, V., and Drbal, K. (2011). PRR7 is a transmembrane adaptor protein expressed in activated T cells involved in regulation of T cell receptor signaling and apoptosis. J Biol Chem *286*, 19617-19629.

Janssen, E., Zhu, M., Zhang, W., Koonpaew, S., and Zhang, W. (2003). LAB: a new membrane-associated adaptor molecule in B cell activation. Nat Immunol *4*, 117-123.

Kantor, A.B., and Herzenberg, L.A. (1993). Origin of murine B cell lineages. Annu Rev Immunol *11*, 501-538.

Kasaian, M.T., and Casali, P. (1993). Autoimmunity-prone B-1 (CD5 B) cells, natural antibodies and self recognition. Autoimmunity *15*, 315-329.

Kirchgessner, H., Dietrich, J., Scherer, J., Isomaki, P., Korinek, V., Hilgert, I., Bruyns, E., Leo, A., Cope, A.P., and Schraven, B. (2001). The transmembrane adaptor protein TRIM regulates T cell receptor (TCR) expression and TCR-mediated signaling via an association with the TCR zeta chain. J Exp Med *193*, 1269-1284.

Klamt, S., Saez-Rodriguez, J., Lindquist, J.A., Simeoni, L., and Gilles, E.D. (2006). A methodology for the structural and functional analysis of signaling and regulatory networks. BMC Bioinformatics *7*, 56.

Koelsch, U., Schraven, B., and Simeoni, L. (2008). SIT and TRIM determine T cell fate in the thymus. J Immunol *181*, 5930-5939.

Kolsch, U., Arndt, B., Reinhold, D., Lindquist, J.A., Juling, N., Kliche, S., Pfeffer, K., Bruyns, E., Schraven, B., and Simeoni, L. (2006). Normal T-cell development and immune functions in TRIM-deficient mice. Mol Cell Biol *26*, 3639-3648.

LeBien, T.W., and Tedder, T.F. (2008). B lymphocytes: how they develop and function. Blood *112*, 1570-1580.

Lindquist, J.A., Simeoni, L., and Schraven, B. (2003). Transmembrane adapters: attractants for cytoplasmic effectors. Immunol Rev *191*, 165-182.

Linnemann, C., Schildberg, F.A., Schurich, A., Diehl, L., Hegenbarth, S.I., Endl, E., Lacher, S., Muller, C.E., Frey, J., Simeoni, L.*, et al.* (2009). Adenosine regulates CD8 T-cell priming by inhibition of membrane-proximal T-cell receptor signalling. Immunology *128*, e728-737.

Liu, Y., and Zhang, W. (2008). Identification of a new transmembrane adaptor protein that constitutively binds Grb2 in B cells. J Leukoc Biol *84*, 842-851.

Love, P.E., and Hayes, S.M. ITAM-mediated signaling by the T-cell antigen receptor. (2010) Cold Spring Harb Perspect Biol *2*, a002485.

Love, P.E., Lee, J., and Shores, E.W. (2000). Critical relationship between TCR signaling potential and TCR affinity during thymocyte selection. J Immunol *165*, 3080-3087.

Malissen, B., Aguado, E., and Malissen, M. (2005). Role of the LAT adaptor in T-cell development and Th2 differentiation. Adv Immunol *87*, 1-25.

Margarit, S.M., Sondermann, H., Hall, B.E., Nagar, B., Hoelz, A., Pirruccello, M., Bar-Sagi, D., and Kuriyan, J. (2003). Structural evidence for feedback activation by Ras.GTP of the Ras-specific nucleotide exchange factor SOS. Cell *112*, 685-695.

Marie-Cardine, A., Kirchgessner, H., Bruyns, E., Shevchenko, A., Mann, M., Autschbach, F., Ratnofsky, S., Meuer, S., and Schraven, B. (1999). SHP2-interacting transmembrane adaptor protein (SIT), a novel disulfide-linked dimer regulating human T cell activation. J Exp Med *189*, 1181-1194.

Marinari, B., Simeoni, L., Schraven, B., Piccolella, E., and Tuosto, L. (2003). The activation of Csk by CD4 interferes with TCR-mediated activatory signaling. Eur J Immunol *33*, 2609-2618.

Martensson, I.L., Almqvist, N., Grimsholm, O., and Bernardi, A.I. (2010). The pre-B cell receptor checkpoint. FEBS Lett *584*, 2572-2579.

Naramura, M., Kole, H.K., Hu, R.J., and Gu, H. (1998). Altered thymic positive selection and intracellular signals in Cbl-deficient mice. Proc Natl Acad Sci U S A *95*, 15547-15552.

Nika, K., Soldani, C., Salek, M., Paster, W., Gray, A., Etzensperger, R., Fugger, L., Polzella, P., Cerundolo, V., Dushek, O.*, et al.* (2010). Constitutively active Lck kinase in T cells drives antigen receptor signal transduction. Immunity *32*, 766-777.

Perchonock, C.E., Fernando, M.C., Quinn, W.J., 3rd, Nguyen, C.T., Sun, J., Shapiro, M.J., and Shapiro, V.S. (2006). Negative regulation of interleukin-2 and p38 mitogen-activated protein kinase during T-cell activation by the adaptor ALX. Mol Cell Biol *26*, 6005-6015.

Pfrepper, K.I., Marie-Cardine, A., Simeoni, L., Kuramitsu, Y., Leo, A., Spicka, J., Hilgert, I., Scherer, J., and Schraven, B. (2001). Structural and functional dissection of the cytoplasmic domain of the transmembrane adaptor protein SIT (SHP2-interacting transmembrane adaptor protein). Eur J Immunol *31*, 1825-1836.

Pivniouk, V.I., and Geha, R.S. (2000). The role of SLP-76 and LAT in lymphocyte development. Curr Opin Immunol *12*, 173-178.

Posevitz, V., Arndt, B., Krieger, T., Warnecke, N., Schraven, B., and Simeoni, L. (2008). Regulation of T Cell Homeostasis by the Transmembrane Adaptor Protein SIT. J Immunol *180*, 1634-1642.

Prasad, A., Zikherman, J., Das, J., Roose, J.P., Weiss, A., and Chakraborty, A.K. (2009). Origin of the sharp boundary that discriminates positive and negative selection of thymocytes. Proc Natl Acad Sci U S A *106*, 528-533.

Priatel, J.J., Chen, X., Huang, Y.H., Chow, M.T., Zenewicz, L.A., Coughlin, J.J., Shen, H., Stone, J.C., Tan, R., and Teh, H.S. (2010). RasGRP1 regulates antigen-induced developmental programming by naive CD8 T cells. J Immunol *184*, 666-676.

Radtke, F., Wilson, A., Stark, G., Bauer, M., van Meerwijk, J., MacDonald, H.R., and Aguet, M. (1999). Deficient T cell fate specification in mice with an induced inactivation of Notch1. Immunity *10*, 547-558.

Roose, J., and Weiss, A. (2000). T cells: getting a GRP on Ras. Nat Immunol *1*, 275-276.

Roose, J.P., Mollenauer, M., Ho, M., Kurosaki, T., and Weiss, A. (2007). Unusual Interplay of Two Types of Ras Activators, RasGRP and SOS, Establishes Sensitive and Robust Ras Activation in Lymphocytes. Mol Cell Biol *27*, 2732-2745.

Saez-Rodriguez, J., Simeoni, L., Lindquist, J.A., Hemenway, R., Bommhardt, U., Arndt, B., Haus, U.U., Weismantel, R., Gilles, E.D., Klamt, S., and Schraven, B. (2007). A logical model provides insights into T cell receptor signaling. PLoS Comput Biol *3*, e163.

Seddon, B., and Zamoyska, R. (2003). Regulation of peripheral T-cell homeostasis by receptor signalling. Curr Opin Immunol *15*, 321-324.

Shapiro, M.J., Nguyen, C.T., Aghajanian, H., Zhang, W., and Shapiro, V.S. (2008). Negative regulation of TCR signaling by linker for activation of X cells via phosphotyrosine-dependent and -independent mechanisms. J Immunol *181*, 7055-7061.

Shores, E.W., Tran, T., Grinberg, A., Sommers, C.L., Shen, H., and Love, P.E. (1997). Role of the multiple T cell receptor (TCR)-zeta chain signaling motifs in selection of the T cell repertoire. J Exp Med *185*, 893-900.

Simeoni, L., Kliche, S., Lindquist, J., and Schraven, B. (2004). Adaptors and linkers in T and B cells. Curr Opin Immunol *16*, 304-313.

Simeoni, L., Lindquist, J.A., Smida, M., Witte, V., Arndt, B., and Schraven, B. (2008). Control of lymphocyte development and activation by negative regulatory transmembrane adapter proteins. Immunol Rev *224*, 215-228.

Simeoni, L., Posevitz, V., Kolsch, U., Meinert, I., Bruyns, E., Pfeffer, K., Reinhold, D., and Schraven, B. (2005a). The transmembrane adapter protein SIT regulates thymic development and peripheral T-cell functions. Mol Cell Biol *25*, 7557-7568.

Simeoni, L., Smida, M., Posevitz, V., Schraven, B., and Lindquist, J.A. (2005b). Right time, right place: the organization of membrane proximal signaling. Semin Immunol *17*, 35-49.

Smith-Garvin, J.E., Koretzky, G.A., and Jordan, M.S. (2009). T cell activation. Annu Rev Immunol *27*, 591-619.

Sosinowski, T., Killeen, N., and Weiss, A. (2001). The Src-like adaptor protein downregulates the T cell receptor on CD4+CD8+ thymocytes and regulates positive selection. Immunity *15*, 457-466.

Starr, T.K., Jameson, S.C., and Hogquist, K.A. (2003). Positive and negative selection of T cells. Annu Rev Immunol *21*, 139-176.

Svec, A., Velenska, Z., and Horejsi, V. (2005). Expression pattern of adaptor protein PAG: correlation between secondary lymphatic follicle and histogenetically related malignant lymphomas. Immunol Lett *100*, 94-97.

Svojgr, K., Burjanivova, T., Vaskova, M., Kalina, T., Stary, J., Trka, J., and Zuna, J. (2009). Adaptor molecules expression in normal lymphopoiesis and in childhood leukemia. Immunol Lett *122*, 185-192.

Svojgr, K., Kalina, T., Kanderova, V., Skopcova, T., Brdicka, T., and Zuna, J. (2012). The adaptor protein NTAL enhances proximal signaling and potentiates corticosteroid-induced apoptosis in T-ALL. Exp Hematol.

Tedoldi, S., Paterson, J.C., Hansmann, M.L., Natkunam, Y., Rudiger, T., Angelisova, P., Du, M.Q., Roberton, H., Roncador, G., Sanchez, L., *et al.* (2006). Transmembrane adaptor molecules: a new category of lymphoid-cell markers. Blood *107*, 213-221.

Theofilopoulos, A.N., Dummer, W., and Kono, D.H. (2001). T cell homeostasis and systemic autoimmunity. J Clin Invest *108*, 335-340.

Togni, M., Swanson, K.D., Reimann, S., Kliche, S., Pearce, A.C., Simeoni, L., Reinhold, D., Wienands, J., Neel, B.G., Schraven, B., and Gerber, A. (2005). Regulation of in vitro and in vivo immune functions by the cytosolic adaptor protein SKAP-HOM. Mol Cell Biol *25*, 8052-8063.

Valk, E., Leung, R., Kang, H., Kaneko, K., Rudd, C.E., and Schneider, H. (2006). T cell receptor-interacting molecule acts as a chaperone to modulate surface expression of the CTLA-4 coreceptor. Immunity *25*, 807-821.

Wang, X., Simeoni, L., Lindquist, J.A., Saez-Rodriguez, J., Ambach, A., Gilles, E.D., Kliche, S., and Schraven, B. (2008). Dynamics of Proximal Signaling Events after TCR/CD8-Mediated Induction of Proliferation or Apoptosis in Mature CD8+ T Cells. J Immunol *180*, 6703-6712.

Wange, R.L. (2000). LAT, the linker for activation of T cells: a bridge between T cell-specific and general signaling pathways. Sci STKE *2000*, RE1.

Warnecke, N., Poltorak, M., Kowtharapu, B.S., Arndt, B., Stone, J.C., Schraven, B., and Simeoni, L. (2012). TCR-mediated Erk activation does not depend on Sos and Grb2 in peripheral human T cells. EMBO Rep. doi: 10.1038/embor.2012.17.

Watanabe, N., Arase, H., Onodera, M., Ohashi, P.S., and Saito, T. (2000). The quantity of TCR signal determines positive selection and lineage commitment of T cells. J Immunol *165*, 6252-6261.

Xu, S., Huo, J., Tan, J.E., and Lam, K.P. (2005). Cbp deficiency alters Csk localization in lipid rafts but does not affect T-cell development. Mol Cell Biol *25*, 8486-8495.

Yablonski, D., and Weiss, A. (2001). Mechanisms of signaling by the hematopoietic-specific adaptor proteins, SLP-76 and LAT and their B cell counterpart, BLNK/SLP-65. Adv Immunol *79*, 93-128.

Yamazaki, T., Arase, H., Ono, S., Ohno, H., Watanabe, H., and Saito, T. (1997). A shift from negative to positive selection of autoreactive T cells by the reduced level of TCR signal in TCR-transgenic CD3 zeta-deficient mice. J Immunol *158*, 1634-1640.

Yasuda, T., and Kurosaki, T. (2008). Regulation of lymphocyte fate by Ras/ERK signals. Cell Cycle *7*, 3634-3640.

Zhu, J., and Paul, W.E. (2008). CD4 T cells: fates, functions, and faults. Blood *112*, 1557-1569.

Zhu, M., Granillo, O., Wen, R., Yang, K., Dai, X., Wang, D., and Zhang, W. (2005). Negative regulation of lymphocyte activation by the adaptor protein LAX. J Immunol *174*, 5612-5619.

Zhu, M., Janssen, E., Leung, K., and Zhang, W. (2002). Molecular cloning of a novel gene encoding a membrane-associated adaptor protein (LAX) in lymphocyte signaling. J Biol Chem *277*, 46151-46158.

Zhu, M., Koonpaew, S., Liu, Y., Shen, S., Denning, T., Dzhagalov, I., Rhee, I., and Zhang, W. (2006a). Negative regulation of T cell activation and autoimmunity by the transmembrane adaptor protein LAB. Immunity *25*, 757-768.

Zhu, M., Rhee, I., Liu, Y., and Zhang, W. (2006b). Negative regulation of Fc epsilonRI-mediated signaling and mast cell function by the adaptor protein LAX. J Biol Chem *281*, 18408-18413.

Acknowledgements

There are many people to whom I owe my gratitude for their support and encouragement over the past ten years.

First, I would like to thank Prof. Burkhart Schraven for his initial scientific guidance and for his continuous support and motivation as well as for giving me the opportunity to work in an outstanding research environment.

In addition, I would like to extend special thanks to my colleague Dr. Jonathan Lindquist for stimulating discussions and helpful suggestions during the past ten years, to Dr. Anja Thielitz for her encouragement to write this work, and to Dr. Börge Arndt, a former member of my group, with whom it has been a great pleasure to work for the preparation of his doctoral thesis.

I also would like to thank Dr. Tilo Beyer and all the members of the Institute for helpful discussions and support received along the way.

Finally, a special thanks and gratitude go to my family. Without their understanding, endless patience, and encouragement this work would not have been possible.

This work was supported by grants from the German Research Society (DFG): FOR521, GRK1167, and SFB854.

Publications for the cumulative Habilitation

1. Pfrepper K.I., Marie-Cardine A., **Simeoni L.**, Kuramitsu Y., Leo A., Spicka J., Hilgert I., Scherer J., and Schraven B. (2001) Structural and functional dissection of the cytoplasmic domain of the transmembrane adaptor protein SIT (SHP2-interacting transmembrane adaptor protein). *Eur J Immunol.* 31:1825-36.

2. Brdicka T, Imrich M., Angelisova P., Brdicková N. Horváth O.; Spicka J., Hilgert I., Luskova P., Draber P., Novak P., Engels N., Wienands J., **Simeoni L.**, Österreicher J., Aguado E., Malissen M., Schraven B. and Horejsi V. (2002) NTAL (Non T-cell Activation Linker), a novel transmembrane adaptor protein involved in immunoreceptor signalling, *J Exp Med*. 196:1617-26.

3. Marinari B., **Simeoni L.**, Schraven B., Piccolella E., and Tuosto L. (2003). The activation of Csk by CD4 interferes with TCR-mediated activatory signalling. *Eur J Immunol.* 33:2609-18.

4. Brdičková N., Brdička T., Angelisová P., Horváth O., Špička J., Hilgert I., Pačes I., **Simeoni L.**, Kliche S., Merten C., Schraven B., and Hořejší V. (2003) LIME: a new membrane raft-associated adaptor protein involved in CD4 and CD8 coreceptor signaling. *J Exp Med*. 198:1453-62.

5. **Simeoni L.**, Posevitz V., Kölsch U., Meinert I., Bruyns E., Pfeffer K., Reinhold D., and Schraven B. (2005) The transmembrane adapter protein SIT regulates thymic development and peripheral T cell functions. *Mol Cell Biol.* 25:7557-68.

6. Togni M., Swanson K.D., Reiman S., Kliche S., Pearce A.C., **Simeoni L.**, Reinhold D., Wienenads J., Neel B.G., Schraven B., and Gerber A. (2005) Regulation of *in vitro* and *in vivo* immune functions by the cytosolic adaptor protein SKAP-HOM. *Mol Cell Biol.* 25:8052-63.

7. Klamt S., Saez-Rodriguez J., Lindquist JA., **Simeoni L.**, and Gilles ED. (2006) A methodology for the structural and functional analysis of signaling and regulatory networks. *BMC Bioinformatics*. 7:56-82.

8. Kölsch U., Arndt B., Reinhold D., Lindquist JA., Jüling N., Kliche S., Pfeffer K., Bruyns E., Schraven B., and **Simeoni L.** (2006) Normal T-cell development and immune functions in TRIM-deficient mice. *Mol Cell Biol.* 26:3639-48.

9. Saez-Rodriguez J., **Simeoni L.**, Lindquist J.A., Hemenway R., Bommhardt U., Arndt B., Haus U.U., Weismantel R., Gilles E.D., Klamt S., and Schraven B. (2007) A logical model provides insights into T-cell signaling. *PLoS Comput Biol.* 3:e163.

10. Grégoire C., Simova S., Wang Y., Sansoni A., Richelme S., Schmidt-Giese A., **Simeoni L.**, Angelisova P., Reinhold D., Schraven B., Horejsi V., Malissen B., and Malissen M. (2007) Deletion of the LIME adaptor protein minimally affects T and B cell development and function. *Eur J Immunol.* 37:3259-69.

11. Posevitz V., Arndt B., Krieger T., Warnecke N., Schraven B., and **Simeoni L.** (2008) Regulation of T-cell homeostasis by the transmembrane adaptor protein SIT. *J Immunol.* 180:1634-1642.

12. Wang X., **Simeoni L.**, Lindquist J.A., Saez-Rodriguez J., Gilles E.D., Kliche S., and Schraven B. (2008) Dynamics of proximal signaling events after TCR/CD8-mediated induction of proliferation or apoptosis in mature CD8+ T-cells. *J Immunol.* 180:6703-6712.

13. Kölsch U., Schraven B., and **Simeoni L.** (2008) SIT and TRIM determine T-cell fate in the thymus. *J Immunol.* 181:5930-5939.

14. Linnemann C., Schildberg F.A., Schurich A., Diehl L., Hegenbarth S.I., Endl E., Lacher S., Müller C.E., Frey J., **Simeoni L.**, Schraven B., Stabenow D., and Knolle P.A. (2009) Adenosine regulates CD8 T-cell priming by inhibition of membrane-proximal T-cell receptor signalling. *Immunology*. 128:e728-737.

15. Horn J., Wang X., Reichardt P., Stradal T.E., Warnecke N., **Simeoni L.**, Gunzer M., Yablonski D., Schraven B., and Kliche S. (2009) Src Homology 2-Domain Containing Leukocyte-Specific Phosphoprotein of 76 kDa Is Mandatory for TCR-Mediated Inside-Out Signaling, but Dispensable for CXCR4-Mediated LFA-1 Activation, Adhesion, and Migration of T Cells. *J Immunol.* 183:5756-5767.

16. Arndt B., Krieger T., Kalinski T., Thielitz A., Reinhold D., Rössner A., Schraven B., and **Simeoni L.** (2011) The transmembrane adaptor protein SIT inhibits TCR-mediated signaling. *PLosONE*, 6: e23761. doi:10.1371/journal.pone.0023761.

17. Warnecke N., Poltorak M., Kowtharapu B.S., Arndt B., Stone J.C., Schraven B., and **Simeoni L.** (2012) TCR-mediated Erk activation does not depend on Sos and Grb2 in peripheral human T cells. *EMBO Rep*, doi: 10.1038/embor.2012.17.

18. Arndt B., Kowtharapu B.S., Wang X., Lindquist J.A., Schraven B., and **Simeoni L.** Analysis of TCR activation kinetics and feedback regulation in primary human T cells upon focal or soluble stimulation. J Immunol., in revision

19. Arndt B., Kalinski T., Reinhold D., Thielitz A., Rössner A., Schraven B., and **Simeoni L.** Cooperative immunoregulatory function of the transmembrane adaptor proteins SIT and LAX, submitted

Appendix 1

Structural and functional dissection of the cytoplasmic domain of the transmembrane adaptor protein SIT (SHP2-interacting transmembrane adaptor protein)

Pfrepper K.I., Marie-Cardine A., **Simeoni L.**, Kuramitsu Y., Leo A., Spicka J., Hilgert I., Scherer J., and Schraven B. (2001) *Eur J Immunol.* 31:1825-36.

Structural and functional dissection of the cytoplasmic domain of the transmembrane adaptor protein SIT (SHP2-interacting transmembrane adaptor protein)

Klaus-Ingmar Pfrepper[1], Anne Marie-Cardine[2], Luca Simeoni[3], Yasuhiro Kuramitsu[1], Albrecht Leo[1], Jiri Spicka[1], Ivan Hilgert[4], Jeanette Scherer[1] and Burkhart Schraven[3]

[1] Immunomodulation Laboratory of the Institute for Immunology, Ruprecht-Karls University Heidelberg, Heidelberg, Germany
[2] Faculté de Médecine de Créteil, INSERM U448, Crétail, France
[3] Institute for Immunology, Otto-von-Goernicke University Magdeburg, Magdeburg, Germany
[4] Institute of Molecular Genetics, Academy of Sciences of the Czech Republik, Prague, Czech Republik

SIT (SHP2-interacting transmembrane adaptor protein) is a recently identified transmembrane adaptor protein, which is expressed in lymphocytes. Its structural properties, in particular the presence of five potential tyrosine phosphorylation sites, suggest involvement of SIT in TCR-mediated recruitment of SH2 domain-containing intracellular signaling molecules to the plasma membrane. Indeed, it has recently been demonstrated that SIT inducibly interacts with the SH2-containing protein tyrosine phosphatase 2 (SHP2) via an immunoreceptor tyrosine-based inhibition motif (ITIM). Moreover, SIT is capable to inhibit TCR-mediated signals proximal of activation of protein kinase C. However, inhibition of T cell activation by SIT occurs independently of SHP2 binding. The present study was performed to further characterize the molecular interaction between SIT and intracellular effector molecules and to identify the protein(s) mediating its inhibitory function. We demonstrate that SIT not only interacts with SHP2 but also with the adaptor protein Grb2 via two consensus YxN motifs. However, mutation of both Grb2-binding sites also does not influence the inhibitory function of SIT. In contrast, mutation of the tyrosine-based signaling motif Y^{168} ASV completely abrogates the ability of SIT to inhibit T cell activation. Co-precipitation experiments revealed that the tyrosine kinase $p50^{csk}$ could represent the negative regulatory effector molecule that binds to this motif.

Received	17/1/01
Accepted	20/3/01

Key words: T cell / Transmembrane adaptor protein / Signaling

1 Introduction

Among the earliest intracellular events that occur after engagement of the T cell receptor (TCR) complex are tyrosine phosphorylations of numerous proteins which result from activation of protein tyrosine kinases (PTK) of the Src (*e. g.* Lck, Fyn), Syk (ZAP-70, Syk) and Tec (*e. g.* Itk) family (for recent reviews see [1–4]). It is now well established that these initial phosphorylations are a prerequisite to allow coupling of the TCR to intracellular signaling pathways such as the Ras/Raf/MAPK pathway or the calcineurin/NF-AT pathway. Moreover, it is well documented that TCR-mediated tyrosine phosphorylations are accompanied by and are required for the translocation of intracellular signaling molecules (*e. g.* Grb2, SHP2, SLP-76 and others) from the cytosol to the inner leaflet of the plasma membrane. The precise molecular mechanisms whereby these cytoplasmic effector and adaptor molecules are targeted to the plasma membrane after TCR engagement were until recently only poorly understood. Major progress in solving this puzzle has been achieved through the identification of a novel group of proteins that has been termed transmembrane adap-

[I 21725]

The first two authors contributed equally to this work.

Abbreviations: Csk: C terminal src kinase **Grb2:** Growth factor receptor binding protein 2 **LAT:** Linker for activation of T cells **NF-AT:** Nuclear factor of activated T cells **PAG:** Phosphoprotein associated with GEM **PAG:** Phosphoprotein associated with GEM **PI3-K:** Phosphatidylinositol 3-kinase **PLC:** Phospholipase C **PTK:** Protein tyrosine kinase **SH:** Src-homology **SHP:** SH2-containing protein tyrosine phosphatase **SHIP:** SH2-domain containing inositol phosphatase **SIT:** SHP2-interacting transmembrane adaptor protein **SLP:** SH2 domain containing leukocyte phosphoprotein

 0014-2980/01/0606-1825$17.50+.50/0

tor proteins. These polypeptides are characterized by very short extracellular domains and comparatively long cytoplasmic tails, which contain several tyrosine-based signaling motifs (between five and ten). Upon phosphorylation by Src and/or Syk-PTK the tyrosine-based signaling motifs become rapidly phosphorylated and then serve as docking sites for SH2 domain-containing intracellular signaling molecules (reviewed in [4, 5]).

The so far best characterized transmembrane adaptor protein is LAT (linker for activation of T cells) [6, 7]. LAT is a type III transmembrane protein that carries 10 tyrosine residues in its cytoplasmic tail, among which 6 represent potential tyrosine-based signaling motifs. LAT becomes rapidly tyrosine phosphorylated after T cell activation by ZAP-70 and then directly interacts with the SH2-domains of Grb2, Gads and PLCγ 1 and indirectly with other intracellular signaling molecules including PI3-kinase, SLP-76 and Cbl [6, 7]. Compelling evidence that LAT is required for the propagation of TCR-mediated signals was provided by the analysis of LAT-deficient Jurkat variants. These cells exhibit severe defects in TCR-mediated phosphorylation and activation of PLCγ1, generation of calcium fluxes, activation of the Ras pathway and IL2-gene expression [8, 9]. Moreover, LAT-deficient mice show an arrest in thymic development at the $CD4^-CD8^-$ stage that results in a loss of mature peripheral blood T-cells [10]. All these data suggest that LAT is indispensable for T cell activation and T cell development.

Shortly after the identification of LAT, the molecular cloning of three additional transmembrane adaptor proteins, TRIM (T cell receptor interacting molecule) [11], SIT (SHP2-interacting transmembrane adaptor protein) [12] and PAG/Cbp (protein associated with GEMs/Csk binding protein) [13, 14] has been reported.

TRIM has been initially indentified as a T cell-specific disulfide-linked homodimer which associates and co-modulates with the TCR/CD3/ζ complex [15, 16]. TRIM becomes tyrosine phosphorylates by Src kinases and then associates with the 85-kDa subunit of PI3-kinase via a typical consensus YxxM motif and possibly via its YGNL and/or YASL motifs with two additional so far non-identified polypeptides of 43 and 50 kDa. However, the function of TRIM remains elusive.

The most recently identified transmembrane adaptor protein PAG/Cbp is a type III transmembrane protein with an extracellular domain of 16 amino acids (aa) and a 397 aa cytoplasmic tail [13, 14]. In contrast to the other transmembrane adaptor proteins known so far, PAG is ubiquitously expressed. In its cytoplasmic tail it carries a total of 10 potential tyrosine-based signaling motifs among which at least one (Y^{317} in human PAG) mediates an association with the PTK Csk, the major negative regulator of Src-family kinases. Thus, PAG/Cbp could be involved in negative regulation of T cell activation by recruiting Csk to the plasma membrane followed by down-regulation of T cell activation. Accordingly, overexpression of PAG in COS or 293T cells attenuates the kinase activity of Src and Fyn via a mechanism that involves binding of Csk [13, 14]. In resting peripheral blood T cells PAG is expressed as a constitutively tyrosine-phosphorylated polypeptide that recruits Csk to the membrane. Perhaps more importantly, immediately after T cell activation PAG becomes dephosphorylated by an unknown protein tyrosine phosphatase and releases Csk [13]. These data suggest that one function of PAG might be to down-regulate the enzymatic activities of Src kinases in resting T cells by recruiting Csk and thus to participate in keeping the cells in a quiescent state.

SIT is a disulfide-linked homodimeric polypeptide which is exclusively expressed in lymphocytes. In contrast to the other transmembrane adaptor proteins known so far, SIT is a heavily glycosylated polypeptide [12]. This could indicate that SIT possesses an external ligand that modulates its function. The cytoplasmic domain of SIT contains five potential tyrosine phosphorylation sites among which one is an ITIM. This motif mediates an inducible interaction with the tyrosine phosphatase SHP2. Importantly, overexpression of SIT in Jurkat T cells inhibits TCR-mediated activation of the nuclear factor of T cells (NF-AT) via a mechanism that is likely located upstream of the activation of phospholipase C (PLC) and protein kinase C (PKC). However, mutation of the tyrosine residue within the ITIM does not prevent SIT-mediated inhibition of NF-AT activity although it almost completely abrogates the interaction between SIT and SHP2 [12]. These data suggest that SIT exerts its inhibitory function via a mechanism that does not involve SHP2 or the ITIM. The present study was conducted to better understand the molecular mechanisms leading to tyrosine phosphorylation of SIT and to elucidate the structural basis for its negative regulatory function during T cell activation.

2 Results

2.1 Identification of the sites of tyrosine phosphorylation within the cytoplasmic domain of SIT

The cytoplasmic domain of SIT carries a total of five potential sites of tyrosine phosphorylation. These are Y^{90}GNL, Y^{128}TSL, VKY^{148}SEV (ITIM), Y^{168}ASV and Y^{188}ANS. To assess which of these five tyrosines represent *in vivo* phosphorylation sites, we generated a series

of chimeric SIT molecules in which the cytoplasmic tail of SIT was fused to the transmembrane and the extracellular domains of CD8. The cytoplasmic domains of the individual CD8/CD8/SIT chimeras corresponded either to wild-type SIT or carried mutations of four of the five potential tyrosine phosphorylation sites. A scheme depicting the various CD8/CD8/4F chimeras that we used in these experiments is shown in Fig. 1 B.

The individual cDNA contracts were transfected into Jurkat T cells by electroporation. Following overnight incubation the expression of the chimeras was assessed by FACS analysis (see *e. g.* Fig. 4) and by anti-SIT Western blotting (Fig. 1 C). Subsequently, the transfectants were either left untreated or were briefly treated with pervanadate, lysed in NP40-containing buffer, subjected to CD8 immunoprecipitation followed by anti-phosphotyrosine

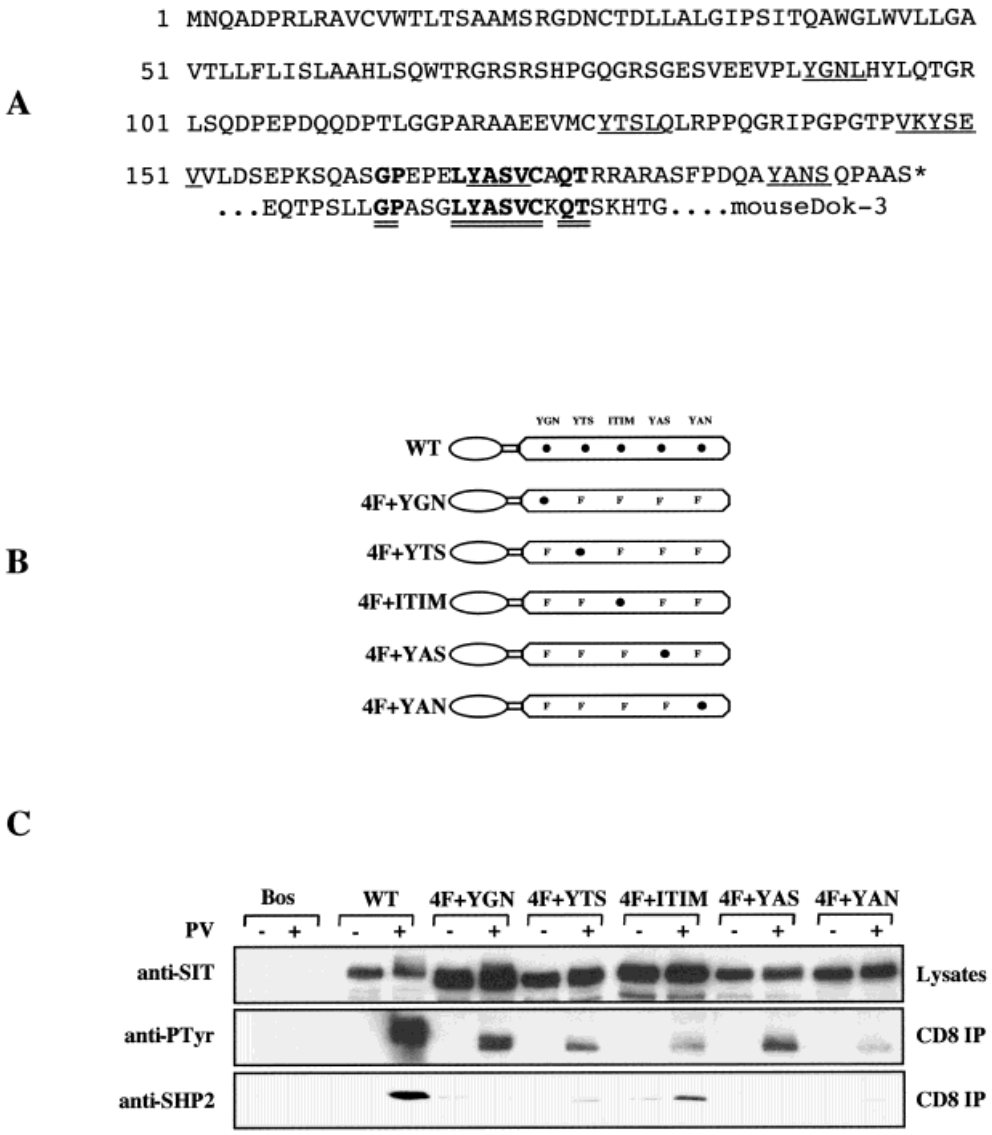

Fig. 1. Identification of the tyrosine phosphorylation sites within in the cytoplasmic domain of SIT. (A) Amino acid sequence of human SIT. The five tyrosine-based signaling motifs are underlined. The amino acids that are conserved between human SIT and Dok-3 (see Sect. 3) are double underlined. (B) A cDNA construct coding for a chimeric molecule encompassing the extracellular and transmembrane domain of human CD8 fused to the cytoplasmic portion of SIT was generated and cloned into the pEF-Bos eukaryotic expression vector. The wild-type CD8/CD8/SIT construct was then used as a template to generate the depicted variants in which individual tyrosine residues (●) were replaced by phenylalanines (F). (C) cDNA constructs encoding the SIT chimeras depicted in (B) were transiently expressed in Jurkat T cells by electroporation. Following overnight incubation, the cells were activated for 2 min with pervanadate (PV). Subsequently cells were lysed in NP 40-containing buffer and subjected to CD8 immunoprecipitation. Following SDS-PAGE, proteins were subjected to sequential anti-PTyr anti-SHP2 and anti-SIT Western blotting.

(PTyr) Western-blotting. Fig. 1 C demonstrates that under these experimental conditions the CD8/CD8/SIT, the CD8/CD8/4F+YGN and the CD8/CD8/4F+YAS chimeras became strongly tyrosine phosphorylated, whereas the phosphorylation of the CD8/CD8/4F+YTS, the CD8/CD8/4F+ITIM and the CD8/CD8/4F+YAN chimeras was much weaker. The overall level of tyrosine phosphorylations was YGNL ≥ YASV > YTSL > ITIM > YANS. The data indicate that the major sites of SIT tyrosine phosphorylation are the YGNL and the YASV motifs. However, the YTSL, the ITIM and the YANS motifs likely also become tyrosine phosphorylated after T cell activation. Indeed, when we analyzed the individual CD8 immunoprecipitates shown in Fig. 1 C for co-precipitation of SHP-2, we observed that SHP2 was recruited by the wild-type CD8/CD8/SIT chimera and the CD8/CD8/4F+ITIM chimera but not by any of the other mutants tested (Fig. 1 C, middle panel). This confirms our previous data which had suggested that the ITIM represents the *in vivo* phosphorylation site mediating the association between SIT and SHP2 ([12] and see also below).

2.2 SIT associates with SHP2 and Grb2 after T cell activation

The YGNL motif of SIT represents a potential binding site for the SH2 domain of the cytosolic adaptor protein Grb2 [17]. Given the above finding that this motif likely represents a major site of tyrosine phosphorylation we next assessed whether SIT, besides recruiting SHP2, would also associated with Grb2 after T cell activation. To this end Jurkat cells were stimulated for increasing periods of time with the clonotypic anti-TCR mAb C305 and then lysed in NP40-containing buffer. Subsequently, anti-SIT immunoprecipitates were prepared and analyzed for SIT tyrosine phosphorylation and co-precipitation of SHP2 and Grb2 by Western blotting. The upper panel of Fig. 2 A demonstrates that an increase in SIT phosphotyrosine content is already detectable after 1 min of TCR-mediated activation of Jurkat T cells and that it remains detectable for at least 1 h. As previously reported [12], the rapid increase in SIT phosphorylation is accompanied by an association between SIT and SHP2 (Fig. 2 A, middle panel). Perhaps more importantly, a time-dependent interaction of SIT with Grb2 was also detectable (Fig. 2 A, lower panel). Densitometric analysis of the blots revealed that the interaction between SIT and SHP2 or Grb2 was peaking at approximately 5 min after TCR engagement, and then slowly declined (Fig. 2 B). These results demonstrate that SIT not only associates with SHP2 but also with Grb2 upon T cell activation.

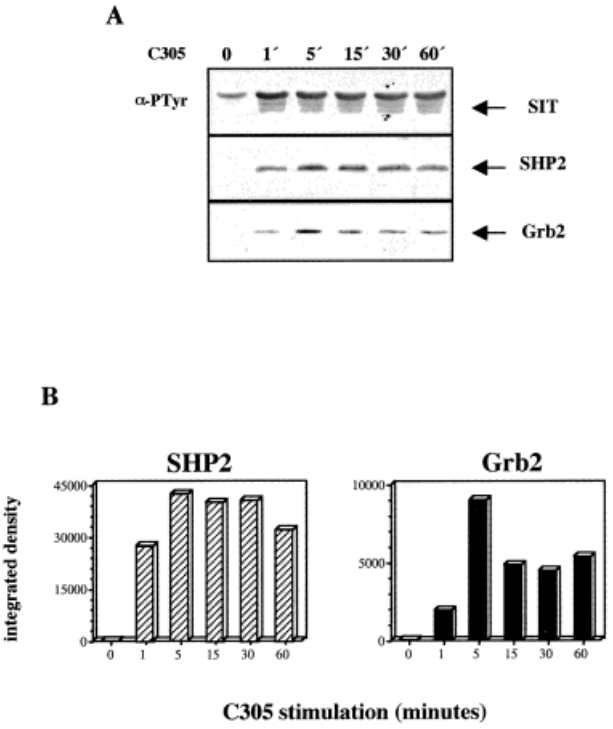

Fig. 2. TCR stimulation of Jurkat cells results in the recruitment of Grb2 and SHP2 to SIT. (A) Jurkat cells (4×10^7) were stimulated with C305 mAb for the indicated periods of time at 37 °C. Lysates were subjected to immunoprecipitation using anti-SIT antibodies, separated on a SDS-10 % PAGE, and immunoblotted with the anti-PTyr mAb 4G10 (upper panel). The membrane was subsequently stripped and reprobed with anti-SHP2 (middle panel) and anti-Grb2 (lower panel) mAbs. (B) Densitometric analysis of the bands corresponding to SHP2 and Grb2 shown in (A).

2.3 Grb2 binds to the YGNL and YANS motifs of SIT

To assess whether the inducible association between SIT and Grb2 is mediated via the YGNL motif we overexpressed CD8/CD8/SIT chimeras in Jurkat T-cells in which single tyrosine residues were mutated to phenylalanine (see Fig. 3 A for a schematic representation of the individual cDNA constructs). Again, the transfectants were left unstimulated or were treated with pervanadate. Subsequently, NP40 lysates were prepared and subjected to anti-CD8 immunoprecipitation. Immunoprecipitates were then analyzed for the presence of SHP2 and Grb2 by Western blotting (Fig. 3 B). These experiments revealed that the YTSL, the ITIM and the YASV motif are dispensable for the association between SIT and Grb2 since almost identical amounts of Grb2 were detectable in CD8 precipitates prepared from transfectants expressing these three mutants compared to cells expressing wild-type SIT (Fig. 3 B).

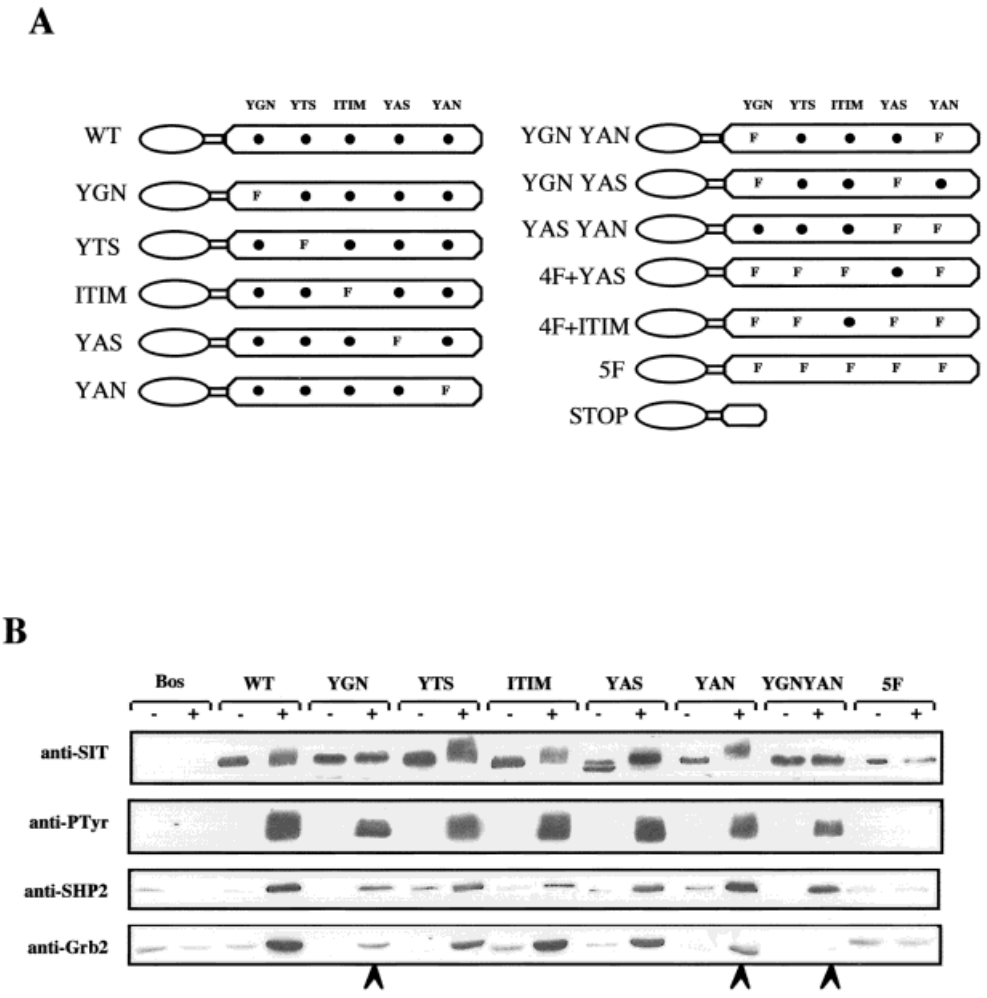

Fig. 3. The YANS and YGNL motifs of SIT mediate the association with Grb2. (A) Schematic representation of the cDNA constructs used for the experiments shown in this figure as well as those shown in Fig. 4 (see legend of Fig. 1 for nomenclature). (B) Jurkat cells were transfected with empty pEF-Bos vector (Bos) or with the indicated constructs. After 18 h, 2×10^6 cells were left unstimulated (–) or treated with pervanadate (+) for 2 min. NP40 lysates were subjected to anti-CD8 immunoprecipitation followed by anti-pTyr Western blot analysis. The blot was then stripped and re-probed with anti-SIT, anti-SHP2 or anti-Grb2 antibodies, as indicated.

In marked contrast, mutation of the YGNL motif resulted in an impaired ability of SIT to recruit Grb2 following T cell activation (arrow in Fig. 3 B), indicating that this motif represents a Grb2 binding site. However, we observed that the CD8/CD8/YAN chimera also had a reduced ability to associate with Grb2 despite the above observation that this motif apparently does not represent a major site of tyrosine phosphorylation. Moreover, concomitant mutation of the YGNL and the YANS motif (CD8/CD8/YGN+YAN chimera) resulted in a complete loss of Grb2 binding while the association with SHP2 was unaffected. These data strongly suggest that the association between SIT and Grb2 occurs on two different sites, namely YGNL and YANS (with YGNL being the major binding site).

2.4 Inhibition of T cell activation by SIT requires an intact YASV motif

Previous data had suggested that SIT might exert an inhibitory function during T cell activation. This hypothesis was based on the finding that overexpression of wild-type SIT or a CD8/CD8/SIT chimera in Jurkat T cells strongly impaired induction of the transcriptional activity of NF-AT after recruitment of the TCR [12]. However, inhibition of T cell activation by SIT is apparently not mediated via SHP2 since a SIT-ITIM mutant or a CD8/CD8/ITIM chimera which had largely lost their ability to bind to SHP2 still inhibited TCR-mediated induction of NF-AT activity [12].

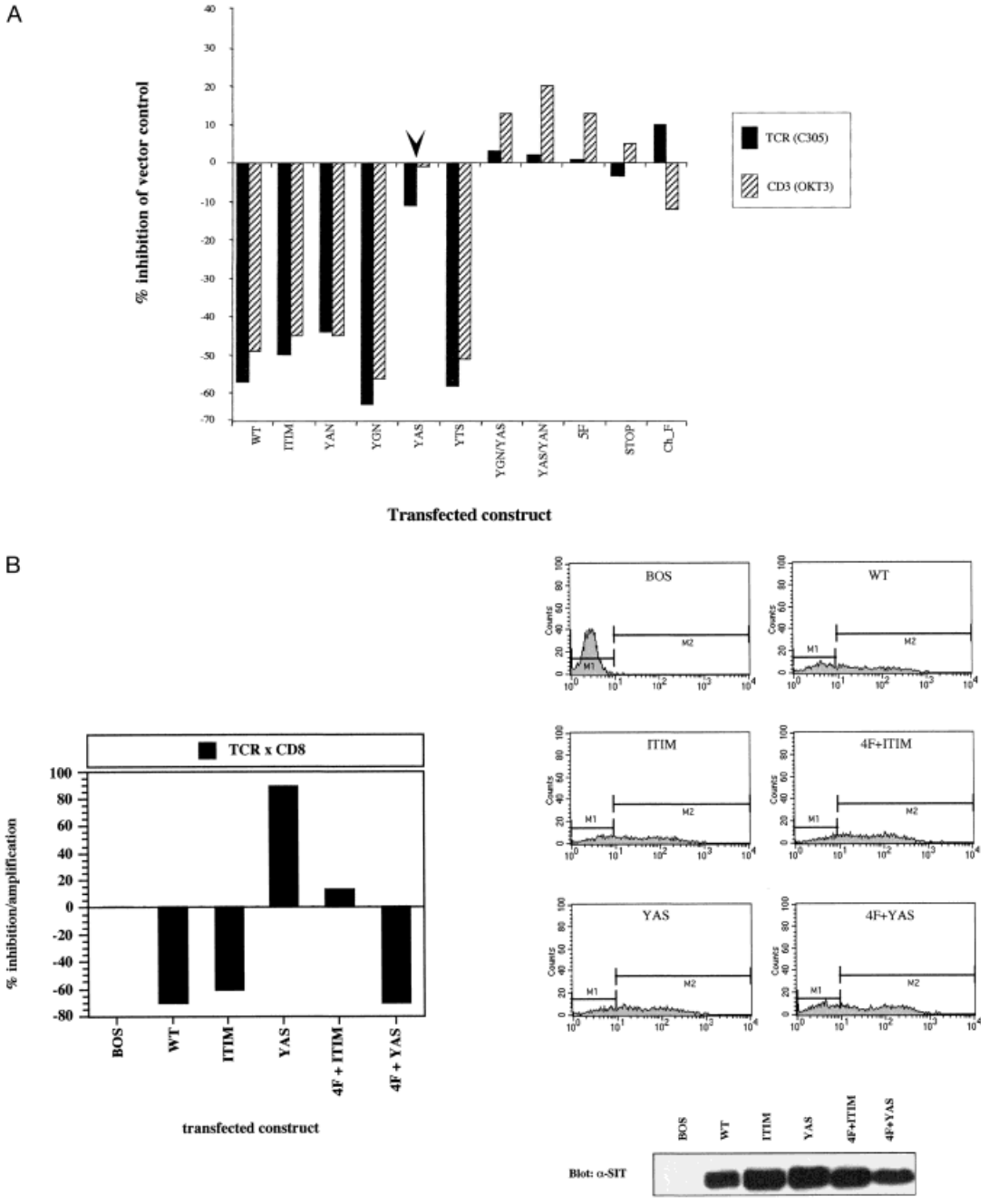

Fig. 4. The YASV-motif is responsible for SIT-mediated inhibition of TCR/CD3-induced NF-AT activation. (A) Jurkat cells were co-transfected with empty vector (pEF-Bos), a cDNA encoding the CD8/CD8/SIT chimera (WT) or the indicated SIT-variants, together with a NF-AT driven luciferase reporter construct. Eighteen hours later, cells were stimulated with crosslinked anti-TCR (C305) or CD3ε (OKT3) mAb for 6 h and then analyzed for luciferase activity as described in Sect. 4. The luciferase units obtained after stimulation of cells transfected with the empty vector were set as 100 %. Shown is the relative inhibition of the response of each transfectant in comparison to the response of the vector transfectant. Equal levels of expression of the individual chimeras were verified by anti-SIT Western blotting and by FACS analysis using an anti-CD8 mAb (not shown but see *e. g.* Fig. 4 B). (B) Cells were transfected with the indicated constructs as described in (A). Transfectants were subsequently stimulated with crosslinked anti-TCR mAb C305 alone or with a combination of crosslinked C305 and CD8 mAb (MEM-31). The luciferase units after stimulation with crosslinked C305 alone were set as 100 %. Shown is the relative inhibition/amplification of this response following co-crosslinking of the CD8-chimera with the TCR. The following equation was used: normalized luciferase units after TCR × CD8 co-stimulation divided by normalized luciferase units after TCR-stimulation alone. The expression of the constructs was verified by anti-SIT immunoblotting (lower panel) and by indirect immunofluorescence using mAb MEM-31.

To examine further the molecular mechanisms underlying the inhibitory function of SIT, the wild-type CD8/CD8/SIT chimera or tyrosine mutants thereof (see Fig. 3 A for details) were transiently overexpressed in Jurkat cells together with a luciferase reporter gene construct that is driven by a triplicated NF-AT binding site of the IL-2 promoter. A truncated version of the CD8/CD8/SIT chimera lacking the entire cytolasmic tail of SIT (CD8/CD8/STOP), a CD8/CD8/SIT chimera in which all five tyrosine phosphorylation sites were mutated to phenlyalanine (CD8/CD8/5F) as well as a chimeric TRIM molecule consisting of the extracellular domain of human HLA-A2 fused to a full-length TRIM molecule (Ch_F), served as negative controls. Following transfection, cells were allowed to rest for 18 h and were then stimulated for 6 h using either the anti-TCR mAb C305 or the CD3ε mAb OKT3. Subsequently, the TCR-mediated induction of NF-AT activity was determined.

As shown in Fig. 4 A, overexpression of the CD8/CD8/SIT chimera induced the previously described decrease in TCR- and CD3ε-mediated activation of NF-AT. Deletion of the entire intracellular domain of SIT (CD8/CD8/STOP) or mutation of all five tyrosine residues (CD8/CD8/5F) abrogated the ability of the chimera to inhibit NF-AT activation. In addition, overexpression of Ch_F did not influence TCR-mediated activation of NF-AT, as previously reported [15]. These data demonstrate that i) inhibition of T cell activation is a specific property of SIT, ii) SIT-mediated inhibition of T cell activation requires an intact cytoplasmic domain and iii) it involves one or more of the five cytoplasmic tyrosine residues of SIT.

As reported previously, overexpression of the CD8/CD8/ITIM-chimera, which is strongly impaired in its ability to bind SHP2 (see *e. g.* Fig. 3 B and [12]) still inhibited T cell activation. The same was true for CD8/CD8/SIT chimeras in which the two Grb2-binding sites (CD8/CD8/YGN or CD8/CD8/YAN chimera) were mutated individually or concomitantly, as well as for the CD8/CD8/YTS chimera. These findings suggested that the YGNL, YTSL, ITIM or YANS motifs do not mediate the inhibitory signal exerted by SIT. In marked contrast, all CD8/CD8/SIT chimeras in which the YASV motif was mutated either alone (arrow) or in combination with other tyrosine residues were strongly impaired in their ability to inhibit TCR responses.

Similar data as shown in Fig. 4 A were obtained when the individual CD8/CD8/SIT chimeras were co-ligated with the TCR (Fig. 4 B). Under these experimental conditions the wild-type CD8/CD8/SIT and the CD8/CD8/ITIM chimera induced an approximately 60–70 % inhibition of NF-AT activity. Perhaps more importantly, an identical down-regulation of NF-AT activity was produced by the CD8/CD8/4F+YAS chimera (in which only the YASV motif is intact), whereas co-crosslinking of the CD8/CD8/4F+ITIM chimera did not influence induction of NF-AT activity. From this experiment as well as from the data shown in Fig. 4 A we conclude that the inhibitory function of SIT is exclusively mediated via the YASV motif.

Surprisingly, we observed that the CD8/CD8/YAS chimera even up-regulated NF-AT activity when it was co-ligated with the TCR. This suggested that in the absence of a functional YASV motif, SIT can provide a positive – rather than a negative – regulatory signal for T cell activation rather (Fig. 4 B). To investigate, which of the remaining four tyrosine residues that are present in the CD8/CD8/YAS chimera is responsible for up-regulation of T cell activation in the absence of YASV, we overexpressed the individual CD8/CD8/4F chimeras in Jurkat T cells and assessed their influence on induction of NF-AT activity after co-crosslinking with the TCR. As shown in Fig. 5 A the CD8/CD8/4F+YTS, the CD8/CD8/4F+ITIM and the CD8/CD8/4F+YAN chimeras had no major impact on NF-AT activity after co-ligation with the TCR. In marked contrast, co-engagement of the CD8/CD8/4F+YGN chimera strongly up-regulated the response under conditions where the CD8/CD8/SIT and the CD8/CD8/4F+YAS chimeras inhibited NF-AT activity. Thus, in the absence of a phosphorylatable YASV motif SIT can exert a positive regulatory function for T cell activation which is mediated via the YGNL motif.

2.5 The PTK Csk binds to the YASV motif

Given the above data indicating a critical role for the YASV motif for SIT-mediated inhibition of T cell activation, we were interested to identify the molecule that binds to this motif. To this end we established Jurkat variants stably expressing the CD8/CD8/SIT or the CD8/CD8/YAS chimera, respectively. The individual transfectants as well as the parental ($CD8^-$) Jurkat cell line were metabolically labeled with a mixture of ^{35}S-cysteine and ^{35}S-methionine and subjected to brief pervanadate treatment. Subsequently, CD8 immunoprecipitates were prepared from postnuclear lysates, subjected to two-dimensional gel electrophoresis and analyzed by autoradiography. By using this approach we repeatedly observed a 45–50-kDa polypeptide (p45) with an estimated isoelectric point of 7.0 co-precipitating with the CD8/CD8/SIT chimera but not with the CD8/CD8/ITIM chimera (not shown).

Both the molecular weight of p45 as well as its isoelectric point are similar to those of the PTK $p50^{csk}$, the major negative regulator of src PTK. Moreover, the YASV motif of SIT shows striking similarities to the tyrosine-based signaling motif Y^{314}SSV which has recently been shown

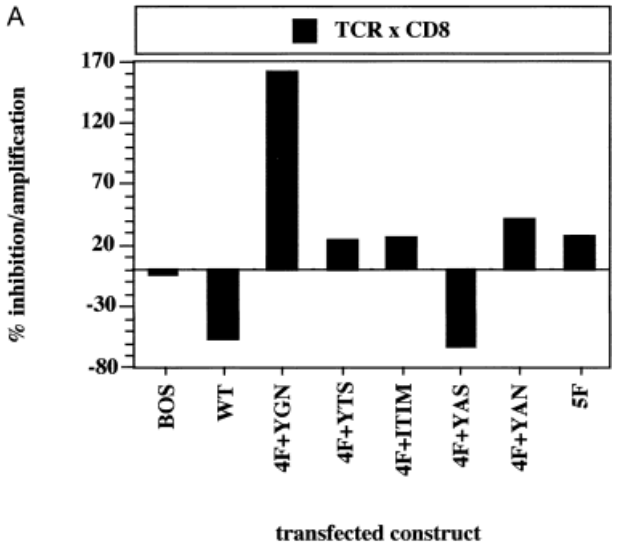

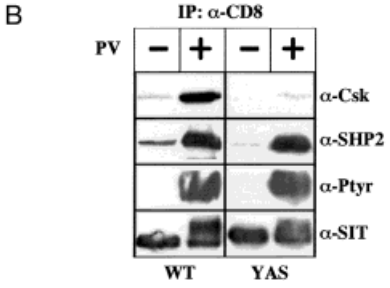

Fig. 5. The YASV – motif is responsible for SIT-mediated inhibition of TCR/CD3-induced NF-AT activation. (A) The same experiment as shown in Fig. 4 B using the CD8/CD8/4F-chimeras. (B) Jurkat cells stably expressing the CD8/CD8/SIT or the CD8/CD8/YAS chimeras were briefly treated with pervanadate. Subsequently, cells were lysed in NP40 containing buffer and subjected to CD8 immunoprecipitation. The tyrosine phosphorylation status of the chimeras as well as the presence of Csk and SHP2 in the immunoprecipitates were assessed by sequential Western -blotting (anti-Ptyr → anti-Csk → anti-SHP-2 → anti-SIT).

to represent the major bindig site for the SH2 domain of Csk within the cytoplasmic domain of the transmembrane adapter protein PAG/Cbp [13, 14]. Therefore we argued that p45 is identical to Csk and that SIT might recruit Csk via the YASV motif. To assess this question we performed anti-Csk Western blot analysis of CD8 immunoprecipitates prepared from the above Jurkat variants after treatment with pervanadate. As shown in Fig. 5 B large amounts of Csk co-precipitated with the CD8/CD8/SIT but not with the CD8/CD8/YASV chimera under these experimental conditions. Thus, Csk is the primary candidate for being the negative regulatory molecule that binds to YASV and mediates the inhibition of T cell activation by SIT.

3 Discussion

During the last years major efforts have been made to understand better the molecular mechanisms controlling the quality of an immune response after engagement of the TCR. The recent identification of a novel group of integral membrane proteins that carry multiple tyrosine-based signaling motifs in their cytoplasmic domains has offered new perspectives to explain how TCR-mediated signals are coupled to intracellular signaling pathways to yield an appropriate cellular response. This group of signaling molecules has collectively been termed transmembrane adaptor proteins and so far comprises LAT, TRIM, PAG/Cbp and SIT.

While it is meanwhile well established that the expression and tyrosine phosphorylation of LAT is essential for T cell activation and T cell development, the cellular functions of TRIM, PAG/Cbp and SIT are less well defined. We thought that one way to better understand the roles of these novel adaptor proteins during T cell activation might be to identify their sites of tyrosine phosphorylation as well as the signaling proteins that inducibly bind to their cytoplasmic domains. In this study we have performed a structure-function analysis of SIT.

The cytoplasmic domain of SIT contains five potential sites of tyrosine phosphorylation. These are Y^{90}GNL, Y^{128}TSL, Y^{148}SEV, Y^{168}ASV and Y^{188}ANS. Overexpression of CD8/CD8/SIT chimeras in Jurkat T cells in which four of these five sites were mutated to phenylalanine (CD8/CD8/4F chimeras) revealed that under optimal conditions (pervanadate stimulation) all five tyrosines can serve as substrates for protein tyrosine kinases. However, the levels of tyrosine phosphorylation of the individual 4F chimeras were quite different. Thus, the YGNL and the YASV motifs clearly seem to represent the preferred phosphorylation sites whereas YTSL, ITIM and YANS become phosphorylated to a much lesser extent (the overall order seems to be: YGNL ≥ YASV > YTSL > ITIM > YANS). At present we do not know whether these differences in tyrosine phosphorylation indeed reflect the *in vivo* situation or whether the lower levels of tyrosine phosphorylation of the YTSL, the ITIM and the YANS motifs are due to the fact that their full phosphorylation can only be achieved after YGNL and YASV have been phosphorylated. This possibility cannot be excluded because our previous experiments had suggested that, although the Syk-PTK ZAP-70 and Syk alone cannot induce detectable tyrosine phosphorylation of SIT in a

COS cell system, optimal tyrosine phosphorylation of SIT apparently requires co-expression of both Src and Syk PTK [12]. Moreover, our previous data as well as the experiments described in this report clearly demonstrate that, besides YGNL and YASV, at least the ITIM and the YANS motifs can bind intracellular effector molecules (SHP2 and Grb2) after T cell activation (Fig. 3).

Based on the studies performed by Songyang et al. [17], we argued that the YGNL motif could mediate an interaction between SIT and the cytoplasmic adaptor molecule Grb2. Indeed, an analysis of SIT immunoprecipitates prepared from TCR-stimulated Jurkat T cells not only corroborated an activation-induced association between SIT and SHP2 but also revealed an interaction between SIT and Grb2 (Fig. 2). By using chimeric CD8/CD8/SIT constructs in which individual tyrosine residues were mutated to phenylalanine we confirmed that Y^{188}GNL represents a Grb2 binding site (Fig. 3 B). However, we also observed that mutation of this site only partially abolished the association between SIT and Grb2. This suggested the existence of at least one additional Grb2 binding site within the cytoplasmic domain of SIT, which we identified as the Y^{188} ANS motif. Thus, simultaneous mutation of both YGNL and YANS motifs completely ablated the ability of SIT to recruit Grb2 whereas single mutation of either motif only partially interfered with the association between the two molecules (Fig. 3 B). These data suggest that after T cell activation Grb2 can interact with SIT via two different sites, namely Y^{90} GNL and Y^{188} ANS.

Previous studies had indicated that overexpression of SIT in Jurkat cells leads to down-regulation of the TCR/CD3-induced activation of NF-AT and that this inhibitory function is dependent on the presence of its cytoplasmic domain. We here extended these initial observations by demonstrating that the inhibitory function of SIT is dependent on tyrosine phosphorylation. Thus, a CD8/CD8/SIT chimera in which all five tyrosines were mutated to phenylalanine (CD8/CD8/5F chimera) had completely lost its capability to inhibit T cell activation (Fig. 4 A).

By mutational analysis we identified the Y^{168} ASV motif as the phosphorylation site that seems to be responsible for SIT mediated inhibition of T cell activation. Overexpression of a CD8/CD8/SIT chimera in which only the YASV motif was mutated (CD8/CD8/YAS chimera) fully rescued the NF-AT response following T cell activation, whereas chimeras carrying mutations in the YGNL, the ITIM, the YTSL or the YANS motifs had no influence on the ability of SIT to inhibit T cell responses (Fig. 4 A). Moreover, co-ligation of a CD8/CD8/SIT chimera, which only contained the YASV motif (CD8/CD8/4F+YAS) with the TCR-inhibited activation of NF-AT in an identical fashion as the wild-type protein (Fig. 4 B). All these data suggest that the inhibitory function of SIT is exclusively mediated via the YASV motif.

However, mutation of the YASV motif has no obvious impact on the binding of SHP2 and/or Grb2 to SIT (Fig. 3 B). Therefore we proposed the existence of a SH2 domain containing negative regulatory effector molecule that selectively binds to the phosphorylated YASV motif and mediates the inhibitory effect on T cell activation. Two-dimensional analysis of CD8 immunoprecipitates prepared from metabolically labeled Jurkat T cells stably expressing either the CD8/CD8/SIT or the CD8/CD8/YAS chimera resulted in the identification of a 45-kDa polypeptide (p45) with an estimated isoelectric point of about 7.0 that specifically co-precipitated with the wild-type chimera but not with the YASV mutant. We argued that p45 may be the tyrosine kinase Csk, which possesses the appropriate molecular weight and isoelectric point. In addition, Csk has recently been demonstrated to bind via a YSSV motif (which is very similar to the YASV-motif of SIT) to human and rat homologoues of the transmembrane adapter protein PAG/Cbp [13, 14]. Based on these molecular properties of Csk it was not surprising that we identified endogenous Csk in CD8 immunoprecipitates prepared from the CD8/CD8/SIT transfectants but not in those obtained from Jurkat T cells expressing the CD8/CD8/YAS mutant (Fig. 5 B). Collectively, these findings suggest that Csk could represent the negative regulatory protein that binds to the YASV motif and mediates the negative regulatory effect exerted by SIT on TCR-induced NF-AT activity.

The obvious question emerging from the finding that Csk is capable to bind to SIT is which TCR-mediated signaling pathway(s) leading to activation of NF-AT is/are controlled by this interaction. In this regard it is important to remember that overexpression of SIT in the Jurkat variant J.HM1.2.2 (which co-expresses a TCR and the human muscarinic receptor type 1) does not inhibit induction of NF-AT activity after triggering of G-protein coupled receptors [12]. This suggests that SIT controls signaling processes mediated via ITAM-containing immunoreceptors. Moreover, we had demonstrated that the inhibitory effect of SIT on TCR-mediated induction of NF-AT activity can be bypassed by treatment of SIT transfectants with a combination of a phorbol ester and ionomycin (which indicates that SIT likely exerts its function upstream of activation of PKC).

However, so far our attempts to show inhibition of (a) proximal tyrosine phosphorylation event(s) as an indicator of Csk-mediated inhibition of Src kinase activity in cells overexpressing SIT have not been successful. For

example we did not observe significant alterations of the global TCR-mediated tyrosine phosphorylation of cellular proteins after overexpression of SIT (either transiently or stably). In addition, tyrosine phosphorylation of TCRζ, LAT, PLCγ and also phosphorylation of Erk after TCR triggering seem to occur normally in cells overexpressing SIT. Collectively, these findings suggest that at least the initial activation of Src kinases occurs normally in cells overexpressing SIT. Therefore, further studies are required to elucidate the question which TCR-mediated signaling pathway(s) is/are controlled by SIT.

It is important to note that the functional activities of SIT show striking similarities to those that have recently been described for the negative regulatory adaptor protein Dok-3 [18]. Like SIT Dok-3 inducibly associates with Csk and down-regulates BCR-mediated activation of NF-AT via an unknown mechanism. The inhibitory effect of Dok-3 depends on the presence of the C-terminal tail of the molecule which contains four potential tyrosine-based signaling motifs among which one is likely responsible for recruitment of Csk [18]. Interestingly, the same YASV motif that mediates the association between SIT and Csk is also expressed in Dok-3 and the amino acids flanking both motifs are well conserved between the two molecules (see Fig. 1 A). It is therefore tempting to speculate that the YASV motif of Dok-3 also mediates its association with Csk and that this motif is involved in the inhibition of BCR-mediated signaling. Furthermore, the overall functional similarities between the two molecules might suggest that they control the same pathways of immunoreceptor-mediated signaling in different types of cells.

Previously we have demonstrated that the cytoplasmic tyrosine phosphatase SHP2 binds to the ITIM within the cytoplasmic domain of SIT. In T cells it is believed that SHP2 is involved in regulation of the MAPK pathway leading to activation of the transcription factor AP-1 [19]. The NF-AT reporter construct that we used in this study contains an AP-1 binding site and therefore we thought that, if SIT-associated SHP2 regulated AP-1 activity, then the CD8/CD8/4F-ITIM chimera should be capable to upregulate NF-AT when overexpressed in T cells. However, this is clearly not the case. Even co-ligation of the CD8/CD8/4F+ITIM chimera with the TCR failed to exert any measurable effect on the activity of the NF-AT reporter construct, although the chimera was capable to bind SHP2 (Fig. 1 C). From these data we conclude that the SIT-associated fraction of SHP2 regulates an (unknown) pathway of T cell activation that does not result in activation of AP-1.

An interesting observation during this study was that the functional effect of the individual CD8/CD8/SIT chimeras could be best demonstrated when the chimeras were co-crosslinked with the TCR using a CD8 antibody (Figs. 4 B and 5 A). As already mentioned above SIT represents a heavily glycosylated molecule that could possess an external ligand. One possibility to explain our results would be that the CD8 antibody mimics the function of this putative ligand. In this scenario engagement of SIT by its ligand would bring SIT in close proximity of the TCR, thus allowing the down-regulation of TCR-mediated signals. However, whether SIT indeed has an external ligand and whether this putative ligand regulates its function requires further investigations.

We also would like to point out that, although our previous studies as well as the experiments described in this report, support the view that SIT represents a negative regulatory adaptor protein, the possibility cannot be excluded that under particular conditions of T cell activation SIT exerts a positive rather than a negative regulatory function.

As shown in Figs. 2 and 3, SIT is capable of recruiting Grb2 via the YGNL motif following T cell triggering. In addition, it seems that YGNL represents a preferred tyrosine phosphorylation site (Figs. 1 and 3). Finally, our experiments using the CD8/CD8/YASV and the CD8/CD8/4F+YGN chimera indicate that in the absence of phosphorylatable YASV, SIT enhances TCR-mediated activation of NF-AT (Figs. 4 B and 5 A). This effect is mediated via the YGNL motif and thus likely involves a Grb2-controlled signaling pathway (Fig. 5 A).

One could imagine a situation in which a preferential (or even exclusive) phosphorylation of YGNL occurs *in vivo*, for example after TCR triggering by a weak agonist. Thus, depending on its state of phosphorylation SIT (as well as other transmembrane and cytosolic adaptor proteins) could serve as a multifunctional protein that helps to integrate the quality of an externally applied signal into an appropriate cellular response. For the further understanding of SIT function it will be important to elucidate the question whether the phosphorylation status of SIT as well as its association with cytosolic effector molecules is influenced by the quality of an externally applied signal. Moreover, it will be important to identify the molecule(s) that bind to the SIT/Grb2 complex. Potential candidates are SOS [20, 21], SLP-76 [22], Dynamin [20], TNF-R1 [23] and SHIP [24] which all have been demonstrated to bind one or two of the Grb2-SH3 domains. Experiments are underway to assess these questions.

4 Materials and methods

4.1 Cells and antibodies

Jurkat cells were maintained in RPMI 1640 supplemented with 10 % FCS, 2 % glutamin and 1 % penicillin-streptomycin (Gibco BRL, Germany). The Jurkat variants stably expressing the CD8/CD8/SIT and the CD8/CD8/YAS chimeras were generated and propagated as previously described [11]. The anti-SIT polyclonal antiserum was raised by immunizing rabbits with a KLH-coupled synthetic peptide corresponding to amino acids 96–114 [12]. After affinity purification on peptide-coupled protein A-Sepharose beads, antibodies were used at 2 μg/ml for Western blotting. Antibodies against SHP2, phosphotyrosine (4G10) (Upstate Biotechnology Inc.), Grb2 (Santa Cruz) and Csk (Santa Cruz) were diluted at 1 μg/ml for immunoblotting. For immunoprecipitation experiments, protein A-Sepharose-purified anti-CD8 mAb AICD8.1 or MEM-31 mAb were covalently coupled to CNBr-activated Sepharose beads (6 mg mAb/ml of packed beads).

4.2 Immunoprecipitation and Western blotting

Untransfected Jurkat T cells (4×10^7 for the experiment shown in Fig. 2) or Jurkat cells (2×10^6) that had been transiently transfected with cDNA encoding the various CD8/CD8/SIT chimeras (see below) were stimulated with culture supernatant of C305 mAb (provided by Dr. A. Weiss, University of California, San Francisco, CA) for the indicated period of time, or with a mixture of 0.1 mM vanadate plus 1 mM H_2O_2 for 2 min, at 37 °C. Immunoprecipitations were performed using the crude polyclonal rabbit antiserum directed at SIT (1 : 100 v/v) followed by collection of the immune complexes using protein A-Sepharose or by using 15 μl of packed beads coupled with protein A-purified CD8 mAb. After several washes, the precipitates were subjected to SDS-PAGE and further processed for Western blot analysis using standard procedures, as described elsewhere [12, 16].

4.3 cDNA constructs and transfection

Generation of the chimeric CD8/CD8/SIT molecule and its cloning into the eukaryotic pEF-Bos expression vector have been previously described [12]. Point mutation of the tyrosine residues (replaced by phenylalanine) within selected signaling motif(s) has been performed using the Quick Change site-directed Mutagenesis kit from Stratagene according to the manufacturer's recommendations.

4.4 Luciferase reporter gene assay

Jurkat cells were transiently transfected by electroporation using 30 μg of the indicated cDNA construct together with 10 μg of the NF-AT reporter construct and 1 μg of a rennilla luciferase reporter gene. Cells were allowed to recover for 18 h and incubated in duplicates (7×10^4 cells/well) with medium, immobilized anti-TCR (C305) or anti-CD3 (OKT3) mAb, or PMA (10^{-8} M) plus ionomycin (1 μg/ml) in a 96-well plate (U96 Maxisorp, Nunc). After 6 h of stimulation, cells were harvested, washed twice in PBS and lysed for 15 min at room temperature. The normalized luciferase activity of the NF-AT reporter gene was measured in each supernatant using the dual luciferase assay system from Promega.

References

1 **Howe, L. R. and Weiss, A.,** Multiple kinases mediate T-cell receptor signaling. *TIBS* 1995. **20:** 59–64.

2 **van Leeuwen, L. E. and Samelson, L. E.,** T cell antigen-receptor signal transduction. *Curr. Opin. Immunol.* 1999. **11:** 242–248.

3 **Tomlinson, M. G., Lin, J. and Weiss, A.,** Lymphocytes with a complex: adapter proteins in antigen receptor signaling. *Immunol. Today* 2000. **21:** 584–591.

4 **Zhang, W. and Samelson, L. E.,** The role of membrane-associated adaptors in T cell receptor signalling. *Semin. Immunol.* 2000. **12:** 35–41.

5 **Schraven, B., Marie-Cardine, A., Hübener, C., Bruyns, E. and Ding, I.,** Integration of receptor-mediated signals in T cells by transmembrane adaptor proteins. *Immunol. Today* 1999. **20:** 431–434.

6 **Weber, J. R., Orstavik, S., Torgersen, K. M., Danbolt, N. C., Berg, S. F., Ryan, J. C., Tasken, K., Imboden, J. B. and Vaage, J. T.,** Molecular cloning of the cDNA encoding pp36, a tyrosine-phosphorylated adapter protein selectively expressed by T cells and natural killer cells. *J. Exp. Med.* 1998. **187:** 1157–1161.

7 **Zhang, W., Sloan-Lancaster, J., Kitchen, J., Trible, R. P. and Samelson, L. E.,** LAT: the ZAP-70 tyrosine kinase substrate that links T cell receptor to cellular activation. *Cell* 1998. **92:** 83–92.

8 **Finco, T. S., Kadlecek, T., Zhang, W., Samelson, L. E. and Weiss, A.,** LAT is required for TCR-mediated activation of PLCγ 1 and the Ras pathway. *Immunity* 1998. **9:** 617–626.

9 **Zhang, W., Irvin, B. J., Trible, R. P., Abraham, R. T. and Samelson, L. E.,** Functional analysis of LAT in TCR-mediated signaling pathways using a LAT-deficient Jurkat cell line. *Int. Immunol.* 1999. **11:** 943–950.

10 **Zhang, W., Sommers, C. L., Burshtyn, D. N., Stebbins, C. C., DeJarnette, J. B., Trible, R. B., Grinberg, A., Tsay, H. C., Jacobs, H. M., Kessler, C. M., Long, E. O., Love, P. E. and Samelson, L. E.,** Essential role of LAT in T cell development. *Immunity* 1999. **10:** 323–332.

11 **Bruyns, E., Kirchgessner, H., Meuer, S. and Schraven, B.,** Biochemical analysis of the CD45-p56^{lck}. and lck complex in Jurkat T cells lacking expression of lymphocyte phosphatase associated phosphoprotein. *Int. Immunol.* 1998. **10:** 185–194.

12 **Marie-Cardine, A., Kirchgessner, H., Bruyns, E., Shevchenko, A., Mann, M., Autschbach, F., Ratnofsky, S., Meuer, S. and Schraven, B.,** SHP2 interacting transmembrane adaptor protein (SIT), a novel disulfied linked dimer regulating human T-cell activation. *J. Exp. Med.* 1999. **189:** 1181–1194.

13 **Brdicka, T., Pavlistova, D., Leo, A., Bruyns, E., Korinek, V., Angelisova, P., Scherer, J., Shevchenko, A., Shevchenko, A., Hilgert, I., Cerny, J., Drbal, K., Kuramitsu, Y., Kornacker, B., Horejsi, V. and Schraven, B.,** Phosphoprotein associated with glycosphingolipid-enriched microdomains (PAG), a novel ubiqui-

touslmy expressed transmembrane adator protein, binds the protein tyrosine kinase Csk and is involved in regulation of T cell activation. *J. Exp. Med.* 2000. **191:** 1591–1604.

14 **Kawabushi, M., Satomi, Y., Takao, T., Shimonishi, Y., Nada, S., Nagai, K., Tarakhovsky, A. and Okada, M.,** Transmembrane phosphoprotein Cbp regulates the activities of Src-family kinases. *Nature* 2000. **404:** 999–1003.

15 **Bruyns, E., Marie-Cardine, A., Kirchgessner, H., Sagolla, K., Shevchenko, A., Mann, M., Autschbach, F., Bensussan, A., Meuer, S. and Schraven, B.,** T cell receptor (TCR) interacting molecule (TRIM), a novel disulfide-linked dimer associated with the TCR-CD3ζ complex, recruits intracellular signaling proteins to the plasma membrane. *J. Exp. Med.* 1998. **188:** 561–575.

16 **Schraven, B., Ratnofsky, S., Gaumont, Y., Lindegger, H., Kirchgessner, H., Bruyns, E., Moebius, U. and Meuer, S. C.,** Identification of a novel dimeric phosphoprotein (pp29/30) associated with signaling receptors in human T lymphocytes and natural killer cells. *J. Exp. Med.* 1994. **180:** 897–906.

17 **Songyang, Z., Shoelsen, S. E., Chaudhuri, M., Gish, G., Pawson, T., Haser, W. G., King, F., Roberts, T., Ratnofsky, S., Lechleider, R. J., Neel, B. G., Birge, R. B., Fajardo, J. E., Chou, M. M., Hanafusa, H., Schaffhausen, B. and Cantley, L. C.,** SH2 domains recognize specific phosphopeptide sequences. *Cell* 1993. **72:** 767–778.

18 **Lemay, S., Davidson, D., Tatour, S. and Veilette, A.,** Dok-3, a novel adapter protein involved in the negative regulation of immunoreceptor signaling. *Mol. Cell. Biol.* 2000. **20:** 2743–2754.

19 **Frearson, J. A. and Alexander, D. R.,** The phosphotyrosine phosphatase SHP-2 participates in a multimeric signaling complex and regulates T cell receptor (TCR) coupling to the Ras/mitogen-activated protein kinase (MAPK) pathway in Jurkat cells. *J. Exp. Med.* 1998. **187:** 1417–1426.

20 **Vidal, M., Montiel, J. L., Cussac, D., Cornille, F., Duchesne, M., Parker, F., Tocque, B., Roques, B. P. and Garbay, C.,** Differential interactions of the growth factor receptor-bound protein 2 N-SH3 domain with son of sevenless and dynamin. Potential role in the Ras-dependent signaling pathway. *J. Biol. Chem.* 1998. **273:** 5343–5348.

21 **Vidal, M., Goudreau, N., Cornille, F., Cussac, D., Gincel, E. and Garbay, C.,** Molecular and cellular analysis of Grb2 SH3 domain mutants: interaction with Sos and dynamin. *J. Mol. Biol.* 1999. **290:** 717–730.

22 **Jackman, J. K., Motto, D. G., Sun, Q., Tanemoto, M., Turck, C. W., Peltz, G. A., Koretzky, G. A. and Findell, P. R.,** Molecular cloning of SLP-76, a 76-kDa tyrosine phosphoprotein associated with Grb2 in T cells. *J. Biol. Chem.* 1995. **270:** 7029–7032.

23 **Hildt, E. and Oess, S.,** Identification of Grb2 as a novel binding partner of tumor necrosis factor (TNF) receptor I. *J. Exp. Med.* 1999. **189:** 1707–1714.

24 **Harmer, S. L. and DeFranco, A. L.,** The src homology domain 2-containing inositol phosphatase SHIP forms a ternary complex with Shc and Grb2 in antigen receptor-stimulated B lymphocytes. *J. Biol. Chem.* 1999. **274:** 12183–12191.

Correspondence: Burkhart Schraven, Institute for Immunology, Otto-von-Guericke-Universität Magdeburg, Leipziger Str. 44, D-39120 Magdeburg, Germany
Fax: 0391 67 158 52
e-mail: burkhart.schraven@medizin.uni-magdeburg.de

K.-I. Pfrepper's present address: Mikrogen GmbH, Dept. for Research and Development, Fraunhoferstr. 20, D-82151 Martinsried, Germany

Appendix 2

NTAL (Non T-cell Activation Linker), a novel transmembrane adaptor protein involved in immunoreceptor signalling

Brdicka T, Imrich M., Angelisova P., Brdicková N. Horváth O.; Spicka J., Hilgert I., Luskova P., Draber P., Novak P., Engels N., Wienands J., **Simeoni L.**, Österreicher J., Aguado E., Malissen M., Schraven B. and Horejsi V. (2002) *J Exp Med*. 196:1617-26.

Non–T Cell Activation Linker (NTAL): A Transmembrane Adaptor Protein Involved in Immunoreceptor Signaling

Tomáš Brdička,[1] Martin Imrich,[1] Pavla Angelisová,[1] Naděžda Brdičková,[1] Ondrej Horváth,[1] Jiří Špička,[1] Ivan Hilgert,[1] Petra Lusková,[1] Petr Dráber,[1] Petr Novák,[2] Niklas Engels,[3] Jürgen Wienands,[3] Luca Simeoni,[4] Jan Österreicher,[5] Enrique Aguado,[6] Marie Malissen,[6] Burkhart Schraven,[4] and Václav Hořejší[1]

[1]*Institute of Molecular Genetics and* [2]*Institute of Microbiology, Academy of Sciences of the Czech Republic, Vídeňská 1083, 142 20 Prague 4, Czech Republic*

[3]*Department of Biochemistry and Molecular Immunology, University of Bielefeld, Universitätsstrasse 25, Bielefeld D-33615, Germany*

[4]*Institute for Immunology, Otto-von-Guericke-University, Leipziger Strasse 26, 39120 Magdeburg, Germany*

[5]*Department of Radiobiology and Immunology, Purkyně Military Medical Academy, Třebešská 1575, 500 01 Hradec Králové, Czech Republic*

[6]*Centre d'Immunologie de Marseille-Luminy, INSERM-CNRS-Univ. Med., Parc Scientifique de Luminy, 13288 Marseille Cedex 9, France*

Abstract

A key molecule necessary for activation of T lymphocytes through their antigen-specific T cell receptor (TCR) is the transmembrane adaptor protein LAT (linker for activation of T cells). Upon TCR engagement, LAT becomes rapidly tyrosine phosphorylated and then serves as a scaffold organizing a multicomponent complex that is indispensable for induction of further downstream steps of the signaling cascade. Here we describe the identification and preliminary characterization of a novel transmembrane adaptor protein that is structurally and evolutionarily related to LAT and is expressed in B lymphocytes, natural killer (NK) cells, monocytes, and mast cells but not in resting T lymphocytes. This novel transmembrane adaptor protein, termed NTAL (non–T cell activation linker) is the product of a previously identified *WBSCR5* gene of so far unknown function. NTAL becomes rapidly tyrosine-phosphorylated upon cross-linking of the B cell receptor (BCR) or of high-affinity Fcγ- and Fcε-receptors of myeloid cells and then associates with the cytoplasmic signaling molecules Grb2, Sos1, Gab1, and c-Cbl. NTAL expressed in the LAT-deficient T cell line J.CaM2.5 becomes tyrosine phosphorylated and rescues activation of Erk1/2 and minimal transient elevation of cytoplasmic calcium level upon TCR/CD3 cross-linking. Thus, NTAL appears to be a structural and possibly also functional homologue of LAT in non–T cells.

Key words: lipid rafts • membrane microdomains • antigen receptors • Fc gamma receptor • Fc epsilon receptor

Introduction

Immunoreceptors (TCR, B cell receptor [BCR],* most Fc-receptors) initiate, upon binding of their agonist ligands, signaling pathways based on an inducible activation of Src-, Syk-, and Tec-family protein tyrosine kinases (1–3). Eventually this leads to activation of further downstream signal-

Preliminary reports (abstracts, poster and oral communications) on some aspects of this work were presented at the EMBO Workshop on Lymphocyte Antigen Receptor and Coreceptor Signalling, Siena, May 4–8, 2002 and at the ELSO2002 Meeting, Nice, June 29–July 3, 2002.

Address correspondence to Václav Hořejší, Institute of Molecular Genetics AS CR, Vídeňská 1083, 142 20 Praha 4, Czech Republic. Phone: 420-2-41729908; Fax: 420-2-44472282; E-mail: horejsi@biomed.cas.cz; or Burkhart Schraven, Institute for Immunology, Otto-von-Guericke-University, Leipziger Strasse 26, 39120 Magdeburg, Germany. Phone: 0391-67-15800; Fax: 0391-67-15852; E-mail: burkhart.schraven@medizin.uni-magdeburg.de

**Abbreviations used in this paper:* BCR, B cell receptor; BMMC, bone marrow mast cell; GEM, glycosphingolipid-enriched microdomain; LAT, linker for activation of T cells; NTAL, non–T cell activation linker; PI3-K, phosphatidylinositol 3-kinase; PLCγ, phospholipase Cγ; PTK, protein tyrosine kinase; P-Tyr, phosphotyrosine.

ing molecules such as phospholipase Cγ (PLCγ), phosphatidylinositol 3-kinase (PI3-K), and other proteins regulating activities of small G-proteins of Ras and Rho families. A key component of the TCR signaling pathway is a transmembrane adaptor protein linker for activation of T cells (LAT) which becomes tyrosine phosphorylated by activated ZAP-70 (4) and then binds several other molecules including PLCγ, Grb2, SLP-76, PI3-K, and Gads (5). LAT is expressed in T cells as a palmitoylated protein and is a characteristic component of detergent-resistant membrane microdomains (6, 7), also called membrane rafts or glycosphingolipid-enriched membrane domains (GEMs) enriched in glycosylphosphatidylinositol (GPI)-anchored proteins, glycosphingolipids, cholesterol, and several species of signaling molecules including Src-family kinases and heterotrimeric G-proteins (8). Association of the ligated TCR (as well as other immunoreceptors) with GEMs seems to be indispensable for the initiation of cellular activation as it facilitates the phosphorylation of immunoreceptor-associated tyrosine-based activation motifs by GEM-associated Src-kinases and several other early signaling steps (9, 10). T cells devoid of LAT are defective in TCR signaling and $LAT^{-/-}$ mice lack mature T cells as their development in thymus is blocked at an early stage (11).

In marked contrast to T cells, B cells of $LAT^{-/-}$ mice are functionally normal because LAT is not expressed in these cells. Furthermore, myeloid and NK cells develop apparently normally in the LAT-deficient animals and at least some aspects of signaling through their Fc-receptors remain functional (11–13). The latter data indicate that another LAT-like molecule may be expressed in non–T cells. Therefore, we were looking for a molecule which might possibly play a LAT-like role in BCR and Fc-receptor signaling.

Materials and Methods

Cells and Antibodies. Human T, B, NK cells, and monocytes were obtained from buffy coats by Ficoll centrifugation and preparative cell sorting using a FACS Vantage™ flow cytometer (Becton Dickinson) and PE-conjugated mAbs to CD3 and CD19 (Serotec), biotinylated anti-CD14 (Serotec), fluoresceinated streptavidin (BD Biosciences), unlabeled CD56 mAb MEM-188 (product of the Prague laboratory), and fluorescein-conjugated $F(ab)_2$ fragments of goat anti–mouse Ig (Caltag). Mouse splenocytes (an unseparated washed suspension containing ~40% B cells) used in functional experiments with B cells were obtained from C57/BL6 mice. Human blood monocytes used in the functional experiments were obtained by preparative cell sorting based solely on their characteristic side and forward scatter properties (i.e., without any antibody staining). Bone marrow mast cells (BMMCs) of wild-type and $Lyn^{-/-}$ mice (14) were provided by Dr. M. Hibbs (Ludwig Institute for Cancer Research, Melbourne, Australia). B cell line Ramos, myeloid cell line THP-1, T cell line Jurkat, and 293T cells were from the cell line collection of the Institute of Molecular Genetics. Jurkat T cell line mutant J.CaM2.5 deficient in the transmembrane adaptor protein LAT (15) was donated by Dr. A. Weiss (University of California at San Francisco, San Francisco, CA).

Antiserum to non–T cell activation linker (NTAL) was produced in the Prague laboratory by immunization of rabbits with bacterially expressed cytoplasmic fragment of human NTAL (amino acids 89–243), mouse mAbs to NTAL were prepared using standard techniques from splenocytes of mice immunized with the same bacterially produced NTAL fragment; some of them cross-reacted also with mouse homologue (unpublished data). In addition, anti-peptide mAbs were prepared directed to the peptide comprising residues 196 to 210 of the human molecule (purchased from Genemed Synthesis Inc.) conjugated to keyhole limpet hemocyanin using a commercial kit (Pierce Chemical Co.). Rabbit polyclonal antibodies to Erk1/2 and phospho-Erk1/2 were from Promega and New England Biolabs, Inc., respectively.

The sources of the other antibodies used were as follows: Jurkat TCR (IgM mAb C305, provided by Dr. A. Weiss), CD28 (IgM mAb 248.23.2; reference 16), Grb2 (mouse mAb; Transduction Laboratories), Sos1 (rabbit polyclonal; Santa Cruz Biotechnology, Inc.), c-Cbl (rabbit polyclonal; Santa Cruz Biotechnology, Inc.), Gab1 (Upstate Biotechnology), ubiquitin (rabbit polyclonal; Sigma-Aldrich), phosphotyrosine (mAbs P-Tyr-01 and P-Tyr-02 prepared in the Prague laboratory; PY-20-horseradish peroxidase conjugate; Transduction Laboratories), CD59 (mAb MEM-43), and CD3ε (mAb MEM-92), both prepared in Prague laboratory.

In Vitro Kinase Assay, Immunoprecipitation, and Other Biochemical Methods. Detergent-resistant microdomains (GEMs) were immunoisolated and in vitro kinase assays performed as described previously (17). Briefly, cells were solubilized with ice-cold isotonic lysis solution containing 1% detergent Nonidet P-40 (NP-40), the postnuclear supernatants containing GEMs were incubated in plastic wells coated with mAb MEM-43 (antibody to a major protein component of GEMs, GPI-anchored protein CD59). After washing, the kinase solution containing [$\gamma-^{32}$P]ATP (ICN Biomedicals) was added and the proteins phosphorylated by GEMs-associated kinases were resolved by SDS-PAGE and autoradiography. Sucrose density gradient-based GEMs isolation was performed as described previously (18).

NTAL and NTAL-containing complexes were immunoprecipitated using postnuclear supernatants of cells solubilized by a detergent effectively disrupting GEMs (laurylmaltoside [n-dodecyl β-D-maltoside]; Calbiochem; lysis buffer: 1% laurylmaltoside in 20 mM Tris [pH 7.5], containing 100 mM NaCl, 10% glycerol, 1 mM 4-(2-aminoethyl)-benzenesulfonyl fluoride, 10 mM EDTA, 50 mM NaF, 1 mM Na_3VO_4) and CNBr-Sepharose beads (Amersham Biosciences) coupled with mAbs purified by Protein A-Sepharose affinity chromatography. These lysates were passed through minicolumns (30–50 μl packed volume) of such immunosorbents; after washing with 10 column volumes of lysis buffer, bound proteins were eluted with 2 column volumes of 2× concentrated SDS-sample buffer and the flow-through and eluted fractions were analyzed by SDS-PAGE followed by Western blotting. In some experiments the cells were solubilized in 2× concentrated SDS-sample buffer, ultracentrifuged (250,000 *g*, 30 min) and the supernatant analyzed by SDS-PAGE and Western blotting. Biosynthetic labeling with [^{3}H]palmitate, SDS-PAGE, and Western blotting were performed as described (18). For enhanced detection of polyubiquitinated NTAL, the blot was autoclaved before immunostaining (19).

Isolation of NTAL and Its Identification by Peptide Mass Mapping. Large-scale isolation of GEMs from NP-40-solubilized THP-1 cells by sucrose density gradient ultracentrifugation and separation of their protein components by two-dimensional

PAGE was performed essentially as described earlier for analogous isolation of the transmembrane adaptor protein PAG (18). Two silver stained spots comigrating with the radioactively labeled in vitro phosphorylated spots were digested directly in the gel by trypsin (Promega) and the resulting peptide mixtures were analyzed on a Bruker BIFLEX II (Bruker-Franzen) MALDI-TOF mass spectrometer equipped with a nitrogen laser (337 nm) and a delayed extraction ion source. A saturated solution of α-cyano-4-hydroxycinnamic acid in aqueous 50% acetonitrile and 1% acetic acid was used as a MALDI matrix. 1 μl of the sample and 1 μl of the matrix solution were mixed on the target and allowed to dry at the ambient temperature. Positive-ion mass spectra of peptide maps were measured in the reflectron mode. Spectra were externally calibrated by using the monoisotopic $[M+H]^+$ ion of peptide standard (somatostatin; Sigma-Aldrich).

DNA Constructs, Transfections. The coding region of human NTAL was amplified from human leukocyte cDNA library (CLONTECH Laboratories, Inc.; primers: 5′ CAGTTCTTGGAAACCCACTCGAG 3′ and 5′ GATGTCGACTAGGCTTCTGTGGCTGCCAC 3′). The PCR product was blunted and cloned into EcoRV site of pBluescript SK vector (Stratagene), the coding sequence was then cut out with HindIII and SmaI, gel-purified, and cloned into the HindIII/EcoRV digested eukaryotic expression vector pFLAG-CMV 5a (Sigma-Aldrich), and sequenced. For stable transfections NTAL coding sequence was subcloned into EcoRI site of pEFIRES-N vector (provided by Dr. S. Hobbs, Institute of Cancer Research, London, UK; reference 20). The FLAG-NTAL construct encoding the full length NTAL containing the COOH-terminal FLAG tag was produced from the pFLAG-CMV 5a construct by site-directed mutagenesis using the QuikChange™ site-directed mutagenesis kit (Stratagene) according to the manufacturer's instructions and the FLAG-NTAL insert was eventually subcloned into the pEFIRES-N vector. The analogous FLAG-LAT construct was obtained from a previously described construct (21) by subcloning the FLAG-LAT insert into the pEFIRES-N vector. The FLAG-TRIM construct in pEF-BOS vector was described earlier (21). For transient transfection of 293T cells, Lipofectamine 2000™ reagent (Invitrogen) was used according to manufacturers instructions. For transfection experiments in 293T cells the following cDNA constructs were used: Myc-tagged Lck or ZAP-70 inserted into pcDNA3 vector (donated by Dr. R. Abraham, Mayo Clinic, Rochester, MN), Syk cloned into the pRK5 vector (provided by Dr. W. Kolanus, Gene Center, Munich, Germany), Myc-tagged Lyn in pcDNA3.1 vector (provided by Dr. S. Watson, University of Oxford, UK), and FLAG-tagged Hck in pcDNA1 vector (provided by Dr. G. Langsley, Institut Pasteur, Paris, France). For bacterial expression, the NTAL intracellular fragment corresponding to amino acids 89–243 was cloned to BamHI site of pET-15b expression vector (Novagen), generating a construct with NH_2-terminal histidine tag.

J.CaM2.5 cells (Jurkat T cell line mutant deficient in the transmembrane adaptor protein LAT) were transfected with non-tagged or FLAG-tagged NTAL, LAT, and TRIM constructs in the above described expression vectors by electroporation; stable transfectants expressing NTAL were selected by growing in 96-well plate in selective medium containing 1 mg/ml G418 (Calbiochem). After 3 wk oligoclonal G418-resistant populations were expanded and checked for NTAL expression by Western blotting. Four independent clones (three expressing high amount of NTAL and one of very low expression) were analyzed in detail. All these clones expressed only trace amounts of LAT (just like the parental J.CaM2.5 cells) and all of them had the same high expression of CD3 as the parental J.CaM2.5 cells or wild-type Jurkat cells (unpublished data). In relevant figures a representative of the NTAL high-expressing clones (which all gave similar results) is compared with wild-type Jurkat cells and to a parental J.CaM2.5 cell line (which behaves essentially identically as the NTAL-low expressing clone).

Mouse Genomic Clones. LAT genomic clones were isolated from a 129/Ola phage library and sequenced. The GenBank/EMBL/DDBJ accession no. corresponding to mouse LAT is AJ438435. Part of the sequence of the mouse *LAT* gene can be found on a contig present in the Ensembl Gene report (Ensembl gene ID: ENSMUSG00000030742; http://www.ensembl.org/Mus_musculus/), allowing the location of the *LAT* gene to chromosome 7.

Confocal Microscopy. THP-1 cells and J.CaM2.5-NTAL transfectants were spun on coverslips coated with poly-L-lysine (Sigma-Aldrich), fixed, and permeabilized 3 min in −20°C methanol and then 5 s in cold acetone. After washing in PBS the slides were blocked with PBS containing 1% bovine serum albumin and 20% human AB serum and incubated for 45 min with mouse mAb to NTAL (NAP-7, 50 μg/ml), followed by 45 min incubation with Alexa 488 goat anti–mouse IgG (Molecular Probes, 500× diluted). Nuclei were stained with propidium iodide (10 min, 0.5 μg/ml). The samples were mounted in PBS and viewed with a Laserscan microscope (Leica TCS SP). Incubation with irrelevant primary antibody served as a negative control.

Tissue Section Immunostaining. Sample of intestinal tissue biopsy from a colorectal carcinoma patient (including a normal tissue with local lymph nodes) was fixed with 10% neutral buffered formalin, embedded into parafin, and 4-μm thick tissue sections were cut. The preparation was dipped into citrate buffer pH 6.0 and treated in a microwave oven (2 × 5 min; 750 W). After blocking endogenous peroxidase activity by 1.5% H_2O_2 in methanol for 20 min, tissue sections were incubated sequentially with hybridoma supernatant containing anti-NTAL mouse monoclonal antibody, biotinylated anti–mouse antibody (Jackson ImmunoResearch Laboratories), streptavidin-conjugated horseradish peroxidase (Biogenex), and 3,3-diaminobenzidine.

Cell Activation. THP-1 cells were incubated 30 min on ice with an irrelevant mouse IgG2a monoclonal antibody (50 μg/ml in HBSS) which binds in the monomeric form selectively to the human high affinity IgG receptor (FcγRI; CD64; reference 22) and then 20 min at 37°C in culture medium. Ligated Fcγ-receptors were then cross-linked with polyclonal goat anti–mouse antibody (Sigma-Aldrich; 20 μg/ml; 2 min at 37°C), cooled down in ice-water bath for 1 min, spun down 1 min at 2°C, and immediately detergent solubilized. In some experiments THP-1 cells were stimulated in the presence of kinase inhibitors. Purified monocytes were stimulated using a similar protocol, except that they were first incubated with human AB serum and the ligated Fcγ-receptors were then cross-linked with polyclonal rabbit anti–human Ig antibody (Jackson ImmunoResearch Laboratories). BMMCs from wild-type mice or from mice with a genetically disrupted Lyn gene (BMMC-$Lyn^{-/-}$) were sensitized with monoclonal IgE (IGEL b4 1; 1 μg/ml) and the ligated FcεRIs were aggregated with 2,4,6-trinitrophenyl (TNP)-BSA conjugate (1 μg/ml; 5 min at 37°C) as described elsewhere (23). Ramos B cells were activated by incubation for 2 min at 37°C with $F(ab)_2$ fragments of goat anti–human IgM (Jackson ImmunoResearch Laboratories). Mouse B cells present in the unseparated splenocyte suspension (10^8 cells/ml) were stimulated 30 s with $F(ab)_2$ fragments of goat anti–mouse IgM (20 μg/ml; Jackson ImmunoResearch

Laboratories). In vitro activation of Jurkat T cells, J.CaM2.5 mutants, and J.CaM2.5-NTAL stable transfectants was performed using soluble IgM anti-CD3 mAb MEM-92 (100–250× diluted ascitic fluid containing approximately 8 mg/ml mAb, at 37°C for 5 min). Activated (phosphorylated) Erk1/2 was determined by immunoblotting of the total cell lysates using phospho-Erk specific antibody (New England Biolabs, Inc.). J.CaM2.5 cells transiently transfected with the FLAG-tagged LAT, NTAL, or TRIM constructs were 18 h after the transfection stimulated for 2 min with a combination of anti-TCR (C305) and anti-CD28 IgM mAbs (hybridoma supernatants) and phospho-Erk1/2 and FLAG epitope were determined in their detergent lysates by Western blotting.

Flow Cytometry Analysis of Calcium Mobilization. Jurkat, J.CaM2.5, and J.CaM2.5-NTAL cells were loaded with fluorescent Ca^{2+} indicators Fura Red and Fluo-4 (9.2 μM and 3.6 μM, respectively; Molecular Probes) in HBSS containing 10 mM HEPES (Sigma-Aldrich) and 4 mM Probenecid (Sigma-Aldrich), for 20 min in dark and at room temperature. The cells were washed twice in HBSS containing 10 mM HEPES and 1% fetal calf serum (HBSS/FCS), resuspended to final concentration of 10^6 per ml, rested for 15 min in dark, and preheated for 15 min at 37°C before the measurement performed at 37°C. After 1 min, anti-CD3 (MEM-92) mAb (100× diluted ascitic fluid containing approximately 8 mg/ml mAb) at 10 μg/ml final concentration was added and the measurement was continued for additional 5 min. Finally, adequacy of cellular loading was verified by treating the cells with ionomycin (Sigma-Aldrich; 2 μg/ml final concentration). Data were acquired on FACSort™ flow cytometer (Becton Dickinson) at 500 ms time points and ratiometric analysis was performed with Flow Jo software (Tree Star).

Results

NTAL Is a Transmembrane Adaptor Protein Similar to LAT. In vitro kinase assays performed on GEMs immunoprecipitated from myeloid cell lines HL-60 and THP-1 revealed the presence of an unidentified 30 kD phosphoprotein (pp30) which was not detectable under similar conditions in T cells (Fig. 1 A). To further characterize this protein, the in vitro labeled proteins were mixed with GEMs prepared from 5×10^8 THP-1 cells as described previously (18). This mixture was then subjected to two-dimensional gel electrophoresis and a doublet of acidic protein spots of 29–30 kD visualized by silver staining was found to colocalize with radiolabeled pp30 (Fig. 1 B). The spots were excised, digested in-gel with trypsin, and resulting peptides were analyzed by mass spectrometry (MALDI-TOF). Database searching revealed that six of the peptides (Table I) fit precisely to those predicted for a so far uncharacterized protein encoded by a previously cloned full-length cDNA corresponding to a broadly expressed human gene termed *WBSCR5* which is located on human chromosome 7 (7q11.23; references 24 and 25). The *WBSCR5* cDNA codes for a polypeptide of 243 amino acid residues (Fig. 2) and a predicted molecular weight of 26.550 daltons while the predicted mouse homologue is shorter by 40 amino acid residues and is encoded by a gene residing on chromosome 5 (25). The protein resembles in its general organization the GEM-associated transmembrane adaptor proteins PAG/Cbp (18, 26) and LAT (4). Thus, it consists of a very short NH_2-terminal extracellular peptide (6aa), a single putative hydrophobic transmembrane domain which is followed by a potential palmitoylation site (a CxxC motif). The predicted cytoplasmic domain contains a total of 10 tyrosines but no other clearly recognizable motifs. Importantly, the mouse *LAT* and *WBSCR5* genes show a strikingly similar organization. Both of them are composed of 11 exons that split the respective coding sequence in a very similar manner (Fig. 3). The two genes (residing on different chromosomes) also display the same splice frame diagrams (Fig. 3) further suggesting that they are closely related and likely are derived from a common ancestor (see Discussion). Because of the structural similarity to LAT and its broad expression we termed to the novel protein NTAL.

Based on the published cDNA sequence of human *WBSCR5*, a full length NTAL cDNA was obtained by PCR from human leukocyte cDNA library and subcloned into bacterial (pET-15b) or eukaryotic (pEFIRES-N) expression vectors. Rabbit polyclonal and mouse monoclonal antibodies raised to the bacterially produced major part of the cytoplasmic domain of NTAL detected a band of the appropriate size in the LAT-deficient Jurkat variant JCaM2.5 following expression of NTAL (Fig. 4 A).

Western blotting further demonstrated absence of NTAL in peripheral blood T cells, moderate expression in monocytes, and strong expression in peripheral blood B lymphocytes and NK cells (Fig. 4 B); NTAL is also strongly expressed in B cell lines Raji and Ramos and myeloid lines

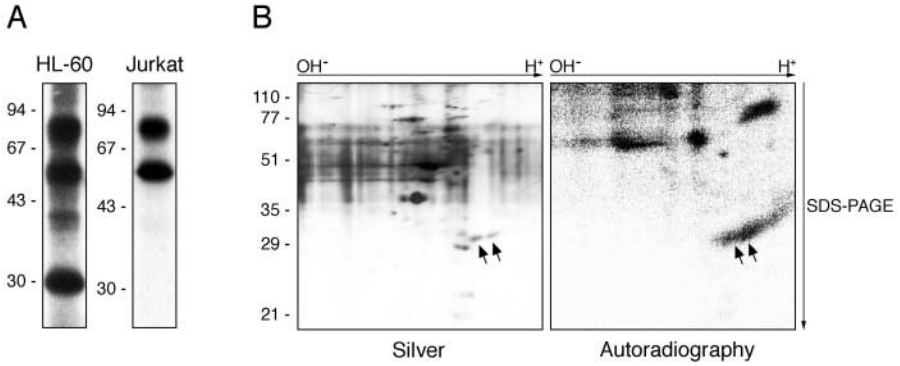

Figure 1. NTAL isolation. (A) Proteins of myeloid cell (HL-60) vs. T cell (Jurkat) membrane microdomains (GEMs) phosphorylated under the conditions of the in vitro kinase assay; a pattern very similar to that of HL-60 was observed also in the case of the THP-1 cell preparation (unpublished data). (B) Proteins of THP-1 GEMs were mixed with the preparation obtained by in vitro kinase assay, separated by 2-dimensional gel electrophoresis and detected by silver staining or autoradiography. Arrows indicate the position of pp30.

Table I. *Tryptic Peptides Identified by Mass Spectrometry*

Position of peptide in the polypeptide chain	Measured masses $[M+H]^+$	Calculated masses $[M+H]^+$
146-161		
$+C_2H_3ON$@Cys[a]	1,677.7	1,677.8
80–94	1,722.8	1,722.9
78–94	1,965.9	1,966.0
57–76	2,131.0	2,131.1
57-76		
+O@Met[b]	2,147.0	2,147.1
57-76		
+20@Met[c]	2,163.0	2,163.1
57–77	2,259.0	2,259.1
57-77		
+O@Met[b]	2,275.0	2,275.1
57-77		
+2O@Met[c]	2,291.0	2,291.1
104–123	2,400.9	2,401.0
104-123		
+O@Met[b]	2,416.9	2,417.0
104-123		
+2O@Met[c]	2,432.9	2,433.0

The six peptides and their derivatives shown in the table fit unequivocally to the WBSCR5 gene product (AAF74978) and covered 30% of its predicted sequence.
[a]Carbamidomethylation of cysteine (due to iodoacetamide present in the lysis buffer).
[b]Mono-oxidation of methionine.
[c]Di-oxidation of methione.

THP-1 and HL-60 but not in T cell lines HPB-ALL and Jurkat (unpublished data). Immunohistochemical staining of paraffin tissue sections revealed a particularly strong expression in germinal centers of human lymph nodes (Fig. 5 A). As expected, NTAL is mostly present in buoyant GEMs (Fig. 5 B), it can be biosynthetically labeled by ^{3}H-palmitate (Fig. 5 C), and clearly localizes to the plasma membrane (Fig. 5 D).

```
  1  MSSGTELLWP GAALLVLLGV AASLCVRCSR PGAKRSEKIY
 41  QQRSLREDQQ SFTGSRTYSL VGQAWPGPLA DMAPTRKDKL
 81  LQFYPSLEDP ASSRYQNFSK GSRHGSEEAY IDPIAMEYYN
121  WGRFSKPPED DDANSYENVL ICKQKTTETG AQQEGIGGLC
161  RGDLSLSLAL KTGPTSGLCP SASPEEDEES EDYQNSASIH
201  QWRESRKVMG QLQREASPGP VGSPDEEDGE PDYVNGEVAA
241  TEA
```

Figure 2. Predicted amino acid sequence of human NTAL (product of the *WBSCR5* gene). The putative transmembrane region is boxed, the potential palmitoylation sequence, the tyrosine-x-asparagine motifs, and all other tyrosines are in bold and underlined. These sequence data are available from GenBank/EMBL/DDBJ under accession no. AAF74978.

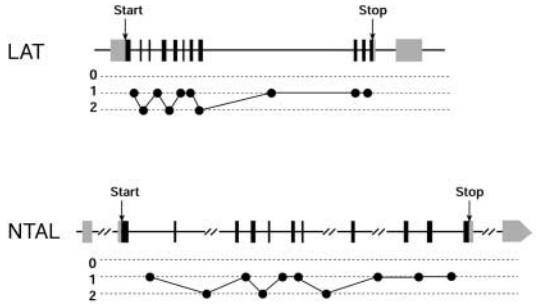

Figure 3. Comparison of the exon-intron organization and of the splice frame diagrams of the mouse genes encoding LAT and NTAL, respectively. Exons are shown by boxes; the positions of the initiation (Start) and termination (Stop) codons are indicated by vertical arrows. Based on splice frame junctions, three types of introns can be distinguished in a given gene: phase 0 intron interrupts the reading frame between two consecutive codons, whereas phase 1 and phase 2 introns interrupt the reading frame between the first and the second nucleotide of a codon or between the second and the third nucleotide of a codon, respectively (reference 40). According to that classification, the phase class of each intron is indicated by a solid circle on the diagram shown below each gene. For the sake of clarity, the length of introns is not drawn to scale. The structure of the mouse NTAL (*WBSCR5*) gene is reported in (reference 25) and that of LAT in this paper.

NTAL Is Tyrosine-phosphorylated after FcγRI, FcεRI, or BCR Cross-linking and Becomes Associated with Other Signaling Proteins. The overall similarity of NTAL to LAT and the results of in vitro kinase assay indicated that NTAL might be inducibly tyrosine-phosphorylated after triggering of immunoreceptors. Indeed, NTAL became tyrosine-phosphorylated and associated with additional phosphoproteins following cross-linking of the high-affinity IgG-receptor (FcγRI/CD64) on human THP-1 myeloid cells and blood monocytes, the high-affinity IgE-receptor (FcεRI) on mouse BMMCs, and the BCR on human Ramos and mouse splenic B cells (Fig. 6 A).

The major proteins inducibly associating with NTAL in cells activated via the BCR or the FcγRI were identified as

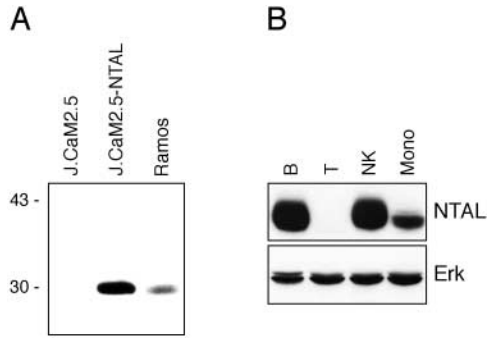

Figure 4. Expression of NTAL. (A) cDNA encoding human NTAL was expressed in J.CaM2.5 cells and the protein product was visualized by Western blotting of the transfectants detergent lysate as compared with Ramos cells (expressing endogenous NTAL). (B) Western blotting of the indicated subpopulations of human peripheral blood cells (immunostaining for NTAL or Erk; the latter was used as a loading control).

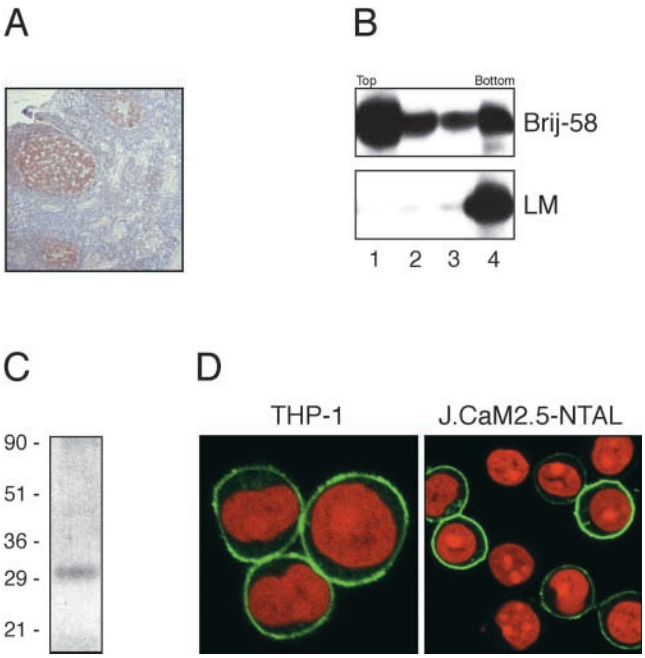

Figure 5. Tissue and subcellular localization of NTAL. (A) Paraffin section of lymphoid tissue immunoperoxidase stained for NTAL; the major positive structures are germinal centers. (B) Localization of NTAL in buoyant detergent-resistant microdomains (GEMs). THP-1 cells were solubilized in the presence of 3% nonionic detergent Brij-58 or 1% laurylmaltoside (LM; a detergent known to disrupt GEMs) and subjected to sucrose density gradient ultracentrifugation; the fractions (numbered from top to bottom) were analyzed by Western blotting. (C) Biosynthetic labeling of NTAL with [^{3}H]palmitate; NTAL immunoprecipitate was analyzed by SDS-PAGE followed by fluorography of the gel. (D) Plasma membrane localization of NTAL (green) as determined by confocal microscopy in THP-1 cells and J.CaM2.5-NTAL transfectants; nuclei are shown in red.

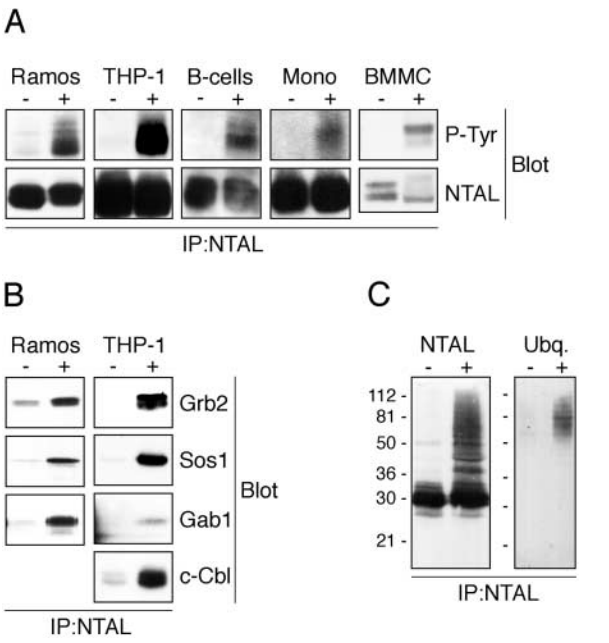

Figure 6. Induction of NTAL tyrosine phosphorylation and association with cytoplasmic signaling proteins. (A) THP-1 cells or purified human monocytes were stimulated via their FcγRI receptors, Ramos cells or murine B lymphocytes via BCR, and mouse BMMC via FcεRI receptors. NTAL was immunoprecipitated from unstimulated (−) or stimulated (+) cells and analyzed by SDS-PAGE and Western blotting using anti-phosphotyrosine antibody to visualize tyrosine-phosphorylated NTAL (top panel). The bottom panel represents immunostaining of NTAL in the same samples and in the same position of the blot (around 30 kD). (B) The same NTAL immunoprecipitates as shown in part A were analyzed by Western blotting using antibodies to the indicated associated molecules. (C) Blots of NTAL immunoprecipitates from unstimulated (−) or anti-BCR-stimulated (+) Ramos cells were immunostained by antibodies to NTAL or ubiquitin (Ubq.). Only the relevant parts of the blots are shown in parts A and B, corresponding to the size of the relevant proteins.

Grb2, Sos1, and Gab1 (in both Ramos and THP-1 cells) and c-Cbl (only in THP-1; Fig. 6 B). A fraction of the NTAL protein immunoprecipitated from detergent lysate of anti-BCR–stimulated Ramos cells exhibited strongly decreased electrophoretic mobility indicative of possible attachment of multiple ubiquitin residues. This was confirmed directly by Western blotting of NTAL immunoprecipitates prepared from BCR-triggered Ramos cells (Fig. 6 C). Maximum level of NTAL tyrosine phosphorylation in Ramos cells was observed already after 15 s of stimulation, whereas the maximal ubiquitinylation was seen after >3 min (unpublished data).

To determine which protein tyrosine kinases (PTKs) are able to phosphorylate NTAL, we treated THP-1 cells with the Src-family PTK inhibitor PP2 or the Syk-family PTK inhibitor piceatannol and then stimulated them via FcγRI cross-linking. As shown in Fig. 7 A, both inhibitors suppressed tyrosine phosphorylation of NTAL. Coexpression of NTAL with Src-family kinases Lck, Lyn, Hck, or Yes and/or Syk or ZAP-70 in 293T-cells indicated that NTAL was, similarly as LAT, most strongly phosphorylated in the presence of simultaneously expressed Lck and ZAP-70 or Lck and Syk (Fig. 7 B). Furthermore, no tyrosine phosphorylation of NTAL was observed in Lyn$^{-/-}$ mouse BMMCs stimulated via FcεRI (compare Fig. 6 A for the wild-type BMMCs) indicating that Lyn is directly or indirectly responsible for NTAL inducible phosphorylation in these cells (unpublished data).

Expression of NTAL Can Partially Compensate for LAT Deficiency in T Cells. To assess whether NTAL could exert a LAT-like function, NTAL was stably expressed in the LAT-deficient Jurkat variant J.CaM2.5 (which also does not express NTAL). After stimulation of the transfectants with an agonistic CD3 mAb, NTAL became rapidly tyrosine-phosphorylated and associated with Grb2, Sos1, and c-Cbl (Fig. 8 A) but not with SLP-76 or PLCγ1 (unpublished data). CD3 stimulation was accompanied by a minimal (but reproducible) and transient increase in cytoplasmic calcium level (Fig. 8 B) and a partial rescue of Erk1/2 phosphorylation (Fig. 8 C). To compare semiquantitatively the effects of NTAL expression with that of LAT, J.CaM2.5 cells were transiently transfected with expression constructs encoding FLAG-tagged LAT, NTAL, TRIM, or with the vector only and activation of Erk1/2 was followed after anti-CD3 plus anti-CD28 stimulation. As shown in Fig. 8 D, NTAL partially rescued activation of

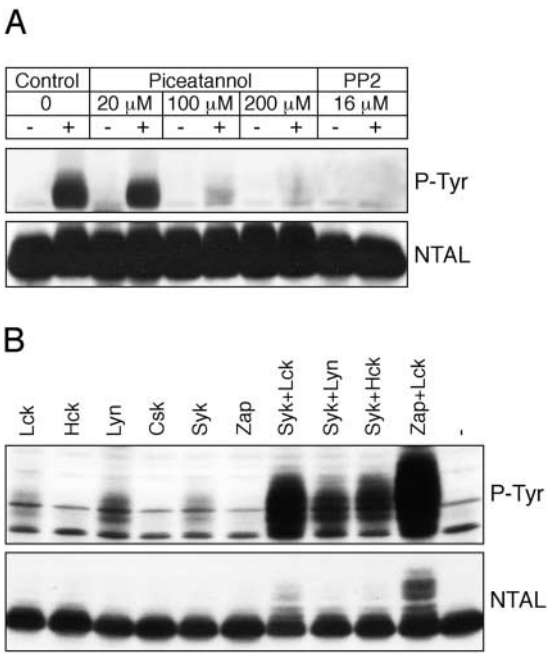

Figure 7. Kinases phosphorylating NTAL. (A) Inhibition of NTAL tyrosine phosphorylation in THP-1 cells stimulated via FcγRI by the indicated PTK inhibitors. NTAL immunoprecipitates prepared from the treated and control cells were analyzed by Western blotting to detect P-Tyr or NTAL, respectively. (B) Phosphorylation of NTAL coexpressed in 293T cells with various Src- and Syk-family kinases. Total cell lysates were analyzed by SDS-PAGE and Western blotting to detect the indicated molecules.

Erk1/2 when expressed at a level comparable to that of LAT under the same conditions while expression of TRIM had no effects even at much higher expression level. Thus, the ectopically expressed NTAL can partially restore at least some aspects of TCR signaling in LAT-deficient mutants.

Discussion

The new transmembrane adaptor protein NTAL described in this paper (a product of the previously described gene *WBSCR5;* references 24 and 25) appears to be structurally closely related to the critical component of the TCR signaling pathway, LAT (4). Moreover, the organization of the genes encoding LAT and NTAL, respectively, is also similar, indicating they probably have a common evolutionary origin. Interestingly, the expression pattern of NTAL in lymphocytes is largely complementary to that of LAT: while LAT is predominantly found in T but not B lymphocytes, the reverse is true for NTAL. Among the important features of the structure of NTAL is a potential palmitoylation site (CxxC) adjacent to the transmembrane domain that is presumably responsible for targeting the protein to membrane microdomains (rafts, GEMs). Furthermore, there are five potential Grb2 binding motifs (YxN). Our data using PTK inhibitors (Fig. 7) and coexpression of NTAL and PTKs in 293T cells indicate that NTAL, again similarly to LAT, is phosphorylated by concerted action of Src- and Syk-family kinases (presumably the Src-family kinases are needed for activation of the Syk family kinases).

Induction of NTAL tyrosine phosphorylation after BCR cross-linking is reminiscent of the phosphorylation of LAT that is induced by TCR ligation (4). Similar to LAT in activated T cells, NTAL immunoprecipitated from BCR-stimulated B lymphocytes is associated with the cytoplasmic linker protein Grb2 and the nucleotide exchange factor of the small G-protein Ras, Sos1 (27). Surprisingly, and in clear contrast to LAT, we never observed an inducible association of NTAL with PLCγ or another cytoplasmic adaptor protein, SLP-76 (or its B cell analogue SLP-65/BLNK; references 28 and 29), both of which are key components of the multicomponent complex that is organized by activated (tyrosine-phosphorylated) LAT (5). This could suggest that the role of NTAL in BCR signaling differs from that of LAT in the TCR signaling; namely, that NTAL may be involved only in activation of the Grb2/Sos1-initiated pathway(s) but not in activation of the PLCγ-Ca^{2+} pathway. The finding of the adaptor protein Gab1 in the NTAL immunoprecipitates may further suggest that the NTAL-Grb2-Gab1 complex possibly regulates the activity of PI3-K in stimulated cells (30–32), but this remains a speculation at this moment.

The lack of association of SLP-65 and PLCγ with phosphorylated NTAL may further indicate that SLP-65 does not require a LAT-like molecule in B cells for being targeted to the plasma membrane. Indeed, recent data suggested that SLP-65 binds directly with its Src-homology 2 (SH2)-domain to a highly conserved non-ITAM tyrosine motif within the cytoplasmic domain of CD79a (Igα; references 33 and 34). Moreover in contrast to SLP-76, phosphorylated SLP-65 binds SH2 domains of PLCγ2 (35). Thus, it is tempting to speculate that the multiple functions that LAT exerts in T cells are shared in B lymphocytes between NTAL and other molecules, for example, CD79a.

Similarly to the situation in B cells, NTAL becomes strongly tyrosine phosphorylated after cross-linking of FcγRI and FcεRI and then associates with Grb2 and Sos1 (but again not with PLCγ and also not with SLP-76). Thus, also in these cells NTAL seems to be involved in linking the activated immunoreceptors to the Grb2/Sos pathway. In contrast to activated B cells, NTAL also interacts with c-Cbl in activated THP-1 cells (Fig. 6). LAT has been shown to be important for processing of the FcγRI and FcεRI mediated signals; however, FcγRI and FcεRI signaling in $LAT^{-/-}$ cells is still partially functional (12, 13). It is therefore tempting to speculate that this residual Fc-receptor signaling capacity in myeloid cells is due to the presence of NTAL. It is important to note that FcγRI (CD64) is the only human Fc-receptor that binds soluble monomeric murine antibodies of the IgG2a isotype with sufficient affinity (22). This indicates that under the used experimental conditions only this Fcγ-receptor became activated in our experiments with the THP-1 cells. Furthermore, an identical pattern of NTAL phosphorylation was observed in the THP-1 cells when FcγRI (CD64) was di-

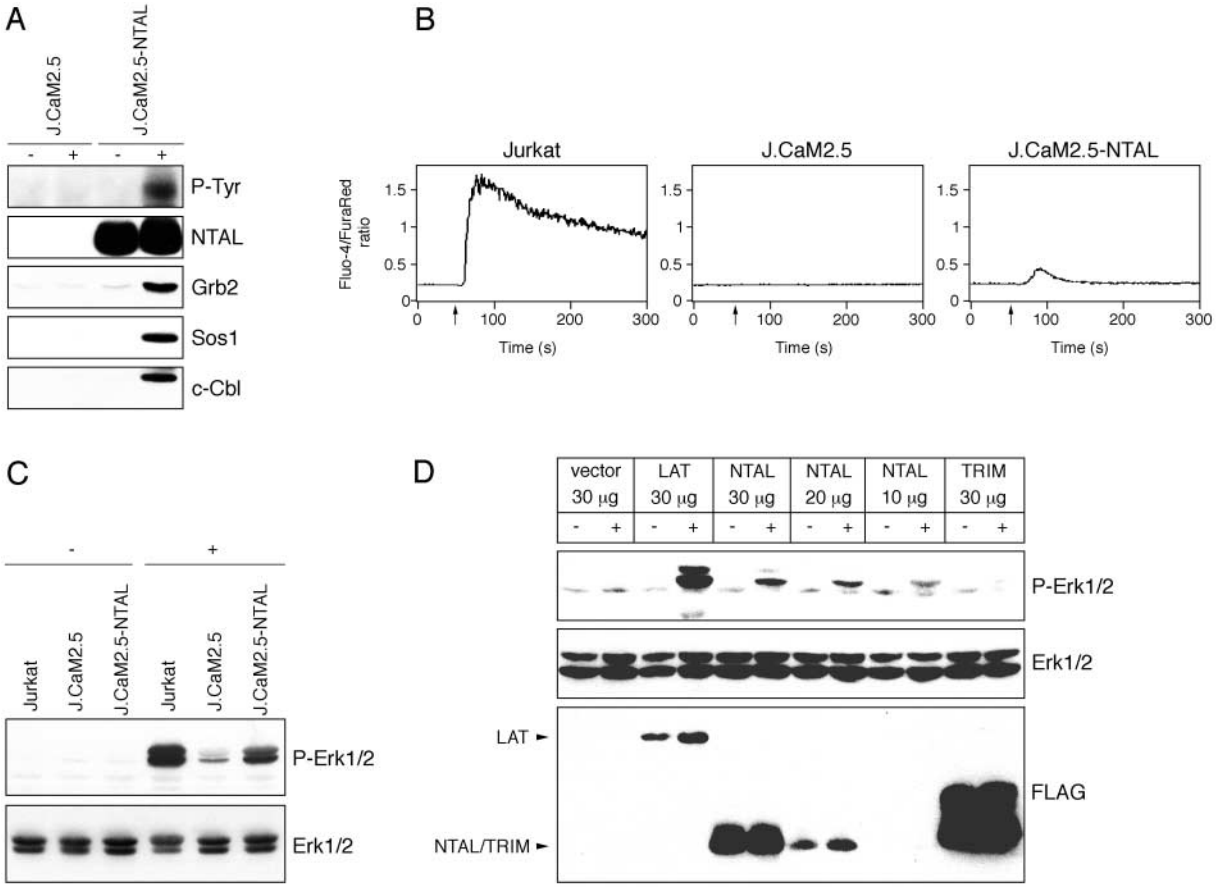

Figure 8. Functional analysis of NTAL in LAT-defective J.CaM2.5 transfectants. (A) NTAL immunoprecipitates obtained from unstimulated (−) or anti-CD3 stimulated (+) J.CaM2.5 mutants and J.CaM2.5-NTAL transfectants were analyzed by Western blotting for the presence of the indicated molecules. The top panel corresponds to tyrosine-phosphorylated NTAL (30 kD). (B) Wild-type Jurkat, J.CaM2.5, and J.CaM2.5-NTAL transfectants were stimulated by anti-CD3 IgM mAb (added at time points indicated by arrows) and increase of cytoplasmic Ca^{2+} was measured. (C) Wild-type Jurkat, J.CaM2.5, and J.CaM2.5-NTAL transfectants were stimulated by optimally diluted anti-CD3 IgM mAb and after 5 min of activation Erk1/2 was detected in the cell lysates by Western blotting using anti-phospho Erk antibody; bottom panel represents control staining by anti-Erk. (D) J.CaM2.5 cells transiently transfected with the indicated FLAG-tagged constructs were stimulated for 2 min by anti-CD3 and anti-CD28 mAbs and activation of Erk1/2 was detected as in C (top panel); presence of equal amounts of Erk1/2 in all samples was ascertained (middle panel) and the level of expression of individual FLAG-tagged proteins was determined (bottom panel).

rectly cross-linked by a CD64-specific monoclonal antibody; in contrast, no phosphorylation was observed after direct mAb-mediated cross-linking of FcγRII (CD32) or FcγRIII (CD16) in these cells (unpublished data).

Our experiments provide preliminary evidence for a functional LAT-like role of NTAL in immunoreceptor signaling: ectopic expression of this protein in LAT-deficient J.CaM2.5 Jurkat T cells partially rescues TCR/CD3-mediated signaling, namely activation of Erk1/2 (Fig. 8). The minimal calcium response accompanying the CD3-mediated stimulation may be in agreement with the observed lack of coprecipitation of PLCγ and SLP-76 with activated NTAL in these transfectants, as discussed above. The striking conservation of the exon-intron organization of the genes encoding LAT and NTAL, respectively (Fig. 3), suggests that they probably derive from a duplication of an ancestral gene. As reported for other gene families, in the course of evolution, the original position of the exon borders has been blurred by splice junction sliding (36). It is important to note that the exon-intron organization and splice frame diagram of genes encoding other transmembrane adaptor proteins involved in immunoreceptor signaling, e.g., SIT (37) or TRIM (38) differ totally from the distinctive organization found in the genes enconing LAT and NTAL. A similar relationship of gene organization was previously noted for the functionally closely related signal transducing subunits of several immunoreceptors (39). Thus, NTAL appears to be structurally, evolutionarily and probably also functionally related to the transmembrane adaptor protein LAT.

We would like to thank Drs. R. Abraham, M. Hibbs, S. Hobbs, W. Kolanus, G. Langsley, S. Watson, and A. Weiss for kindly providing us with cells and constructs as specified in Materials and Methods.

This work was supported from the projects Center of Molecular and Cellular Immunology (LN00A026) and grant no. 1131000001 from Ministry of Education, Youth and Sports of the Czech Re-

public, grant J1116W24Z from the Wellcome Trust (to V. Hořejší), Research Center Immunology Magdeburg/Halle, Sachsen-Anhalt (supported by grant 01 ZZ 0110 of the Bundesministerium für Bildung und Forschung to B. Schraven); P. Dráber is supported by an International Research Scholar's Award from Howard Hughes Medical Institute, M. Malissen is supported by Centre National de la Recherche Scientifique and Institut National de la Sante et de la Recherche Medicale, and E. Aguado was supported by a fellowship from the European Communities.

Submitted: 13 August 2002
Revised: 30 October 2002
Accepted: 6 November 2002

References

1. van Leeuwen, J.E., and L.E. Samelson. 1999. T cell antigen-receptor signal transduction. *Curr. Opin. Immunol.* 11:242–248.
2. Reth, M. 2001. Oligomeric antigen receptors: a new view on signaling for the selection of lymphocytes. *Trends Immunol.* 22:356–360.
3. Turner, H., and J.P. Kinet. 1999. Signalling through the high-affinity IgE receptor FcεRI. *Nature.* 402:B24–B30.
4. Zhang, W., J. Sloan-Lancaster, J. Kitchen, R.P. Trible, and L.E. Samelson. 1998. LAT: the ZAP-70 tyrosine kinase substrate that links T cell receptor to cellular activation. *Cell.* 92: 83–92.
5. Zhang, W., R.P. Trible, M. Zhu, S.K. Liu, C.J. McGlade, and L.E. Samelson. 2000. Association of Grb2, Gads, and phospholipase C-γ1 with phosphorylated LAT tyrosine residues. Effect of LAT tyrosine mutations on T cell angigen receptor-mediated signaling. *J. Biol. Chem.* 275:23355–23361.
6. Zhang, W., R.P. Trible, and L.E. Samelson. 1998. LAT palmitoylation: its essential role in membrane microdomain targeting and tyrosine phosphorylation during T cell activation. *Immunity.* 9:239–246.
7. Brdička, T., J. Černý, and V. Hořejší. 1998. T cell receptor signalling results in rapid tyrosine phosphorylation of the linker protein LAT present in detergent-resistant membrane microdomains. *Biochem. Biophys. Res. Commun.* 248:356–360.
8. Harder, T. 2001. Raft membrane domains and immunoreceptor functions. *Adv. Immunol.* 77:45–92.
9. Cherukuri, A., M. Dykstra, and S.K. Pierce. 2001. Floating the raft hypothesis: lipid rafts play a role in immune cell activation. *Immunity.* 14:657–660.
10. Langlet, C., A.M. Bernard, P. Drevot, and H.T. He. 2000. Membrane rafts and signaling by the multichain immune recognition receptors. *Curr. Opin. Immunol.* 12:250–255.
11. Zhang, W., C.L. Sommers, D.N. Burshtyn, C.C. Stebbins, J.B. DeJarnette, R.P. Trible, A. Grinberg, H.C. Tsay, H.M. Jacobs, C.M. Kessler, et al. 1999. Essential role of LAT in T cell development. *Immunity.* 10:323–332.
12. Tridandapani, S., T.W. Lyden, J.L. Smith, J.E. Carter, K.M. Coggeshall, and C.L. Anderson. 2000. The adapter protein LAT enhances Fcγ receptor-mediated signal transduction in myeloid cells. *J. Biol. Chem.* 275:20480–20487.
13. Saitoh, S., R. Arudchandran, T.S. Manetz, W. Zhang, C.L. Sommers, P.E. Love, J. Rivera, and L.E. Samelson. 2000. LAT is essential for FcεRI-mediated mast cell activation. *Immunity.* 12:525–535.
14. Hibbs, M.L., D.M. Tarlinton, J. Armes, D. Grail, G. Hodgson, R. Maglitto, S.A. Stacker, and A.R. Dunn. 1995. Multiple defects in the immune system of Lyn-deficient mice, culminating in autoimmune disease. *Cell.* 83:301–311.
15. Finco, T.S., T. Kadlecek, W. Zhang, L.E. Samelson, and A. Weiss. 1998. LAT is required for TCR-mediated activation of PLCγ1 and the Ras pathway. *Immunity.* 9:617–626.
16. Liang, Q., G. Schurmann, M. Betzler, and S.C. Meuer. 1991. Activation and signaling status of human lamina propria T lymphocytes. *Gastroenterology.* 101:1529–1536.
17. Cinek, T., and V. Hořejší. 1992. The nature of large noncovalent complexes containing glycosyl-phosphatidylinositol-anchored membrane glycoproteins and protein tyrosine kinases. *J. Immunol.* 149:2262–2270.
18. Brdička, T., D. Pavlištová, A. Leo, E. Bruyns, V. Kořínek, P. Angelisová, J. Scherer, A. Shevchenko, I. Hilgert, J. Černý, et al. 2000. Phosphoprotein associated with glycosphingolipid-enriched microdomains (PAG), a novel ubiquitously expressed transmembrane adaptor protein, binds the protein tyrosine kinase Csk and is involved in regulation of T cell activation. *J. Exp. Med.* 191:1591–1604.
19. Swerdlow, P.S., D. Finley, and A. Varshavsky. 1986. Enhancement of immunoblot sensitivity by heating of hydrated filters. *Anal. Biochem.* 156:147–153.
20. Hobbs, S., S. Jitrapakdee, and J.C. Wallace. 1998. Development of a bicistronic vector driven by the human polypeptide chain elongation factor 1alpha promoter for creation of stable mammalian cell lines that express very high levels of recombinant proteins. *Biochem. Biophys. Res. Commun.* 252:368–372.
21. Kirchgessner, H., J. Dietrich, J. Scherer, P. Isomaki, V. Korinek, I. Hilgert, E. Bruyns, A. Leo, A.P. Cope, and B. Schraven. 2001. The transmembrane adaptor protein TRIM regulates T cell receptor (TCR) expression and TCR-mediated signaling via an association with the TCR zeta chain. *J. Exp. Med.* 193:1269–1283.
22. van de Winkel, J.G., and P.J. Capel. 1993. Human IgG Fc receptor heterogeneity: molecular aspects and clinical implications. *Immunol. Today.* 14:215–221.
23. Kovářová, M., P. Tolar, R. Arudchandran, L. Dráberová, J. Rivera, and P. Dráber. 2001. Structure-function analysis of Lyn kinase association with lipid rafts and initiation of early signaling events after Fcε receptor I aggregation. *Mol. Cell. Biol.* 21:8318–8328.
24. Osborne, L.R., D. Martindale, S.W. Scherer, X.M. Shi, J. Huizenga, H.H. Heng, T. Costa, B. Pober, L. Lew, J. Brinkman, et al. 1996. Identification of genes from a 500-kb region at 7q11.23 that is commonly deleted in Williams syndrome patients. *Genomics.* 36:328–336.
25. Martindale, D.W., M.D. Wilson, D. Wang, R.D. Burke, X. Chen, V. Duronio, and B.F. Koop. 2000. Comparative genomic sequence analysis of the Williams syndrome region (LIMK1-RFC2) of human chromosome 7q11.23. *Mamm. Genome.* 11:890–898.
26. Kawabuchi, M., Y. Satomi, T. Takao, Y. Shimonishi, S. Nada, K. Nagai, A. Tarakhovsky, and M. Okada. 2000. Transmembrane phosphoprotein Cbp regulates the activities of Src-family tyrosine kinases. *Nature.* 404:999–1003.
27. Cullen, P.J., and P.J. Lockyer. 2002. Integration of calcium and Ras signalling. *Nat. Rev. Mol. Cell Biol.* 3:339–348.
28. Wienands, J., J. Schweikert, B. Wollscheid, H. Jumaa, P.J. Nielsen, and M. Reth. 1998. SLP-65: a new signaling component in B lymphocytes which requires expression of the antigen receptor for phosphorylation. *J. Exp. Med.* 188:791–

795.
29. Fu, C., C.W. Turck, T. Kurosaki, and A.C. Chan. 1998. BLNK: a central linker protein in B cell activation. *Immunity*. 9:93–103.
30. Liu, Y., and L.R. Rohrschneider. 2002. The gift of Gab. *FEBS Lett*. 515:1–7.
31. Ingham, R.J., M. Holgado-Madruga, C. Siu, A.J. Wong, and M.R. Gold. 1998. The Gab1 protein is a docking site for multiple proteins involved in signaling by the B cell antigen receptor. *J. Biol. Chem*. 273:30630–30637.
32. Ingham, R.J., L. Santos, M. Dang-Lawson, M. Holgado-Madruga, P. Dudek, C.R. Maroun, A.J. Wong, L. Matsuuchi, and M.R. Gold. 2001. The Gab1 docking protein links the B cell antigen receptor to the phosphatidylinositol 3-kinase/Akt signaling pathway and to the SHP2 tyrosine phosphatase. *J. Biol. Chem*. 276:12257–12265.
33. Engels, N., B. Wollscheid, and J. Wienands. 2001. Association of SLP-65/BLNK with the B cell antigen receptor through a non-ITAM tyrosine of Ig-α. *Eur. J. Immunol*. 31: 2126–2134.
34. Kabak, S., B.J. Skaggs, M.R. Gold, M. Affolter, K.L. West, M.S. Foster, K. Siemasko, A.C. Chan, R. Aebersold, and M.R. Clark. 2002. The direct recruitment of BLNK to immunoglobulin α couples the B-cell antigen receptor to distal signaling pathways. *Mol. Cell. Biol*. 22:2524–2535.
35. Ishiai, M., H. Sugawara, M. Kurosaki, and T. Kurosaki. 1999. Association of phospholipase C-2 Src homology 2 domains with BLNK is critical for B cell antigen receptor signaling. *J. Immunol*. 163:1746–1749.
36. Kolkman, J.A., and W.P. Stemmer. 2001. Directed evolution of proteins by exon shuffling. *Nat. Biotechnol*. 19:423–428.
37. Hubener, C., A. Mincheva, P. Lichter, B. Schraven, and E. Bruyns. 2001. Complete sequence, genomic organization, and chromosomal localization of the human gene encoding the SHP2-interacting transmembrane adaptor protein (SIT). *Immunogenetics*. 53:337–341.
38. Hubener, C., A. Mincheva, P. Lichter, B. Schraven, and E. Bruyns. 2000. Genomic organization and chromosomal localization of the human gene encoding the T-cell receptor-interacting molecule (TRIM). *Immunogenetics*. 51:154–158.
39. Malissen, B., and A.M. Schmitt-Verhulst. 1993. Transmembrane signalling through the T-cell-receptor-CD3 complex. *Curr. Opin. Immunol*. 5:324–333.
40. Sharp, P.A. 1981. Speculations on RNA splicing. *Cell*. 23: 643–646.

Appendix 3

The activation of Csk by CD4 interferes with TCR-mediated activatory signalling

Marinari B., **Simeoni L.**, Schraven B., Piccolella E., and Tuosto L. (2003). *Eur J Immunol.* 33:2609-18.

The activation of Csk by CD4 interferes with TCR-mediated activatory signaling

Barbara Marinari[1], Luca Simeoni[2], Burkhart Schraven[2], Enza Piccolella[1] and Loretta Tuosto[1]

[1] Department of Cellular and Developmental Biology, "La Sapienza" University, I-00185 Rome, Italy
[2] Insitute of Immunology Otto-von-Guericke University, Magdeburg, Germany

CD4-Lck recruitment to TCR/CD3, as well as Lck activation is essential for T cell activation. Indeed, the blockage of CD4-Lck recruitment to TCR during antigen recognition exerts a drastic inhibitory effect on T cell activation by interfering with both early and late phases of T cell signaling. In the present work, we report a novel inhibitory mechanism by which CD4 can shut down proximal T cell-activating signals. Indeed, we show that upon ligation of CD4 by antibodies the inhibitory kinase, $p50^{csk}$, is strongly induced and prolonged during the time. In contrast, $p50^{csk}$ was not activated when TCR and CD4 were properly engaged by their ligands. We also demonstrate that anti-CD4 treatment stimulated Csk kinase associated to the membrane adapter, PAG/Cbp, without affecting the total amount of Csk bound to PAG/Cbp. As a consequence, early tyrosine phosphorylation events as well as downstream signaling pathways leading to IL-2 gene expression induced by TCR were inhibited in anti-CD4 pretreated cells. We suggest a new model to explain the activation of negative signals by CD4 molecule.

Received	31/3/03
Revised	13/6/03
Accepted	24/7/03

Key words: CD4 / Csk / TCR

1 Introduction

The coreceptor molecule CD4 plays a crucial role in the early events of T cell activation by contributing to both MHC recognition and intracellular signal transduction. CD4 binds to both engaged TCR and non-polymorphic regions of MHC class II molecules [1, 2], and its cytoplasmic tail interacts with the Src family tyrosine kinase $p56^{lck}$ [3] that is necessary to initiate the immunoreceptor signaling. The earliest event induced by TCR recognition of peptide-MHC molecules is the phosphorylation of tyrosine residues in the immunoreceptor tyrosine-based activation motifs (ITAM) of the CD3 subunits and TCR-associated ζ chain, which leads to the recruitment and activation of ZAP-70 kinase [4]. CD4-associated $p56^{lck}$ contributes to the initial tyrosine phosphorylation of ITAM and interacts with the ζ/ZAP-70 complex, mechanisms proposed to favor CD4 recruitment to the activated TCR [5]. Moreover, $p56^{lck}$ is also involved in the phosphorylation and activation of ζ-associated ZAP-70, which in turn phosphorylates several adapter proteins (*i.e.* LAT and SLP-76) resulting in the activation of downstream signaling events that lead to functional T cell responses [6].

In addition to initiate immunoreceptor signaling, CD4-associated $p56^{lck}$ can also have inhibitory roles. Indeed, CD4 ligation by mAb or HIV gp120 transmits negative signals able to both inhibit TCR signaling [7, 8] and activate apoptotic programs [9, 10]. Several mechanisms have been proposed for the CD4-mediated inhibitory effects, including sequestration of $p56^{lck}$ to the actin-cytoskeleton [11] or sequestration of key components of the TCR/CD3 by the CD4-Lck complexes [8]. A still open question is whether the modulation of CD4-associated Lck kinase activity modifies TCR-dependent kinase signaling cascades by transforming activatory signals into suppressive ones.

Lck kinase activity is regulated by an inhibitory C-terminal tyrosine residue (Tyr505) that when phosphorylated associates with the SH2 domain of $p56^{lck}$ itself, thus leading to the down-regulation of its catalytic activity [12, 13]. A balance between phosphorylated and dephosphorylated $p56^{lck}$ at this C-terminal residue must be maintained to avoid hypo– as well as hyper-reactivity in response to TCR engagement. The tyrosine kinase Csk phosphorylates the inhibitory Tyr505 residue,

[DOI 10.1002/eji.200324064]

Abbreviations: PAG: Glycosphingolipid-enriched microdomains **Cbp:** Csk binding protein **SEE:** Staphylococcal enterotoxin E

 0014-2980/03/0808-2609$17.50+.50/0

whereas the CD45 tyrosine phosphatase antagonizes Csk by dephosphorylating this inhibitory residue [14]. $p50^{csk}$ is a cytoplasmic tyrosine kinase expressed ubiquitously, albeit in greater amounts in hemopoietic cells [15]. $p50^{csk}$ contains an SH3 domain, an SH2 domain and a C-terminal kinase domain. Elimination of $p50^{csk}$ in thymocytes abrogates the requirement for preTCR-mediated signals for the development of mature $\alpha\beta$ T cells [16]. $p50^{csk}$ overexpression strongly inhibits TCR signaling, an effect correlated with its ability to phosphorylate and inactivate Lck and Fyn [17]. More recently, a cooperation between $p50^{csk}$ and the associated proline-enriched protein tyrosine phosphatase PEP, in inhibiting Src kinase mediated signals in T cells, has been described [18]. To negatively regulate Src kinase activities, $p50^{csk}$ must translocate from the cytoplasm to the membrane, specifically to the glycosphingolipid-enriched domains or lipid rafts, which play an important role for the initiation of receptor-mediated signaling, and where the majority of Src kinases are localized [19–21]. One mechanism that has been proposed relies on the interaction of $p50^{csk}$ with a recently cloned phosphoprotein associated with glycosphingolipid-enriched microdomains (PAG) or Csk binding protein (Cbp) [22, 23]. Indeed, in resting normal T cells $p50^{csk}$ is present in lipid rafts through interaction with tyrosine phosphorylated PAG/Cbp, thus inducing a tonic inhibition of T cell activation. The dephosphorylation of PAG/Cbp induced by TCR engagement leads to the dissociation of Csk from lipid rafts and to Lck activation [24]. Therefore, the signals that activate Csk and at the same time inhibit its dissociation from membrane PAG/Cbp may interfere with Lck activation by blocking TCR activating signaling.

Here we report a novel inhibitory mechanism by which CD4 can shut down proximal T cell activating signals. Indeed, we show that upon ligation of CD4 $p50^{csk}$ kinase activity was strongly induced and prolonged during the time. On the contrary, $p50^{csk}$ was not activated when TCR was properly stimulated. We also demonstrate that anti-CD4 treatment induced PAG/Cbp-associated Csk kinase activity without affecting the total amount of Csk bound to PAG/Cbp. As a consequence, TCR-mediated early tyrosine phosphorylation events as well as downstream signaling pathways, which lead to IL-2 gene expression, were inhibited in anti-CD4 pretreated cells. These results support data on the negative effects mediated by Csk, and provide a new model to explain the activation of negative signals by CD4 molecule.

2 Results

2.1 CD4 dissociation from TCR inhibits both earliest and late TCR-mediated signaling events in staphylococcal enterotoxin E-stimulated Jurkat cells

To elucidate the molecular mechanisms regulating anti-CD4 antibodies-mediated inhibition of T cell responses, we used $CD3^+CD4^+CD28^+$ Jurkat cells that, when stimulated with staphylococcal enterotoxin E (SEE) presented by $B7^+$ HLA-DR1-expressing cells (5-3.1/B7) or EBV-B cells, provide a good physiological model of T cell activation [10]. CD4 ligation by Leu3a mAb separately from TCR inhibited both NF-AT- and IL-2-luciferase activities induced by SEE (Fig. 1A, B). The tyrosine phosphorylation of TCR-associated CD3 subunits and ζ chains is one

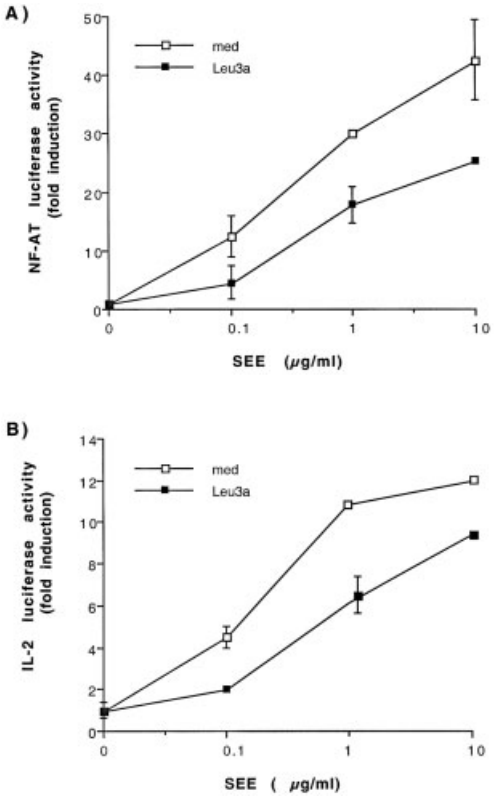

Fig. 1. CD4 engagement by Leu3a inhibits TCR-induced NF-AT and IL-2 promoter activity. (A, B) Jurkat cells were transfected with 10 μg NF-AT (A) or IL-2 (B) luciferase reporter constructs. Cells were then pre-cultured for 15 min in the presence or absence of Leu3a (1:100 dilution) and then stimulated for 8 h with 5-3.1/B7 cells pulsed with different concentrations of SEE. The results are expressed as fold induction over the basal luciferase activity after normalization to β-galactosidase values. The results express the mean ± SD of three different experiments.

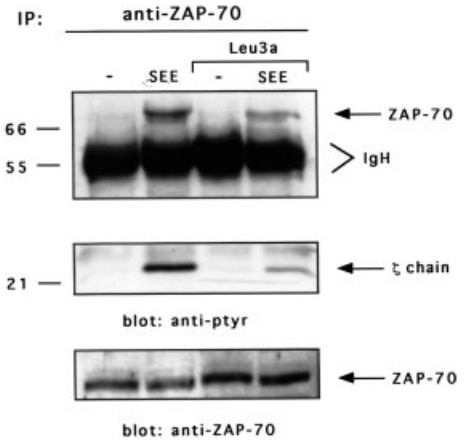

Fig. 2. CD4 engagement by Leu3a inhibits TCR-induced ZAP-70 tyrosine phosphorylation. Jurkat cells were pre-cultured for 15 min in the presence or absence of Leu3a (1:100 dilution) and then stimulated with EBV-B cells pulsed with 1 μg/ml SEE. ZAP-70 was immunoprecipitated and anti-phosphotyrosine Western blotting was performed (upper and middle panels). Each sample was analyzed by Western blotting with anti ZAP-70 antibodies (lower panel). Sizes are indicated in kilodaltons. The results are representative of three independent experiments.

of the earliest events that precede the activation of the downstream signaling pathways regulating T cell activation. Tyrosine phosphorylated ζ chains in turn recruit ZAP-70 that is itself tyrosine phosphorylated by the receptor-associated src kinases, and activated [4]. To determine whether the inhibition of NF-AT and IL-2 promoter activity reflected a blockage of early TCR signaling, Jurkat cells were both untreated or treated with Leu3a and then stimulated with EBV-B cells pre-pulsed with an optimal concentration of SEE. ZAP-70 was then immunoprecipitated and tyrosine phosphorylation was analyzed by Western blotting. As shown in Fig. 2, Leu3a treatment inhibited the tyrosine phosphorylation of both ZAP-70 (upper panel) and coprecipitating ζ chain (middle panel, lane 4 *vs.* 2). Similar to that observed in primary T cells [25], CD4 engagement before TCR triggering inhibits in Jurkat cells the earliest TCR-induced tyrosine phosphorylation events necessary for IL-2 gene expression.

2.2 CD4 engagement by antibodies induces Csk kinase activity

In most T cells, immunoreceptor signaling is dependent on full activation of Src family tyrosine kinases [4]. In contrast, the activation of Csk inhibits TCR signaling [17]. Thus, we verified whether the inhibitory signals induced by dissociating CD4 from TCR following Leu3a treatment were associated to the activation of $p50^{csk}$. To test this hypothesis, Jurkat cells were treated with Leu3a for different times and both $p56^{lck}$ and $p50^{csk}$ kinase activities were measured *in vitro*. Fig. 3A shows that cross-linking of CD4 by Leu3a results in a twofold increase of Lck kinase activity that rapidly decreased to nearly the basal level after 15 min of stimulation (upper panel, lanes 1–4). In contrast, CD4 engagement induced a high and sustained activation of Csk (Fig. 3A upper panel, lanes 5–8). CD4-induced activation of Csk was independent of Lck as demonstrated by the absence of any detectable Lck in anti-Csk immunoprecipitates (Fig. 3B, lower panel), and was also observed using a second anti-Csk antiserum (Fig. 3C, upper panel, lanes 1–4). Similar results were obtained in primary $CD4^+$ T cells (Fig. 3D), indicating that CD4-mediated activation of Csk was not peculiar to Jurkat cells but was also a feature of normal T lymphocytes.

Although Leu3a mAb was an IgG1, with a low binding affinity for protein A, and lysates were subjected to two preclearing steps with protein A-Sepharose beads before Csk immunoprecipitation, we ensured that the kinase activity observed was exclusively due to immunoprecipitated Csk. Thus, we performed *in vitro* competition assays using the Csk peptide used for generating the anti-Csk antibodies. The anti-Csk antibodies were incubated overnight at 4°C with a saturating concentration of blocking peptide, and anti-Csk immunoprecipitations were performed in unstimulated or Leu3a-activated Jurkat cells. As shown in Fig. 4A, the addition of blocking peptide strongly reduced the total amount of immunoprecipitated Csk (lower panel, lanes 3 and 4 *vs.* 1 and 2) as well as the kinase activity observed in Leu3a stimulated Jurkat cells (upper panel, lanes 3 and 4 *vs.*1 and 2). In contrast, the same peptide did not inhibit either CD4-associated Lck activity (Fig. 4A, upper panel, lane 6 *vs.* 5) or the amount of CD4-bound Lck (lower panel). The ability of Csk to undergo strong autophosphorylation *in vitro* has been previously shown [26], but no obvious sites of tyrosine autophosphorylation were found in Csk. Thus, we verified whether the robust autophosphorylation of Csk induced by anti-CD4 antibodies was also accompanied by an increase of its ability to phosphorylate a specific exogenous substrate. CD4 stimulation increased Csk kinase activity on the exogenous substrate pEY (Fig. 4B, upper panel). This peptide has been previously described to be highly specific for Csk [26]. Indeed, pEY was not phosphorylated by CD4-associated Lck (Fig. 4C, upper panel lanes 3 and 4), despite the strong Lck kinase activity observed in anti-CD4 immunoprecipitates (Fig. 4C, upper panel, lanes 1 and 2). Altogether these data clearly demonstrate that CD4 stimulation of both Jurkat cells and primary $CD4^+$ T cells induced the activation of Csk.

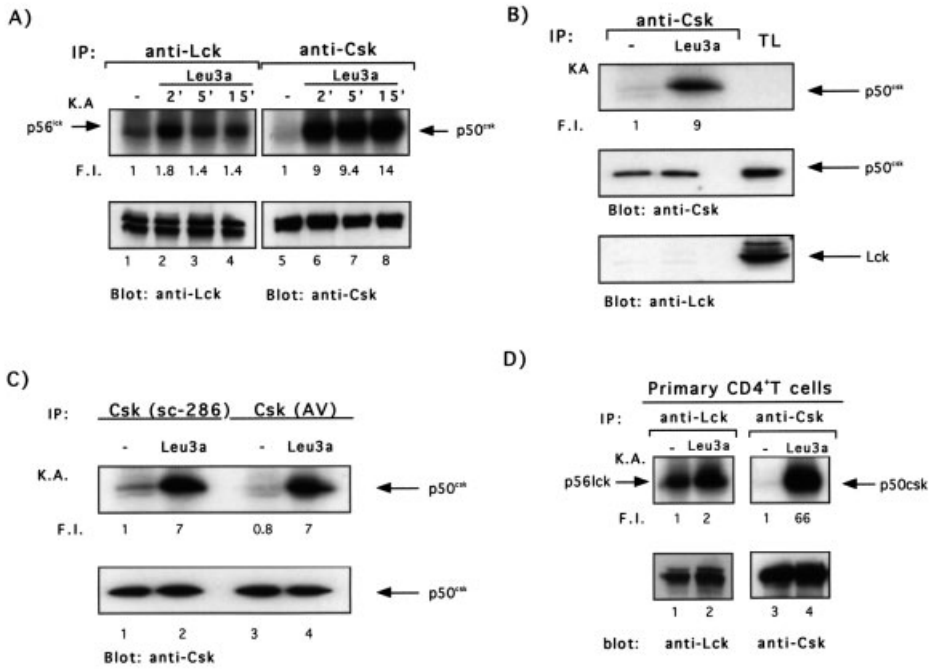

Fig. 3. Csk kinase activity is induced following CD4 engagement in T cells. (A) Jurkat cells were stimulated for different times with Leu3a and *in vitro* kinase assays were performed in anti-p56^{lck} (lanes 1–4) or anti-p50^{csk} (lanes 5–8) immunoprecipitates. (B) Jurkat cells were stimulated for 5 min with Leu3a and Csk was immunoprecipitated by using sc-286 antibody (lanes 1–2). The kinase activities of immunoprecipitated Csk was evaluated *in vitro* (upper panel). (C) Jurkat cells were stimulated for 5 min with Leu3a and Csk was immunoprecipitated by using sc-286 antibody (lanes 1–2) or anti-Csk antiserum from A. Veillette's Laboratory (AV, lanes 3–4). The kinase activities of immunoprecipitated Csk were evaluated *in vitro* (upper panel). (D) Primary CD4$^+$ T cells were stimulated for 5 min with Leu3a and the kinase activities of Lck and Csk were measured as in (A). Fold induction over the basal kinase activity (F.I.) was quantitated by phosphorimager. Each IP was analyzed for Lck or Csk content using specific antibodies followed by peroxidase-conjugated protein A. The results are representative of three independent experiments.

We next examined the effect of CD4 cross-linking on Csk kinase activity in TCR stimulated Jurkat cells. Jurkat cells were pretreated for 15 min with Leu3a and then stimulated with 5-3.1/B7 cells pulsed with an optimal dose of SEE. Consistent with several lines of evidence that for an efficient TCR signaling Csk must not be active [17, 18], SEE stimulation did not induce a significant up-regulation of Csk kinase activity (Fig. 5, upper panel, lanes 1–4). No Csk activity was observed when Jurkat cells were stimulated with an optimal concentration of SEE (10 μg/ml, data not shown). In contrast, when Leu3a engaged CD4 before SEE stimulation, Csk kinase activity increases of at least 23-fold (Fig. 5, upper panel, lanes 5–7). Similar results were obtained in normal CD4$^+$ T cells stimulated with anti-CD3 Ab (data not shown). These data demonstrate that the inhibitory signals elicited by CD4 engagement, separately from TCR, are associated at a very early step with the induction of Csk kinase activity, which through the negative regulation of Src kinases abolishes TCR activation.

2.3 Leu3a treatment induces Csk kinase activity associated to PAG/Cbp without affecting the ratio of PAG/Cbp-Csk complexes

The relocation of Csk to the lipid rafts, where Src kinases are active, is essential for its role as negative regulator of TCR signaling. Indeed, the identification of lipid rafts-associated protein PAG/Cbp, which when tyrosinephosphorylated binds Csk [22, 23] and up-regulates its kinase activity [27], has suggested a mechanism by which Csk may turn off the signaling events initiated by Src kinases. PAG/Cbp was immunoprecipitated from both Jurkat cells and primary CD4$^+$ T cells treated with Leu3a, and Csk kinase activity was measured. CD4 engagement by Leu3a increased PAG/Cbp-associated Csk autophosphorylation (Fig. 6A, upper panel). We were sure that the autophosphorylated band was PAG/Cbp-associated Csk and not CD4-bound Lck on the basis of their different migration mobility on 7% SDS-PAGE (data not shown). The increase of *in vitro* PAG/Cbp-associated Csk autophosphorylation was also accompanied by an increase of Csk kinase activity on the exogenous sub-

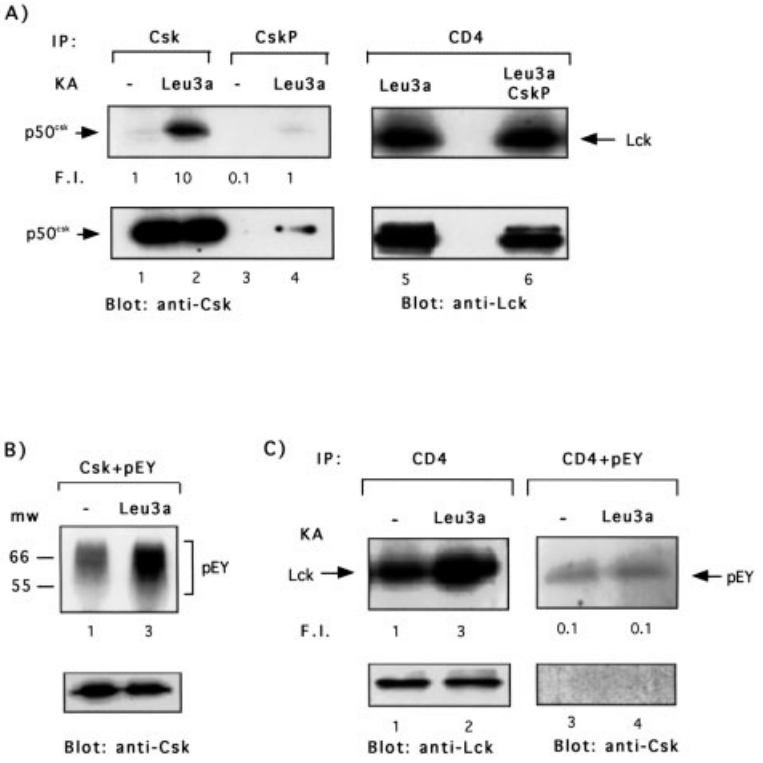

Fig. 4. CD4 engagement increases Csk kinase activity on exogenous substrates. (A) Jurkat cells were stimulated for 5 min with Leu3a, Csk and CD4 were immunoprecipitated with specific antibodies (upper panel, lanes 1, 2 and 5) or specific antibodies incubated overnight with a tenfold excess of Csk blocking peptide (CskP) (upper panel, lanes 3, 4 and 6) and *in vitro* kinase assays were performed. (B) Csk was immunoprecipitated from both unstimulated or anti-CD4 activated Jurkat cells and the kinase activity was measured on the exogenous substrate poly(Glu, Tyr) (pEY). Position of molecular weight markers (mw) are shown in kDa. (C) CD4 was immunoprecipitated from both unstimulated or anti-CD4 activated Jurkat cells and *in vitro* kinase assays for Lck activity (upper panel, lanes 1, 2) or on the exogenous substrate pEY (upper panel, lanes 3, 4) were performed. F.I. and IP were determined as in legend for Fig. 3. The results are representative of three independent experiments.

strate pEY (Fig. 6B, upper panel). Similar results were obtained in primary $CD4^+$ T cells (Fig. 6C). The induction of Csk kinase activity induced by Leu3a was not associated to an increase of Csk binding to PAG/Cbp as demonstrated by the equal amounts of Csk coprecipitated with PAG/Cbp in both unstimulated and Leu3a-treated cells (Fig. 6, middle panels). We next examined if CD4 treatment before TCR engagement was also able to activate PAG/Cbp-associated Csk activity. Jurkat cells were pretreated for 15 min with Leu3a and then stimulated for different times with 5-3.1/B7 cells prepulsed with an optimal concentration of SEE. As shown in Fig. 7, SEE stimulation did not affect PAG/Cbp-associated Csk kinase activity (upper panel, lanes 1–3). It is interesting to note that in contrast to the results obtained using anti-CD3 and anti-CD28 mAb as stimulators [22], the amount of PAG/Cbp-associated Csk did not change in Jurkat cells physiologically activated with SEE presented by $B7^+$ APC (Fig. 7, middle panel). Interestingly, PAG/Cbp-associated Csk kinase activity was up-regulated in SEE-

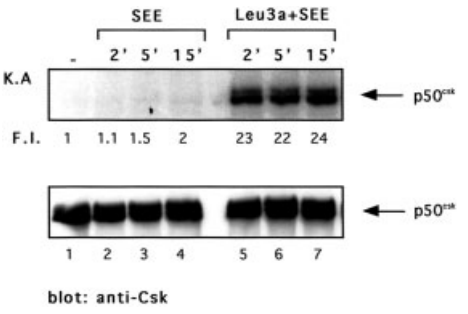

Fig. 5. CD4 ligation before TCR engagement induces Csk kinase activity. Jurkat cells were pre-cultured for 15 min in the presence or absence of Leu3a and then stimulated with adherent 5-3.1/B7 cells prepulsed with 1 μg/ml SEE for the indicated times. Csk was immunoprecipitated and the kinase activity was measured by *in vitro* kinase assays. F.I. and IP were determined as in legend for Fig. 3. The results are representative of three independent experiments.

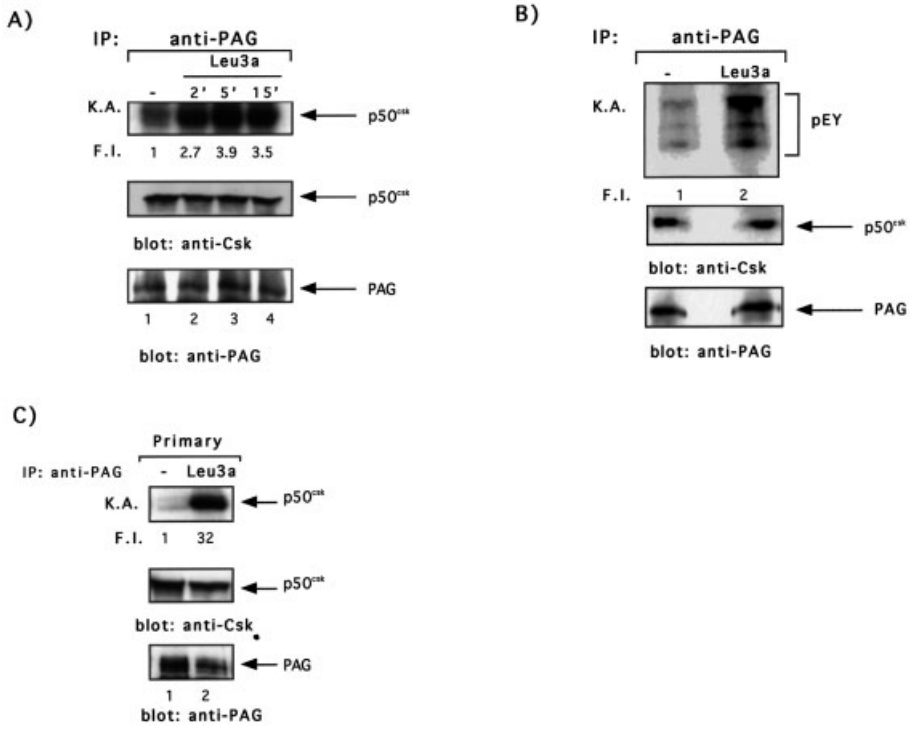

Fig. 6. CD4 ligation induces the activation of PAG/Cbp-associated Csk without affecting the amount of Csk bound to PAG/Cbp. (A) Jurkat cells were activated with Leu3a for the indicated times. Cells were lysed in buffer containing n-octyl β-glucopiranoside, PAG/Cbp was immunoprecipitated using specific antibodies and *in vitro* kinase assays were performed. (B) Jurkat cells were activated with Leu3a for 5 min and Csk activity was measured in anti-PAG/Cbp immunoprecipitates using pEY as substrate. (C) Primary CD4$^+$ T cells were activated with Leu3a for 5 min and PAG/Cbp-associated Csk kinase activity was evaluated as in (A). Each IP was analyzed for Csk and PAG content using specific antibodies followed by peroxidase-conjugated protein A. The results are representative of three independent experiments.

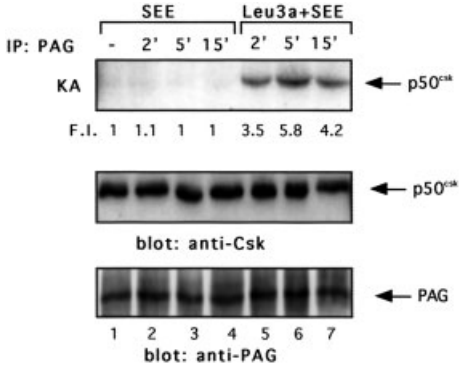

Fig. 7. CD4 engagement separately from TCR increases PAG/Cbp-associated Csk kinase activity. Jurkat cells were pre-cultured in the presence or absence of Leu3a and then stimulated with adherent 5-3.1/B7 cells prepulsed with 1 μg/ml SEE. Csk kinase activity in anti-PAG/Cbp immunoprecipitates was measured. Each IP was analyzed for Csk or PAG/Cbp content using specific antibodies. The results are representative of three independent experiments.

stimulated Jurkat cells pretreated with Leu3a (upper panel, lanes 5–7 vs. 1–4). Thus, CD4 engagement was able to up-regulate PAG/Cbp-associated Csk kinase activity also in SEE-stimulated cells without affecting the amount of Csk bound to PAG/Cbp.

To assess the significance of Csk activation by CD4 in inhibiting TCR-mediated signaling, Jurkat cells were transfected with a NF-AT-luciferase reporter construct together with a Csk mutant lacking its kinase activity (Csk KR). Overexpression of Csk (KR) increased NF-AT basal activity (at least tenfold) and completely reverted Leu3a-mediated inhibition of NF-AT activity in SEE-stimulated Jurkat cells (Fig. 8, panel A).

3 Discussion

The reorganization of surface receptors and signaling molecules at the T cell/APC interface plays a key role in T cell activation. This process, known as immunological synapse (IS) formation, co-ordinates engagement of the

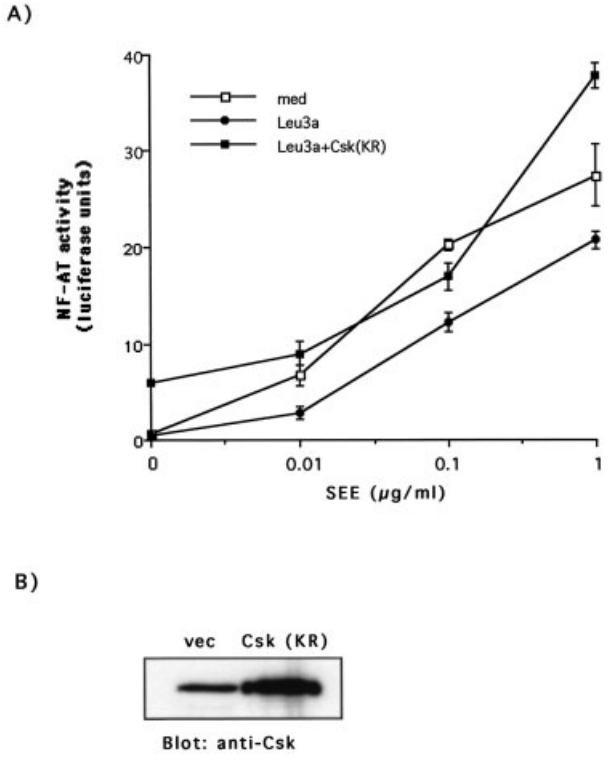

Fig. 8. Expression of dominant negative Csk (KR) restores TCR-induced NF-AT activation in Leu3a-treated cells. (A) Jurkat cells were transfected with NF-AT luciferase reporter construct together with vector control or dominant negative Csk (KR) mutant and after 24 h cells were stimulated for additional 8 h with SEE-pulsed 5-3.1/B7 cells. The results are expressed as the mean of arbitrary units of the luciferase activity ± SD. The data represent at least four independent experiments. (B) The overexpression of Csk (KR) mutant was analyzed by western blotting using anti-Csk antibodies.

TCR by peptide/MHC complex, thus facilitating signaling through the TCR. Recent models suggest that the main role of CD4 is to "boost" TCR recognition [28], facilitating the rapid recruitment of Lck to TCR/CD3, an event that is essential to initiate signaling and trigger the early phase of T cell activation [29]. Indeed, Lck is autophosphorylated and activated during IS formation, an event that require both CD4 and CD28 [29]. The blockage of CD4-Lck recruitment to TCR by anti-CD4 antibodies or HIV gp120 during antigen recognition exerts a drastic inhibitory effect on T cell activation by interfering with both early and late phases of T cell signaling [7, 30]. Several mechanisms have been proposed to explain the inhibitory effects mediated by CD4 on TCR signaling, such as decreased cellular levels of $p56^{lck}$ [31], sequestration of CD4-associated $p56^{lck}$ to the cytoskeleton [11], or sequestration of crucial components of the TCR/CD3 signaling pathway to the CD4-$p56^{lck}$ complexes [8]. Less is known about the regulation of $p56^{lck}$ kinase activity following CD4 engagement separately from TCR. Here we present evidence that a mechanism regulating $p56^{lck}$ activity relies on the induction of Csk kinase activity by CD4.

$p56^{lck}$ kinase activity is regulated by a conserved tyrosine residue, Tyr505, within the C-terminal tail that, when phosphorylated, inhibits kinase activity. CD45, a transmembrane tyrosine phosphatase expressed by all hemopoietic cells, appears to be required for activation of $p56^{lck}$ by dephosphorylating its inhibitory site [32]. In contrast, the tyrosine kinase $p50^{csk}$ phosphorylates the Tyr505, thus inhibiting $p56^{lck}$ kinase activity [15]. CD45 and Csk are both constitutively active enzymes. However, data from CD45-deficient mice indicate that the balance between CD45 and Csk is a net dephosphorylation of the inhibitory site at the steady state [33]. A current model proposes that, under resting conditions, CD45 maintains a basal level of CD4-Lck activity that is responsible for generating the p21 ζ phosphoisoform associating inactive ZAP-70 [34]. Engagement of TCR by peptide-MHC molecules brings CD4-Lck into closer proximity of CD3/TCR-ζ, thus leading to the generation of p23 ζ phosphoisomer, and phosphorylation and activation of ζ-bound ZAP-70 by $p56^{lck}$ [35]. The subsequent interaction between ZAP-70 and $p56^{lck}$ will result in the activation of both proteins [36, 37]. In this model, if the balance between CD45 and Csk will shift in favor of Csk, the dominance of Tyr505-phosphorylated $p56^{lck}$ species in a "closed" conformation and with a reduced ability of their SH2/SH3 domains to dock with the TCR/ZAP-70 complex will be induced. Indeed, we show that CD4 engagement by anti-CD4 mAb induced a reduction of both ZAP-70 and ZAP-70-associated TCR-ζ tyrosine phosphorylations (Fig. 2). These events were associated to a transient increase of Lck kinase activity. In contrast, CD4 stimulation induced a stronger and persistent increase of Csk kinase activity that was not observed when cells were correctly stimulated through TCR (Fig. 5). Although, a direct correlation between CD4-induced Csk activation and the impairment of TCR-mediated signaling cannot be made, our data on the loss of CD4-mediated inhibition of TCR signaling in kinase-deficient Csk-overexpressing cells, strongly support this hypothesis. Moreover, it is intriguing that the reduction in TCR-ζ phosphorylation and ZAP-70 recruitment in anti-CD4-treated cells is similar to that observed in Csk-overexpressing cells [18].

Similarly to the Src kinases, Csk consists of an SH3 domain, an SH2 domain and a kinase domain, but lacks the C-terminal regulatory tyrosine residue as well as the N-terminal myristoylation signal for targeting to lipid rafts. Recently, a transmembrane protein known as PAG or Cbp has been identified that, when phosphorylated,

can recruit Csk via its SH2 domain to the membrane lipid rafts where the Src kinases are located [22, 23]. PAG/Cbp is involved not only in the membrane recruitment of Csk but also in Csk-mediated inhibition of Src, by directly activating Csk [27]. In unstimulated T cells, PAG/Cbp is constitutively tyrosine phosphorylated and associated to Csk. TCR engagement by antibodies has been described to induce the rapid dephosphorylation of PAG/Cbp, thus leading to a transient displacement of Csk from lipid rafts. This event has been reported to allow a stronger and prolonged activation of Src kinases and sustained TCR signaling [22, 24]. Physiological stimulation of Jurkat cells by SEE presented on $B7^+$ APC did not affect either the amount of PAG/Cbp-associated Csk or PAG/Cbp-associated Csk kinase activity. The failure to see PAG dephosphoryation in Jurkat cells following TCR stimulation may be due to the fact that Jurkat express not very much PAG/Cbp but a lot of phosphatases, which results in a constitutive dephosphorylation of PAG/Cbp. Indeed, when the expression levels of PAG/Cbp are raised, PAG becomes dephosphorylated after TCR stimulation also in Jurkat cells [38]. In contrast, CD4 engagement alone or before TCR stimulation was able to activate PAG/Cbp-associated Csk kinase activity, again without modifying the total amount of Csk bound to PAG/Cbp (Fig. 6, 7). It may be possible that Lck activated by Leu3a phosphorylates PAG, thus inducing an increase of Csk recruitment and activation. However, our results showing that Leu3a did not change the amount of Csk associated with PAG suggest that Csk kinase activity may be regulated by another mechanism. Csk has also been described to down-regulate Src activity by redistributing to sites of Src activation through a direct interaction with tyrosine phosphorylated GTPase-activating protein (GAP)-associated $p62^{dok}$ [39, 40]. In T cells, $p62^{dok}$ is tyrosine phosphorylated following CD2 [41] or CD28 stimulation [42]. Recent data from Nemorin et al. have shown that $p62^{dok}$ tyrosine phosphorylation is mediated by Lck [41] and that $p62^{dok}$ overexpression impairs both CD3- and CD2-induced NF-AT activation and IL-2 secretion [43]. Thus, the transient increase of Lck kinase activity induced by Leu3a may lead to the tyrosine phosphorylation of $p62^{dok}$, which in turn may recruit and activate Csk thus leading to the termination of Lck activity. CD4 engagement by Leu3a induced in Jurkat cells the tyrosine phosphorylation of a $\sim$62 kDa protein that may be $p62^{dok}$ (data not shown). Experiments are in progress to verify this hypothesis.

A disregulation between CD3- and CD4-mediated signals has been observed following exposure of T lymphocytes to IL-16, a natural ligand of CD4 [44], or in lymphocytes derived from HIV-1-infected patients. Moreover, binding of HIV gp120 with CD4 separately from TCR results in the activation of programmed cell death [9, 45]. An increase of Csk kinase activity has also been observed in T cells committed to apoptosis [46]. Our data represent the first demonstration that CD4 may regulate the activity of an inhibitory kinase that, altering the proximal signaling events generated by TCR, gives rise to a dominant negative signals that, in some circumstances, may contribute to the death of T cells [47]. This characterizes a novel biological role for CD4 that may contribute to a greater understanding of TCR signaling both in normal and pathological conditions.

4 Materials and methods

4.1 Cell lines, antibodies and reagents

$CD4^+$ Jurkat T cell line was maintained in RPMI 1640 supplemented with 10% FCS, L-glutamine, penicillin and streptomycin (Gibco). The L cell transfectants expressing HLA-DRB1*0101 (5-3.1) and co-transfected with human B7.1 (5-3.1/B7) were previously described [45]. Human peripheral blood $CD4^+$ T cells were purified by negative selection using an indirect magnetic cell sorting kit (Miltenyi Biotec, Auburn, CA). Mouse anti-CD4 mAb (Leu3a) was from Becton Dickinson (Mountain View, CA). Mouse anti-$p56^{lck}$ (3A5), rabbit anti-$p56^{lck}$, rabbit anti-$p50^{csk}$ antibodies and the Csk blocking peptide were purchased from Santa Cruz Biotechnology (Santa Cruz, CA). Rabbit anti-Csk antiserum was kindly provided by A. Veillette (IRCM, Montreal, Canada). Anti-human ZAP-70 and ζ chain mAb were from Upstate Biotechnology (Lake Placid, NY). Anti-PAG antibodies were generated as previously described [22]. SEE was purchased from Toxin Technology (Sarasota, FL).

4.2 Plasmids, cell transfection, activation and luciferase assay

The NF-AT luciferase reporter construct containing the luciferase gene under the control of the human IL-2 promoter NF-AT binding site was kindly provided by C. Baldari (University of Siena, Siena, Italy). The IL-2 luciferase construct [48] was kindly provided by J.F. Peyron (Faculté de Medicine Pasteur, Nice, France). Kinase-dead Csk, Csk (K222R), was kindly provided by A. Veillette (IRCM). The pSVβ-gal vector (Promega Corp., Madison, WI) contains the β-galactosidase gene driven by the SV40 promoter/enhancer.

Transient transfections were performed by electroporating (at 260 V, 960 μF) 10^7 Jurkat cells in 0.5 ml RPMI 1640 supplemented with 20% FCS with 10 μg of the indicated reporter constructs together with 20 μg pSV-βgal plasmid, keeping the total amount of DNA constant (50 μg) with empty vector. At 24 h after transfection 10^5 cells were pretreated for 15 min with medium or Leu3a (1:100 dilution) at 37°C and then stimulated for 8 h with confluent 5-3.1/B7 cells cultured overnight with the indicated concentration of

SEE in round-bottom 96-well plates. β-Galactosidase and luciferase assays were performed according to the manufacturer's instruction (Promega). Luciferase activity, determined in triplicates samples using an automated luminometer (Lumat LB 9501, EG&G Berthold, Wildbad, Germany) was expressed as fold induction over the basal activity of cells cultured with medium alone or in arbitrary units (AU) after normalization to the β-galactosidase values.

4.3 Cell stimulation, immunoprecipitation and *in vitro* kinase assay

Jurkat cells were washed twice, resuspended in medium (10^8/ml) and incubated at 37°C in the presence or absence of Leu3a mAb for different times. When indicated, Leu3a pretreated cells were then stimulated with adherent 5-3.1/B7 cells pulsed with different concentration of SEE. At the end of incubation, cells were harvested and lysed for 30 min on ice in 1% NP40 lysis buffer containing 20 mM Tris-HCl pH 7.5, 150 mM NaCl, 1 mM EGTA in the presence of inhibitors of proteases and phosphatases: 10 μg/ml leupeptin, 10 μg/ml aprotinin, 1 mM Pefabloc-sc, 50 mM NaF, 10 mM $Na_4P_2O_7$ and 1 mM $NaVO_4$. Cells were lysed in buffer containing 60 mM N-octyl β-glucopiranoside (Sigma) instead of 1% NP-40 for co-immunoprecipitation experiments of PAG/Csk complexes. Post-nuclear lysates were subjected to two rounds of preclearing with protein A-Sepharose beads before immunoprecipitations with anti-Csk, or anti-Lck or anti-PAG antibodies preadsorbed on protein A-Sepharose beads. In the competition assays with the Csk blocking peptide, the anti-Csk antibodies were incubated overnight at 4°C with a tenfold excess of peptide before immunoprecipitation. The kinase activity of immunoprecipitated $p56^{lck}$ or $p50^{csk}$ was assayed at 30°C for 15 min in 25 μl $p56^{lck}$ kinase buffer (1 mM Tris-HCl pH 7.5, 7.5 mM NaCl, 25 mM Hepes pH 7.3, 10 mM $MnCl_2$, 0.05% NP-40) or $p50^{csk}$ kinase buffer (50 mM Hepes, pH 7.4, 5 mM $MgCl_2$, 0.05% NP-40) in the presence of 10 μCi [γ–^{32}P]ATP (10 Ci/mmol). Similar assays with the same buffer were performed with the synthetic polyamino acid poly(Glu, Tyr) 4:1 (Sigma), abbreviated pEY (0.5 μg), as substrate of Csk. The reactions were terminated with 2× Laemmli sample buffers. Samples were analyzed by sodium dodecylsulfate-polyacrylamide gel electrophoresis (SDS-PAGE). Gels were fixed, treated with 1 M KOH for 1 h at 55°C to remove the alkali-labile phosphate groups from serine and threonine-phosphorylated proteins, dried and autoradiographed. Radioactivity in the phosphorylated proteins was quantitated by a phosphorimager. Immunoblotting and detections of proteins by enhanced chemiluminescence (Amersham Pharmacia Biotech) were performed as previously described [5]. For anti-Csk and anti-Lck Western blotting, peroxidase-conjugated protein A was used instead of secondary Ab to avoid Ig heavy chain nonspecific binding.

Acknowledgements: We thank C. Baldari, J. F. Peyron and A. Veillette for providing reagents. This work was supported by grants from the National Health Ministry research project on AIDS (2001), the Ministry for the University and Scientific and Technological Research (MIUR-COFIN 2001, and "Progetto Giovani Ricercatori 2000"), and the National Council of Research (CNR, "Progetto Giovani Ricercatori 2000").

References

1 **Cammarota, G., Scheirle, A., Takacs, B., Doran, D. M., Knorr, R., Bannwarth, W., Guardiola, J. and Sinigaglia, F.,** Identification of a CD4 binding site on the beta 2 domain of HLA-DR molecules. *Nature* 1992. **356:** 799–801.

2 **Konig, R., Huang, L. Y. and Germain, R. N.,** MHC class II interaction with CD4 mediated by a region analogous to the MHC class I binding site for CD8. *Nature* 1992. **356:** 796–798.

3 **Turner, J. M., Brodsky, M. H., Irving, B. A., Levin, S. D., Perlmutter, R. M. and Littman, D. R.,** Interaction of the unique N-terminal region of tyrosine kinase p56lck with cytoplasmic domains of CD4 and CD8 is mediated by cysteine motifs. *Cell* 1990. **60:** 755–765.

4 **Kane, L. P., Lin, J. and Weiss, A.,** Signal transduction by the TCR for antigen. *Curr. Opin. Immunol.* 2000. **12:** 242–249.

5 **Duplay, P., Thome, M., Hervé, F. and Acuto, O.,** $p56^{lck}$ interacts via its src homology 2 domain with the ZAP-70 kinase. *J. Exp. Med.* 1994. **179:** 1163–1172.

6 **Clements, J. L. and Koretzky, G. A.,** Recent developments in lynphocyte activation: linking kinases to downstream signaling events. *J. Clin. Invest.* 1999. **103:** 925–929.

7 **Bonnard, M., Haughn, L. and Julius, M.,** CD4-mediated inhibition of IL-2 production in activated T cells. *J. Immunol.* 1999. **162:** 1252–1260.

8 **Sanzenbacher, R., Kabelizt, D. and Janssen, O.,** SLP-76 binding to $p56^{lck}$: a role for SLP-76 in CD4-induced desensitization of the TCR/CD3 signaling complex. *J. Immunol.* 1999. **163:** 3143–3152.

9 **Banda, N. K., Bernier, J., Kurahara, D. K., Kurrle, R., Haigwood, N., Sekaly, R. P. and Finkel, T. H.,** Crosslinking CD4 by human immunodeficiency virus gp120 primes T cells for activation-induced apoptosis. *J. Exp. Med.* 1992. **176:** 1099–1106.

10 **Tuosto, L. and Acuto, O.,** CD28 affects the earliest signaling events generated by TCR engagement. *Eur. J. Immunol.* 1998. **28:** 2131–2142.

11 **Goldman, F., Crabtree, J., Hollenback, C. and Koretzky, G.,** Sequestration of p56(lck) by gp120, a model for TCR desensitization. *J. Immunol.* 1997. **158:** 2017–2024.

12 **Xu, W., Harrison, S. C. and Eck, M. J.,** Three-dimensional structure of the tyrosine kinase c-Src. *Nature* 1997. **385:** 595–602.

13 **Yamaguchi, H. and Hendrickson, W. A.,** Structural basis for activation of human lymphocytes kinase Lck upon tyrosine phosphorylation. *Nature* 1996. **384:** 484–489.

14 **Ostergaard, H. L., Shackelford, D. A., Hurley, T. R., Johnson, P., Hyman, R., Sefton, B. M. and Trowbridge, I. S.,** Expression of CD45 alters phosphorylation of the lck-encoded tyrosine protein kinase murine lymphoma T cell lines. *Proc. Natl. Acad. Sci. USA* 1989. **86:** 8959–8963.

15 **Chow, L. M. L. and Veillette, A.,** The Src and Csk families of tyrosine kinases in hemopoietic cells. *Semin. Immunol.* 1995. **7:** 207–226.

16 **Schmedt, C. and Tarakhovsky, A.,** Autonomous maturation of α/β T lineage cells in the absence of COOH-terminal Src kinase (Csk). *J. Exp. Med.* 2001. **193:** 815–825.

17 **Chow, L. M. L., Fournel, M., Davidson, D. and Veillette, A.,** Negative regulation of T cell receptor signalling by protein tyrosine kinase p50^{csk}. *Nature* 1993. **365:** 156–160.

18 **Cloutier, J.-F. and Veillette, A.,** Cooperative inhibition of T cell antigen receptor signaling by a complex between a kinase and a phosphatase. *J. Exp. Med.* 1999. **189:** 111–121.

19 **Ilangumaran, S., Arni, S., van Echten-Deckert, G., Borisch, B. and Hoessli, D. C.,** Microdomain-dependent regulation of Lck and Fyn protein-tyrosine kinases in T lymphocyte plasma membranes. *Mol. Biol. Cell.* 1999. **10:** 891–905.

20 **Simons, K. and Ikonen, E.,** Functional rafts in cell membrane *Nature* 1997. **387:** 569–572.

21 **Viola, A.,** The amplification of TCR signalling by dynamic membrane microdomains. *Trends Immunol.* 2001. **22:** 322–327.

22 **Brdicka, T., Palvistova, D., Leo, A., Bruyns, E., Korinek, V., Angelisova, P., Sherer, J., Shevchenko, A., Shevchenko, A., Hilgert, I., Cerny, J., Drbal, K., Kuramitsu, Y., Kornacker, B., Horejsi, V. and Schraven, B.,** Phosphoprotein associated with glycosphingolipid-enriched microdomain (PAG), a novel ubiquitously expressed transmembrane adaptor protein, binds the protein tyrosine kinase csk and is involved in regulation of T cell activation. *J. Exp. Med.* 2000. **191:** 1591–1604.

23 **Kawabuchi, M., Satomi, Y., Takao, T., Shimonishi, Y., Nada, S., Nagai, K., Tarakhovsky, A. and Okada, M.,** Transmembrane phosphoprotein Cbp regulates the activities of Src-family tyrosine kinases. *Nature* 2000. **404:** 999–1003.

24 **Torgersen, K. M., Vang, T., Abrahamsen, H., Yaqub, S., Horejsi, V., Schraven, B., Rostald, B., Mustelin, T. and Taskén, K.,** Release from tonic inhibition of T cell activation through transient displacement of c-terminal Src kinase (Csk) from lipid rafts. *J. Biol. Chem.* 2001. **276:** 29313–29318.

25 **Harding, S., Lipp, P. and Alexander, D. R.,** A therapeutic CD4 monoclonal antibody inhibits TCR-zeta chain phosphorylation, zeta-associated protein of 70-kDa Tyr319 phosphorylation, and TCR internalization in primary human T cells. *J. Immunol.* 2002. **169:** 230–238.

26 **Vang, T., Taskén, K., Skalhegg, B. S., Hansson, V. and Levy, F. O.,** kinetic properties of the C-terminal Src kinase, p50^{csk}. *Biochim. Biophys. Acta* 1998. **1384:** 285–293.

27 **Takeuchi, S., Takayama, Y., Ogawa, A., Tamura, K. and Okada, M.,** Transmembrane phosphoprotein CbP positively regulates the activity of the carboxyl-terminal Src kinase, Csk. *J. Biol. Chem.* 2000. **275:** 29183–29186.

28 **Krummel, M. F., Sjaastad, M. D., Wülfing, C. and Davis, M. M.,** Differential clustering of CD4 and CD31562; during T cell recognition. *Science* 2000. **289:** 1349–1352.

29 **Holdorf, A. D., Lee, K. -H., Burack, W. R., Allen, P. M. and Shaw, A. S.,** Regulation of Lck activity by CD4 and CD28 in the immunological synapse. *Nat. Immunol.* 2002. **3:** 259–264.

30 **Jabado, N., Pallier, A., Le deist, F., Bernard, F., Fischer, A. and Hivroz, C.,** CD4 ligands inhibit the formation of multifunctinal transduction complexes involved in T cell activation. *J. Immunol.* 1997. **158:** 94–103.

31 **Cayota, A., Vuiller, F., Siciliano, J. and Dighiero, G.,** Defective protein tyrosine phosphorylation and altered levels of p59^{fyn} and p56^{lck} in CD4 T cells from HIV-1 infected patients. *Int. Immunol.* 1994. **6:** 611–621.

32 **Thomas, M. L. and Brown, E. J.,** Positive and negative regulation of Src-family membrane kinases by CD45. *Immunol. Today* 1999. **20:** 406–411.

33 **Stone, J. D., Conroy, L. A., Byth, K. F., Hederer, R. A., Howlet, S., Takemoto, Y., Holmes, N. and Alexander, D. R.,** Aberrant TCR-mediated signaling in CD45-null thymocytes involves dysfunctional regulation of Lck, Fyn, TCR-zeta and ZAP-70. *J. Immunol.* 1997. **158:** 5773–5782.

34 **Alexander, D. R.,** The CD45 tyrosine phosphatase: a positive and negative regulator of immune cell function. *Semin. Immunol.* 2000. **12:** 349–359.

35 **Van Oers, N. S. C., Killen, N. and Weiss, A.,** ZAP-70 is constitutively associated with tyrosine-phosphorylated TCR-zeta inmurine thymocytes and lymph-node T cells. *Immunity* 1994. **1:** 675–685.

36 **Di Bartolo, V., Mege, D., Germain, V., Pelosi, M., Dufour, E., Michel, F., Magistrelli, G., Isacchi, A. and Acuto, O.,** Tyrosine 319, a newly identified phosphorylation site of ZAP-70, plays a critical role in T cell antigen receptor signalling. *J. Biol. Chem.* 1999. **274:** 6285–6294.

37 **Pelosi, M., Di Bartolo, V., Mounier, V., Mege, D., Pascussi, J. M., Dufour, E., Blondel, A. and Acuto, O.,** Tyrosine 319 in the interdomain B of ZAP-70 is a binding site for the Src homology 2 domain of Lck. *J. Biol. Chem.* 1999. **274:** 14229–14237.

38 **Itoh, K., Sakakibara, M., Yamasaki, S., Takeuchi, A., Arase, H., Miyazaki, M., Nakajima, N., Okada, M. and Saito, T.,** Negative regulation of immune synapse formation by anchoring lipid raft to cytoskeleton through Cbp-EBP50-ERM assembly. *J. Immunol.* 2002. **168:** 541–544.

39 **Neet, K. and Hunter, T.,** The nonreceptor protein-tyrosine kinase CSK complexes directly with the GTPase-activating protein-associated p62 protein in cells expressing v-Src or activated c-Src. *Mol. Biol. Cell.* 1995. **15:** 4908–4920.

40 **Vuica, M., Desiderio, S. and Schneck, J. P.,** Differential effects of B cell receptor and B cell receptor-FCγRIIB1 engagement on docking of Csk to GTPase-activating protein (GAP)-associated p62. *J. Exp, Med.* 1997. **186:** 259–267.

41 **Nemorin, J.-G. and Duplay, P.,** Evidence that Lck-mediated phosphorylation of p56^{dok} and p62^{dok} may play a role in CD2 signaling. *J. Biol. Chem.* 2000. **275:** 14590–14597.

42 **Yang, W. C., Ghiotto, M., Barbarat, B. and Olive, D.,** The role of Tec protein-tyrosine kinase in T cell signalling. *J. Biol. Chem.* 1999. **274:** 607–617.

43 **Nemorin, J. -G., Laporte, P., Berube, G. and Duplay, P.,** p62^{dok} negatively regulates CD2 signaling in Jurkat cells *J. Immunol.* 2001. **166:** 4408–4415.

44 **Center, D. M., Kornfeld, H. and Cruikshank, W. W.,** Interleukin 16 and its function as a CD4 ligand. *Immunol. Today* 1996. **17:** 476–481.

45 **Tuosto, L., Gilardini Montani, M. S., Lorenzetti, S., Cundari, E., Moretti, S., Lombardi, G. and Piccolella, E.,** Differential susceptibility to monomeric HIV gp120-mediated apoptosis in antigen-activated CD4$^+$ T cell population. *Eur. J. Immunol.* 1995. **25:** 2907.

46 **Orchansky, P. L., Wang, D. H., Johnson, P. and Teh, H.-S.,** Increase in the specific activity of p50^{csk} in proliferating T cells correlates with decreased specific activity of p56^{lck} and p59^{fyn} and reduced phosphorylation of CD3 subunits. *Mol. Immunol.* 1996. **33:** 531–540.

47 **Tuosto, L., Marinari, B. and Piccolella, E.,** CD4-Lck through TCR and in the absence of Vav exchange factor induces Bax increase and mitochondrial damage. *J. Immunol.* 2002. **168:** 6106–6112.

48 **Peyron, J. F., Verma, S., de Waal Malefyt, R., Sancho, J., Terhorst, C. and Spits, H.,** The CD45 protein tyrosine phosphatase is required for the completion of the activation program leading to lymphokine production in the Jurkat human T cell line. *Int. Immunol.* 1991. **3:** 1357–1366.

Correspondence: Loretta Tuosto, Department of Cellular and Developmental Biology, University of Rome "La Sapienza", Rome Italy
Fax: +39-06-49917594
e-mail: tuosto@uniroma1.it

Appendix 4

LIME: a new membrane raft-associated adaptor protein involved in CD4 and CD8 coreceptor signaling

Brdičková N., Brdička T., Angelisová P., Horváth O., Špička J., Hilgert I., Pačes I., **Simeoni L.**, Kliche S., Merten C., Schraven B., and Hořejší V. (2003) *J Exp Med*. 198:1453-62.

The Journal of Experimental Medicine

LIME: A New Membrane Raft-associated Adaptor Protein Involved in CD4 and CD8 Coreceptor Signaling

Naděžda Brdičková,[1] Tomáš Brdička,[1] Pavla Angelisová,[1] Ondrej Horváth,[1] Jiří Špička,[1] Ivan Hilgert,[1] Jan Pačes,[1] Luca Simeoni,[2] Stefanie Kliche,[2] Camilla Merten,[2] Burkhart Schraven,[2] and Václav Hořejší[1]

[1]*Institute of Molecular Genetics, Academy of Sciences of the Czech Republic, 142 20 Prague 4, Czech Republic*
[2]*Institute for Immunology, Otto-von-Guericke-University, 39120 Magdeburg, Germany*

Abstract

Lymphocyte membrane rafts contain molecules critical for immunoreceptor signaling. Here, we report identification of a new raft-associated adaptor protein LIME (Lck-interacting molecule) expressed predominantly in T lymphocytes. LIME becomes tyrosine phosphorylated after cross-linking of the CD4 or CD8 coreceptors. Phospho-LIME associates with the Src family kinase Lck and its negative regulator, Csk. Ectopic expression of LIME in Jurkat T cells results in an increase of Csk in lipid rafts, increased phosphorylation of Lck and higher Ca^{2+} response to CD3 stimulation. Thus, LIME appears to be involved in regulation of T cell activation by coreceptors.

Key words: membrane microdomains • Lck • Csk • signal transduction • phosphorylation

Introduction

Membrane microdomains, also called lipid rafts or glycolipid-enriched microdomains, are small areas of cell membranes that can be distinguished from the rest of the membrane by unique lipid and protein composition. They are enriched in lipids containing long saturated fatty acid residues (mainly sphingomyelin and glycosphingolipids) and cholesterol, glycosylphosphatidylinositol-anchored proteins, and several cytoplasmic proteins associated with the inner leaflet of the membrane via covalently attached fatty acid residues. Among these cytoplasmic proteins are, e.g., Src family kinases (possessing NH_2-terminal double acylation) and heterotrimeric G proteins. The integrity of membrane rafts seems to be maintained by lateral interactions of their constituent lipids which form, together with cholesterol, a more organized "liquid ordered" phase in the membrane. Membrane rafts can be easily isolated due to their relative insolubility in solutions of common mild detergents of the polyoxyethylene type (such as Triton X-100, Brij series, NP-40) at low temperature and their ability to float when such detergent lysates are ultracentrifuged in sucrose density gradient. Conversely, membrane rafts are readily solubilized by alkyl-glycosidic type of detergents (for general review on the rafts and their role in immunoreceptor signaling see references 1–3). Most transmembrane proteins are excluded from lipid rafts, exceptions being few molecules palmitoylated on cytoplasmic membrane-proximal cysteine residues, such as the pre-TCR (4), the CD4 and CD8 coreceptors (5, 6), and the three recently discovered transmembrane adaptor proteins, linker for activation of T cells (LAT) (7, 8), phosphoprotein associated with glycosphingolipid-enriched microdomains (PAG) (9), or Csk-binding protein (Cbp) (10) and non–T cell activation linker (NTAL) (11) or linker for activation of B cells (LAB) (12).

Because of the presence of several key signal-transducing molecules (Src family kinases, transmembrane adaptor proteins LAT, NTAL/LAB, and PAG/Cbp), membrane rafts have been shown recently to play an essential role in initiation of immunoreceptor (TCR, BCR, FcR) signaling (1–3). To identify novel lipid raft-associated transmembrane adaptor

Address correspondence to Václav Hořejší, Institute of Molecular Genetics, AS CR, Vídenská 1083, 142 20 Praha 4, Czech Republic. Phone: 420-2-41729908; Fax: 420-2-44472282; email: horejsi@biomed.cas.cz; or Burkhart Schraven, Institute for Immunology, Otto-von-Guericke-University, Leipziger Strasse 44, 39120 Magdeburg, Germany. Phone: 0391-67-15800; Fax: 0391-67-15852; email: burkhart.schraven@medizin.uni-magdeburg.de

Preliminary reports (abstracts, poster, and oral communications) on some aspects of this work were presented at the ELSO2002 Meeting, Nice, June 29–July 3, 2002, 5th EFIS Tatra Immunology Conference, Tatranske Zruby, September 7–11, 2002, and 15th EFIS Meeting, Rhodes, June 2003.

Abbreviations used in this paper: Cbp, Csk-binding protein; LAT, linker for activation of T cells; LAB, linker for activation of B cells; LIME, Lck-interacting molecule; NTAL, non–T cell activation linker; PAG, phosphoprotein associated with glycosphingolipid-enriched microdomains; PBL, peripheral blood leukocytes; PHA, phytohemagglutinin; PLCγ, phospholipase Cγ; PTK, protein tyrosine kinase; P-Tyr, phosphotyrosine; SH Src homology; TRAP, transmembrane adaptor protein; TRIM, TCR-interacting molecule.

 J. Exp. Med. © The Rockefeller University Press • 0022-1007/2003/11/1453/10 $8.00
Volume 198, Number 10, November 17, 2003 1453–1462
http://www.jem.org/cgi/doi/10.1084/jem.20031484

proteins, we have searched public databases for molecules sharing the structural features characteristic of raft-targeted transmembrane adaptor proteins. One of the proteins identified by this approach was Lck-interacting molecule (LIME), a molecule of unknown function whose amino acid sequence has been deposited in the databases since 1998. In the present study we describe the first biochemical and functional characterization of LIME.

Materials and Methods

Cells and Antibodies. T, B, and NK cells and monocytes were obtained from buffy coats by Ficoll centrifugation and preparative cell sorting using a FACS Vantage™ flow cytometer (Becton Dickinson) and PE-conjugated mAbs to CD3 and CD19 (Serotec), biotinylated anti-CD14 (Serotec), fluoresceinylated (FITC) streptavidin (BD Biosciences), unlabeled CD56 mAb MEM-188, and fluorescein-conjugated $F(ab)_2$ fragments of goat anti–mouse Ig (Caltag). Single-positive ($CD4^+8^-$, $CD4^-8^+$), double-positive ($CD4^+8^+$), and double-negative ($CD2^+CD4^-CD8^-CD19^-$) thymocytes were isolated by flow sorting using anti–CD4-FITC (MEM-241), anti–CD8-PE (BD Biosciences), anti–CD2-PE (Immunotech), anti–CD4-biotin (Serotec), anti–CD8-biotin (Serotec), anti–CD19-biotin (Serotec), and Streptavidin-FITC (BD Biosciences) mAbs. Purity of all sorted thymocyte subpopulations used in subsequent experiments was >99%. In some experiments, the peripheral blood leukocytes (PBLs) obtained by Ficoll centrifugation were passed through nylon wool column, the nonadhering T and NK cells were recovered and are referred to as peripheral blood T cells. 293T cells were from the cell line collection of the Institute of Molecular Genetics. T cell line J77 ($CD4^+$ Jurkat) was provided by Dr. O. Acuto (Institut Pasteur, Paris, France).

Antiserum to LIME was produced in the Prague laboratory by immunization of rabbits with bacterially expressed and Talon purified (CLONTECH Laboratories, Inc.) cytoplasmic fragment of human LIME (described under constructs), and mouse mAbs to LIME were prepared using standard techniques from splenocytes of mice immunized with the same bacterially produced LIME fragment. In addition, antipeptide mAbs were prepared against the COOH-terminal peptide comprising residues 281–296 of the human molecule (purchased from PolyPeptide Laboratories) conjugated to keyhole limpet hemocyanin using a commercial kit (Pierce Chemical Co.). Rabbit antiserum to LAT (13) was provided by Dr. L. Samelson (National Institute of Child Health and Human Development, National Institutes of Health, Bethesda, MD).

The sources of the other antibodies used were as follows: mAb to phosphotyrosine (4G10; UBI), rabbit polyclonal antibodies to Erk1/2 (Promega), phospho-Lck (Tyr^{505}) and phospho-Src family (Tyr^{416}) (New England Biolabs, Inc.), Csk (Santa Cruz Biotechnology, Inc.), mAbs to CD3 (OKT3; Ortho), CD28 (IgM isotype; provided by Dr. U. Moebius, University of Heidelberg, Germany), and CD4 (B66.1; donated by Dr. C.T. Baldari, University of Siena, Siena, Italy). mAbs to Lck (LCK-01), CD4 (MEM-16, MEM-115, MEM-241), CD8 (MEM-31), CD3ε (MEM-92, MEM-57), CD20 (MEM-97), and CD56 (MEM-188) were all prepared in the Prague laboratory.

Immunoprecipitation, In Vitro Kinase Assay, and Other Biochemical Methods. LIME and LIME-containing complexes were immunoprecipitated from postnuclear supernatants of cells solubilized by a detergent effectively disrupting lipid rafts (laurylmaltoside [*N*-dodecyl β-D-maltoside]; Calbiochem) (lysis buffer: 1% laurylmaltoside in 20 mM Tris, pH 7.5, containing 100 mM NaCl, 10% glycerol, 1 mM 4-[2-aminoethyl]-benzenesulfonyl fluoride, 10 mM EDTA, 50 mM NaF, 1 mM Na_3VO_4) using CNBr-Sepharose beads (Amersham Biosciences) coupled with mAbs purified by protein A–Sepharose affinity chromatography. The lysates were passed through minicolumns (30–50 μl packed volume) of such immunosorbents; after washing with 10 column volumes of lysis buffer, bound proteins were eluted with 2 column volumes of 2× concentrated SDS sample buffer and the flow-through, and eluted fractions were analyzed by SDS-PAGE followed by Western blotting.

In vitro kinase assays were performed as described before (14). Briefly, cells were solubilized in ice cold 1% laurylmaltoside lysis buffer (see previous paragraph), and the postnuclear supernatants were incubated in plastic wells coated with appropriate mAbs. After washing, the kinase solution (20 mM Hepes, pH 7.4, 5 mM $MgCl_2$, 5 mM $MnCl_2$, 0.1% detergent Igepal [Sigma-Aldrich]) containing 0.1 μCi [γ-^{32}P]ATP (ICN) per well was added, and the proteins phosphorylated by kinases present in the immunoprecipitates were resolved by SDS-PAGE followed by autoradiography and immunoblotting. In some cases, purified cytoplasmic domain of TCR-interacting molecule (TRIM) protein (15) (30 μg/ml) was used as an exogenous Lck substrate and added together with 0.5 μCi [γ-^{32}P]ATP per well. At the end of the test, the content of the wells was taken and processed for SDS-PAGE and autoradiography. For control, the wells were then washed, and phosphorylated proteins in immunoprecipitates were resolved as in the standard kinase assay. Lipid raft separation by sucrose gradient ultracentrifugation was performed essentially as described before, using 3% Brij-58 detergent for membrane solubilization; the density gradient fractions were analyzed by SDS PAGE and Western blotting (9). In some experiments, cells were directly solubilized in 2× concentrated SDS sample buffer, ultracentrifuged (250,000 *g*, 30 min), and the supernatant was analyzed by SDS-PAGE and Western blotting. Biosynthetic labeling with ^{3}H-palmitate, SDS-PAGE, and Western blotting were performed as described (11).

PCR. Nested PCR with two sets of primers (first 5′-GAGAATTCTGCACAAAGACCTTCCTGG-3′ plus 5′-GAGAATTCACAGGTCCTTGAGTGTTCAG-3′ and then the same 5′ end primer plus 5′-GCAGCACCCTAGAACCCAGA-3′ primer) was used to detect the LIME cDNA in the Multiple Tissue Panels I and II and the Immune System Panel (CLONTECH Laboratories, Inc.).

DNA Constructs and Transfections. The coding region of human LIME was amplified from human leukocyte cDNA library (CLONTECH Laboratories, Inc.) (primers: 5′-GAGAATTCTGCACAAAGACCTTCCTGG-3′ and 5′-GAGAATTCACAGGTCCTTGAGTGTTCAG-3′). The PCR product was cloned into EcoRI site of pBluescript SK vector (Stratagene) and sequenced. For bacterial expression, the LIME intracellular fragment corresponding to aa 141–295 was cloned into XhoI and BamHI sites of pET-15b expression vector (Novagen), generating a construct with NH_2-terminal histidine tag. For expression in eukaryotic cells, LIME coding sequence was subcloned into EcoRI site of pEFIRES-N vector (16) (provided by Dr. S. Hobbs, Institute of Cancer Research, London, UK). For transient transfection of 293T cells, Lipofectamine 2000™ reagent (Invitrogen) was used according to manufacturer's instructions. For transfection experiments in 293T cells, the following cDNA constructs were used: Flag-tagged Lck and Myc-tagged ZAP-70 inserted into pcDNA3 vector (donated by Dr. R. Abraham, Mayo Clinic, Rochester, Minnesota), Fyn cloned in pSRα expression

vector (provided by Dr. A. da Silva, Dana Farber Cancer Institute, Boston, MA), Csk in pEF-BOS vector (9), Syk cloned into the pRK5 vector (provided by Dr. W. Kolanus, Gene Center, Munich, Germany), Myc-tagged Lyn in pcDNA3.1 vector (provided by Dr. S. Watson, University of Oxford, Oxford, UK), and Flag-tagged Hck in pcDNA1 vector (provided by Dr. G. Langsley, Institut Pasteur, Paris, France).

J77 cells (Jurkat T cell line expressing CD4; essentially devoid of endogenous LIME expression) were transfected with the LIME-pEFIRES-N construct by electroporation, and stable transfectants were selected by growing the cells in 96-well plate in selective medium containing 1 mg/ml G418 (Calbiochem). After 3 wk, oligoclonal G418-resistant populations were expanded and checked for LIME expression by Western blotting. Single Tyr→Phe mutants were produced by site-directed mutagenesis using the QuickChange XL Site-Directed Mutagenesis kit (Stratagene) according to the manufacturer's protocol. COOH-terminally FLAG-tagged NTAL was produced by site-directed mutagenesis using the same kit; FLAG-tagged LIME construct was generated by PCR using the primer containing sequence for FLAG. All mutated nucleotide sequences were verified by full-length sequencing and subcloned to pEFIRES-N.

For overexpression in peripheral blood T cells, LIME was subcloned into EcoRI site of pXJ41 vector (17), and the transfection was performed using the nucleofector apparatus and human T cell nucleofector kit (Amaxa Biosystems) according to the manufacturer's instructions.

Confocal Microscopy. J77-LIME transfectants were spun on coverslips coated with poly-L-lysine (Sigma-Aldrich), and fixed and permeabilized 3 min in −20°C methanol and then 5 s in cold acetone. After washing in PBS, the slides were blocked in PBS containing 1% BSA and incubated 45 min with mouse mAb to LIME (LIME-1, 50 μg/ml), followed by 45 min incubation with Alexa 488 goat anti–mouse IgG (Molecular Probes, 500× diluted). Nuclei were stained with propidium iodide (Molecular Probes, 10 min, 0.5 μg/ml). The samples were mounted in PBS and viewed on a Laserscan microscope (Leica TCS SP). Incubation with irrelevant primary antibody and staining of nontransfected J77 cells served as a negative control.

Cell Activation. Peripheral blood T cells were stimulated by 2 min incubation with anti-CD3 (MEM-92) or anti-CD4 (MEM-16) IgM mAbs (~10 μg/ml) at 37°C. In some experiments, a combination of anti-CD4 mAbs (MEM-16 + MEM-115 [IgG] + MEM-241 [IgG]; ~10 μg/ml each) for 2 min at 37°C was used. When IgG mAbs alone were used (anti-CD4 [MEM-241], anti CD8 [MEM-31]), the cells were first preincubated 30 min on ice with the primary antibody (~10 μg/ml), washed with ice cold medium, and stimulated by cross-linking with 10 μg/ml goat anti–mouse polyclonal antibody (ICN) for 2 min at 37°C. The cells were then lysed, subjected to LIME immunoprecipitation, and LIME phosphorylation was determined by anti-phosphotyrosine (P-Tyr) immunoblotting. In some experiments the cells were pretreated for 7–20 min with 2.5–10 μg/ml of the Src kinase family inhibitor PP2 (Calbiochem).

For long term activation, culture dishes were precoated with purified sterile anti-CD3 mAb MEM-57 (IgG2a; final concentration 10 μg per ml of 0.1 M Tris, pH 9.5) for 4 h at 37°C. Dishes were washed three times with RPMI medium without serum, and 5 million T cells, resuspended in 5 ml RPMI supplemented with FCS and 500 IU IL-2 (Chiron), were seeded per 5-cm dish. Cells were then cultured, harvested, and lysed at indicated time points. Where indicated, cells were removed from the anti–CD3-coated dish, washed, and cultured in a new uncoated dish in the presence of IL-2 (100 IU/ml). For phytohemagglutinin (PHA) stimulation, PBLs were cultured for 3 d in RPMI medium with 10% FCS and PHA (Wellcome Reagents; commercial stock solution diluted for optimal activity 50×).

To measure Ca^{2+} response to anti-CD3 activation, J77 cells were electroporated either with FLAG-tagged LIME or NTAL expression constructs or with an empty pEFIRES-N vector. After 48 to 72 h in culture, the cells were transferred to Hepes-buffered Hank's balanced salt solution with 1% FCS and loaded with Fluo-4 and Fura Red dyes (Molecular Probes, each 1 μg/100 μl containing 10^6 cells) for 20 min at room temperature. The cells were washed in the same buffer incubated for 10 min at room temperature and then warmed for 10 min at 37°C. The measurement was performed on the FACSort™ flow cytometer (Becton Dickinson) in a heated holder (37°C); after measuring the baseline, the anti-CD3 IgM mAb MEM-92 (10^5 diluted ascitic fluid) was added, and eventually, when the response subsided the calcium ionophore ionomycin (Molecular Probes) was used to determine the absolute maximal response. The analysis was performed using the FlowJo program (Tree Star, Inc.). From a kinetic curve constructed from ratios of Fluo-4 to FuraRed fluorescence, the average baseline, the maximum after anti-CD3 stimulation, and the average response to ionomycin were deduced.

Results

LIME, A Novel Lipid Raft-Associated Transmembrane Adaptor Protein. Public databases were searched for proteins possessing the following structural features: (a) an NH_2-terminal peptide consisting of 5–50 amino acids followed by a transmembrane helix; (b) a palmitoylation motif (CxxC) starting 0–4 amino acids downstream from the transmembrane helix; and (c) at least one tyrosine-based motif (Yxx[I/L/V]) in the COOH-terminal (presumably cytoplasmic) portion of the protein. This approach yielded a number of candidate proteins, most of them being false positives (e.g., proteins with NH_2-terminal signal peptide). However, the search identified also the already known transmembrane adaptors PAG/Cbp and NTAL/LAB. Among several other potentially interesting molecules we identified a protein carrying the GenBank/EMBL/DDBJ accession no. BAA91148. BLAST search revealed that the sequence of its murine homologue, LIME (standing for "Lck interacting molecule") is also available under GenBank/EMBL/DDBJ accession no. AAG35210. Although Hur et al. (18) submitted the sequence to the database already in 1998, no biochemical or functional characterization of LIME has been reported up to now.

The human *LIME* cDNA codes for a strongly basic polypeptide (predicted pI 9.7) of 295 amino acid residues and a predicted molecular weight of 31,229 daltons (Fig. 1). The leaderless type III protein consists of a very short NH_2-terminal extracellular peptide (4 aa), a single putative hydrophobic transmembrane domain (23 aa), which is followed by a potential palmitoylation site (a CxxC motif) and two arginine residues. The predicted cytoplasmic domain contains a total of five tyrosines, all potentially phosphorylated by Src family kinases. Two of the tyrosine-based signaling motifs (Y^{200} and Y^{235}, respectively) potentially represent immunoreceptor tyrosine-based inhibition motifs.

```
  1   MGLPVSWAPP ALWVLGCCAL LLSLWALCTA CRRPEDAVAP
 41   RKRARRQRAR LQGSATAAEA SLLRRTHLCS LSKSDTRLHE
 81   LHRGPRSSRA LRPASMDLLR PHWLEVSRDI TGPQAAPSAF
121   PHQELPRALP AAAATAGCAG LEATYSNVGL AALPGVSLAA
161   SPVVAEYARV QKRKGTHRSP QEPQQGKTEV TPAAQVDVLY
201   SRVCKPKRRD PGPTTDPLDP KGQGAILALA GDLAYQTLPL
241   RALDVDSGPL ENVYESIREL GDPAGRSSTC GAGTPPASSC
281   PSLGRGWRPL PASLP
```

Figure 1. Predicted amino acid sequence of human LIME. The putative transmembrane region is boxed, and the potential palmitoylation sequence and tyrosine motifs are in bold and underlined.

LIME transcripts were detected by PCR in cDNA prepared from PBLs, various lymphoid tissues, and liver but not other tissues (Fig. 2, A and B). In Western blotting experiments, both polyclonal and monoclonal antibodies directed to COOH-terminal fragments of LIME recognized a zone of the appropriate size in peripheral blood T cells, which strongly increased in intensity after overexpression of LIME (Fig. 2 C). Strong expression of LIME was also observed in purified $CD56^+$ cells (mixture of NK cells and NK T cells). However, when further separated NK cells (CD3-negative) were found to express only little LIME compared with NK T cells (unpublished data). Similarly, purified blood B lymphocytes express only low amounts of LIME, and the molecule seems to be absent in monocytes (Fig. 2 D). In addition, all thymocyte subsets (double negative, double positive, single positive) contained comparable amounts of LIME, and no marked differences in the level of LIME expression could be detected in purified subsets of peripheral blood T cells ($CD4^+$, $CD8^+$, $CD45RA^+$, $CD45RO^+$, $CD4^+CD25^+$, $CD4^+CD25^-$, γδ Tcells; not depicted). Among the T cell lines tested (Jurkat, HPB ALL, HUT-78, SupT1, Molt-4, and CEM), only Jurkat cells are essentially negative for LIME protein expression (not depicted). Expression of LIME strongly decreased when peripheral blood T cells were activated in vitro for several days using PHA or plastic-immobilized CD3 mAb (Fig. 2, E and F). When the stimulated T cells were transferred in new culture dishes and cultivated further in the absence of external stimuli, LIME became rapidly and strongly reexpressed (Fig. 2 F). These data suggest that expression of LIME in peripheral blood T cells is controlled by external stimuli mediated via the TCR (or other PHA-responsive cell surface receptors).

As shown in Fig. 3, LIME is mostly present in buoyant lipid rafts (Fig. 3 A) and can be biosynthetically labeled by ^{3}H-palmitate (Fig. 3 B), indicating that the membrane-proximal putative palmitoylation motif is used for targeting the protein into lipid rafts. Moreover, LIME clearly localizes to the plasma membrane as judged from confocal microscopy of Jurkat T cells stably overexpressing the molecule (Fig. 3C). Collectively, these data suggest that LIME represents an integral membrane protein associated with lipid rafts.

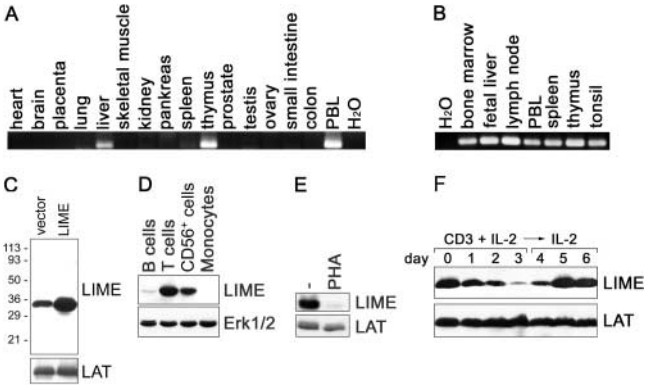

Figure 2. Expression of LIME. (A) Presence of LIME mRNA in various tissues as detected by PCR from the Multiple Tissue cDNA Panels I and II (CLONTECH Laboratories, Inc.) and (B) the Immune System Panel (CLONTECH Laboratories, Inc.). (C) Western blotting of vector- and LIME-transfected peripheral blood T cells (immunostaining for LIME and LAT; the latter was used as a loading control). (D) Western blotting of indicated subpopulations of human peripheral blood cells (immunostaining for LIME and Erk1/2; the latter was used as a loading control). (E) Western blotting of resting and PHA-activated peripheral blood T cells (immunostaining for LIME and LAT; the latter was used as a control). (F) Kinetics of LIME downmodulation in peripheral blood T cells stimulated by immobilized anti-CD3 mAb and LIME reexpression after removal of the cells from anti-CD3–coated wells (after day 3) and further culturing in the presence of IL-2. Cell lysates were analyzed by Western blotting for the presence of LIME and LAT. The same results were obtained when IL-2 was not added to the culture medium (not depicted).

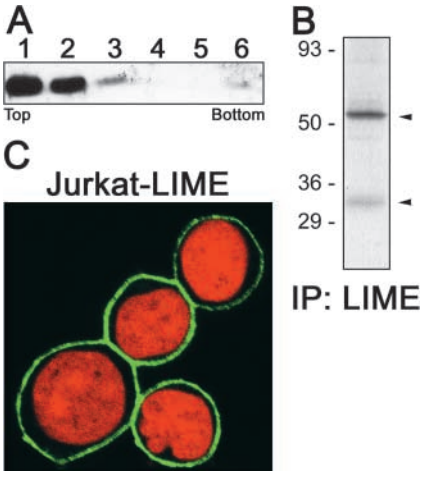

Figure 3. Subcellular localization of LIME. (A) Localization of LIME in buoyant detergent-resistant microdomains (lipid rafts). Peripheral blood T cells were solubilized in the presence of 3% nonionic detergent Brij-58 and subjected to sucrose density gradient ultracentrifugation; the fractions (numbered from top to bottom) were analyzed by Western blotting. (B) Biosynthetic labeling of LIME with ^{3}H-palmitate; LIME immunoprecipitate was analyzed by SDS-PAGE followed by fluorography of the gel (the 56-kD zone corresponds probably to associated Lck). (C) Plasma membrane localization of LIME (green) as determined by confocal microscopy in J77-LIME.

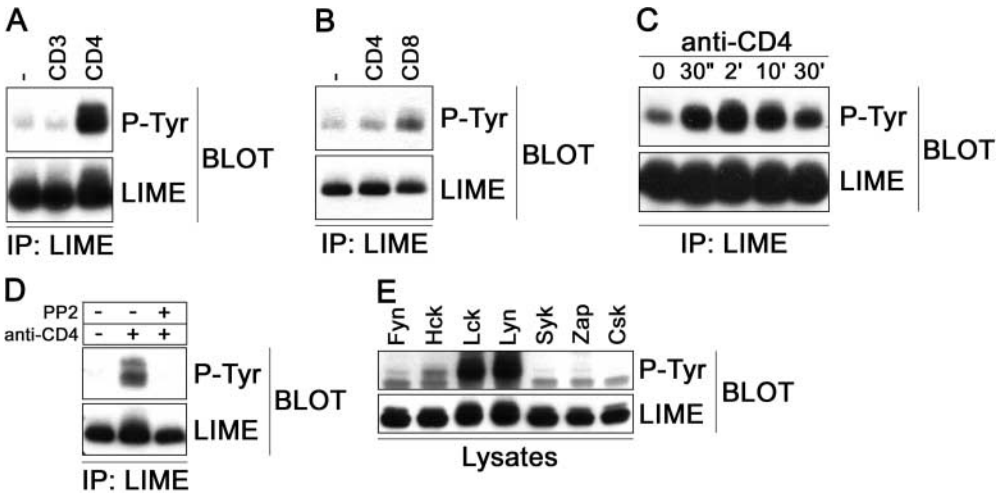

Figure 4. Induction of LIME tyrosine phosphorylation. (A) Peripheral blood T cells were left unstimulated (−) or stimulated via CD3 or CD4, and LIME was immunoprecipitated from lauryl-maltoside lysates and analyzed by Western blotting to visualize tyrosine-phosphorylated LIME (top) and total LIME (bottom). (B) As in A but using purified $CD8^+$ T cells stimulated by mAbs to CD4 (negative control), CD8, or not stimulated (−). (C) Kinetics of LIME phosphorylation after T cell stimulation via CD4; stimulation was stopped after the indicated times (0–30 min). Immunoprecipitated LIME was analyzed by Western blotting using antibodies to P-Tyr (top) or LIME (bottom). (D) Inhibition of anti–CD4-induced LIME phosphorylation in T cells by the inhibitor of Src kinases PP2. LIME immunoprecipitates were analyzed by Western blotting for P-Tyr and LIME. (E) Kinases phosphorylating LIME were examined by cotransfection of constructs encoding LIME, and the indicated kinases in 293T cells; total cell lysates were analyzed by Western blotting using antibodies to P-Tyr (top) or LIME (bottom). Expression of all the kinases was verified separately (not depicted).

Engagement of the CD4 or CD8 Coreceptors Induces Tyrosine Phosphorylation of LIME and Its Association with Protein Tyrosine Kinases Lck and Csk. The overall similarity between LIME, LAT, PAG/Cbp, and NTAL/LAB indicated that LIME might be inducibly tyrosine phosphorylated after ligation of some cell surface receptor(s). To identify such receptors, a broad screening involving antibody-mediated cross-linking of multiple lymphocyte surface molecules was performed. This approach revealed that LIME becomes tyrosine-phosphorylated exclusively after antibody-mediated engagement of the CD4 or CD8 coreceptors (Fig. 4) but not after triggering CD2, CD3, CD5, CD7, LFA-1, CD43, CD45, or MHC class I (not depicted). Cocross-linking of CD4 and CD3 consistently produced lower levels of LIME tyrosine phosphorylation than CD4 cross-linking alone (not depicted).

As shown in Fig. 4 C, after cross-linking of CD4 phosphorylation of LIME was maximal after 2 min and slowly declined thereafter. LIME became also tyrosine phosphorylated after cross-linking of CD4 on the surface of anti-CD3 activated, IL-2–propagated T cell blasts (not depicted).

To determine which protein tyrosine kinases (PTKs) might be responsible for phosphorylation of LIME, we treated human peripheral blood T cells with the Src family PTK inhibitor PP2 before CD4 cross-linking. As shown in Fig. 4 D, pretreatment with PP2 strongly suppressed the CD4-mediated tyrosine phosphorylation of LIME. In agreement with this result, coexpression of LIME with the protein tyrosine kinases Fyn, Lck, Lyn, Hck, Csk, Syk, or ZAP-70 in 293T-cells revealed that LIME represents a substrate for PTKs of the Src family, in particular Lck or Lyn (Fig. 4 E).

The next series of experiments was performed to assess molecular interactions between LIME and other signaling molecules expressed in T cells. These experiments indicated that the Src family kinase Lck and the negative regulator of Src kinases, the Csk kinase, specifically associate with phosphorylated LIME in CD4-stimulated T lymphocytes (Fig. 5 A). Analysis of the LIME immunoprecipitates using phosphospecific antibodies further suggested that LIME-associated Lck was phosphorylated on both the COOH-terminal inhibitory and the activating tyrosine residues (Y^{505} and Y^{394}, respectively; Fig. 5 A). The inducible association of LIME with PTK activity was also demonstrated by an in vitro kinase assay using LIME immunoprecipitates prepared from unstimulated or anti-CD4–stimulated T cells (Fig. 5 B).

Strikingly, when stably expressed in the CD4-positive Jurkat T cell line (J77), LIME displayed constitutive strong tyrosine phosphorylation and bound Lck, Csk, and also Fyn (Fig. 6) even without CD4 cross-linking; constitutive tyrosine phosphorylation of LIME was observed also in all

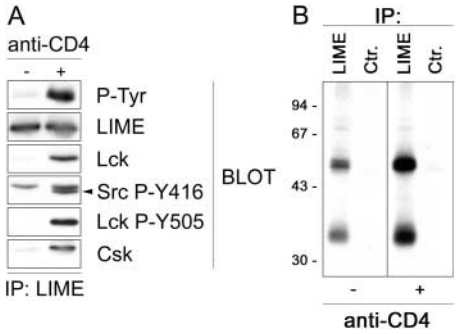

Figure 5. Proteins associated with phosphorylated LIME. (A) LIME immunoprecipitates prepared from unstimulated (left) or anti–CD4-stimulated (right) T cells (solubilized under raft-dissociating conditions) were analyzed by Western blotting using antibodies to the indicated molecules. (B) In vitro kinase assay of the LIME immunoprecipitates obtained from unstimulated and anti–CD4-stimulated T cells; as a negative control (Ctr.) an irrelevant antibody (anti-CD20) was used for the immunoprecipitation.

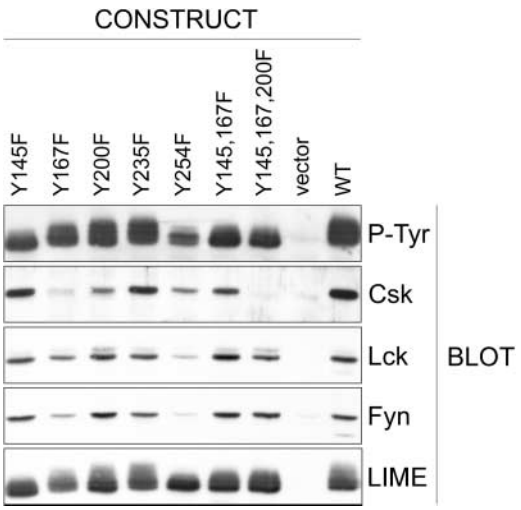

Figure 6. Identification of the P-Tyrs involved in binding of Lck, Fyn, and Csk. LIME immunoprecipitates from lysates of J77 cells stably transfected with the indicated Tyr to Phe mutants of LIME were analyzed by Western blotting for the presence of the indicated molecules.

T cell lines expressing LIME naturally [unpublished data]). Moreover, the level of LIME phosphorylation and its association with Lck and Csk, respectively, did not change significantly in these transfectants after CD4 cross-linking. However, brief pretreatment of these transfectants with the Src family PTK inhibitor PP2 led to a substantial decrease of the constitutive phosphorylation of LIME; in such pretreated cells, LIME rephosphorylation could be achieved by cross-linking of CD4 by antibodies or recombinant HIV-derived gp120 (not depicted). The reason for the constitutive tyrosine phosphorylation of LIME in J77 is unclear at present but might be due to a deregulation of the membrane-proximal signaling pathways in the transformed cells (see Discussion).

To assess which tyrosine residues of LIME mediate its interaction with Lck and Csk, respectively, a series of stable J77 transfectants were generated expressing tyrosine mutants of LIME. It could be demonstrated that Y^{254} represents the binding site for Lck (and Fyn) (Fig. 6). Indeed, this site corresponds to a high stringency binding site for Lck and Fyn as predicted by the scansite program (http://scansite.mit.edu) (19). In contrast, phosphorylated Y^{167} and potentially also Y^{200} appear to mediate the interaction between LIME and Csk. These tyrosine-based signaling motifs readily fit the consensus sequence that is found in various Cbps and the consensus sequence selected from peptide libraries (Table I).

Further analysis of the J77-LIME transfectant indicated that the amounts of lipid rafts-associated Lck and Csk are either slightly (in the case of Lck) or strongly increased (in the case of Csk) in these cells compared with WT J77 cells (Fig. 7 C). These data confirm that tyrosine-phosphorylated LIME is capable of targeting Lck and Csk to lipid rafts.

The data shown in Fig. 7 A demonstrate that in J77-LIME transfectants the LIME-associated fraction of Lck is more strongly phosphorylated on the inhibitory tyrosine Y^{505} compared with the total pool of Lck. In addition, an in vitro kinase assay of Lck immunoprecipitates prepared from J77-LIME cells results in a much stronger phosphorylation of Lck than in WT J77 cells (Fig. 7 B). Furthermore, LIME-associated Lck was even stronger phosphorylated than Lck immunoprecipitated from the total pool of Lck in the J77-LIME cells (Fig. 7 B). This could be either due to a higher enzymatic activity of the LIME-associated Lck (resulting in a higher level of autophosphorylation) or due to an increased phosphorylation of Lck by LIME-associated Csk.

Table I. *Comparison of Published Csk Binding Sequences*

Protein name and binding site position	Csk binding sequence	Reference
LIME Y^{167}	V A E **Y** A R V Q K R K	This paper
LIME Y^{200}	D V L **Y** S R V C K P K	This paper
Paxillin Y^{118}	E H V **Y** S F P N K Q K	39
Caveolin Y^{14}	G H L **Y** T V P I R E Q	40
PTP-HSCF Y^{354}	A D T **Y** A V V Q K R G	41
PTP-HSCF Y^{381}	T P I **Y** S Q V A P R A	41
IGF-IR Y^{943}	G V L **Y** A S V N P E Y	42
IGF-IR Y^{1316}	R Q P **Y** A H M N G G R	42
InsulinR Y^{1322}	H I P **Y** T H M N G G K	42
p62dok Y^{449}	S A L **Y** S Q V Q K S G	43
PAG Y^{317}	S A M **Y** S S V N K P G	9
SIT Y^{169}	P E L **Y** A S V C A Q T	44
Hic-5 Y^{60}	D H L **Y** S T V C K P R	45
Peptide library	**Y**[T/A/S][K/R/Q/N][M/I/V/R]	46

Critical tyrosines are bolded, other amino acids participating in the putative consensus motif are underlined.

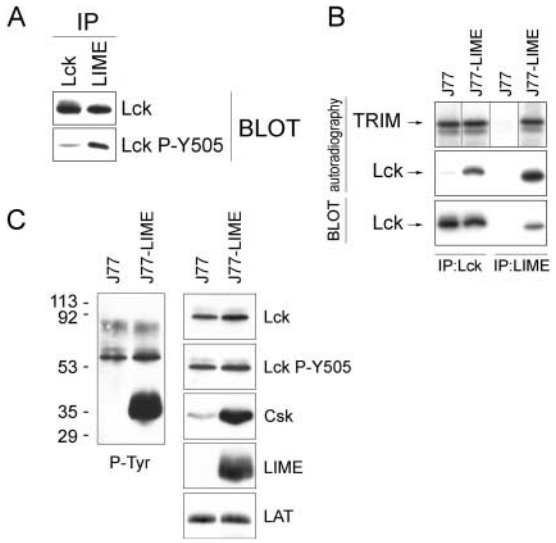

Figure 7. Effects of LIME on Lck and Csk in J77-LIME stable transfectants. (A) The concentration of directly immunoprecipitated Lck was adjusted to equate on the Western blot to the amount of Lck coprecipitated with LIME (top), and the blot was then stained with antibody specifically recognizing the phosphorylated Tyr^{505}. (B) In vitro kinase assay was performed using purified cytoplasmic domain of TRIM protein as an exogenous substrate for Lck immunoprecipitated from J77-LIME transfectants or from cells transfected with an empty vector. The phosphorylated proteins in immunoprecipitates were also resolved to check content (immunoblotting) and phosphorylation status (autoradiography) of Lck. The dividing lines in the TRIM panel indicate that these lanes were not adjacent in the original gel, and the far right-hand lane is from a different gel, which was processed simultaneously. (C) Localization of Lck and Csk in lipid rafts of J77-LIME transfectants or cells transfected with an empty vector. Cells were solubilized in the presence of 3% nonionic detergent Brij-58 and subjected to sucrose density gradient ultracentrifugation; the fractions (numbered from top to bottom) were analyzed by Western blotting.

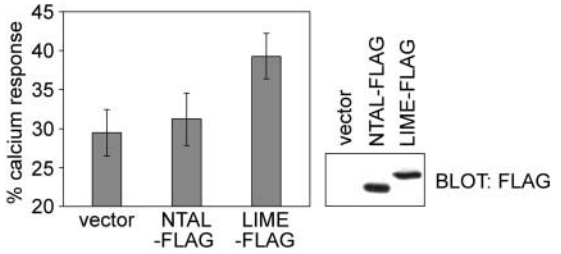

Figure 8. Effects of LIME on anti–CD3-induced Ca^{2+} response. J77 cells transiently transfected with the indicated constructs were stimulated by cross-linking of CD3. The results are presented as a proportion of the peak anti-CD3 response to the maximum response induced by Ca^{2+} ionophore ionomycin after correction for basal level. The results are representative of three independent experiments and show the mean and SD of four measurements. The observed increase is statisticaly significant at the 5% level (Student's *t* test). The right panel shows the comparable level of LIME and NTAL expression as determined by Western blotting and immunostaining of FLAG tag.

To distinguish between these possibilities, we assessed the capability of Lck to phosphorylate an exogenous substrate (the cytoplasmic domain of the transmembrane adaptor protein TRIM, which has been shown to be an excellent substrate for Lck in vivo [20]). As shown in Fig. 7 B (top), the ability of Lck to phosphorylate TRIM appears to be the same in J77-LIME cells and in J77 cells transfected with an empty vector. These data collectively support the hypothesis that the higher levels of tyrosine phosphorylation of LIME-associated Lck primarily result from phosphorylation of Y^{505} by the LIME-associated Csk. Moreover, they suggest that expression of LIME in Jurkat T cells leads to increased phosphorylation of Lck by Csk without dramatically altering the enzymatic activity of Lck. This finding can be best explained by the fact that the Src homology (SH)2 domain of Lck is not available for interaction with phospho-Y^{505} because it is engaged by phosphorylated LIME (Y^{254}), and therefore, the closed inactive conformation of Lck cannot be formed.

LIME Increases Ca^{2+} Response After Stimulation of J77 Cells. Transient expression of LIME in J77 cell leads to a significantly higher Ca^{2+} response to anti-CD3 stimulation compared with cells transfected with an empty vector, whereas another raft-associated transmembrane adaptor protein NTAL, expressed at the same level, does not change this response significantly (Fig. 8).

Discussion

Transmembrane adaptor proteins (TRAPs) are emerging as important molecules involved in coupling immunoreceptors to intracellular signaling pathways (1–3). Two types of TRAPs can be distinguished, namely those that are excluded from the rafts (TRIM [20], SHP2-interacting transmembrane adaptor [21], and linker for activation of X [LAX] [22]) and those that are targeted to rafts via juxtamembrane palmitoylation of a di-cysteine motif CxxC (LAT [7, 8], PAG/Cbp [9, 10], NTAL/LAB [11, 12], and LIME). The increasing number of the raft-associated TRAPs is in agreement with the currently recognized importance of membrane rafts in receptor signaling and other cellular processes (1–3). LAT and NTAL/LAB are involved in signaling initiated by immunoreceptors (TCR and BCR or Fc receptors, respectively [11, 12, 23]), whereas PAG/Cbp participates more generally in negative regulation of Src family kinases and thus indirectly controls immunoreceptor signaling (9, 10, 24–26).

LIME, the novel TRAP described herein, appears not to be a direct target of immunoreceptor-mediated signaling events. Rather, its phosphorylation and association with intracellular signaling and effector molecules (Lck and Csk) seems to be controlled in primary T cells by the coreceptors CD4 and CD8. Csk and Lck (plus Fyn) also associate with LIME when the molecule is expressed in the J77 Jurkat T cell line; notably, in these transfectants LIME is constitutively tyrosine phosphorylated, and its phosphorylation status apparently does not change upon CD4 (nor CD3) cross-linking. Importantly, the Lck molecules that associate with phosphorylated LIME are phosphorylated both on the COOH-terminal negative regulatory Y^{505} and on the positive regulatory Y^{394} and exhibit somewhat paradoxically an increased autophosphorylation activity. It seems likely that the inhibitory phospho-Y^{505} is unable to exert its inhibitory

function, since the Lck SH2 domain is bound to the phospho-LIME (see further discussion of this point below). Interestingly, despite the presence of two putative immunoreceptor tyrosine-based inhibition motifs in the cytoplasmic tail of LIME, so far we could not detect any SH2 domain containing phosphatase (SHP-1, SHP-2, or SHIP) in LIME immunoprecipitates prepared from activated (even pervanadate-treated) cells.

What are possible biological functions of this novel raft-associated adaptor? Induction of tyrosine phosphorylation and association with Lck and Csk after CD4 or CD8 cross-linking strongly indicates that LIME plays a role in regulation or propagation of coreceptor signaling.

The roles of the coreceptors (so far studied mainly for CD4) may be twofold, depending on whether the coreceptor is coengaged with the TCR or cross-linked separately. Cocross-linking of CD4 with the TCR generally potentiates TCR-mediated signaling events, obviously due to bringing the CD4-associated fraction of Lck into the proximity of the cytoplasmic tails of the CD3 complex and the ζ chains (27, 28). LIME might play a potentiating role in this physiological signaling. This view is supported by our observation that transient overexpression of LIME in J77 Jurkat T cells increases Ca^{2+} responses after CD3 stimulation. Moreover, when stably expressed in J77 cells LIME is expressed as a constitutively phosphorylated protein. This could correspond to the situation that occurs in primary T cells after coreceptor engagement.

In contrast to coengagement with the TCR, separate cross-linking of CD4 either by antibodies to suitable CD4 epitopes or by HIV gp120 is known to inhibit or markedly modify the outcome of the subsequent signaling induced by TCR engagement (29, 30). Moreover, in rodent models selective ligation of CD4 in vivo by certain antibodies results in remarkably robust alloantigen-specific immunosuppression and induction of specific transplantation tolerance, which is apparently mediated by regulatory T cells secreting suppressive cytokines (31, 32). Finally, CD4 signaling may also modify LFA-1–dependent adhesivity (33). Little is known about the molecular mechanisms underlying these inhibitory functions of CD4. However, CD4 cross-linking alone can induce signaling pathways similar to those triggered by TCR (activation of Lck and Fyn, initiation of the Ras-Raf-MAPK, and phospholipase Cγ-PKC-Ca^{2+} pathways, resulting in activation of the NF AT, NFκB, and AP-1 transcription factors) (34, 35). The final result of signaling mediated solely via CD4 may be either induction of apoptosis or presensitization of T cells to CD3-mediated apoptosis (34, 36, 37).

It is tempting to speculate that LIME is involved in these inhibitory aspects of CD4 signaling: it may, for example, compete with CD4 for Lck and at the same time it may bring more Csk to membrane rafts (Fig. 7 C). This could eventually result in inhibition of Src family kinases, which are needed for TCR signaling. This model of LIME function is, however, not very well compatible with our observation that Lck isolated from J77-LIME transfectants and

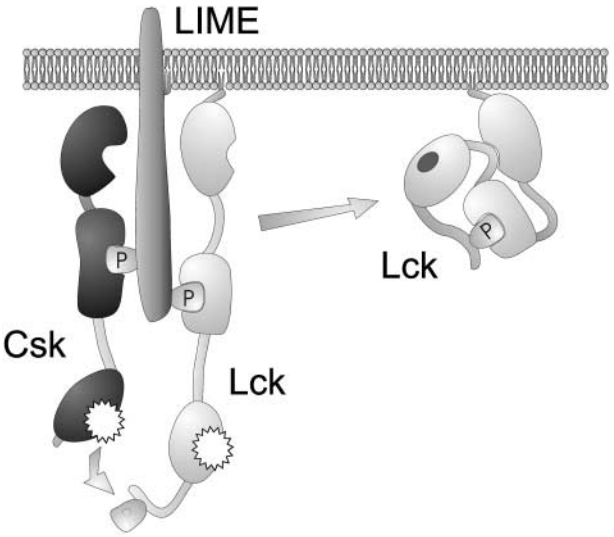

Figure 9. Hypothetical mechanism of LIME involvement in regulation of Lck activity.

LIME-associated Lck (which is more phosphorylated on the COOH-terminal inhibitory tyrosine) has a kinase activity comparable to Lck from control cells. Nevertheless, it is possible to propose the following model for LIME function (Fig. 9): cross-linking of CD4 induces aggregation or reorganization of lipid rafts containing LIME, CD4-Lck, and free Lck. By this, Lck (free or CD4-associated) is brought into proximity of LIME and phosphorylates the adaptor. Now, cytoplasmic Csk and free Lck bind to tyrosine-phosphorylated LIME via their SH2 domains. In the resulting complex, Csk phosphorylates Lck on Y^{505} (either on the same LIME adaptor or on a different LIME molecule in close proximity). However, the Lck phosphorylated on Y^{505} remains enzymatically active because its SH2 domain is bound to phospho-LIME and thus cannot be engaged by phospho-Y^{505} (with the consequence that the inactivating "closed" conformation of Lck cannot be formed). LIME-associated, "open" Lck could phosphorylate additional molecules thus propagating the CD4-mediated signal. In addition (or alternatively), phospho-Y^{505} of LIME-bound Lck could serve as a docking site for additional signaling proteins (including Lck or Fyn). Recruitment of these molecules to the LIME–Csk–Lck complex could further amplify the CD4-mediated signal. Subsequently, the phosphorylated Lck may dissociate from LIME, assume the "closed" conformation, and remain inactive in the lipid raft. A model in which LIME-associated Lck recruits and activates lipid raft-associated Fyn might explain the recent report that the activation of Fyn within the lipid microdomains is preceded (and requires) translocation of Lck to lipid rafts (38).

A remarkable feature of LIME is its downmodulation in T cells after stimulation with PHA or immobilized anti-CD3 antibodies and its reappearance after removal of the stimulating agents. A plausible explanation could be that down-regulation of LIME serves to limit CD3/TCR-

mediated activation processes by blunting coreceptor signaling. Such a mechanism could help to prevent hyperactivation of T cells that have already seen antigen and start to differentiate into effector T-lymphocytes.

In summary, we suggest that the newly described lipid raft-associated transmembrane adaptor protein LIME may have regulatory function(s) in T cells. At the beginning of an immune response where coreceptor signaling is required to activate T cells, LIME rapidly becomes tyrosine-phosphorylated, transiently increases the activity of Lck by blocking formation of its inactive conformation, and thus amplifies TCR-mediated signals. Upon prolonged stimulation, LIME helps to accumulate inhibited Lck in lipid rafts, thereby preventing hyperactivation of T cells. In the case of antigen persistence, T cells down-regulate expression of LIME. This may be a mechanism to prevent premature termination of the immune response by blunting membrane recruitment of enzymatically active Lck. Furthermore, one may speculate that strongly positive nonphosphorylated LIME may possibly interact with membrane phospholipids or other negatively charged cytoplasmic molecules (e.g., phosphoproteins) and thereby modify their interactions with other signaling molecules. To fully understand the role of LIME during T cell activation, it will be necessary to explore its possible functional interactions with PAG/Cbp, another raft-associated transmembrane adaptor that regulates the activity of Src kinases by recruiting Csk (10, 11). Moreover, more definitive answers regarding the physiological role of LIME in T cell activation should be provided by LIME knock-out mice, currently under construction.

We would like to thank Drs. R. Abraham, O. Acuto, S. Hobbs, W. Kolanus, G. Langsley, L. Samelson, A. da Silva, and S. Watson for providing us with cells and constructs as specified in Materials and Methods.

This work was supported from the project Center of Molecular and Cellular Immunology (LN00A026) of the Czech Ministry of Education, Youth and Sports, grant J1116W24Z from the Wellcome Trust to V. Hořejší, and grant SCH 533/6-1 from Deutsche Forschungsgemeinschaft to B. Schraven.

Submitted: 28 August 2003
Accepted: 10 September 2003

References

1. Harder, T. 2001. Raft membrane domains and immunoreceptor functions. *Adv. Immunol.* 77:45–92.
2. Cherukuri, A., M. Dykstra, and S.K. Pierce. 2001. Floating the raft hypothesis: lipid rafts play a role in immune cell activation. *Immunity.* 14:657–660.
3. Horejsi, V. 2003. The roles of membrane microdomains (rafts) in T cell activation. *Immunol. Rev.* 191:148–164.
4. Saint-Ruf, C., M. Panigada, O. Azogui, P. Debey, H. von Boehmer, and F. Grassi. 2000. Different initiation of pre-TCR and γδTCR signalling. *Nature.* 406:524–527.
5. Fragoso, R., D. Ren, X. Zhang, M.W. Su, S.J. Burakoff, and Y.J. Jin. 2003. Lipid raft distribution of CD4 depends on its palmitoylation and association with Lck, and evidence for CD4-induced lipid raft aggregation as an additional mechanism to enhance CD3 Signaling. *J. Immunol.* 170:913–921.
6. Arcaro, A., C. Gregoire, N. Boucheron, S. Stotz, E. Palmer, B. Malissen, and I.F. Luescher. 2000. Essential role of CD8 palmitoylation in CD8 coreceptor function. *J. Immunol.* 165: 2068–2076.
7. Brdicka, T., J. Cerny, and V. Horejsi. 1998. T cell receptor signalling results in rapid tyrosine phosphorylation of the linker protein LAT present in detergent-resistant membrane microdomains. *Biochem. Biophys. Res. Commun.* 248:356–360.
8. Zhang, W., R.P. Trible, and L.E. Samelson. 1998. LAT palmitoylation: its essential role in membrane microdomain targeting and tyrosine phosphorylation during T cell activation. *Immunity.* 9:239–246.
9. Brdicka, T., D. Pavlistova, A. Leo, E. Bruyns, V. Korinek, P. Angelisova, J. Scherer, A. Shevchenko, I. Hilgert, J. Cerny, et al. 2000. Phosphoprotein associated with glycosphingolipid-enriched microdomains (PAG), a novel ubiquitously expressed transmembrane adaptor protein, binds the protein tyrosine kinase Csk and is involved in regulation of T cell activation. *J. Exp. Med.* 191:1591–1604.
10. Kawabuchi, M., Y. Satomi, T. Takao, Y. Shimonishi, S. Nada, K. Nagai, A. Tarakhovsky, and M. Okada. 2000. Transmembrane phosphoprotein Cbp regulates the activities of Src-family tyrosine kinases. *Nature.* 404:999–1003.
11. Brdicka, T., M. Imrich, P. Angelisova, N. Brdickova, O. Horvath, J. Spicka, I. Hilgert, P. Luskova, P. Draber, P. Novak, et al. 2002. Non–T cell activation linker (NTAL): a transmembrane adaptor protein involved in immunoreceptor signaling. *J. Exp. Med.* 196:1617–1626.
12. Janssen, E., M. Zhu, W. Zhang, and S. Koonpaew. 2003. LAB: A new membrane-associated adaptor molecule in B cell activation. *Nat. Immunol.* 4:117–123.
13. Zhang, W., J. Sloan-Lancaster, J. Kitchen, R.P. Trible, and L.E. Samelson. 1998. LAT: the ZAP-70 tyrosine kinase substrate that links T cell receptor to cellular activation. *Cell.* 92: 83–92.
14. Cinek, T., and V. Horejsi. 1992. The nature of large noncovalent complexes containing glycosyl- phosphatidylinositol-anchored membrane glycoproteins and protein tyrosine kinases. *J. Immunol.* 149:2262–2270.
15. Kirchgessner, H., J. Dietrich, J. Scherer, P. Isomaki, V. Korinek, I. Hilgert, E. Bruyns, A. Leo, A.P. Cope, and B. Schraven. 2001. The transmembrane adaptor protein TRIM regulates T cell receptor (TCR) expression and TCR-mediated signaling via an association with the TCR ζ chain. *J. Exp. Med.* 193:1269–1284.
16. Hobbs, S., S. Jitrapakdee, and J.C. Wallace. 1998. Development of a bicistronic vector driven by the human polypeptide chain elongation factor 1α promoter for creation of stable mammalian cell lines that express very high levels of recombinant proteins. *Biochem. Biophys. Res. Commun.* 252:368–372.
17. Zheng, X.M., Y. Wang, and C.J. Pallen. 1992. Cell transformation and activation of $pp60^{c\text{-}src}$ by overexpression of a protein tyrosine phosphatase. *Nature.* 359:336–339.
18. Hur, E.M., M. Son, O.-H. Lee, Y.B. Choi, C. Park, H.S. Lee, and Y. Yun. 2003. LIME, a novel transmembrane adaptor protein, associates with $p56^{lck}$ and mediates T cell activation. *J. Exp. Med.* 198:1463–1473.
19. Yaffe, M.B., G.G. Leparc, J. Lai, T. Obata, S. Volinia, and L.C. Cantley. 2001. A motif-based profile scanning approach for genome-wide prediction of signaling pathways. *Nat. Bio-*

technol. 19:348–353.
20. Bruyns, E., A. Marie-Cardine, H. Kirchgessner, K. Sagolla, A. Shevchenko, M. Mann, F. Autschbach, A. Bensussan, S. Meuer, and B. Schraven. 1998. T cell receptor (TCR) interacting molecule (TRIM), a novel disulfide-linked dimer associated with the TCR–CD3-ζ complex, recruits intracellular signaling proteins to the plasma membrane. *J. Exp. Med.* 188: 561–575.
21. Marie-Cardine, A., H. Kirchgessner, E. Bruyns, A. Shevchenko, M. Mann, F. Autschbach, S. Ratnofsky, S. Meuer, and B. Schraven. 1999. SHP2-interacting transmembrane adaptor protein (SIT), a novel disulfide-linked dimer regulating human T cell activation. *J. Exp. Med.* 189:1181–1194.
22. Zhu, M., E. Janssen, K. Leung, and W. Zhang. 2002. Molecular cloning of a novel gene encoding a membrane-associated adaptor protein (LAX) in lymphocyte signaling. *J. Biol. Chem.* 277:46151–46158.
23. Samelson, L.E. 2002. Signal transduction mediated by the T cell antigen receptor: the role of adapter proteins. *Annu. Rev. Immunol.* 20:371–394.
24. Baumgartner, M., P. Angelisova, N. Setterblad, N. Mooney, D. Werling, V. Horejsi, and G. Langsley. 2003. Constitutive exclusion of Csk from Hck-positive membrane microdomains permits Src kinase-dependent proliferation of *Theileria*-transformed B-lymphocytes. *Blood.* 101:1874–1881.
25. Ohtake, H., N. Ichikawa, M. Okada, and T. Yamashita. 2002. Cutting Edge: Transmembrane phosphoprotein Csk-binding protein/phosphoprotein associated with glycosphingolipid-enriched microdomains as a negative feedback regulator of mast cell signaling through the FcεRI. *J. Immunol.* 168:2087–2090.
26. Torgersen, K.M., T. Vang, H. Abrahamsen, S. Yaqub, V. Horejsi, B. Schraven, B. Rolstad, T. Mustelin, and K. Tasken. 2001. Release from tonic inhibition of T cell activation through transient displacement of C-terminal Src kinase (Csk) from lipid rafts. *J. Biol. Chem.* 276:29313–29318.
27. Owens, T., B. Fazekas de St Groth, and J.F. Miller. 1987. Coaggregation of the T-cell receptor with CD4 and other T-cell surface molecules enhances T-cell activation. *Proc. Natl. Acad. Sci. USA.* 84:9209–9213.
28. Eichmann, K., J.I. Jonsson, I. Falk, and F. Emmrich. 1987. Effective activation of resting mouse T lymphocytes by cross-linking submitogenic concentrations of the T cell antigen receptor with either Lyt-2 or L3T4. *Eur. J. Immunol.* 17:643–650.
29. Bank, I., and L. Chess. 1985. Perturbation of the T4 molecule transmits a negative signal to T cells. *J. Exp. Med.* 162: 1294–1303.
30. Harding, S., P. Lipp, and D.R. Alexander. 2002. A therapeutic CD4 monoclonal antibody inhibits TCR-ζ chain phosphorylation, ζ-associated protein of 70-kDa Tyr319 phosphorylation, and TCR internalization in primary human T cells. *J. Immunol.* 169:230–238.
31. Benjamin, R.J., and H. Waldmann. 1986. Induction of tolerance by monoclonal antibody therapy. *Nature.* 320:449–451.
32. Laub, R., R. Brecht, M. Dorsch, U. Valey, K. Wenk, and F. Emmrich. 2002. Anti-human CD4 induces peripheral tolerance in a human $CD4^+$, murine $CD4^-$, $HLA\text{-}DR^+$ advanced transgenic mouse model. *J. Immunol.* 169:2947–2955.
33. Mazerolles, F., C. Barbat, M. Trucy, W. Kolanus, and A. Fischer. 2002. Molecular events associated with CD4-mediated down-regulation of LFA-1-dependent adhesion. *J. Biol. Chem.* 277:1276–1283.
34. Milia, E., M.M. Di Somma, M.B. Majolini, C. Ulivieri, F. Somma, E. Piccolella, J.L. Telford, and C.T. Baldari. 1997. Gene activating and proapoptotic potential are independent properties of different CD4 epitopes. *Mol. Immunol.* 34:287–296.
35. Ulivieri, C., S. Pacini, S. Bartalini, S. Valensin, J.L. Telford, and C.T. Baldari. 1999. Obligatory cross-talk with the tyrosine kinases assembled with the TCR/CD3 complex in CD4 signal transduction. *Eur. J. Immunol.* 29:2625–2635.
36. Newell, M.K., L.J. Haughn, C.R. Maroun, and M.H. Julius. 1990. Death of mature T cells by separate ligation of CD4 and the T-cell receptor for antigen. *Nature.* 347:286–289.
37. Tuosto, L., B. Marinari, and E. Piccolella. 2002. CD4-Lck through TCR and in the absence of Vav exchange factor induces Bax increase and mitochondrial damage. *J. Immunol.* 168:6106–6112.
38. Filipp, D., J. Zhang, B.L. Leung, A. Shaw, S.D. Levin, A. Veillette, and M. Julius. 2003. Regulation of Fyn through translocation of activated Lck into lipid rafts. *J. Exp. Med.* 197:1221–1227.
39. Schaller, M.D., and J.T. Parsons. 1995. $pp125^{FAK}$-dependent tyrosine phosphorylation of paxillin creates a high-affinity binding site for Crk. *Mol. Cell. Biol.* 15:2635–2645.
40. Cao, H., W.E. Courchesne, and C.C. Mastick. 2002. A phosphotyrosine-dependent protein interaction screen reveals a role for phosphorylation of caveolin-1 on tyrosine 14: recruitment of C-terminal Src kinase. *J. Biol. Chem.* 277:8771–8774.
41. Wang, B., S. Lemay, S. Tsai, and A. Veillette. 2001. SH2 domain-mediated interaction of inhibitory protein tyrosine kinase Csk with protein tyrosine phosphatase-HSCF. *Mol. Cell. Biol.* 21:1077–1088.
42. Arbet-Engels, C., S. Tartare-Deckert, and W. Eckhart. 1999. C-terminal Src kinase associates with ligand-stimulated insulin-like growth factor-I receptor. *J. Biol. Chem.* 274:5422–5428.
43. Shah, K., and K.M. Shokat. 2002. A chemical genetic screen for direct v-Src substrates reveals ordered assembly of a retrograde signaling pathway. *Chem. Biol.* 9:35–47.
44. Pfrepper, K.I., A. Marie-Cardine, L. Simeoni, Y. Kuramitsu, A. Leo, J. Spicka, I. Hilgert, J. Scherer, and B. Schraven. 2001. Structural and functional dissection of the cytoplasmic domain of the transmembrane adaptor protein SIT (SHP2-interacting transmembrane adaptor protein). *Eur. J. Immunol.* 31:1825–1836.
45. Ishino, M., H. Aoto, H. Sasaski, R. Suzuki, and T. Sasaki. 2000. Phosphorylation of Hic-5 at tyrosine 60 by CAKβ and Fyn. *FEBS Lett.* 474:179–183.
46. Songyang, Z., S.E. Shoelson, J. McGlade, P. Olivier, T. Pawson, X.R. Bustelo, M. Barbacid, H. Sabe, H. Hanafusa, T. Yi, et al. 1994. Specific motifs recognized by the SH2 domains of Csk, 3BP2, fps/fes, GRB-2, HCP, SHC, Syk, and Vav. *Mol. Cell. Biol.* 14:2777–2785.

Appendix 5

The transmembrane adapter protein SIT regulates thymic development and peripheral T cell functions

Simeoni L., Posevitz V., Kölsch U., Meinert I., Bruyns E., Pfeffer K., Reinhold D., and Schraven B. (2005) *Mol Cell Biol.* 25:7557-68.

MOLECULAR AND CELLULAR BIOLOGY, Sept. 2005, p. 7557–7568 Vol. 25, No. 17
0270-7306/05/$08.00+0 doi:10.1128/MCB.25.17.7557–7568.2005

The Transmembrane Adapter Protein SIT Regulates Thymic Development and Peripheral T-Cell Functions

Luca Simeoni,[1]* Vilmos Posevitz,[1] Uwe Kölsch,[1] Ines Meinert,[1] Eddy Bruyns,[2] Klaus Pfeffer,[3] Dirk Reinhold,[1] and Burkhart Schraven[1]

Otto von Guericke University, Institute of Immunology, Leipziger Str. 44, 39120 Magdeburg, Germany[1]; FOCUS Clinical Drug Development GmbH, Im Neuenheimer Feld 515, 69120 Heidelberg, Germany[2]; and Heinrich Heine University, Institute of Medical Microbiology, Universitäts Str. 1, 40225 Düsseldorf, Germany[3]

Received 21 December 2004/Returned for modification 15 February 2005/Accepted 25 May 2005

SIT is a transmembrane adapter protein that modulates signals emanating from the T-cell receptor (TCR). Here, we have used gene-targeted mice to assess the role of SIT for T-cell development and peripheral T-cell functions. SIT$^{-/-}$ double-positive thymocytes show an upregulation of the activation markers CD5 and CD69, suggesting that SIT negatively regulates TCR-mediated signals at the CD4$^+$ CD8$^+$ stage of thymic development. This assumption is further supported by the observation that in female H-Y TCR transgenic mice, positive selection is enhanced and even converted to negative selection. Similarly, mature peripheral T cells are hyperresponsive towards TCR-mediated stimuli and produce larger amounts of T-helper 1 (TH1) cytokines, and SIT-deficient mice show an increased susceptibility to develop experimental autoimmune encephalomyelitis, a mouse model of multiple sclerosis. These results demonstrate that SIT is a critical negative regulator of TCR-mediated signaling and finely tunes the signals required for thymic selection and peripheral T-cell activation.

The recognition of specific antigen/major histocompatibility complex (MHC) complexes by the clonotypic T-cell receptor (TCR) initiates a number of signaling cascades which ultimately culminate in gene transcription. The proper function of these signal transduction pathways requires the coordinated action of many molecules. During the last years, the understanding of the membrane-proximal signaling events leading to T-cell activation has significantly advanced. For example, it has been demonstrated that the activation of protein tyrosine kinases belonging to the Src, Syk, and Tec families are among the earliest biochemical events that initiate cellular activation upon antigen recognition (reviewed in references 12 and 37) Also, major progress was made in elucidating how Src and Syk kinase-mediated signals are further processed to induce appropriate cellular responses. In this regard, the identification of a novel group of integral membrane molecules named transmembrane adapter proteins (TRAPs) was a major achievement (18).

All TRAPs known to date have a common molecular structure. They possess very short extracellular domains and comparatively long cytoplasmic tails containing several (up to 10) tyrosine-based signaling motifs (TBSMs) (18). After immunoreceptor engagement, the core tyrosine residues within the TBSMs become rapidly phosphorylated and thereby serve as docking sites for cytoplasmic signaling proteins carrying SH2 domains. By recruiting SH2 domain-containing proteins to the plasma membrane, the TRAPs function as molecular biochips which sort and coordinately propagate externally applied signals into the cell. Thus, the identification of the TRAPs has clarified the question of how signal-transducing receptors such as the TCR are connected with intracellular signaling pathways.

Presently, the family of TRAPs includes LAT, LAX, LIME, NTAL/LAB, PAG/Cbp, SIT, and TRIM. LAT represents the most well-characterized transmembrane adapter protein and appears to be primarily involved in positively regulating TCR-mediated signaling. By recruiting cytoplasmic signaling molecules such as Grb2, GADS, SLP-76, and phospholipase C-γ to the plasma membrane, LAT assembles a signaling complex that is required for coupling the T-cell receptor to the major intracellular signaling pathways leading to transcription of the T-cell growth factor interleukin-2 (16, 34, 48). The generation of LAT-deficient mice has further revealed the indispensable role of this transmembrane adapter protein for T-cell development (49).

Conversely to LAT, the transmembrane adapter proteins LAX and PAG seem to exert negative regulatory functions on TCR-mediated signaling either by recruiting the most important negative regulator of Src kinase activity, the cytosolic protein tyrosine kinase Csk, to the plasma membrane (PAG) (8, 22, 43) or by inhibiting TCR-mediated activation of p38 mitogen-activated protein kinase (LAX) (50).

In addition to the regulation of antigen receptor signaling, it appears that some transmembrane adapters may regulate signals initiated after coreceptor engagement. This has most recently been shown for the lipid raft-associated transmembrane adapter protein LIME, which exclusively becomes phosphorylated after external engagement of the CD4 or CD8 coreceptors (9, 21). However, the biological relevance of this phosphorylation has not yet been revealed.

Two transmembrane adapters, TRIM and SIT, differ from

* Corresponding author. Mailing address: Otto von Guericke University, Institute of Immunology, Leipziger Strasse 44, 39120 Magdeburg, Germany. Phone: 49 391 67 17894. Fax: 49 391 6715852. E-mail: luca.simeoni@medizin.uni-magdeburg.de.

the other TRAPs known so far as they represent disulfide-linked homodimers. TRIM associates with the TCR complex, preferentially through an interaction with the TCR-ζ chain, and when overexpressed in Jurkat T cells, TRIM inhibits the spontaneous internalization of the TCR (10, 26). However, the precise function that TRIM plays during T-cell activation remains elusive.

SIT has been reported to act as a modulator of TCR-mediated signaling (29, 35). Indeed, when overexpressed in Jurkat T cells, wild-type (wt) SIT exerts strong negative regulatory effects upon TCR-mediated activation of the transcription factor NF-AT (29, 35) This inhibitory effect seems to be exclusively mediated via a single TBSM within the SIT cytoplasmic domain (YASV) that binds a still-to-be-defined ligand. In contrast, overexpression of a SIT mutant lacking the YASV motif strongly amplifies TCR signals. This effect is mediated via another tyrosine-based signaling motif, YGNL, which seems to control a Grb2-mediated signaling pathway (35). Collectively, the currently available data suggest that SIT serves as a multifunctional adapter that finely tunes signals emanating from the TCR.

The aim of the present study was to assess the role of SIT during T-cell development and T-cell activation using an in vivo model. To this end, we generated SIT-deficient mice. Our data confirm that SIT primarily acts as a negative regulator of TCR-mediated signals and sets signaling thresholds necessary for positive selection within the thymus. In addition, SIT seems to be involved in the maintenance of peripheral T-cell homeostasis, as demonstrated by the hypersensitivity of SIT-deficient T cells in response to TCR stimulation and increased susceptibility of SIT-deficient mice to autoimmunity in a murine model of multiple sclerosis.

MATERIALS AND METHODS

Mice. The targeting construct was transfected into 129-derived embryonic stem cells. Targeted embryonic stem clones were selected and processed as previously described (2). Positive clones were injected into C57BL/6 blastocysts. Animals containing the disrupted *SIT* allele were crossed onto C57BL/6 (Charles River) for more than 10 generations. Genotype was determined by PCR using a mixture of three primers, 5′ SIT (CCT GAC TCT CAC ACC AGC AGC), 3′ SIT (GGT CCA CTG GGA CAA GAG TGC AGC C), and 3′ NEO (GAC GTG CTA CTT CCA TTT GTC ACG TCC) (BioTeZ Berlin-Buch GmbH). OT-I and OT-II TCR transgenic (tg) mice were kindly provided by Percy Knolle, P14 mice were provided by Thomas Kammerthoens, and H-Y TCR transgenic mice were kindly provided by Gary Koreztky. For TCR transgenic studies, $SIT^{-/-}$ mice × TCR tg mice were obtained by crossing $SIT^{-/-}$ mice with $SIT^{+/-}$ mice for TCR heterozygote transgenics. All mice analyzed were between 5 and 10 weeks of age.

Flow cytometry. For each sample, 1×10^6 cells were stained with antibodies and analyzed on a FACSCalibur using the CellQuest software (Becton Dickinson). All antibodies were purchased from BD Biosciences except for H-Y–fluorescein isothiocyanate (clone T3.70; eBioscience). For flow cytometric determination of extracellular signal-regulated kinase (ERK) activation, thymocytes were surface labeled with anti-CD4-CyChr and anti-CD8-phycoerythrin, fixed, and permeabilized in phosphate-buffered saline (PBS) containing 3.7% formaldehyde and 0.2% saponin for 15 min at room temperature. After being washed in PBS containing 0.1% saponin, 0.1% NaN_3, and 0.2% BSA/c, cells were stained with anti-phospho-p44/42 mitogen-activated protein kinase (Cell Signaling) in PBS supplemented with bovine serum albumin (10 mg/ml), 0.2% BSA/c, 0.1% saponin, and 0.1% NaN_3 for 45 min at room temperature. Bound antibody was detected with fluorescein isothiocyanate-conjugated anti-rabbit immunoglobulin G (IgG) (Jackson ImmunoResearch Laboratories).

Apoptosis assay. Thymocytes (5×10^5) were cultured in 96-well flat-bottomed plates coated with 10 μg/ml anti-CD3 (145-2C11; BD Biosciences) or 10 μg/ml anti-CD3 plus 10 μg/ml anti-CD28 (37.51; BD Biosciences). For concanavalin A (ConA) stimulation, a final concentration of 1 μg/ml was used. Samples were then incubated at 37°C for 24 h before analysis. After harvesting, the living cells were analyzed by forward scatter and side scatter flow cytometry parameters. Cells were also harvested, washed, and stained with annexin V and propidium iodide according to the manufacturer's instructions (Bender MedSystems).

Proliferation assay and cytokine determination. T-cell purification was performed using a Pan T-cell Isolation kit and an AutoMacs magnetic separation system (Miltenyi Biotec). Purified T cells (2.5×10^4 cells/well) were cultured in RPMI medium (supplemented with 10% fetal calf serum, antibiotics, and 2-β-mercaptoethanol) in a U-bottomed 96-well plate (Costar) in the presence of plate-bound anti-mouse CD3ε (145-2C11; BD Biosciences) or phorbol myristate acetate (PMA) and ionomycin. Cells were cultured for 72 h and labeled with 0.5 μCi/well of [^{3}H]thymidine during the last 6 h. Supernatants from anti-CD3-stimulated T cells were collected after 48 h and assessed for cytokines by cytometric bead array (BD Biosciences).

Induction of active EAE. Myelin oligodendrocyte glycoprotein (MOG) p35-55, corresponding to the mouse sequence MEVGWYRSPFSRVVHLYRNGK, was synthesized by standard 9-fluorenylmethoxycarbonyl chemistry and purified by high-performance liquid chromatography. Active experimental autoimmune encephalomyelitis (EAE) was induced in 8- to 12-week-old mice by immunization with 200 μg of MOG p35-55 in complete Freund's adjuvant (Sigma-Aldrich, Taufkirchen, Germany) containing 800 μg of killed *Mycobacterium tuberculosis* (Difco Laboratories, Detroit, MI). In addition, 200 ng of pertussis toxin (List Biological Laboratories, Campbell, CA) dissolved in 200 μl PBS was injected intraperitoneally on the day of immunization and again 2 days postimmunization.

Statistics. Statistical analyses were performed using GraphPad Prism (GraphPad Software Inc., San Diego, CA). *P* values were determined by an unpaired two-tailed Student's *t* test.

RESULTS

SIT is expressed predominantly in thymocytes. Previously, we have shown that SIT is selectively expressed in lymphoid cell lines (29). To assess the expression of SIT in primary cells from different murine lymphoid organs, anti-SIT Western blotting was performed. As shown in Fig. 1A, the highest levels of SIT protein expression are detectable in the thymus, and lower levels are detected in spleen. We next analyzed whether SIT expression is different in T lymphocytes compared to B lymphocytes and whether immature T cells express different amounts of SIT than mature T cells. Figure 1A shows that SIT expression is much higher in purified $CD3^+$ splenic T cells than in $B220^+$ B cells. In addition, the expression of SIT within the thymus (containing approximately 80% immature T cells) is much higher than in mature splenic T cells. Conversely, SIT is not expressed in the $Gr\text{-}1^+$ myeloid lineage in the bone marrow (data not shown). In conclusion, SIT is expressed at the highest levels in immature thymocytes.

$SIT^{-/-}$ mice show normal B-cell but altered T-cell development. To elucidate the function of SIT within the immune system, we generated SIT-deficient mice by homologous recombination. The SIT gene was disrupted in embryonic stem cells by using a standard gene-targeting strategy. As shown in Fig. 1B, the entire coding sequence of the SIT gene (19) was replaced with a neomycin resistance cassette, and the expected mutation was confirmed by PCR (Fig. 1C) and anti-SIT Western blotting (Fig. 1D).

SIT-deficient mice are born at the expected Mendelian frequency, and they are viable, are fertile, show normal growth, and present no obvious abnormalities. Flow cytometry analysis further revealed that the distribution of B-cell subsets in the bone marrow, spleen, and lymph nodes is normal (Table 1 and Fig. 2). B-cell precursor fractions such as pro-B cells ($B220^+$ $CD43^+$), immature B cells ($B220^+$ IgM^+), and recirculating mature B cells ($B220^{high}$ IgM^+) from $SIT^{-/-}$ bone marrow are comparable to those of wt mice (Fig. 2A). In the spleen, the

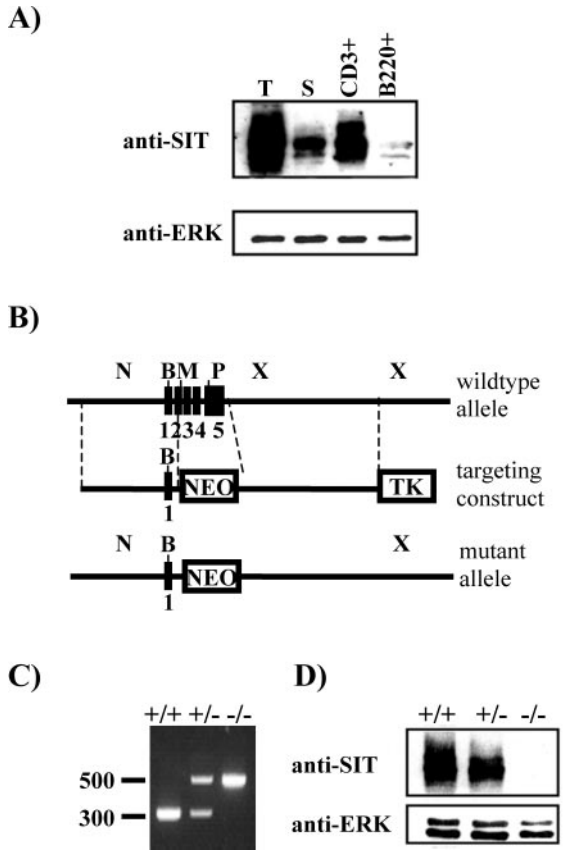

FIG. 1. Expression of SIT in mouse lymphocytes and generation of SIT-deficient mice. (A) Lysates prepared from freshly isolated thymocytes (T), splenocytes (S), purified splenic T cells ($CD3^+$), or purified splenic B cells ($B220^+$) were separated by sodium dodecyl sulfate-polyacrylamide gel electrophoresis and blotted with an anti-SIT MAb. To demonstrate equal amounts of protein loading, the blot was stripped and reprobed with an anti-Erk polyclonal antibody. (B) Partial restriction map of the SIT locus and the targeting cassette. Filled boxes represent exons. Restriction sites are indicated as follows: N, NotI; B, BamHI; M, MluI; P, PstI; X, XbaI. Abbreviations: NEO, neomycin resistance cassette; TK, thymidine kinase. (C) PCR analysis of *SIT* wild-type (+/+), heterozygous (+/−), and homozygous (−/−) mutant alleles. (D) Anti-SIT Western blot analysis showing absence of SIT protein in $SIT^{-/-}$ mice. Postnuclear lysates were prepared from thymocytes, separated by sodium dodecyl sulfate-polyacrylamide gel electrophoresis, and blotted with an anti-SIT MAb. The blot was successively stripped and reprobed with an anti-ERK1/2 antibody as a loading control.

total B-cell distribution ($B220^+$ IgM^+) as well as the percentages of B-cell subpopulations such as immature (IgM^{high} IgD^{low}), transitional (IgM^{high} IgD^{high}), and mature (IgM^{low} IgD^{high}) are also not affected by SIT deficiency (Fig. 2F). Moreover, B1 lymphocytes ($CD5^+$ $B220^+$) in the peritoneal cavity also show a normal distribution (Fig. 2C). In addition, basal immunoglobulin levels as well as those obtained after immunization of SIT-deficient mice were normal (data not shown). Collectively, these data suggest that SIT is dispensable for normal B-cell development and peripheral B-cell functions.

To address the question of whether SIT plays a role in T-cell development, we investigated single-cell suspensions of thymocytes from wild-type animals and SIT-deficient littermates by

TABLE 1. Cell numbers of lymphocyte subpopulations in thymus and lymph nodes[a]

Genotype and *P* value	No. of mice examined	No. (10^6) of cells ± SD								
		Thymus				Lymph nodes				
		Total	$CD4^-$ $CD8^-$	$CD4^+$ $CD8^+$	$CD4^+$ $CD8^-$	$CD4^-$ $CD8^+$	Total	$CD4^+$	$CD8^+$	$\gamma\delta TCR^+$	$B220^+$	$NK1.1^+$
$SIT^{+/+}$	15	135.2 ± 34.1	3.7 ± 1.7	109.2 ± 44.1	16.1 ± 6.1	5.3 ± 2.4	12.7 ± 3.8	4.9 ± 1.4	4.1 ± 1.0	0.14 ± 0.07	3.1 ± 1.5	0.15 ± 0.06
$SIT^{-/-}$	15	174.3 ± 51.2	3.5 ± 1.0	154.6 ± 48.2	13.0 ± 3.2	3.4 ± 1.7	8.3 ± 3.3	2.9 ± 1.2	2.0 ± 0.7	0.43 ± 0.1	2.4 ± 1.2	0.20 ± 0.1
P value		**0.03**	0.8	**0.02**	0.1	**0.03**	**0.0009**	**0.002**	**<0.0001**	**<0.0001**	0.2	0.3

[a] Values that are indicated in boldface type are statistically significant.

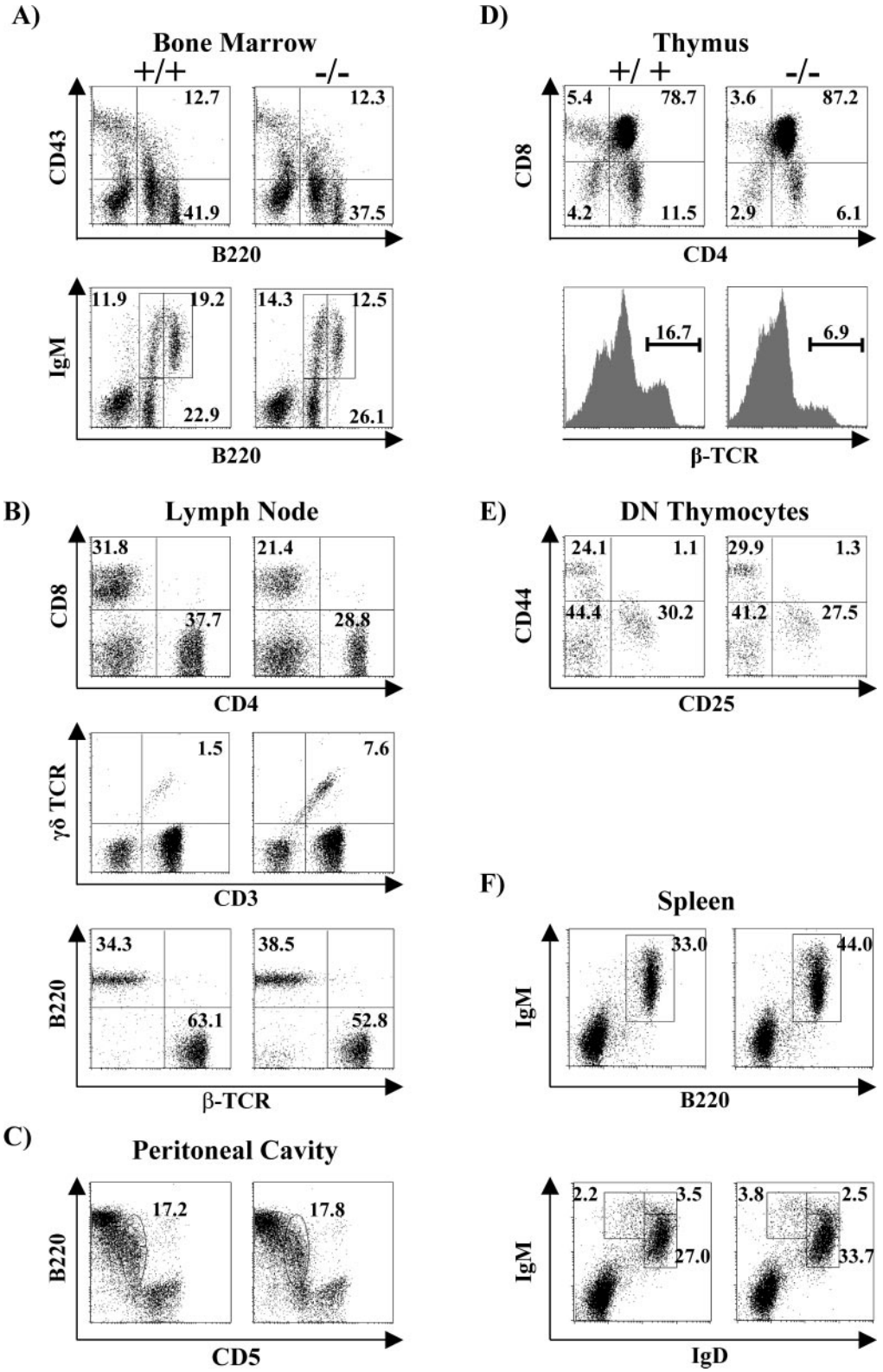

FIG. 2. Lymphocyte development in SIT-deficient mice. Bone marrow cells (A), lymph nodes cells (B), peritoneal cavity cells (C), thymocytes (D), double-negative thymocytes (E), and splenocytes (F) from 5- to 8-week-old mice were stained with MAbs for CD43, B220, IgM, CD4, CD8, TCR-β, CD44, CD25, γδTCR, IgD, and CD5 and analyzed by flow cytometry. Numbers represent the percentages of cells that fall into the indicated boxes or quadrant areas of total gated living cells.

flow cytometry. Table 1 shows that the cellularity of SIT-deficient thymi is moderately increased. Fluorescence-activated cell sorter analysis further revealed an alteration in the composition of thymocyte subpopulations (Fig. 2D), with clearly reduced proportions of both $CD4^+$ and $CD8^+$ mature single-positive (SP) thymocytes and an increase of $CD4^+$ $CD8^+$ (double-positive [DP]) immature thymocytes in $SIT^{-/-}$ mice. In agreement with this observation, a significant decrease of thymocytes expressing high levels of TCR (as a measure of terminal maturation) was found in the knockout animals (Fig. 2D). Due to the increase in total thymic cellularity, we calculated the absolute numbers of the individual thymocyte subsets. As summarized in Table 1, $SIT^{-/-}$ mice show an approximate 40% increase in the total number of immature DP thymocytes and a slight reduction in the number of mature SP thymocytes. In contrast, the numbers of double-negative thymocytes (Table 1) as well as their CD25/CD44 fluorescence-activated cell sorter profiles are normal (Fig. 2E). The latter finding suggests that SIT is dispensable during the earliest steps of thymic development. Thus, the higher total numbers of thymocytes in SIT-deficient mice are primarily caused by an increase in the DP subset. The alteration in the DP/SP ratio suggests a subtle defect in thymic selection.

Upregulation of cell surface molecules involved in thymic selection processes on $SIT^{-/-}$ DP thymocytes. To obtain further insight into the molecular mechanism underlying the altered thymic development in $SIT^{-/-}$ mice, we analyzed the expression levels of surface markers whose expression is known to be regulated during thymic development.

The expression of CD5 has been reported to directly correlate with the intensity of pre-TCR- and TCR-mediated signals (5, 6). Thus, high levels of CD5 expression are found in thymocytes of transgenic mice which express TCRs with a high affinity/avidity for their selecting ligands (5, 6) or on DP thymocytes of mice lacking negative regulatory cytosolic adapters such as c-Cbl or SLAP (32, 38). Therefore, it appears that CD5 serves as a negative-feedback regulator of TCR-mediated signals and that its expression is required to regulate signaling processes during thymocyte selection (5, 6, 42). As shown in Fig. 3, the expression of CD5 is upregulated on SIT-deficient DP thymocytes, indicating an enhanced signaling capability of the TCR in the absence of SIT.

CD69 is another maturation marker that becomes upregulated after TCR engagement by ligands presented by thymic stromal cells during both negative and positive selection (4, 31, 41, 47). Similar to CD5, DP thymocytes of SIT-deficient mice express higher levels of CD69 than wt littermates (Fig. 3). This further corroborates our hypothesis that TCR-mediated signaling is augmented in SIT-deficient thymocytes. In contrast to CD5 and CD69, the expression profiles of CD4, CD8, heat-stable antigen (HSA), CD45RB, and CD62L are normal in $SIT^{-/-}$ thymocytes (data not shown).

SIT deficiency alters positive selection in H-Y and P14 TCR transgenic mice. Within the thymus, the majority of cells belong to the DP stage. Moreover, it is during this stage that autoreactive thymocytes are eliminated by negative selection, while thymocytes with the appropriate specificity for self-peptide/MHC complexes are positively selected and further develop to the SP stage. It is known from multiple studies that TCR transgenic mice expressing a defined αβTCR are well suited to study thymic selection processes (13, 27). Given the above-described findings, which suggested that loss of SIT affects thymic development by enhancing TCR-mediated signals, we wished to obtain a more detailed insight into SIT-mediated regulation of thymic selection processes. To this end, we crossed $SIT^{-/-}$ mice with mice expressing transgenic TCRs (P14, H-Y, OT-I, and OT-II) and evaluated the effect of SIT deficiency on selection processes.

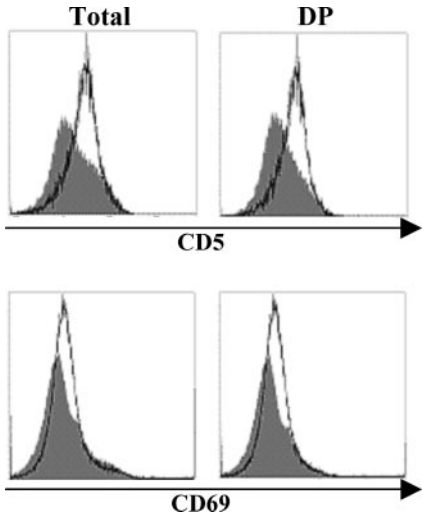

FIG. 3. Enhanced expression of CD5 and CD69 on $SIT^{-/-}$ DP thymocytes. Ungated (total) or $CD4^+$ $CD8^+$-gated (DP) thymocytes were assessed for surface expression of CD5 and CD69. The histograms represent profiles of cells from a representative $SIT^{+/+}$ (shaded) and $SIT^{-/-}$ (thick lines) mouse. All data are representative of a minimum of 10 individual experiments.

As shown in Fig. 4A, higher levels of CD5 are expressed on DP and in particular on positively selected $CD8^+$ SP H-Y tg thymocytes of $SIT^{-/-}$ mice than in their $SIT^{+/+}$ counterparts. Since CD5 expression on mature SPs has been proposed to result from TCR-mediated signals that are delivered during the selection processes (6), the enhanced expression of CD5 on $SIT^{-/-}$ SP cells indicates that, similar to the situation seen in the non-TCR tg mice, loss of SIT also enhances signaling via the TCR in the H-Y TCR tg model.

Figure 4A further demonstrates that the positively selected $CD8^+$ SP TCR tg cells express strikingly lower levels of HSA than the corresponding cells from $SIT^{+/+}$ animals. This indicates that SIT-deficient CD8 SP cells are more mature than $SIT^{+/+}$ cells, likely because of enhanced positive selection (see below).

According to the currently proposed model, the activation/phosphorylation status of the dual-specificity kinase ERK directly correlates with the efficiency of positive selection (7, 23, 28, 33). Figure 4B depicts that ex vivo phosphorylation of ERK in DP thymocytes of SIT-deficient mice is stronger than in the corresponding SIT-positive animals (mean fluorescence intensity [MFI] of 59.5 versus 30.4). In contrast, the levels of Erk phosphorylation are similar after in vitro stimulation with PMA (MFI of 170 versus 183), which rules out the possibility that the cells express different amounts of phosphorylatable Erk. Note that the histograms shown in Fig. 4B were obtained from cells that had not been activated in vitro; thus, the ex-

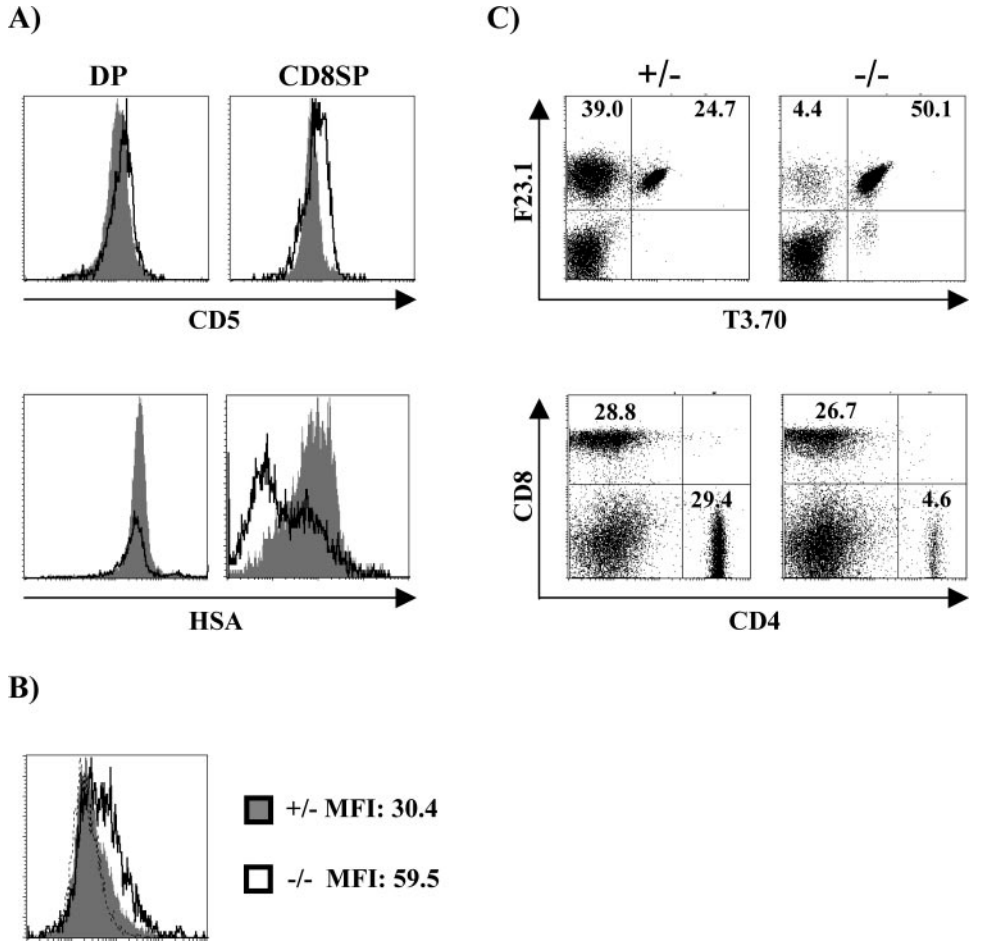

FIG. 4. Enhanced positive selection in the absence of SIT. (A) Thymocytes from H-Y female mice were stained with CD4 and CD8 and assessed for the expression of CD5 and HSA on gated DP and CD8 SP cells. The histograms represent overlaid profiles of cells from a representative $SIT^{+/-}$ (shaded) and $SIT^{-/-}$ (thick lines) mouse. (B) Enhanced ERK1/2 activation in $SIT^{-/-}$ H-Y thymocytes. Single-cell suspensions from thymi were immediately fixed and stained for CD4, CD8, and phospho-ERK1/2. Numbers indicate MFI from one representative experiment out of four. Dotted lines indicate the levels of staining with the secondary antibody alone. (C) Representative dot plots of the expression of the clonotypic transgenic TCRα chain (T3.70) and transgenic TCRβ (F23.1) (upper panels) or CD4 and CD8 (lower panels) in lymph node cells. Numbers indicate the percentages of cells in each subset.

pression levels of phospho-ERK indeed reflect the in vivo situation within the thymus. Since the H-Y TCR is known to signal rather inefficiently (36), it is therefore not surprising that the mean peaks of fluorescence (as a sign of Erk phosphorylation) are not very high. Nevertheless, both the more mature phenotype of SP cells and the enhanced activation of ERK on DP thymocytes strongly suggest that loss of SIT enhances the efficiency of positive selection in female H-Y TCR tg mice.

This assumption is even further supported by the finding that the proportions of non-TCR tg T cells are strongly decreased in SIT-deficient mice (Fig. 4C). The non-TCR tg pool in the H-Y mice is composed of CD4 cells in which the transgenic TCR-β chain is paired with an endogenous (non-tg) TCR-α chain (Fig. 4C). This pairing occurs in the H-Y tg mice because the transgenic TCR has only a weak affinity for the selecting ligands, and therefore, it transduces a weak signal that is not sufficient to properly suppress the rearrangement of the *Tcra* locus (20). The enhanced ratio of tg (CD8 $H\text{-}Y^{+}$) to non-tg (CD4 $H\text{-}Y^{-}$) T cells in $SIT^{-/-}$ mice therefore indicates that in the absence of SIT, the H-Y TCR signals stronger, resulting in a more efficient suppression of the rearrangement of the endogenous TCR-α chain.

Besides the above-described signs of enhanced positive selection, we also observed a significant reduction in the total number of H-Y–TCR tg DP thymocytes in SIT-deficient mice (Fig. 5A). This finding could indicate that the loss of SIT not only enhances the efficiency of positive selection but even partially converts positive selection to negative selection. Importantly, similar data as shown in Fig. 5A for the H-Y TCR tg model were found in a second TCR tg model, P14 (Fig. 5B). However, in the P14 TCR tg system, loss of SIT resulted in an even more dramatic reduction of thymic cellularity. This could suggest that in this system, the conversion from positive to negative selection caused by loss of SIT is even stronger than in the H-Y TCR tg model. In any case, both TCR tg models demonstrate that the loss of SIT alters thymic selection processes, likely by enhancing positive selection and also by partially converting positive selection to negative selection. In

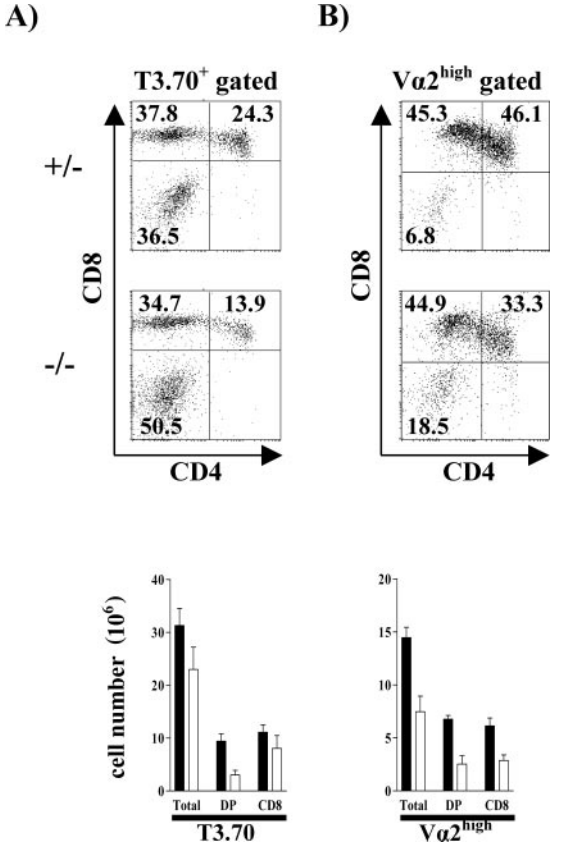

FIG. 5. The absence of SIT partially converts positive selection to negative selection. Flow cytometric analysis of positive selection in thymus is shown. Thymocytes from H-Y (A) and P14 (B) TCR SIT$^{-/-}$ or SIT$^{+/-}$ transgenic mice were analyzed for transgenic TCR expression by staining with T3.70, a clonotypic antibody specific for H-Y TCRα chain, or $V_{\alpha}2$, the P14 TCRα chain. The dot plots show CD4 and CD8 profiles of cells gated on TCR^{high}. Numbers indicate percentages of cells in each subset. One representative animal for each group is shown. The graphs show the mean cellularity of TCR transgenic thymocyte subsets from seven SIT$^{+/-}$ and seven SIT$^{-/-}$ H-Y^{+} tg mice and three SIT$^{+/-}$ and three SIT$^{-/-}$ P14^{+} tg mice.

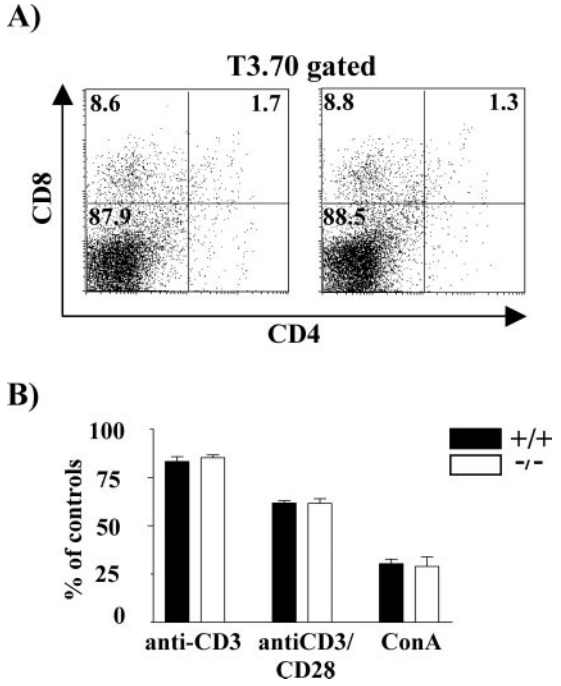

FIG. 6. SIT is dispensable for negative selection. (A) Flow cytometric analysis of CD4/CD8 profiles of the T3.70^{+} population in H-Y TCR transgenic male mice. (B) DP thymocyte deletion in response to TCR cross-linking. Thymocytes were cultured in 24-well plates coated with anti-CD3 or anti-CD3 plus anti-CD28 or in the presence of ConA for 24 h, and their viability was determined. One of two independent experiments is shown, each using three pairs of mice. Black and open bars represent wild-type and knockout mice, respectively.

contrast to the H-Y and the P14 system, SIT deficiency did not alter the outcome of selection processes in a class I-restricted TCR tg model with higher affinity (OT-I) and class II-restricted TCR tg models (OT-II) (data not shown).

Normal negative selection in the absence of SIT. We also investigated whether SIT deficiency would directly influence negative selection. To assess this question in vivo, we took further advantage of the H-Y TCR transgenic model (27). In male H-Y TCR transgenic mice, the CD4^{+} CD8^{+} DP thymocytes are efficiently depleted by negative selection, and therefore, mature CD8 SP cells are barely detectable. However, some CD8 SP thymocytes downregulate the CD8 coreceptor and escape negative selection, thus permitting a small population of thymocytes to colonize the periphery. Figure 6A demonstrates that loss of SIT does not alter the cellular composition of the thymus in male H-Y TCR tg mice. Similarly, no differences were observed in the periphery of SIT-deficient H-Y TCR tg male mice (data not shown). These data strongly suggest that negative selection proceeds normally in the absence of SIT.

However, since the deletion process in the H-Y male model occurs at a very high efficiency and only extremely low numbers of DP cells are detectable in the mice, it is difficult to unmask augmented negative selection in this system. To circumvent this problem, we mimicked negative selection in vitro by stimulating freshly isolated thymocytes with CD3 and CD3 plus CD28 monoclonal antibodies (MAbs) or with the polyclonal mitogen ConA. Figure 6B shows that the survival rates of the in vitro-activated thymocytes were comparable between wild-type and SIT$^{-/-}$ mice. Thus, SIT seems to be dispensable for negative selection within the thymus as well as for in vitro deletion of immature T lymphocytes.

Alterations of the peripheral T-cell pools in SIT$^{-/-}$ mice. To obtain further insight into the consequences of SIT deficiency, we examined the cellular composition of the peripheral lymphoid system. These experiments revealed normal sizes, architectures, and cellularities of spleen, Peyer's patches, and bone marrow (data not shown). Moreover, the numbers of B (B220^{+}), αβT (TCRβ^{+}), CD4, CD8, and NK (NK1.1^{+}) cells were also unaffected in the absence of SIT (Fig. 2F and data not shown). In marked contrast, both superficial and mesenteric lymph nodes of SIT$^{-/-}$ mice show an approximate 50% decrease in total cellularity (Table 1). Anatomical analysis of these lymph nodes did not show alterations in global architecture. However, a significant reduction in the number of

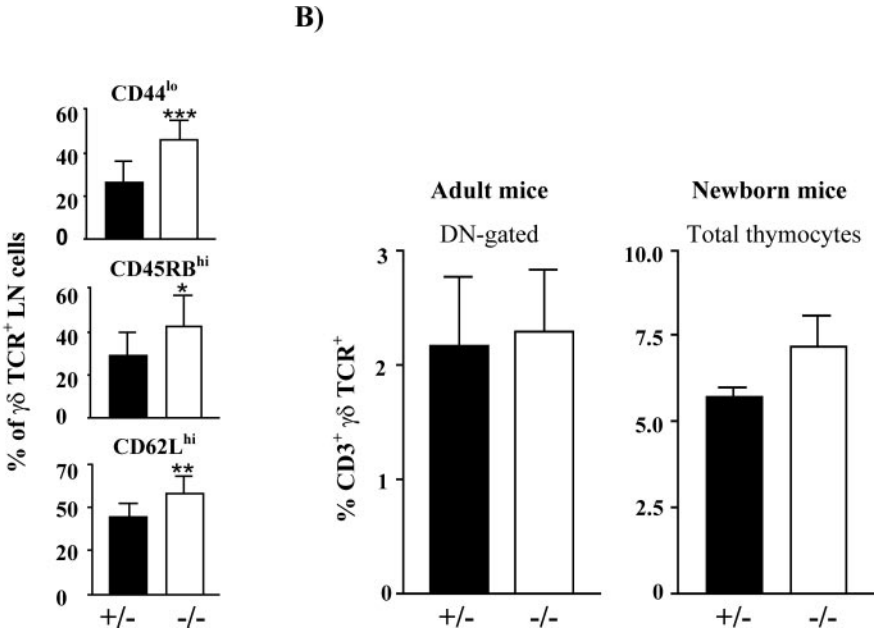

FIG. 7. γδ T-cell populations in SIT$^{-/-}$ mice. (A) Proportion of CD3$^+$ γδ TCR$^+$ lymph node cells expressing CD44, CD45RB, and CD62L. Ten mice for each genotype were included in the groups. ***, $P = 0.0003$; **, $P = 0.0038$; *, $P = 0.0352$. (B) γδ T-cell distribution in thymi from adult or newborn mice. Black bars and open boxes represent wt and SIT-deficient mice, respectively.

αβTCR$^+$ lymphocytes in both the CD4 and CD8 subpopulations (Table 1 and Fig. 2B) was found by flow cytometry, whereas the numbers of B and NK cells as well as the expression levels of CD24, CD25, CD44, CD45RB, CD62L, and CD69 cells (Table 1, Fig. 2B, and data not shown) were all normal. Thus, the decrease in total cellularity of lymph nodes is due to a selective reduction in conventional αβTCR$^+$ T lymphocytes.

Further analysis of the secondary lymphatic organs revealed an increase in both the distribution and the absolute numbers of γδTCR$^+$ lymphocytes in SIT-deficient lymph nodes, spleen, Peyer's patches, blood, and bone marrow (Table 1, Fig. 2B, and data not shown). Moreover, the SIT$^{-/-}$ γδ T-cell subset contains a higher proportion of CD44^{low}, CD45RB^{hi}, and CD62L^{hi} cells which correspond with a naive phenotype (25, 44) (Fig. 7A). γδ T cells develop very early in the thymus during embryonal life through a unique developmental pathway (3, 17). The first two waves of γδ T cells lack junctional diversity and migrate to the skin and to mucosal tissue. At the end of the fetal life, a third wave of γδ cells is produced. After exiting the thymus, these cells populate the spleen and the lymph nodes of adult mice. To assess whether SIT deficiency alters γδ T-cell development, we analyzed thymocyte suspensions from newborn and adult mice by flow cytometry. These experiments revealed no alteration of the numbers of CD3$^+$ γδTCR$^+$ cells within the thymus of SIT-deficient mice (Fig. 7B). Similarly, the distribution of intraepithelial gut lymphocytes, which are also mostly γδ T cells, was found to be unaffected in SIT-deficient mice (not shown). Collectively, these data suggest that SIT regulates the expansion of peripheral γδT cells rather than being involved in the homing of these cells to the gut or in their thymic development.

SIT negatively regulates peripheral T-cell responses. The altered distribution of peripheral T-cell subpopulations in SIT-deficient mice prompted us to investigate whether T cells function normally in the absence of SIT. To this end, we analyzed proliferation of purified splenic T cells that were stimulated with different concentrations of plate-bound anti-CD3 MAb by means of [^{3}H]thymidine incorporation. As shown in Fig. 8A, compared to wild-type littermates, T cells of SIT$^{-/-}$ mice exhibit a ~50% enhancement in proliferation upon CD3 stimulation that is most evident at intermediate antibody concentrations. Similarly, SIT-deficient T cells produce strikingly higher amounts of gamma interferon, interleukin-2, and tumor necrosis factor alpha after CD3 stimulation (Fig. 8B), strongly suggesting that SIT deficiency skews the peripheral T-cell repertoire towards the TH1 (T-helper 1) lineage.

To assess whether the altered peripheral T-cell function of SIT-deficient mice primes the organism for the development of autoimmune diseases, we investigated the clinical course of EAE in wild-type and SIT$^{-/-}$ mice. EAE is a T-cell-mediated autoimmune disease of the central nervous system that is characterized by inflammation, demyelination, and relapsing/remitting courses of paralysis (30). It represents a well-established animal model for multiple sclerosis and is believed to primarily be a TH1-mediated disease. As shown in Fig. 8C, analysis of the clinical EAE score following immunization with MOG shows a more severe disease in SIT$^{-/-}$ mice than in control animals. Thus, the absence of SIT not only affects selection processes within the thymus and peripheral T-cell functions but also aggravates the susceptibility of the organism to develop autoimmune diseases. Surprisingly, however, even a detailed biochemical analysis of most important membrane-proximal signaling events of SIT-deficient T cells (e.g., global

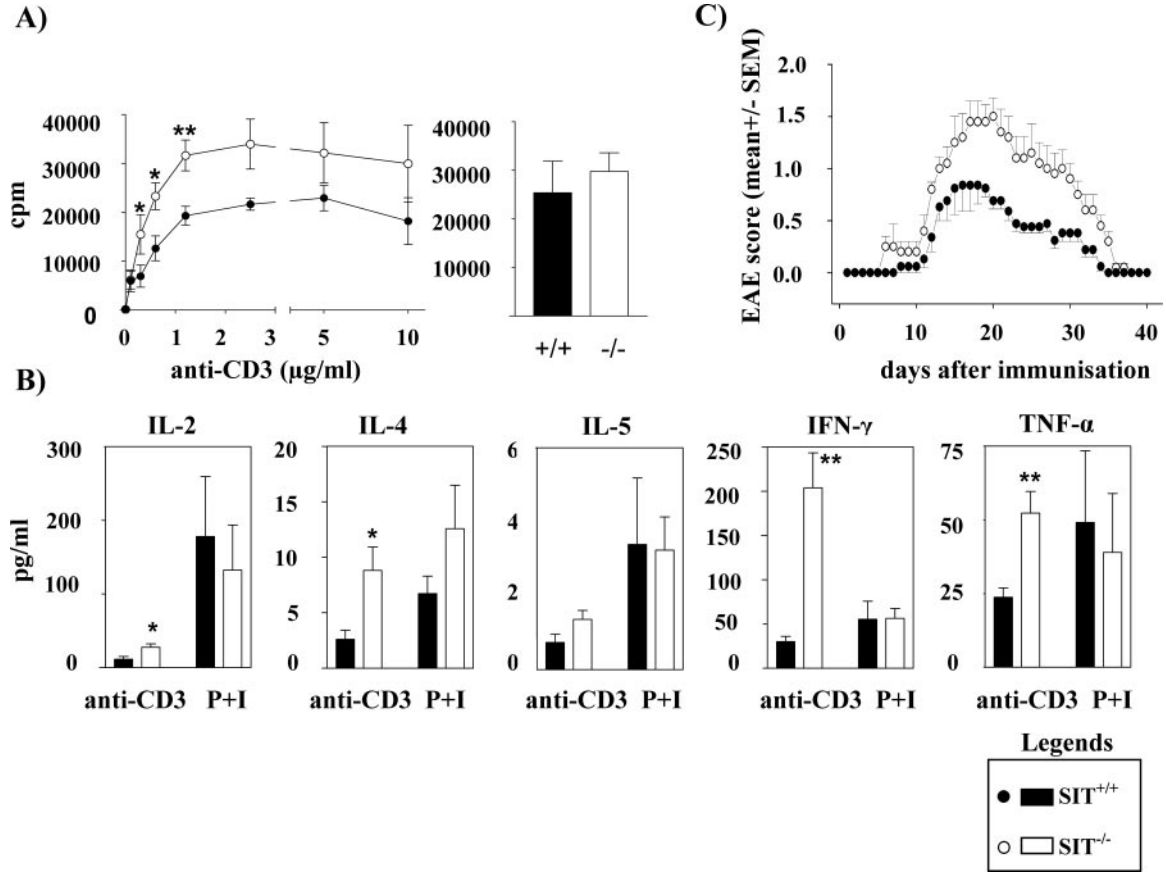

FIG. 8. Altered peripheral T-cell function in SIT$^{-/-}$ mice. (A) Enhanced T-cell proliferation. Purified splenic T cells were stimulated in 96-well plates coated with anti-CD3 antibody or PMA and ionomycin (P+I), pulsed with [^{3}H]thymidine, and processed for standard scintillation counting. Results from seven wild-type and nine knock-out mice are shown as mean counts per minute (cpm). One of two independent experiments is shown. *, $P = 0.01$; **, $P = 0.007$. (B) Augmented cytokine production by anti-CD3-stimulated SIT$^{-/-}$ T cells. T cells were purified and stimulated with 0.3 μg/ml anti-CD3 or PMA and ionomycin (P+I). Results from 8 wild-type and 10 knockout mice are shown. IL-2, interleukin-2; IFN-γ, gamma interferon; TNF-α, tumor necrosis factor alpha. *, $P = 0.02$; **, $P < 0.005$. (C) Increased incidence of EAE in the absence of SIT. Mice were examined daily for signs of disease and graded on a scale of increasing severity from 0 to 5 as follows: 0, no signs; 0.5, partial tail weakness; 1, limp tail or slight slowing of righting from supine position; 1.5, limp tail and slight slowing of righting; 2, partial hind-limb weakness or marked slowing of righting; 2.5, dragging of hind limb(s) without complete paralysis; 3, complete paralysis of at least one hind limb; 3.5, hind-limb paralysis and slight weakness of forelimbs; 4, severe forelimb weakness; 5, moribund or dead.

tyrosine phosphorylation; TCR-mediated Ca^{2+} flux; LAT phosphorylation; activation of ERK, June N-terminal protein kinase, and p38; IκB degradation, etc.) did not reveal any significant changes compared to wt littermates (data not shown). Thus, the mechanisms by which SIT controls T-cell function remain elusive, although the biochemical analysis of TCR-mediated signals within the thymic compartment suggests that SIT primarily regulates TCR-mediated activation of Erk.

DISCUSSION

In this study, we report the characterization of mice lacking the transmembrane adapter molecule SIT. Our findings support our previous hypothesis that SIT primarily acts as a negative regulator of TCR-mediated signaling (29, 35). Because SIT is most highly expressed in thymocytes, we initially investigated the function of SIT during thymic selection processes. Non-TCR transgenic SIT-deficient thymocytes showed higher levels of CD5 and CD69 than wild-type animals. Upregulation of these two activation markers has been proposed to reflect the activation status of the cells within the thymus, and the expression levels of CD5 on thymocytes have been shown to directly correlate with the strength of TCR-mediated signals (6, 32, 38). Therefore, the enhanced expression of CD5 on SIT-deficient thymocytes suggests that not only in Jurkat T cells (29, 35) but also in vivo, SIT primarily acts as a negative regulator of T-cell activation. Furthermore, it indicates that one physiologic function of SIT is to finely tune signals that emanate from the TCR during thymic development. Clearly, the possibility that SIT directly regulates the expression levels of CD5 or CD69 cannot be completely ruled out. However, the observation that the expression levels of CD5 and CD69 are normal in SIT-deficient OT-I and OT-II TCR transgenic mice (data not shown) makes this possibility unlikely.

The enhanced expression of CD5 and CD69 (together with the slightly increased thymic cellularity) in non-TCR tg mice initially suggested that loss of SIT enhances TCR-mediated

signals, thereby leading to subtle alterations of the thymic selection processes. This hypothesis was confirmed in the low-affinity H-Y TCR tg model system, where we demonstrated that in female H-Y TCR tg animals, loss of SIT apparently enhances the efficiency of positive selection. This hypothesis was deduced from different observations. First, SIT-deficient $CD8^+$ SPs show enhanced expression of CD5 (as a sign of enhanced TCR-mediated signaling during the selection processes [6]). Second, the positively selected $CD8^+$ SP cells in the female mice are more mature than their SIT-expressing counterparts (as assessed by lower levels of HSA expression). Third, ex vivo-isolated thymocytes show enhanced constitutive phosphorylation of the dual-specificity kinase ERK, whose activity has been reported to directly correlate with the efficiency of positive selection (1, 36, 40). Fourth, loss of SIT induces a more efficient silencing of the TCRα locus that results in a decrease of non-TCR tg $CD4^+$ SP T-cells (20). Thus, the H-Y data are compatible with the hypothesis that loss of SIT enhances TCR-mediated signals and thereby facilitates positive selection. It is interesting that similar effects on positive selection as shown here for SIT have previously been observed in mice lacking expression of CD5 (in the H-Y and the P14 TCR tg models [5, 42]). Thus, it appears as if negative regulators such as SIT and CD5 serve to set the signaling thresholds for positive selection during thymic development.

In addition to enhanced positive selection, we found a decrease in DP cells in female H-Y TCR tg mice. This could suggest that in the H-Y system (and even more pronounced in the P14 system), loss of SIT not only enhances positive selection but even partially converts positive selection to negative selection. Although further experiments are required to prove this hypothesis, the idea that loss of SIT partially converts positive selection to negative selection is strongly supported by recent data that we obtained in our laboratory using female H-Y TCR tg SIT/TRIM double-knockout mice. TRIM is a second non-lipid-raft transmembrane adapter protein with unknown function that carries similar tyrosine-based signaling motifs in its cytoplasmic domain as SIT (10).

Importantly, the thymi of the female H-Y TCR tg TRIM/SIT double-knockout mice are almost indistinguishable from the thymi of wild-type male H-Y TCR tg animals, in which almost all DP thymocytes are eliminated by negative selection (due to expression of the endogenous male autoantigen). Thus, in the female H-Y TCR tg mice, concomitant loss of both TRIM and SIT completely converts positive selection to negative selection (L. Simeoni et al., unpublished data). The fact that this conversion is only incomplete in SIT-single-deficient mice (note that loss of TRIM by itself has a null effect on thymic development in either male or female H-Y TCR tg mice [Simeoni et al., unpublished]) suggests that the loss of SIT is partially compensated for by other transmembrane adapter proteins, TRIM being one potential candidate (see below).

It is also possible that SIT may regulate thymocyte survival. However, two observations argue against this hypothesis. First, the thymic cellularity in the OT-I and OT-II transgenic systems is normal. Second, we did not observed any differences in the survival rate of thymocytes after treatment with various apoptotic stimuli (e.g., dexamethasone, etoposide, and anti-Fas).

Compensatory mechanisms might also explain why SIT deficiency does not enhance positive selection (or convert positive selection to negative selection) in the OT-I and OT-II TCR transgenic models. Alternatively, it simply might suggest that the fine-tuning function of SIT becomes negligible beyond a certain strength of the TCR-mediated input signal. In line with a gatekeeper function of SIT only in low-strength signaling systems might be the finding that the loss of SIT apparently does not influence negative selection processes in any model that we investigated (i.e., the strong TCR-mediated signals that induce negative selection apparently can no longer be influenced by SIT).

Besides regulating thymic development, SIT seems to partially control the size of the peripheral T-cell pool. Thus, the loss of SIT leads to an expansion of γδ T cells in peripheral lymphoid organs without enhancing the production of γδ T cells within the thymus or impairing their homing to the gut. In addition, SIT-deficient mice show diminished numbers of αβ T cells, selectively in lymph nodes. The latter finding could be due either to a reduced production of αβ T cells within the thymus or to a defect in peripheral T-cell homeostasis or to both. The mild reduction in the numbers of SP thymocytes in nontransgenic $SIT^{-/-}$ mice could in fact be partially responsible for the reduced numbers of mature peripheral T cells. However, it is also known that similarly to immature thymocytes, naive T cells require continuous contact with self-peptide/MHC molecules (low-affinity signals) to prevent death by neglect (15, 39). Thus, low-affinity ligands dictate positive selection in immature thymocytes and survival in naive peripheral T cells. Loss of a negative regulatory molecule such as SIT could enhance the strength of TCR-mediated signaling in the presence of low-affinity peptides, thereby altering the survival/death rate of peripheral T cells.

Independently of the mechanism that underlies altered homeostasis of the peripheral T-cell pool, the absence of SIT results in hyperreactivity of peripheral T cells towards TCR-mediated stimuli, with the consequence of enhanced production of the TH1 cytokines tumor necrosis factor alpha and gamma interferon in vitro. In line with this, loss of SIT significantly enhances the clinical course of EAE, a TH1-mediated autoimmune disease of the central nervous system.

How SIT regulates peripheral T-cell functions and how it balances TH1 versus TH2 T-helper cells in the periphery is not known at present. Indeed, despite considerable effort, we could not reveal significant alterations of membrane-proximal signaling events in SIT-deficient peripheral T cells. One possibility to explain the hyperreactivity of peripheral T cells was based on our previous observation that in Jurkat T cells, SIT exerts its negative regulatory function via the tyrosine-based signaling motif YASV (29, 35). Moreover, in the Jurkat system, it was shown that upon pervanadate stimulation, the tyrosine kinase Csk, the major negative regulator of Src protein tyrosine kinases, is capable of binding to this motif. Therefore, Csk represented an attractive candidate for mediating the inhibitory function of SIT on TCR signaling. However, so far, we could not show an association between SIT and Csk in human or mouse T cells under more physiological conditions of stimulation (e.g., CD3 MAb instead of pervanadate [data not shown]). Similarly, we did not observe an upregulation of the enzymatic activity of Lck, a crucial substrate of Csk in peripheral T cells of $SIT^{-/-}$ mice. Furthermore, CD3-mediated phosphorylation

of the TCR-ζ chain is not impaired in SIT-deficient thymocytes. Collectively, these data suggest that SIT is not involved in the inhibition of Src kinases (either directly or indirectly by recruiting Csk).

Another possibility to explain the negative regulatory role of SIT was based on our previous observation that SIT is capable of recruiting cytosolic protein tyrosine phosphatases (e.g., SHP2) to the plasma membrane (29). However, extensive biochemical analysis of SIT-deficient T cells did not reveal alteration of TCR-mediated membrane targeting of SHP1 or SHP2 (data not shown). This largely rules out the possibility that impaired membrane targeting of SHP1 or SHP2 underlies the enhanced signaling capacity of $SIT^{-/-}$ T cells. Nevertheless, the fact that SIT-deficient T cells react normally after stimulation with PMA and ionomycin suggests (and confirms our previous data) that SIT exerts its negative regulatory role upstream of activation of protein kinase C and production of IP3.

Although the molecular mechanism(s) underlying SIT-mediated inhibition of signaling is still unknown, it appears as if SIT would negatively regulate TCR-mediated activation of ERK in thymocytes. Indeed, ex vivo-isolated H-Y transgenic SIT-deficient thymocytes show enhanced phosphorylation of ERK1/2, and $SIT^{-/-}$ DP thymocytes display higher expression levels of CD5 and CD69, both molecules whose expression is regulated via the ERK-dependent transcription factors Ets-1 (14, 45) and AP-1 (11, 24). In light of these observations, it is important that we have previously demonstrated that SIT can bind the cytosolic adapter protein Grb2, an upstream activator of Erk, via a membrane-proximal YGNL motif. However, when overexpressed in Jurkat T cells, a CD8/CD8/SIT chimera (extracellular domain/transmembrane domain/intracellular domain) that carries an isolated YGNL motif does not inhibit T-cell functions (35). Rather, when this chimera is co-cross-linked with the TCR, it strongly upregulates TCR-mediated activation of the transcription factor NFAT. This suggests a positive rather than a negative regulatory role of the YGNL motif. However, further experiments are required to assess the role of the YGNL motif for SIT-mediated T-cell function.

Another possibility to explain enhanced TCR-mediated signaling in the absence of SIT would be to assume that SIT exerts its negative regulatory role in normal cells through sequestration of key signaling molecules from the lipid raft to the nonraft fraction, thereby limiting the numbers of signaling molecules in the lipid rafts. Loss of SIT within the nonraft fraction could then result in a redistribution of these signaling molecules to the lipid rafts. This would then permit enhanced signaling. A redistribution of molecules from nonrafts to rafts has most recently been proposed to cause the augmented FcεRIII-mediated signaling in NTAL/LAB-deficient mast cells (46, 51).

However, another recent report suggested that when present in the nonraft fraction of chicken DT-40 cells, Grb2 inhibits B-cell receptor (BCR)-mediated signals via an unknown mechanism (38a). Targeting of Grb2 to the lipid rafts (e.g., by ectopic expression of the lipid raft-associated transmembrane adapter NTAL) rescues the BCR from the Grb2-mediated inhibitory signal, thus facilitating BCR-mediated responses. If this model would also apply for T cells, then it would be reasonable to assume that SIT inhibits TCR-mediated signaling by enhancing the inhibitory pool Grb2 in the nonraft fraction. The fact that we did not observe major alterations of biochemical signaling events following CD3 stimulation of SIT-deficient peripheral T cells does not necessarily contradict this hypothesis, simply because the subtle changes that are induced by loss of SIT might be too weak to be detected by standard biochemical techniques. In addition, loss of SIT might be to a large extent compensated by other non-raft-associated transmembrane adapter proteins exerting similar functions, such as TRIM and LAX.

Although the molecular mechanism(s) underlying SIT function is still elusive, it is obvious that SIT controls signaling pathways at different levels within the immune system. First, SIT-mediated signals are required to maintain a proper T-cell repertoire; second, they are mandatory to maintain the composition of the peripheral T-cell pools; third, they regulate the activation thresholds of peripheral T cells; and fourth, they control cytokine production/expansion of particular peripheral T-cell populations. In all cases, SIT seems to act as a fine tuner of TCR-mediated signaling processes.

The only mild alterations of thymic selection processes as well as the rather moderate hyperreactivity of peripheral T cells in SIT-deficient mice might be due to a functional redundancy among those transmembrane adapter proteins that serve as negative regulators during TCR-mediated signaling. In this regard, other nonraft transmembrane adapter proteins, for example, TRIM and LAX, might compensate for the loss of SIT. TRIM shares not only structural properties with SIT (both molecules are disulfide-linked homodimers) but also two tyrosine-based signaling motifs (YGNL and YASV, which is YASL in TRIM) (18). Similarly, LAX is also capable of binding, e.g., Grb2, and has been reported to negatively regulate TCR-mediated signals via an unknown mechanism (50). Therefore, the analysis of the SIT/LAX or SIT/TRIM double knockout or the SIT/LAX/TRIM triple knockout will possibly help to elucidate the biochemical pathways that are controlled by these transmembrane adapter proteins. Nevertheless, it is tempting to speculate that SIT as well as other transmembrane adapter proteins play important roles in priming the organism for the development of autoimmune diseases either by regulating peripheral tolerance or by altering the generation of an appropriate T-cell repertoire. In this regard, it will be important to assess the genetic status and the phosphorylation status of SIT and other negative regulatory transmembrane adapter proteins in patients suffering from autoimmune disease.

ACKNOWLEDGMENTS

We are grateful to Jonathan Lindquist for critically reading the manuscript and helpful discussion; to Gary Koretzy, Thomas Kammerthoens, and Percy Knolle for TCR transgenic lines; to Reinhold Foerster and Oliver Pabst for investigation of gammadelta IEL; to Andrew Cope and Weiguo Zhang for reagents; and to the employees of the animal facility for maintenance of the animals. The help of Robert Enders, Evi Schaller, Agnes Fütterer, and Jennifer Meinecke is highly appreciated.

The work was supported by Deutsche Forschungsgemeinschaft (DFG)-funded research group 521 (research grants to L.S. and B.S.) and by DFG grants to K.P.

REFERENCES

1. **Alberola-Ila, J., K. A. Hogquist, K. A. Swan, M. J. Bevan, and R. M. Perlmutter.** 1996. Positive and negative selection invoke distinct signaling pathways. J. Exp. Med. **184:**9–18.

2. **Alimzhanov, M. B., D. V. Kuprash, M. H. Kosco-Vilbois, A. Luz, R. L. Turetskaya, A. Tarakhovsky, K. Rajewsky, S. A. Nedospasov, and K. Pfeffer.** 1997. Abnormal development of secondary lymphoid tissues in lymphotoxin beta-deficient mice. Proc. Natl. Acad. Sci. USA **94:**9302–9307.
3. **Allison, J. P.** 1993. Gamma delta T-cell development. Curr. Opin. Immunol. **5:**241–246.
4. **Anderson, G., K. J. Hare, and E. J. Jenkinson.** 1999. Positive selection of thymocytes: the long and winding road. Immunol. Today **20:**463–468.
5. **Azzam, H. S., J. B. DeJarnette, K. Huang, R. Emmons, C. S. Park, C. L. Sommers, D. El Khoury, E. W. Shores, and P. E. Love.** 2001. Fine tuning of TCR signaling by CD5. J. Immunol. **166:**5464–5472.
6. **Azzam, H. S., A. Grinberg, K. Lui, H. Shen, E. W. Shores, and P. E. Love.** 1998. CD5 expression is developmentally regulated by T cell receptor (TCR) signals and TCR avidity. J. Exp. Med. **188:**2301–2311.
7. **Bommhardt, U., Y. Scheuring, C. Bickel, R. Zamoyska, and T. Hunig.** 2000. MEK activity regulates negative selection of immature CD4+CD8+ thymocytes. J. Immunol. **164:**2326–2337.
8. **Brdicka, T., D. Pavlistova, A. Leo, E. Bruyns, V. Korinek, P. Angelisova, J. Scherer, A. Shevchenko, I. Hilgert, J. Cerny, K. Drbal, Y. Kuramitsu, B. Kornacker, V. Horejsi, and B. Schraven.** 2000. Phosphoprotein associated with glycosphingolipid-enriched microdomains (PAG), a novel ubiquitously expressed transmembrane adaptor protein, binds the protein tyrosine kinase csk and is involved in regulation of T cell activation. J. Exp. Med. **191:**1591–1604.
9. **Brdickova, N., T. Brdicka, P. Angelisova, O. Horvath, J. Spicka, I. Hilgert, J. Paces, L. Simeoni, S. Kliche, C. Merten, B. Schraven, and V. Horejsi.** 2003. LIME: a new membrane Raft-associated adaptor protein involved in CD4 and CD8 coreceptor signaling. J. Exp. Med. **198:**1453–1462.
10. **Bruyns, E., A. Marie-Cardine, H. Kirchgessner, K. Sagolla, A. Shevchenko, M. Mann, F. Autschbach, A. Bensussan, S. Meuer, and B. Schraven.** 1998. T cell receptor (TCR) interacting molecule (TRIM), a novel disulfide-linked dimer associated with the TCR-CD3-zeta complex, recruits intracellular signaling proteins to the plasma membrane. J. Exp. Med. **188:**561–575.
11. **Castellanos, M. C., C. Munoz, M. C. Montoya, E. Lara-Pezzi, M. Lopez-Cabrera, and M. O. de Landazuri.** 1997. Expression of the leukocyte early activation antigen CD69 is regulated by the transcription factor AP-1. J. Immunol. **159:**5463–5473.
12. **Chu, D. H., C. T. Morita, and A. Weiss.** 1998. The Syk family of protein tyrosine kinases in T-cell activation and development. Immunol. Rev. **165:**167–180.
13. **Clarke, S. R., M. Barnden, C. Kurts, F. R. Carbone, J. F. Miller, and W. R. Heath.** 2000. Characterization of the ovalbumin-specific TCR transgenic line OT-I: MHC elements for positive and negative selection. Immunol. Cell Biol. **78:**110–117.
14. **Dittmer, J.** 2003. The biology of the Ets1 proto-oncogene. Mol. Cancer **2:**29.
15. **Ernst, B., D. S. Lee, J. M. Chang, J. Sprent, and C. D. Surh.** 1999. The peptide ligands mediating positive selection in the thymus control T cell survival and homeostatic proliferation in the periphery. Immunity **11:**173–181.
16. **Finco, T. S., T. Kadlecek, W. Zhang, L. E. Samelson, and A. Weiss.** 1998. LAT is required for TCR-mediated activation of PLCgamma1 and the Ras pathway. Immunity **9:**617–626.
17. **Hayday, A. C.** 2000. [gamma][delta] cells: a right time and a right place for a conserved third way of protection. Annu. Rev. Immunol. **18:**975–1026.
18. **Horejsi, V., W. Zhang, and B. Schraven.** 2004. Transmembrane adaptor proteins: organizers of immunoreceptor signalling. Nat. Rev. Immunol. **4:**603–616.
19. **Hubener, C., A. Mincheva, P. Lichter, B. Schraven, and E. Bruyns.** 2001. Complete sequence, genomic organization, and chromosomal localization of the human gene encoding the SHP2-interacting transmembrane adaptor protein (SIT). Immunogenetics **53:**337–341.
20. **Huesmann, M., B. Scott, P. Kisielow, and H. von Boehmer.** 1991. Kinetics and efficacy of positive selection in the thymus of normal and T cell receptor transgenic mice. Cell **66:**533–540.
21. **Hur, E. M., M. Son, O. H. Lee, Y. B. Choi, C. Park, H. Lee, and Y. Yun.** 2003. LIME, a novel transmembrane adaptor protein, associates with p56lck and mediates T cell activation. J. Exp. Med. **198:**1463–1473.
22. **Itoh, K., M. Sakakibara, S. Yamasaki, A. Takeuchi, H. Arase, M. Miyazaki, N. Nakajima, M. Okada, and T. Saito.** 2002. Cutting edge: negative regulation of immune synapse formation by anchoring lipid raft to cytoskeleton through Cbp-EBP50-ERM assembly. J. Immunol. **168:**541–544.
23. **Jameson, S. C., K. A. Hogquist, and M. J. Bevan.** 1995. Positive selection of thymocytes. Annu. Rev. Immunol. **13:**93–126.
24. **Karin, M.** 1995. The regulation of AP-1 activity by mitogen-activated protein kinases. J. Biol. Chem. **270:**16483–16486.
25. **Kelly, K. A., M. Pearse, L. Lefrancois, and R. Scollay.** 1993. Emigration of selected subsets of gamma delta + T cells from the adult murine thymus. Int. Immunol. **5:**331–335.
26. **Kirchgessner, H., J. Dietrich, J. Scherer, P. Isomaki, V. Korinek, I. Hilgert, E. Bruyns, A. Leo, A. P. Cope, and B. Schraven.** 2001. The transmembrane adaptor protein TRIM regulates T cell receptor (TCR) expression and TCR-mediated signaling via an association with the TCR zeta chain. J. Exp. Med. **193:**1269–1284.
27. **Kisielow, P., H. Bluthmann, U. D. Staerz, M. Steinmetz, and H. von Boehmer.** 1988. Tolerance in T-cell-receptor transgenic mice involves deletion of nonmature CD4+8+ thymocytes. Nature **333:**742–746.
28. **Mariathasan, S., S. S. Ho, A. Zakarian, and P. S. Ohashi.** 2000. Degree of ERK activation influences both positive and negative thymocyte selection. Eur. J. Immunol. **30:**1060–1068.
29. **Marie-Cardine, A., H. Kirchgessner, E. Bruyns, A. Shevchenko, M. Mann, F. Autschbach, S. Ratnofsky, S. Meuer, and B. Schraven.** 1999. SHP2-interacting transmembrane adaptor protein (SIT), a novel disulfide-linked dimer regulating human T cell activation. J. Exp. Med. **189:**1181–1194.
30. **Martin, R., H. F. McFarland, and D. E. McFarlin.** 1992. Immunological aspects of demyelinating diseases. Annu. Rev. Immunol. **10:**153–187.
31. **Merkenschlager, M., D. Graf, M. Lovatt, U. Bommhardt, R. Zamoyska, and A. G. Fisher.** 1997. How many thymocytes audition for selection? J. Exp. Med. **186:**1149–1158.
32. **Naramura, M., H. K. Kole, R. J. Hu, and H. Gu.** 1998. Altered thymic positive selection and intracellular signals in Cbl-deficient mice. Proc. Natl. Acad. Sci. USA **95:**15547–15552.
33. **O'Shea, C. C., T. Crompton, I. R. Rosewell, A. C. Hayday, and M. J. Owen.** 1996. Raf regulates positive selection. Eur. J. Immunol. **26:**2350–2355.
34. **Paz, P. E., S. Wang, H. Clarke, X. Lu, D. Stokoe, and A. Abo.** 2001. Mapping the Zap-70 phosphorylation sites on LAT (linker for activation of T cells) required for recruitment and activation of signalling proteins in T cells. Biochem. J. **356:**461–471.
35. **Pfrepper, K. I., A. Marie-Cardine, L. Simeoni, Y. Kuramitsu, A. Leo, J. Spicka, I. Hilgert, J. Scherer, and B. Schraven.** 2001. Structural and functional dissection of the cytoplasmic domain of the transmembrane adaptor protein SIT (SHP2-interacting transmembrane adaptor protein). Eur. J. Immunol. **31:**1825–1836.
36. **Priatel, J. J., S. J. Teh, N. A. Dower, J. C. Stone, and H. S. Teh.** 2002. RasGRP1 transduces low-grade TCR signals which are critical for T cell development, homeostasis, and differentiation. Immunity **17:**617–627.
37. **Schaeffer, E. M., and P. L. Schwartzberg.** 2000. Tec family kinases in lymphocyte signaling and function. Curr. Opin. Immunol. **12:**282–288.
38. **Sosinowski, T., N. Killeen, and A. Weiss.** 2001. The Src-like adaptor protein downregulates the T cell receptor on CD4+CD8+ thymocytes and regulates positive selection. Immunity **15:**457–466.

38a. **Stork, B., M. Engelke, J. Frey, V. Horejsi, A. Hamm-Baarke, B. Schraven, T. Kurosaki, and J. Wienands.** 2004. Grb2 and the non-T cell activation linker NTAL constitute a Ca^{2+}-regulating signal circuit in B lymphocytes. Immunity **21:**681–691.

39. **Surh, C. D., and J. Sprent.** 2000. Homeostatic T cell proliferation: how far can T cells be activated to self-ligands? J. Exp. Med. **192:**F9–F14.
40. **Swan, K. A., J. Alberola-Ila, J. A. Gross, M. W. Appleby, K. A. Forbush, J. F. Thomas, and R. M. Perlmutter.** 1995. Involvement of p21ras distinguishes positive and negative selection in thymocytes. EMBO J. **14:**276–285.
41. **Swat, W., M. Dessing, H. von Boehmer, and P. Kisielow.** 1993. CD69 expression during selection and maturation of CD4+8+ thymocytes. Eur. J. Immunol. **23:**739–746.
42. **Tarakhovsky, A., S. B. Kanner, J. Hombach, J. A. Ledbetter, W. Muller, N. Killeen, and K. Rajewsky.** 1995. A role for CD5 in TCR-mediated signal transduction and thymocyte selection. Science **269:**535–537.
43. **Torgersen, K. M., T. Vang, H. Abrahamsen, S. Yaqub, V. Horejsi, B. Schraven, B. Rolstad, T. Mustelin, and K. Tasken.** 2001. Release from tonic inhibition of T cell activation through transient displacement of C-terminal Src kinase (Csk) from lipid rafts. J. Biol. Chem. **276:**29313–29318.
44. **Tough, D. F., and J. Sprent.** 1998. Lifespan of gamma/delta T cells. J. Exp. Med. **187:**357–365.
45. **Tung, J. W., S. S. Kunnavatana, L. A. Herzenberg, and L. A. Herzenberg.** 2001. The regulation of CD5 expression in murine T cells. BMC Mol. Biol. **2:**5.
46. **Volna, P., P. Lebduska, L. Draberova, S. Simova, P. Heneberg, M. Boubelik, V. Bugajev, B. Malissen, B. S. Wilson, V. Horejsi, M. Malissen, and P. Draber.** 2004. Negative regulation of mast cell signaling and function by the adaptor LAB/NTAL. J. Exp. Med. **200:**1001–1013.
47. **Yamashita, I., T. Nagata, T. Tada, and T. Nakayama.** 1993. CD69 cell surface expression identifies developing thymocytes which audition for T cell antigen receptor-mediated positive selection. Int. Immunol. **5:**1139–1150.
48. **Zhang, W., B. J. Irvin, R. P. Trible, R. T. Abraham, and L. E. Samelson.** 1999. Functional analysis of LAT in TCR-mediated signaling pathways using a LAT-deficient Jurkat cell line. Int. Immunol. **11:**943–950.
49. **Zhang, W., C. L. Sommers, D. N. Burshtyn, C. C. Stebbins, J. B. DeJarnette, R. P. Trible, A. Grinberg, H. C. Tsay, H. M. Jacobs, C. M. Kessler, E. O. Long, P. E. Love, and L. E. Samelson.** 1999. Essential role of LAT in T cell development. Immunity **10:**323–332.
50. **Zhu, M., E. Janssen, K. Leung, and W. Zhang.** 2002. Molecular cloning of a novel gene encoding a membrane-associated adaptor protein (LAX) in lymphocyte signaling. J. Biol. Chem. **277:**46151–46158.
51. **Zhu, M., Y. Liu, S. Koonpaew, O. Granillo, and W. Zhang.** 2004. Positive and negative regulation of FcepsilonRI-mediated signaling by the adaptor protein LAB/NTAL. J. Exp. Med. **200:**991–1000.

Appendix 6

Regulation of *in vitro* and *in vivo* immune functions by the cytosolic adaptor protein SKAP-HOM

Togni M., Swanson K.D., Reiman S., Kliche S., Pearce A.C., **Simeoni L.**, Reinhold D., Wienenads J., Neel B.G., Schraven B., and Gerber A. (2005) *Mol Cell Biol.* 25:8052-63.

MOLECULAR AND CELLULAR BIOLOGY, Sept. 2005, p. 8052–8063 Vol. 25, No. 18
0270-7306/05/$08.00+0 doi:10.1128/MCB.25.18.8052–8063.2005

Regulation of In Vitro and In Vivo Immune Functions by the Cytosolic Adaptor Protein SKAP-HOM

M. Togni,[1]† K. D. Swanson,[2]† S. Reimann,[1] S. Kliche,[1] A. C. Pearce,[3] L. Simeoni,[1] D. Reinhold,[1] J. Wienands,[4] B. G. Neel,[2] B. Schraven,[1]* and A. Gerber[1]

Institute of Immunology, Otto von Guericke University, Magdeburg,[1] and Cellular and Molecular Immunology, Georg August University, Göttingen,[4] Germany; Cancer Biology Program, Division of Hematology-Oncology, Department of Medicine, Beth Israel Deaconess Medical Center, Harvard Medical School, Boston, Massachusetts[2]; and Centre for Cardiovascular Sciences, Division of Medical Sciences, Institute of Biomedical Research, Wolfson Drive, The Medical School, University of Birmingham, Edgbaston, Birmingham, United Kingdom[3]

Received 24 March 2005/Returned for modification 6 May 2005/Accepted 17 June 2005

SKAP-HOM is a cytosolic adaptor protein representing a specific substrate for the Src family protein tyrosine kinase Fyn. Previously, several groups have provided experimental evidence that SKAP-HOM (most likely in cooperation with the cytosolic adaptor protein ADAP) is involved in regulating leukocyte adhesion. To further assess the physiological role of SKAP-HOM, we investigated the immune system of SKAP-HOM-deficient mice. Our data show that T-cell responses towards a variety of stimuli are unaffected in the absence of SKAP-HOM. Similarly, B-cell receptor (BCR)-mediated total tyrosine phosphorylation and phosphorylation of Erk, p38, and JNK, as well as immunoreceptor-mediated Ca^{2+} responses, are normal in SKAP-HOM$^{-/-}$ animals. However, despite apparently normal membrane-proximal signaling events, BCR-mediated proliferation is strongly attenuated in the absence of SKAP-HOM$^{-/-}$. In addition, adhesion of activated B cells to fibronectin (a ligand for β1 integrins) as well as to ICAM-1 (a ligand for β2 integrins) is strongly reduced. In vivo, the loss of SKAP-HOM results in a less severe clinical course of experimental autoimmune encephalomyelitis following immunization of mice with the encephalitogenic peptide of MOG (myelin oligodendrocyte glycoprotein). This is accompanied by strongly reduced serum levels of MOG-specific antibodies and lower MOG-specific T-cell responses. In summary, our data suggest that SKAP-HOM is required for proper activation of the immune system, likely by regulating the cross-talk between immunoreceptors and integrins.

Adaptor proteins are multifunctional signaling molecules which are capable of coupling engaged immunoreceptors (e.g., the T-cell receptor [TCR] or the B-cell receptor [BCR]) to intracellular signaling pathways and effector systems. In general, adaptor proteins do not exert enzymatic or transcriptional activities. Rather, they contain a variety of modular domains that mediate constitutive or inducible protein-protein or protein-lipid interactions after engagement of signal-transducing receptors.

Several cytosolic adaptor proteins have been identified during the last years which appear to be involved in reorganization of the cytoskeleton and/or integrin-mediated adhesion after external engagement of immunoreceptors. In T cells, these include the cytosolic adaptor proteins ADAP (adhesion and degranulation promoting adaptor protein) (27) and SKAP55 (Src-kinase-associated phosphoprotein of 55 kDa) (31).

ADAP was among the first adaptor proteins shown to translate TCR stimulation to avidity modulation of β1 and β2 integrins (a mechanism called inside-out signaling). Thus, despite almost normal proximal signaling events (global tyrosine phosphorylation, TCR-mediated increases in intracellular calcium, Erk activation, actin polymerization, and TCR clustering), TCR-mediated clustering of integrins and the adhesion of T cells to the β1 and β2 integrin ligands fibronectin and ICAM-1 were found to be strongly impaired in ADAP-deficient T cells. The failure to activate integrins via inside-out signaling leads to a defect in TCR-mediated proliferation, interleukin-2 (IL-2) production, and a strongly impaired T-cell response in vivo (9, 27).

While ADAP is expressed in T cells and myeloid cells, SKAP55 is expressed exclusively in T lymphocytes (5, 20). SKAP55 comprises a pleckstrin homology domain, a C-terminal SH3 domain, and an interdomain that carries three tyrosine-based signaling motifs (21). Overexpression experiments in Jurkat T cells suggested that SKAP55 interacts with the protein tyrosine phosphatase CD45 and possibly regulates the mitogen-activated protein kinase pathway (32, 33). More recently it was demonstrated that SKAP55 is capable of regulating integrin-mediated adhesion, conjugate formation between T cells, and antigen-presenting cell (APC)- and TCR-mediated clustering of LFA-1 in mouse T cells (15, 31). Thus, the functional effects of SKAP55 and ADAP seem to be similar.

In line with this assumption is the observation that in primary T cells and in the Jurkat T-cell line, SKAP55 tightly associates with ADAP. This interaction involves the SH3 domain of SKAP55 and a proline-rich segment in ADAP (17, 21). Biochemical analysis had further suggested that all SKAP55 molecules expressed in T lymphocytes associate with ADAP. All these data indicate that in T lymphocytes, SKAP55 and

* Corresponding author. Mailing address: Institute of Immunology, Otto von Guericke University, Magdeburg, Leipziger Strasse 44, 39120 Magdeburg, Germany. Phone: 49 391 67 15800. Fax: 49 391 67 15852. E-mail: burkhart.schraven@medizin.uni-magdeburg.de.

† M. Togni and K. D. Swanson contributed equally to this work.

ADAP form a functional unit and that a role of this unit is to modulate T-cell adhesion after engagement of the TCR/CD3 complex. However, it is still unknown whether regulation of adhesion is the only task that is fulfilled by SKAP55 and ADAP during an ongoing immune response.

In contrast to SKAP55, the cytosolic adaptor SKAP-HOM (SKAP55 homologue) or SKAP55R (SKAP55 related) is an adaptor protein that is more widely expressed within the hematopoetic system (4, 16, 23). SKAP-HOM comprises an almost identical structure as SKAP55, except for a unique N-terminal putative coiled-coil region and only two tyrosine-based signaling motifs in the interdomain. Similar to SKAP55, SKAP-HOM has been reported to associate with ADAP via its SH3 domain and to represent a specific substrate for the Src family protein tyrosine kinase p59Fyn (17, 23).

An involvement of SKAP-HOM in integrin-mediated signaling was initially suggested by the analysis of murine bone marrow-derived macrophages (BMM) in which tyrosine phosphorylation of SKAP-HOM (and of ADAP) was induced after adhesion to fibronectin (1, 30). Moreover, in BMM from mice homozygous for the "motheaten" (me) mutation (these me/me mice lack expression of the cytosolic tyrosine phosphatase SHP-1), ADAP and SKAP-HOM were found to be expressed as constitutively tyrosine phosphorylated proteins, and this augmented phosphorylation correlates well with the known hyperadhesiveness of me/me macrophages (28, 30). Finally, enteropathogenic species of *Yersinia enterocolitica* exert resistance to phagocytosis by injecting the virulence factor YopH, a protein tyrosine phosphatase, into host cells. In these cells YopH apparently dephosphorylates ADAP and SKAP-HOM. Either by itself or in concert with other mechanisms, this leads to abrogation of the phagocytic process and causes cellular detachment and rounding up (1, 6). Thus, not only ADAP and SKAP55 but also SKAP-HOM seem to be involved in integrin-mediated signaling pathways. However, the function of SKAP-HOM within the immune system remains elusive.

To gain further insight into the physiologic role of SKAP-HOM, we investigated the immune system of SKAP-HOM-deficient mice. T-cell, platelet, and macrophage functions appear to be unaffected by loss of SKAP-HOM. In marked contrast, despite apparently normal membrane-proximal signaling events, both in vitro and in vivo B-cell responses are impaired in the absence of SKAP-HOM. Indeed, after antibody-mediated stimulation of the BCR, SKAP-HOM-deficient B cells show reduced in vitro proliferation and an impaired capability to adhere to either fibronectin or ICAM, two physiologic ligands for β1 and β2 integrins. Moreover, when challenged in vivo, SKAP-HOM-deficient mice display a decrease in clinical severity of experimental autoimmune encephalomyelitis (EAE) and a strongly reduced production of MOG (myelin oligodendrocyte glycoprotein)-specific immunoglobulins. Taken together, our findings indicate an important role for SKAP-HOM in regulating homeostasis of the immune system. Moreover, they suggest that SKAP-HOM might be an attractive target for therapeutic intervention in autoimmune diseases such as multiple sclerosis.

MATERIALS AND METHODS

Mice strains. The SKAP-HOM-deficient mouse was generated by retrovirus-based gene trap technology (Lexicon Genetics Inc.) (34). Mice were backcrossed to C57BL/6JBom (Taconics) for a minimum of six generations. In all experiments, 8- to 12-week-old littermate mice were used. All procedures were conducted according to protocols approved by the local authorities. Mice were genotyped by two independent PCRs using the following primer sequences: neomycin sense, 5′GAT GCC GCC GTG TTC C; neomycin antisense, 5′GCC CCT GAT GCT CTT CGT C; SKAP-HOM sense, 5′CCT GCG GCC TTT GAT GGT G; SKAP-HOM antisense, 5′ACT GCT TTG CTG GGG GTG GTG TT.

Determination of hematological parameters. To measure blood cell parameters, whole blood was collected by heart puncture in tubes containing heparin and analyzed on an automatic hematology counter (Cell-Dyn 1600; Abbott).

Cell preparations. The spleens were passed through a fine mesh filter to obtain a single cell suspension. In all assays, total splenocytes were isolated, and B and T cells were purified by negative selection using mouse B-cell isolation kits or mouse T-cell isolation kits and AutoMACS (Miltenyi Biotec), respectively. CD4- and CD8-positive splenocytes were prepared by positive selection using anti-CD4 or anti-CD8 microbead-coupled antibody and AutoMACS. Purity was >90% as checked by flow cytometry. The cells were cultured in RPMI 1640 medium supplemented with 10% fetal calf serum, 100 U/ml penicillin, 100 μg/ml streptomycin (all from Biochrom AG), and 50 μM 2-mercaptoethanol.

Adhesion assay. For fibronectin binding, the central area of a 35-mm diameter tissue culture dish (Falcon) was coated with 50 μl fibronectin (100 μg/ml; Roche Diagnostics) for 90 min at room temperature. For ICAM-1 binding, tissue culture dishes were precoated for 16 h at 4°C with goat anti-human immunoglobulin G (IgG) Fc fragment (7.2 μg/ml; Dianova) to allow directional coating. After washing, dishes were coated with 12.5 μg/ml recombinant murine ICAM-1 human Fc chimera (R&D Systems) for 90 min at room temperature. After coating, dishes were washed three times with phosphate-buffered saline (PBS) (without Ca^{2+} or Mg^{2+}) and blocked with 1% bovine serum albumin (BSA) in PBS for an additional 2 h.

Cells (5×10^6) were washed with Hanks balanced salt solution (HBSS) and either left unstimulated or stimulated with tetradecanoyl phorbol acetate (50 ng/ml), $MnCl_2$ (2 mM), or anti-mouse IgM $F(ab')_2$ (2 μg/ml) for 30 min at 37°C. Cells were plated on the dishes and incubated at 37°C for 30 min. Nonadherent cells were removed by washing the dishes three times with HBSS. Cell adhesion was measured by counting six independent fields by microscopy using an ocular counting reticule. Specific adhesion was expressed as the increase over unstimulated control samples.

Proliferation assay. Freshly isolated mouse cells were resuspended in complete medium and seeded in quadruplicate at 1×10^5 cells in 96-well round-bottomed microtiter plates (Costar). Cells were either left unstimulated or stimulated for 72 h at 37°C with the indicated concentrations of affinity-purified goat anti-mouse IgM or the corresponding $F(ab')_2$ fragment (Jackson ImmunoResearch), lipopolysaccharide (LPS; 2.5 μg/ml; Sigma), IL-4 (20 ng/ml; Peprotech Inc.), anti-mouse CD40 (1 μg/ml; Pharmingen), phorbol myristate acetate (PMA) (2×10^{-8} M; Sigma), and ionomycin (500 ng/ml; Calbiochem). For the last 8 h, 0.5 μCi [^{3}H]thymidine was added to the cultures. After harvesting, the radioactivity incorporated into the DNA was measured by liquid scintillation counting (1450 MicroBeta Trilux; PerkinElmer Wallac GmbH). The stimulation index was calculated as the ratio of counts per minute (cpm) of stimulated to unstimulated proliferation.

Measurement of bone marrow-derived macrophage proliferation in response to macrophage colony-stimulating factor (M-CSF) and granulocyte-macrophage colony-stimulating factor (GM-CSF). BMMs from mice of the indicated genotypes were differentiated ex vivo as previously described (10) with some modification. Specifically, bone marrow cells were preplated for 48 h on tissue culture plates, and cells remaining in suspension were enumerated. Cells (1×10^6) were seeded onto 35-mm petri plates. The cells were incubated at 37°C in Dulbecco's modified Eagle medium containing 10% heat-inactivated serum supplemented with either 10 ng/ml M-CSF or 20 ng/ml of GM-CSF (Peprotech). Cells were fed every 2 days. At the indicated time, cells were rinsed with PBS, harvested in trypsin-EDTA, and counted using a Z2 Coulter Counter.

FcR and complement receptor-mediated phagocytosis. To opsonize sheep red blood cells (RBCs) with IgG, RBCs were washed and resuspended in veronal-buffered saline (Sigma-Aldrich) containing 1:2,500 rabbit anti-RBC serum and incubated at 37°C for 1.5 to 2 h. To opsonize RBCs with complement, RBCs were incubated with anti–sheep RBC IgM for 1 h (1:5,000), followed by incubation with 10% C5-deficient serum (Sigma-Aldrich) for 20 min. Opsonized RBCs were washed with veronal-buffered saline and resuspended in DMEM at ~5×10^7 RBCs/ml. BMMs (7 to 8 days old) were seeded in 24-well plates (3×10^5/well) for 24 h, starved for 2 h, and incubated with 0.4 ml of opsonized RBCs at 37°C for 20 min. Phagocytosis was terminated by lysing nonphagocytosed RBCs with H_2O for 40 s, and BMMs were fixed in 4% paraformaldehyde. To visualize internalized RBCs, the cells were permeabilized with 0.5% Triton X-100 for 5

min, rinsed three times in PBS, pH 7.4, and incubated with rabbit anti-RBC serum (1:10,000) and rhodamine phalloidin. After washing, the cells were incubated in fluorescein isothiocyanate (FITC)-conjugated anti-rabbit Ig and washed three times prior to being photographed using a Zeiss microscope. Four-hundred cells were counted in three randomly chosen fields. The percentage of active cells (greater than 3 RBCs/cell) and the average number of RBCs per active cell were determined for each field.

Flow cytometry. The cells were stained with the following antibodies: anti-CD3, anti-CD5, anti-CD11a, anti-CD18, anti-CD21, anti-CD23, anti-CD29, anti-CD45R/B220, anti-CD49d, anti-IgM, and anti-IgD (all from Pharmingen). Flow cytometry was performed on a FACSCalibur using CellquestPro software (Becton Dickinson).

Western blotting. Western blotting was performed as previously described (22). For immunodetection, the following primary antibodies were used: anti-phospho-Tyr (4G10; Upstate Biotechnology), anti-phospho-Erk1/2, anti-Erk1/2, anti-phospho-JNK, anti-JNK, anti-phospho-p38, anti-p38, anti-phospho-Akt (Cell Signaling Technology, Inc.), and anti-SKAP55 (BD Biosciences). Goat polyclonal anti-ADAP sera were previously described (25). Affinity-purified rabbit polyclonal anti-SKAP-HOM antiserum was prepared as described elsewhere (23). Specific binding was detected using peroxidase-conjugated goat anti-mouse or goat anti-rabbit antibodies by applying the enhanced chemiluminescence system (Amersham Biosciences) according to the manufacturer's protocol.

Calcium flux. Purified splenic B cells were resuspended at 1×10^6 cells/ml in RPMI 1640 without phenol red, supplemented with 10% fetal calf serum, and loaded with 3.75 μM indo-1 acetoxymethyl ester (Molecular Probes) for 45 min at 37°C. Cells were washed, resuspended in the same RPMI medium, and incubated for an additional 30 min at 37°C. After establishing a stable baseline level, B cells were stimulated with 10 μg/ml affinity-purified goat anti-mouse IgM $F(ab')_2$ fragment (Jackson ImmunoResearch). Equal loading of samples was checked by treatment of cells with 100 nM ionomycin (Calbiochem). The ratio of indo-1 violet/blue was analyzed by flow cytometry using LSR (Becton Dickinson). Data analysis was performed using FloJo software (Tree Star).

Enzyme-linked immunosorbent assays (ELISAs). For the determination of spontaneous levels of IgM and IgG isotypes, microtiter plates (MaxiSorb; Nunc, Wiesbaden, Germany) were coated with 3.6 μg/ml goat anti-mouse IgG plus IgM (heavy plus light chains) (Dianova, Hamburg, Germany) at 4°C overnight and blocked with 1% BSA. Sera were serially diluted in duplicate. Isotype-specific antibodies were detected with the respective alkaline phosphatase-conjugated goat anti-mouse antibodies to IgG1, IgG2a, IgG2b, IgG3, or IgM (Southern Biotechnology Associates, Inc.). The substrate *p*-nitrophenyl phosphate (Sigma Aldrich) was used for color development, and after 30 min the absorbance was read at 405 nm on an ELISA plate reader (Dynatech). Immunoglobulin concentrations were calculated by interpolation from a standard curve using the respective isotype controls from mouse myeloma (Sigma-Aldrich).

For the determination of specific anti-2,4-dinitrophenyl (DNP) and anti-MOG p35-55, IgG and IgM plates were coated with 3 μg/ml DNP-BSA or 10 μg/ml MOG in bicarbonate buffer, respectively, overnight at 37°C. After blocking with 1% BSA, the plates were incubated with serial dilutions of mouse serum overnight at 4°C. Specific binding was detected using alkaline phosphatase-labeled goat anti-mouse IgM (μ chain specific; Serotec) or goat anti-mouse IgG (subclasses 1 plus 2a plus 2b plus 3; Fcγ fragment specific; Dianova).

Immunization of mice. Twelve-week-old mice were immunized intraperitoneally (i.p.) with 100 μg of 2,4-dinitrophenyl-conjugated keyhole limphet hemocyanin (DNP-KLH; Calbiochem) in complete Freund's adjuvant (CFA; Sigma-Aldrich, Taufkirchen, Germany) and were boosted 21 days later. Mice were bled before and after boosting (day 21 and day 28), and hapten-specific serum antibody levels were measured by ELISA (see above). Also, mice were immunized i.p. with 100 μg of 2,4,6-trinitrophenyl (TNP)-LPS in saline. Mice were bled before and 5 and 10 days after immunization, and hapten-specific serum antibody levels were measured by ELISA.

Induction of EAE and clinical evaluation. MOG p35-55 corresponding to a mouse sequence (MEVGWYRSPFSRVVHLYRNGK) was synthesized on a peptide synthesizer by standard 9-fluorenylmethoxycarbonyl chemistry and purified by high-performance liquid chromatography (HPLC). Active EAE was induced in 8- to 12-week-old mice by immunization with 200 μg MOG p35-55 emulsified in complete Freund's adjuvant (CFA; Sigma-Aldrich, Taufkirchen, Germany) containing 800 μg of heat-killed *Mycobacterium tuberculosis* (Difco Laboratories, Detroit, Mich.). The emulsion was administered subcutaneously as four 50-μl injections into the flanks of each leg. In addition, 200 ng of pertussis toxin (List Biological Laboratories, Campbell, CA) dissolved in 200 μl PBS was injected i.p. on days 0 and 2. Mice were weighed daily, monitored for clinical signs of EAE, and graded on a scale of increasing severity from 0 to 5 by blinded investigators as described earlier (29). Daily clinical scores were calculated as the average of all individual disease scores of each group, including mice not developing clinical signs of EAE.

Cytokine concentration. Levels of cytokines in culture supernatants were determined using the mouse inflammatory cytometric bead array kit (Becton Dickinson).

Conjugation assay. Splenic B cells obtained from wild-type or knock-out littermates were cultured at a concentration of 2×10^6 cells/ml in RPMI 1640 medium supplemented with 10% fetal calf serum, 100 U/ml penicillin, 100 μg/ml streptomycin (all from Biochrom AG), and 50 μM 2-mercaptoethanol for 16 h with (loaded) or without (unloaded) 0.2 mg/ml chicken ovalbumin 323-339 peptide ($OVA_{323-339}$). Cells were then washed and set to 1×10^6 cells/ml in the same medium. T cells enriched by negative selection using a T-cell kit (Miltenyi Biotec) obtained from OT-II mice were loaded with 5 (and 6-)-carboxfluorescein diacetate succinimidyl ester (CFSE). After loading, T cells were diluted to 1×10^6 cells/ml RPMI 1640 medium supplemented with 10% fetal calf serum, 100 U/ml penicillin, 100 μg/ml streptomycin (all from Biochrom AG), and 50 μM 2-mercaptoethanol. Peptide-loaded or unloaded B cells (100 μl) were mixed with equal volume of T cells in a 96-well plate. After coincubation for 8 h, cells were fixed by adding 200 μl of 4% paraformaldehyde. After 20 min at 37°C, cells were carefully transferred into Falcon tubes and measured by a fluorescence-activated cell sorter. Events with positive CFSE staining and increased forward scatter were counted as conjugates.

Actin polymerization. Purified splenic B cells (100 μl; 2×10^6 cells/ml in PBS) were stimulated with 10 μg/ml affinity-purified goat anti-mouse IgM $F(ab')_2$ fragment. At the end of the stimulation, 100 μl 4% formaldehyde, 0.2% saponin, and 100 μl FITC-phalloidin (5 μg/ml) were added. The tubes were vortexed and kept at room temperature for 15 min. After washing, cells were resuspended in 300 μl paraformaldehyde. Actin polymerization was measured by flow cytometry and expressed as an increase in mean fluorescence intensity.

Statistical analysis. Values are expressed as the means ± standard errors of the means (SEM) of at least three independent experiments. One-way analysis of variance was used to assess the statistical significance of the differences. Probability (*P*) values of <0.05 (*) and <0.01 (**) were considered significant.

RESULTS

Expression of SKAP-HOM within the hematopoietic system. In order to asses the in vivo function of SKAP-HOM, we generated SKAP-HOM$^{-/-}$ mice by a retrovirus-based gene trap technology (Lexicon Genetics Inc.) (Fig. 1A). SKAP-HOM deficiency was confirmed by PCR and by anti-SKAP-HOM Western blotting (Fig. 1B and C). SKAP-HOM$^{-/-}$ mice were born healthy at the expected Mendelian frequency and did not show any obvious abnormalities. Moreover, the total numbers of leukocytes or of different leukocyte subsets (lymphocytes, monocytes, and granulocytes) were normal in the peripheral blood of SKAP-HOM-deficient animals (Table 1). Similarly, the numbers of splenocytes, thymocytes, and lymph node cells were unaffected in the absence of SKAP-HOM. Platelet counts were slightly (but not significantly) lower in SKAP-HOM-deficient mice compared to wild-type animals. Within the lymphatic organs of wild-type mice, SKAP-HOM was found to be expressed in T cells, B cells, $CD4^+$ T cells, $CD8^+$ T cells, and, to a lesser extent, thymocytes (Fig. 1D). Unfortunately, we could not analyze the expression pattern of SKAP-HOM within the T-cell compartment in more detail (e.g., whether SKAP-HOM is selectively expressed in particular T-cell subsets), because the polyclonal antiserum we used for Western blotting was not suitable for flow cytometry or for microscopy.

Recently it had been demonstrated that loss of ADAP in the T-cell line Jurkat induces a concomitant loss of its binding partner SKAP55, likely because SKAP55 is subjected to degradation when not complexed with ADAP (13). Since SKAP-HOM is also expressed in T-cells and, similar to SKAP55, is capable of associating with ADAP, we had to formally exclude

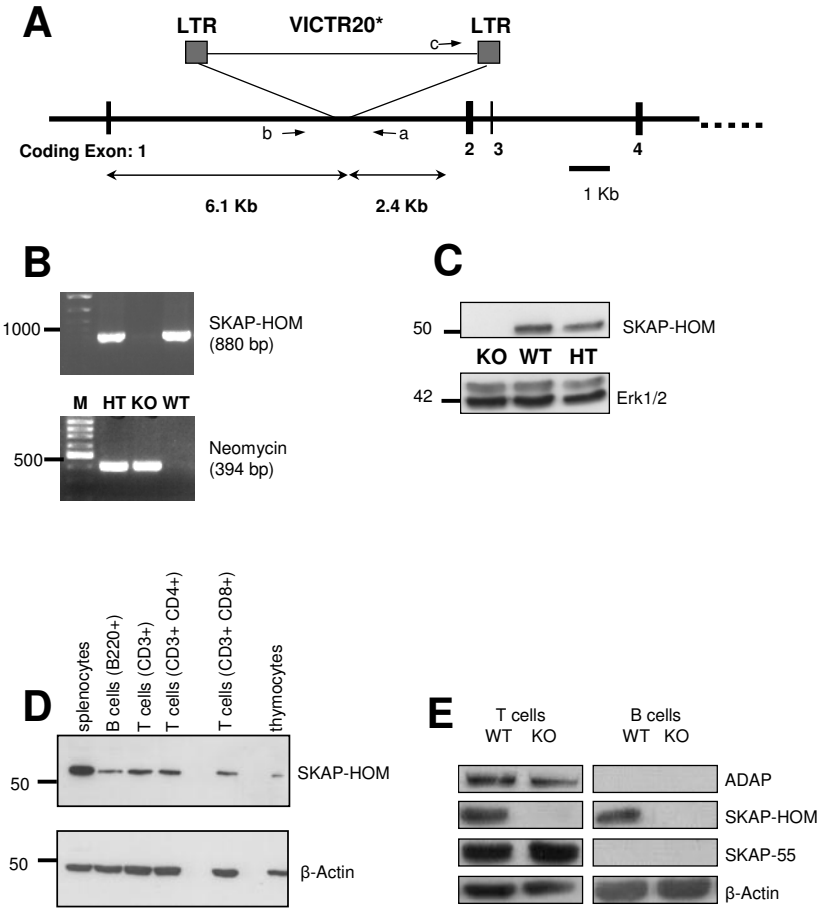

FIG. 1. Scheme showing the retroviral insertion into the SKAP-HOM locus, the expression pattern of SKAP-HOM in lymphoid organs, and the loss of SKAP-HOM protein in SKAP-HOM-deficient mice. (A) The VICTR20 retroviral insertion site in the SKAP-HOM locus was determined by restriction site mapping and comparing the wild-type and retroviral-targeted alleles. PCR products generated by oligonucleotide primers (a to c; also used for genotyping) positioned as shown were sequenced to identify the precise site of retroviral integration. Only the first 4 out of 12 coding exons are shown. (B) Mice were genotyped by PCR detecting the wild-type SKAP-HOM allele and the recombinant allele containing the neomycin resistance cassette. (C) Postnuclear lysates of total splenocytes of knock-out, wild-type, and heterozygous animals were resolved by sodium dodecyl sulfate-polyacrylamide gel electrophoresis followed by blotting onto nitrocellulose sheets. Immunoblots were probed with a polyclonal rabbit anti-SKAP-HOM antiserum. (D) Total splenocytes and thymocytes were prepared from wild-type animals. Splenic B cells and T cells were obtained by negative selection with microbeads. $CD4^+$ T cells and $CD8^+$ T cells were obtained by positive selection with microbeads. Postnuclear lysates were resolved by sodium dodecyl sulfate-polyacrylamide gel electrophoresis, and the resulting blots were probed as for panel C. (E) Loss of SKAP-HOM does not affect expression of ADAP and SKAP55 in the T-cell compartment. Postnuclear lysates of purified splenic T- and B-cell populations were separated by sodium dodecyl sulfate-polyacrylamide gel electrophoresis followed by anti-SKAP-HOM, anti-ADAP, and anti-SKAP55 Western blotting. LTR, long terminal repeat; KO, knockout; WT, wild-type; HT, heterozygous.

the possibility that loss of SKAP-$HOM^{-/-}$ in T and/or B cells influences the expression levels of either ADAP or SKAP55. Figure 1E shows that this is not the case. Indeed, T-cells of SKAP-HOM-deficient mice express normal amounts of both ADAP and SKAP55. While these data exclude the possibility that the expression of ADAP or SKAP55 is dependent on SKAP-HOM, they also indicate that loss of SKAP-HOM within the T-cell compartment could be compensated for by the ADAP/SKAP55 complex. In contrast to T cells (and as reported previously), B lymphocytes express SKAP-HOM but not ADAP or SKAP55 (5, 20, 23).

Lymphocyte populations of spleen, lymph nodes, and bone marrow of SKAP-HOM-deficient mice were further analyzed by flow cytometry with a panel of lineage- and stage-specific monoclonal antibodies. The number and distribution of T cells

TABLE 1. Hematopoietic cellularity in 8- to 12-week-old wild-type and SKAP-HOM-deficient littermates[a]

Hematopoietic cellularity	Mouse	
	Wild type (n = 12)	SKAP-$HOM^{-/-}$ (n = 10)
Splenocyte number (10^6)	148 ± 15	182 ± 30
Thymocyte number (10^6)	154 ± 12	184 ± 18
Lymph node cells (10^6) (inguinal + axillary)	12 ± 2	11 ± 2
White blood cells (10^3 cells/μl)	4.4 ± 0.5	4.5 ± 0.7
Lymphocytes (10^3 cells/μl)	3.6 ± 0.4	3.9 ± 0.5
Monocytes (10^3 cells/μl)	0.4 ± 0.1	0.3 ± 0.1
Granulocytes (10^3 cells/μl)	0.4 ± 0.1	0.3 ± 0.1
Platelets (10^3 cells/μl)	555 ± 105	442 ± 102

[a] Note that the differences in platelet counts did not reach statistical significance as assessed by one-way analysis of variance.

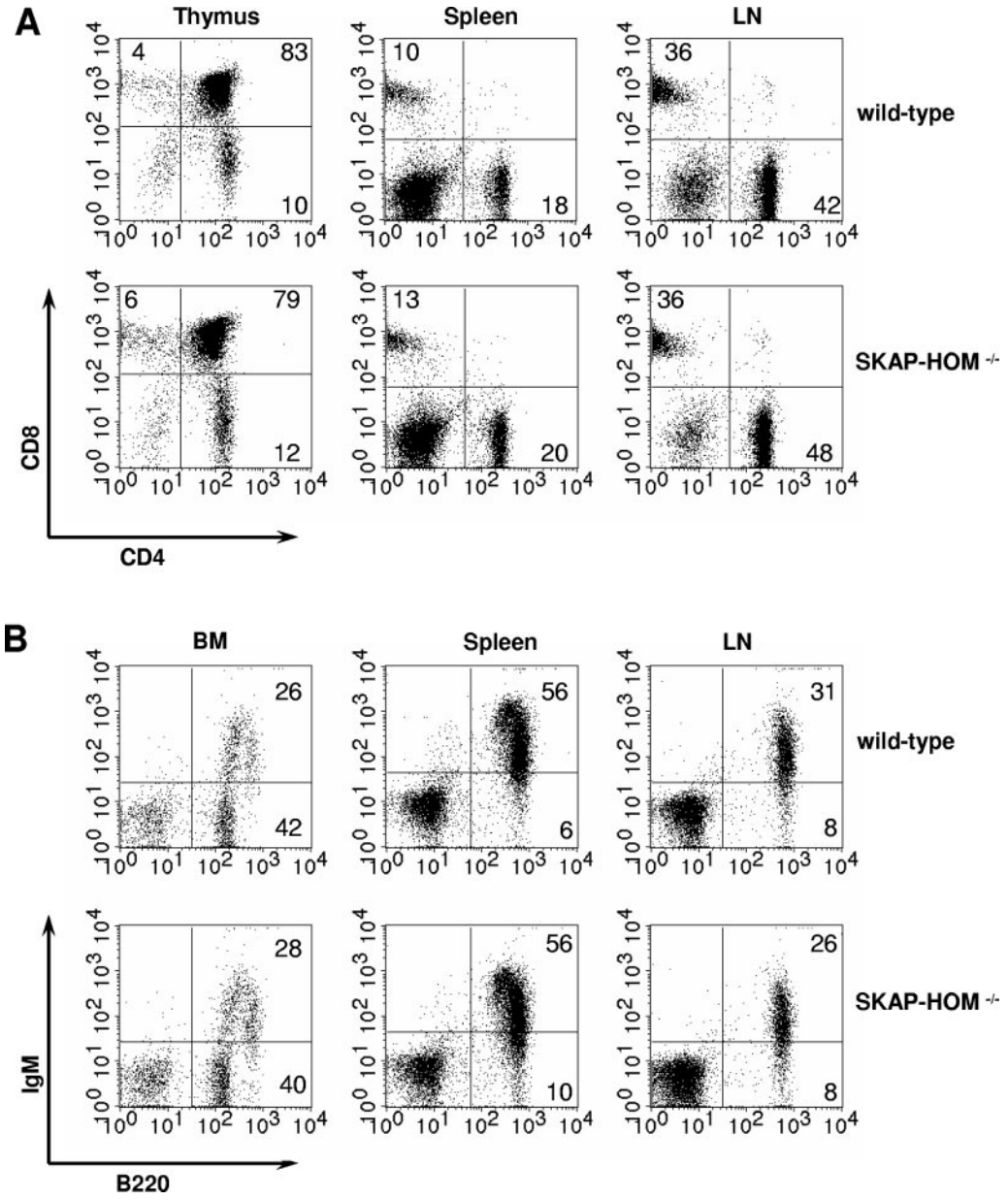

FIG. 2. Normal T- and B-lymphocyte differentiation in SKAP-HOM-deficient mice. (A) Thymic T-cell precursors, splenic T cells, and lymph node T cells were analyzed by flow cytometry after staining with CD4-FITC and CD8-phycoerythrin. (B) Bone marrow B-cell precursors, splenic B cells, and lymph node B cells were analyzed after staining with B220-FITC and IgM-phycoerythrin. The percentages of cells within each lymphocyte population are indicated. BM, bone marrow; LN, lymph node.

in the various immunological organs (thymus, spleen, lymph nodes, and bone marrow) as well as the CD4/CD8 ratio was normal in SKAP-HOM$^{-/-}$ mice. Also, developmental and maturation markers of B cells (including marginal zone B cells and B1 cells) showed no abnormalities in bone marrow, spleen, lymph nodes, and the peritoneal cavity (Fig. 2 and data not shown). Thus, although SKAP-HOM is ubiquitously expressed within the hematopoietic system, its absence is either dispensable for normal hematopoietic cell development or can be compensated for by other molecules.

Impaired B-cell responses in SKAP-HOM$^{-/-}$ mice. We next assessed the consequences of SKAP-HOM deficiency in various hematopoietic cell populations known to express SKAP-HOM. These experiments revealed that T-cell proliferation (as judged by [^{3}H]thymidine incorporation) towards a variety of different stimuli (anti-βTCR, anti-CD3ε, PMA plus ionomycin) was comparable between SKAP-HOM-deficient mice and control animals (Fig. 3A). Note that the apparent hyperproliferation of PMA-ionomycin-stimulated T cells is due to variability within the different samples and did not reach significance. There was also no difference in the production of tumor necrosis factor α, IL-4, IL-5, gamma interferon, and IL-2 by stimulated T cells between knock-out and wild-type mice (data not shown). This strongly suggests that loss of SKAP-HOM

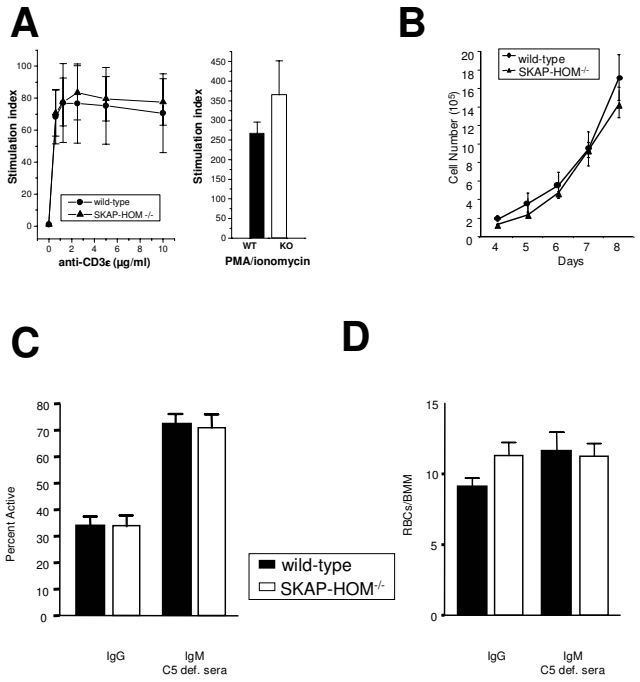

FIG. 3. Normal T-cell and BMM proliferation and normal Fc- and complement receptor-mediated phagocytosis in SKAP-HOM-deficient mice. (A) Purified splenic T cells were stimulated with increasing concentrations of CD3ε MAbs or with a combination of PMA plus ionomycin. Data of quadruplicate cultures are shown as means ± SEM; $n = 5$. (B) BMMs isolated from wild-type or knockout mice were cultured for 2 days and then plated in replicates in the presence of 10 ng/ml M-CSF. Cells were harvested at the indicated times and counted. (C) BMMs were incubated with sheep red blood cells opsonized with either IgG or IgM and C5-deficient (def.) sera. BMMs were scored for the percent of phagocytically active cells and for the ability of active cells to phagocytize RBCs (D). Results are representative of three separate experiments.

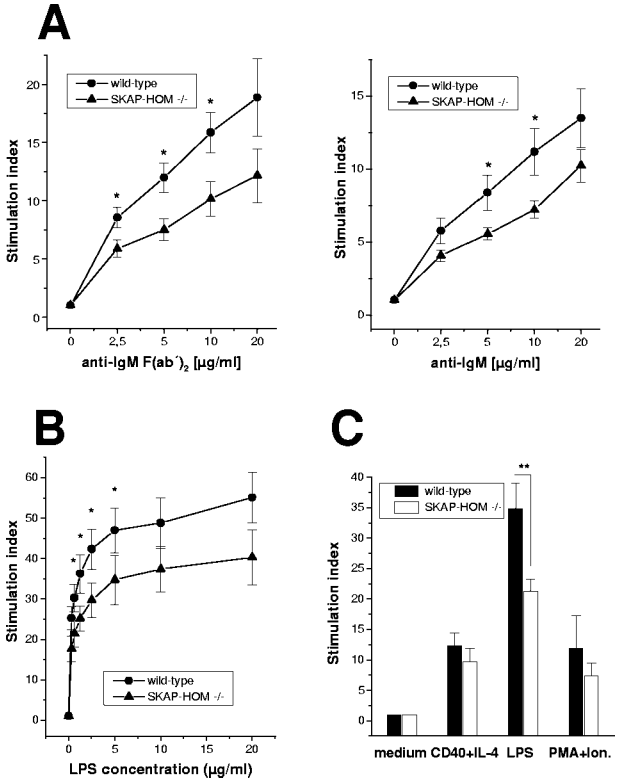

FIG. 4. Impaired B-cell proliferation in SKAP-HOM-deficient mice. (A) Purified splenic B cells from wild-type or SKAP-HOM-deficient mice were stimulated with the indicated concentration of soluble anti-IgM $F(ab')_2$ or soluble anti-IgM; $n = 10$; results are means ± SEM. The mean counts per minute of maximally IgM $F(ab')_2$-stimulated wild-type B cells was 7,045 ± 893 cpm versus 407 ± 69 cpm of unstimulated cells. For SKAP-HOM-deficient B cells, the mean counts per minute was 6,417 ± 663 versus 628 ± 60, respectively. (B) Purified splenic B cells were stimulated with the indicated concentration of LPS (0.31 to 20 μg/ml). (C) Purified splenic B cells were activated with either anti-CD40+IL-4, LPS (2.5 μg/ml), or PMA plus ionomycin (Ion.). The stimulation index was calculated as the ratio of counts per minute (cpm) of stimulated to unstimulated proliferation. Nonstimulated B cells are shown as controls; $n = 8$; shown are means ± SEM. *, $P < 0.05$; **, $P < 0.01$.

does not alter in vitro T-cell functions, possibly because its loss is compensated for by the ADAP/SKAP55 complex (see above).

Similar to T cells, stimulation of SKAP-HOM deficient platelets with collagen-related peptide (a ligand for the ITAM-coupled receptor glycoprotein VI [GPVI]) or thrombin (which activates the G protein-coupled receptors protease-activated receptors 3 and 4 [PAR3 and PAR4]) exhibited normal aggregation and α-granule secretion. Platelet spreading on collagen and fibrinogen was also normal in SKAP-HOM-deficient mice. Likewise, tyrosine phosphorylation of LAT, SLP-76, and PLGγ2 after stimulation of GPVI with collagen-related peptide was unaffected (data not shown). These findings suggest that SKAP-HOM is also dispensable for platelet function.

SKAP-HOM is expressed in macrophages, and previous overexpression studies had suggested that in myeloid cells it negatively regulates cytokine-mediated growth (2, 4). To assess whether loss of SKAP-HOM alters growth of ex vivo-isolated myeloid cells, we measured M-CSF-induced proliferation of BMM prepared from wild-type, heterozygous, and SKAP-HOM-deficient mice. As shown in Fig. 3B, BMMs of SKAP-HOM$^{-/-}$ mice and wild-type mice showed almost identical growth rates after stimulation with M-CSF and GM-CSF (data not shown). Thus, SKAP-HOM does not seem to play a major role in regulating cytokine-mediated growth of BMMs. Moreover, analysis of SKAP-HOM-deficient BMMs did not reveal significant differences in Fc- or complement receptor-mediated phagocytosis of IgG- or IgM-coated sheep red blood cells (Fig. 3C and D).

In marked contrast to T cells, platelets, and macrophages, the proliferative responses of anti-IgM stimulated B lymphocytes were significantly decreased in SKAP-HOM$^{-/-}$ mice (Fig. 4A). Similarly, the response to LPS, which is mediated via toll-like receptor 4 (TLR4), was strongly impaired (Fig. 4B). In contrast, the same cells responded normally after stimulation with PMA-ionomycin or a combination of CD40 monoclonal antibody (MAb) plus IL-4, ruling out a general defect in the capability of B cells to become activated (Fig. 4C). These results were confirmed with CFSE staining, excluding the possibility that the decreased proliferation observed was due to increased apoptosis (data not shown). Rather, the data suggest

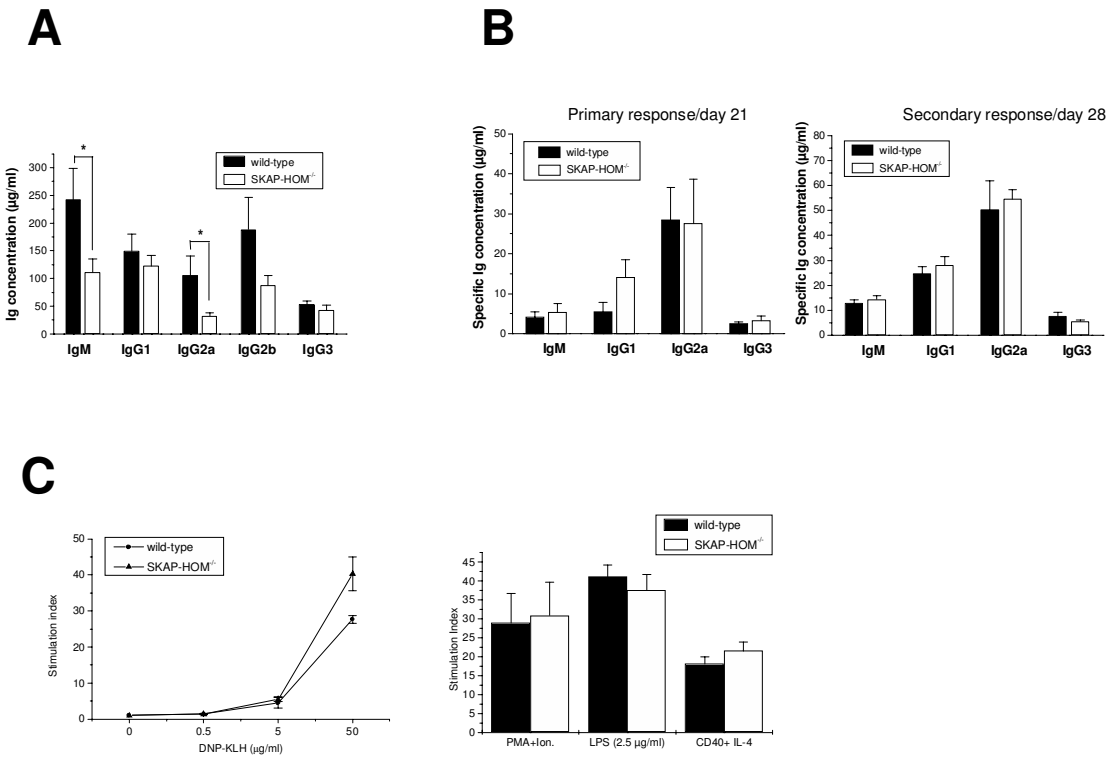

FIG. 5. Constitutive serum immunoglobulin levels and humoral immune responses in SKAP-HOM-deficient mice. (A) Constitutive serum immunoglobulin levels in nonimmunized wild-type and SKAP-HOM-deficient animals; $n = 11$; shown are means ± SEM. (B) Humoral immune response after immunization with the T-dependent antigen DNP-KLH. Twelve-week-old mice were injected at days 0 and day 21 intraperitoneally with DNP-KLH. Mice were bled before boostering (on day 21, corresponding to primary response) and after boostering (on day 28, corresponding to secondary response). Anti-DNP-specific levels of IgM, IgG1, IgG2a, and IgG3 were measured by ELISA. Four animals were investigated for each group. (C) Proliferative response of splenocytes after the secondary immunization to DNP-KLH. Lymphocytes isolated from the spleen at day 28 (after boostering) were stimulated with the indicated concentrations of DNP-KLH for 72 h. Results are given as the mean stimulation index of three independent experiments (means ± SEM). Ion., ionomycin.

that SKAP-HOM is involved in the regulation of BCR- and TLR4-mediated activation of B lymphocytes.

In summary, the data shown in Fig. 3 and 4 indicate that loss of SKAP-HOM primarily alters B-cell functions.

Reduced levels of serum immunoglobulins in SKAP-HOM$^{-/-}$ mice. The impaired proliferative in vitro response of SKAP-HOM-deficient B cells prompted us to assess the spontaneous and induced production of immunoglobulins in wild-type and SKAP-HOM-deficient animals. As shown in Fig. 5, considerably lower concentrations of constitutive serum immunoglobulins were found in SKAP-HOM$^{-/-}$ mice compared to wild-type littermates. This was in particular true for the IgM, IgG2a, and IgG2b isotypes (Fig. 5A).

To investigate the humoral response after in vivo immunization, wild-type and SKAP-HOM-deficient animals were immunized with a T-dependent (DNP-KLH) or a T-independent model antigen (TNP-LPS). In the former case, the primary immune response was measured 21 days after the first immunization. On the same day the mice received a second immunization (boostering), and the secondary immune response was assessed 7 days later. As shown in Fig. 5B, the magnitude of DNP-KLH-specific IgM, IgG1, IgG2a, and IgG3 was similar in wild-type and SKAP-HOM$^{-/-}$ animals with regard to both the primary and the secondary immune response. Moreover, DNP-KLH and mitogen-induced in vitro proliferation of splenocytes after the second immunization was unaffected in SKAP-HOM-deficient animals (Fig. 5C).

Similar to the response after immunization with DNP-KLH, SKAP-HOM-deficient mice responded normally after immunization with the T-independent antigen TNP-LPS (data not shown). Collectively, these data indicate that loss of SKAP-HOM affects basal immunoglobulin production, whereas SKAP-HOM-deficient mice are able to mount normal nitrophenyl-specific primary and secondary responses to all immunoglobulin isotypes.

Normal proximal signaling in SKAP-HOM$^{-/-}$ B cells. Despite the apparently normal B-cell response after immunization with T-dependent and T-independent antigens, the impaired B-cell proliferation following anti-IgM and LPS stimulation suggested that loss of SKAP-HOM results in a subtle failure(s) of the BCR to be coupled to intracellular signaling pathways. To further elucidate the molecular mechanism underlying the functional alterations of SKAP-HOM-deficient B cells, we analyzed membrane-proximal signaling events downstream of the BCR. First, we assessed the ability of SKAP-HOM$^{-/-}$ B cells to elicit a calcium response upon stimulation with an anti-IgM MAb. As shown in Fig. 6A, at an antibody concentration at which impaired B-cell proliferation

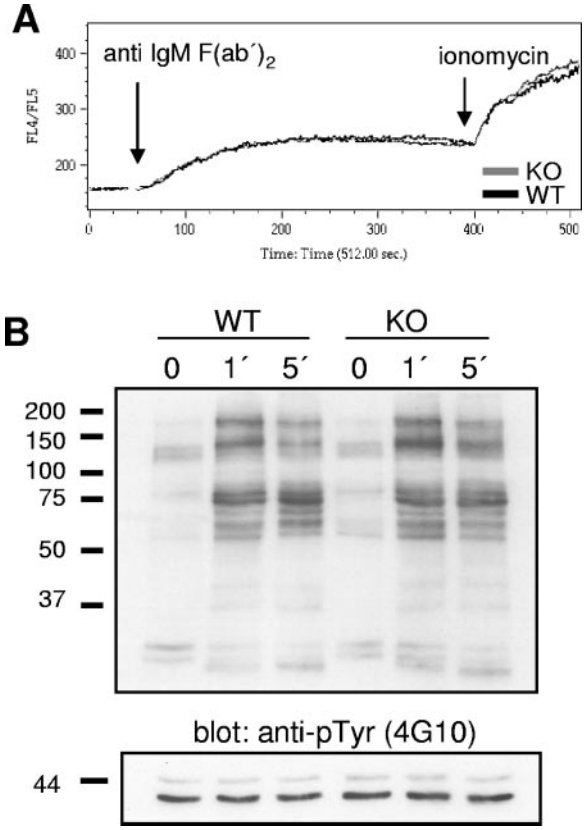

FIG. 6. Normal proximal BCR-mediated signaling in the absence of SKAP-HOM. (A) Freshly isolated, indo-1-loaded splenic B cells were stimulated with anti-IgM $F(ab')_2$ (10 μg/ml) or, as a positive control, with ionomycin (100 nM). Intracellular calcium levels were measured by flow cytometry. (B) Purified splenic B cells were left unstimulated or treated with soluble anti-IgM $F(ab')_2$ (10 μg/ml) for the indicated minutes. Cellular lysates were resolved by sodium dodecyl sulfate-polyacrylamide gel electrophoresis, and blots were probed with anti-phosphotyrosine (anti-pTyr) MAb 4G10. The expression levels of total Erk1 and Erk2 are shown as loading controls in the lower panel (additional data not shown). KO, knockout; WT, wild type.

of SKAP-HOM deficient B-cells was clearly evident, no differences in BCR-mediated calcium flux were discernible between splenic B cells of wild-type and SKAP-HOM$^{-/-}$ mice. Similarly, BCR stimulation did not reveal any significant differences in global tyrosine phosphorylation (Fig. 6B) as well as in the phosphorylation of Erk1/2, JNK, p38, and PKB/Akt after short-time (up to 10 min) as well as after long-time stimulation (up to 60 min; data not shown). Thus, loss of SKAP-HOM does not affect the major membrane-proximal signaling events downstream of the BCR.

Impaired adhesion of SKAP-HOM$^{-/-}$ mice B cells. A strongly reduced proliferation after immunoreceptor engagement in combination with almost normal membrane-proximal signaling events is reminiscent of the situation that has been described for T cells lacking the cytosolic adaptor protein ADAP (9, 27). ADAP$^{-/-}$ T cells are severely compromised in their ability to adhere to ligands of β1 and β2 integrins, such as ICAM-1 and fibronectin. Similarly, downregulation of SKAP55 (e.g., by RNA interference) has the same effect (15 and S. Kliche and B. Schraven, unpublished data).

To assess whether loss of SKAP-HOM alters B-cell adhesion, purified splenic B lymphocytes were stimulated via the BCR and then allowed to adhere to fibronectin (a ligand of the β1 integrin VLA-4) or to ICAM-1 (a ligand of the β2 integrin LFA-1). As shown in Fig. 7A and B, BCR-induced adhesion to both fibronectin and ICAM-1 was strongly attenuated in SKAP-HOM$^{-/-}$ B cells. In contrast, treatment of the same cells with manganese chloride (which induces a conformational change of the extracellular domain of integrins, thereby switching them to the high-affinity state) or phorbol ester (which induces the high-affinity state of the integrins via inside-out signaling by bypassing membrane-proximal signaling events) induced adhesion comparable to that of wild-type cells. The latter finding excludes the possibility that loss of SKAP-HOM generates an intrinsic functional defect of either β1 or β2 integrins. Moreover, flow cytometry analysis did not reveal alterations in cell surface expression of CD11a/CD18 (LFA-1) and CD49d/CD29 (VLA-4) in SKAP-HOM$^{-/-}$ B cells (data not shown), which rules out the possibility that loss of adhesiveness of SKAP-HOM-deficient B cells is caused by blunted expression of integrins. Rather, it appeared that, similar to ADAP/SKAP55 in T cells, SKAP-HOM is involved in coupling the BCR to integrin activation.

To investigate whether the adhesion defect of SKAP-HOM$^{-/-}$ B cells could be attributed to impaired dynamics of the actin cytoskeleton, we compared BCR-induced actin polymerization in wild-type and SKAP-HOM-deficient B cells. To this end, activated B cells were permeabilized with saponin and subsequently stained with phalloidin-tetramethyl rhodamine isocyanate, a probe specifically reacting with polymerized F-actin. The amount of polymerized F-actin within the cells was subsequently determined by flow cytometry. Figure 7C depicts that actin polymerization occurs normally in the absence of SKAP-HOM, which suggests that SKAP-HOM is dispensable for BCR-mediated reorganization of the cytoskeleton.

The β2 integrin LFA-1 has been shown to be involved in the formation of the immunological synapse in T cells and in conjugate formation between B and T cells at the onset of an immune response (12). To assess whether loss of SKAP-HOM impairs conjugate formation, we loaded freshly isolated splenic B cells with the model peptide $OVA_{323-339}$ and then incubated the peptide-loaded B cells with T cells of OT-II TCR-transgenic mice. Subsequently, conjugate formation between T and B cells was evaluated by flow cytometry. Figure 7D shows that conjugate formation is not impaired in SKAP-HOM-deficient B lymphocytes. In addition, the formation of the B-cell synapse and the clustering of LFA-1 after MAb-mediated activation of the BCR also seem to occur normally in the absence of SKAP-HOM (F. Batista, personal communication). Thus, SKAP-HOM seems to be dispensable for conjugate formation between T cells and APCs and for formation of the immunological synapse after antibody-mediated triggering of the BCR.

Decreased severity of EAE in SKAP-HOM$^{-/-}$ mice. Although EAE is considered to primarily represent a Th1-mediated autoimmune disease, a number of studies have suggested a role for B cells and autoantibodies in EAE (7, 8, 14). To asses the consequences of SKAP-HOM deficiency in this autoimmune model, wild-type mice and SKAP-HOM$^{-/-}$ mice were immunized with the encephalitogenic peptide MOG 35-55.

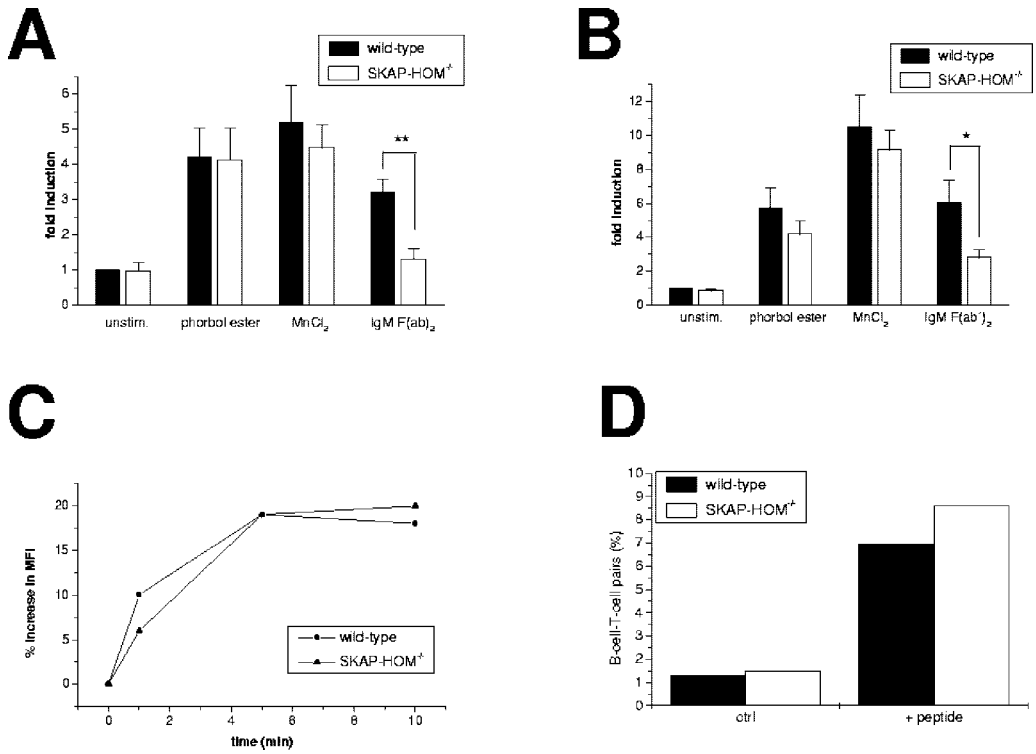

FIG. 7. Attenuated BCR-mediated adhesion but normal F-actin polymerization and conjugate formation of SKAP-HOM-deficient B cells. (A) Purified splenic B cells were stimulated with anti-IgM F(ab′)$_2$ and then allowed to adhere to tissue cell culture dishes coated with either fibronectin (A) or recombinant murine ICAM-1 (B). Adherent cell numbers were determined by microscopy. Results are expressed as means ± SEM of six independently performed experiments. (C) Purified B cells were treated with anti-IgM F(ab′)$_2$, permeabilized with saponin, and then stained with FITC-phalloidin. The cellular F-actin polymerization was assayed by flow cytometry after 1, 5, and 10 min. Results are expressed as percent increase of mean fluorescence intensity (MFI). The shown graph is representative of five independently performed experiments. (D) Purified B cells were loaded with OVA peptide overnight. T cells of OT-II TCR-transgenic mice were loaded with CFSE and coincubated with the peptide-pulsed B cells for 8 h. Conjugate formation was subsequently assessed by flow cytometry. Results are expressed as percentages of loaded B cells conjugated with T cells. The shown graph is representative of four independently performed experiments. unstim., unstimulated.

Figure 8A demonstrates that both groups of mice showed maximal disease scores at days 15 to 17 after immunization, which was followed by a remission phase. However, despite the fact that the first clinical signs of disease appeared somewhat earlier in SKAP-HOM$^{-/-}$ animals (Fig. 8A and the inset table), the mean clinical score of EAE was clearly more severe in wild-type animals (mean score of 2.2 in wild-type animals versus 1.2 in SKAP-HOM$^{-/-}$ animals at day 17, respectively; $P < 0.05$). Thus, SKAP-HOM$^{-/-}$ mice are not only impaired in their ability to activate B lymphocytes in vitro but also show a blunted immune response after immunization with the encephalitogenic peptide MOG in vivo.

To further elucidate the mechanisms underlying the altered response of SKAP-HOM-deficient mice in the EAE model, we measured the in vivo levels of the MOG-specific autoantibodies at day 15 after immunization. Figure 8B shows that the levels of MOG-specifc IgG and, to a lesser extent, MOG-specifc IgM antibodies in the serum were much lower in SKAP-HOM$^{-/-}$ mice compared to wild-type animals. In addition, a decreased MOG-specific proliferation of lymph node cells was observed (Fig. 8C). These findings suggest that loss of SKAP-HOM within the hematopoietic system leads to an attenuated clinical course of EAE which is accompanied by reduced production of MOG-specific immunoglobulins as well as a reduced MOG-induced T-cell response.

DISCUSSION

In this study we investigated the immune system of mice deficient in expression of the cytosolic adaptor protein SKAP-HOM. SKAP-HOM represents the ubiquitously expressed homologue of the T-cell-specific adaptor protein SKAP55, a physiological binding partner of the integrin-regulating adaptor ADAP (17, 21). Mice lacking SKAP-HOM$^{-/-}$ are viable and fertile and exhibit no obvious abnormalities. Therefore, it is likely that SKAP-HOM$^{-/-}$ is not required during development of the growing organism or the hematopoietic system.

Although no anatomic abnormalities were observed in the primary and secondary lymphoid organs, SKAP-HOM$^{-/-}$ mice showed reduced levels of spontaneous immunoglobulins in the serum. The constitutive defect in the production of IgM, IgG2a, and IgG2b apparently does not result from loss of a particular B-cell population but rather is due to a reduced ability of SKAP-HOM-deficient B cells to proliferate after stimulation of the BCR or TLR4.

Our attempts to identify the signaling defect(s) underlying

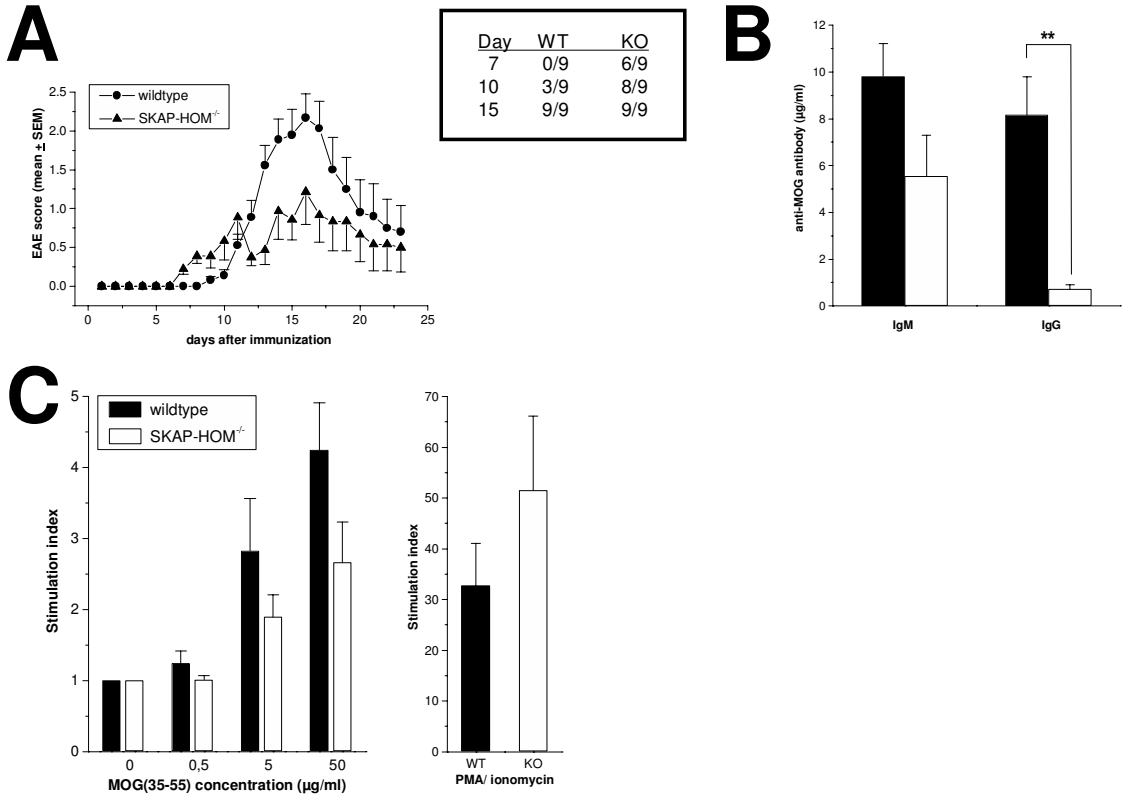

FIG. 8. SKAP-HOM-deficient mice show reduced severity of EAE. (A) EAE was induced following immunization with MOG 35-55 (200 μg MOG in CFA). The severity of EAE is presented as mean clinical scores (means ± SEM; $n = 9$). The accompanying table in the box shows the incidence of EAE within the experimental groups at days 7, 10, and 15, respectively. The shown graph is representative of three independently performed experiments. The difference in the mean clinical score was significant at days 7, 8, 13, 15, and 17 ($P < 0.05$). (B) Serum levels of anti-MOG-specific antibodies in sera collected at day 14 after immunization of mice with MOG 35-55. Concentration of specific IgM and IgG were measured by ELISA. (C) Proliferative response to MOG 35-55 of lymphocytes isolated from draining lymph nodes at day 14 following immunization with MOG 35-55 ($n = 5$). Lymph node cells were cultured with or without MOG 35-55 for 72 h. The mean counts per minute of maximally MOG-stimulated wild-type lymph node cells was 4,431 ± 856 cpm versus 1,059 ± 211 cpm of unstimulated cells. For SKAP-HOM$^{-/-}$ lymph node cells, the mean cpm was 1,969 ± 860 versus 610 ± 191, respectively. WT, wild type; KO, knockout.

the reduced ability of SKAP-HOM-deficient B cells to respond to external stimuli did not reveal significant alterations of BCR-mediated global tyrosine phosphorylation, calcium flux, or activation of the mitogen-activated protein kinase pathways. These data collectively suggest that the major membrane-proximal signaling events regulating B-cell activation are not impaired in the absence of SKAP-HOM. However, we found that the lack of SKAP-HOM results in a severely compromised ability to couple the BCR to regulation of β1 and β2 integrins, thereby causing reduced adhesion of B cells to fibronectin and to ICAM-1. It is tempting to speculate that these adhesion defects are the major reason for the observed alterations of both the in vivo and in vitro B-cell responses that we see in the SKAP-HOM$^{-/-}$ mice.

Both SKAP-HOM and SKAP55 are reported to form a complex with the cytosolic adaptor protein ADAP (17, 21). In T cells, the association between SKAP55 and ADAP has been shown to be mediated via the SH3 domain of SKAP55 and the proline-rich domain of ADAP (17, 21). Moreover, loss of ADAP in T cells results in a failure of integrin-mediated adhesion as well as impaired T-cell proliferation after TCR stimulation (9, 27). Preliminary data obtained by RNA interference approaches in the T-cell line suggest a similar adhesion-regulating function for SKAP55 (15 and S. Kliche and B. Schraven, unpublished). Moreover, a recent report had demonstrated that overexpression of SKAP55 augments both T-cell adhesion to fibronectin and ICAM-1 as well as conjugate formation between T cells and APCs (31). Thus, it appears as if in T cells ADAP and SKAP55 form a functional unit that couples the TCR to integrin activation, thereby regulating T-cell adhesion. Our finding that B-cell adhesion is impaired in SKAP-HOM-deficient mice strongly suggests that SKAP-HOM fulfils a similar function in B lymphocytes as SKAP55 and ADAP in T-cells. One of the major challenges for the future will be to assess whether a B-cell homologue of ADAP (ADAP-HOM) exists that constitutively interacts with SKAP-HOM in B lymphocytes and couples the BCR to integrin activation.

It is, however, important to note that the adhesion defect caused by loss of SKAP-HOM is apparently less severe than the T-cell adhesion defect that is observed in ADAP-knockout mice. This could indicate that ADAP regulates adhesion not only via SKAP55 but also through another, as yet unidentified signaling molecule(s). Alternatively, the possibility has to be considered that loss of SKAP-HOM in B cells is partially

compensated for by another protein(s) that regulate(s) B-cell adhesion.

Although additional studies are required to solve this puzzle, it appears as if the impaired adhesion of B cells in vitro does not affect the ability of B cells to populate the different lymphoid organs in vivo. This could be explained by the fact that the regulated induction of adhesion and migration in vivo results from complex interactions of different signaling pathways and that in the orchestra of events regulating, e.g., homing of lymphocytes, the absence of one player can be compensated for by others. In line with this hypothesis is the finding that also in ADAP$^{-/-}$ mice (in which T cells show a strongly impaired adhesion to ICAM-1 and ICAM-2, VCAM-1, and fibronectin after TCR engagement) the colonization of the lymphoid organs appears to be almost normal (9, 27).

The unaltered response of the SKAP-HOM-deficient animals after immunization with DNP-KLH versus the clearly reduced in vitro response of SKAP-HOM-deficient B lymphocytes and the lower levels of anti-MOG antibodies after immunization of the animals with MOG-peptide seem to be contradictory. However, it is important to note that the DNP-KLH immunization for inducing a humoral immune response and, e.g., the immunization with MOG peptide that is used for induction of EAE are not directly comparable. The different nature of antigen (hapten plus carrier versus peptide), the different routes of application (intraperitoneal versus subcutaneous), and the different immunization protocols (booster dose versus single application) may explain these diverging results.

In this regard, an elegant recent in vitro study showed that integrin (e.g., LFA-1)-mediated adhesion is primarily important for B-cell activation under suboptimal conditions of stimulation (e.g., when either low-affinity antigens are used for stimulation or when the concentration of the activating peptide is very low) (3). Possibly, in terms of the B-cell response, subcutaneous immunization with MOG peptide represents a "suboptimal" condition in which the contribution of integrin-mediated adhesion is important to allow appropriate B-cell activation. In contrast, i.p. immunization with optimal doses of high-affinity T-dependent or T-independent antigens might reflect conditions of stimulation in which the contribution of integrin-mediated adhesion is less important. The elucidation of these possibilities requires immunization of the animals with different doses of T-dependent or T-independent antigens and subsequent monitoring of the B-cell response. Additionally, or alternatively, SKAP-HOM-deficient mice could be crossed with mice carrying a transgenic BCR, as described previously (3). Ex vivo-isolated B cells from such double transgenic animals could be stimulated with different concentrations of peptide or with altered peptides, followed by analysis of B-cell functions (microscopic analysis of the B-cell synapse and/or functional readouts such as CD86 expression). We are currently preparing to assess these possibilities.

Nevertheless, the impaired in vitro response of SKAP-HOM-deficient B lymphocytes, the lower constitutive concentrations of serum immunoglobulins, and the strongly reduced antibody response in the EAE model suggest that SKAP-HOM plays an important role in the generation of an appropriate immune response after challenge with particular antigens (see also below).

Loss of SKAP-HOM attenuates the clinical course of EAE. This is accompanied by a decreased synthesis of MOG-specific antibodies and a reduced secondary MOG-specific proliferation of lymph node cells. The apparently normal in vitro functions of SKAP-HOM-deficient T cells might suggest that the attenuated course of EAE is mainly due to an altered B-cell response. However, EAE is primarily considered to represent a Th1-mediated autoimmune disease, and the pathophysiolgic role of B cells and autoantibodies is controversial. For example, B-cell-deficient mice immunized with rodent MOG 35-55 develop a course of EAE that is indistinguishable from that of wild-type mice. This suggests that B cells do not play a major role in EAE (11). By contrast, passive transfer of activated B cells or serum from wild-type mice immunized with MOG restores the susceptibility of B-cell-deficient mice to develop EAE. This indicates that MOG-specific B cells and anti-MOG antibodies seem to contribute to the pathology of EAE (18, 19, 26). In line with the latter assumption is a recent report by Filatreau et al. which clearly showed a role of B cells in regulating the clinical course of EAE (7). Thus, further studies are required to assess whether impaired B-cell responses alone are responsible for the altered outcome of EAE in SKAP-HOM-deficient mice.

Indeed, it might well be that not only blunted B-cell functions but also an altered cooperation between T and B cells results in an incomplete T-cell activation leading to an attenuated MOG-specific immune response in SKAP-HOM-deficient mice. In addition (or alternatively), the possibility cannot be excluded that the altered course of EAE in the SKAP-HOM$^{-/-}$ mice is in part (if not primarily) due to an impaired cooperation between dendritic cells (DC), macrophages, and T cells. Although further experiments are required to precisely assess the functions of SKAP-HOM$^{-/-}$ DCs and macrophages, two preliminary pieces of evidence argue against a severe functional alteration of antigen-presenting cells in the absence of SKAP-HOM. First, we did not find significant impairments of Fc- or complement receptor-mediated phagocytosis in SKAP-HOM-deficient macrophages, which suggests that antigen uptake (at least via these receptors) is not dependent on SKAP-HOM. Moreover, conjugate formation between $OVA_{323-339}$-loaded DCs and the corresponding OT-II TCR transgenic T cells is not affected in the absence of SKAP-HOM. However, whether it also applies for DCs loaded with MOG or other (suboptimal) peptides requires further analysis.

Finally, despite apparently normal functions in vitro (which might be due to the fact that loss of SKAP-HOM is compensated for by the presence of SKAP55, whose expression is not affected in T cells of SKAP-HOM-deficient mice), the possibility cannot be excluded that SKAP-HOM-deficient T cells are also slightly impaired in their ability to respond to specific antigens (such as MOG) in vivo. In summary, further studies (including the analysis of microglia cells which express SKAP-HOM) are required to answer the question of how loss of SKAP-HOM attenuates the clinical course of EAE. In addition, it will be necessary to assess the question of whether loss of SKAP-HOM exclusively alters the clinical outcome of EAE or whether it also affects the course of other model diseases (e.g., infection with *Yersinia enterocolitica*). Experiments are under way to address these questions.

Nevertheless, we have shown here that loss of SKAP-HOM

attenuates B-cell functions and that it impairs the cross-talk between the BCR and integrins. These findings might be important in light of recent data showing that the α4 integrin (VLA-4) antagonistic monoclonal antibody Natalizumab reduces the development of brain lesions in murine EAE as well as in controlled clinical trials with patients suffering from multiple sclerosis (24). VLA-4 is expressed on activated T cells, B cells, and monocytes. Our data demonstrating loss of adhesion to the VLA-4 ligand fibronectin in SKAP-HOM-deficient B lymphocytes and attenuated EAE in SKAP-HOM-deficient mice might suggest that the beneficial effect of Natalizumab is partially due to an inhibition of B-cell invasion into the central nervous system. Although further histopathological studies are required to analyze the nature and the numbers of infiltrating immunocompetent cells in the central nervous system of wild-type and SKAP-HOM-deficient mice during EAE, our data indicate that interference with SKAP-HOM functions might be an attractive new avenue for pharmaceutical intervention in autoimmune diseases such as multiple sclerosis.

ACKNOWLEDGMENTS

The studies were supported by Deutsche Forschungsgemeinschaft DFG grants Schr 533/5-1 and Schr 533/5-2 and by NIH grants P01 DK50654 and R01 DK50693 to B.G.N. A.C.P. is funded by the Wellcome Trust.

REFERENCES

1. **Black, D. S., A. Marie-Cardine, B. Schraven, and J. B. Bliska.** 2000. The Yersinia tyrosine phosphatase YopH targets a novel adhesion-regulated signalling complex in macrophages. Cell Microbiol. **2:**401–414.
2. **Bourette, R. P., J. Therier, and G. Mouchiroud.** 2005. Macrophage colony-stimulating factor receptor induces tyrosine phosphorylation of SKAP55R adaptor and its association with actin. Cell Signal. **17:**941–949.
3. **Carrasco, Y. R., S. J. Fleire, T. Cameron, M. L. Dustin, and F. D. Batista.** 2004. LFA-1/ICAM-1 interaction lowers the threshold of B cell activation by facilitating B cell adhesion and synapse formation. Immunity **20:**589–599.
4. **Curtis, D. J., S. M. Jane, D. J. Hilton, L. Dougherty, D. M. Bodine, and C. G. Begley.** 2000. Adaptor protein SKAP55R is associated with myeloid differentiation and growth arrest. Exp. Hematol. **28:**1250–1259.
5. **Da Silva, A. J., Z. Li, C. de Vera, E. Canto, P. Findell, and C. E. Rudd.** 1997. Cloning of a novel T-cell protein FYB that binds FYN and SH2-domain-containing leukocyte protein 76 and modulates interleukin 2 production. Proc. Natl. Acad. Sci. USA **94:**7493–7498.
6. **Fallman, M., F. Deleuil, and K. McGee.** 2002. Resistance to phagocytosis by Yersinia. Int. J. Med. Microbiol. **291:**501–509.
7. **Fillatreau, S., C. H. Sweenie, M. J. McGeachy, D. Gray, and S. M. Anderton.** 2002. B cells regulate autoimmunity by provision of IL-10. Nat. Immunol. **3:**944–950.
8. **Genain, C. P., B. Cannella, S. L. Hauser, and C. S. Raine.** 1999. Identification of autoantibodies associated with myelin damage in multiple sclerosis. Nat. Med. **5:**170–175.
9. **Griffiths, E. K., C. Krawczyk, Y. Y. Kong, M. Raab, S. J. Hyduk, D. Bouchard, V. S. Chan, I. Kozieradzki, A. J. Oliveira-Dos-Santos, A. Wakeham, P. S. Ohashi, M. I. Cybulsky, C. E. Rudd, and J. M. Penninger.** 2001. Positive regulation of T cell activation and integrin adhesion by the adapter Fyb/Slap. Science **293:**2260–2263.
10. **Gu, H., R. J. Botelho, M. Yu, S. Grinstein, and B. G. Neel.** 2003. Critical role for scaffolding adapter Gab2 in Fc gamma R-mediated phagocytosis. J. Cell Biol. **161:**1151–1161.
11. **Hjelmstrom, P., A. E. Juedes, J. Fjell, and N. H. Ruddle.** 1998. B-cell-deficient mice develop experimental allergic encephalomyelitis with demyelination after myelin oligodendrocyte glycoprotein sensitization. J. Immunol. **161:**4480–4483.
12. **Hogg, N., M. Laschinger, K. Giles, and A. McDowall.** 2003. T-cell integrins: more than just sticking points. J. Cell Sci. **116:**4695–4705.
13. **Huang, Y., D. D. Norton, P. Precht, J. L. Martindale, J. K. Burkhardt, and R. L. Wange.** 2005. Deficiency of ADAP/FYB/SLAP130 destabilizes SKAP55 in Jurkat T cells. J. Biol. Chem. **280:**23576–23583.
14. **Iglesias, A., J. Bauer, T. Litzenburger, A. Schubart, and C. Linington.** 2001. T- and B-cell responses to myelin oligodendrocyte glycoprotein in experimental autoimmune encephalomyelitis and multiple sclerosis. Glia **36:**220–234.
15. **Jo, E. K., H. Wang, and C. E. Rudd.** 2005. An essential role for SKAP-55 in LFA-1 clustering on T cells that cannot be substituted by SKAP-55R. J. Exp. Med. **201:**1733–1739.
16. **Kouroku, Y., A. Soyama, E. Fujita, K. Urase, T. Tsukahara, and T. Momoi.** 1998. RA70 is a src kinase-associated protein expressed ubiquitously. Biochem. Biophys. Res. Commun. **252:**738–742.
17. **Liu, J., H. Kang, M. Raab, A. J. Da Silva, S. K. Kraeft, and C. E. Rudd.** 1998. FYB (FYN binding protein) serves as a binding partner for lymphoid protein and FYN kinase substrate SKAP55 and a SKAP55-related protein in T cells. Proc. Natl. Acad. Sci. USA **95:**8779–8784.
18. **Lyons, J. A., M. J. Ramsbottom, and A. H. Cross.** 2002. Critical role of antigen-specific antibody in experimental autoimmune encephalomyelitis induced by recombinant myelin oligodendrocyte glycoprotein. Eur. J. Immunol. **32:**1905–1913.
19. **Lyons, J. A., M. San, M. P. Happ, and A. H. Cross.** 1999. B cells are critical to induction of experimental allergic encephalomyelitis by protein but not by a short encephalitogenic peptide. Eur. J. Immunol. **29:**3432–3439.
20. **Marie-Cardine, A., E. Bruyns, C. Eckerskorn, H. Kirchgessner, S. C. Meuer, and B. Schraven.** 1997. Molecular cloning of SKAP55, a novel protein that associates with the protein tyrosine kinase p59fyn in human T-lymphocytes. J. Biol. Chem. **272:**16077–16080.
21. **Marie-Cardine, A., L. R. Hendricks-Taylor, N. J. Boerth, H. Zhao, B. Schraven, and G. A. Koretzky.** 1998. Molecular interaction between the Fyn-associated protein SKAP55 and the SLP-76-associated phosphoprotein SLAP-130. J. Biol. Chem. **273:**25789–25795.
22. **Marie-Cardine, A., H. Kirchgessner, C. Eckerskorn, S. C. Meuer, and B. Schraven.** 1995. Human T lymphocyte activation induces tyrosine phosphorylation of alpha-tubulin and its association with the SH2 domain of the p59fyn protein tyrosine kinase. Eur. J. Immunol. **25:**3290–3297.
23. **Marie-Cardine, A., A. M. Verhagen, C. Eckerskorn, and B. Schraven.** 1998. SKAP-HOM, a novel adaptor protein homologous to the FYN-associated protein SKAP55. FEBS Lett. **435:**55–60.
24. **Miller, D. H., O. A. Khan, W. A. Sheremata, L. D. Blumhardt, G. P. Rice, M. A. Libonati, A. J. Willmer-Hulme, C. M. Dalton, K. A. Miszkiel, and P. W. O'Connor.** 2003. A controlled trial of natalizumab for relapsing multiple sclerosis. N. Engl. J. Med. **348:**15–23.
25. **Musci, M. A., L. R. Hendricks-Taylor, D. G. Motto, M. Paskind, J. Kamens, C. W. Turck, and G. A. Koretzky.** 1997. Molecular cloning of SLAP-130, an SLP-76-associated substrate of the T cell antigen receptor-stimulated protein tyrosine kinases. J. Biol. Chem. **272:**11674–11677.
26. **Oliver, A. R., G. M. Lyon, and N. H. Ruddle.** 2003. Rat and human myelin oligodendrocyte glycoproteins induce experimental autoimmune encephalomyelitis by different mechanisms in C57BL/6 mice. J. Immunol. **171:**462–468.
27. **Peterson, E. J., M. L. Woods, S. A. Dmowski, G. Derimanov, M. S. Jordan, J. N. Wu, P. S. Myung, Q. H. Liu, J. T. Pribila, B. D. Freedman, Y. Shimizu, and G. A. Koretzky.** 2001. Coupling of the TCR to integrin activation by Slap-130/Fyb. Science **293:**2263–2265.
28. **Roach, T. I., S. E. Slater, L. S. White, X. Zhang, P. W. Majerus, E. J. Brown, and M. L. Thomas.** 1998. The protein tyrosine phosphatase SHP-1 regulates integrin-mediated adhesion of macrophages. Curr. Biol. **8:**1035–1038.
29. **Steinbrecher, A., D. Reinhold, L. Quigley, A. Gado, N. Tresser, L. Izikson, I. Born, J. Faust, K. Neubert, R. Martin, S. Ansorge, and S. Brocke.** 2001. Targeting dipeptidyl peptidase IV (CD26) suppresses autoimmune encephalomyelitis and up-regulates TGF-beta 1 secretion in vivo. J. Immunol. **166:**2041–2048.
30. **Timms, J. F., K. D. Swanson, A. Marie-Cardine, M. Raab, C. E. Rudd, B. Schraven, and B. G. Neel.** 1999. SHPS-1 is a scaffold for assembling distinct adhesion-regulated multi-protein complexes in macrophages. Curr. Biol. **9:**927–930.
31. **Wang, H., E. Y. Moon, A. Azouz, X. Wu, A. Smith, H. Schneider, N. Hogg, and C. E. Rudd.** 2003. SKAP-55 regulates integrin adhesion and formation of T cell-APC conjugates. Nat. Immunol. **4:**366–374.
32. **Wu, L., J. Fu, and S. H. Shen.** 2002. SKAP55 coupled with CD45 positively regulates T-cell receptor-mediated gene transcription. Mol. Cell. Biol. **22:**2673–2686.
33. **Wu, L., Z. Yu, and S. H. Shen.** 2002. SKAP55 recruits to lipid rafts and positively mediates the MAPK pathway upon T cell receptor activation. J. Biol. Chem. **277:**40420–40427.
34. **Zambrowicz, B. P., G. A. Friedrich, E. C. Buxton, S. L. Lilleberg, C. Person, and A. T. Sands.** 1998. Disruption and sequence identification of 2,000 genes in mouse embryonic stem cells. Nature **392:**608–611.

Appendix 7

A methodology for the structural and functional analysis of signaling and regulatory networks

Klamt S., Saez-Rodriguez J., Lindquist JA., **Simeoni L.**, and Gilles ED. (2006) *BMC Bioinformatics*. 7:56-82.

BMC Bioinformatics

Methodology article

Open Access

A methodology for the structural and functional analysis of signaling and regulatory networks

Steffen Klamt*†[1], Julio Saez-Rodriguez†[1], Jonathan A Lindquist[2], Luca Simeoni[2] and Ernst D Gilles[1]

Address: [1]Max-Planck Institute for Dynamics of Complex Technical Systems, Sandtorstrasse 1, D-39106 Magdeburg, Germany and [2]Institute for Immunology, University of Magdeburg, Leipziger Strasse 44, D-39120 Magdeburg, Germany

Email: Steffen Klamt* - klamt@mpi-magdeburg.mpg.de; Julio Saez-Rodriguez - saezr@mpi-magdeburg.mpg.de; Jonathan A Lindquist - Jon.Lindquist@Medizin.Uni-Magdeburg.de; Luca Simeoni - Luca.Simeoni@Medizin.Uni-Magdeburg.de; Ernst D Gilles - gilles@mpi-magdeburg.mpg.de

* Corresponding author †Equal contributors

Published: 07 February 2006

*BMC Bioinformatics*2006, **7**:56 doi:10.1186/1471-2105-7-56

Received: 28 July 2005
Accepted: 07 February 2006

This article is available from: http://www.biomedcentral.com/1471-2105/7/56

Abstract

Background: Structural analysis of cellular interaction networks contributes to a deeper understanding of network-wide interdependencies, causal relationships, and basic functional capabilities. While the structural analysis of metabolic networks is a well-established field, similar methodologies have been scarcely developed and applied to signaling and regulatory networks.

Results: We propose formalisms and methods, relying on adapted and partially newly introduced approaches, which facilitate a structural analysis of signaling and regulatory networks with focus on functional aspects. We use two different formalisms to represent and analyze interaction networks: interaction graphs and (logical) interaction hypergraphs. We show that, in interaction graphs, the determination of feedback cycles and of all the signaling paths between any pair of species is equivalent to the computation of elementary modes known from metabolic networks. Knowledge on the set of signaling paths and feedback loops facilitates the computation of intervention strategies and the classification of compounds into activators, inhibitors, ambivalent factors, and non-affecting factors with respect to a certain species. In some cases, qualitative effects induced by perturbations can be unambiguously predicted from the network scheme. Interaction graphs however, are not able to capture AND relationships which do frequently occur in interaction networks. The consequent logical concatenation of all the arcs pointing into a species leads to Boolean networks. For a Boolean representation of cellular interaction networks we propose a formalism based on logical (or signed) interaction hypergraphs, which facilitates in particular a logical steady state analysis (LSSA). LSSA enables studies on the logical processing of signals and the identification of optimal intervention points (targets) in cellular networks. LSSA also reveals network regions whose parametrization and initial states are crucial for the dynamic behavior.

We have implemented these methods in our software tool *CellNetAnalyzer* (successor of *FluxAnalyzer*) and illustrate their applicability using a logical model of T-Cell receptor signaling providing non-intuitive results regarding feedback loops, essential elements, and (logical) signal processing upon different stimuli.

Conclusion: The methods and formalisms we propose herein are another step towards the comprehensive functional analysis of cellular interaction networks. Their potential, shown on a realistic T-cell signaling model, makes them a promising tool.

Background

Evolution has equipped cells with exquisite signaling systems which allow them to sense their environment, receive and process signals in a hierarchically organized manner and to react accordingly [1]. The complexity of the corresponding molecular machineries, in accordance with the complicated tasks they have to perform, is overwhelming. In the last few years, as a key element to the growing popularity of systems biology, mathematical tools have been applied to the analysis of signaling data [2]. Ordinary differential equations relying on kinetic descriptions of the underlying molecular interactions are arguably the most used approach for modeling signaling networks (e.g. [3-6]). A number of theoretical methods have been devised and employed for the reconstruction (reverse engineering) of signaling or, more generally, interaction networks (which may represent signaling but also other types or abstractions of cellular networks such as genetic regulatory networks) based on perturbation experiments [7]. The approaches rely on methods ranging from Bayesian networks (e.g. [8]) to metabolic control analysis [9,10].

Relatively few methods have been proposed so far for analyzing the structure of a *given* signaling (or any interaction) network. This is somewhat surprising since structural analysis of metabolic networks is a well-established field and proved to be successful to recognize relationships between structure, function, and regulation of metabolic networks [11]. Structural analysis will be particularly useful in large signaling networks, where a simple visual inspection is not possible and at the same time the construction of precise quantitative models is practically infeasible due to the huge amount of required, but generally unknown, kinetic parameters and concentration values. However, the reconstruction of large signaling networks is still in its first stages [2,12].

Structural or qualitative approaches that have been employed for interaction networks include statistical large-scale analyses in protein-protein networks (e.g. [13]). These studies are important for examining statistical properties of the interaction graph and for understanding its global organization but they provide relatively few insights into the function of the network. Papin and coworkers [14,15] were the first to adapt methods from the constraint-based approach (frequently used for structural analysis of metabolic networks [11]) to analyze stoichiometric models of signaling pathways. Recently, graph-theoretical descriptions of signaling networks have been examined [16-18]. Finally, Boolean networks as discrete approximations of quantitative models have been used for logical analyses of small signaling networks e.g. [19]. However, the majority of studies relying on the Boolean approach deal with genetic interaction networks, many of which have a relatively small size (ca. 10 species; e.g. [20,21]), however, recently more complicated networks have also been investigated [22,23].

In this contribution, we propose formalisms for representing signaling and other interaction networks mathematically and present a collection of methods facilitating structural analysis of the respective network models. Rather than introducing completely new concepts, we will systematize and adapt existing formalisms and methods, often motivated from structural analyses of metabolic networks, towards a *functional* analysis of the structure of a signaling network. Issues that can be addressed with the proposed methods include:

• check of the plausibility and consistency of the network structure

• identification of all or particular signaling pathways, feedback loops and crosstalks

• network-wide functional interdependencies between network elements

• identification of the different modes of (logical) input/output behavior

• predicting responses (phenotypes) after changes in network structure

• finding targets and intervention points in the network for repressing or provoking a certain behavior or response

• analysis of structural network properties like redundancy and robustness

Structural analysis is not based on quantitative and dynamic properties and can thus only provide qualitative answers. However, some insights into the dynamic properties can nevertheless often be obtained, because fundamental properties of the dynamic behavior are often governed by the network structure [24]. While we will focus on signaling networks, the methods can be easily applied to any kind of interaction network, including gene regulatory systems. Apart from a toy model, we will exemplify our methods on a model of signaling pathways in T-cells.

Results and discussion

Mass and signal flows in cellular interaction networks

The reader familiar to the structural analysis of stoichiometric networks may notice that, in the case of metabolic networks, many of the issues in the task list of the previous section have been handled by the constraint-based approach [11]. For example, the identification of func-

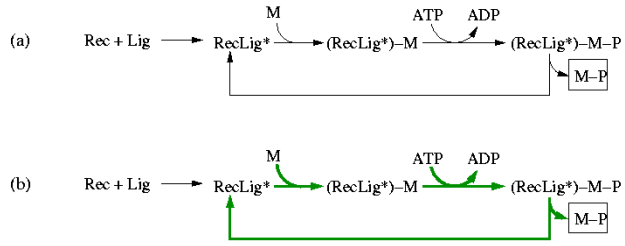

Figure 1
(a) Example of a typical signaling pathway where mass and signal flow occur simultaneosly (Rec = receptor; Lig = ligand; RecLig* = (active) receptor-ligand-complex; M = molecule; M-P = phosphorylated molecule M). (b) The (only) elementary mode in this example which follows when M, M-P, ADP, ATP, Rec and Lig are considered as external (boundary) species. The involved reactions are indicated by green, thick arrows. In its net stoichiometry, this elementary mode converts M and ATP into M-P and ADP, whereas RecLig* is recycled in the overall process. Importantly, the mandatory process of building the receptor-ligand-complex RecLig* (hence, the causal dependeny of M-P from the availability of Rec and Lig) is not reflected by this mode.

tional pathways and studying the input (substrates)/output (products) behavior of stoichiometric reaction networks is facilitated by elementary-modes analysis [25,26]. Flux Balance Analysis is another related technique often used for phenotype predictions of metabolic mutants [11,27]. Recently, the concept of minimal cut sets has been introduced for identifying targets in metabolic networks [28,29]. Therefore, it seems reasonable to apply these methods to signaling networks. However, some fundamental differences in the way the network elements interact may complicate a direct transfer:

(1) The constraint-based framework assumes steady-state, while in signaling networks a transient behavior can often be observed. (However, as will be discussed below, many useful insights of signaling networks can be obtained from using a static approach.)

(2) In stoichiometric networks, any arrow (reaction) leading from educts to products can be seen as an "activating" (producing) connection for the products. Therefore, employing stoichiometric framework it is difficult or only indirectly possible to express an inhibitory action of a species onto another.

(3) Probably the most significant difference is that the edges (i.e. the connections between the species) in metabolic networks carry flows of *mass* whereas edges in signaling networks may carry mass *and/or* information (signal) flow. Of course, at the molecular level, any interaction between species in the cell can be written as a stoichiometric equation. However, whereas mass flow is connected to a real consumption of participating compounds, signal flow is usually characterized by a recycling of certain species (e.g. enzymes) so that these species can mediate the signal transfer continuously (until they are degraded).

A typical example, namely the activation of a receptor tyrosine kinase (Figure 1(a)) [30], illustrates the simultaneous occurrence of mass and signal flow. A ligand (Lig) binds to the extracellular domain of a receptor (Rec) yielding a receptor-ligand complex which can undergo further changes (e.g. by autophosphorylation or/and dimerization). We denote the outcome by RecLig*. This complex is now able to phosphorylate another molecule (M). Accordingly, M binds to RecLig* and becomes phosphorylated (M-P) by the expense of ATP. At the end, M-P is released, recycling also the activated receptor-ligand complex RecLig*.

The first step in this scheme can be considered as a mass flow. However, the cycle in which RecLig* phosphorylates M, is a mass flow with respect to M and ATP, but a signaling flow with respect to RecLig*, as the latter is indeed required for driving this cycle but not consumed (because recycled) in the overall stoichiometry.

In performing a structural analysis we are interested in extracting signaling paths from the network scheme. Therefore, it may seem reasonable to compute elementary modes, which typically represent pathways in reaction networks with mass flow [25]. A basic property of elementary modes is that the (relative) mass flow represented by an elementary mode keeps the "internal" species in a balanced state. Internal species (here: RecLig*, RecLig*-M, RecLig*-M-P) are within the system's boundary, whereas the external species (here: Rec, Lig, M, M-P, ADP, ATP) are considered as pools which are balanced by processes lying outside the system's boundaries. Computing the elementary modes from the respective stoichiometric model of Figure 1(a) gives exactly one mode which reflects the discussed role of RecLig* as a kinase (Figure 1(b)): in its net stoichiometry, this elementary mode converts the external species M and ATP into M-P and ADP, whereas RecLig* is recycled. Since RecLig* is neither consumed nor produced in the overall process, the first step (building the receptor-ligand complex) is not involved in this mode simply because a continuous synthesis of RecLig* would lead to an accumulation of this species, which is inconsistent with the steady-state assumption of elementary modes. Thus, the causal dependency of M-P from the availability of Rec and Lig is not reflected by the mass flow concept of elementary modes. Note that exactly the same conceptual problem would arise when enzymes and enzyme synthe-

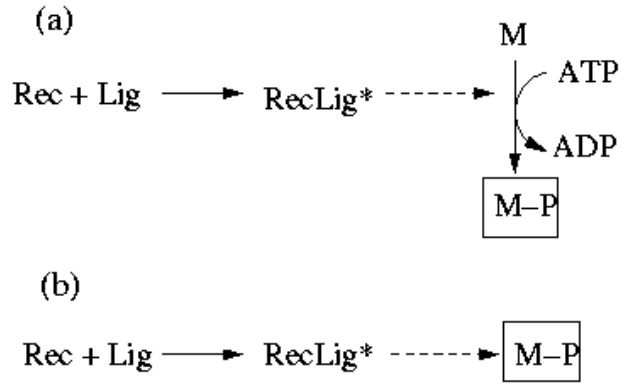

Figure 2
Interpretation of Figure 1 as an interaction network.

sis would be considered explicitly in stoichiometric studies of metabolic networks.

The example demonstrates that we require a framework with the ability to account for mass *and* signal flows. Handling both mass and signal flows formally equivalent as *interactions* could be a suitable approach. Interpreting Figure 1(a)) as a diagram of interactions we could redraw it as depicted in Figure 2(a). The dashed arrow indicates that RecLig* catalyzes the phosphorylation of M to M-P. If we assume that ADP, ATP, and M are always present, we get the simple chain shown in Figure 2(b) expressing that Rec and Lig are required to obtain RecLig* (or to activate RecLig*), and that RecLig* is required to get M-P. If we do not further distinguish between the two types of arrows and thus consider mass and signal flows as formally equivalent, the causal connections between the species would, nevertheless, still be captured correctly. This abstract representation of different types of interactions will thus be used herein.

The following two sections will deal first with interaction *graphs* and later with the more general (logical) interaction *hypergraphs*. The basic difference between these two related approaches can be illustrated by how they deal with a connection such as "Rec + Lig" in Figure 2(b). If we interpret it as "Rec activates RecLig* and Lig activates RecLig*" then the concept of *interaction graphs* is applicable (discussed in the following section). However, it would be more accurate to say that "Rec AND Lig are required *simultaneously* for building RecLig*", and it is this more refined approach that leads to the concept of *interaction hypergraphs*, which will be discussed in further details later on.

Analyzing interaction graphs

Definition of interaction graphs

Interaction (or causal influence) graphs are frequently used to show direct dependencies between species in signaling, genetic, or protein-protein interaction networks. The nodes in these graphs may represent, depending on the network type and the level of abstraction, receptors, ligands, effectors, kinases, genes, transcription factors, metabolites, proteins, and other compounds, while each edge describes a relation between *two* of these species. In signaling and gene regulatory networks, two further characteristics are usually specified for each edge: a *direction* (which species influences which) and a *sign* ("+" or "- ", depending on whether the influence is activating (level increasing) or inhibiting (level decreasing)). Formally, we represent a directed interaction or causal influence graph as a signed directed graph $G = (V, A)$, where V is the set of vertices or nodes (species) and A the set of labeled directed edges [31,32]. Directed edges are usually called arcs and an arc from vertex i (*tail*) to j (*head*) is denoted by an ordered tuple $\{i,j,s\}$ with $i, j \in V$ and $s \in \{+,-\}$.

Sometimes, for example in protein-protein interaction networks, the directions of the edges remain unspecified. We will not consider such undirected interaction graphs explicitly, however, many of the issues discussed in the following can be transferred to undirected graphs (e.g. by representing an undirected edge by two (forward and backward) arcs).

The structure of a signed graph can be stored conveniently by an m x q incidence matrix **B** in which the columns correspond to the q arcs (interactions) and the rows to the m nodes (species), similar as in stoichiometric matrices of metabolic reaction networks [33]. For the k-th arc $\{i, j, s\}$ a (-1) is stored in the k-th column of **B** for the tail vertex (i) and (+1) for the head vertex (j) of arc k. Hence, $\mathbf{B}_{i,k} = -1$ and $\mathbf{B}_{j,k} = 1$ and $\mathbf{B}_{l,k} = 0$ ($l \neq i, j$). For storing the signs, a q-vector **s** is introduced whose k-th element is (+1) if arc k is positive and (-1) if k is negative.

Self-loops (arcs connecting a species with itself) are not considered here but could be stored in a separate list since they would appear as a zero column in the incidence matrix.

Note that, as far as the memory requirement is concerned, the structure of a graph can be stored more efficiently than by an incidence matrix, e.g. by using adjacency lists [34]. However, since we will present methods directly operating on the incidence matrix, we refer herein to this representation.

Signal transduction networks are usually characterized by an input, intermediate, and output layer (cf. [16]). The

input domain consists only of species having no predecessor, which can thus not be activated from other species in the graph. Such *sources* (typical representatives are receptors and ligands) are starting points of signal transduction pathways and can easily be identified from the incidence matrix since their corresponding row contains no positive entry. In contrast, the output layer consists only of nodes having no successor. These *sinks*, usually corresponding to transcription factors or genes, are identifiable as rows in **B** which have no negative entry. The set of source and sink nodes define the boundaries of the network under investigation. They play here a similar role as the external metabolites in stoichiometric studies [33]. The intermediate layer functions as the actual signal transduction and processing unit. It consists of the intermediate species, all of which have at least one predecessor and at least one successor, i.e. they are influenced and they influence other elements. Such species contain both -1 and +1 entries in the incidence matrix. In reconstructed signaling networks, the detection of all sink and source species may help to detect gaps in the network, e.g. when a species should be an intermediate but is classified as a sink or source.

The presence of sinks and sources are a consequence of setting borders to the system of interest. Sometimes there are no sinks or/and no sources, especially in models of gene regulatory networks (see e.g. the networks studied in [21]), but this does not impose limitations to the approaches presented here.

A toy example of a (directed) interaction graph that will serve for illustrations throughout this paper is given in Figure 3. This interaction graph, called TOYNET, consists of two sources (I1, I2), two sinks (O1, O2), 7 intermediate species (A,..., G), two inhibiting (arcs 2 and 7) and 11 activating interactions. Incidence matrix **B** of TOYNET reads (the sign vector **s** is given on the top of **B**):

$$\mathbf{B} = \begin{array}{c} \begin{matrix} + & - & + & + & + & + & - & + & + & + & + & + & + \end{matrix} \\ \begin{pmatrix} -1 & -1 & 0 & 0 & 0 & 0 & 0 & 0 & 0 & 0 & 0 & 0 & 0 \\ 0 & 0 & -1 & 0 & 0 & 0 & 0 & 0 & 0 & 0 & 0 & 0 & 0 \\ 0 & 0 & 0 & -1 & 0 & 0 & 1 & 0 & 0 & 0 & 0 & 0 & 0 \\ 1 & 0 & 0 & 1 & -1 & 0 & 0 & 0 & 0 & 0 & 0 & 0 & 0 \\ 0 & 0 & 0 & 0 & 1 & -1 & 0 & 1 & 0 & 0 & 0 & -1 & 0 \\ 0 & 0 & 0 & 0 & 0 & 1 & -1 & 0 & 0 & 0 & 0 & 0 & 0 \\ 0 & 1 & 1 & 0 & 0 & 0 & 0 & -1 & -1 & 0 & 0 & 0 & \mathbf{0} \\ 0 & 0 & 0 & 0 & 0 & 0 & 0 & 0 & 1 & -1 & 1 & 0 & 0 \\ 0 & 0 & 0 & 0 & 0 & 0 & 0 & 0 & 0 & 1 & -1 & 0 & -1 \\ 0 & 0 & 0 & 0 & 0 & 0 & 0 & 0 & 0 & 0 & 0 & 1 & 0 \\ 0 & 0 & 0 & 0 & 0 & 0 & 0 & 0 & 0 & 0 & 0 & 0 & 1 \end{pmatrix} \end{array} \begin{matrix} \text{I1} \\ \text{I2} \\ \text{A} \\ \text{B} \\ \text{C} \\ \text{D} \\ \text{E} \\ \text{F} \\ \text{G} \\ \text{O1} \\ \text{O2} \end{matrix} \quad (1)$$

Identification of feedback loops

Even though some analysis methods (e.g. Bayesian networks) rely on acyclic networks where feedbacks are not allowed, one of the most important features of signaling and regulatory networks are their feedback loops [3,5,18,21,35-38]. Positive feedbacks are responsible and even required [39] for multiple steady state behavior in dynamical systems. In biological systems, multistationarity plays a central role in differentiation processes and for epigenetic and switch-like behavior. In contrast, negative feedback loops are essential for homeostatic mechanisms (i.e. for adjusting and maintaining levels of system variables) or for generating oscillatory behavior [35].

Most reports demonstrating the role and consequences of feedback loops analyze relatively small networks where the cycles can be easily recognized from the network scheme but rather few works address the question of how feedback cycles can be identified systematically. This is particularly important in large interaction graphs, where a detection by simple visual inspection is impossible, especially when feedback loops overlap.

A feedback loop is, in graph theory, a *directed cycle* or *circuit*. A circuit is defined as a sequence $C = \{\mathbf{a}_1,...,\mathbf{a}_w\}$ of arcs that starts and ends at the same vertex k and visits (with the exception of k) no vertex twice, i.e. $C = \{\mathbf{a}_1,...,\mathbf{a}_w\} = \{\{k, l_1\}, \{l_1,l_2\},..., \{l_{w-1},k\}\}$ such that all nodes k, l_1, l_2 ... l_{w-1} are distinct. The parity of the number of negative signs of the arcs in C determines whether the feedback loop is negative (odd number of negative signs) or positive (even). In the example TOYNET two feedback loops can be found: (i) the arc sequence {4,5,6,7} which is negative (since one negative arc (7) is involved), and (ii) the sequence {10,11}, which is positive (because the signs of both arcs in this circuit are positive). Obviously, sinks and sources (and all arcs connected to these nodes) can never be involved in any circuit.

Computing all directed cycles in large graphs is computationally a difficult task. Algorithms that can be found in the literature usually rely on backtracking strategies (e.g. [16,40]). Here, we introduce a different approach where the circuits are identified as elementary modes establishing a direct link to metabolic network analysis. Circuits can be formally represented by a q-vector **c** in which $c_i = 1$ if arc i is involved in the circuit and $c_i = 0$ otherwise. A circuit vector fulfills the equation

$$\mathbf{B}\,\mathbf{c} = \mathbf{0} \quad (2)$$

and hence, lies in the null space of the incidence matrix of the graph [32,41]. Generally, any vector **c** obeying (2) fulfills a so-called conservation law and is called a *circulation* which may be envisioned as a flow cycling around in the network [42]. Eq. (2) is strongly related to the mass balance equation of metabolic networks in steady state. In fact, considering the graph as a reaction network with the

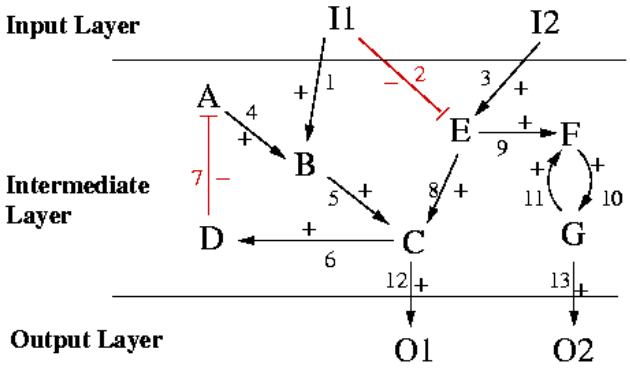

Figure 3
Example of a directed interaction graph (TOYNET). Arcs 2 and 7 indicate inhibiting interactions, while all others are activating.

arcs being irreversible mono-molecular reactions, the incidence matrix would be equivalent to the stoichiometric matrix and any circulation would be equivalent to a stationary flux distribution. Note that not all circulations are circuits: the linear combinations of circuit vectors do also yield circulations but are not (elementary) circuits. Precisely, circuits are special circulations having two additional properties. First, they must be admissible with respect to the directions of the involved arcs, i.e. only non-negative values are allowed for **c**:

$c_i \geq 0$ for all i. (3)

Second, circuits are *non-decomposable* circulations, i.e. the set of arcs building up the circuit **c**, expressed by $P(\mathbf{c}) = \{i: c_i > 0\}$, is irreducible:

There is no non-zero vector **d** fulfilling eqs. (2) and (3) and $P(\mathbf{d}) \subset P(\mathbf{c})$ (4)

Eqs. (2) and (3) and condition (4) close the complete analogy to elementary modes. In fact, cycles or circuits are the elementary modes in the special case of graphs (elementary modes are defined for *any* matrix in eq. (2), not only for the very special shape of incidence matrices related to graphs). Any feasible stationary flux vector in a metabolic network can be obtained by non-negative linear combinations of elementary modes. Equivalently, any circulation vector can be decomposed into a non-negative linear combination of circuit vectors. Note that, multiplying a (circuit) vector **c**, that fulfills (2)-(4), by a scalar $b>0$ yields another vector $\mathbf{v} = b\mathbf{c}$ which represents the same circuit because the same arcs compose it (are unequal to zero). Moreover, all non-zero components in a circuit vector are equal to each other. Therefore we can always normalize the vector in such a way that we obtain the binary representative of this circuit where all components are either "1" or "0".

In metabolic networks, elementary modes reveal not only internal cycles but also, even with higher relevance, metabolic pathways connecting input and output species. Continuing with the analogy to interaction graphs, in the next subsection we will see that elementary modes can be used to identify not only feedback loops but also signaling paths.

Signaling (influence) paths between two species

When the interaction graph is very large it becomes difficult to see whether a species S1 can influence (activate or inhibit) another species S2 and via which distinct pathways this can happen. Computing the complete set of directed paths between a given pair (S1, S2) of species is therefore often desirable. A path $P = \{\mathbf{a}_1,...,\mathbf{a}_w\}$ is, similarly to a feedback circuit, a sequence of arcs where none of the nodes is visited more than once, but in the case of a signaling path the start node S1 is distinct from the end node S2, i.e. $P = \{\mathbf{a}_1,...,\mathbf{a}_w\} = \{\{S1,l_1\}, \{l_1,l_2\}, ..., \{l_{w-1},S2\}\}$ such that all nodes $S1$, $S2$, l_1, l_2 ... l_{w-1} are distinct.

To obtain the signaling pathways from S1 to S2 we proceed as follows (Figure 4(a)): we add an "input arc" for S1 (i.e. a new column in the incidence matrix **B** containing only zeros except a (+1) for S1) and an "output arc" for S2 (another new column in **B** containing only zeros except a (-1) for S2. Then, computation of the elementary modes in this network will provide the original feedback loops without participation of the input and the output arc (as shown above) and additionally all paths starting with the input arc at S1 and ending with the output arc at S2, with the latter revealing all possible routes between S1 and S2.

Admittedly, the introduced input and output arcs have no tail or no head, respectively, and would therefore not be edges in the graph-theoretical sense, but this has no consequence for the analysis described within this contribution. In fact, this procedure is equivalent to adding in the incidence matrix a "dummy" node representing the environment (ENV), an "input arc" from ENV to S1 and an "output arc" from S2 to ENV (Figure 4(b)). Computing the elementary modes from the resulting incidence matrix would produce the feedback circuits as well as the circuits running over ENV. The latter represent the paths leading from S1 to S2. In the procedure described above ENV is simply removed from the incidence matrix leading to the same results.

In order to obtain only the paths from S1 to S2 (without the feedback loops), one can enforce the input and output arc to be involved by using an extension of the algorithm for computing elementary modes [43].

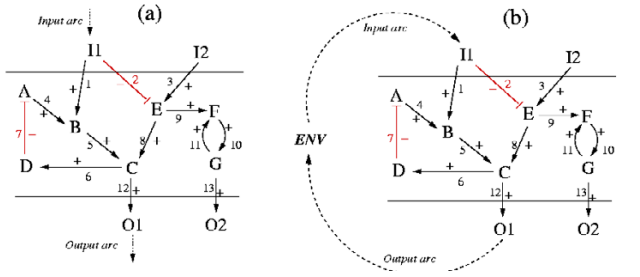

Figure 4
Computation of all signaling paths between two species (here: between I1 and O1). (a) via the incorporation of a "simplified" input and output arc; (b) with explicit introduction of an ENV („environment") node. Computing the elementary modes from the respective incidence matrix for (a) and (b) yields basically the same result, namely all paths between I1 and O1, as well as the two feedback circuits in the intermediate layer.

Furthermore, we may also add several input and output edges simultaneously. For example, if we are interested in all the paths connecting the input layer with the output layer, i.e. all routes leading from a source to a sink node, we add to each source an input edge and to each sink an output edge and compute the elementary modes (and, optionally, discard the feedback circuits where neither a source nor a sink participates). In this way we obtain the same set of signaling paths as if the elementary modes would be computed separately for each possible pair of source and sink nodes. Figure 5 shows the complete set of signaling paths connecting the input with the output layer of TOYNET.

Analogously to the feedback loops, we assign to each signaling path an "overall sign" indicating whether A activates (+) or inhibts (-) B along this path. Again, the parity of the signs of the arcs in the path determine whether the influence is positive (even number of negative signs) or negative (odd number of signs).

To sum up, feedback loops and influence paths in interaction graphs can be identified as elementary modes (or, equivalently, as extreme rays of convex cones [44]) from the respective incidence matrix. Similar conclusions have recently been drawn by Xiong et al. [45], albeit the authors computed paths only between sink and source nodes and only within unsigned graphs (i.e. they did not consider inhibitory effects). Feedback circuits were also not considered. Hence, here we extend and generalize those results.

The equivalence of signaling paths and loops to elementary modes allows one the advantage to use the highly optimized algorithms for computing elementary modes [43,44,46].

Combinatorial studies on signaling paths

The computation of all paths between a pair of species helps us to recognize all the different ways in which a signal can propagate between two nodes. In metabolic pathway analysis, a statistical or combinatorial analysis of the participation and co-occurrences of reactions in elementary modes proved to be useful for obtaining system-wide properties, such as the detection of essential reactions/enzymes or correlated reaction sets (enzyme subsets) [11,26,47].

In principle, similar features are of interest also for signaling paths and feedback loops. However, two important issues arise in interaction graphs that require a special treatment. First, we have two different types of pathways, positives and negatives. Owing to their opposite meanings we often need to analyze them separately in statistical assessments. Second, in metabolic networks we are particularly interested in the reactions (edges), because they correspond to enzymes that are subject to regulatory processes and can be knocked-out in experiments. In contrast, in interaction graphs we are usually more interested in the nodes, since they are often knocked-out in experiments or medical treatments, either via mutations, siRNA or by specific inhibitors. An edge in signaling networks represents mostly a direct interaction between a pair of species and has therefore no mediator. In some cases, an edge can directly be targeted by e.g. a mutation at the corresponding binding site of one of the two nodes species involved. Here, we will focus on species participation, albeit similar computations can be made for the edges.

As mentioned several times, in signaling networks we are often interested in all the different ways by which a certain transcription factor (or any other species from the output layer) can be activated or inhibited by signals arriving the input layer. For this purpose, we compute all signaling paths leading from source nodes located in the input layer down to a certain sink species s of interest. We denote the set of all these paths by I_s, which can be dissected in the two disjoint subsets of activating and inhibiting paths: $I = I_s^+ \cdots I_s^-$. Each source species i can then be classified into one of the following four influence classes with respect to s:

(1) activator of s (i is involved in at least one path of I_s^+ and in no path of I_s^-)

(2) inhibitor of s (i is involved in at least one path of I_s^- and in no path of I_s^+)

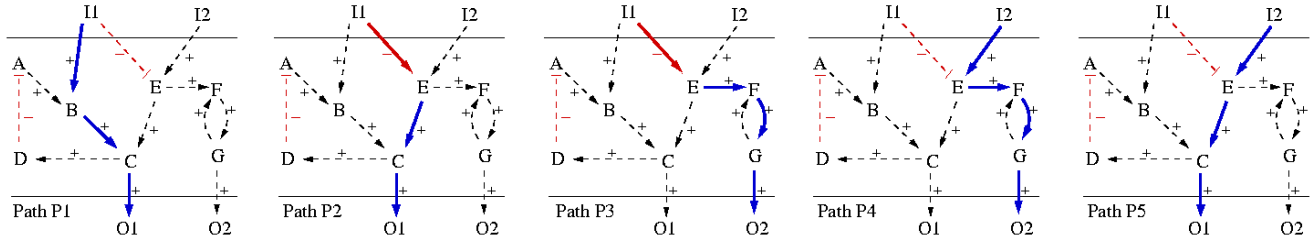

Figure 5
All signaling paths linking the input layer (source species) with the output layer (sink species) in TOYNET.

(3) ambivalent factor for s (i is involved in at least one (inhibiting) path of I_s^- and in at least one (activating) path of I_s^+)

(4) without any influence on s (i is not involved in any path of I_s)

In TOYNET, we see from Figure 5 that I2 is a pure activator and I1 an ambivalent factor for O1. With respect to O2, I1 is an inhibitor and I2 again an activator. The qualitative response of s after perturbing the level of a non-affecting species, or of an inhibitor or activator can be predicted unambiguously (namely unchanged or decreasing or increasing, respectively) as long as the network has no negative feedback loop. Negative feedback loops limit such qualitative predictions for activators (or inhibitors): if there is any path from an activator (inhibitor) to s that touches a negative feedback loop (i.e. at least one species on the path is involved in a negative feedback) then the resulting effect in perturbation experiments can not be predicted uniquely (cf. [36]). This case occurs in TOYNET for I2 with respect to O1: I2 is an activator of O1 but the only connecting path (P5 in Figure 5) goes through species C which participates in the negative feedback circuit. Thus, although at least a transient increase in O1 can be expected after up-regulating I2, we cannot exclude that the negative feedback drives the level of O1 below its initial level at a certain time point after increasing the level of I2. We therefore call an activator (inhibitor) p of s a *total activator* (*total inhibitor*) of s if there is no path from p to a species in a negative feedback circuit that is in turn connected to s.

Positive feedbacks do not limit these qualitative up/down-predictions because they cannot change the monotone effect of the respective input signal, e.g. when increasing the level of I2 in TOYNET we can expect an increase in the level of O2 after some time.

To summarize, regarding the influence of a species p on another species s we have 6 possible cases: total and non-total activator, total and non-total inhibitor, ambivalent factor and non-influencing species. Note that, by computing the connecting signaling paths, this classification procedure can be applied not only between a source and a sink node but also between any pair of species, e.g. between a source and an intermediate, an intermediate and a sink, and two intermediates. In TOYNET, for example, F is a total activator of O2 and has no influence on O1, whereas D is an inhibitor but not a total one of O1 because it is connected to (even involved in) a negative feedback circuit.

Additionally, as the complement of incoming paths, we can also determine the paths starting in a certain species s showing us which nodes and arcs are reachable from (and influenceable by) s. As a further generalization, sets of incoming and/or outgoing paths can also be defined not only for a single species s but also for a set S of species. This might be useful, for example, when we are interested in all paths ending (starting) in a certain subset of the sink (source) nodes.

Investigations of influence and signaling paths as proposed above provide, apart from pair-pair relationships (e.g. "a is a (total) activator of b" or "a has no influence on b"), global properties (e.g. a is a (total) activator of all sink species). Some other useful structural features and constraints can be detected by a statistical or combinatorial analysis of certain path sets (partially, similar ideas have been proposed by [14] for stoichiometric models of signaling networks):

• Essential species (arcs): When focussing on a specific signaling event, e.g. the activation of a certain species by signals from the input layer, we may identify essential species (or arcs) with respect to this event. For example, species E and arc 9 are essential for activating O2 but non-essential for the activating paths leading to O1 in TOYNET.

• Species (arc) participation: A more quantitative measure can be obtained by giving percentages of all those activating and/or inhibiting pathways, in which the species or

Table 1: Shortest length of positive/negative paths in TOYNET (∞= no path exists). Values in the diagonal indicate whether the respective element is involved in a positive/negative feedback loop. See also the dependency matrix in Figure 6.

	I1	I2	A	B	C	D	E	F	G	O1	O2
I1	∞/∞	∞/∞	4/4	1/∞	2/2	3/3	∞/1	∞/2	∞/3	3/3	∞/4
I2	∞/∞	∞/∞	∞/4	∞/5	2/∞	3/∞	1/∞	2/∞	3/∞	3/∞	4/∞
A	∞/∞	∞/∞	∞/4	1/∞	2/∞	3/∞	∞/∞	∞/∞	∞/∞	3/∞	∞/∞
B	∞/∞	∞/∞	∞/3	∞/4	1/∞	2/∞	∞/∞	∞/∞	∞/∞	2/∞	∞/∞
C	∞/∞	∞/∞	∞/2	∞/3	∞/4	1/∞	∞/∞	∞/∞	∞/∞	1/∞	∞/∞
D	∞/∞	∞/∞	∞/1	∞/2	∞/3	∞/4	∞/∞	∞/∞	∞/∞	∞/4	∞/∞
E	∞/∞	∞/∞	∞/3	∞/4	1/∞	2/∞	∞/∞	1/∞	2/∞	2/∞	3/∞
F	∞/∞	∞/∞	∞/∞	∞/∞	∞/∞	∞/∞	∞/∞	2/∞	1/∞	∞/∞	2/∞
G	∞/∞	∞/∞	∞/∞	∞/∞	∞/∞	∞/∞	∞/∞	1/∞	2/∞	∞/∞	1/∞
O1	∞/∞	∞/∞	∞/∞	∞/∞	∞/∞	∞/∞	∞/∞	∞/∞	∞/∞	∞/∞	∞/∞
O2	∞/∞	∞/∞	∞/∞	∞/∞	∞/∞	∞/∞	∞/∞	∞/∞	∞/∞	∞/∞	∞/∞

arc is involved. One may only relate the relative participation to the paths where the respective species or arc is involved or to the complete set of paths. For example, I2 is involved in 50% of all positive paths coming from the input layer and activating O1, while I2 is involved in 100% of all paths activating O2 (but only 50% of the paths coming from I2 lead to O2). Arc 9 is involved in one activating and one inhibiting path leading to O2. Thus, only 50% of the paths running over this arc are activating, however, it is involved in all (100%) activating paths connecting sources with O2. Similar considerations can be done regarding feedback loops: in TOYNET, species D and A as well as arcs 6, 7 and 11 are not involved in paths connecting input with output layers and have thus a special importance in establishing the negative (D, A, arcs 6 and 7) and positive (arc 11) feedback. (Note that a similar measure for the importance of a species or arc is betweenness centrality [48]. This importance measure is well-known in graph theory and checks how many *shortest* paths between pairs of nodes are running over the respective node or arc.)

• Redundancy: The total number of paths activating (inhibiting) a species is a measure for the redundancy in the system.

• Path length: The length distribution of signaling paths provides a rough idea on the compactness of the network [18].

• Crosstalk: Using our framework, crosstalk might be defined as a place (node) where paths from different source nodes cross each other for the first time. For example, E is a crosstalk species in TOYNET (signals of I1 and I2 cross) whereas F and G are not. In some cases, however, crosstalk is a more complex phenomenon where different nodes are involved. For example, at species C a path coming from I1 via B and another path from I2 via E meet each other. However, I1 and I2 have also met earlier in E and, additionally, the action of I1 on C via B is already influenced by I2 in species B since I2 can act on B via the path visiting E, C, D and A.

Distance matrix and dependency matrix

Some applications presented in this section require exhaustive enumerations of signaling paths becoming computationally challenging in large networks. However, in some cases we only want to know whether *any* activating and/or *any* inhibiting path between two nodes exists or whether there is any positive or any negative feedback circuit in which a certain species is involved. For such "existence questions" we can often apply standard methods from graph theory. A very useful object is the distance matrix **D** which can be obtained with low computational demand by computing the shortest distances (shortest path lengths) between each pair of species (e.g. Dijkstra's algorithm [32]). **D** has dimension $m \times m$ and the element $\mathbf{D}_{ij}$ stores the length of the shortest path for traveling from node i to node j, being $\mathbf{D}_{ij} = \infty$ if no paths exists between i and j. The distance matrix shows immediately

• which elements can be influenced by species i (the i-th row of **D**)

• which nodes can influence species i (i-th column of **D**)

• whether feedback circuits exist: if the distance $\mathbf{D}_{ii}$ from a node i back to itself is finite, then i is involved in at least one feedback loop. Furthermore, if $\mathbf{D}_{ij}$ and the transposed element $\mathbf{D}_{ji}$ are finite, $\mathbf{D}_{ij}$, $\mathbf{D}_{ji} \neq \infty$, then a feedback between species i and j exists.

By an extension of the usual shortest path algorithm (not shown), we may also compute separately a matrix $\mathbf{D}^{pos}$ for the shortest *positive* paths and another $\mathbf{D}^{neg}$ for the shortest *negative* paths. Table 1 shows the distance matrices $\mathbf{D}^{pos}$ and $\mathbf{D}^{neg}$ from TOYNET.

Note that by taking the minimum values from $\mathbf{D}^{pos}$ and $\mathbf{D}^{neg}$, **D** can be obtained. Moreover, the two matrices $\mathbf{D}^{pos}$ and $\mathbf{D}^{neg}$, whose computation is reasonably possible in very large networks, are sufficient to classify all species into (total/non-total) activators, (total/non-total) inhibitors, ambivalent factors, and non-influencing nodes with respect to a certain compound *y*. The reason is that this classification requires only knowledge on the *existence* of positive and negative paths between species pairs and on the *existence* of negative feedback loops. For example, a species *x* is a total activator of *y* if (i) at least one positive path from *x* to *y* exits ($\mathbf{D}^{pos}_{x,y} \neq \infty$) and if (ii) no negative path from *x* to *y* exists ($\mathbf{D}^{neg}_{x,y} = \infty$) and if (iii) for any species *z* that is influenced by *x* ($\mathbf{D}_{x,z} \neq \infty$) and connected to *y* ($\mathbf{D}_{z,y} \neq \infty$) it holds, that *z* is not involved in a negative feedback ($\mathbf{D}^{neg}_{z,z} = \infty$).

For representing species dependencies in a compact manner, we introduce the *dependency matrix* **M**, which shows all the pair-wise dependencies, e.g. by using 6 different colors (for the 6 possible cases). Thereby, the color of matrix element $\mathbf{M}_{xy}$ indicates whether species *x* is a total/non-total activator or a total/non-total inhibitor or an ambivalent factor or a non-influencing node for species *y*. Again, $x = y$ is allowed, indicating feedbacks. Figure 6 shows the dependency matrix for TOYNET.

Although the distance and dependency matrices store a wealth of structural information in a very condensed manner, some applications still require a full enumeration of all available signaling paths. One case is the systematic determination of minimal cut sets.

Minimal cut and intervention sets in interaction graphs

Searching for intervention strategies in signaling networks is of high relevance in experimental and, in particular, medical applications. Recently, the concept of *minimal cut sets* has been introduced, which facilitates the identification of efficient intervention strategies (cuts) and, at the same time, the recognition of potential failure modes in a given biochemical reaction network [28,29]. Basically, in the most general version, a minimal cut set (MCS) is defined as a minimal (irreducible, non-decomposable) set of cuts (or failures) of edges or/and nodes that represses a certain functionality or behavior in the system [29]. For example, assume we want to prevent the activation of the sink node O1 in TOYNET. By removing nodes {B, E} one can be sure that an activation of O1 by an external stimulus becomes infeasible. The set {B, E} would thus be a cut set for preventing the activation of O1. Moreover, it is minimal since neither the removal of only B nor the removal of only E can guarantee that the "inhibition task" is achieved. Another minimal cut set would be {C}. C is thus essential for activating O1, as would be confirmed by participation analysis of all paths activating O1. A general algorithmic scheme for a systematic enumeration of MCSs in stoichiometric networks was given in [29]:

(i) Define a *deletion task*

(ii) Compute all minimal functional units (elementary modes) and specify the set of *target modes* that have to be attacked in order to achieve the deletion task

(iii) Compute the so-called *minimal hitting sets* of the target modes

We could proceed here in a similar way. First, a deletion task specifying the goal of our intervention is defined. In our example, the deletion task is "Prevent the activation of O1 by any external input". Hence, the signaling paths from the input layer to O1 are computed, which are P1, P2, and P5 (see Figure 5). However, according to our deletion task, the target set comprises only the paths P1 and P5, because only these two activate O1. Finally, the minimal hitting sets of the target paths have to be computed, which are the MCSs [26,29]. When cutting species, a hitting set ***T*** is a set of species that "hits" all target paths in a minimal way, i.e. for each target path there is at least one species that is contained in ***T*** and in the path. To be a *minimal* hitting set, no proper subset of ***T*** fulfills the hitting set condition. The minimal hitting sets of the target paths and hence the MCSs of our deletion task would be: {C}, {B, E}, {I2, B}, {I1, E} and {I1, I2}. Deletion tasks may be more complicated: for example, in TOYNET we might be interested to repress the activation of O1 *and* O2. Accordingly, the target paths would increase by one (P4 in Figure 5) resulting in another set of MCSs.

This example might suggest that we can use the same procedure as in metabolic networks, namely computing the minimal hitting sets with respect to the target paths. This naive approach works indeed for the case where the target paths do only involve positive arcs (as in our example). It can also be applied for interrupting any set of feedback circuits. For example, removing {A} interrupts the negative feedback circuit and deleting {D, F} interrupts both feedback circuits in TOYNET. However, in general, negatively signed arcs occurring in interaction graphs require a special treatment. Even the following simple activating path leading from a source species I to a sink species O contains pitfalls:

$I \xrightarrow{+} A \xrightarrow{-} B \xrightarrow{-} C \xrightarrow{+} O$. If the activation of O is to be repressed, the signal flow along this path must be

interrupted. Removal of one species in the chain should be sufficient. However, not all nodes are allowed to be cut. If species B is removed, its negative action on C would be interrupted, enabling in turn C to activate O. The reason is that B, according to the definitions, is an inhibitor of O and is therefore not a proper cut candidate. In fact, we could *add* (constitutively provide or activate) B to stop an activation of O. Generally, for attacking an *activating* path, only the species that have an activating effect on the end node of this path are proper cut candidates, whereas species inhibiting the end node should instead be kept at a high level to prevent an activation along this path. Hence, as a generalization of (minimal) cut sets, we define *(minimal) intervention sets* (MISs) in interaction networks as (minimal) sets of elements that are to be removed *or* to be added in order to achieve a certain *intervention task*. By allowing only the removal of elements, the set of MISs coincides with the MCSs.

The computation of the MISs (or the smaller set of MCSs) for a set of activating target paths that involve *negatively* signed arcs is a more difficult task than computing only minimal hitting sets. Indeed, each MIS will still represent a hitting set, because at least one species in each target path must be removed or constitutively provided. The difficulty arises by ambivalent factors which have in some target paths an activating and in others an inhibitory effect upon the end node. We could therefore restrict the interventions to those species that are either pure activators with respect to the target paths (these are allowed to be removed) or pure inhibitors (these are allowed to be added). Using only these species, the MISs could again be computed as the minimal hitting sets.

However, for computing MISs that may also act on ambivalent factors, we present a more general algorithm (here for a given set of *activating* target paths):

(1) In each target path, the involved nodes are labeled by +1 (if the species influences the end node *of the respective path* positively) or by -1 (if the species has a negative influence on the end node *of the respective path*).

(2) Combinations C_i of one, two, three, ... distinct removed or activated species are constructed systematically. For each combination C_i, it is checked for each target path whether the signal flow from the start node to the end node is interrupted properly. A requirement is that at least one of the positive (+1) species of each path is removed or at least one negative (-1) species is provided (added) by C_i (hitting set property). If, for a certain path, C_i contains several nodes that are visited by this paths then it is only checked whether the node closest to the end node is attacked properly. When all paths have been attacked (hit) properly by a combination C_i, then a new MIS has been found. When constructing further combinations of larger cardinality, the algorithm has to ensure that none of the new combinations contains an earlier found MISs completely.

Of course, this enumerative algorithm is even more time consuming than computing minimal hitting sets and it will become infeasible to compute all MISs in large networks. We may then restrict ourselves to MISs of low cardinality and/or to the subset of MCSs. Besides, the determination of MISs can become even more complicated: it might happen that a MIS attacks all activating target paths correctly but simultaneously destroys an inhibiting path (not contained in the set of target paths) which might then become an activating path. The MCS {I1, I2} of our example represents such a problematic case: it hits the two activating paths to O1 as demanded, but it also attacks the inhibiting path leading from I1 to O1. Thus, the inhibition of E through I1 would be interrupted and it could be sufficient to retain E in an active state enabling the activation of O1. Hence, we would not be sure about the activation status of O1 after removing this cut set. To avoid such side-effects, we may extend our algorithm given above by checking also the consequence of each intervention C_i with respect to the non-target paths and exclude combinations that do not fulfill certain criteria.

In a completely analogous fashion, we can also determine MCSs or MISs that repress *inhibitory* paths. For example, removing {I1} is a MCS that attacks the only inhibiting path to O1, alternatively we might use the MISs {#E} or {#C}, where # stands for "constitutively provided". The same issues as discussed above must be taken into account when interrupting a negative path: here, in each target path, only the inhibiting species of the final sink source should be removed whereas the activating nodes can be added. Furthermore, we may also define more complicated intervention tasks, e.g. where some activating and some inhibiting paths are selected as target paths.

Jacobian matrix and interaction graph

Several works have highlighted the strong relationships between interaction graphs and the Jacobian matrix **J**, the latter obtained from a dynamical model of the network under investigation [10,35,39]. A dynamic model of a signaling (or any kind of interaction) network is usually described by a system of ordinary differential equations that model the evolution of the m network components x_1 ... x_m with the time:

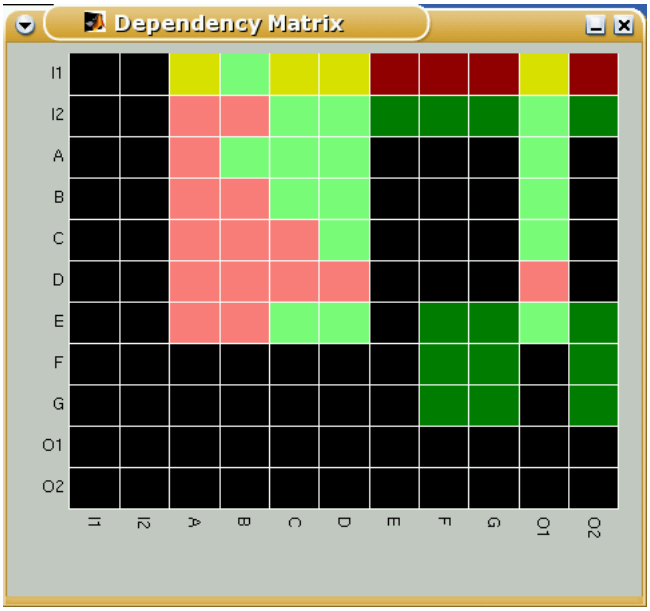

Figure 6
Dependency matrix of TOYNET. The color of a matrix element $\mathbf{M}_{xy}$ has the following meaning: (i) dark green: x is an total activator of y; (ii) light green: x is a (non-total) activator of y; (iii) dark red: x is a total inhibitor of y; (iv) light red: x is a (non-total) inhibitor of y; (v) yellow: x is an ambivalent factor for y; (vi) black: x does not influence y;

$$\dot{\mathbf{x}} = \frac{d\mathbf{x}}{dt} = \begin{pmatrix} \dot{x}_1 \\ \vdots \\ \dot{x}_m \end{pmatrix} = F(\mathbf{x},t) = \begin{pmatrix} f_1(\mathbf{x},t) \\ \vdots \\ f_m(\mathbf{x},t) \end{pmatrix} \qquad (5)$$

The $m \times m$ Jacobian matrix $\mathbf{J}(\mathbf{x})$ collects the partial derivatives of F with respect to $\mathbf{x}$:

$$\mathbf{J}_{ik}(\mathbf{x}) = \frac{df_i}{dx_k}(\mathbf{x}) \qquad (6)$$

The sign of $\mathbf{J}_{ik}(\mathbf{x})$ tells whether x_k has a (direct) positive or negative influence on x_i and $\text{sign}(\mathbf{J}(\mathbf{x}))$ can thus be seen as the *adjacency* matrix of the underlying interaction graph. In an adjacency matrix $\mathbf{Y}$, a non-zero entry for $\mathbf{Y}_{ik}$ indicates an edge from node i to k. Adjacency and incidence matrix are equivalent for describing a graph structure and can be converted into each other: each non-zero element $\mathbf{Y}_{ik}$ gets a corresponding column in the incidence matrix.

The sign structure of the Jacobian matrix is, in biological systems, typically constant and reflects, despite its very qualitative nature, fundamental properties of the dynamic system. For example, multistationarity can only occur if a positive circuit exists in the associated interaction graph [39]. Methods for the detection of multistability in a special class of dynamical systems – monotone I/O systems – have been developed by Sontag et al. [36]. Monotone I/O systems possess a monotonicity property that can be checked from the interaction graph spanned by the Jacobian matrix. In fact, having one source species and one sink species, the required monotonicity property is equivalent to our definition of a *total activator* of the sink node. Thus, the methods developed in the previous section may support such studies, where the structure of the Jacobian matrix is analyzed. Having the absolute values of the Jacobian matrix available (which change over time), arcs, paths, and feedback circuits could be assigned an interaction strength useful to identify key elements in the network.

Boolean networks and (logical) interaction hypergraphs

Definitions

The methods described above consider an interaction as a dependency between two species allowing to employ tools from graph theory. However, in cellular networks, an interaction (edge) often represents a relationship among more than two species (nodes). A typical example is a bimolecular reaction of the form A+B→ C, where three species are involved. The binding of the ligand to the receptor in Figure 2(b) (Rec+Lig→ RecLig*) is such a bimolecular interaction. Using an interaction graph, this reaction is modeled with two arcs (Figure 7(a)), namely Rec→ RecLig* and Lig→ RecLig*, capturing correctly that Rec and Lig have an influence on RecLig*. However, this relaxed representation has shortcomings for a functional interpretation of the network. To exemplify this, consider the minimal cut sets repressing the phosphorylation of M in Figure 7(a). As explained in the previous section, we need to attack all positive paths leading to M-P. There are two positive paths, one starting from Rec and the other from Lig and, thus, {Rec, Lig} would be a minimal cut set. But, intuitively, this cut set is *not* minimal for the real system because both Rec and Lig are required for activating M, and removing only one of the two species is thus sufficient to interrupt the activation of M. (In other words, the existence of a signaling path in an interaction graph does not ensure that a signal can flow along this path.)

This example reveals that a proper consideration of AND-connections between species is required. However, AND-relationships are not possible in graphs but in hypergraphs, which are generalizations of graphs. Similar to a directed graph, a directed hypergraph $H=(V, A)$ consists of a set V of nodes and a set A of hyperarcs (= directed hyperedges [49]). A hyperarc a connects two subsets of nodes: $a = \{S,E\}$; $S,E \subset V$. S comprises the tail (start) nodes and E the head (end) nodes of the connection. S and E can have arbitrary cardinality, and a graph is a special case of a

hypergraph where the cardinality of ***S*** and ***E*** is 1 for all edges.

In our context, without loss of generality, we will usually have only one end node in ***E*** and we interpret a hyperarc as an interaction in which the compound contained in ***E*** is activated by a combined action of the species contained in ***S***. Figure 7(b) depicts the example with the receptor-ligand-complex as a hypergraph in which a hyperarc captures now the AND-connection between Rec and Lig yielding RecLig*.

AND connections facilitate a refined representation of stoichiometric conversions within interaction networks, albeit the precise stoichiometric coefficients are not captured here. Apart from stoichiometric interactions, AND connections allow the description of other dependencies, for example, the case where only the presence of an activator AND the absence of an inhibitor leads to the activation of a certain protein.

In TOYNET, the four nodes (B, C, E, F) have more than one incoming arc (Figure 3). In these nodes it is undetermined how the different stimuli are combined, e.g. whether B AND E are required to activate C or whether one of both is sufficient (B OR E).

We could therefore concatenate all incoming edges in a node by logical operations leading to *Boolean networks* [21,31]. An assumption underlying Boolean networks is to consider only discrete (concentration/activation) levels for each species; in the simplest case a species can only be "off" (= 0 = "inactive" or "absent") and "on" (= 1 = "active" or "present"). Hence, each species is considered as a binary (logical) variable. Next, a Boolean function f_i is defined for each node i which determines under which conditions i is on or off, respectively. f_i depends only on those nodes in the interaction graph from which an arc points into species i. In general, for constructing a Boolean function, all logical operations like AND, OR, NOT, XOR, NAND can be used. However, here we express each Boolean function by a special representation known as sum of products (SOP; also called (minimal) disjunctive normal form (DNF)) which is possible for any Boolean function [50]. SOP representations require only AND, OR and NOT operators. In a SOP expression, *literals*, which are Boolean variables or negated Boolean variables, are connected by AND's giving *clauses*. Several such AND clauses are then in turn connected by OR's. Using the usual symbols '·' for AND, '+' for OR and '!' for NOT, an example of a SOP expression would be: $f_i = x \cdot y \cdot z + x \cdot !z$ stating that f_i gets value "1" if (x AND y AND z are active) OR (if x is active AND z is NOT) and "0" else. The SOP expression $f_i = x \cdot !y + !x \cdot y$ mimics an XOR gate.

In our context, writing a Boolean function as a SOP has several advantages. First, many biological mechanisms that lead to the activation of a species correspond directly to SOP representations. Second, by using SOPs, the structure of a Boolean network can be represented and depicted intuitively as a hypergraph: each hyperarc pointing into a node i is an AND clause of other nodes and represents one way of activating i; hence, all hyperarcs ending in i are OR'ed together. A hyperarc carries a signal flow to its end node and the binary value of the flow depends on the state of all its start nodes. In the following, such a hypergraph induced by a minimal SOP representation of a Boolean network will be called a *logical interaction hypergraph (LIH)*.

In Figure 8 a possible instance of a LIH compatible with the interaction graph of TOYNET in Figure 3 is depicted. In each of the four nodes with more than one incoming arc, the logical concatenation has now been specified. For example, B is now activated if A AND I1 are active simultaneously (hyperarc "1&4"). In contrast, C is activated if B OR E is present (active), and F is active if E OR G are in an active state. Hence, C and F retain their graph-like structure.

Inhibiting arcs in the interaction graph are interpreted in the corresponding LIH as NOT-operations. Thus, arc 7 is now interpreted as "A is active if D is not present". Since arc 2 and 3 in Figure 3 have been combined with an AND in Figure 8, we interpret this new hyperarc as "E becomes activated if I2 is present AND I1 NOT". Hence, in contrast to inhibiting arcs in interaction graphs, in general we do not assign a minus sign (a NOT) to the complete hyperarc, but to its negative branches (see hyperarc 2&3 in Figure 8), whereas all other branches get positive signs. Due to the assignment of signs LIHs can formally be seen as *signed directed hypergraphs*.

The pure logical description of a signaling or regulatory network works well when the activation (inhibition) of a species by others follows a sigmoid curve [21]. Problems that might arise while describing a real network within the logical framework and possible solutions are discussed in a later section.

LIHs can be formally represented and stored in a similar way as interaction graphs. The underlying hypergraph is stored by an $m \times n$ incidence matrix $\mathbf{B}$ in which the rows correspond to the species and the columns to the n hyperarcs. If species i is contained in the set of start (tail) nodes of a hyperarc k then $\mathbf{B}_{ik} = -1$, if i is the endpoint (head) of hyperarc k then $\mathbf{B}_{ik} = 1$, and if i is not involved in k we have $\mathbf{B}_{ik} = 0$. For storing the NOTs operating on certain species in a hyperarc we may use another $m \times n$ matrix $\mathbf{U}$ that stores in $\mathbf{U}_{ik}$ a "1" if species i enters the hyperarc k with its

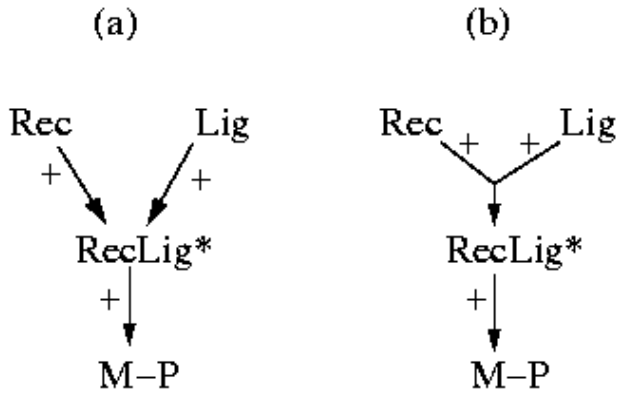

Figure 7
(a) the graphical and (b) the more correct hypergraphical representation of the simple interaction network shown in Figure 1 and 2.

negated value and "0" else. Accordingly, the incidence matrix **B** for the LIH of TOYNET (Figure 8) reads

$$\mathbf{B} = \begin{array}{c} \begin{array}{cccccccccccc} 1\,\&\,4 & 2\,\&\,3 & 5 & 6 & 7 & 8 & 9 & 10 & 11 & 12 & 13 & \end{array} \\ \begin{pmatrix} -1 & -1(*) & 0 & 0 & 0 & 0 & 0 & 0 & 0 & 0 & 0 \\ 0 & -1 & 0 & 0 & 0 & 0 & 0 & 0 & 0 & 0 & 0 \\ -1 & 0 & 0 & 0 & 1 & 0 & 0 & 0 & \mathbf{0} & 0 & 0 \\ 1 & 0 & -1 & 0 & 0 & 0 & 0 & 0 & 0 & 0 & 0 \\ 0 & 0 & 1 & -1 & 0 & 1 & 0 & 0 & 0 & -1 & 0 \\ 0 & 0 & 0 & 1 & -1(*) & 0 & 0 & 0 & 0 & 0 & 0 \\ 0 & 1 & 0 & 0 & 0 & -1 & -1 & 0 & 0 & 0 & 0 \\ 0 & \mathbf{0} & 0 & 0 & 0 & 0 & 1 & -1 & 1 & 0 & 0 \\ 0 & 0 & 0 & 0 & 0 & 0 & 0 & 1 & -1 & 0 & -1 \\ 0 & 0 & 0 & 0 & 0 & 0 & 0 & 0 & 0 & 1 & 0 \\ 0 & 0 & 0 & 0 & 0 & 0 & 0 & 0 & 0 & 0 & 1 \end{pmatrix} \begin{array}{c} \text{I1} \\ \text{I2} \\ \text{A} \\ \text{B} \\ \text{C} \\ \text{D} \\ \text{E} \\ \text{F} \\ \text{G} \\ \text{O1} \\ \text{O2} \end{array} \end{array} \quad (7)$$

To be concise, the two non-zeros entries of **U** are indicated by an asterisk in the incidence matrix.

Representing a Boolean network as a LIH we can easily reconstruct the underlying interaction graph from the matrices **B** and **U:** we simply split up the hyperarcs having more than one start node (or/and more than one end node in the general case). Thus, a hyperarc with d start and g end nodes is converted into $d \cdot g$ arcs in the interaction graph. The sign of each arc in the graph model can be obtained from **U**. The reverse, the reconstruction of the LIH from the interaction graph, is not possible in a unique manner underlining the non-deterministic nature of interaction graphs.

Time in Boolean networks

A *logical interaction hypergraph* describes only the static structure of a Boolean network. However, it is the *dynamic* behavior of Boolean networks that has been analyzed intensely in the context of biological (especially genetic) systems [21,31,51]. For studying the evolution of a logical system we need to introduce the (discrete) time variable t and a state vector $\mathbf{x}(t)$ that captures the logical values of the m species at time point t. Two fundamental strategies exist to derive the new state vector $\mathbf{x}(t+1)$ from the current state $\mathbf{x}(t)$. In the *synchronous* model, the logical value of each node i is updated by evaluating its Boolean function f_i with the current state vector: $x_i(t+1) = f_i(\mathbf{x}(t))$. Synchronous models are deterministic but assume for all interactions the same time delay which is often too unrealistic for biological systems [21]. In the *asynchronous* model, we select any (but only one) node i whose current state is unequal to its associated Boolean function: $x_i(t) \neq f_i(\mathbf{x}(t))$. Only this node switches in the next iteration. Since there are, in general, degrees of freedom in choosing the switching node, this description is non-deterministic. The advantage is that the complete spectrum of potential trajectories is captured, albeit the graph of sequences is usually very dense, complicating its analysis in large systems. The asynchronous description becomes (more) deterministic if time delays for activation and inhibition events are known [21].

We are now approaching the main part of this section.

Logical steady-state analysis

An important characteristic of the dynamic behavior of Boolean networks, which is equivalent for both asynchronous and synchronous descriptions, is the set of *logical steady states (LSSs)*. LSSs are state vectors $\mathbf{x}^s$ obeying $x_i^s = f_i(\mathbf{x}^s)$ for all nodes i. Hence, in LSS, the state of each node is consistent with the value of its associated Boolean function and, therefore, once a Boolean network has moved into a logical steady state, it will stop to switch and then retain this state.

In the following, we will focus on logical steady state analysis (thus circumventing any interpretation problems that might arise by choosing synchronous or asynchronous description), which suffices for a number of applications, especially for predicting potential functional states in signaling or regulatory networks.

Given a Boolean network we may enumerate all possible LSSs [52]. However, this is computationally difficult in large networks. Besides, we are often interested in particular LSSs that can be reached from a given initial state $\mathbf{x}^0$. In some cases, we only know a fraction of all initial node values. For example, a typical scenario in signaling networks would be that initial values from species in the input layer are known (specifying which external signals reach the cell and which not), and we would like to know how the

Table 3: All negative and positive feedback loops in the T-cell model as determined by CellNetAnalyzer. Negative influences are indicated by "", positive influences are expressed by "→".

1 (negative)	TCRbind → TCRphos → ZAP70 → cCbl TCRbind
2 (negative)	TCRbind → Fyn → TCRphos → ZAP70 → cCbl TCRbind
3 (negative)	TCRbind PAGCsk Lck → ZAP70 → cCbl TCRbind
4 (negative)	TCRbind PAGCsk Lck → TCRphos → ZAP70 → cCbl TCRbind
5 (negative)	PAGCsk Lck → Fyn → PAGCsk
6 (negative)	TCRbind PAGCsk Lck → Fyn → TCRphos → ZAP70 → cCbl TCRbind
7 (negative)	cCbl ZAP70 → cCbl
8 (positive)	TCRbind → Fyn → PAGCsk Lck → TCRphos → ZAP70 → cCbl TCRbind
9 (positive)	TCRbind → Fyn → PAGCsk Lck → ZAP70 → cCbl TCRbind

(logical) integration and propagation of these input signals generate a certain logical pattern in the output layer. Of course, we have to "wait" until the signals reach the bottom of the network and, for obtaining a unique answer, there should be a time point from which the states will not change in the future. This is equivalent to determining the LSS in which the network will run from a given starting point.

In a possible scenario for TOYNET, the initial values of the source species I1 and I2 might be known to be $x_{I1}^0 = 0$ and $x_{I2}^0 = 1$, whereas the initial states of all other nodes are unknown (Figure 9(a)). The states of I1 and I2 will not change anymore because I1 and I2 have no predecessor in the hypergraph model. Assuming that each interaction has a finite time delay, E must become active and B inactive. From these fixed values we can conclude that C and F will definitely become active (by E) at a certain time point and not change this state in the future. Proceeding further in the same way, we can resolve the complete LSS resulting from the given initial values of I1 and I2 (Figure 9(b)).

The last example illustrated that partial knowledge on initial values, especially from the source nodes, can be sufficient to determine the resulting LSS uniquely. However, in general, several LSSs might result from a given set of initial values or a LSS may not exist at all. For example, if we only know $x_{I2}^0 = 1$ in TOYNET nothing can be concluded regarding a LSS (except that I2 will retain its state). If no complete LSS can be concluded uniquely from initial values, there might nevertheless be a subset of nodes that will reach a state in which they will remain for the future. For example, setting $x_{I1}^0 = 1$ E will definitely become inactivated after some time (again, finite time delay is assumed). Since in this scenario nothing further can be derived for other nodes, we would say that $x_{I1} = 1$ and $x_E = 0$ are *partial LSSs* for the initial value set $\{ x_{I1}^0 = 1\}$. Note that these two partial steady states would not change when we specified more or even all initial values.

We have conceived an algorithm which derives partial LSSs that follow from a given set of initial values (if for each node a partial LSS can be found, then a unique and complete LSS exists for the set of initial values). The iterative algorithm uses the following rules in the logical hypergraph model:

• initial values of source nodes will not change in the future, hence, are partial LSSs

• if species *i* has a proved partial LSS of 0, all hyperarcs in which *i* is involved with its non-negated value have a zero flow

• if species *i* has a proved partial LSS of 1, all hyperarcs in which *i* is involved with its negated value have a zero flow

• if all hyperarcs pointing into node *i* have a zero flow, then *i* has a partial LSS of 0

• if all start nodes of a hyperarc have a partial LSS of 1 (or of 0 for those start nodes entering the hyperarc with the negated value) then a partial LSS of 1 follows for the end node of this hyperarc

• knowing all the positive feedback circuits in the system, we can check whether there is a "self-sustaining" positive circuit where the known initial state values of the involved nodes guarantee a partial LSS for all the nodes in this cycle (see comments below)

In each loop, the algorithm tries to identify new partial LSSs (following from the current set of partial LSSs already identified) until no further ones can be found. Setting initial values in the input layer, this can be envisioned as a propagation of signals through the interaction network

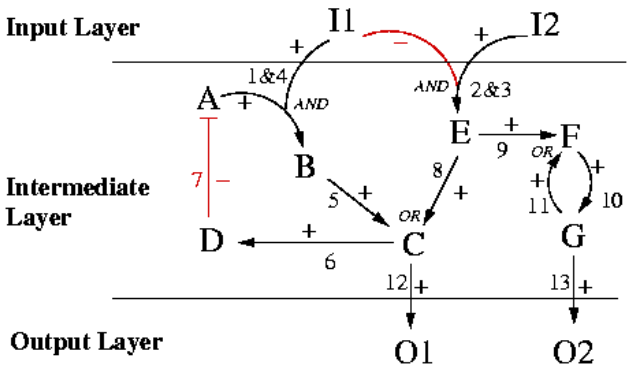

Figure 8
Logical interaction hypergraph of TOYNET (compare with interaction graph in Figure 3).

until signals reach nodes where the available information is not sufficient to derive a unique LSSs.

Generally, in logical interaction hypergraphs where the underlying interaction graph has no feedback loop (i.e. is acyclic), specification of the initial values of all the source nodes will always result in a unique and complete LSS since the signals can be propagated step by step from top-down to the output layer. In general, if all initial values are known for the input layer, non-uniqueness or even non-existence of partial LSSs can only be generated by feedback loops. The partial LSSs of nodes involved in positive feedbacks do often depend on the initial values of all the nodes in this loop. For example, defining $x^0_{I2} = 0$ we can conclude a partial LSSs of zero for E in TOYNET (Figure 8), but, among others, the values of F, G and O2 remain unknown although the only connection to a source node leads via E. The reason is that F and G build up a positive feedback loop which cannot be resolved without knowledge on further initial values. If we know, additionally to $x^0_{I2} = 0$, that $x^0_F = x^0_G = 1$ then F and G will always keep each other activated so that we can infer a partial LSS of 1 for F, G and O2 (this is the last rule in the list given above). If we have instead $x^0_F = x^0_G = 0$, we derive a 0 for the partial LSS of these three nodes. If one of the two nodes F and G has an initial value of 1 and the other 0, nothing can be derived since the positive loop might become fully activated or fully deactivated. However, what can be confirmed in these simple examples is that positive feedback loops induce multistationarity. It is noteworthy that continuous dynamic models of networks with positive feedbacks will depend, apart from kinetic parameters, in a similar fashion on initial state values.

In contrast, negative feedback loops are not sensitive against initial values but they can be the source of oscillations, preventing hence the existence of LSSs. In TOYNET we have one negative feedback loop which can potentially generate oscillations, for example, when we set $x^0_{I1} = 1$. Then, C cannot be activated via E. Assuming an initial value of 0 for C (the same conclusion would be drawn with 1), D becomes deactivated and thus A actived. Due to the partial LSS of 1 for I1 we get an activation of B and then of C and D which in turn inhibits A leading in the next round to a deactivation of B, C and D and so on. The logical states within this circuit and downstream of it (O1) will thus never reach a steady state. As shown in [21], oscillatory behavior in logical models corresponds to oscillations or a stable equilibrium (lying somehow between the fully activated and fully inactivated level) in the associated continuous model, depending on the chosen parameters. Negative feedback loops can thus impede predictions on the basis of logical steady states, but they also point to network structures whose parametrization will have great impact on the dynamic behavior.

Note that feedback loops do not always prevent predictions on (partial) LSSs as can be seen by the example in Figure 9, it depends on the given initial values.

Such a logical steady state or "signal flow" analysis (SFA) as presented herein shares similarities with the established method of metabolic flux analysis [53]. In MFA, uptake and excretion rates of cells are measured in order to reconstruct the intracellular flux distribution within a metabolic network. MFA relies on the quasi-steady state assumption, similarly as SFA relies on LSS. However, whereas MFA tries to reconstruct the reaction rates along the edges and nothing can be said on the states of the species, the goal of SFA is to determine the steady states of the nodes (belonging to a given activation scheme) from which then the signal flows along the edges follow. It is noteworthy that the calculability of unknown reaction rates in MFA depends only on the *set* of known rates [54], whereas in SFA the set of given initial states *and their respective values* determine the unique calculability of (partial) LSSs.

Applications of logical steady state analysis

The LSS analysis introduced herein offers a number of applications for studying functional aspects in cellular interaction networks:

Input-output behavior

Imposing different patterns of signals in the input layer one may check which species become activated or inhibited in the intermediate and, in particular, in the output layer. This can also be simulated in combination with different initial state values for certain intermediate nodes, albeit this will have an influence on the LSS only in connection with positive feedbacks, as shown above.

Mutants and interventions

The changes in signals flows and in the input-output behavior occurring in a manipulated or malfunctioning network can be studied by removing or adding elements or by fixing the states of certain species in the network. In TOYNET, for example, if we want to study the effect of a mutant missing F (or the effect of adding an inhibitor for F) we may remove species F from the network (or, equivalently, fix the state of F to zero) and compute then the partial LSSs again. We will see that, independently of a given pattern in the input layer, G and O1 will be assigned a partial LSS of 0. Removing elements often changes not only the *values*, but also the *determinacy* of partial LSSs.

Minimal cut sets (MCSs) and minimal intervention sets (MISs)

The definiton of MCSs and MISs in logical interaction hypergraphs is similar as in interaction graphs: a MCS is a minimal (irreducible) set of species whose removal will prevent a certain response or functionality as defined by an intervention goal. In the more general MISs we permit, additionally to cuts, also the constitutive *activation* of certain compounds. Two examples in TOYNET: removing F is a MCS for repressing an activation of G and O2. Assuming an initial state of zero for the species in the intermediate layer, adding I1 and removing B would be a proper MIS for repressing the activation of O1 and O2. Note that in the interaction graph of TOYNET, this intervention would not suffice to attack all activating paths leading from the input layer to O1 and O2 (path P4 not attacked, Figure 5). This example underscores again that MCSs and MISs in interaction hypergraphs are usually smaller than those obtained from the underlying interaction graph, simply because more constraints are added by logical combinations. However, the determination of MCSs, and let alone MISs, in logical interaction hypergraphs is combinatorially complicated as in interaction graphs, in particular when negative signs (NOTs) occur. Here, we can only propose a "brute-force" approach where the LSS analysis serves algorithmically as an oracle: we check systematically for each combination of one, two, three ... knocked out (for MISs also of permanently activated) nodes in the network how this affects the (partial) LSSs, possibly in combination with a given scenario of initial states. From the resulting partial LSSs we can decide whether our intervention goal has been achieved or not. To compute only *minimal* cut or intervention sets, further combinations with a cut or intervention set already satisfying our intervention goal have to be avoided. The algorithm can be stopped when a user-given maximum cardinality for the MCSs/MISs has been reached.

Backward propagation

The methods described above compute partial LSSs actually only by forward propagation of signals, but one may also do the opposite, e.g. fixing values in the output layer and tracing back the required states of nodes in the intermediate and input layer using similar rules as for forward propagation.

Network expansion methods

There is an interesting relationship between our LSS analysis and network expansion methods proposed by Ebenhöh et al. [55]. Network expansion allows for checking which metabolites can in principle be produced from a provided set of start species within a metabolic (stoichiometric) reaction network. This is a special case in our logical framework. Briefly, metabolic networks are per se hypergraphs and can thus be represented as a LIH by using only AND's (each reaction is an AND clause of its reactants; stoichiometric coefficients are not considered) and OR's. Hence, no inhibiting interactions exist. We may then put the supplied set of available species in the input layer, set the initial values of all other species to zero and compute then the LSS. Note that, according to the explanations given above, a complete LSS will always be found since all initial values are given and no negative feedback circuit exists. Therefore, the computed LSS indicates which species can be produced from the input set and which not.

Extensions for the logical description of interaction networks

Several extensions and refinements of the logical framework can be introduced which allow a more appropriate description of real signaling and regulatory networks:

(1) As already proposed and applied by Thomas et al. [21], the discretization in more than two levels is in principle possible. This mimics the fact, that in reality multiple relevant threshold values for a species may exist. A refined discretization could be relevant, for instance, for a species that activates/inhibits more than one species (with different threshold levels). Another relevant situation occurs if a species can be activated via two paths (connected by an OR; see species C in TOYNET): the activation via *both* paths might be significantly stronger than by only *one*. However, considering several activation levels for a certain species forces one to often consider multiple levels for elements downstream or/and upstream of this species, increasing hence the complexity of the network, and requiring detailed knowledge which is often not available.

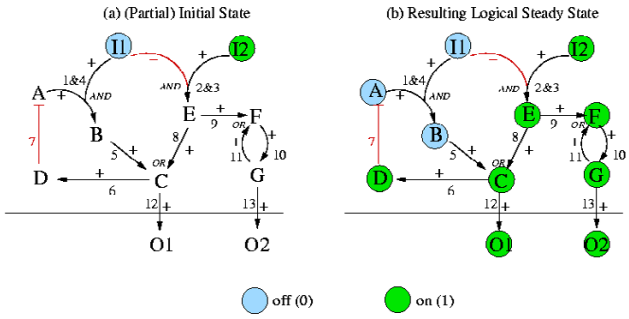

Figure 9
Example of a logical steady state in TOYNET resulting from a particular set of initial states in the input layer.

(2) As we have seen, negative feedback can limit the predictability in LSS analysis. However, in cellular networks, negative feedbacks become activated often upon a certain time period after an activation event occurs, for example, when gene expression is involved. This might be considered by classifying species and/or hyperedges by assigning a discrete *time constant* (or time scale) τ to each element telling us whether this network element appears in an early ($\tau = 1$) or late ($\tau = 2$) state. Using the sub-network with all elements having a time constant of $\tau = 1$ for the first simulation and then using the computed LSSs as initial values for computing the second round (where the complete network is considered) leads often to more realistic results. As in the case of multiple levels, this extension requires a more detailed knowledge about the network under consideration. An example in TOYNET (Figure 8): we may assume that D is a factor that is transcriptionally regulated by C, thus, arc 6 has a time constant of $\tau = 2$ and all others have $\tau = 1$. Setting the initial values I1 = 1, I2 = 0 and D = 0 and computing the LSSs for $\tau = 1$ activation of C and O1 occurs. We can then fix the state of D (D = 1) and get then a complete deactivation of C and O1.

(3) In real signaling and regulatory networks, it is sometimes difficult to decide whether arcs from the interaction graph have to be linked by an AND or an OR in the interaction hypergraph. For example, in TOYNET, species E is inhibited by factor I1 and activated by factor I2. If I1 has a very strong inhibiting effect on E we may formulate the hyperarc as done in Figure 8, suggesting that I1 must not be active for activating E. However, if the interaction strength of both I1 and I2 with respect to E is at the same level (i.e. additive) neither "NOT(I1) OR I2" nor "NOT(I1) AND I2" would reflect the real situation. Indeed, this is a recurring situation in signaling networks, where often a balance between different signals determines the activation of a certain element. At this point it could be helpful to use logical operations that have a partially incomplete truth table. In the latter example we could say that E is active if (NOT(I1) AND I2) and E is inactive if (I1 AND NOT(I2)). For the other two possible cases, no decision could be made along this hyperedge. Of course, modeling uncertainty in this way will limit the determinacy but on the other hand a determined result with this model allows a safer interpretation.

Analyzing interaction networks using CellNetAnalyzer

We have integrated many of the methods and algorithms described herein in our software tool *CellNetAnalyzer*, which is a MATLAB package and the successor of *FluxAnalyzer* [56]. Whereas *FluxAnalyzer* was originally developed for structural and functional analysis of metabolic networks, *CellNetAnalyzer* extends these capabilities consequently to the structural analysis of signaling and regulatory networks. Apart from stoichiometric (metabolic) reaction networks, *CellNetAnalyzer* supports now also the composition of logical interaction hypergraphs using AND, OR and NOT connections. Whenever needed, the underlying interaction graph can be deduced from the interaction hypergraph. Alternatively, by using only OR's and NOT's, arbitrary interaction graphs can be constructed. As in *FluxAnalyzer*, the network model can be linked with externally created graphics visualizing the network. User interfaces (text boxes) enable data input and output directly in these interactive maps (see screenshot in Figure 10). New functions for graph-theoretical and logical analysis have been integrated into the user menu; the results from computations are directly displayed within the interaction maps or in separate windows. The functions include:

• large-scale computation of all (positive and negative) signaling paths connecting inputs with outputs or of all signaling paths between a given pair of nodes; statistical analysis of these paths

• large-scale computation of all (positive and negative) feedback loops; statistical analysis of these routes

• computation of minimal cut sets for a given set of paths or/and loops

• computation of distance (shortest paths) matrices – separately for positive and negative paths

• large-scale dependency analysis: identification of (total) activators, (total) inhibitors and ambivalent factors for a given species; display of the dependency matrix

• computation of (partial) logical steady states from a given set of initial state values

• computation of (logical) minimal cut sets repressing or provoking a user-defined behavior in the logical network

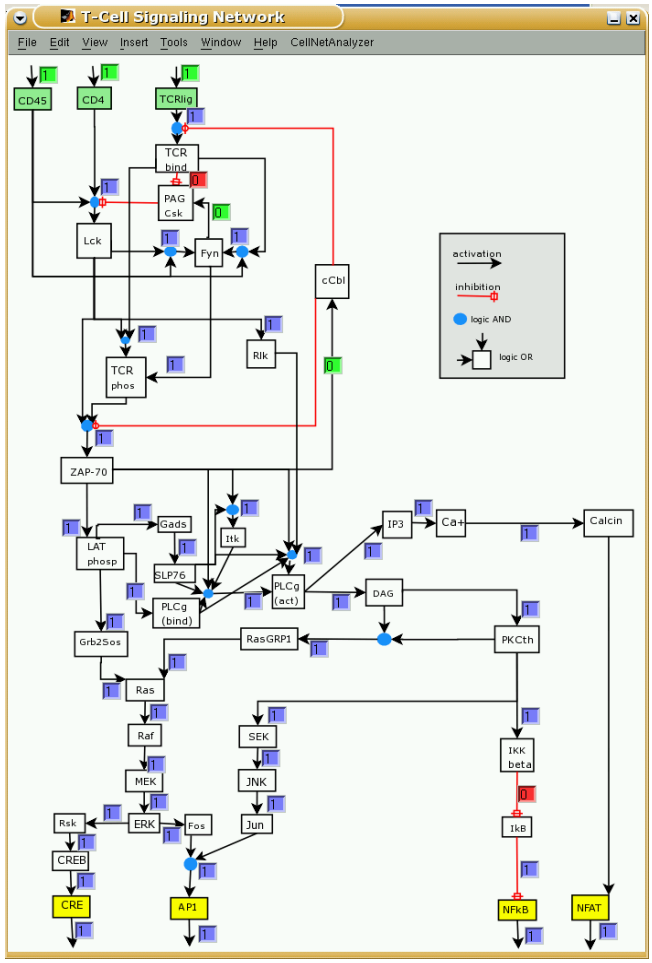

Figure 10
Screenshot of the *CellNetAnalyzer* model for T-cell activation. Each arrow finishing on a species box represents a hyperarc and all the hyperarcs pointing into a species box are OR connected. In the shown "early-event" scenario, the feedbacks were switched off whereas all input arcs are active. The resulting logical steady state was then computed. Text boxes display the signal flows along the hyperarcs (green boxes: fixed values prior computation; blue boxes: hyperarcs activating a species (signal flow is 1); red boxes: hyperarcs which are not active (signal flow is 0)).

To illustrate the ability of our approach to deal with real complex signaling networks, we have set-up and analyzed in *CellNetAnalyzer* a logical model of T-cell activation (Figure 10), which will be discussed in the next section.

CellNetAnalyzer is free for academic purposes (see web-site [57]).

Logical model of T-cell activation

T-cell activation and the molecular mechanisms behind

T-lymphocytes play a key role within the immune system: Cytotoxic, $CD8^+$, T-cells destroy cells infected by viruses or malignant cells, and $CD4^+$ helper T-cells coordinate the functions of other cells of the immune system, such as B-lymphocytes and monocytes [58]. Loss or dysfunction, especially of $CD4^+$ T-cells (as it occurs e.g. in the course of HIV infection or in immuno-deficiencies) has severe consequences for the organism and results in susceptibility to viral and fungal infections as well as in the development of malignancies. The importance of T-cells for immune homeostasis is due to their ability to specifically recognize foreign, potentially dangerous, agents and, subsequently, to initiate a specific immune response that is aimed at eliminating them. T-cells detect foreign antigens by means of their T-Cell Receptor (TCR) which recognizes peptides only when presented on MHC (Major Histocompatibility Complex) molecules. The peptides that are recognized by the TCR are typically derived from foreign (e.g. bacterial, viral) proteins and are generated by proteolytic cleavage within so called antigen presenting cells (APCs). Subsequent to their production the peptides are loaded onto the MHC-molecules and the assembled peptide/MHC-complex is then transported to the cell surface of the APC were it can be recognized by T-cells. The whole process of antigen uptake, proteolytic cleavage, peptide loading onto MHC, transport of the peptide/MHC complex to the surface of the APC and the recognition of the peptide/MHC-complex by the TCR is called antigen presentation and provides the molecular basis for the fine specificity of the adaptive immune response.

The binding of peptide/MHC to the TCR, and the additional binding of a different region of the MHC molecules to so called co-receptors (CD4 in the case of helper T-cells and CD8 in the case of cytotoxic T-cells), initiates a plethora of signaling cascades within the T-cell. As a result, several transcription factors – most importantly, AP1, NFAT and NFκB – are activated. These transcription factors, in turn, control the cell's fate, e.g. whether it becomes activated and proliferates [59] or not.

In the following, a logical model describing some of the main steps involved in the activation of $CD4^+$ helper T-cells (also applicable for $CD8^+$ cytotoxic T-cells) will be briefly introduced and analyzed (see Figure 10 and Table 2). Several players, in particular, some whose role and activation is not completely understood, are not included in our model and thus their effects are not considered or lumped with others. Additionally, in several, currently still controversial cases, we have assumed one of the possible hypotheses; however, this does not mean that we propose this to be the correct description of the TCR-induced signaling network; we just want to demonstrate

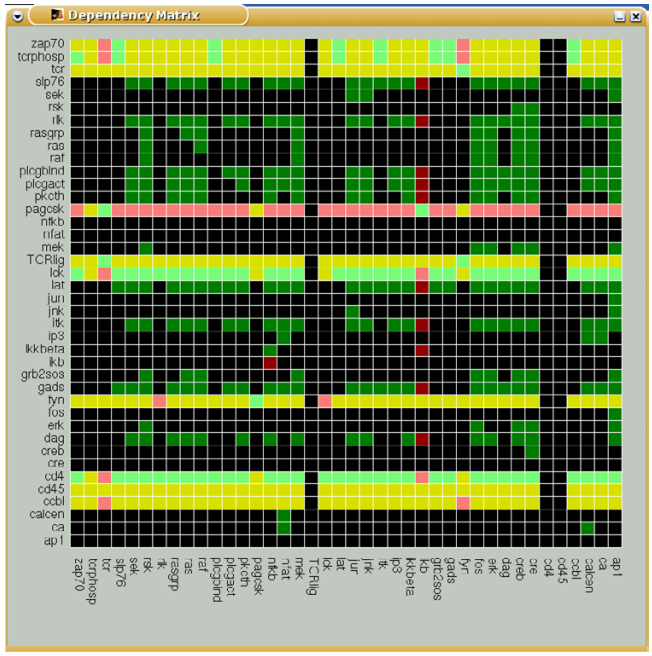

Figure 11
Dependency matrix for the T-cell model. The meaning of the different colors is the same as in Figure 6.

the applicability of our approach on a realistic, complex case. It is out of the scope of this paper to analyze the complete, highly-complex signaling machinery of a T-cell.

Here, the biochemical steps included in the signaling pathway will be described briefly; for a detailed description we refer the reader to reviews such as [59,60] and the references therein:

• Upon binding of peptide/MHC to the TCR, the first main step in the TCR-mediated signaling cascade is the activation of the Src-family protein tyrosine kinase $p56^{lck}$ (in the following termed Lck), although the exact mechanism is still unclear. We have included one well accepted mechanism [61], which probably plays a major role but may be combined with others (cf. Figure 10):

➢ In resting T-cells, the major negative regulator of Lck, the protein tyrosine kinase Csk (C-terminal Src-kinase) is bound via a SH2-domain to the constitutively tyrosine phosphorylated transmembrane adaptor protein PAG (Protein Associated with Glycosphingolipid enriched microdomains) and consequently inhibits membrane-bound Lck by phosphorylating a C-terminal negative regulatory tyrosine residue of the Src kinase.

➢ Upon ligand binding, PAG is dephosphorylated by a so far unknown protein tyrosine phosphatase, thereby leading to the detachment of Csk from PAG, and hence releasing Lck from the inhibitory effect of Csk. The release of Csk from PAG, together with the activity of the membrane associated tyrosine phosphatase CD45 (which dephosphorylates Lck on the same inhibitory residue that is phosphorylated by Csk), and the concomitant binding of the MHC molecule to the coreceptor CD4, leads to full activation of Lck (see Figure 10).

➢ However, both CD4 and the TCR can also be stimulated individually, e.g. by using monoclonal antibodies specifically directed at either of the molecules or using cell lines expressing mutated forms of CD4 that cannot bind MHC or cannot transmit signals.

➢ A regulation of the enzymatic activity of CD45 is not included in the model (basically because it is not yet clear how CD45 is regulated *in vivo*), but, since CD45 is an important regulatory element for T-cells, it is included as an input signal, allowing the analysis of its effect and the performance of CD45 knock-out experiments.

➢ After a few minutes, PAG is rephosphorylated [62], probably by the Src-kinase Fyn, and subsequently Csk is re-recruited to PAG inhibiting Lck again.

• Activated Lck can phosphorylate another member of the Src-protein kinases, $p59^{fyn}$, in the following termed Fyn (Fyn can probably also be activated in a Lck-independent, TCR-dependent manner [63]). Additionally, Lck phosphorylates the so called ITAMs (Immunoreceptor Tyrosine-based Activation Motifs) that are present in the cytoplasmic domains of the TCR-complex (the latter if the TCR is close to Lck, i.e., if there is a concurrent activation of the TCR). Subsequently, the Syk-family protein tyrosine kinase ZAP70 (Zeta Associated Phosphoprotein of 70 kDa) binds to the phosphorylated ITAMs and, if Lck is active, becomes activated by Lck-mediated tyrosine phosphorylation. Thus, during the initial phase of signal transduction via the TCR three tyrosine kinases become activated in a sequential manner, first Lck and Fyn and then ZAP70. Together these three kinases propagate the TCR-mediated signal by phosphorylating a number of membrane associated and cytosolic signaling proteins.

• Active ZAP70 can phosphorylate LAT (Linker for Activation of T-cells), a second transmembrane adapter protein, at four different tyrosine residues. Subsequently, cytoplasmic signaling molecules containing SH2-domains, including the scaffolding proteins Grb2, Gads, and the lipid kinase PLCγ1 (Phospholipase gamma 1), can bind to phosphorylated LAT. Additionally, Grb2 binds to the

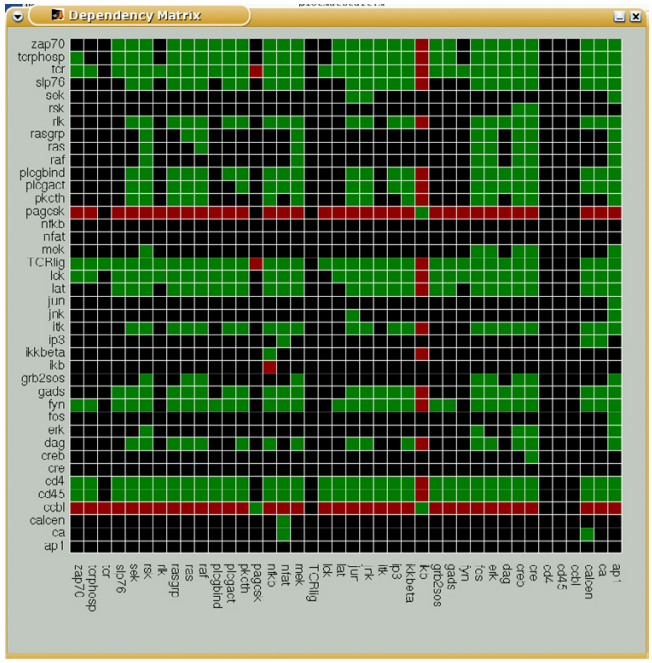

Figure 12
Dependency matrix for the T-cell model for the early event scenario (τ = *1: the feedback loops are not active*). The meaning of the different colors is the same as in Figure 6.

nucleotide exchange factor Sos (here we lumped Grb2 and Sos in one activation step), and Gads to the adapter protein SLP76. The latter, upon phosphorylation by ZAP70, can bind to the Tec-family tyrosine kinase Itk. Binding to SLP76 and additional phosphorylation by ZAP70 activates Itk.

• For the activation of PLCγ1, the following conditions have to be fulfilled: PLCγ1 is bound to LAT, SLP76 bound to Gads, ZAP70 is activated (which hence phosphorylates SLP76, allowing PLCγ1 to bind to SLP76), and Itk is active, and hence is able to phosphorylate and thereby to fully activate PLCγ1. Since all these conditions are needed, a logical AND was included in the model (see Figure 10). Rlk, another Lck-dependent Tec-family tyrosine kinase, can also phosphorylate PLCγ1, hence Rlk has a redundant role to Itk with regard to the activation of PLCγ1 [64].

• Activated PLCγ1 hydrolyses phosphatidyl-inositol-4,5 biphosphate (PIP_2), which is considered an ubiquitous membrane associated phospholipid and is therefore not modeled, thereby generating the second messenger molecules diacyloglycerol (DAG) and inositol trisphosphate (IP3) [59,61].

• IP_3 mediates calcium flux. Calcium (together with calmodulin) activates the serine phosphatase calcineurin, which dephosphorylates the cytosolic form of the transcription factor NFAT (Nuclear Factor of Activated T-cells). The calcineurin-mediated removal of phosphate groups allows NFAT to translocate to the nucleus and to regulate gene expression.

• The second messenger DAG activates PKCθ and (together with PKCθ[65]) activates the nucleotide exchange factor RasGRP1.

• RasGRP1 and Sos (the latter if it is close to the membrane, that is, if it is bound to LAT by means of Grb2), can activate Ras, which in turn activates the Raf/MEK/ERK MAPK Cascade.

• PKCθ is involved in the activation of JNK, as well as the essential transcription factor NFκB (via phosphorylation and subsequent degradation of the NFκB inhibitor, Iκ B, by the PKCθ-activated Iκ B-kinase, IKK).

• ERK, activated by the Ras/Raf/MEK cascade, activates the transcription factor CRE and (together with JNK) the essential transcription factor AP1.

• The E3 ubiquitin ligase cCbl is important for shutting off TCR-mediated signaling processes by ubiquitination of key proteins, which are subsequently targeted for degradation [66]. One important target of cCbl is ZAP70; upon tyrosine phosphorylation of ZAP70, cCbl binds to ZAP70, leading to ZAP70's ubiquitination and degradation as well as to the downregulation of the TCR.

From these biological facts we constructed a logical hypergraph model, containing 40 nodes and 49 hyperarcs, and implemented it in *CellNetAnalyzer* (Figure 10). The model is summarized in Table 2.

Remarks on the logical T-cell activation model

Note that a species can represent different states of a molecule: for example, CD45 refers to the availability of CD45 to act on its substrates (Lck and Fyn), PLCg(bind) refers to PLCγ1 bound to LAT, and PLCg(act) to the active (bound to LAT and phosphorylated) form of PLCγ1. It is also important to realize that several steps can be lumped together or expressed in higher detail; for example, the formation of the complex LAT:Grb2:Sos is considered as one step, but intermediate steps could be considered. This would be reasonable, for example, if Grb2 would have other functions apart from binding Sos. Similarly, the two steps of cCbl's effect (ubiquitination and degradation) are lumped in the hyperarcs pointing to its targets ZAP70 and TCR.

Also note that some of the logical operators could be modeled in a different manner, as in the case of Sos and

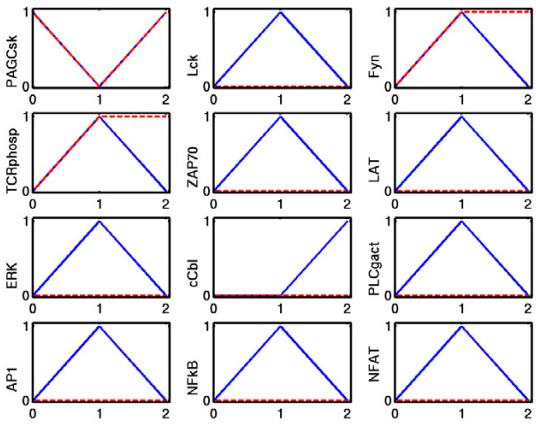

Figure 13
Simulation results of LSS analysis of key elements of the T-cell model using the two time-scales explained in the text. Blue line: upon TCR+CD4+CD45 activation; dashed red line: only TCR+CD45 activation.

RasGRP for the activation of Ras (where we prefer an OR since both can independently activate Ras, although both (AND) may be needed for full Ras activation).

Furthermore, our model describes the full activation of the cascade which leads to proliferation; it is known that e.g. stimulation of TCR with antibodies against its CD3 subunits produces a certain activation of the cascade (where probably Fyn overtakes Lck's role [63]) but does not lead to full activation. Therefore, in our model, as an approximation, activated Fyn can phosphorylate the ITAMs of the TCR, but is not able to activate ZAP70. Here a model with more than 2 levels could be envisioned, where activation of Fyn would be enough to produce a weak (level 1) activation of ZAP70 and hence the whole cascade downstream, while full activation via Lck would activate the cascade to a level 2 (full activation).

The model has two extracellular input signals (one for the TCR and one for the coreceptor CD4). Additionally, an input arc for CD45 is included because the regulation of CD45 is not modeled, as described above. Therefore, mathematically speaking, the model contains 3 elements in the input layer. On the other hand, the output layer contains 4 transcription factors (CRE, AP1, NFAT and NFκB).

As explained in the theoretical section, one reasonable way to deal with the effect of negative feedbacks is to consider the different time scales of the processes. Hence, since PAG rephosphorylation takes place after a few minutes [62], and cCbl mediated degradation is an even slower process, we can define several scenarios:

-τ = 0, resting-state (no inputs, no feedbacks),

-τ = 1, early-events (input(s), no feedbacks), and

-τ = 2, mid-time events (input(s), feedbacks). Here, the state of the feedback loops (activation of PAG/Csk by Fyn and recruitment of cCbl to phosphorylated ZAP70) will depend on the state of the respective activators at τ = 1. This can be considered either by fixing manually the state values of cCbl and PAG/Csk for τ = 2 upon inspection at τ = 1 (as was done herein) or by inclusion of a positive self-loop.

We use the term mid-time event since one can also envision a long-term scenario (τ = 3), where slow gene expression mechanisms (not considered here) are active.

Analysis of the T-cell signaling cascade

In the interaction graph underlying the hypergraphical model, there are 1158 paths from the input to the output layer and 9 (7 negative and 2 positive) feedbacks loops, which are listed in Table 3. cCbl is involved in most (88%) of the loops, in accordance to its important role in the regulation of the signaling cascade. Not surprisingly, since the only feedback mechanisms included are the effect of cCbl on ZAP70 and TCR and of Fyn on PagCsk, no loop goes downstream of ZAP70, and a suitable minimal cut set attacking all the feedback loops would consist of Fyn and cCbl.

We further analyze the interaction graph by computing the dependency matrix (Figure 11). Since downstream of ZAP70 there are only positive connections (except at node IκB), all the elements downstream of ZAP70 are total activators (except of IκB, which is a total inhibitor of NfκB) with respect to the transcription factors in the output layer, that is, they can have only positive effects. Therefore, for these species, a negative intervention via e.g. inhibitors or iRNA would unambiguously lead to a decrease in the activation levels of the transcription factors. For considering the early-events scenario (τ = 1: the feedback loops are not active), we recompute the dependency matrix where the action of Fyn on PAGCsk and of ZAP70 on cCbl is not considered (Figure 12). Then, all inputs (CD45, TCRlig and CD4) are total activators for all species in the output layer. This is not the case when the feedbacks become active (Figure 11): TCRlig and CD45 become then ambivalent factors, i.e. have negative connections to the sink species, whereas CD4 is still an activator but no longer a total one, as it is now connected to a negative feedback loop.

Table 2: The hyperarcs of the logical T-cell signaling model (see Figure 10). Exclamation mark ('!') denotes a logical NOT and dots within the equations indicate AND operations.

→ CD45
→ CD8
→ TCRlig
AP1 →
Ca → Calcin
Calcin → NFAT
CRE →
CREB → CRE
DAG → PKCth
ERK → Fos
ERK → Rsk
Fyn → PAGCsk
Fyn → TCRphos
Gads → SLP76
Grb2Sos → Ras
!IkB → NFkB
!IKKbeta → IkB
IP3 → Ca
JNK → Jun
Jun·Fos → AP1
LAT → Gads
LAT → Grb2Sos
LAT → PLCgbind
Lck·CD45 → Fyn
Lck → Rlk
MEK → ERK
NFAT →
NFkB →
!PAGCsk·CD8·CD45 → Lck
PKCth·DAG → RasGRP1
PKCth → IKKbeta
PKCth → SEK
PLCg(act) → DAG
PLCg(act) → IP3
Raf → MEK
Ras → Raf
RasGRP1 → Ras
Rsk → CREB
SEK → JNK
TCRbind·CD45 → Fyn
TCRbind·Lck → TCRphos
!TCRbind → PAGCsk
TCRlig·!cCbl → TCRbind
TCRphos·Lck·!cCbl → ZAP70
ZAP70·SLP76·PLCg(bind)·Itk → PLCg(act)
ZAP70·SLP76 → Itk
ZAP70 → cCbl
ZAP70 → LAT
ZAP70·SLP76·Rlk·PLCg(bind) → PLCg(act)

A further analysis of the interaction graph provides that there is no minimal cut set containing only one (essential) species whose removal would interrupt all the positive paths to all the outputs. In fact, all minimal cut sets satisfying this intervention task would contain at least two species, for example MCS1 = {Rlk, ZAP70} and MCS2 = {LAT, PLCg(act)}. The latter examples agree only partially with biological knowledge: removal of MCS1 or MCS2 would indeed prevent the activation of any output, however, from experimental observations one knows that for example LAT alone is essential in TCR signaling [60]. Thus, MCS2 would not be minimal.

Interpreting the *hypergraphical (logical)* model (Figure 10) reveals that, due to several AND connections, the additional removal of PLCg(act) would indeed be redundant

because PLCg can anyway not be activated if LAT is removed. This example illustrates the limitations of graph-based methods and we computed therefore the (logical) minimal cut sets from the logical interaction hypergraph revealing that not only LAT, but also ZAP70, Lck, TCR, the ligand for the TCR, TCRphosp, CD4 and CD45 are essential for full T-cell activation. This result is in good agreement with the current knowledge: the T-cell receptor, its ligand, and the ability of the receptor to get phosphorylated are required for T-cell activation; and CD4 (since it binds Lck thus recruiting it to the membrane) and CD45 (which dephosphorylates Lck inhibitory regulatory site) are required for the activation of the essential kinase Lck.

Next we performed a logical steady state analysis for the different time scales given above. These simulations provide a rough approximation to the dynamics of the signaling cascade. Figure 10 shows the particular situation in the early-event scenario ($\tau = 1$) as displayed in *CellNetAnalyzer*. Figure 13 summarizes the logical steady state values of important components obtained for the three different time scales. The blue line shows the case for TCR+CD4+CD45 stimulation, whereas the dashed red line represents the case when only TCR+CD45 is stimulated in the input layer. Similar analysis can be performed using different scenarios, for example, in a cell where a certain element has been knocked-out.

Conclusion

In this contribution we have presented a collection of methods for the functional analysis of the structure of cellular signaling and regulatory networks. As discussed in the theoretical sections, different abstractions and formalisms can be used to encode and analyze the topology of interaction networks. The simplest representations are interaction graphs, which are restricted to one-to-one relationships but do yet capture important functional and causal dependencies in the system under study. We have shown that arguably the most important features of interaction graphs, namely feedback circuits and signaling (or influence) pathways, can systematically be identified by the concept and algorithm of elementary modes known from stoichiometric (metabolic) network analysis. Feedback cycles are mainly responsible for the dynamic behavior of the system, whereas signaling paths reveal network-wide dependencies between species. In some cases, analysis of feedback cycles and signaling paths may allow one to predict unambiguously the qualitative effect upon perturbations of certain species (independently of kinetic parameters and mechanisms). Falsification experiments may then be used to identify missing or incorrect interactions. Knowledge on all the signaling paths also facilitates a systematic identification of optimal intervention strategies. Again, a concept known from metabolic networks, minimal cut sets, can be adapted and employed here. However, inhibitory actions make this kind of analysis more complicated and we therefore generalized the formalism of minimal cut sets leading to minimal intervention sets.

The applicability of tools from metabolic network analysis to interaction graphs relies on the fact that metabolic networks are hypergraphs, which in turn are generalizations of graphs. In our opinion, the importance of hypergraphs in structural analyses of cellular interaction networks has been underestimated. In fact, whenever AND-connections occur in interactions of species, hypergraphical approaches become essential.

Boolean networks describe interaction networks in a more constrained and deterministic manner than interaction graphs, enabling discrete simulations. Herein we have demonstrated that signed directed hypergraphs are capable to represent the logical structure of any Boolean network. The hypergraphical coding of Boolean networks, which relies on the sum-of-product representation of Boolean networks (using only AND, OR and NOT operations), has several advantages: it is rather intuitive, it mostly corresponds to the underlying molecular mechanisms, and it is easy to store and to handle. A hypergraphical representation of a Boolean network also establishes a direct link to the corresponding (underlying) interaction graph which can easily be derived from the hypergraph. Finally, it facilitates a logical signal flow (or steady state) analysis in Boolean networks which, as demonstrated in this report, is useful for studying and predicting the qualitative input-output behavior of signaling networks with respect to a given, possibly incomplete, set of initial state values. This can be achieved here without an explicit enumeration and/or simulation of all possible trajectories.

In general, Boolean networks rely on stronger assumptions and knowledge than interaction graphs and a pure logical description of all interactions is not always possible. We have suggested extensions of the Boolean framework, such as incomplete truth tables of logical operations, to handle these problems.

As pointed out by many authors (e.g. [67-69]) the logical description and analysis of large signaling networks has a strong relationship to electrical circuit analysis; however, there still seems to be a large potential in employing theoretical and software tools from electrical engineering and Boolean logic for investigating interaction networks. Signal flow analysis as introduced herein might be another step in this direction.

Describing signal and mass flows equivalently as interactions, as done herein, offers high flexibility and enables

one to integrate several types of cellular networks (such as metabolic, signalling or regulatory ones) into one framework. However, the higher level of abstraction comes with the price that some molecular mechanisms are not always precisely represented, as, for instance, the stoichiometric coefficients in mass flows.

The potential of the introduced methods were demonstrated on a model of a small part of the signaling machinery of T-cells. The size and complexity of the model was chosen so that the methods could be tested on a case study of real size and complexity, while at the same time the results could be (at least in part) intuitively understood and proofed. If enough information is available, similar models could be set up for any other signaling network.

Certainly, these tools will be especially useful in larger interaction networks. Our current and future work aims to expand and subsequently analyse the T-cell model, with hopes that further understanding of this complex network can improve current knowledge about important illnesses, such as autoimmune diseases and leukemia. This is certainly a challenging task, but the potential described here makes it a worthy endeavour.

Availability and requirements

For academic purposes,*CellNetAnalyzer* can be obtained for free via the website

http://www.mpi-magdeburg.mpg.de/projects/cna/cna.html

Note that *CellNetAnalyzer* requires MATLAB® version 6.1 or higher.

List of abbreviations

LIH: logical interaction hypergraph

LSS(s): logical steady state(s)

MCS(s): minimal cut set(s)

MIS(s): minimal intervention set(s)

Authors' contributions

SK elaborated the framework and the methods for studying interaction graphs and logical interaction hypergraphs and implemented algorithms in *CellNetAnalyzer*. JSR mainly constructed the logical model of T-cell signalling and he also contributed to the methods' development. JL and LS assisted in the construction of the T-cell model. EDG initiated the project on methods for structural analysis of signaling networks. SK and JSR prepared the manuscript jointly. All authors have read and accepted the manuscript.

Acknowledgements

The work was supported by grants from the Deutsche Forschungsgemeinschaft (FOR521) and Bundesministerium für Bildung und Forschung. Thanks to the signaling group at the Institute of Immunology, especially to B. Schraven, for helpful discussions on the T-cell signaling model and to J. Gagneur, J. Behre, U.U. Haus, R. Weismantel and Annegret Wagler for fruitful discussions on theoretical issues. We thank R. Hemenway for critical reading the manuscript.

References

1. Downward J: **The ins and outs of signalling.** *Nature* 2001, **411:**759-762.
2. Papin JA, Hunter T, Palsson BO, Subramaniam S: **Reconstruction of cellular signalling networks and analysis of their properties.** *Nat Rev Mol Cell Biol* 2005, **6:**99-111.
3. Kholodenko BN: **Negative feedback and ultrasensitivity can bring about oscillations in the mitogen-activated protein kinase cascades.** *Eur J Biochem* 2000, **267:**1583-8.
4. Schoeberl B, Eichler-Jonsson C, Gilles ED, Müller G: **Computational modeling of the dynamics of the MAP kinase cascade activated by surface and internalized EGF receptors.** *Nat Biotech* 2002, **20:**370-375.
5. Sauro HM, Kholodenko BN: **Quantitative analysis of signaling networks.** *Biophysics & Molecular Biology* 2004, **86:**5-43.
6. Sasagawa S, Ozaki Y, Fujita K, Kuroda S: **Prediction and validation of the distinct dynamics of transient and sustained ERK activation.** *Nat Cell Biol* 2005, **7:**365-373.
7. Styczynski MP, Stephanopoulos G: **Overview of computational methods for the inference of gene regulatory networks.** *Computers & Chemical Engineering* 2005, **29:**519-534.
8. Sachs K, Perez O, Pe'er D, Lauffenburger D, Nolan GP: **Causal protein signaling networks dreived from multiparamter single-cell data.** *Science* 2005, **308:**523-529.
9. de la Fuente A, Brazhnik P, Mendes P: **Linking the genes: inferring quantitative gene networks from microarray data.** *Trends Genet* 2002, **18:**395-398.
10. Sontag E, Kiyatkin A, Kholodenko BN: **Inferring dynamic architecture of cellular networks using time series of gene expression, protein and metabolite data.** *Bioinformatics* 2004, **20:**1877-1886.
11. Price ND, Reed JL, Palsson BO: **Genome-scale models of microbial cells: evaluating the consequences of constraints.** *Nat Rev Microbiol* 2004, **2:**886-897.
12. Oda K, Matsuoka Y, Funahashi A, Kitano H: **A comprehensive pathway map of epidermal growth factor receptor signaling.** *Molecular Systems Biology* . 10.1038/msb4100014
13. Jeong H, Mason SP, Barabasi AL, Oltvai ZN: **Lethality and centrality in protein networks.** *Nature* 2001, **411:**41-42.
14. Papin JA, Palsson BO: **Topological analysis of mass-balanced signaling networks: a framework to obtain emergent network properties including crosstalk.** *J Theor Biol* 2004, **227:**283-297.
15. Papin JA, Palsson BO: **The JAK-STAT Signaling Network in the Human B-Cell: An Extreme Signaling Pathway Analysis.** *Biophys J* 2004, **87:**37-46.
16. Zevedei-Oancea I, Schuster S: **A theoretical framework for detecting signal transfer routes in signalling networks.** *Computers & Chemical Engineering* 2005, **29:**597-617.
17. Binder B, Heinrich R: **Interrelations between dynamical properties and structural characteristics of signal transduction networks.** *Genome Inform* 2004, **15:**13-23.
18. Wagner A, Wright J: **Compactness and cycles in signal transduction and transcriptional regulation networks: a signature of natural selection?** *Advances in Complex Systems* 2005, **7:**419-432.
19. Kaufman M, Andris F, Leo O: **A logical analysis of T cell activation and anergy.** *Proc Natl Acad Sci U S A* 1999, **96:**3894-3899.
20. Mendoza L, Thieffry D, Alvarez-Buylla ER: **Genetic control of flower morphogenesis in Arabidopsis thaliana: a logical analysis.** *Bioinformatics* 1999, **15:**593-606.
21. Thomas R, D'Ari R: *Biological feedback* Boca Raton: CRC Press; 1990.
22. Albert R, Othmer HG: **The topology of the regulatory interactions predicts the expression pattern of the Drosophila segment polarity genes.** *J Theor Biology* 2003, **223:**1-18.
23. Espinosa-Soto C, Padilla-Longoria P, Alvarez-Buylla ER: **A gene regulatory network model for cell-fate determination during**

Arabidopsis thaliana flower development that is robust and recovers experimental gene expression profiles. *Plant Cell* 2004, **16:**2923-2939.
24. Gagneur J, Casari G: **From molecular networksto qualitative cell behavior.** *FEBS Letter* 2005, **579:**1867-1871.
25. Schuster S, Fell DA, Dandekar T: **A general definition of metabolic pathways useful for systematic organization and analysis of complex metabolic networks.** *Nat Biotechnol* 2000, **18:**326-332.
26. Stelling J, Klamt S, Bettenbrock K, Schuster S, Gilles ED: **Metabolic network structure determines key aspects of functionality and regulation.** *Nature* 2002, **420:**190-193.
27. Kauffman KJ, Prakash P, Edwards JS: **Advances in flux balance analysis.** *Curr Opin Biotechnol* 2003, **14:**491-496.
28. Klamt S, Gilles ED: **Minimal cut sets in biochemical reaction networks.** *Bioinformatics* 2004, **20:**226-234.
29. Klamt S: **Generalised concept of minimal cut sets in biochemical networks.** *Biosystems* 2006, **83:**233-247.
30. Schlessinger J: **Cell signaling by receptor tyrosine kinases.** *Cell* 2000, **103:**211-25.
31. de Jong H: **Modeling and simulation of genetic regulatory systems: a literature overview.** *J Comp Biol* 2002, **9:**67-103.
32. Gross JL, Yellen J: *Handbook of graph theory* Boca Raton: CRC Press; 2004.
33. Heinrich R, Schuster S: *The Regulation of Cellular Systems* New York: Chapman & Hall; 1996.
34. Bollabas B: *Modern graph theory* New York, Springer-Verlag; 1998.
35. Thomas R, Kaufman M: **Multistationarity, the basis of cell differentiation and memory. I Structural conditions of multistationarity and other non-trivial behavior.** *Chaos* 2001, **11:**170-179.
36. Angeli D, Ferrell JE, Sontag ED: **Detection of multistability, bifurcations and hysteresis in a large class of biological positive-feedback systems.** *PNAS* 2004, **101:**1822-1827.
37. Reth M, Brummer T: **Feedback regulation of lymphocyte signalling.** *Nat Rev Immunol* 2004, **4:**269-77.
38. Xiong W, Ferrel JR Jr: **A positive-feedback-based bistable 'memory module' that governs a cell fate decision.** *Nature* 2003, **426:**460-5.
39. Soule C: **Graphic requirements for multistationarity.** *ComPlexUs* 2003, **1:**123-133.
40. Tarjan R: **Enumeration of the elementary circuits of a directed graph.** *SIAM J Comput* 1973, **2:**211-216.
41. Gleiss PM, Stadler PF, Wagner A, Fell DA: **Relevant cycles in chemical reaction networks.** *Adv Complex S* 2001, **4:**207-226.
42. Lawler E: *Combinatorial Optimization – Networks and Matroids* Mineola: Dover Publications; 2001.
43. Klamt S, Gagneur J, Kamp A: **Algorithmic approaches for computing elementary modes in large biochemical reaction networks.** *IEE Proceedings Systems Biology* 2005, **152(4):**249-255.
44. Gagneur J, Klamt S: **Computation of elementary modes: a unifying framework and the new binary approach.** *BMC Bioinformatics* 2004, **5:**175.
45. Xiong M, Jinying Z, Xiong H: **Network-based regulatory pathways analysis.** *Bioinformatics* 2004, **20:**2056-2066.
46. Urbanczik R, Wagner C: **An improved algorithm for stoichiometric network analysis: theory and applications.** *Bioinformatics* 2005, **21:**1203-1210.
47. Pfeiffer T, Sánchez-Valdenebro I, Nuño JC, Montero F, Schuster S: **METATOOL: For studying metabolic networks.** *Bioinformatics* 1999, **15:**251-257.
48. Newman MEJ: **Scientific collaboration networks: II. Shortest paths, weighted networks and centrality.** *Phys Rev E* 2001, **64:**016132.
49. Zeigarnik AV: **On hypercycles and hypercircuits in hypergraphs.** In *Discrete Mathematical Chemistry Volume 51*. Edited by: Hansen P, Fowler PW, Zheng M. DIMACS series in discrete mathematics and theoretical computer science; 2000:377-383.
50. Mendelson E: *Schaum's outline of Boolean algebra and switching circuits* McGraw-Hill, New York; 1970.
51. Kauffman SA: **Metabolic stability and epigenesis in randomly constructed genetic nets.** *J Theor Biol* 1969, **22:**437-467.
52. Devloo V, Hansen P, Labbe M: **Identification of all steady states in large networks by logical analysis.** *Bulletin of Mathematical Biology* 2003, **65:**1025-1051.
53. Stephanopoulos GN, Aristidou AA, Nielsen J: *Metabolic Engineering* Academic Press, San Diego; 1998.
54. Klamt S, Schuster S, Gilles ED: **Calculability analysis in underdetermined metabolic networks illustrated by a model of the central metabolism in purple nonsulfur bacteria.** *Biotechnol Bioeng* 2002, **77:**734-751.
55. Ebenhöh O, Handorf T, Heinrich R: **Structural analysis of expanding metabolic networks.** *Genome Informatics* 2004, **15:**35-45.
56. Klamt S, Stelling J, Ginkel M, Gilles ED: **FluxAnalyzer: exploring structure, pathways, and flux distributions in metabolic networks on interactive flux maps.** *Bioinformatics* 2003, **19:**261-269.
57. [http://www.mpi-magdeburg.mpg.de/projects/cna/cna.html].
58. Benjamini E, Coico R, Sunshine G: *Immunology-A short course* Wiley-Liss; 2000.
59. Huang Y, Wange RL: **T cell receptor signaling: beyond complex complexes.** *J Biol Chem* 2004, **279:**28827-30.
60. Togni M, Lindquist J, Gerber A, Kolsch U, Hamm-Baarke A, Kliche S, Schraven B: **The role of adaptor proteins in lymphocyte activation.** *Mol Immunol* 2004, **41:**615-630.
61. Horejsi V, Zhang W, Schraven B: **Transmembrane adaptor proteins: organizers of immunoreceptor signalling.** *Nat Rev Immunol* 2004, **4:**603-16.
62. Torgersen KM, Vang T, Abrahamsen H, Yaqub S, Horejsi V, Schraven B, Rolstad B, Mustelin T, Tasken K: **Release from tonic inhibition of T cell activation through transient displacement of C-terminal Src kinase (Csk) from lipid rafts.** *J Biol Chem* 2001, **276:**29313-29318.
63. Filipp D, Julius M: **Lipid rafts: resolution of the "fyn problem"?** *Mol Immunol* 2004, **41:**645-56.
64. Schaeffer EM, Debnath J, Yap G, McVicar D, Liao XC, Littman DR, Sher A, Varmus HE, Lenardo MJ, Schwartzberg PL: **Requirement for Tec kinases Rlk and Itk in T cell receptor signaling and immunity.** *Science* 1999, **284:**638-41.
65. Roose JP, Mollenauer M, Gupta VA, Stone J, Weiss A: **A diacylglycerol-protein kinase C-RasGRP1 pathway directs Ras activation upon antigen receptor stimulation of T cells.** *Mol Cell Biol* 2005, **25:**4426-41.
66. Duan L, Reddi AL, Ghosh A, Dimri M, Band H: **The Cbl Family and Other Ubiquitin Ligases Destructive Forces in Control of Antigen Receptor Signaling.** *Immunity* 2004, **21:**7-17.
67. Genoud T, Santa Cruz MBT, Metraux JP: **Numeric simulation of plant signaling networks.** *Plant Physiology* 2001, **126:**1430-1437.
68. Hasty J, McMillen D, Collins JJ: **Engineered gene circuits.** *Nature* 2002, **420:**224-230.
69. Lok L: **Software for signaling networks, electronic and cellular.** *Science's STKE* 2002, **122:**PE11.

Appendix 8

Normal T-cell development and immune functions in TRIM-deficient mice

Kölsch U., Arndt B., Reinhold D., Lindquist JA., Jüling N., Kliche S., Pfeffer K., Bruyns E., Schraven B., and **Simeoni L.** (2006) *Mol Cell Biol.* 26:3639-48.

MOLECULAR AND CELLULAR BIOLOGY, May 2006, p. 3639–3648 Vol. 26, No. 9
0270-7306/06/$08.00+0 doi:10.1128/MCB.26.9.3639–3648.2006

Normal T-Cell Development and Immune Functions in TRIM-Deficient Mice

Uwe Kölsch,[1†] Börge Arndt,[1] Dirk Reinhold,[1] Jonathan A. Lindquist,[1] Nicole Jüling,[1] Stefanie Kliche,[1] Klaus Pfeffer,[2] Eddy Bruyns,[3] Burkhart Schraven,[1] and Luca Simeoni[1]*

Otto von Guericke University, Institute of Immunology, Leipziger Str. 44, 39120 Magdeburg,[1] FOCUS Clinical Drug Development GmbH, Im Neuenheimer Feld 515, 69120 Heidelberg,[2] and Heinrich Heine University, Institute of Medical Microbiology, Universitätsstr. 1, 40225 Düsseldorf,[3] Germany

Received 2 December 2005/Returned for modification 27 January 2006/Accepted 13 February 2006

The transmembrane adaptor molecule TRIM is strongly expressed within thymus and in peripheral CD4$^+$ T cells. Previous studies suggested that TRIM is an integral component of the T-cell receptor (TCR)/CD3 complex and might be involved in regulating TCR cycling. To elucidate the in vivo function of TRIM, we generated TRIM-deficient mice by homologous recombination. TRIM$^{-/-}$ mice develop normally and are healthy and fertile. However, the animals show a mild reduction in body weight that appears to be due to a decrease in the size and/or cellularity of many organs. The morphology and anatomy of nonlymphoid as well as primary and secondary lymphoid organs is normal. The frequency of thymocyte and peripheral T-cell subsets does not differ from control littermates. In addition, a detailed analysis of lymphocyte development revealed that TRIM is not required for either positive or negative selection. Although TRIM$^{-/-}$ CD4$^+$ T cells showed an augmented phosphorylation of the serine/threonine kinase Akt, the in vitro characterization of peripheral T cells indicated that proliferation, survival, activation-induced cell death, migration, adhesion, TCR internalization and recycling, TCR-mediated calcium fluxes, tyrosine phosphorylation, and mitogen-activated protein family kinase activation are not affected in the absence of TRIM. Similarly, the in vivo immune response to T-dependent and T-independent antigens as well as the clinical course of experimental autoimmune encephalomyelitis, a complex Th1-mediated autoimmune model, is comparable to that of wild-type animals. Collectively, these results demonstrate that TRIM is dispensable for T-cell development and peripheral immune functions. The lack of an evident phenotype could indicate that TRIM shares redundant functions with other transmembrane adaptors involved in regulating the immune response.

Upon ligation of the T-cell receptor (TCR) by peptide/major histocompatibility complex complexes, a plethora of signaling cascades are initiated within T cells that finally result in T-cell activation. It is well established that the TCR itself is not capable of transducing signals, as it possesses only a short intracellular tail that lacks any known signaling motif. Rather, signal transduction via the TCR is accomplished by the invariant CD3γ, CD3δ, CD3ε, and ζ subunits, which all possess particular amino acid motifs named ITAMs (immunoreceptor tyrosine-based activation motifs) in their cytoplasmic domains (17, 35). Overall, the TCR/CD3/ζ complex is organized in dimers (CD3εδ and CD3εγ dimers that noncovalently associate with the TCRαβ heterodimer and the TCRζ homodimer) and contains in total 10 ITAMs: 1 in each of the CD3γ, CD3δ, and CD3ε subunits and 3 in each of the two TCRζ chains. Upon phosphorylation by Src family kinases, the ITAMs are converted into high-affinity binding sites for the cytosolic protein tyrosine kinase ZAP-70, which is in turn recruited from the cytosol to the activated TCR by its tandem SH2 domains. After binding to the phosphorylated ITAMs, ZAP-70 serves as a substrate for Src kinases and becomes activated by phosphorylation. The biochemical cascade originating from the ligated TCR is then further propagated by the transmembrane adaptor protein LAT (linker for activation of T cells) which links the TCR to the mitogen-activated protein kinase (MAPK) and Ca^{2+} pathways after phosphorylation by ZAP-70 (12, 37).

In addition to being the signal transducing subunits of the TCR, the CD3 and TCRζ chains are also required for the correct expression of the TCR at the plasma membrane (for a review, see reference 1). TCR assembly begins in the endoplasmic reticulum with the pairing of CD3ε with either CD3γ or CD3δ. Once the εδ and εγ heterodimers are formed, they noncovalently associate with the TCRα/β heterodimer. The last component to be incorporated in the complex is the TCRζ homodimer, which overrides an endoplasmic reticulum retention signal within the CD3ε chain, thus allowing the complex to be transported to the plasma membrane (9).

Recent findings have indicated that the invariant chains of the TCR/CD3 complex might associate with a variety of additional molecules. For example, the TCRζ chain has been proposed to interact with SLAP-2 (26), TRIM (4, 20), CTLA4 (7), and Unc119 (5, 14), while CD3ε apparently complexes with CAST (36) and Nck (13). The physiological relevance of these interactions is so far not completely understood. However, it has been proposed that they could serve to integrate or regulate the signal capability of the TCR/CD3 complex or to modulate the expression levels of the T-cell receptor.

The nonraft transmembrane adaptor protein TRIM (T-cell receptor interacting molecule) is exclusively expressed in T

* Corresponding author. Mailing address: Institute of Immunology, Otto von Guericke University, Leipziger Str. 44, 39120 Magdeburg, Germany. Phone: 49-391-6717894. Fax: 49-391-6715852. E-mail: luca.simeoni@medizin.uni-magdeburg.de.

† Present address: Clinic of Pediatric and Neonatology, Otto von Guericke University, 39112 Magdeburg, Germany.

lymphocytes. TRIM has been shown to coprecipitate with the TCR/CD3 complex under mild detergent conditions, and, similar to the TCR, its expression is downregulated after TCR triggering (4). A recent study demonstrated that TRIM preferentially interacts with the TCR complex via the TCRζ chain and that all three domains of TRIM (extracellular, transmembrane, and cytoplasmic domains) are required for this interaction (20).

The functional relevance of the association between TRIM and TCRζ has been addressed by overexpressing TRIM in the Jurkat T cell line (20). These experiments revealed that cells overexpressing TRIM show a considerable increase in cell surface expression of TCRαβ and CD3ε caused by TRIM-mediated inhibition of spontaneous TCR internalization (20). As expected, the enhanced expression levels of the TCR in TRIM transfectants concomitantly lead to an increased TCR-mediated Ca^{2+} flux. Based upon these data, it was proposed that TRIM regulates TCR-mediated signaling by modulating the expression levels of the TCR on the cell surface.

TRIM possesses three tyrosine-based signaling motifs (TBSMs) within its cytoplasmic domain that are potentially involved in regulating TCR-mediated signal transduction. One of these motifs (YEQM) represents a consensus motif for the p85 subunit of phosphatidylinositol 3-kinase (PI3K) and, indeed, TRIM is capable of binding p85 via the YEQM motif after phosphorylation by Src kinases (4). Similarly, the two other TBSMs also become phosphorylated upon TCR engagement, but the molecules binding to these motifs are yet to be identified (20).

To study the function of TRIM in vivo, we generated TRIM-deficient mice by homologous recombination. Collectively, the functional and biochemical characterization of $TRIM^{-/-}$ mice suggest that TRIM is dispensable for the development and the function of the immune system.

MATERIALS AND METHODS

Mice. $TRIM^{-/-}$ mice were generated by homologous recombination by replacing a part of exon 1 (including ATG) and exon 2 (coding for the entire transmembrane region) with a NEO cassette. The linearized targeting construct was transfected into SVJ129-derived embryonic stem cells, and G418-selected clones were transferred into C57BL/6 blastocysts as previously described (2). Germ line mutated animals were backcrossed onto the C57BL/6 background for more than 10 generations in a conventional animal facility. Animals were genotyped by PCR using the following primers: 5′TRIM (CGT CTC TGC TTC TCT ACA TAG TGG), 3′TRIM (GCT CTG GAT GCC CCT TCT TCC), and 3′Neo (GAC GTG CTA CTT CCA TTT GTC ACG TCC) (BioTez GmbH).

OT-I and OT-II TCR transgenic mice were kindly provided by Percy Knolle, P14 mice were provided by Thomas Kammerthoens, and H-Y TCR transgenic mice were provided by Gary Koreztky. For TCR transgenic studies, $TRIM^{-/-}$ mice crossed with TCR transgenic mice were obtained by crossing $TRIM^{-/-}$ mice with $TRIM^{+/-}$ mice with TCR heterozygote transgenics.

Flow cytometry analysis. Single-cell suspensions were obtained from thymus, lymph nodes, spleen, and bone marrow by dissociation of isolated tissues through a 70-μm mesh. Cells were stained with fluorescence-labeled monoclonal antibodies against CD3 (145-2C11), CD4 (RM4-5), CD5 (53-7.3), CD8 (53-6.7), CD25 (7D4), CD44 (IM7), CD45RB (363.16A), CD62L (MEL-14), CD69 (H1.2F3), TCRβ (H57-597), TCRγδ (GL3), B220 (RA3-6B2), and TCRVα2 (B20.1), all obtained from BD Biosciences, or with fluorescein isothiocyanate (FITC)-labeled HY-TCR (T3.70) (eBiosciences) for 30 min at 4°C. Cell-associated fluorescence was analyzed by a FACSCalibur and Cell Quest Pro software (BD Biosciences).

Immunoblotting. For all biochemical analyses, $CD4^+$ T cells were purified by an AutoMACS magnetic isolation system according to the manufacturer's instructions (Miltenyi). Cells were either left unstimulated, stimulated with 10 μg/ml of biotinylated CD3ε antibody (145-2C11; BD Biosciences), or stimulated with CD3 plus 10 μg/ml of biotinylated CD28 (BD Biosciences) monoclonal antibody (MAb) followed by cross-linking with 25 μg/ml of streptavidin (Dianova) at 37°C. Cells were lysed in lysis buffer containing 1% NP-40, 1% laurylmaltoside (*N*-dodecyl β-D-maltoside), 50 mM Tris, pH 7.5, 140 mM NaCl, 10 mM EDTA, 10 mM NaF, 1 mM phenylmethylsulfonyl fluoride, 1 mM Na_3VO_4. Proteins were separated by sodium dodecyl sulfate-polyacrylamide gel electrophoresis, transferred onto polyvinylidene difluoride or nitrocellulose membranes, and blotted with the following antibodies: anti-phosphotyrosine (4G10), anti-ERK1/2 (pT202/pT204), anti-JNK (pT183/pY185), anti-p38 (pT180/pT182), anti-phospho-Akt (S473), anti-Akt, all from Cell Signaling, and anti-ZAP70 (clone Z24820; Transduction Laboratories), anti-ERK1/2 (Cell Signaling), or β-actin (Sigma). Where PI3K inhibitor was used, $CD4^+$ T cells were preincubated with 100 nM wortmannin (Calbiochem) for 30 min at 37°C prior to stimulation.

Ca^{2+} flux. For Ca^{2+} measurement, cells were incubated for 30 min with 3.75 μg/ml indo-1-AM (Molecular Probes) in phenol red-free RPMI 1640 medium (GIBCO BRL) containing 10% fetal calf serum (FCS). After washing, the cells were incubated for 30 min at 37°C in RPMI 1640 and stained with CD4 and CD8 and incubated with 10 μg/ml biotinylated CD3 (145-2C11) MAbs at 4°C. Calcium fluxes were induced by cross-linking the TCR/CD3 complex with 75 μg/ml streptavidin and were measured using an LSR flow cytometer (BD Biosciences).

Proliferation assay. $CD4^+$ T cells were purified from single-cell suspensions of splenocytes by an AutoMACS magnetic isolation system according to the manufacturer's instructions (Miltenyi). Cells were stimulated for 72 h with either the indicated concentrations of plate-bound CD3 MAb (145-2C11), 4 μg/ml concanavalin A (ConA) (Calbiochem), or 2.5 μg/ml staphylococcal enterotoxin B (SEB; Sigma), or with 2×10^{-9} M phorbol-12-myristate-13-acetate (PMA) (Calbiochem) and 0.5 μg/ml ionomycin (Calbiochem) in 96-well U-bottomed plates (Corning Costar) at a density of 25×10^4 cells per well in 200 μl of RPMI medium supplemented with penicillin, streptomycin, β-mercaptoethanol, and 10% FCS. Cells were pulsed with 1 μCi [^{3}H]thymidine per well during the last 8 h.

Cell survival assays. Thymocytes or purified splenic $CD4^+$ T cells were incubated for 24 h in the presence of the following stimuli: plate-bound CD3 MAb (145-2C11), $CD3^+$ CD28 MAb (37.51), 1 μM etoposide (Sigma), 1 μg/ml Fas MAb (BD Biosciences) plus 30 μg/ml cycloheximide (Calbiochem), or 2 nM dexamethasone (Sigma). Cells were harvested and stained with annexin V and propidium iodide (BenderMedSystem) according to the manufacturer's instructions. Apoptotic cells were defined as annexin V-positive and propidium iodide-negative cells.

For activation-induced cell death (AICD), 2×10^6 $CD4^+$ lymphocytes were stimulated with 5 μg/ml plate-bound CD3 MAb in RPMI in flat-bottomed 24-well plates (Corning Costar) for 2 days. Cells were then grown in medium containing 5 IU/ml recombinant human interleukin-2 (rIL-2) (PeproTech) for an additional 2 days in flat-bottomed 24-well plates, and 1×10^6 cells were restimulated overnight with 5 μg/ml plate-bound CD3 MAb in new 24-well plates with medium containing 5 IU/ml rIL-2. Apoptosis was measured as described above.

Migration assay. Cell migration was performed in a 24-well Transwell plate (Corning Costar) with 3-μm-pore polycarbonate filters. Freshly isolated lymph node cells were resuspended at a density of 4×10^7 cells/ml in RPMI containing 0.5% bovine serum albumin (BSA). One hundred microliters of cell suspension was placed in the upper chamber, and 600 μl of medium was placed in the lower chamber. After equilibration at 37°C for 1 h, 50 nM of mouse recombinant SDF1β (PeproTech) was added to the wells, and the plates were incubated for an additional 3 h. Cells were then harvested, stained with anti-CD4 and anti-CD8, and counted by fluorescence-activated cell sorting (FACS). Duplicates were used for each condition.

Mouse immunization and ELISA. Two- to 3-month-old mice were immunized intraperitoneally with 20 μg/animal 2,4-dinitrophenyl (DNP)–keyhole limpet hemocyanin (KLH) (Calbiochem) in 200 μl complete Freund's adjuvant (Sigma) and were boosted 10 days later with 20 μg/animal DNP-KLH in 200 μl incomplete Freund's adjuvant (Sigma). Before and after immunization, mice were bled and the amount of hapten-specific immunoglobulins was determined by enzyme-linked immunosorbent assay (ELISA) as previously described (31). Briefly, plates were coated with 3 μg/ml DNP-BSA in bicarbonate buffer overnight at 4°C. Nonspecific binding was prevented by blocking the plates with 1% BSA for 2 h at room temperature. Serial dilutions of mouse sera were incubated overnight at 4°C, and the specific binding was detected using alkaline-phosphatase-labeled goat anti-mouse immunoglobulin M (IgM; Serotec) or goat anti-mouse IgG (subclasses 1, 2a, 2b, 3; Dianova).

Basal levels of immunoglobulins were measured as previously described (31).

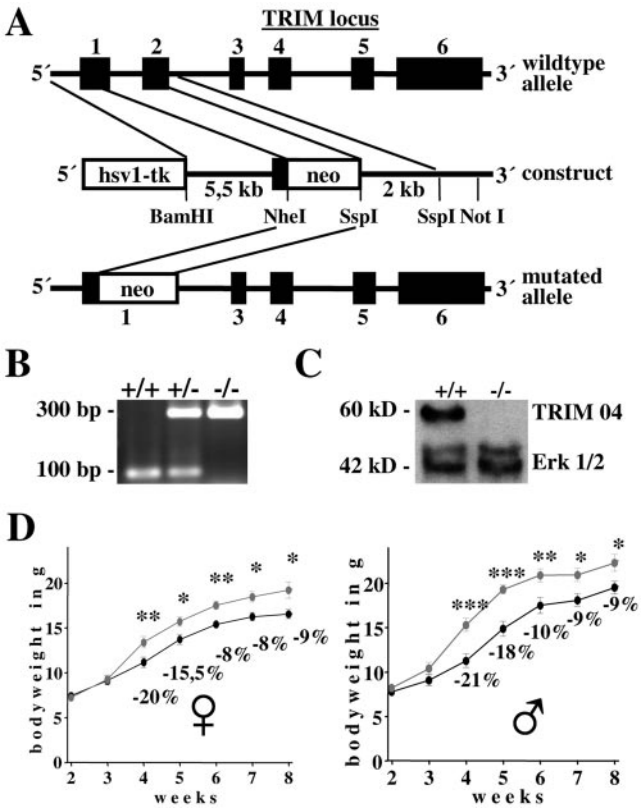

FIG. 1. Generation of TRIM-deficient mice. (A) Partial restriction map of the TRIM locus and the targeting construct. Exons are represented by filled boxes. Neo, neomycin resistance cassette; Tk, thymidine kinase. (B) PCR analysis of TRIM wild type, heterozygous, and knockout mice. (C) Western blot analysis of cell lysates prepared from wild-type and TRIM$^{-/-}$ thymocytes. The blot was probed with the monoclonal anti-TRIM antibody TRIM04 and with the polyclonal anti-ERK1/2 antibody to show equal loading. (D) TRIM-deficient mice display lower body weights. Shown are growth curves of female and male TRIM$^{+/+}$ or TRIM$^{-/-}$ animals ($n = 15$ mice per group). Statistically significant differences are indicated: *, $P < 0.05$; **, $P < 0.005$; ***, $P < 0.001$.

TCR internalization and recycling. For TCR internalization assays, 2×10^6 lymph node cells were precoated for 30 min at 4°C with phycoerythrin (PE)-labeled TCRβ (H57-597) MAb in RPMI containing 10% FCS, 50 μM β-mercaptoethanol, penicillin, and streptomycin. After washing, cells were plated in 96-well plates at a density of 1×10^6 cells per 200 μl of medium and incubated at 37°C for the indicated times. TCR internalization was measured as previously described (10). Briefly, TCR internalization was stopped by washing the cells in ice-cold phosphate-buffered saline (PBS) containing 0.1% sodium azide and 1% BSA. The surface-bound antibody was removed by washing lymphocytes in stripping buffer (100 mM Glycin, 100 mM NaCl, pH 2.5). The intracellular fluorescence was measured by FACS. To distinguish the different lymphocyte subsets, cells were stained with CD4-FITC and CD8-CyChrome MAbs after stripping. Internalization of the TCR was calculated according to the following equation, as previously published (10, 16, 32): % internalization = 100 × [(acid-resistant fluorescence at t − cellular autofluorescence)/(fluorescence of cells stained with TCRβ-PE MAb − cellular autofluorescence)], where t is time.

A TCR recycling assay was performed as reported previously (24). Briefly, 4×10^6 freshly isolated lymph node cells were stained at 37°C with 1 μg/ml PE-labeled anti-TCRβ for 1 h. After washing, surface-bound antibody was stripped as reported above. To allow reexpression of the internalized receptor, cells were then incubated at 37°C for different times, washed in ice-cold PBS containing 0.1% sodium azide and 1% BSA, and again stripped in low-pH buffer. Lymphocytes were stained for CD4 and CD8 and analyzed by FACS. Recycled TCR was calculated using the following formula: % recycled = 100 × [(acid-resistant fluorescence after second low-pH buffer treatment − autofluorescence)/(acid-resistant fluorescence after first low-pH buffer treatment)].

EAE. Experimental autoimmune encephalomyelitis (EAE) was induced and scored as previously described (28, 31).

RESULTS AND DISCUSSION

Generation of TRIM-deficient mice. To assess the role of TRIM within the immune system, the *TRIM* gene was disrupted by homologous recombination in embryonic stem (ES) cells (Fig. 1A). The targeting vector replaced part of exon 1 and exon 2 of the *TRIM* gene with a *neomycin* selection cassette. The deleted region contained the translation start site as well as the entire extracellular and transmembrane regions of TRIM. The linearized targeting vector was introduced into ES cells by electroporation, and cells were selected with G418 and ganciclovir. Successfully targeted ES clones were injected into C57BL/6 blastocysts. To avoid potential phenotypic bias due to inbred genetics, germ line-competent chimeric mice were backcrossed on a C57BL/6 genetic background for more than 10 generations. Mutation of the *TRIM* gene was confirmed by genomic PCR (Fig. 1B). To ensure that the targeted allele results in loss of protein, lysates were prepared from thymocytes of null and wild-type mice and analyzed by anti-TRIM Western blotting with two different monoclonal or two polyclonal anti-TRIM reagents, all directed at particular regions of the cytoplasmic tail of TRIM. Under all conditions tested, we did not detect any anti-TRIM-reactive product, corresponding either to the full-length or to a truncated (cytoplasmic) form in TRIM$^{-/-}$ thymocytes (Fig. 1C and data not shown). These data demonstrate that the *TRIM* gene was indeed successfully inactivated. Analysis of genotypes at weaning revealed that the mutated allele segregates with the expected Mendelian frequency, thus indicating that TRIM does not cause embryonic lethality. Indeed, among the 608 viable offspring obtained by breeding TRIM$^{+/-}$ mice, 149 (24.5%) were TRIM$^{+/+}$, 290 (47.7%) were TRIM$^{+/-}$, and 169 (27.8%) were TRIM$^{-/-}$.

TRIM$^{-/-}$ mice are viable and fertile but display a smaller body size. Anatomical and histological analysis of hematoxylin-eosin sections of liver, muscle, smooth muscle from heart, brain, testis, gut, and primary and secondary lymphoid organs such as thymus, spleen, and lymph nodes from TRIM-deficient mice did not reveal any detectable abnormalities (data not shown). Moreover, TRIM$^{-/-}$ mice were viable and fertile. However, compared to sex-matched wild-type littermates, TRIM-deficient mice displayed a mild reduction (about 10 to 20%) in body weight which became evident at 3 weeks of age and remained constant throughout the aging process (Fig. 1D). Accordingly, we found a decrease (about 10 to 20%) in the size of several organs, such as thymus, spleen, lymph nodes, liver, kidney, and heart (data not shown). Because TRIM$^{-/-}$ and TRIM$^{+/-}$ mice maintain constant organ-to-body-mass ratios, the difference in body weight could be due to an overall reduction in cell size or in cellularity.

Analysis of lymphoid organs (thymus, lymph nodes, spleen, and bone marrow) revealed that cell sizes were normal, whereas cell numbers within the organs were significantly reduced (about 20% [Tables 1 and 2 and data not shown]). This indicates that loss of TRIM results in a reduction of organ cellularity and consequently in body mass. Since TRIM ap-

TABLE 1. T-cell subsets in thymus[a]

TRIM status	*n*	Total no. of cells (10^6)	No. of cells with indicated phenotype				CD4/CD8 ratio
			$CD4^-$ $CD8^-$	$CD4^+$	$CD8^+$	$CD4^+$ $CD8^+$	
$TRIM^{+/+}$	19	119.8 (9.7)	3.9 (0.4)	11.8 (1.1)	3.4 (0.4)	100.6 (8.3)	3.8 (0.2)
$TRIM^{-/-}$	20	92.0 (9.2)	2.8 (0.3)	8.9 (1.2)	2.7 (0.3)	77.5 (8.0)	3.5 (0.2)

[a] The numbers of lymphocyte subsets were determined on the basis of the total cell count and flow cytometric analysis shown in Fig. 2. Data represent means and standard errors of the means (in parentheses).

pears to be exclusively expressed in T cells, the reason for this unexpected observation remains elusive. At present, it is not known whether the immune system is directly involved in the regulation of body weight (particularly in healthy animals such as TRIM-deficient mice, which also do not show any histological signs of chronic inflammation that could be responsible for reduced body weight). A decrease in body mass has been observed in several knockout strains of mice in which molecules that are expressed in T cells (3, 6, 8, 15, 22, 23) were eliminated. However, in these models, the reduction in body weight is caused by alterations of organ development or by altered hormone action (as the molecules under investigation are also expressed outside of the hematopoietic system) but not by impaired immune functions. One possible explanation for our observation, therefore, could be that TRIM is not only expressed in T cells but also in other types of cells, e.g., hormone-producing cells. In this regard it is worth mentioning that Ikaros, a well-known lymphoid transcription factor, has recently been found to be expressed in cells of the pituitary gland (11). It appears that Ikaros is required not only for the development of the immune system but also for the regulation of the endocrine pituitary-adrenocortical system and body weight (11). Possibly a similar situation holds true for TRIM. Experiments are in progress to assess this possibility.

TRIM-deficient T cells show normal TCR/CD3 surface levels and normal TCR dynamics. Previously, we had shown that overexpression of TRIM in Jurkat T cells enhances the expression levels of the TCR on the cell surface by altering spontaneous TCR internalization (4, 20). To address the question of whether TRIM exerts a similar function in nontransformed primary mouse T cells, we investigated the expression levels of the TCR on thymocytes and peripheral T cells of wild-type and TRIM-deficient mice by flow cytometry. As shown in Fig. 2A and B, the absence of TRIM had no impact on the expression levels of the TCR (or CD3ε [data not shown]). We next investigated whether internalization of the TCR or TCR recycling after antibody-mediated internalization was affected in $TRIM^{-/-}$ T lymphocytes. Figure 2C shows that the internalization of the TCR in peripheral lymph node T cells and in thymocytes (data not shown) occurred at normal rates in the absence of TRIM. In addition, the reexpression kinetics of the internalized TCR pool at the cell surface was comparable in wild-type and TRIM-deficient T cells (Fig. 2D). These data suggest that in contrast to Jurkat T cells, TRIM is dispensable for both the internalization and the recycling of the TCR in primary mouse T cells. A possible explanation could be that the regulation of TCR expression-downregulation-internalization by TRIM can only be observed in an overexpression system or in transformed cell lines, such as Jurkat. Alternatively, it might be that primary T cells possess other molecules that compensate for the absence of TRIM.

Normal T-cell development in $TRIM^{-/-}$ mice. To assess the role of TRIM during T-cell development, flow cytometric analyses of lymphocyte suspensions prepared from thymus, spleen, and lymph nodes (Tables 1 and 2 and Fig. 3) were performed. As depicted in Table 1, the total cellularity of the thymus was found to be slightly reduced in $TRIM^{-/-}$ mice. However, the distribution of thymic subpopulations, as defined by CD4 and CD8 coreceptor expression, was similar between $TRIM^{-/-}$ animals and control littermates Fig. 3A. Moreover, we did not observe a significant alteration in the CD4/CD8 ratio (Table 1), and there was also no difference in CD25 and CD44 expression within the double negative thymocyte population (Fig. 3B). Collectively, these findings suggest that TRIM is dispensable for thymic development.

To corroborate this assumption and, in particular, to rule out subtle alterations in the selection processes in the absence of TRIM, we crossed $TRIM^{-/-}$ mice onto different TCR transgenic backgrounds. As shown in Fig. 4, the loss of TRIM did not influence positive selection in class I (HY)- or class II (OT-II)-restricted TCR transgenic models. We also tested positive selection using OT-I and P14 class I-restricted TCRs, which possess higher affinities for the selecting ligands than the HY TCR, and again we did not observe any alteration in TRIM-deficient animals (data not shown). Thus, TRIM appears to be dispensable for positive selection. Similarly, the loss of TRIM had no influence on the efficiency of negative selection in $TRIM^{-/-}$ HY male animals (Fig. 4C) or when negative selection was mimicked by intraperitoneal injection of the CD3ε MAb 145-2C11 (data not shown). In addition, the

TABLE 2. T-cell subsets in peripheral lymph nodes[a]

TRIM status	*n*	Total no. of cells (10^6)	No. of cells with indicated phenotype				CD4/CD8 ratio	CD3/B220 ratio
			$CD4^+$	$CD8^+$	$CD3^+$	$B220^+$		
$TRIM^{+/+}$	11	28.3 (3.5)	10.8 (1.3)	10.4 (1.7)	21.1 (2.7)	6.2 (0.7)	1.12 (0.1)	3.38 (0.2)
$TRIM^{-/-}$	12	20.3 (2.5)	7.0 (0.7)	7.9 (1.1)	15.5 (2.0)	4.1 (0.5)	0.92 (0.04)	3.78 (0.3)

[a] The numbers of lymphocyte subsets were determined on the basis of the total cell count and flow cytometric analysis shown in Fig. 2. Data represent means and standard errors of the means (in parentheses).

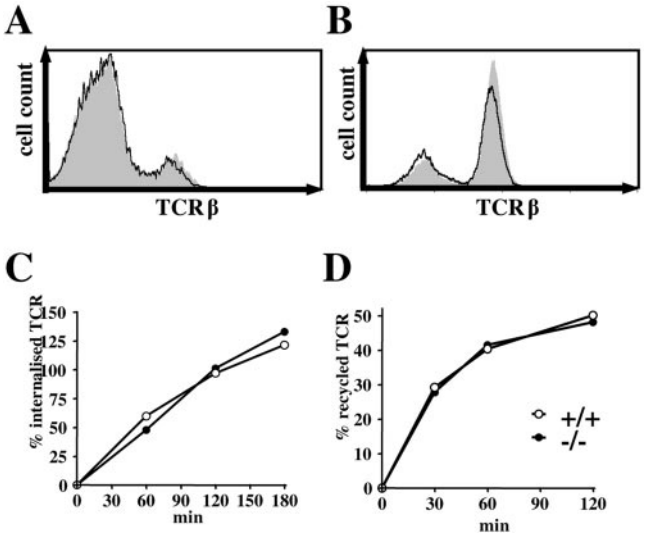

FIG. 2. TCR expression, internalization, and recycling are normal in TRIM-deficient mice. Thymocytes (A) and lymph node cells (B) were stained with anti-TCRβ MAb and analyzed by flow cytometry. The histograms represent profiles of cells from representative $TRIM^{+/+}$ (shaded) and $TRIM^{-/-}$ (thick lines) mice. (C) Measurement of TCR internalization. Lymph node T cells were incubated with PE-labeled anti-TCRβ antibody (H57-597) for 30 min on ice. Cells were then washed to remove unbound antibody and placed at 37°C for 0, 30, 60, 90, and 180 min. Surface-bound antibody was removed by low-pH washes, and internalized antibody in $CD4^+$ cells was quantified by flow cytometry. (D) Reexpression of previously internalized anti-TCRβ antibody. To label an internalized pool of TCRβ, lymph node T cells were stained with PE-labeled anti-TCRβ antibody, cultured for 90 min at 37°C (to allow optimal TCR internalization), and stripped at low pH to remove cell surface TCR-bound antibody as described for panel C. Cells were then incubated at 37°C for various time points. TCR/anti-TCRβ-PE complexes recycling to the cell surface of $CD4^+$ cells were quantified as the fluorescence lost after a second low-pH wash at the indicated time point and the fluorescence at time zero.

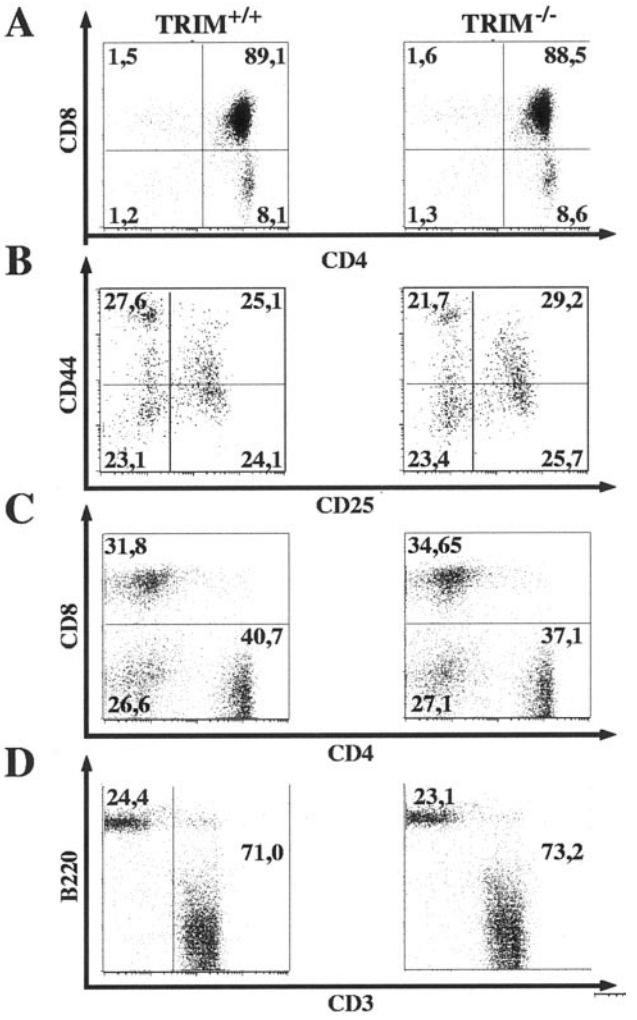

FIG. 3. Development of lymphoid organs in TRIM-deficient mice. Thymocytes (A), double negative thymocytes (B), and peripheral lymph node cells (C and D) from 6- to 10-week-old mice were stained with MAbs for CD3, CD4, CD8, CD25, CD44, and B220 and analyzed by flow cytometry. Numbers represent percentages of cells falling into the indicated quadrant of total living cells.

survival of $TRIM^{-/-}$ thymocytes after in vitro application of different apoptotic stimuli was found to be normal (Fig. 4D). Finally, membrane-proximal TCR-mediated signaling events (global tyrosine phosphorylation and calcium fluxes) in thymocytes were also unaffected in $TRIM^{-/-}$ thymocytes (data not shown). In summary, these data corroborate that TRIM is dispensable for both positive and negative selection as well as for thymocyte responses to either TCR-mediated or TCR-independent apoptotic stimuli.

We next analyzed peripheral lymphocyte populations prepared from secondary lymphoid organs. Similar to the situation within the thymus, $TRIM^{-/-}$ mice showed slightly reduced numbers of all lymphocyte subsets in the spleen and lymph nodes (Table 2 and data not shown), while the distributions of T- and B-cell subsets were normal (Fig. 3C and D and data not shown). In addition, we did not observe major alterations in the CD4/CD8 or the T-cell/B-cell ratios (Table 2) in $TRIM^{-/-}$ animals. A detailed expression analysis of a variety of lineage- and activation-specific markers (including CD5, CD25, CD44, CD45RB, CD62L, CD69, TCRαβ, TCRγδ, and NK1.1) also did not reveal any differences between $TRIM^{-/-}$ animals and control littermates. Similarly, TRIM deficiency had no influence on the expression levels of the accessory receptor CD28 or of the negative regulatory receptor CTLA4 (data not shown). Together, these results indicate a nonessential role for TRIM in the development, maturation, and distribution of peripheral T lymphocytes.

Analysis of in vitro and in vivo peripheral lymphocyte functions. We have previously reported that TRIM is exclusively expressed in lymphoid organs (thymus, lymph node, and spleen) (4, 19). As shown in Fig. 5A, within the T-cell compartment TRIM is strongly expressed in thymocytes and in mature peripheral $CD4^+$ T cells, whereas mature $CD8^+$ cells express only minute amounts of the protein. These findings are in line with a recent report showing higher expression levels of TRIM mRNA in human and mouse $CD4^+$ peripheral T lymphocytes than $CD8^+$ T cells (29) (http://symatlas.gnf.org/SymAtlas/).

To assess whether TRIM deficiency affects the function of peripheral $CD4^+$ T cells, we investigated membrane-proximal TCR-mediated signaling events. Figures 5B and C demon-

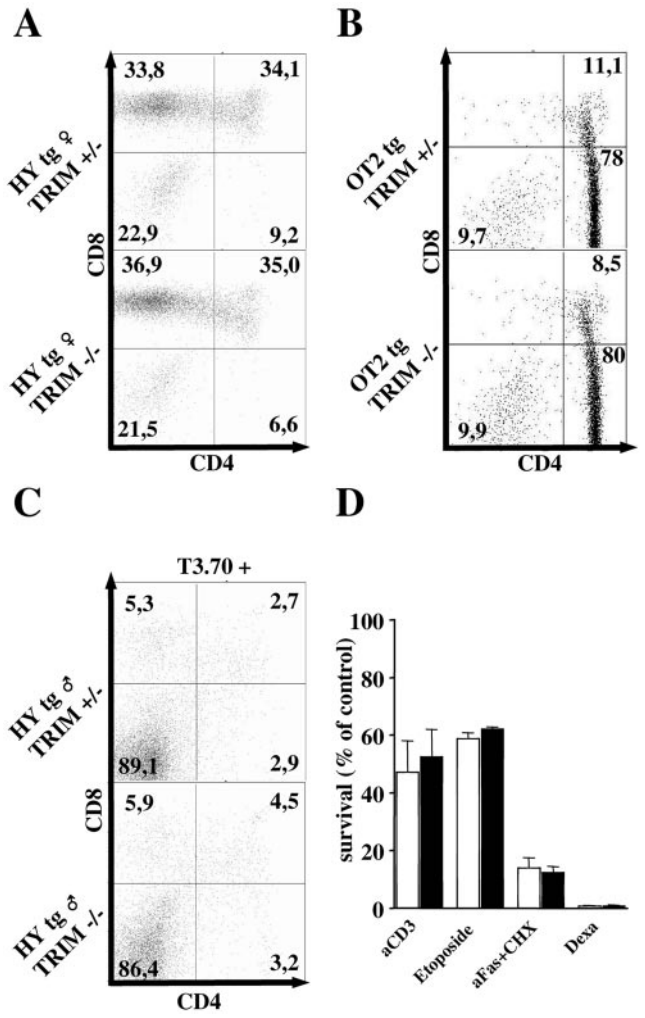

FIG. 4. Positive and negative selection in TRIM$^{-/-}$ mice. Normal positive selection in female HY (A) and OT-II (B) TCR transgenic (tg) mice. Thymocytes were stained with anti-HY (T3.70) and anti-Vα_2 antibodies, and the CD4/CD8 profiles of transgenic TCR-gated cells are shown in panels A and B, respectively. (C) Normal negative selection in HY TCR tg TRIM$^{-/-}$ male mice. Profiles of thymocytes gated on T3.70$^+$ cells and then examined for CD4 and CD8 expression. (D) Response to death-inducing signals within the thymocyte population. Freshly isolated thymocytes were incubated for 24 h in 24-well plates and were stimulated with 10 μg/ml plate-bound CD3 plus CD28 MAbs or incubated either with etoposide, anti-Fas plus cycloheximide (aFas+CHX), or dexamethasone (Dexa). Cell viability was measured by annexin V and propidium iodide staining.

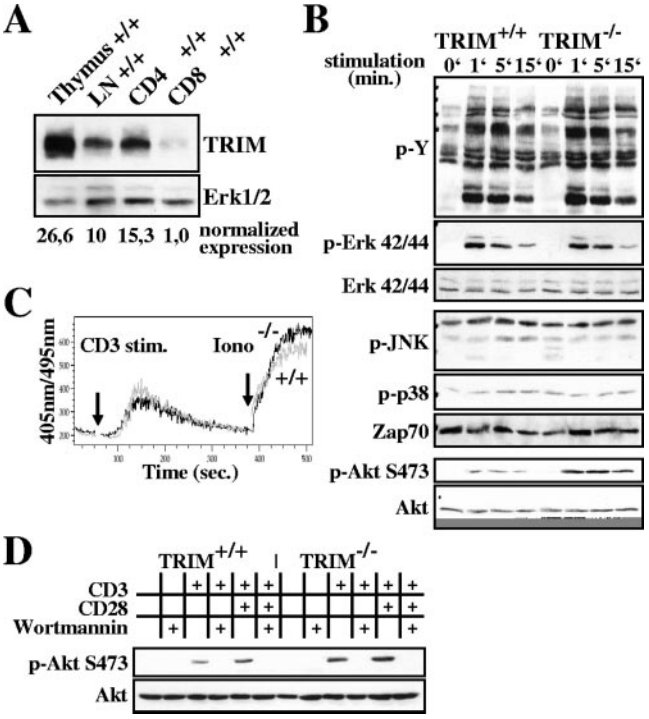

FIG. 5. TCR-mediated signaling in TRIM-deficient CD4$^+$ T cells. (A) TRIM expression in T cells. Postnuclear lysates were prepared from freshly isolated thymocytes, lymph node cells (LN), or purified CD4$^+$ and CD8$^+$ splenocytes, separated on sodium dodecyl sulfate-polyacrylamide gel electrophoresis, and blotted with TRIM04 MAb. The blot was reprobed with anti-Erk1/2 to demonstrate equal loading. Numbers below the blot represent relative TRIM expression compared to the lowest. (B) Global tyrosine phosphorylation and MAP family kinase activation are normal, but Akt phosphorylation is enhanced in TRIM-deficient mice. Purified CD4$^+$ splenic T cells were stimulated for the indicated periods of time with the CD3 MAb 145-2C11. The cells were lysed and processed for Western blot analysis. The blots were probed with anti-phosphospecific antibodies and then stripped and reprobed with anti-Erk1/2, anti-ZAP-70, and anti-Akt to show equal loading. Data are representative of five separate experiments. (C) Analysis of Ca^{2+} mobilization. Purified splenic CD4$^+$ cells were loaded with indo-1-AM and incubated with 10 μg/ml of biotinylated anti-CD3 (145-2C11). The arrows indicate the addition of streptavidin and ionomycin (Iono), respectively. (D) TRIM regulation of Akt phosphorylation depends on PI3K activity. Purified CD4$^+$ splenic T cells were stimulated for 2 min with CD3 MAb alone or with CD3 plus CD28 MAbs in the presence or absence of the PI3K inhibitor wortmannin. The level of Akt activation was measured by using a phosphospecific anti-Akt antibody and the equal loading by using an anti-Akt antibody. stim., stimulation.

strate that TCR-mediated global tyrosine phosphorylation, the activation of MAPKs, and the elevation of intracellular calcium ions are all normal in TRIM$^{-/-}$ CD4$^+$ T cells. Since TRIM has been shown to recruit the p85 regulatory subunit of PI3 kinase (4) and, therefore, may be involved in the regulation of PI3K activity, we also investigated TCR-mediated activation-phosphorylation of the serine/threonine kinase Akt/protein kinase B as a surrogate marker of PI3K activity. Surprisingly, TRIM-deficient T lymphocytes showed an augmented and prolonged phosphorylation of Akt compared to control cells. Since wortmannin treatment completely abolished Akt phosphorylation in both wild-type and TRIM-deficient CD4$^+$ T cells (Fig. 5D), we conclude that PI3K activity is indeed augmented in TRIM$^{-/-}$ T lymphocytes.

The PI3 kinase/Akt pathway is involved in many biological processes, including cell survival, proliferation, differentiation, and migration (25). To assess whether the augmented activity of Akt in the absence of TRIM would alter apoptotic responses, we stimulated mature peripheral CD4$^+$ T cells with CD3 MAbs, corticosteroids, CD95 MAbs, ConA, or etoposide. Figure 6A shows that the survival of TRIM$^{-/-}$ T cells is indistinguishable from that of control T cells. To further investigate whether TRIM deficiency alters apoptosis of preactivated T cells (a phenomenon known as AICD), CD4$^+$ T cells were

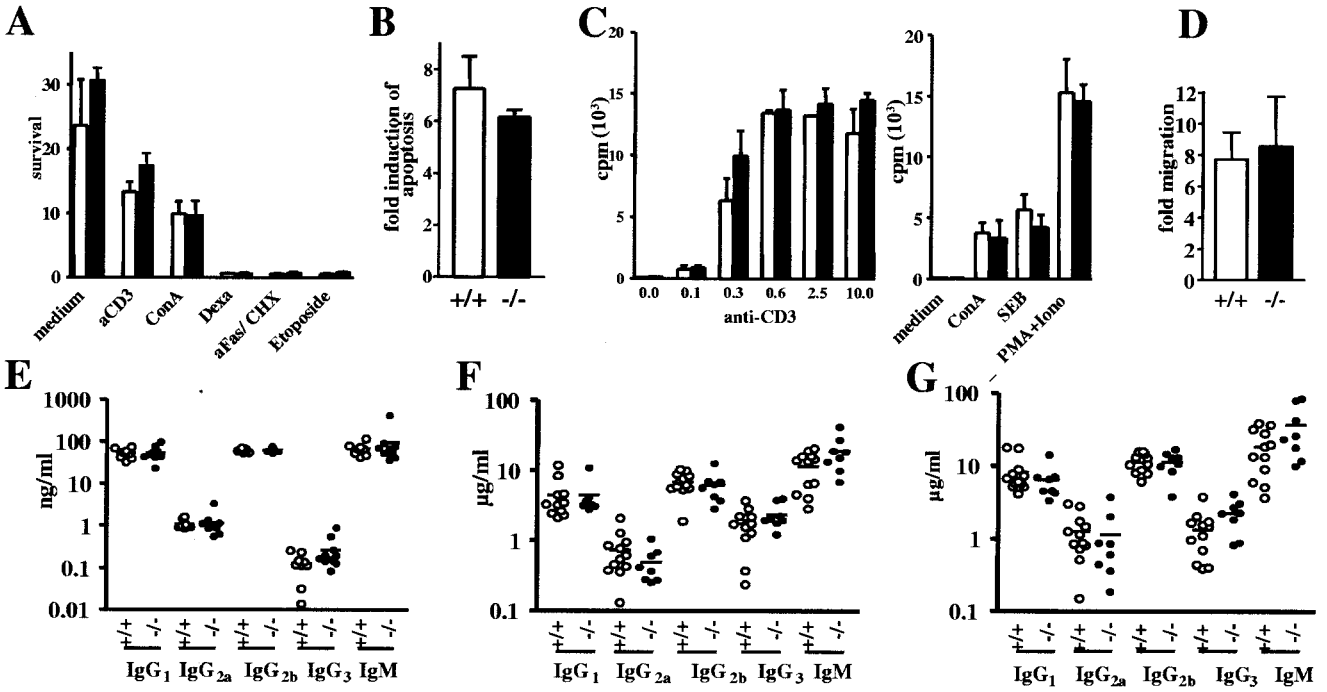

FIG. 6. T-cell responses in vitro and in vivo. (A) Normal survival of peripheral $CD4^+$ T cells upon stimulation with CD3 MAb (aCD3), ConA, etoposide, anti-Fas plus cycloheximide (aFas/CHX), or dexamethasone (Dexa). One representative out of two experiments is shown. (B) Activation-induced cell death (AICD). $CD4^+$ T cells were stimulated in CD3 MAb-coated plates, grown in IL-2, and restimulated overnight with CD3 antibody. Apoptosis was measured by annexin V and propidium iodide staining. The data are expressed as induction of apoptosis relative to control samples that were not restimulated. (C) Normal T-cell proliferation in TRIM-deficient mice. Purified $CD4^+$ splenic T cells were stimulated in CD3 MAb-coated 96-well plates or with ConA, SEB, or PMA plus ionomycin (Iono) for 72 h, pulsed with $[H^3]$thymidine, and processed for standard scintillation counting. One out of five independent experiments is shown. Three mice of each genotype were included in each experiment. (D) Migration assay. Freshly isolated lymph node cells were added to the insert of a transwell plate, with the lower chamber containing medium alone or medium supplemented with SDF1α. After 3 h, cells that had migrated into the lower wells were collected and counted by flow cytometry. The data shown are representative for three independently performed experiments. The migration is expressed as induction relative to that of control samples incubated with medium alone. (E) Serum immunoglobulin titers. The concentration of serum immunoglobulins was measured by ELISA. Bars represent mean values. (F and G) Humoral immune response. Mice were immunized with the T-dependent antigen DNP-KLH, and DNP-specific immunoglobulins were analyzed at day 10 (F), or they were reimmunized at day 14 with the same antigen and DNP-specific immunoglobulins were measured at day 28 (G) as described in Materials and Methods.

stimulated in CD3 MAb-coated wells for 2 days. The activated cells were then grown in the presence of IL-2 for an additional 2 days and finally restimulated overnight with CD3 MAbs. The induction of apoptosis was subsequently measured by staining the cells with annexin V and propidium iodide. The data shown in Fig. 6B demonstrate that the absence of TRIM does not influence AICD.

We next assessed the in vitro proliferative response after stimulation with a variety of mitogenic stimuli, such as CD3 MAbs, ConA, SEB, and CD3/CD28 costimulation. As shown in Fig. 6C, TRIM-deficient $CD4^+$ T cells responded as efficiently as wild-type T cells to all applied stimuli. Similarly, the concentrations of IL-2, IL-4, tumor necrosis factor α, and gamma interferon in the culture supernatants were found to be normal (data not shown). Note that similar results were obtained when unfractionated splenic T cells were analyzed instead of purified $CD4^+$ T cells (data not shown).

To investigate whether TRIM regulates the migration of peripheral T lymphocytes, we used a transwell system and allowed lymphocytes to migrate through fibronectin-coated polycarbonate meshes in response to the chemokine SDF1. Again, $TRIM^{-/-}$ T cells migrated with an efficiency similar to that of wild-type lymphocytes (Fig. 6D). Similarly, the constitutive and the CD3-mediated adhesion of β1 and β2 integrins to fibronectin or ICAM-I-coated plastic dishes were normal in $TRIM^{-/-}$ mice (data not shown). Collectively, these data suggest that the absence of TRIM does not influence T-cell proliferation, survival, migration, and adhesion.

In summary, the data shown in Fig. 6 demonstrate that despite the enhanced activity of PI3K in $TRIM^{-/-}$ mice, T-cell functions are unaffected under a variety of experimental conditions. A possible explanation for this somewhat unexpected observation could be that the slight augmentation of PI3K activity that occurs in the absence of TRIM is, per se, not sufficient to significantly alter downstream signaling cascades and thus cellular responses. It is also possible, however, that the augmented PI3K activity in $TRIM^{-/-}$ cells is partially compensated for by another nonraft transmembrane adaptor protein(s) exerting similar functions, the transmembrane adaptor protein LAX being a likely candidate. LAX also binds the p85 regulatory subunit of PI3K (40), and similar to the situation described here, $LAX^{-/-}$ T cells show a slightly augmented PI3K activity after TCR engagement (39). Thus, it appears as if both TRIM and LAX jointly regulate PI3K activity in pe-

TABLE 3. Clinical observations of MOG peptide-induced EAE[a]

Group	Incidence of EAE	Avg score	No. of deaths
Wild type	26/32	1.95 ± 0.2	10/32
TRIM$^{-/-}$	25/33	1.75 ± 0.2	8/33

[a] Disease severity was scored according to a scale from 0 to 5: 0, no signs; 0.5, partial tail weakness; 1, limp tail or slight slowing of righting from supine position; 2, paresis of hind limb or marked slowing of righting; 2.5, dragging of hind limb(s) without complete paralysis; 3, complete paralysis of hind limb; 4, severe forelimb paralysis; 5, moribund or dead. In respect of the animal protection laws, mice were killed when they reached a score of 3 and received this last score until the end of the experiment.

ripheral T cells. Combined deletion of the TRIM and LAX genes will be required to assess whether both molecules indeed share redundant functions with regard to the TCR-mediated activation of PI3K or not.

One possibility to explain the enhanced activity of PI3K in the absence of either TRIM or LAX could be that in normal T cells both molecules are involved in sequestering the p85 subunit of PI3K from the lipid rafts to the nonraft fraction. Loss of TRIM or LAX might then cause a redistribution of PI3K from the nonraft to the raft fraction, thereby enhancing its activity. It is important to note that a similar "redistribution" phenomenon has recently been proposed to underlie the augmented response of mast cells that lack expression of the transmembrane adaptor protein NTAL/LAB (33).

The impact of TRIM deficiency on in vivo immune functions was further tested by challenging TRIM$^{-/-}$ mice and control littermates with the T-dependent antigen DNP-KLH at days 0 and 21. The levels of hapten-specific IgG1, IgG2a, IgG2b, IgG3, and IgM antibodies were measured 10 and 28 days after immunization. As shown in Fig. 6, both the primary (Fig. 6F) and the secondary (Fig. 6G) humoral responses of mutant and wild-type mice were comparable, indicating that T-helper functions are not affected in TRIM$^{-/-}$ mice.

To finally study the immune function of TRIM-deficient T cells in a disease model, we assessed the clinical course of experimental autoimmune encephalomyelitis (EAE), a murine model of multiple sclerosis, in wild-type and TRIM-deficient animals. EAE is a well-established Th1-mediated disease that can be induced in C57BL/6 mice by immunization with MOG(35-55) peptide. The pathophysiology of EAE is characterized by T-cell-mediated demyelinization of axons in the central nervous system, which is followed by a progressive paralysis of the tail and the limbs (21). Due to the complex nature of the disease, which integrates many aspects of T-cell function, EAE represents a sensitive model system to detect even subtle alterations of immune functions. Indeed, we recently could show clear differences in the clinical course of EAE in knockout mice in which both T-dependent and T-independent immune responses were unaffected (28, 31).

To induce EAE, matched groups of TRIM$^{-/-}$ and wild-type mice were immunized with MOG(35-55) peptide, and the clinical score of EAE was assessed over time in a blinded study. As shown in Table 3, TRIM-deficient mice showed a normal course of EAE both with regard to the onset of disease as well as with regard to the clinical score, which ranged between 1.7 and 1.9 in both TRIM$^{-/-}$ and TRIM$^{+/+}$ mice. Together with the normal response after immunization with T-dependent antigens, these data suggest a nonessential role of TRIM within the immune system.

Normal B-cell development and B-cell functions in TRIM-deficient mice. Although TRIM expression has been reported to be limited to T lymphocytes (4), we also investigated the generation and the functions of B cells in TRIM$^{-/-}$ animals. These experiments were aimed to exclude the possibility that TRIM is expressed as a functional protein in particular B-cell subsets or in B-cell precursors as had previously been shown for the transmembrane adaptor protein LAT and the tyrosine kinase ZAP-70 (27, 30). However, the development of B cells within the bone marrow as well as the in vitro proliferation of purified splenic B cells after anti-IgM, lipopolysaccharide, anti-CD40, and IL-4 stimulation was not affected by loss of TRIM (data not shown). Similarly, the serum Ig levels (Fig. 6E) and the humoral immune response after immunization with the T-independent antigen DNP-lipopolysaccharide was normal in TRIM$^{-/-}$ mice (data not shown). Thus, in contrast to LAT, TRIM is not involved in regulating B-cell development and B-cell functions both in vivo and in vitro.

Concluding remarks. Among the seven TRAPs known to date, LAT clearly represents the master switch that critically regulates T-cell development and peripheral T-cell activation (12, 37, 38). In contrast, other transmembrane adaptors such as LAX, NTAL, and SIT rather appear to be involved in the fine-tuning of antigen receptor-mediated signaling within immune cells (28, 34, 39). The same seems to apply for the nonraft transmembrane adaptor protein investigated here, TRIM.

TRIM is strongly expressed in thymocytes and, as shown here, in peripheral CD4$^+$ T cells. Previous reports suggested that TRIM might be involved in the regulation of TCR expression in Jurkat T cells (4, 20). In addition, TRIM was shown to undergo tyrosine phosphorylation after T-cell activation and to recruit the p85 regulatory subunit of PI3K to the plasma membrane (4, 20). Together, these observations suggested that TRIM might represent an important regulator of T-cell development and T-cell responses. However, the data presented in this report suggest that TRIM does not play an essential role within the (murine) immune system.

Although our study did not reveal major alterations of immune functions in the absence of TRIM, we certainly cannot exclude the possibility that TRIM regulates immunological processes that we have not investigated (for example, TRIM could be involved in pathways that emerge from signaling receptors distinct from the TCR). However, given the fact that several in vivo models (immunization with T-dependent antigens as well as induction of the autoimmune disease EAE) did not show abnormalities in TRIM-deficient animals, we believe this possibility to be unlikely.

To date, seven TRAPs have been identified: LAT, LAX, LIME, NTAL/LAB, PAG/CBP, SIT, and TRIM (for a review, see reference 18). Among them, LAX, SIT, and TRIM are localized in the nonraft fraction of the plasma membrane. Recently published data showed that both LAX and SIT function as negative regulators of antigen receptor-mediated signaling. Thus, LAX-deficient T and B lymphocytes are hyperresponsive to CD3- or anti-IgM-mediated stimuli (39). Similarly, we have most recently shown that SIT functions as a negative regulator of TCR-mediated signaling (28). The mo-

lecular mechanisms underlying LAX- and SIT-mediated negative regulation of TCR signaling are still unclear. One possibility is that LAX and SIT affect signaling within T cells by sequestering cytoplasmic effector molecules from the lipid rafts to the nonraft fraction or that they blunt T-cell responses by recruiting negative regulatory molecules to the plasma membrane.

The very mild phenotypes of the SIT and LAX knockout mice plus the almost nonexistent phenotype of the TRIM mouse described in this report indicate that each of the nonraft-associated TRAPs by itself plays a rather subtle role within the immune system. However, the orchestrated activities of all negative regulatory transmembrane adaptor proteins might play a major role in controlling cell growth and differentiation. The apparent redundancy among the different nonraft TRAPs may serve as a safety mechanism to guarantee the integrity of the system even when one component is missing or altered. In this regard, the analysis of TRIM/SIT double-deficient mice (note that TRIM and SIT share two tyrosine-based signaling motifs within their cytoplasmic tails, YGNL and YASV/L), of TRIM/LAX double-deficient mice (as both molecules are capable of binding PI3K and each of the single knockouts shows augmented activity of PI3K), or even of triple knockouts (as all three molecules carry YXN motifs that might bind the cytosolic adaptor protein Grb2) might shed further light onto the question of how TRAPs regulate homeostasis within the immune system.

ACKNOWLEDGMENTS

We are grateful to Gary Koretzy, Thomas Kammerthoens, and Percy Knolle for TCR transgenic lines and to the employees of the animal facility for maintenance of the animals. The help of Robert Enders, Evi Schaller, Agnes Fütterer, and Jennifer Meinecke is also highly appreciated.

The work was supported by the Deutsche Forschungsgemeinschaft (DFG)-funded research group 521 (research grants to L.S. and B.S.) and by DFG grants to K.P.

REFERENCES

1. **Alarcon, B., D. Gil, P. Delgado, and W. W. Schamel.** 2003. Initiation of TCR signaling: regulation within CD3 dimers. Immunol. Rev. **191:**38–46.
2. **Alimzhanov, M. B., D. V. Kuprash, M. H. Kosco-Vilbois, A. Luz, R. L. Turetskaya, A. Tarakhovsky, K. Rajewsky, S. A. Nedospasov, and K. Pfeffer.** 1997. Abnormal development of secondary lymphoid tissues in lymphotoxin beta-deficient mice. Proc. Natl. Acad. Sci. USA **94:**9302–9307.
3. **Barton, L. F., H. A. Runnels, T. D. Schell, Y. Cho, R. Gibbons, S. S. Tevethia, G. S. Deepe, Jr., and J. J. Monaco.** 2004. Immune defects in 28-kDa proteasome activator gamma-deficient mice. J. Immunol. **172:**3948–3954.
4. **Bruyns, E., A. Marie-Cardine, H. Kirchgessner, K. Sagolla, A. Shevchenko, M. Mann, F. Autschbach, A. Bensussan, S. Meuer, and B. Schraven.** 1998. T cell receptor (TCR) interacting molecule (TRIM), a novel disulfide-linked dimer associated with the TCR-CD3-zeta complex, recruits intracellular signaling proteins to the plasma membrane. J. Exp. Med. **188:**561–575.
5. **Cen, O., M. M. Gorska, S. J. Stafford, S. Sur, and R. Alam.** 2003. Identification of UNC119 as a novel activator of SRC-type tyrosine kinases. J. Biol. Chem. **278:**8837–8845.
6. **Chen, W. S., P. Z. Xu, K. Gottlob, M. L. Chen, K. Sokol, T. Shiyanova, I. Roninson, W. Weng, R. Suzuki, K. Tobe, T. Kadowaki, and N. Hay.** 2001. Growth retardation and increased apoptosis in mice with homozygous disruption of the Akt1 gene. Genes Dev. **15:**2203–2208.
7. **Chikuma, S., J. B. Imboden, and J. A. Bluestone.** 2003. Negative regulation of T cell receptor-lipid raft interaction by cytotoxic T lymphocyte-associated antigen 4. J. Exp. Med. **197:**129–135.
8. **Cho, H., J. L. Thorvaldsen, Q. Chu, F. Feng, and M. J. Birnbaum.** 2001. Akt1/PKBalpha is required for normal growth but dispensable for maintenance of glucose homeostasis in mice. J. Biol. Chem. **276:**38349–38352.
9. **Delgado, P., and B. Alarcon.** 2005. An orderly inactivation of intracellular retention signals controls surface expression of the T cell antigen receptor. J. Exp. Med. **201:**555–566.
10. **D'Oro, U., I. Munitic, G. Chacko, T. Karpova, J. McNally, and J. D. Ashwell.** 2002. Regulation of constitutive TCR internalization by the zeta-chain. J. Immunol. **169:**6269–6278.
11. **Ezzat, S., R. Mader, S. Yu, T. Ning, P. Poussier, and S. L. Asa.** 2005. Ikaros integrates endocrine and immune system development. J. Clin. Investig. **115:**1021–1029.
12. **Finco, T. S., T. Kadlecek, W. Zhang, L. E. Samelson, and A. Weiss.** 1998. LAT is required for TCR-mediated activation of PLCgamma1 and the Ras pathway. Immunity **9:**617–626.
13. **Gil, D., W. W. Schamel, M. Montoya, F. Sanchez-Madrid, and B. Alarcon.** 2002. Recruitment of Nck by CD3 epsilon reveals a ligand-induced conformational change essential for T cell receptor signaling and synapse formation. Cell **109:**901–912.
14. **Gorska, M. M., S. J. Stafford, O. Cen, S. Sur, and R. Alam.** 2004. Unc119, a novel activator of Lck/Fyn, is essential for T cell activation. J. Exp. Med. **199:**369–379.
15. **Han, J., J. W. Shui, X. Zhang, B. Zheng, S. Han, and T. H. Tan.** 2005. HIP-55 is important for T-cell proliferation, cytokine production, and immune responses. Mol. Cell. Biol. **25:**6869–6878.
16. **Harding, S., P. Lipp, and D. R. Alexander.** 2002. A therapeutic CD4 monoclonal antibody inhibits TCR-zeta chain phosphorylation, zeta-associated protein of 70-kDa Tyr319 phosphorylation, and TCR internalization in primary human T cells. J. Immunol. **169:**230–238.
17. **Hombach, J., T. Tsubata, L. Leclercq, H. Stappert, and M. Reth.** 1990. Molecular components of the B-cell antigen receptor complex of the IgM class. Nature **343:**760–762.
18. **Horejsi, V., W. Zhang, and B. Schraven.** 2004. Transmembrane adaptor proteins: organizers of immunoreceptor signalling. Nat. Rev. Immunol. **4:**603–616.
19. **Huynh, T., A. Wurch, E. Bruyns, V. Korinek, B. Schraven, and K. Eichmann.** 2001. Developmentally regulated expression of the transmembrane adaptor protein trim in fetal and adult T cells. Scand. J. Immunol. **54:**146–154.
20. **Kirchgessner, H., J. Dietrich, J. Scherer, P. Isomaki, V. Korinek, I. Hilgert, E. Bruyns, A. Leo, A. P. Cope, and B. Schraven.** 2001. The transmembrane adaptor protein TRIM regulates T cell receptor (TCR) expression and TCR-mediated signaling via an association with the TCR zeta chain. J. Exp. Med. **193:**1269–1284.
21. **Linington, C.** 1997. Actively induced models of central nervous system autoimmune disease, p. 1696–1700. *In* I. Lefkovits (ed.), Immunological methods - the comprehensive sourcebook of techniques, vol. 3. Harcourt Brace & Company, Basel, Switzerland.
22. **Mikkers, H., M. Nawijn, J. Allen, C. Brouwers, E. Verhoeven, J. Jonkers, and A. Berns.** 2004. Mice deficient for all PIM kinases display reduced body size and impaired responses to hematopoietic growth factors. Mol. Cell. Biol. **24:**6104–6115.
23. **Molero, J. C., T. E. Jensen, P. C. Withers, M. Couzens, H. Herzog, C. B. Thien, W. Y. Langdon, K. Walder, M. A. Murphy, D. D. Bowtell, D. E. James, and G. J. Cooney.** 2004. c-Cbl-deficient mice have reduced adiposity, higher energy expenditure, and improved peripheral insulin action. J. Clin. Investig. **114:**1326–1333.
24. **Myers, M. D., L. L. Dragone, and A. Weiss.** 2005. Src-like adaptor protein down-regulates T cell receptor (TCR)-CD3 expression by targeting TCR{zeta} for degradation. J. Cell Biol. **170:**285–294.
25. **Okkenhaug, K., and B. Vanhaesebroeck.** 2003. PI3K in lymphocyte development, differentiation and activation. Nat. Rev. Immunol. **3:**317–330.
26. **Pandey, A., N. Ibarrola, I. Kratchmarova, M. M. Fernandez, S. N. Constantinescu, O. Ohara, S. Sawasdikosol, H. F. Lodish, and M. Mann.** 2002. A novel Src homology 2 domain-containing molecule, Src-like adapter protein-2 (SLAP-2), which negatively regulates T cell receptor signaling. J. Biol. Chem. **277:**19131–19138.
27. **Schweighoffer, E., L. Vanes, A. Mathiot, T. Nakamura, and V. L. Tybulewicz.** 2003. Unexpected requirement for ZAP-70 in pre-B cell development and allelic exclusion. Immunity **18:**523–533.
28. **Simeoni, L., V. Posevitz, U. Kolsch, I. Meinert, E. Bruyns, K. Pfeffer, D. Reinhold, and B. Schraven.** 2005. The transmembrane adapter protein SIT regulates thymic development and peripheral T-cell functions. Mol. Cell. Biol. **25:**7557–7568.
29. **Su, A. I., T. Wiltshire, S. Batalov, H. Lapp, K. A. Ching, D. Block, J. Zhang, R. Soden, M. Hayakawa, G. Kreiman, M. P. Cooke, J. R. Walker, and J. B. Hogenesch.** 2004. A gene atlas of the mouse and human protein-encoding transcriptomes. Proc. Natl. Acad. Sci. USA **101:**6062–6067.
30. **Su, Y. W., and H. Jumaa.** 2003. LAT links the pre-BCR to calcium signaling. Immunity **19:**295–305.
31. **Togni, M., K. D. Swanson, S. Reimann, S. Kliche, A. C. Pearce, L. Simeoni, D. Reinhold, J. Wienands, B. G. Neel, B. Schraven, and A. Gerber.** 2005. Regulation of in vitro and in vivo immune functions by the cytosolic adaptor protein SKAP-HOM. Mol. Cell. Biol. **25:**8052–8063.
32. **Urba, W. J., C. Ewel, W. Kopp, J. W. Smith, R. G. Steis, J. D. Ashwell, S. P. Creekmore, J. Rossio, M. Sznol, and W. Sharfman.** 1992. Anti-CD3 monoclonal antibody treatment of patients with CD3-negative tumors: a phase IA/B study. Cancer Res. **52:**2394–2401.
33. **Volna, P., P. Lebduska, L. Draberova, S. Simova, P. Heneberg, M. Boubelik,**

V. Bugajev, B. Malissen, B. S. Wilson, V. Horejsi, M. Malissen, and P. Draber. 2004. Negative regulation of mast cell signaling and function by the adaptor LAB/NTAL. J. Exp. Med. **200:**1001–1013.

34. **Wang, Y., O. Horvath, A. Hamm-Baarke, M. Richelme, C. Gregoire, R. Guinamard, V. Horejsi, P. Angelisova, J. Spicka, B. Schraven, B. Malissen, and M. Malissen.** 2005. Single and combined deletions of the NTAL/LAB and LAT adaptors minimally affect B-cell development and function. Mol. Cell. Biol. **25:**4455–4465.
35. **Weiss, A.** 1993. T cell antigen receptor signal transduction: a tale of tails and cytoplasmic protein-tyrosine kinases. Cell **73:**209–212.
36. **Yamazaki, T., Y. Hamano, H. Tashiro, K. Itoh, H. Nakano, S. Miyatake, and T. Saito.** 1999. CAST, a novel CD3epsilon-binding protein transducing activation signal for interleukin-2 production in T cells. J. Biol. Chem. **274:** 18173–18180.
37. **Zhang, W., J. Sloan-Lancaster, J. Kitchen, R. P. Trible, and L. E. Samelson.** 1998. LAT: the ZAP-70 tyrosine kinase substrate that links T cell receptor to cellular activation. Cell **92:**83–92.
38. **Zhang, W., C. L. Sommers, D. N. Burshtyn, C. C. Stebbins, J. B. DeJarnette, R. P. Trible, A. Grinberg, H. C. Tsay, H. M. Jacobs, C. M. Kessler, E. O. Long, P. E. Love, and L. E. Samelson.** 1999. Essential role of LAT in T cell development. Immunity **10:**323–332.
39. **Zhu, M., O. Granillo, R. Wen, K. Yang, X. Dai, D. Wang, and W. Zhang.** 2005. Negative regulation of lymphocyte activation by the adaptor protein LAX. J. Immunol. **174:**5612–5619.
40. **Zhu, M., E. Janssen, K. Leung, and W. Zhang.** 2002. Molecular cloning of a novel gene encoding a membrane-associated adaptor protein (LAX) in lymphocyte signaling. J. Biol. Chem. **277:**46151–46158.

Appendix 9

A logical model provides insights into T-cell signaling

Saez-Rodriguez J., **Simeoni L.**, Lindquist J.A., Hemenway R., Bommhardt U., Arndt B., Haus U.U., Weismantel R., Gilles E.D., Klamt S., and Schraven B. (2007) *PLoS Comput Biol.* 3:e163.

A Logical Model Provides Insights into T Cell Receptor Signaling

Julio Saez-Rodriguez[1], Luca Simeoni[2], Jonathan A. Lindquist[2], Rebecca Hemenway[1], Ursula Bommhardt[2], Boerge Arndt[2], Utz-Uwe Haus[3], Robert Weismantel[3], Ernst D. Gilles[1], Steffen Klamt[1*], Burkhart Schraven[2*]

1 Max Planck Institute for Dynamics of Complex Technical Systems, Magdeburg, Germany, 2 Institute of Immunology, Otto-von-Guericke University, Magdeburg, Germany, 3 Institute for Mathematical Optimization, Otto-von-Guericke University, Magdeburg, Germany

Cellular decisions are determined by complex molecular interaction networks. Large-scale signaling networks are currently being reconstructed, but the kinetic parameters and quantitative data that would allow for dynamic modeling are still scarce. Therefore, computational studies based upon the structure of these networks are of great interest. Here, a methodology relying on a logical formalism is applied to the functional analysis of the complex signaling network governing the activation of T cells via the T cell receptor, the CD4/CD8 co-receptors, and the accessory signaling receptor CD28. Our large-scale Boolean model, which comprises 94 nodes and 123 interactions and is based upon well-established qualitative knowledge from primary T cells, reveals important structural features (e.g., feedback loops and network-wide dependencies) and recapitulates the global behavior of this network for an array of published data on T cell activation in wild-type and knock-out conditions. More importantly, the model predicted unexpected signaling events after antibody-mediated perturbation of CD28 and after genetic knockout of the kinase Fyn that were subsequently experimentally validated. Finally, we show that the logical model reveals key elements and potential failure modes in network functioning and provides candidates for missing links. In summary, our large-scale logical model for T cell activation proved to be a promising in silico tool, and it inspires immunologists to ask new questions. We think that it holds valuable potential in foreseeing the effects of drugs and network modifications.

Citation: Saez-Rodriguez J, Simeoni L, Lindquist JA, Hemenway R, Bommhardt U, et al. (2007) A logical model provides insights into T cell receptor signaling. PLoS Comput Biol 3(8): e163. doi:10.1371/journal.pcbi.0030163

Introduction

Understanding how cellular networks function in a holistic perspective is the main purpose of systems biology [1]. Dynamic models provide an optimal basis for a detailed study of cellular networks and have been applied successfully to cellular networks of moderate size [2–5]. However, for their construction and analysis they require an enormous amount of mechanistic details and quantitative data which, until now, has been often lacking in large-scale networks. Therefore, there has been considerable effort to develop methods based exclusively on the often well-known network topology [6,7]. One may distinguish between studies on the statistical properties of graphs [8–10] and approaches aiming at predicting functional or dysfunctional states and modes. For the latter, a large corpus of methods has been developed for metabolic networks mainly relying on the constraints-based approach [11,12]. However, for signaling networks, methods facilitating a similar functional analysis—including predictions on the outcome of interventions— have been applied to a much lesser extent [6].

Here we demonstrate that capturing the structure of signaling networks by a recently introduced logical approach [13] allows the analysis of important functional aspects, often leading to predictions that can be verified in knock-out/perturbation experiments. Logical networks have until now been used for studying artificial (random) networks [14] or relatively small gene regulatory networks [15–18]. In contrast, herein we study a large-scale signaling network, structured in input (e.g., receptors), intermediate, and output (e.g., transcription factors) layers. Compared with gene regulatory networks, the behavior of signaling networks is mainly governed by their input layer, shifting the interest to input–output relationships. Addressing these issues requires partially different techniques, as compared with gene regulatory networks. We use a special and intuitive representation of logical networks (called *logical interaction hypergraph* (LIH); see Methods), which is well-suited for this kind of input–output analysis. By applying *logical steady state analysis*, one may predict how a combination of signals arriving at the input layer leads to a certain response in the intermediate and the output layers. Additionally, this approach facilitates predictions of the effect of interventions and, moreover, allows one to search for interventions that repress or provoke a certain logical response [13]. Furthermore, each logical network has a unique underlying interaction graph from which other important network properties such as feedback loops, signaling paths, and network-wide interdependencies can be evaluated.

Editor: Rob J. De Boer, Utrecht University, The Netherlands

Received February 6, 2007; **Accepted** July 5, 2007; **Published** August 24, 2007

A previous version of this article appeared as an Early Online Release on July 5, 2007 (doi:10.1371/journal.pcbi.0030163.eor).

Abbreviations: LIH, logical interaction hypergraph; MHC, Major Histocompatibility Complex; MIS, Minimal intervention set; TCR, T cell receptor

* To whom correspondence should be addressed. E-mail: inquiries regarding the mathematical methodology should be addressed to Steffen Klamt, klamt@mpi-magdeburg.mpg.de, and regarding the biological and experimental data to Burkhart Schraven, Burkhart.Schraven@med.ovgu.de

Author Summary

T-lymphocytes are central regulators of the adaptive immune response, and their inappropriate activation can cause autoimmune diseases or cancer. The understanding of the signaling mechanisms underlying T cell activation is a prerequisite to develop new strategies for pharmacological intervention and disease treatments. However, much of the existing literature on T cell signaling is related to T cell development or to activation processes in transformed T cell lines (e.g., Jurkat), whereas information on non-transformed primary T cells is limited. Here, immunologists and theoreticians have compiled data from the existing literature that stem from analysis of primary T cells. They used this information to establish a qualitative Boolean network that describes T cell activation mechanisms after engagement of the TCR, the CD4/CD8 co-receptors, and CD28. The network comprises 94 nodes and can be extended to facilitate interpretation of new data that emerge from experimental analysis of T cell activation. Newly developed tools and methods allow in silico analysis, and manipulation of the network and can uncover hidden/unforeseen signaling pathways. Indeed, by assessing signaling events controlled by CD28 and the protein tyrosine kinase Fyn, we show that computational analysis of even a qualitative network can provide new and non-obvious signaling pathways which can be validated experimentally.

Importantly, we consider here a logical model to be constructed by collecting and integrating well-known *local* interactions (e.g., a kinase phosphorylates an adaptor molecule). The logical model is then employed to derive *global* information (e.g., stimulation of a receptor leads to the activation of a certain transcription factor via several logical connections). Thus, the available data on the global network behavior is not used to construct the model; instead, it is used to *verify* the model. The model may then be employed to *predict* global responses that have not yet been studied experimentally.

Here, we apply the logical framework to a carefully constructed model of T cell receptor (TCR) signaling. T-lymphocytes play a key role within the immune system: cytotoxic, $CD8^+$, T cells destroy cells infected by viruses or malignant cells, and $CD4^+$ T helper cells coordinate the functions of other cells of the immune system [19]. The importance of T cells for immune homeostasis is due to their ability to specifically recognize foreign, potentially dangerous, agents and, subsequently, to initiate a specific immune response. T cell reactivity must be exquisitely regulated as either a decrease (which weakens the defense against pathogens with the consequence of immunodeficiency) or an increase (which can lead to autoimmune disorders and leukemia) can have severe consequences for the organism.

T cells detect foreign antigens by means of the TCR, which recognizes peptides only when presented upon MHC (Major Histocompatibility Complex) molecules. The peptides that are recognized by the TCR are typically derived from foreign (e.g., bacterial, viral) proteins and are generated by proteolytic cleavage within so-called antigen presenting cells (APCs). Binding of the TCR to peptide/MHC complexes and the additional binding of a different region of the MHC molecules by the co-receptors (CD4 in the case of T helper cells and CD8 in the case of cytotoxic T cells), together with costimulatory molecules such as CD28, initiates a plethora of signaling cascades within the T cell. These cascades give rise to a complex signaling network, which controls the activation of several transcription factors. These transcription factors, in turn, control the cell's fate, particularly whether the T cell becomes activated and proliferates or not [20]. Therefore, we chose to focus on a limited number of receptors that are known to be central to the decision making process. The high number of kinases, phosphatases, adaptor molecules, and their interactions give rise to a complex interaction network which cannot be interpreted via pure intuition and requires the aid of mathematical tools. Since no sufficient basis of kinetic data is available for setting up a dynamic model of this network, we opted to use logical modeling as a qualitative and discrete modeling framework. Note that there are kinetic models dealing with a smaller part of the network (e.g., [5,21,22]), as well as models of the gene regulatory network governing T cell activation [23].

We recently introduced our approach for the logical modeling of signaling networks [13], and, to exemplify it, we presented a small logical model for T cell activation (40 nodes). However, this model only served to demonstrate applicability and was too incomplete to address realistic complex input–output patterns. In contrast, the model presented herein has been significantly expanded to 94 nodes and refined by a careful reconstruction process (see below). It is thus realistic enough to be verified with diverse experimental data and to test its predictive power.

In this report, the large-scale logical model describing T cell activation and the analysis performed therewith will be presented. First we will show that a number of important structural features can be identified with this model. Then we will show that the model not only reproduces published data on wet lab experiments, but it also predicts non-intuitive and previously unknown responses.

Results

Setup of a Curated, Comprehensive Logical Model of T Cell Receptor Signaling

We have constructed a logical model describing T cell signaling (see Methods and Figure 1), which comprises the main events and elements connecting the TCR, its coreceptors CD4/CD8, and the costimulatory molecule CD28, to the activation of key transcription factors in T cells such as AP-1, NFAT, and NFκB, all of which determine T cell activation and T cell function. In general, the model includes the following signaling steps emerging from the above receptors: the activation of the Src kinases Lck and Fyn, followed by the activation of the Syk-related protein tyrosine kinase ZAP70, and the subsequent assembly of the LAT signalosome, which in turn triggers activation of PLCγ1, calcium cascades, activation of RasGRP, and Grb2/SOS, leading to the activation of MAPKs [20]. Additionally, it includes the activation of the PI3K/PKB pathway that regulates many aspects of cellular activation and differentiation, particularly survival. For the activation of elements that play an important role, but whose regulation is not well-known yet (e.g., Card11, Gadd45), an external input was added. These elements can be considered as points of future extension of the model.

As mentioned above, our model, which is documented in a detailed manner in Tables S1 and S2, is based upon *local* interactions (e.g., kinase ZAP70 phosphorylates the adaptor molecule LAT) that are well-established for primary T cells in

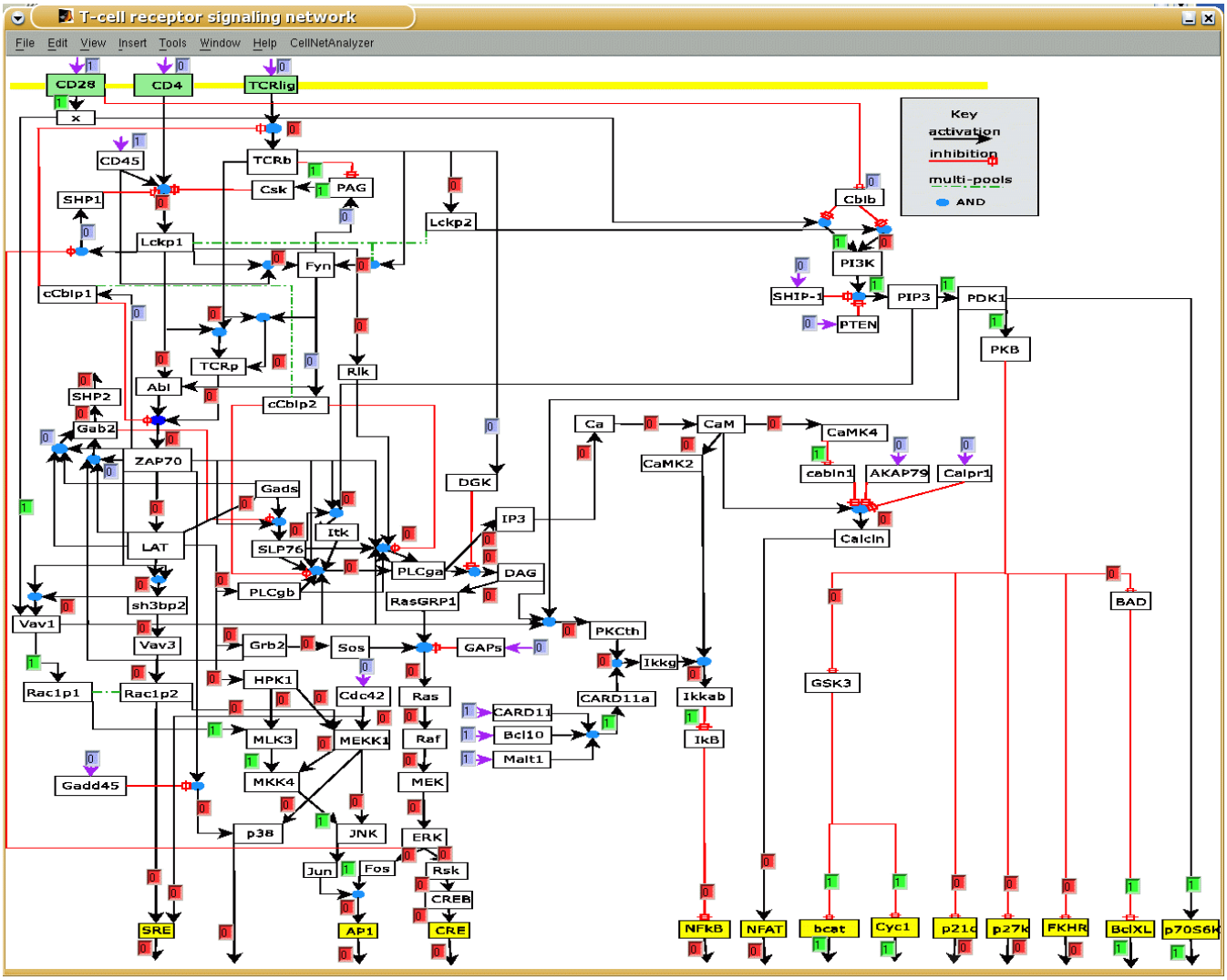

Figure 1. Logical Model of T Cell Activation (Screenshot of CellNetAnalyzer)

Each arrow pointing at a species box is a so-called hyperarc representing one possibility to activate that species (see Methods). All the hyperarcs pointing at a particular species box are OR connected. Yellow species boxes denote output elements, while green ones represent (co)receptors. In the shown "early-event" scenario, the feedback loops were switched off, and only the input for the costimulatory molecule CD28 is active (scenario in column 2 of Table 1). The resulting logical steady state was then computed. Small text boxes display the signal flows along the hyperarcs (blue boxes: fixed values prior to computation; green boxes: hyperarcs activating a species (signal flow is 1); red boxes: hyperarcs which are not active (signal flow is 0)).
doi:10.1371/journal.pcbi.0030163.g001

the literature. We did not use the known *global* information (e.g., stimulation of a receptor leads to the activation of a certain transcription factor) for the model construction. Instead, in simulations, the local interactions give rise to a global behavior which can be compared with available experimental observations (and was thus used to *verify* the model).

Each component in the logical model can be either ON ("1") or OFF ("0"). We consider a compound to be ON only if it is fully activated and able to trigger downstream events properly; otherwise, it is OFF. Furthermore, we consider two timescales [13]: early ($\tau = 1$) and late ($\tau = 2$), involving processes occurring during or after the first minutes of activation, respectively (the time-scale for each interaction is given in Table S2). Some key regulatory processes such as the degradation of signaling proteins mediated by the E3 ubiquitin ligase c-Cbl [24–26] occur after a certain time, and are thus assigned $\tau = 2$. Therefore, as will be shown later, analysis of signal propagation during the early events reveals which elements become activated, and the consideration of the late events allows a rough approximation to the dynamic behavior (sustained versus transient) of the network.

The model comprises 94 different compounds and 123 interactions that give rise to a complex map of interactions (Figure 1). It is, to the best of our knowledge, the largest Boolean model of a cellular network to date.

Interaction-Graph-Based Analyses

The first step in our analysis was to examine the interaction graph underlying the logical model. The former can be easily derived from the latter when a special representation of Boolean networks is used (see Methods). The interaction graph is less constrained than the Boolean network since it only captures direct (positive or negative) *effects* of one

molecule upon another. Thus, unlike the logical model, the interaction graph cannot describe how different causal effects converging at a certain species are combined. For example, in an interaction graph we may say that A and B have a positive influence on another node C; the logical network is more precise because it expresses that A AND B (or A OR B) are required to activate C. Accordingly, compared with the logical model, an interaction graph requires less a priori knowledge about the network under study which comes at the price that functional predictions are limited. Nevertheless, as demonstrated in this section, a number of important functional features can be revealed from the graph model.

First we studied global properties of the graph. As expected, the graph is connected (i.e., neglecting the arc directions, there is always a path from one node to all others). However, the directed graph contains as a core one strongly connected component with 33 nodes (i.e., for each pair (*a*,*b*) of nodes taken from this component there is a path from *a* to *b* and from *b* to *a*). This structural organization is related with the bow-tie structure found in other cellular networks (e.g., [7,27]) and implies that the rest of the network (not contained in the strongly connected component) mainly consists in relatively simple input and output layers (including branching cascades) feeding to and from this component.

We continued the interaction-graph-based analysis by computing the feedback loops. Feedback loops are of major importance for the dynamic behavior and functioning of biological networks. Negative feedback loops control homeostatic response and can give rise to oscillations, while positive feedbacks govern multistable behavior (connected to irreversible decision-making and differentiation processes) [15,28–30]. The interaction graph underlying the logical T cell model has 172 feedback loops, 89 thereof being negative. Remarkably, all feedback loops are only active in the second timescale because each loop contains at least one process of the second timescale. The elements of the MAPK cascade are involved in 92% of the feedback loops. This is due to the fact that there is a connection from ERK to the phosphatase SHP1 from the bottom to the top of the network [5]. Due to this connection, the resulting feedback can return to ERK via many different paths, thereby leading to a high number of loops. Indeed, if the ERK → SHP1 connection is not considered, the number of loops is reduced dramatically from 172 to 13 (with only 11 being negative), all located in the upper part of the network. c-Cbl is involved in ~85% of them, thus underscoring the importance of c-Cbl in the regulation of signaling processes [25,26].

There are 4,538 paths, each connecting one of the three compounds from the input layer (TCR, CD4/CD8, CD28) with one compound in the output layer (transcription factors and other elements controlling T cell activation). The high number of negative paths (2,058) can be traced back to the presence of two negative connections (via DGK and Gab2). In fact, considering the early signaling events within the network, where DGK and Gab2 are not active yet, the number of paths is reduced to 1,530, with only six of them being negative. These paths are from the TCR and CD28 to negative regulators of the cell cycle (p21, p27, and FKHR), having thus a positive effect on T cell proliferation. These and other global effects can be graphically inspected via the dependency matrix [13,31], depicted in Figure 2. Importantly, when considering the timescale $\tau = 1$, there is no ambivalent effect (i.e., via positive *and* negative paths) between any ordered pair (A,B) of species, i.e., A is either a pure activator of B (only positive paths from A to B), or a pure inhibitor of B (only negative paths from A to B), or has no direct or indirect influence on B at all. For example, during early activation, the TCR can only have a positive effect upon AP1 (the array element (TCRb, AP1) in Figure 2 is green). Note that this changes for timescale $\tau = 2$ where, in several cases, a compound influences another species in an ambivalent manner.

Analysis of the Logical Model

An important aspect that can be studied with a logical model is signal processing and signal propagation and the corresponding response (activation/inactivation) of the nodes upon external stimuli and perturbations (see Methods). One starts the analysis of a scenario by defining a pattern of input stimuli, possibly in combination with a set of nodes that are knocked-out or knocked-in. Then, by an iterative evaluation of the Boolean rules in each node, the signal is propagated through the network, switching each node ON or OFF, respectively (see [13] and Methods). For example, since CD28 (an input) is (permanently) ON in the scenario shown in Figure 1, it will (permanently) activate node X, which will in turn (permanently) activate Vav1, and so forth. In the same scenario, since the input CD4 is OFF, Lckp1 and therefore Abl, ZAP70, and other components cannot become activated and therefore are in the OFF state. In the ideal case, each node can be assigned a uniquely determined state that follows from a given input pattern. In terms of Boolean networks, the set of determined node values then represents a logical steady state. In some cases, in particular when negative feedback loops are active, only a fraction of the elements can be assigned a unique steady state value, whereas other (or even all) nodes might oscillate [15]. However, since in the T cell model all negative feedback loops become active only during timescale $\tau = 2$ (as described above), a complete logical steady state follows for arbitrary input patterns when considering $\tau = 1$.

Using this kind of logical steady state analysis, we first analyzed the activation pattern of key elements upon different stimuli (activation of the TCR and/or CD4 and/or CD28; Table 1) for timescale $\tau = 1$. The model was able to reproduce data from both the literature and our own experiments, providing a holistic and integrated interpretation for a large body of data. The model also predicted a non-obvious signaling event, namely that the activation of the costimulatory molecule CD28 alone leads not only to the activation of PI3K—which is to be expected from a large body of literature dealing with CD28 signaling showing that PI3K binds to the motif YxxM of CD28 [32,33]—but also to the selective activation of JNK, but not ERK. The model predicts a pathway from CD28 to JNK which gives a holistic explanation for this result: the pathway does NOT involve the LAT signalosome, activation of PLCγ1, and Calcium flux, but clearly depends on the activation of the nucleotide exchange factor Vav1 which activates MEKK1 via the small G-protein Rac1 (Figure 1). Clearly, the activating pathway shown in Figure 1 could be identified by a visual inspection of the map (note that we have intentionally drawn the network in such a way that this route can be easily seen). However, in large-scale

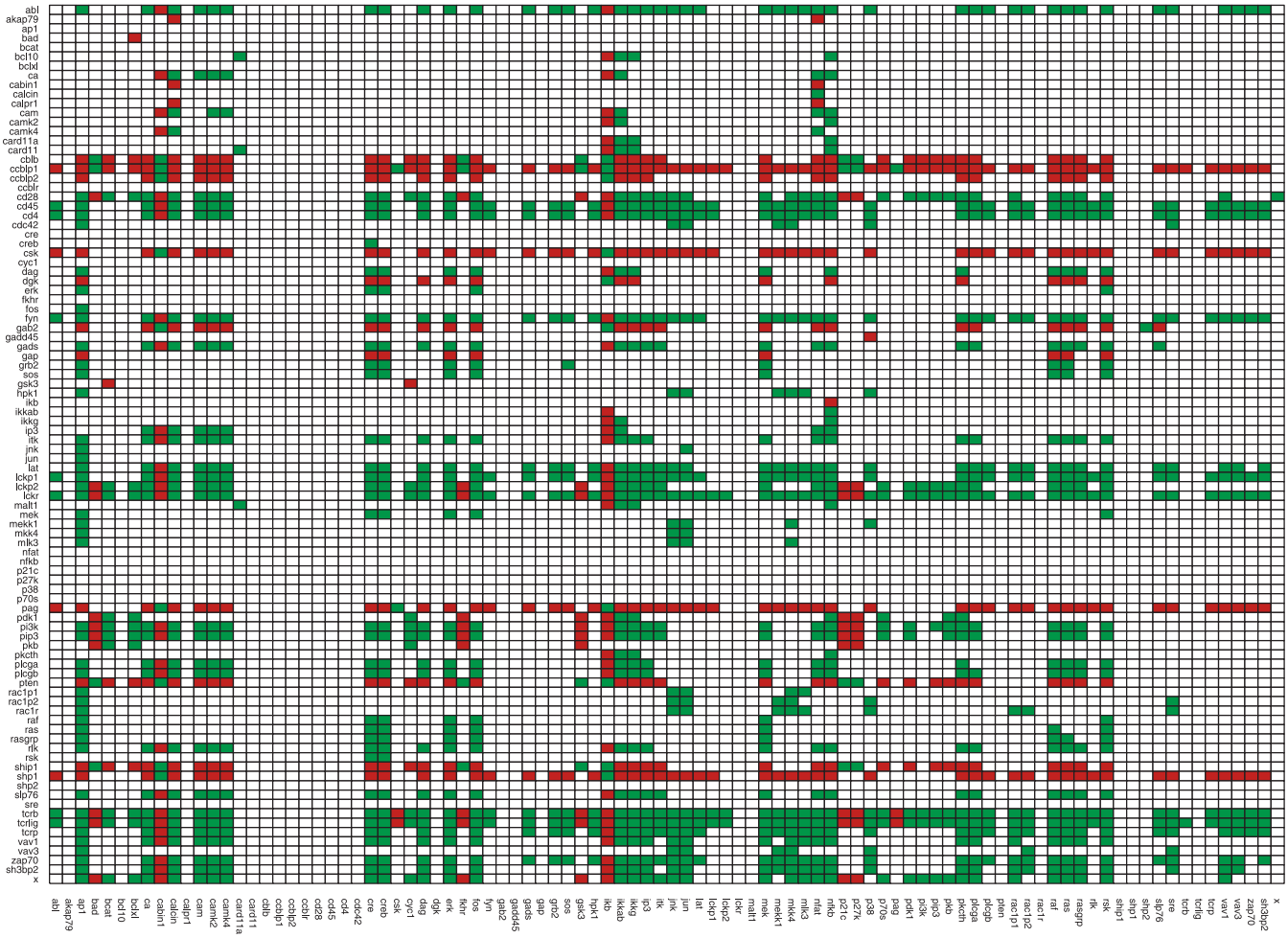

Figure 2. Dependency Matrix of the Logical T Cell Signaling Model (Figure 1) for the Early Events Scenario ($\tau = 1$)

The color of a matrix element M_{xy} has the following meaning [13]: (i) dark green: x is a total activator of y; (ii) dark red: x is a total inhibitor of y; (iii) white: no (direct or indirect) influence from x on y.

doi:10.1371/journal.pcbi.0030163.g002

networks the identification of long-distance pathways by simply following all possible routes becomes infeasible and is particularly complicated if AND connections are involved. Furthermore, since the CD28-induced JNK activation pathway was not expected, one would probably not have searched specifically for this pathway, while the algorithm reveals the whole response of the network.

The prediction made by the model is particularly surprising in light of published data which either suggest that CD28 stimulation alone does NOT activate JNK [34,35] or induces only a weak activation [36]. Driven by this surprising prediction, we performed the corresponding experiments in vitro. As shown in Figure 3A, stimulation of mouse primary T cells with a non-superagonistic CD28 antibody induced an evident and sustained JNK phosphorylation, thus confirming almost perfectly the predicted binary response. Note, the model also predicted that JNK activation does not depend on the activation of PI3K. Again, this prediction was verified by applying a pharmacological inhibitor of PI3K (Figure 3D). The discrepancies with the literature could be due either to the different cellular systems (primary T cells versus T cell lines) or to the different stimulation conditions.

The nature of the kinase involved in CD28-mediated signaling remains unclear. Indeed, application of the Src-kinase inhibitor PP2 that inactivates both Lck + Fyn [37], showed that Src-kinases, which were proposed to mediate CD28 signaling [38], are dispensable for the CD28-mediated activation of JNK (Figure 4). To fit the Src-kinase inhibitor data with the model, it would have been possible to simply bypass the Src-kinase and to draw a causal connection from CD28 to Vav. Such a connection would indeed be justified since it is well established that triggering of CD28 leads to the activation of Vav ([39]; for more details, see Table S2, reactions 35 and 48). However, we preferred to include a to-be-identified kinase X that gets activated by CD28 (Figure 1), in order to keep within the model the information that there is a component to be identified. Potential candidates for kinase X would be members of the Tec-family of PTKs. However, it is difficult to study the signaling properties of these kinases in primary non-transformed cells since specific inhibitors for Tec kinases are not yet available and the corresponding knock-out mice show defects in thymic development. Therefore, as we focused during model generation on well-established data from primary T cells and excluded data obtained from knockout mice showing alterations of thymic development, we did not include it.

Table 1. Summary of Predicted Activation Pattern upon Different Stimuli and Knock-Out Conditions

Input/ Output		WT	WT	WT	PI3K	PI3K	PI3K	SLP76	Fyn	Fyn	Fyn	Rlk and Itk	Lck and Fyn	Lck and Fyn	Lck and Fyn
Input	TCR	1	0	1	1	0	1	1	1	1	1	1	1	0	1
	CD4	0	0	0	0	0	0	0	0	1	0	0	0	0	0
	CD28	0	1	1	0	1	1	0	0	0	1	0	0	1	1
Output	ZAP	1	0	1	1	0	1	1	0	1	0	1	0	0	0
	LAT	1	0	1	1	0	1	1	0	1	0	1	0	0	0
	PLCga	1	0	1	0	0	0	0	0	1	0	0	0	0	0
	ERK	1	0	1	0	0	0	0	0	1	0	0	0	0	0
	JNK	1	1	1	1	1	1	1	0	1	1	1	0	1	1
	PKB	1	1	1	0	0	0	1	1	1	1	1	0	1	1
	AP1	1	0	1	0	0	0	0	0	1	0	0	0	0	0
	NFKB	1	0	1	0	0	0	0	0	1	0	0	0	0	0
	NFAT	1	0	1	0	0	0	0	0	1	0	0	0	0	0
	Reference	Figure 3A, 3C	Figure 3A, 3D	Figures 3A, 4	Figure 3C	Figure 3D	Figure 4	[49]	Figure 3B, [50]	Figure 3B, [50]	Figure 3B, [50]	[51]	Figure 4	Figure 4	Figure 4

The headings denote the perturbed (switched-off) element. In the case of PI3K and Lck and Fyn, the perturbation was done via a chemical inhibitor, and for the rest it was through a genetic knock-out. The "Input" rows show the stimuli, and "Output" the predictions of the model for key elements of the network. Here, blue numbers denote results corroborated by published data, while green ones were confirmed by our own data. The red number shows a discrepancy between model and experiment (see discussion in the main text). Finally, the row labeled Reference indicates the Figure where the experimental results are shown or points to the literature reference.

doi:10.1371/journal.pcbi.0030163.t001

The ability of the model to recapitulate the T cell phenotype of a variety of previously described knock-out mice was also tested (Table 1). Indeed, the model could reproduce the phenotype of several knock-outs and again reported a rather unexpected result: activation of the TCR in Fyn-deficient cells selectively triggers the PI3K/PKB pathway. This prediction was subsequently tested using peripheral primary T cells prepared from spleen of Fyn-deficient mice. As shown in Figure 3B, the wet-lab experiments corroborated the model result again.

However, there was an experimental result which the model could not reproduce: TCR-mediated JNK activation is blocked by an inhibitor of PI3K (Figure 3C). In fact, this result is not in accordance with the network because PI3K has no influence upon JNK (see dependency matrix, Figure 2).

To identify potential connections that would explain the experimental data, we applied the concept of Minimal Intervention Sets (MISs; see Methods). A MIS is a irreducible collection of actions (e.g., activation or inactivation of certain compounds), that, if applied, guarantees that a certain goal (a desired behavior) is fulfilled [13]. Here, we computed the MISs by which JNK becomes activated under the experimentally obtained constraint (see Figure 3C) that PI3K is OFF (describing the effect of the PI3K inhibitor), ZAP70 is ON, and that the TCR has been activated. These MISs (Table 2) thus provide a list of minimal combinations of elements that should be directly or indirectly affected by PI3K and thus allow us to explain the observed response of JNK upon inhibiting PI3K. Some of them are obvious, e.g., the first MIS in Table 2 suggests that JNK activation could be directly interacting with PI3K or elements that are located downstream of PI3K (e.g., PIP3). There is currently no convincing experimental evidence for an effect of PI3K on JNK, though. Other MISs in Table 2 suggest that a PI3K-mediated activation of Vav (both 1 and 3 isoforms) is involved, which would be an attractive possibility to explain the experimental data. Indeed, Vav possesses a PH domain which can bind to PIP3, and this mechanism could be important for Vav activation [40], thus making it a reasonable extension of the model.

Another molecule that could be involved in PI3K-mediated

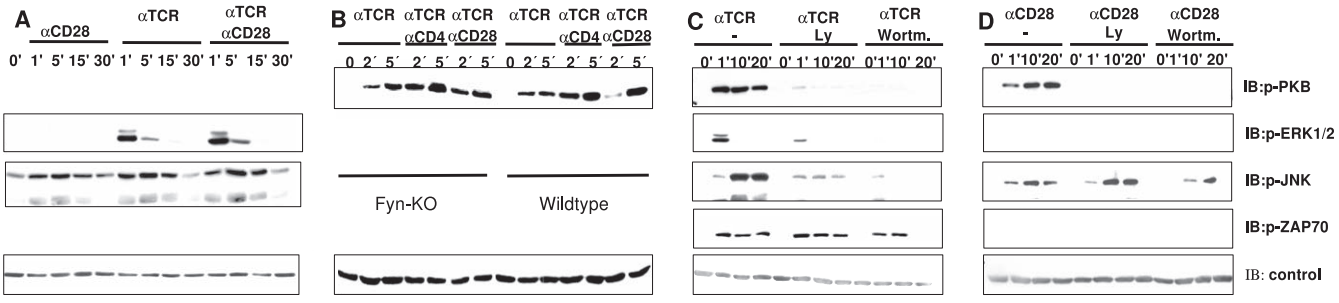

Figure 3. In Vitro Analysis of Model Predictions

(A) Activation of ERK and JNK upon CD28, TCR (CD3), or TCR + CD28 stimulation in mouse splenic T cells.
(B) Activation of PKB upon TCR, TCR+ CD4, and TCR + CD28 stimulation in Fyn-deficient and heterozygous splenic mouse T cells.
(C) Inhibition of PI3K with both Ly294002 and Wortmannin blocks the phosphorylation of PKB, ERK, and JNK, but not ZAP-70 in human T cells.
(D) Inhibition of PI3K with both Ly294002 and Wortmannin blocks the phosphorylation of PKB, but not of JNK in human T cells upon CD28 stimulation.
As a control, the total amount of ZAP70 (A) or β-actin (B–D) was determined. One representative experiment (of three) is shown.

doi:10.1371/journal.pcbi.0030163.g003

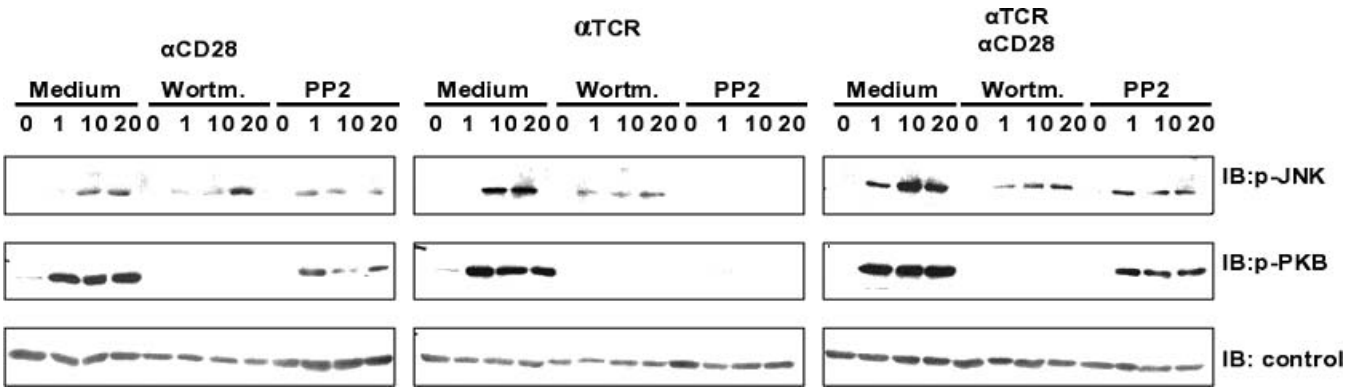

Figure 4. In Vitro Analysis of Src-Kinase Inhibition

Inhibition of Src-Kinases (Lck and Fyn) with PP2 blocks TCR-induced but affects only moderately CD28-induced PKB and JNK activation in human T cells; therefore, we concluded that CD28 signaling is not strictly Src-kinase– dependent. The effect was compared with PI3K inhibition via Wortmannin (ccf. Figure 3C and 3D), which blocks the phosphorylation of PKB but not of JNK. β-actin was included as the loading control. One representative experiment (of three) is shown.

doi:10.1371/journal.pcbi.0030163.g004

activation of JNK is the serine/threonine kinase HPK1 (see Figure 1 and Tables S1 and S2). Interestingly, HPK1 is phosphorylated by Protein Kinase D1 (PKD1) [41], a kinase whose activation depends on PKC (which in turn is dependent on DAG, downstream of PI3K) for activation. Since the regulation and functional roles of both PKD1 and PKC (with the exception of the θ isoform) are not yet well-established in T cells, we did not include them in the model, but a connection PI3K → PIP3 → Itk → PLCγ → DAG → PKC → PKD1 → HPK1 would be plausible (in which the path from PKC to HPK1 via PKD1 would be new). An alternative could be a Rac-dependent activation of HPK1 [42]; however, this is again a not-well-established connection and thus was not considered.

Definitely, the model requires a direct or indirect connection from PI3K to JNK, and additional experiments are required to assess which of the candidate links predicted by the MISs are relevant in peripheral T cells. This particular example illustrates another useful and important application of our approach: the model not only reveals that a link is missing, but also suggests candidates that can be verified experimentally. Thus, MIS analysis is capable of guiding the experimentalist and helps to plan the corresponding experiments.

As an additional application of MISs, we computed combinations of failures (constitutive activation or inactivation of elements caused for example by mutations) which lead to sustained T cell activation without external stimuli. These failure modes would cause uncontrolled proliferation and thus may be connected to diseases such as leukemia or autoimmunity. Interestingly, components occurring in the MISs with few elements (Table 3) are in fact known oncogenes: ZAP70 [43], PI3K [44], Gab2 [45], and PLCγ1 [46] (and SLP76 is directly involved in PLCγ1 activation).

Table 2. Application of the Minimal Intervention Sets To Identify Candidates To Fill the Gap between PI3K and JNK

MIS		
jnk		
hpk1	rac1r	
hpk1	sh3bp2	
mekk1	mkk4	
mekk1	mlk3	
hpk1	mekk1	rac1p1
hpk1	mekk1	vav1
hpk1	mkk4	rac1p2
hpk1	mlk3	vav3
hpk1	rac1p1	rac1p2
hpk1	rac1p1	vav3
hpk1	rac1p2	vav1
hpk1	vav1	vav3
hpk1	mlk3	rac1p2

The MISs of maximal size 3 to obtain JNK off under the conditions (i) TCR *on*, (ii) PI3K *off*, and (iii) ZAP70 *on* (as shown in the experiment, see Figure 3D and Table 1) were computed, setting the rest of conditions to the standard values for the early events. Here, each MIS represents one set of molecules that should be influenced by PI3K in order to be consistent with the fact that PI3K inhibition blocks JNK activation. For species abbreviations, see Tables S1 and S2.

doi:10.1371/journal.pcbi.0030163.t002

Robustness and Sensitivity Analysis of the Logical Model

Strongly related to the idea of MISs is a systematic evaluation of the network response if the model is confronted with failures. By considering a failure as something that happens to the cell by an internal or external event (e.g., a mutation), we may assess the *robustness*—one of the most important properties of living systems [47]—of the network. In contrast, if we consider the failure as an error that has been introduced during the modeling process (due to incomplete knowledge), then we are assessing the *sensitivity* of the model with respect to the predictions it makes. Accordingly, to study robustness and sensitivity issues, we (i) removed systematically each single interaction from the network, (ii) recomputed the scenarios given in Table 1, and (iii) compared the new predictions with the 126 original predictions (Table 1), ranking the interactions according to the number of introduced changes produced (Table 4). As an average value, 4.76 errors were introduced per simulated failure, which corresponds to 3.78% of the total numbers of predictions. The most sensitive interactions are mainly located in the upper part of the network and activate components such as the T cell receptor (TCRb), ZAP70, LAT, Fyn, or Abl. It is intuitively clear that the network is very

Table 3. Minimal Intervention Sets To Produce the Full Activation Pattern in T Cells

MIS		
!gab2	pi3k	zap70
!gab2	pip3	zap70
pi3k	plcga	zap70
pi3k	slp76	zap70
pip3	slp76	zap70
pip3	plcga	zap70
pdk1	plcga	zap70

The MISs of maximal size 3 that induce sustained full activation (namely: ap1, bcat, bclxl, cre, cyc1, nfkb, p70s, sre, and nfat are *on*, whereas fkhr, p21c, and p27k are *off*) of T cells without external stimuli. The MISs were computed using *CellNetAnalyzer*. Note that the exclamation mark "!" denotes "deactivation"; species without this symbol have to be activated (constitutively). Interestingly, the compounds involved in these MISs are involved in oncogenesis (ZAP70, PI3K, Gab2, and PLCγ1 are oncogenes, and SLP76 is directly involved in PLCγ1 activation, see Figure 1 and main text). Note that since PIP3 is a second messenger and not "mutable", for the purpose of this analysis the MISs involving its activation can be considered equivalent to those involving its activator PI3K (i.e., these MISs are equivalent).
doi:10.1371/journal.pcbi.0030163.t003

sensitive to failures (again, caused either by internal/external events or modeling errors) in these upper nodes because all pathways branching downstream are governed by them. Accordingly, the validation of our model (with the data from Table 1) is most sensitive to modeling errors in the upper part of the network. We also note that species that can be activated by more than one interaction (e.g., PI3K) are significantly less sensitive to single interaction failures since alternative pathways exist. Regarding robustness, it is worth emphasizing that in the worst case about 30% of the original predictions are affected after removal of an interaction, indicating that there is no "all-or-nothing" interaction in the network.

We have also performed the same analysis for the removal of a species (instead of an interaction) which basically led to the same results (unpublished data). However, the removal of a node can be seen as a stronger intervention in the network than deleting an interaction, as the former simulates the simultaneous removal of all interactions pointing at that species. Accordingly, deleting nodes implies some stronger deviations from the original predictions.

Qualitative Description of the Dynamics

So far we have analyzed which elements within the signaling network get activated upon signal triggering (i.e., for the first timescale $\tau = 1$). This is due to the fact that a large corpus of data for these conditions is available (see Table 1). However, it is important to note that the model is also able to roughly predict the dynamics upon different stimuli and conditions.

The modus operandi goes as follows: first, one computes the steady state values with no external input ($\tau = 0$). Subsequently, the steady state for $\tau = 1$ is computed as described above. Finally, one computes the state of the "slow" interactions (those only active at $\tau = 2$) as a function of the values at $\tau = 1$, and subsequently recomputes the steady states. This provides the response at late events, $\tau = 2$. The results obtained can be plotted in a time-dependent manner (Figure 5). Here, one can also investigate the effect of different knock-outs. For example, the absence of PAG has no effect on key downstream elements of the cascade, due to the redundant role of other negative regulatory mechanisms (specifically, the degradation via c-Cbl and Cbl-b, and Gab-2–mediated inhibition of PLCγ1). Only a multiple knock-out of these regulatory molecules leads to sustained activation of key elements. Thus, these results point to a certain degree of redundancy in negative feedbacks for switching off signaling.

This sort of qualitative analysis of the dynamics shows the ability of the Boolean approach to reproduce the key dynamic properties (transient versus sustained) of a signaling process.

Table 4. Robustness Analysis: Ranked List of the Most Sensitive Interactions

Interaction	Caused Errors if Removed
!ccblp1 + tcrlig → tcrb	39
!ccblp1 + tcrp + abl → = zap70	34
zap70 → lat	27
tcrb + lckr → fyn	26
tcrb+fyn → tcrp	26
fyn → abl	26
pi3k + !ship1 + !pten → pip3	21
lat → plcgb	15
zap70 + !gab2 + gads → slp76	15
lat → gads	15
pip3 → pdk1	13
lckp2 + !cblb → pi3k	11
lckr + tcrb → lckp2	11
!ikkab → ikb	11
zap70 + lat → sh3bp2	10
plcgb + !ccblp2 + slp76 + zap70 + vav1 + itk → plcga	10
pdk1 → pkb	10
pip3 + zap70 + slp76 → itk	10
zap70 + sh3bp2 → vav1	10
!dgk + plcga → dag	9
!shp1 + cd45 + cd4 + !csk + lckr → lckp1	8
cd28 → x	8
tcrb + lckp1 → tcrp	8
lckp1 → abl	8
mek → erk	6
ras → raf	6
ca → cam	6
dag → rasgrp	6
ip3 → ca	6
lat → grb2	6
grb2 → sos	6
plcga → ip3	6
raf → mek	6
sos + !gap + rasgrp → ras	6
x → vav1	5
mkk4 → jnk	5
mlk3 → mkk4	5
rac1p1 → mlk3	5
rac1r + vav1 → rac1p1	5

Each single non-input interaction was removed from the network followed by a recomputation of the scenarios given in Table 1. The number of deviations from the 126 predictions made in Table 1 is shown. For abbreviations and comments on the interactions, see Tables S1 and S2.
doi:10.1371/journal.pcbi.0030163.t004

Discussion

In this contribution, a logical model describing a large signaling network was established and analyzed. We set up a

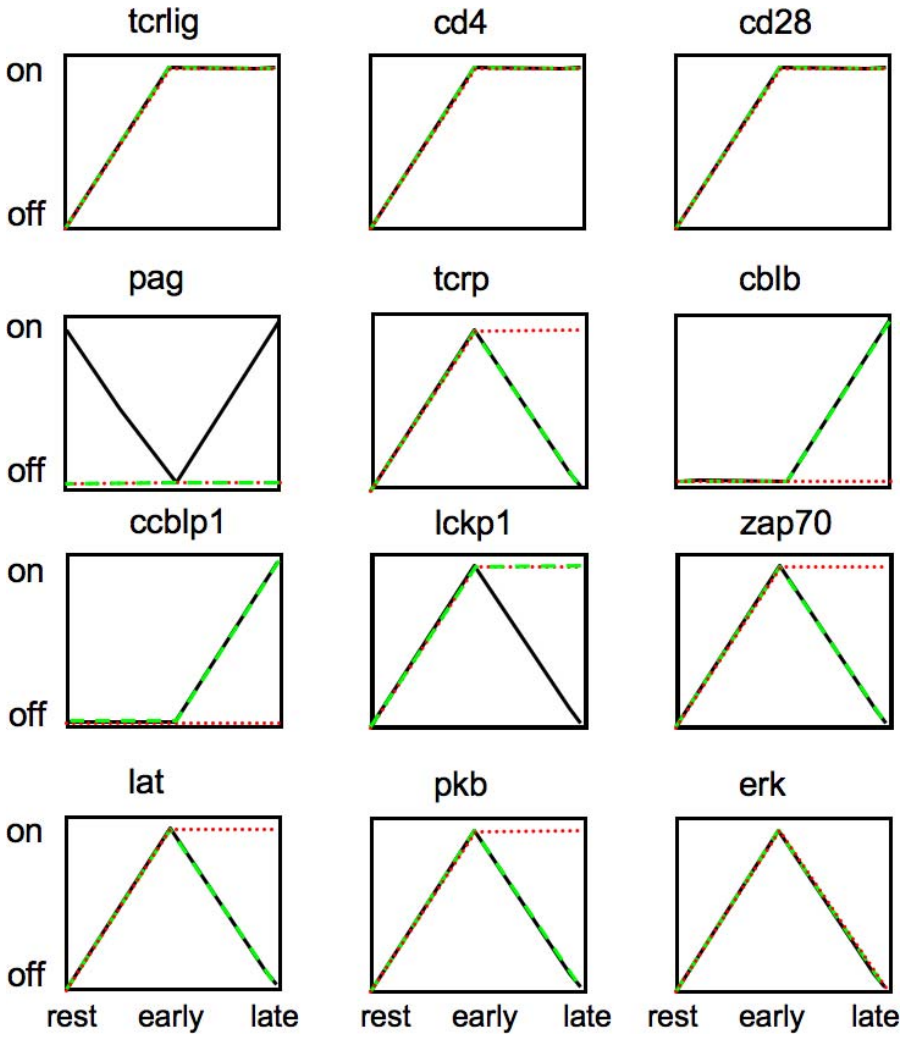

Figure 5. Considering Different Time Scales, a Rough Description of the Dynamics Can Be Obtained

The activation of key elements upon activation of the TCR, the coreceptor CD4, and the costimulatory molecule CD28 is represented at the resting state, $\tau = 0$ (no inputs); early events $\tau = 1$ (input(s), no feedback loops); and later-time events, $\tau = 2$ (input(s), feedback loops). The black lines correspond to a wild type while the green ones to a PAG KO. Note that the absence of PAG has no effect on key downstream elements of the cascade, due to the redundant role of other negative regulatory mechanisms (degradation via c-Cbl and Cbl-b, Gab-2 mediated inhibition of PLCγ1). Multiple knock-out of these regulatory molecules leads to sustained activation of key elements (red lines).

doi:10.1371/journal.pcbi.0030163.g005

comprehensive Boolean model describing T cell signaling and performed logical steady state analyses unraveling the processing of signals and the global input–output behavior. Moreover, by converting the logical model into an interaction graph, we extracted further important features, such as feedback loops, signaling paths, and network-wide interdependencies. The latter can be captured in a dependency matrix (as in Figure 2) which provides thousands of qualitative predictions that can be falsified in perturbation experiments. The logical model reproduces the global behavior of this complex network for both natural and perturbed conditions (knock-outs, inhibitors, mutations, etc.). Its validity has been proven by reproducing published data and by predicting unexpected results that were then verified experimentally. Table 1 summarizes the results of 14 different scenarios, in which the logical model predicted 126 states. For 44 of them, experimental data was available (15 from literature and 29 from our own experiments) confirming the predictions, except in the case discussed above.

Furthermore, we clearly show that the concept of intervention sets allows one (a) to identify missing links in the network, (b) to reveal failure modes that can explain the effects of a physiological dysfunction or disease, and (c) to search for suitable intervention strategies, while keeping track of potential side effects, which is valuable for drug target identification.

Compared with a kinetic model based on differential equations, a Boolean approach is certainly limited regarding the analysis of quantitative and dynamical aspects, and it certainly cannot answer the same questions. However, to establish such a model requires mainly the topology and only a relatively small amount of quantitative data; hence, a combination of information which is currently available in large-scale networks. Although the model itself is qualitative (i.e., discrete), it enables us not only to study qualitative aspects of signaling networks, but it can also be validated by semi-quantitative measurements such as those in Figures 3 and 4. In summary, with the network involved in T cell activation as a case study, our approach proved to be a

promising in silico tool for the analysis of a large signaling network, and we think that it holds valuable potential in foreseeing the effects of drugs and network modifications. Although sometimes the results of a logical model may (afterward) appear to be obvious (as in the case of the CD28-mediated JNK connection), it enables an exhaustive and rigorous analysis of the information processing taking place within a signaling network. Such a systematic analysis becomes infeasible for a human being in large-scale systems. In addition, the LIH can represent the situation of varying cofactor functions; for example, that two substances A AND B are required to activate a third substance C, but activation of C in the presence of A and a fourth substance D requires B not to be present.

Certainly, the logical model for T cell activation is far from complete. We are just at the beginning of the reconstruction process and other receptors and their pathways need to be included. However, we feel that already in its current state, the model may prove useful to inspire immunologists to ask new questions which may first be answered in silico. Furthermore, the model may also provide a framework for those who may endeavor to quantitatively model TCR signaling.

Methods

Logical network representation and analysis. We began construction of the signaling network for primary T cells by collecting data from the literature and from our own experiments providing well-established connections (Tables S1 and S2). As a first (intermediate) result, we obtain an interaction graph. Interaction graphs are signed directed graphs with the molecules (such as receptor, phosphatase, or transcription factor) as nodes and signed arcs denoting the direct influence of one species upon another, which can either be activating (+) or inhibiting (−). For example, a positive arc leads from MEK to ERK because the first phosphorylates and thereby activates the second (Figure 1). From the incidence matrix of an interaction graph we can identify important features such as feedback loops as well as signaling paths and network-wide interdependencies between pairs of species (e.g., perturbing A may have no effect on B as there is no path connecting A to B). Algorithms related to these analyses are well-known [48] and were recently presented in the context of signaling networks [13]. However, from interaction graphs we cannot conclude which combinations of signals reaching a species along the arcs are required to activate that species. For example, in Figure 1, Jun AND Fos are required to form active AP1.

For a refined representation of such relationships, we use a logical (or Boolean) model in which we introduce discrete states for the species (here the simplest (binary) case: 0 = inactive or not present; 1 = active or present) and assign to each species a Boolean function. Here we use a special representation of Boolean functions known as disjunctive normal form (DNF, also called "sum of product" representation) which uses exclusively AND, OR, and NOT operators. A Boolean network with Boolean functions in disjunctive normal form can be intuitively drawn and stored as a hypergraph (LIH) [13], which is well-suited for studying the information flows and input–output relationships in signal transduction networks (Figure 1). In this hypergraph, each hyperarc connects its start nodes with an AND operation (indicated by a blue circle in Figure 1) and each hyperarc represents one possibility for how its end node can be activated or produced (note that hyperacs may also have only one start node, i.e., they are then "graph-like" arcs). Red branches indicate species that enter the hyperarc with their negated value. For example, PLCγ-1 (PLCga in Figure 1) AND NOT DGK activates DAG (see Figure 1). Note that each LIH has a unique underlying interaction graph (which can be easily derived from the LIH representation by splitting the AND connections), whereas the opposite is, in general, not true.

Within this logical framework we may study the effect of a set of input stimuli (typically ligands) on downstream signaling by computing the logical steady state [13] that results by propagating the signals through the network from the input to the output layer. It seems worthwhile to remark that the updating assumption (synchronous versus asynchronous [14,15])—which must usually be made when dealing with dynamic Boolean networks—is not relevant here as we focus on the logical steady states, which are equivalent in both cases. Sometimes a logical steady state is not unique or does not exist due to the presence of feedbacks loops. However, many feedback loops become active only in a longer timescale justifying setting them OFF in the first wave of signal propagation (allowing them to be switched ON for the second timescale). This has been used here for several feedback loops (see main text and Table S2). The effect of knocking-out a species can be tested by re-computing the (new) logical steady state for the respective stimuli. MISs satisfying a given intervention goal can be computed by systematically testing sets of permanently activated or/and deactivated nodes [13,31].

All mathematical analyses and computations have been performed with our software tool *CellNetAnalyzer* [31], a comprehensive user interface for structural analysis of cellular networks. *CellNetAnalyzer* and the T cell model can be downloaded for free (for academic use) from http://www.mpi-magdeburg.mpg.de/projects/cna/cna.html.

Immunoblotting. Human or mouse T cells were purified using an AutoMACS magnetic isolation system according to the manufacturer's instructions (Miltenyi, http://www.miltenyibiotec.com). Mouse T cells were stimulated with 10 μg/ml of biotinylated CD3ε (a subunit of the TCR) antibody (145–2C11, BD Biosciences, http://www.bdbiosciences.com/), 10 μg/ml of biotinylated CD28 antibody (37.51, BD Biosciences), CD3 plus CD28 mAbs, or with CD3 plus 10 μg/ml of biotinylated CD4 (GK1.5, BD Biosciences) followed by crosslinking with 25 μg/ml of streptavidin (Dianova, http://www.dianova.de) at 37 °C for the indicated periods of time. Human T cells were stimulated with CD3ε mAb MEM92 (IgM, kindly provided by Dr. V. Horejsi, Prague, Czech Republic) or with CD3 plus CD28 mAbs (248.23.2). Cells were lysed in buffer containing 1% NP-40, 1% laurylmaltoside (N-dodecyl β-D-maltoside), 50 mM Tris pH 7.5, 140 mM NaCl, 10mM EDTA, 10 mM NaF, 1 mM PMSF, 1 mM Na_3VO_4. Proteins were separated by SDS/PAGE, transferred onto membranes, and blotted with the following antibodies: anti-phosphotyrosine (4G10), anti-ERK1/2 (pT202/pT204), anti-JNK (pT183/pY185), anti-phospho-Akt (S473) (all from Cell Signaling, http://www.cellsignal.com/), anti-ZAP70 (pTyr 319, Cell Signaling), anti-ZAP70 (cloneZ24820, Transduction Laboratories, http://www.bdbiosciences.com/), or against β-Actin (Sigma, http://www.sigmaaldrich.com/). Where PI3K and src-kinase inhibitors were used, T cells were treated with 100 nM Wortmannin (Calbiochem, http://www.emdbiosciences.com) or 10 μM PP2 (Calbiochem) for 30 min at 37 °C prior to stimulation. All experiments have been repeated three times and reproduced the shown results.

Supporting Information

Table S1. List of Compounds in the Logical T Cell Model

Model name corresponds to the name in Figure 1 and Table S2. Common abbreviations are those usually used in the literature, while name is the whole name. Type classifies the molecules, if applies, as follows: K = Kinase, T = Transcription Factor, P = Phosphatase, A = Adaptor Protein, R = Receptor, G = GTP-ase. In the case where two pools of a molecule were considered, a "reservoir" was included which was required for both pools. This allows us to perform a simultaneous knock-out of both pools.

Found at doi:10.1371/journal.pcbi.0030163.st001 (56 KB PDF).

Table S2. Hyperarcs of the Logical T Cell Signaling Model (see Figure 1 and Methods)

Exclamation mark ("!") denotes a logical NOT, and dots within the equations indicate AND operations. The names of the substances in the explanations are those used in the model and Figure 1; the biological names are displayed in Table S1. In the case where two pools of a molecule were considered (e.g., lckp1 and lckp2), a "reservoir" (lckr) was included which was required for both pools. This allows us to perform a simultaneous knock-out of both pools acting on the reservoir.

Found at doi:10.1371/journal.pcbi.0030163.st002 (183 KB PDF).

Acknowledgments

The authors would like to thank the members of the signaling group at the Institute of Immunology (M. Smida, X. Wang, S. Kliche, R. Pusch, M.

Togni, A. Posevitz, V. Posevitz, T. Drewes, U. Kölsch, S. Engelmann) and I. Merida and J. Huard for essential biological input into the model.

Author contributions. JSR set up the model and performed the analysis. LS, JAL, UB, BA, and BS, with the help of the signaling group at the Institute of Immunology, gathered the biological details of the model and analyzed the correctness of the results. LS and BA performed the wet-lab experiments. RH supported the model setup, analysis, and documentation. SK developed the theoretical methods and tools (*CellNetAnalyzer*) and supported the analysis. UUH and RW contributed to the theoretical methods with useful insights. EDG, BS, and RW coordinated the project.

Funding. The authors are thankful for the support of the German Ministry of Research and Education to EDG (Hepatosys), the German Research Society to BS and EDG (FOR521), and the Research Focus Dynamical Systems funded by the Saxony-Anhalt Ministry of Education.

Competing interests. The authors have declared that no competing interests exist.

References

1. Kitano H (2002) Computational systems biology. Nature 420: 206–210.
2. Alon U, Surette MG, Barkai N, Leibler S (1999) Robustness in bacterial chemotaxis. Nature 397: 168–171.
3. Wiley HS, Shvartsman SY, Lauffenburger DA (2003) Computational modeling of the EGF-receptor system: A paradigm for systems biology. Trends Cell Biol 13: 43–50.
4. Sasagawa S, Ozaki Y, Fujita K, Kuroda S (2005) Prediction and validation of the distinct dynamics of transient and sustained ERK activation. Nat Cell Biol 7: 365–373.
5. Altan-Bonnet G, Germain RN (2005) Modeling T cell antigen discrimination based on feedback control of digital ERK responses. PLoS Biol 3: 356.
6. Papin JA, Hunter T, Palsson BO, Subramaniam S (2005) Reconstruction of cellular signalling networks and analysis of their properties. Nat Rev Mol Cell Biol 6: 99–111.
7. Oda K, Matsuoka Y, Funahashi A, Kitano H (2005) A comprehensive pathway map of epidermal growth factor receptor signaling. Mol Syst Biol. doi:10.1038/msb4100014
8. Jeong H, Mason SP, Barabasi AL, Oltvai ZN (2001) Lethality and centrality in protein networks. Nature 411: 41–42.
9. Milo R, Shen-Orr S, Itzkovitz S, Kashtan N, Chklovskii D, et al. (2002) Network motifs: Simple building blocks of complex networks. Science 298: 824–827.
10. Ma'ayan A, Jenkins SL, Neves S, Hasseldine A, Grace E, et al. Formation of regulatory patterns during signal propagation in a Mammalian cellular network. Science 309: 1078–1083.
11. Stelling J, Klamt S, Bettenbrock K, Schuster S, Gilles ED (2002) Metabolic network structure determines key aspects of functionality and regulation. Nature 420: 190–193.
12. Price ND, Reed JL, Palsson BO (2004) Genome-scale models of microbial cells: Evaluating the consequences of constraints. Nat Rev Microbiol 2: 886–897.
13. Klamt S, Saez-Rodriguez J, Lindquist J, Simeoni L, Gilles ED (2006) A methodology for the structural and functional analysis of signaling and regulatory networks. BMC Bioinformatics 7: 56.
14. Kauffman SA (1969) Metabolic stability and epigenesis in randomly constructed genetic nets. J Theor Biol 22: 437–467.
15. Thomas R, D'Ari R (1990) Biological feedback. Boca Raton (Florida): CRC Press.
16. Mendoza L, Thieffry D, Alvarez-Buylla ER (1999) Genetic control of flower morphogenesis in *Arabidopsis thaliana*: A logical analysis. Bioinformatics 15: 593–606.
17. Albert R, Othmer HG (2003) The topology of the regulatory interactions predicts the expression pattern of the *Drosophila* segment polarity genes. J Theor Biology 223: 1–18.
18. Chaves M, Albert R, Sontag ED (2005) Robustness and fragility of Boolean models for genetic regulatory networks. J Theor Biol 235: 431–449.
19. Benjamini E, Coico R, Sunshine G (2000) Immunology—A short course. New York: Wiley-Liss.
20. Huang Y, Wange RL (2004) T cell receptor signaling: Beyond complex complexes. J Biol Chem 279: 28827–28830.
21. Lee KH, Holdorf AD, Dustin ML, Chan AC, Allen PM, et al. (2003) T cell receptor signaling precedes immunological synapse formation. Science 295: 1539–1542.
22. Chan C, Stark J, George AT (2004) Feedback control of T-cell receptor activation. Proc Biol Sci 271: 931–939.
23. Mendoza L (2006) A network model for the control of the differentiation process in Th cells. Biosystems 84: 101–114.
24. Meng W, Sawasdikosol S, Burakoff SJ, Eck MJ (1999) Structure of the amino-terminal domain of Cbl complexed to its binding site on ZAP-70 kinase. Nature 398: 84–90.
25. Duan L, Reddi AL, Ghosh A, Dimri M, Band H (2004) The Cbl family and other ubiquitin ligases destructive forces in control of antigen receptor signaling. Immunity 21: 7–17.
26. Thien CB, Langdon WY (2005) c-Cbl and Cbl-b ubiquitin ligases: Substrate diversity and the negative regulation of signalling responses. Biochem J 15: 153–166.
27. Csete M, Doyle J (2004) Bow ties, metabolism and disease. Trends Biotechnol 22: 44–450.
28. Reth M, Brummer T (2004) Feedback regulation of lymphocyte signalling. Nat Rev Immunol 4: 269–277.
29. Cinquin O, Demongeot J (2002) Positive and negative feedback: Striking a balance between necessary antagonists. J Theor Biol 216: 229–241.
30. Remy E, Ruet P (2006) On differentiation and homeostatic behaviours of Boolean dynamical systems, Lect Notes Comput Sci 4230: 153–162.
31. Klamt S, Saez-Rodriguez J, Gilles ED (2007) Structural and functional analysis of cellular networks with CellNetAnalyzer. BMC Systems Biology 1: 2.
32. Cai YC, Cefai D, Schneider H, Raab M, Nabavi N, et al. (1995) CD28pYMNM mutations implicate phosphatidylinositol 3-kinase in CD86-CD28-mediated costimulation. Immunity 3: 417–426.
33. Rudd CE, Raab M (2003) Independent CD28 signaling via VAV and SLP-76: A model for in trans costimulation. Immunol Rev 192: 32–41.
34. Su B, Jacinto E, Kallunki T, Karin M, Ben-Neriah Y (1994) JNK is involved in signal integration during costimulation of T lymphocytes. Cell 77: 727–736.
35. Harlin H, Podack E, Boothby M, Alegre ML (2002) TCR-Independent CD30 signaling selectively induces IL-13 production via a TNF receptor-associated factor/p38 mitogen-activated protein kinase-dependent mechanism J Immunol 169: 2451–2459.
36. Gravestein LA, Amsen D, Boes M, Calvo CR, Kruisbeek AM, et al. (1998) The TNF receptor family member CD27 signals to Jun N-terminal kinase via Traf-2. Eur J Immunology 28: 2208–2216.
37. Hanke JH, Gardner JP, Dow RL, Changelian PS, Brissette WH, et al. (1996) Discovery of a novel, potent, and Src family-selective tyrosine kinase inhibitor. Study of Lck- and FynT-dependent T cell activation. J Biol Chem 271: 695–701.
38. Holdorf AD, Green JM, Levin SD, Denny MF, Straus DB, et al. (1999) Proline residues in CD28 and the Src homology (SH)3 domain of Lck are required for T cell costimulation. J Exp Med 190: 375–384.
39. Kovacs B, Parry RV, Ma Z, Fan E, Shivers DK, et al. (2005) Ligation of CD28 by its natural ligand CD86 in the absence of TCR stimulation induces lipid raft polarization in human CD4 T cells. J Immunol. 175: 7848–7854.
40. Tybulewicz VL (2005) Vav-family proteins in T-cell signalling. Curr Opin Immunol 17: 267–274.
41. Arnold R, Patzak IM, Neuhaus B, Vancauwenbergh S, Veillette A, et al. (2005) Activation of hematopoietic progenitor kinase 1 involves relocation, autophosphorylation, and transphosphorylation by protein kinase D1. Mol Cell Biol 25: 2364–2383.
42. Hehner SP, Hofmann TG, Dienz O, Droge W, Schmitz ML (2000) Tyrosine-phosphorylated Vav1 as a point of integration for T-cell receptor- and CD28-mediated activation of JNK, p38, and interleukin-2 transcription. J Biol Chem 275: 18160–18171.
43. Herishanu Y, Kay S, Rogowski O, Pick M, Naparstek E, et al. (2005) T-cell ZAP-70 overexpression in chronic lymphocytic leukemia (CLL) correlates with CLL cell ZAP-70 levels, clinical stage and disease progression. Leukemia 19: 1289–1291.
44. Chang F, Lee JT, Navolanic PM, Steelman LS, Shelton JG, et al. (2003) Involvement of PI3K/Akt pathway in cell cycle progression, apoptosis, and neoplastic transformation: A target for cancer chemotherapy. Leukemia 17: 590–603.
45. Bentires-Alj M, Gil SG, Chan R, Wang ZC, Wang Y, et al. A role for the scaffolding adapter GAB2 in breast cancer. Nat Med 12: 114–121.
46. Noh DY, Kang HS, Kim YC, Youn YK, Oh SK, et al. (1998) Expression of phospholipase C-gamma 1 and its transcriptional regulators in breast cancer tissues. Anticancer Res 18: 2643–2648.
47. Stelling J, Sauer U, Szallasi Z, Doyle FJ III, Doyle J (2004) Robustness of cellular functions. Cell 118: 675–685.
48. Schrijver A (2003) Combinatorial optimization. Berlin: Springer.
49. Yablonski D, Kuhne MR, Kadlecek T, Weiss A (1998) Uncoupling of nonreceptor tyrosine kinases from PLC-gamma1 in an SLP-76-deficient T cell. Science 281: 413–416.
50. Sugie K, Jeon MS, Grey HM (2004) Activation of naive CD4 T cells by anti-CD3 reveals an important role for Fyn in Lck-mediated signaling. Proc Natl Acad Sci U S A 101: 14859–14864.
51. Schaeffer EM, Debnath J, Yap G, McVicar D, Liao XC, et al. (1999) Requirement for Tec kinases Rlk and Itk in T cell receptor signaling and immunity. Science 284: 638–641.

Appendix 10

Deletion of the LIME adaptor protein minimally affects T and B cell development and function

Grégoire C., Simova S., Wang Y., Sansoni A., Richelme S., Schmidt-Giese A., **Simeoni L.**, Angelisova P., Reinhold D., Schraven B., Horejsi V., Malissen B., and Malissen M. (2007) *Eur J Immunol.* 37:3259-69.

European Journal of Immunology

Deletion of the LIME adaptor protein minimally affects T and B cell development and function

Claude Grégoire[1,2,3], Sarka Simova[4], Ying Wang[1,2,3], Amandine Sansoni[1,2,3], Sylvie Richelme[1,2,3], Anja Schmidt-Giese[5], Luca Simeoni[5], Pavla Angelisova[4], Dirk Reinhold[5], Burkhart Schraven[5], Vaclav Horejsi[4], Bernard Malissen[1,2,3] and Marie Malissen[1,2,3]

[1] Centre d'Immunologie de Marseille-Luminy, Université de la Méditerranée, Marseille, France
[2] INSERM, U631, Marseille, France
[3] CNRS, UMR6102, Marseille, France
[4] Institute of Molecular Genetics, Academy of Sciences of the Czech Republic, Prague, Czech Republic
[5] Institute for Immunology, Otto-von-Guericke-University, Magdeburg, Germany

LIME (Lck-interacting membrane protein) is a transmembrane adaptor that associates with the Lck and Fyn protein tyrosine kinases and with the C-terminal Src kinase (Csk). To delineate the role of LIME *in vivo*, LIME-deficient mice were generated. Although *Lime* transcripts were expressed in immature and mature B and T cells, the absence of LIME impeded neither the development nor the function of B and T cells. TCR transgenic mice deprived of LIME showed, however, a 1.8-fold enhancement in positive selection. Since B cells and activated T cells express LIME and the related adaptor NTAL, mice lacking both adaptors were generated. Double-deficient mice showed no defect in the development and function of B and T cells, and the lack of LIME had no effect on the autoimmune syndrome that develops in aged NTAL-deficient mice. In contrast to a previous report, we further showed that this autoimmune syndrome develops in the absence of T cells. Therefore, our *in vivo* results refute all the previous roles postulated for LIME on the basis of studies of transformed B and T cells and demonstrate that LIME has no seminal role in the signaling cassette operated by antigen receptors and coreceptors.

Received 13/6/07
Revised 31/7/07
Accepted 14/9/07

[DOI 10.1002/eji.200737563]

Key words: B cells · Knockout · Signaling · T cells · Transmembrane adaptor

Introduction

Transmembrane adaptor proteins (TRAP) represent a group of molecules participating in immunoreceptor signaling. They possess a short extracellular domain, a transmembrane region, and a long cytoplasmic tail carrying up to ten potential tyrosine phosphorylation sites. In contrast to the signaling subunits that are associated with immunoreceptors and that contain immunoreceptor tyrosine activation motif (ITAM), the known TRAP carry no ITAM and do not associate directly with immunoreceptors. So far four TRAP have been identified as components of membrane lipid rafts and denoted as 'linker of activation of T cells' (LAT, also

Correspondence: Bernard Malissen, Centre d'Immunologie de Marseille-Luminy, INSERM-CNRS, Université de la Méditerranée, Parc Scientifique de Luminy, Case 906, 13288 Marseille Cedex 9, France
Fax : +33-4-9126–9430
e-mail: bernardm@ciml.univ-mrs.fr

Abbreviations: Csk: C-terminal Src kinase · **LAT:** linker of activation of T cells · **LIME:** Lck-interacting membrane protein · **NTAL:** non-T cell activation linker · **PAG:** phosphoprotein associated with glycolipid-enriched membranes · **TRAP:** transmembrane adaptor protein(s)

called LAT1), phosphoprotein associated with glycolipid-enriched membranes (PAG, also known as Cbp), non-T cell activation linker (NTAL, also called LAB or LAT2), and Lck-interacting membrane protein (LIME) (reviewed in [1]). These TRAP possess two palmitoylated cysteine residues in the membrane proximal segment of their cytoplasmic tail that target them to lipid rafts. Upon tyrosine phosphorylation, which is mostly due to Src- and Syk-family protein tyrosine kinases, TRAP bind several SH2 domain-containing cytoplasmic signaling molecules. This results in the assembly of membrane proximal complexes that regulate immunoreceptor signaling in a positive or negative manner.

So far little is known about the biological functions of LIME [2–4]. In humans, LIME is expressed predominantly in T cells and becomes tyrosine phosphorylated by Src-family kinases. This phosphorylation occurs exclusively after cross-linking of the CD4 and CD8 co-receptors by antibodies, or by the HIV glycoprotein 120 in the case of CD4 [3]. Overexpression of LIME in Jurkat T cells amplifies TCR-mediated calcium flux, phosphorylation of Erk and transcriptional activation of the *IL-2*-gene promoter [3]. It is therefore possible that LIME plays a positive role in the sequential activation of Lck and Fyn that occurs in the lipid rafts of T cells [5]. Considering that inhibitory signals are induced when CD4 is cross-linked in the absence of TCR engagement [6], the ensuing tyrosine phosphorylation of LIME could also generate inhibitory signals. Finally, LIME may also account for the remarkable ability of certain anti-CD4 antibodies to induce a state of antigen-specific tolerance through the induction of regulatory T cells [7].

The published data on mouse LIME are somewhat different. High expression of LIME was observed in the lung. In T cells, LIME expression was rapidly up-regulated following TCR-cross-linking and LIME was localized at the contact site between T cells and antigen-presenting cells (APC) [2]. A recent report further indicated that LIME might be involved in BCR-mediated B cell activation [4]. Suppression of LIME expression by siRNA resulted in inhibition of BCR-mediated activation of MAPK, PI3K, calcium flux, NFAT, and NF-κB. To further elucidate the function of LIME *in vivo*, we have generated LIME-deficient mice and have analyzed them for the development and function of B and T lymphocytes.

Results

LIME expression in mouse B and T cells

Previous studies contain several inconsistencies with regards to the pattern of expression of LIME [2, 8]. To settle this issue, populations corresponding to several stages of mouse B and T cell differentiation were prepared by cell sorting and analyzed by quantitative RT-PCR for their relative levels of *Lime* transcripts (Fig. 1A). The same cell populations were also analyzed for the presence of *Lat* and *Ntal* transcripts. As shown in Fig. 1A, $CD4^+CD8^+$ thymocytes expressed *Lime* transcripts at lower levels than mature, resting $CD4^+$ and $CD8^+$ T cells. A recent study analyzing whole B cells isolated from the spleen showed that LIME is expressed in mouse B cells [4]. To more precisely determine the pattern of LIME expression within mature B cells, splenic B cells were sorted according to IgM and IgD expression. IgM^{high} IgD^{low} or transitional 1 (T1) cells, are recent immigrant from the bone marrow that develop into IgM^{high} IgD^{high} transitional 2 (T2) cells, some of which differentiate further into mature IgM^{low} IgD^{high}, or follicular recirculating B cells [9]. As shown in Fig. 1, *Lime* transcripts were expressed in T1, T2, and mature B cells, albeit at lower levels than in mature T cells. Plasma cells also expressed *Lime* transcripts at levels comparable to those found in their direct follicular B cell precursors (Fig. 1A). Moreover, Lime transcripts were expressed during early stages of B cell differentiation in the bone marrow (Fig. 1A).

T cell development in LIME-deficient mice

To explore the role of LIME in B and T cell development and function, we generated mice deprived of LIME. As depicted in Fig. 2, our knockout approach resulted in the replacement of the whole LIME coding sequence with a *loxP* sequence. Mice homozygous for this mutation, $Lime^{-/-}$, were born at the expected Mendelian frequencies and were deprived of detectable LIME protein (Fig. 2F). Analysis of $Lime^{-/-}$ mice showed that their thymi, spleens, and lymph nodes were of normal size. Monitoring CD4, CD8, CD44, CD25, CD62L, CD5, TCRαβ, TCRγδ and CD49b (DX5) expression, showed no major alteration in the T cell, NK T cell, and NK cell populations from thymus and secondary lymphoid organs (Fig. 3 and data not shown). T cell proliferation and IL-2 production in response to graded concentrations of anti-CD3 antibody, or to a suboptimal dose of anti-CD3 antibody in combination with increasing concentrations of anti-CD28 antibody were similar in LIME-sufficient and -deficient T cells (Fig. 4A and B). Upon CD3 cross-linking, $Lime^{-/-}$ thymocytes and $CD4^+$ T cells showed calcium responses of the same magnitude as those observed in wild-type counterparts (Fig. 4D and data not shown). In line with these data, the clinical course of experimental autoimmune encephalitis (EAE), a mouse model of human multiple sclerosis, was not influenced by the absence of LIME (data not shown). We also evaluated whether the loss of LIME affects the ability of the CD4 molecule to deliver inhibitory signals

when cross-linked prior to the engagement of the TCR. When CD4 expressed on LIME-sufficient and -deficient T cells was cross-linked for 45 min before stimulation with anti-CD3 antibodies, the same inhibitory signals were delivered by the cross-linked molecules CD4 (Fig. 4C and D). Therefore, the absence of LIME does not detectably affect a large panel of events associated with T cell development and function.

LIME deficiency improves positive selection of Marilyn TCR transgenic thymocytes

To analyze with a higher sensitivity the effect of the *Lime*-deficiency on intrathymic positive and negative selection events, *Lime*$^{-/-}$ mice were backcrossed into transgenic mice expressing an MHC class II-restricted TCR and maintained on a RAG-deficient background. We used the Marilyn TCR transgenic line because it expresses a monoclonal population of Vβ6$^+$ CD4$^+$ T cells specific for Dby, a male H-Y antigen presented by I-A^b molecules, and permits positive and negative selection among the same littermates to be readily analyzed [10]. Moreover, since *in vitro* experiments showed that LIME is heavily tyrosine phosphorylated after CD4 cross-linking [3], using the Marilyn TCR transgenic line we could gauge the role of LIME in a CD4-dependent physiological set-up. Comparison of the thymi of LIME-sufficient and -deficient Marilyn female mice for their cellularity, CD4-CD8 staining profile, and levels of CD3 and of Vβ6$^+$ TCR showed that LIME deficiency improves the selection of mature CD4$^+$ SP cells expressing transgenic TCR (Fig. 5A). *Lime*$^{-/-}$ Marilyn female mice showed a 1.8-fold increase in the number of clonotype-positive CD4$^+$ SP cells [$15.1 \pm 4.5 \times 10^6$ in wild-type Marilyn female thymi (n=4) *versus* $27.5 \pm 2.1 \times 10^6$ in *Lime*$^{-/-}$ Marilyn female thymi (n=6)]. Consistent with this observation, comparison of the spleen from LIME-deficient and -sufficient Marilyn female mice showed that the absence of LIME resulted in a threefold increase in the number of clonotype-positive CD4$^+$ cells [$1.6 \pm 0.5 \times 10^6$ in wild-type Marilyn female spleen (n=4) *versus* $5.2 \pm 1.6 \times 10^6$ in *Lime*$^{-/-}$ Marilyn female spleen (n=6)]. In LIME-sufficient, Marilyn male mice, negative selection results in the absence of TCR^{high} DP and of CD4$^+$ SP cells, and, as a consequence, the periphery is deprived of clonotype-positive CD4$^+$ T cells. As shown in Fig. 5A, in LIME-deficient, Marilyn male mice, the lack of LIME had no measurable impact on negative selection. As documented in other TCR transgenic model, a minute population of clonotype-

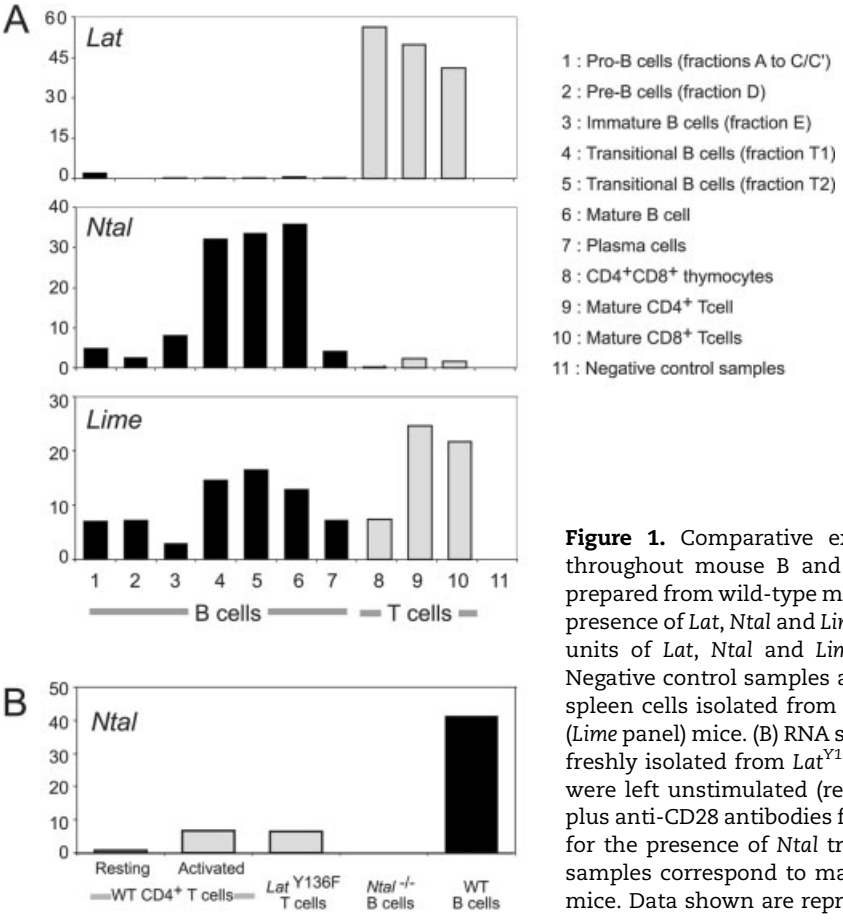

Figure 1. Comparative expression of *Lime*, *Lat* and *Ntal* transcripts throughout mouse B and T cell development. (A) RNA samples were prepared from wild-type mice and analyzed by quantitative RT-PCR for the presence of *Lat*, *Ntal* and *Lime* transcripts. Results are expressed as relative units of *Lat*, *Ntal* and *Lime* mRNA normalized using *Hprt* transcripts. Negative control samples are shown on lane 11 and corresponds to total spleen cells isolated from *Lat*$^{-/-}$ (*Lat* panel), *Ntal*$^{-/-}$ (*Ntal* panel) or *Lime*$^{-/-}$ (*Lime* panel) mice. (B) RNA samples were prepared from CD4$^+$ Th2 effectors freshly isolated from *Lat*^{Y136F} mice and from wild-type CD4$^+$ T cells that were left unstimulated (resting) or stimulated (activated) with anti-CD3 plus anti-CD28 antibodies for 40 h prior to analysis by quantitative RT-PCR for the presence of *Ntal* transcripts. Positive (+) and negative (-) control samples correspond to mature B cells isolated from wild-type or *Ntal*$^{-/-}$ mice. Data shown are representative of two independent experiments.

positive, $CD4^-CD8^-$ T cells is found in the periphery of Marilyn male mice and is not affected by the lack of LIME (Fig. 5A). Despite the presence of slightly lower levels of clonotypic TCR on their surface (Fig. 5A), the mature $CD4^+$ cells found in the periphery of *Lime*$^{-/-}$ Marilyn female mice were capable of proliferating and producing IL-2 in response to their cognate antigen, and slightly higher responses were even observed in the absence of LIME (Fig. 5B and C).

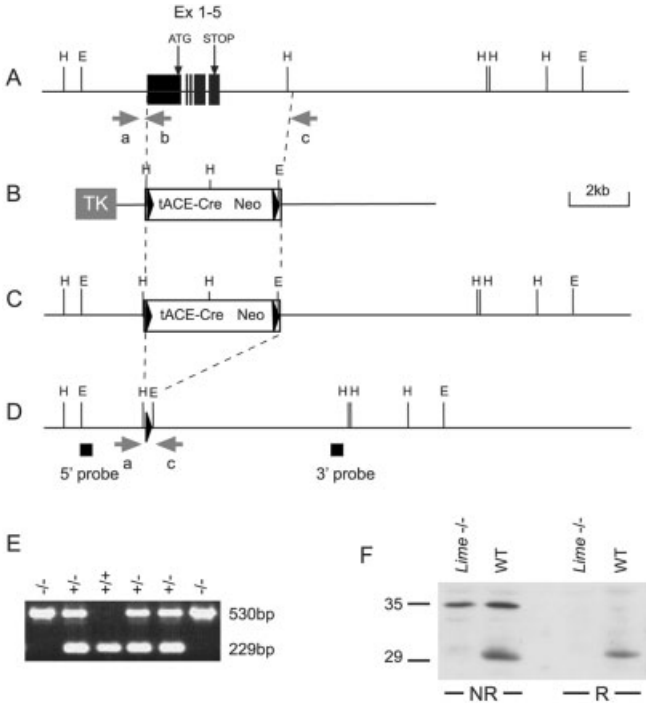

Figure 2. Generation and identification of *Lime* deficient mice. (A–D) Strategy used to delete the *Lime* gene. (A) Partial restriction map of the wild-type *Lime* gene. Exons are shown as filled boxes. Exons containing the initiation (ATG) and stop codon are specified (E: EcoRI, H: HindIII). (B) Targeting vector used for the deletion of exons 1–5. Shaded and open boxes correspond to the thymidine kinase gene (TK) and to the loxP-flanked-Cre-Neo^r cassette, respectively. LoxP sites are shown as triangles. (C) Structure of the targeted allele following homologous recombination. (D) Final structure of the targeted allele after self-excision of the Cre-Neo^r cassette. The 5′ and 3′ single-copy probes used to verify 5′ and 3′ targeting events are indicated. The position of the PCR primers used to genotype the resulting mice are indicated by arrows. (E) PCR genotyping of *Lime*-deficient and -sufficient littermates using primers indicated in (D). (F) Lack of LIME expression in T cells from *Lime*$^{-/-}$ mice as detected by Western blotting. Total cell lysates were processed under reducing (R) or non-reducing (NR) conditions, and revealed with a rabbit antiserum directed at mouse LIME. The position of LIME (29 kDa) and of a non-specifically reactive protein of 35 kDa is indicated. The intensity of this last band demonstrates that each lane was loaded with comparable amounts of total proteins.

B cell development and function in LIME-deficient mice

Although LIME is expressed in immature and mature B cells, analysis of splenic B cell populations showed that they are capable of properly reaching the T1, T2, and follicular stages in the absence of LIME (Fig. 6A). Consistent with these results, basal levels of IgG1, IgG2a, IgG2b, IgG3 and IgE, and antibody responses to a T-dependent antigen were normal in LIME-deficient mice (data not shown). Importantly, NTAL, another raft-associated TRAP is expressed in T1, T2, and follicular B cells [11]. Young mice deprived of NTAL showed no defect in B cell differentiation and function [11, 12]. Because NTAL and LIME are coincidently expressed in immature and mature B cells (Fig. 1), the product of the other may have backed up the function of the missing one. Therefore, to analyze whether some redundancy exists between NTAL and LIME in mouse B cells, *Lime*$^{-/-}$ and *Ntal*$^{-/-}$ mice were bred to generate double-deficient mice. Analysis of the B cell compartment in *Lime*$^{-/-}$ *Ntal*$^{+/+}$, *Lime*$^{+/+}$ *Ntal*$^{-/-}$, and *Lime*$^{-/-}$ *Ntal*$^{-/-}$ mutant mice revealed no major difference with wild-type littermates (Fig. 6A). Moreover, mature B cells isolated from wild-type, *Lime*$^{-/-}$ *Ntal*$^{+/+}$, *Lime*$^{+/+}$ *Ntal*$^{-/-}$, and *Lime*$^{-/-}$ *Ntal*$^{-/-}$ mutant mice showed similar proliferative responses upon stimulation with $F(ab')_2$ fragments of an anti-IgM antibody or lipopolysaccharide (Fig. 6B and data not shown), and similar Ca^{2+} influx following BCR cross-linking (Fig. 6C and data not shown). Thus, single or combined deletions of LIME and NTAL do not detectably affect B cell development and function.

Lack of autoimmunity in LIME-deficient mice

Even though NTAL is barely detectable in naive T cells, it could be detected in activated T cells [13]. As shown in Fig. 1B, *Ntal* transcripts are indeed expressed in activated T cells, including Th2 effector cells from *Lat*^{Y136F} mice, albeit at lower levels than in mature B cells. Therefore, the NTAL and LIME TRAP are coincidently expressed in activated T cells. However, combined deletions of LIME and NTAL do not detectably affect early and late events of T cell activation (Fig. 6D and E).

Aged (>6 -month-old) *Ntal*$^{-/-}$ mice showed hyper-activated T cells that were thought to activate B cells and thus be responsible for the presence of anti-DNA antibodies in the sera of these mice [13]. Using an independently derived line of *Ntal*$^{-/-}$ mice [14], we failed to document an enlargement of the spleen and the presence of hyperactivated T cells in 25–30-week-old *Ntal*$^{-/-}$ mice (Fig. 7A and data not shown). However, we confirmed the presence of anti-nuclear antibodies when the sera of 6-month-old *Ntal*$^{-/-}$ mice were used to stain fixed HEp-2000 cells. The presence of anti-nuclear

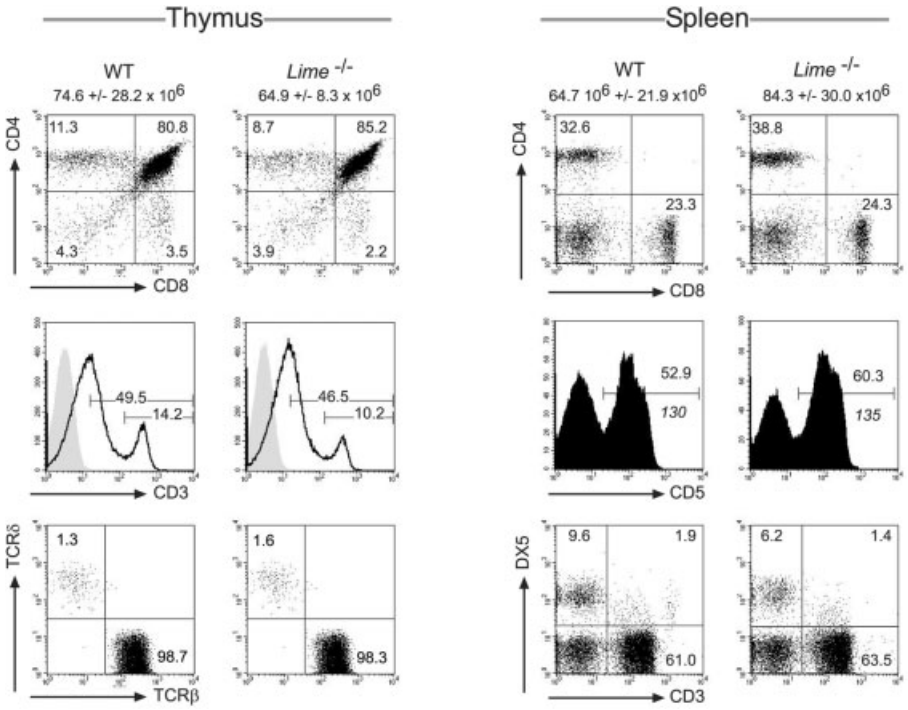

Figure 3. Flow cytometric analysis of T cell populations in thymus and spleen of 7-week-old wild-type and *Lime*$^{-/-}$ mice. Single-cell suspensions were stained with the indicated antibodies and analyzed by flow cytometry. Numbers indicate the percentages of cells in the specified quadrants or gates. In the single-color histograms representing CD5 staining on splenocytes, the values in italic correspond to the mean fluorescence of CD5^{+} cells. The thymocytes analyzed in the TCRβ *versus* TCRδ dot plot corresponded to CD3^{high} cells. The total number of thymocytes and splenocytes are shown above dot plots (averaged from three experiments).

antibodies in the absence of hyperactivated T cells questions the contribution of NTAL-deficient T cells to the development of anti-nuclear antibodies. Considering that *Ntal*$^{-/-}$ *Lat*$^{-/-}$ mice lack T cells but possess a normal B cell compartment [11], we further analyzed the sera of 6-month-old *Ntal*$^{-/-}$ *Lat*$^{-/-}$ mice for the presence of anti-nuclear antibodies. As shown in Fig. 7E, anti-nuclear antibodies were readily detected in the sera of 6-month-old *Ntal*$^{-/-}$ *Lat*$^{-/-}$ mice. Therefore, in contrast to the conclusions reached by Zhu and colleagues [13], NTAL has an intrinsic negative regulatory role within B cells that contributes to regulate their activity in aged mice. Importantly, aged *Lime*$^{-/-}$ mice showed no sign of T or B cell activation and their sera contained no detectable anti-DNA antibodies (Fig. 7E). Furthermore, the absence of LIME was without effect on the development of anti-nuclear antibodies that occurs in aged *Ntal*$^{-/-}$ mice (Fig. 7E).

Discussion

By assembling signalosomes, the four raft-associated TRAP (LAT, NTAL, PAG and LIME) coordinate intracellular programs that control the development and activation of immunocytes. Consistent with these views, LAT plays a seminal role during T cell development and function and is also critical for FcεRI signaling in mast cells [15–17]. In contrast, it has been difficult to define the role of the three other raft-associated TRAP and deletion of their genes resulted in either subtle or no detectable phenotype. NTAL functions primarily as a negative regulator of FcεRI-, BCR- and TREM-1-mediated signaling [11, 12, 14, 18]. Despite a wealth of biochemical data supporting an important role of PAG in regulation of Src-family protein tyrosine kinases, PAG appears dispensable for T cell development and function [19, 20]. We report here that LIME is also dispensable for the development and function of B and T cells. The only robust effect due to the lack of LIME was noted when a null mutation of the *Lime* gene was bred into mice in which αβ TCR variability was neutralized by expressing a TCR transgene previously calibrated in a LIME-sufficient thymus. Under those conditions, the loss of LIME enhanced both positive selection and the number of mature T cells found in the periphery. Therefore, under sensitized conditions LIME likely contributes to dampening TCR signals.

The loss of C-terminal Src kinase (Csk) at early stages of T cell development unleashed the activity of Lck and Fyn, and resulted in TCR-deficient T cells that accumulate in peripheral lymphoid organs [21]. Considering

that the SH2 domain of Csk could bind both PAG and LIME [1], it remains possible that some functional complementation exists between LIME and PAG and thus accounts for the different phenotype observed in mice that lack Csk or have a deletion of the *Pag* or *Lime* gene. In that regard, generation of mice with a combined deletion of *Lime* and *Pag* should be particularly informative.

In this study, besides a 1.8-fold enhancement in T cell-positive selection, we have failed to document any blatant effect resulting from the loss of LIME as well as from the combined loss of LIME and NTAL. These results obtained using *in vivo* assays or freshly isolated T and B cells contrast with previous results obtained using transformed B and T cell lines and refute all the roles postulated for LIME on the basis of the analysis of transformed cell lines. In contrast, using a wealth of *in vivo* sensitized experimental conditions, LIME was found to have no seminal role in the signaling cassette operated by antigen receptors and coreceptors.

Materials and methods

Mice

Mice deficient in recombination activation gene 2 ($Rag2^{-/-}$ mice) [22], in CD3ε ($Cd3^{\Delta5/\Delta5}$ mice) [23], in LAT ($Lat^{-/-}$ mice) [24] and in NTAL ($Ntal^{-/-}$ mice) [11] have been described. Mice homozygous for a mutation that replaced tyrosine 136 of LAT with phenylalanine (Lat^{Y136F} mice) have been described [25]. The Marilyn TCR transgenic line was obtained from O. Lantz [10]. Mice have been crossed onto a C57BL/6 back-

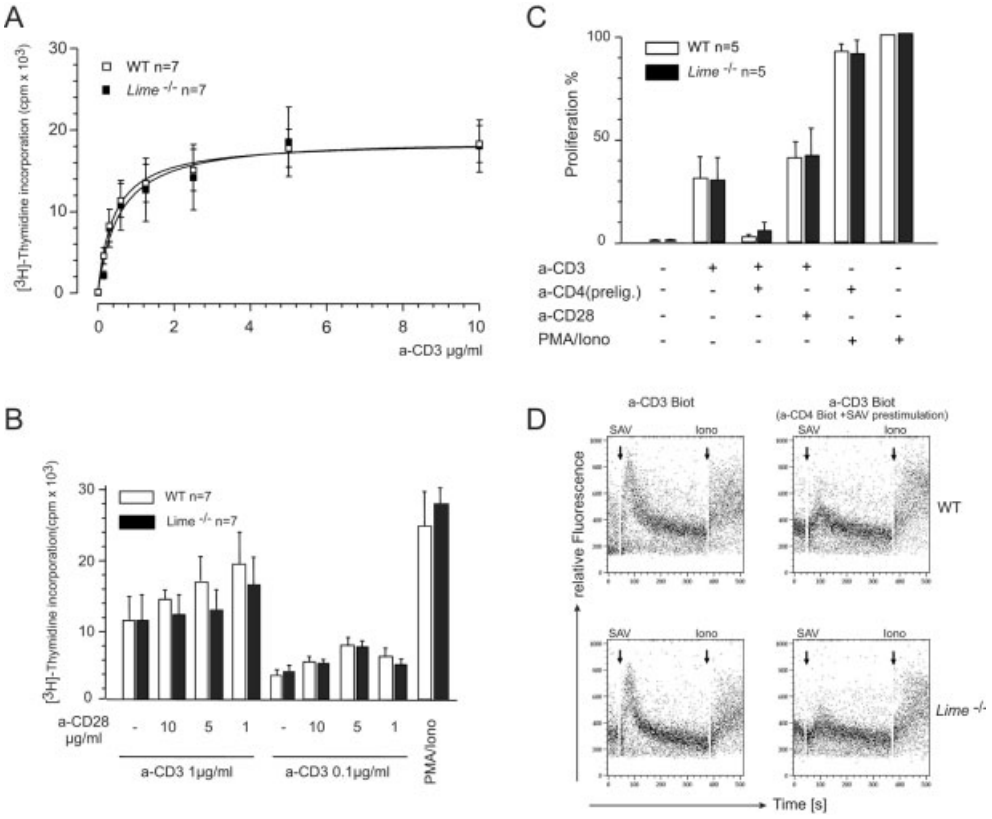

Figure 4. Proliferative responses, IL-2 production, and Ca^{2+} responses in lymph node T cells from wild-type and $Lime^{-/-}$ mice. (A) T cells purified from 7-week-old wild-type and $Lime^{-/-}$ mice were stimulated with graded concentrations of anti-CD3 antibody. After 72 h, the extent of T cell proliferation was measured by determining levels of [^{3}H]thymidine uptake. (B) Purified T cells were stimulated with a fixed concentration (1 µg/mL or 0.1 µg/mL) of anti-CD3 antibody with or without graded concentrations of anti-CD28 antibody. Also shown is the level of T cell proliferation obtained following stimulation with phorbol-myristate-acetate and ionomycin (PMA/Iono). (C) $CD4^+$ T cells purified from wild-type and $Lime^{-/-}$ mice were stimulated with anti-CD3 antibodies. When specified [a-CD4 (prelig)], CD4 molecules were cross-linked for 45 min before stimulation with anti-CD3 antibodies. The extent of proliferation was measured after 72 h of culture. Values have been normalized as % of the proliferation value observed following stimulation with PMA and Iono. In A–C, the data shown are representative of five independent experiments and the values correspond to the mean ± SD from quadruplicate samples. (D) Calcium flux analysis in response to TCR stimulation in wild-type and $Lime^{-/-}$ lymph node $CD4^+$ T cells. The diagram depicts calcium flux (*y* axis) as a function of time (*x* axis). Arrows indicate the time point of addition of streptavidin (SAV) to cross-link the biotinylated anti-CD3 antibody, or of ionomycin (Iono). In the right panels, CD4 molecules were cross-linked for 45 min prior to stimulation with anti-CD3 antibodies. Data shown are representative of four independent experiments.

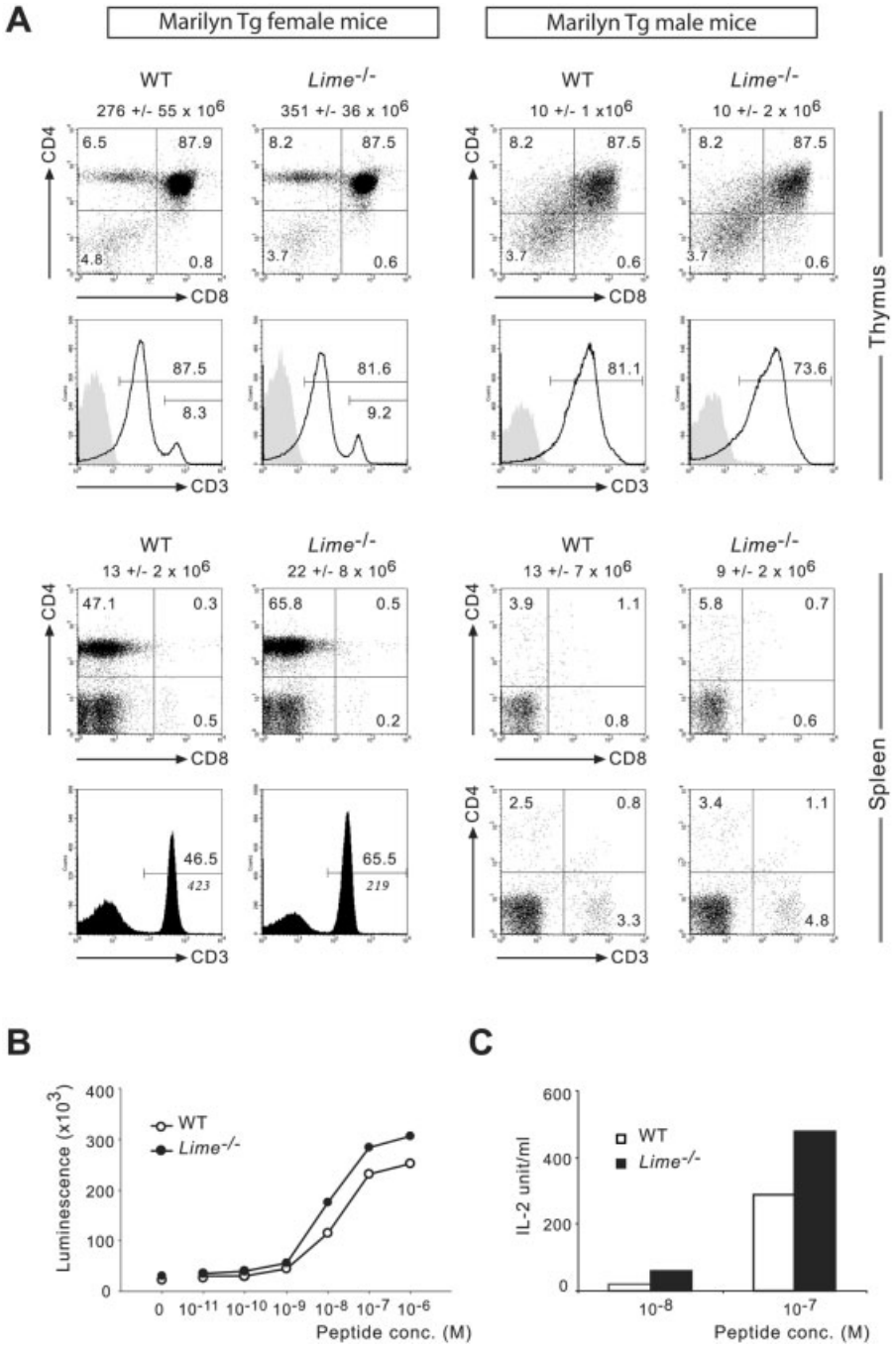

Figure 5. T cell development in wild-type and *Lime*$^{-/-}$ mice expressing the Marilyn transgenic TCR. (A) Thymocytes and splenocytes from LIME-sufficient (WT) and -deficient (*Lime*$^{-/-}$) female or male mice expressing the Marilyn transgenic TCR were analyzed by flow cytometry for expression of CD4, CD8, and CD3ε. The genotypes and the total number of cells in the thymus or spleen [averaged from 4 (WT) and 6 (*Lime*$^{-/-}$) age-matched mice] are indicated above dot plots. The percentages of cells within each quadrants or gates are indicated. Single-color histograms represent CD3ε staining on total thymocytes and splenocytes. The percentage of CD3ε^{int} and CD3ε^{high} thymocytes are indicated. In the case of the spleen, the percentage and mean fluorescence (italicized values) of CD3$^+$ cells are indicated. All the mice were maintained on a *Rag-2*$^{-/-}$-deficient background, and were between 6 and 8 weeks of age. (B, C) CD4$^+$ T cells found in the periphery of WT and *Lime*$^{-/-}$ Marilyn female mice were analyzed for their capacity to proliferate (B) and produce IL-2 (C) after stimulation with graded concentrations of agonistic peptide. CD4$^+$ T cells were purified from secondary lymphoid organs and incubated with A^b-positive APC prepulsed with the Dby agonist peptide. The extent of cell proliferation (B) and IL-2 content (C) were determined after 40 h and 24 h, respectively. Data shown in (B) and (C) are representative of three independent experiments.

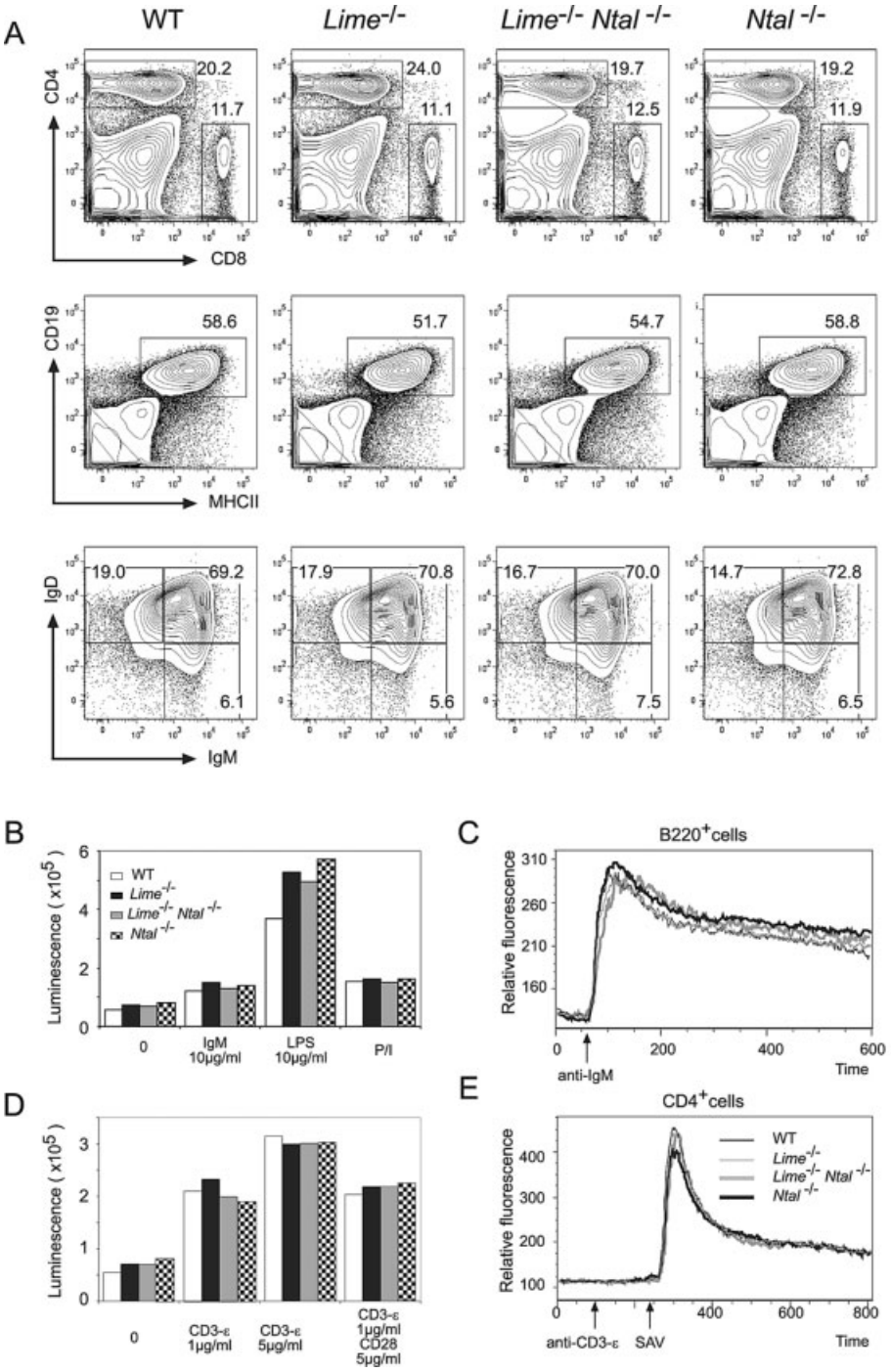

Figure 6. Analysis of B and T cell development and function in mice with single and combined deletion of LIME and NTAL. (A) Splenocytes from wild-type (WT), LIME-deficient (*Lime*$^{-/-}$), NTAL-deficient (*Ntal*$^{-/-}$) mice and mice lacking both LIME and NTAL (*Lime*$^{-/-}$ *Ntal*$^{-/-}$) were stained with the indicated antibodies and analyzed by flow cytometry. Genotypes are specified over the dot plots. In the CD19 *versus* MHC class II staining, the percentages of B cells (CD19^{+}MHCII^{+}) are indicated. In the IgM *versus* IgD staining profiles, CD19^{+}MHCII^{+}-gated B cells were categorized into IgM^{high} IgD^{low}, IgM^{high} IgD^{high}, and IgM^{low} IgD^{high} cells. (B) Spleen B cells from mice of the specified genotypes were left unstimulated (0) or stimulated with lipopolysaccharide (LPS, 10 μg/mL), goat F(ab′)$_2$ anti-mouse IgM antibody (IgM, 10 μg/mL), or with phorbol myristate acetate and ionomycin (P/I). After 40 h of culture, the extent of cell proliferation was determined. (D) Spleen T cells from mice of the specified genotype were left unstimulated (0) or stimulated with anti-CD3ε antibody at two different doses (1 μg/mL and 5 μg/mL), and with a mix of anti-CD3ε and anti-CD28 antibodies. After 40 h of culture, the extent of cell proliferation was determined. (C, E) Calcium responses analysis following to antigen receptor stimulation of B (C) and T (E) cells isolated from mice of the specified genotypes.

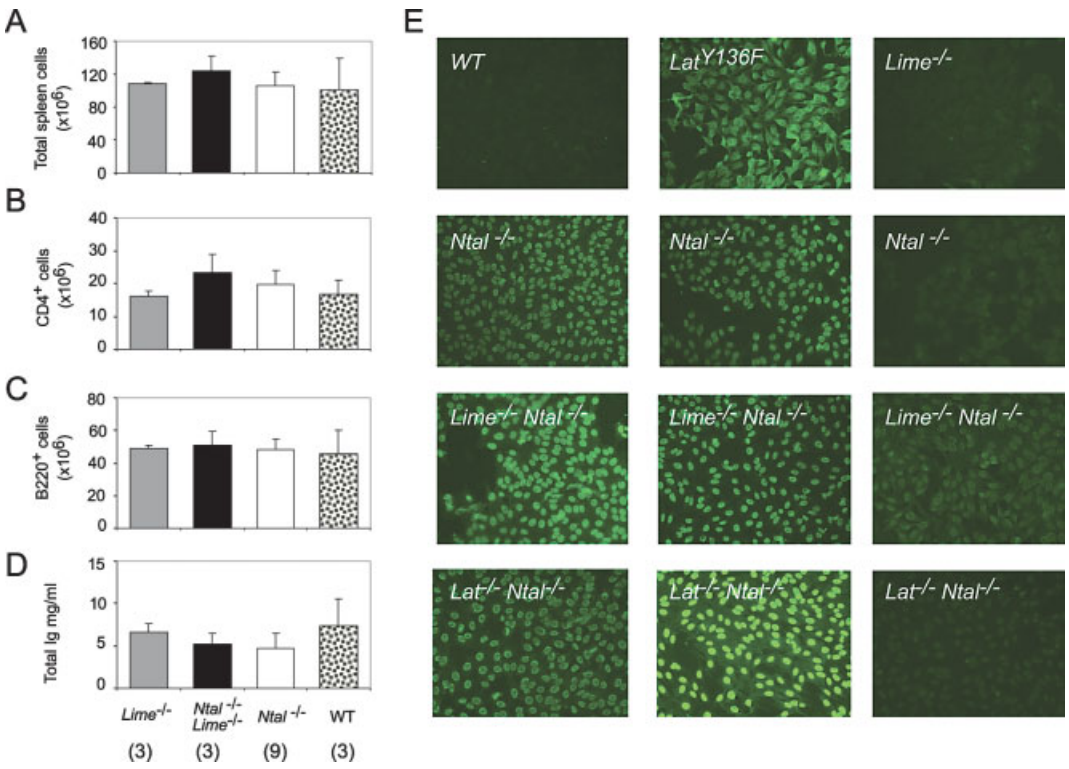

Figure 7. Lime-deficient mice do not develop autoimmune syndrome and splenomegaly upon aging. Spleen from 25- to 30-week-old wild-type (WT), LIME-deficient (*Lime*$^{-/-}$), NTAL-deficient (*Ntal*$^{-/-}$), LIME-NTAL double-deficient (*Lime*$^{-/-}$ *Ntal*$^{-/-}$) mice were assayed for total cellularity (A) and for their content in CD4$^+$ T cells (B) and in B cells (C). Sera from the same mice were analyzed for the concentration of total IgG (D). Data shown are representative of three to nine animals as indicated in parenthesis. (E) Sera from 25- to 36-week-old mice of the specified genotype were used at a 1:80 dilution to stain HEp-2000 cells. The presence of nuclear antibodies was revealed using a FITC-conjugated goat F(ab′)$_2$ anti-mouse IgG. All sera from wild-type (n=4) and *Lime*$^{-/-}$ (n=7) mice gave no staining of HEp-2000 cells. Sera from *Ntal*$^{-/-}$ mice gave fluorescence signals the magnitude of which is similar to the signals obtained with sera of *Lat*^{Y136F} mice that develop early-onset autoantibodies [29, 30]. In line with a previous report [13], some interindividual variations were observed in the content of autoantibodies. In the case of sera from *Ntal*$^{-/-}$ (n=7) mice: four showed strong positive fluorescence signals, one gave clearly positive signals, and two sera gave no detectable staining. *Ntal*$^{-/-}$ *Lat*$^{-/-}$ (n=6) and *Ntal*$^{-/-}$ *Lime*$^{-/-}$ (n=6) mice showed the same frequency of animals containing anti-nuclear antibodies as *Ntal*$^{-/-}$ mice.

ground for at least seven generations, and housed in a specific pathogen-free animal facility. All procedures were in accordance with protocols approved by French Laws and the European Directives.

Vector construction

The targeting construct used for disruption of the *Lime* gene is shown in Fig. 2. The 5′ homologous sequences correspond to a gene segment encompassing nucleotide positions 8079–9024 (sequence available from GenBank/EMBL/DDBJ under accession number F131462). The 3′ homologous sequences correspond to a gene segment encompassing nucleotide positions 13 800–18 812 (sequence available from GenBank/EMBL/DDBJ under accession number F131462). In the targeting vector, exons 1–5 of the *Lime* gene were replaced by a *loxP*-flanked, Cre-Neo^r auto-deleter cassette [26].

Isolation of recombinant embryonic stem cell clones and production of mutant mice

After electroporation of CK35 129/Sv embryonic stem cells [27] and selection in G418 and gancyclovir, colonies were screened for homologous recombination by Southern blot analysis. The 5′ single-copy probe corresponds to a 392-bp fragment that encompasses nucleotide position 6857–7249. It was amplified using the following oligonucleotides: 5′-CGG AAT TCG TGG CAC CAC ACT GTA GAG AG-3′ and 5′-GCT CTA GAC TGT GCA CAC TCC TGA CAA CTC-3′. When tested on HindIII-digested DNA, it hybridized either to a 7.4-kb wild-type fragment or to a 2.7-kb recombinant fragment. The presence of an appropriate homologous recombination event at the 3′ side was assessed using a 357-bp fragment encompassing nucleotide positions 19201–19558. It was amplified using the following oligonucleotides: 5′-CGG AAT TCT GGC TGC AGA CAT GAA CAC AC-3′ and 5′-GCT CTA GAT TGT AGG AAG GCT ATT TCA GG-3′. When tested on EcoRI-digested DNA, this fragment hybridized either to a 16.6-kb wild-type fragment or to a 9.6-kb recombinant fragment. A Neo probe was also used to ensure that adventitious non-homologous recombination

events had not occurred in the selected clones. Screening of mice for the presence of the *Lime* null mutation was performed by PCR using the following oligonucleotides: (a): 5′-ACC TGC TTT GTT CAC CTC ATT AAT GGG TAT-3′, (b): 5′-ACA GCC AGG AAG ATC TTT GTG GGC TGC TGG-3′, and (c): 5′-GTG ACC ACC CTG TCC TGC CCA ACC TAG AGG-3′. The wild-type *Lime* allele is visualized as a 229-bp fragment using the a-b pair of oligonucleotides, whereas the mutant allele is visualized as a 530-bp fragment using the a-c pair of oligonucleotides.

Immunoblotting

Splenocytes from wild-type or $Lime^{-/-}$ mice were solubilized in the presence of 1% laurylmaltoside. Lysates were subjected to SDS/PAGE followed by Western blotting. The blot was immunostained with a rabbit antiserum directed to the cytoplasmic domain of mouse LIME (amino acids 86–202), followed by goat anti-rabbit Ig conjugated to horseradish peroxidase.

Flow cytometry and intracellular staining

Lymphocyte suspensions were prepared from thymus or lymphoid peripheral organs and stained with the specified antibodies (BD Pharmingen and Caltag laboratories). Cells were analyzed on FACSCalibur and BD^{TM} LSRI flow cytometers (Becton Dickinson). Data acquisition and analysis were performed using CellQuest (Becton Dickinson) or FlowJO (Treestar) software.

RNA preparation and quantitative RT-PCR

Purification of immature and mature B and T cell fractions, RNA isolation and real-time RT-PCR were performed as described [11]. The pairs of primers used to amplify the *Hprt*, *Lat*, and *Ntal* transcripts have been reported [11]. *Lime* transcripts were amplified with the following oligonucleotides: *Lime* sense, 5′-GAA GCA CAA AGG GAC AGA GC- 3′ and *Lime* antisense, 5′-CAG GTT CAG CTG GTC TGT GA- 3′. Relative expression values were expressed as $2^{-\Delta CT}$ where ΔC_T is the difference between the mean C_T value of duplicates of the test sample and of the endogenous HPRT control.

Cell purification

Splenic T cells were purified by negative selection using magnetic cell sorting (Miltenyi Biotec). Purity was analyzed by flow cytometry and was >90%.

Ca^{2+} flux measurement

For B cells, Ca^{2+} flux measurements were as described [11], and data acquisition and analysis were performed with CellQuest (Becton Dickinson) or FlowJO (Treestar), respectively. T cells were incubated for 30 min with 3.75 μg/mL indo-1-AM (Molecular Probes) in phenol red-free RPMI 1640 medium (GIBCO BRL) containing 10% fetal calf serum. Cells were subsequently stained with CD4 and CD8 and incubated with 10 μg/mL biotinylated anti-CD3 antibody (clone 145–2C11) at 4°C. Calcium fluxes were induced by cross-linking the TCR/CD3 complex with 75 μg/mL streptavidin and were measured using an LSR flow cytometer (BD Biosciences). In some instances, prior to stimulation with anti-CD3 antibodies, CD4 molecules were cross-linked for 45 min using a biotinylated rat anti-mouse CD4 antibody (clone RM 4–5) and streptavidin.

Proliferative responses and IL-2 production of T cells

Purified T cells were cultured in 96-well round-bottom plates (2.5×10^4 cells per well) and stimulated with graded concentrations of rat anti-mouse CD3 antibodies. After 72 h, plates were pulsed for 8 h with 0.5 μCi [^{3}H]thymidine per well. Incorporation of [^{3}H]thymidine into DNA was measured by liquid scintillation counting (1450 MicroBeta Trilux, Perkin Elmer Wallac GmbH). To assess the effect of CD28 costimulation, graded concentrations of anti-CD28 antibodies were added to T cells stimulated with a fixed concentration (0.1 or 1 μg/mL) of rat anti-mouse CD3 antibodies. When specified, T cells were stimulated with PMA (0.05 μg/mL) and ionomycin (2 nM). In the case of Marilyn TCR transgenic T cells, antigen-induced proliferation was measured using I-A^b-positive, spleen cells from $Cd3^{\Delta 5/\Delta 5}$ mice as APC. Spleen cells were irradiated and pulsed with various concentration of the Dby peptide [28]. Purified $CD4^+$ cells (5×10^4) were stimulated with 5×10^5 antigen-pulsed APC. After 40 h, cultures were assayed for their content of ATP. Briefly, 100 μL CellTiterGlo reagent (Promega) was added to the culture and the resulting luminescence, which is proportional to the ATP content of the culture, was measured with a Victor2 luminometer (Wallac, Perkin Elmer Life Science). The level of IL-2 contained in the supernatant after 20 h was determined using the CTL-L line. Values were converted into IL-2 units using a recombinant mouse IL-2 standard (Pharmingen).

B cell responses and ELISA

They were performed as described [11].

Detection of anti-nuclear antibodies

The presence of anti-nuclear antibodies was determined using human HEp-2000 cells (Immunoconcepts). HEp-2000 cells were incubated with the indicated mouse serum dilution for 30 min. Slides were then washed and incubated for 30 min with a FITC-labeled goat $F(ab')_2$ anti-mouse IgG antibody (Beckman-Coulter). Slides were analyzed by fluorescence microscopy.

Acknowledgements: We thank O. Lantz for mice, M. Mingueneau, A. Gillet, A. Kissenpfennig, N. Brun, and P.Grenot for discussion. Supported by CNRS, INSERM, ARC, ANR, FRM, Plate-forme RIO/MNG, and the European Communities (MUGEN Network of Excellence) (to B.M.), the Deutsche Forschungsgemeinschaft (to B.S. and L.S.), the Center of Molecular and Cellular Immunology (1M6837805001) and Academy of Sciences of the Czech Republic (AV0Z50520514) (to V.H.).

Conflict of interest: The authors declare no financial or commercial conflicts of interest.

References

1 **Horejsi, V., Zhang, W. and Schraven, B.,** Transmembrane adaptor proteins: organizers of immunoreceptor signalling. *Nat. Rev. Immunol.* 2004. **4:** 603–616.

2 **Hur, E. M., Son, M., Lee, O. H., Choi, Y. B., Park, C., Lee, H. and Yun, Y.,** LIME, a novel transmembrane adaptor protein, associates with p56lck and mediates T cell activation. *J. Exp. Med.* 2003. **198:** 1463–1473.

3 **Brdickova, N., Brdicka, T., Angelisova, P., Horvath, O., Spicka, J., Hilgert, I., Paces, J. *et al.*,** LIME: A new membrane Raft-associated adaptor protein involved in CD4 and CD8 coreceptor signaling. *J. Exp. Med.* 2003. **198:** 1453–1462.

4 **Ahn, E., Lee, H. and Yun, Y.,** LIME acts as a transmembrane adapter mediating BCR-dependent B-cell activation. *Blood* 2006. **107:** 1521–1527.

5 **Filipp, D., Zhang, J., Leung, B. L., Shaw, A., Levin, S. D., Veillette, A. and Julius, M.,** Regulation of Fyn through translocation of activated Lck into lipid rafts. *J. Exp. Med.* 2003. **197:** 1221–1227.

6 **Harding, S., Lipp, P. and Alexander, D. R.,** A therapeutic CD4 monoclonal antibody inhibits TCR-zeta chain phosphorylation, zeta-associated protein of 70-kDa Tyr319 phosphorylation, and TCR internalization in primary human T cells. *J. Immunol.* 2002. **169:** 230–238.

7 **Graca, L., Le Moine, A., Cobbold, S. P. and Waldmann, H.,** Antibody-induced transplantation tolerance: The role of dominant regulation. *Immunol. Res.* 2003. **28:** 181–191.

8 **Brdicka, T., Imrich, M., Angelisova, P., Brdickova, N., Horvath, O., Spicka, J., Hilgert, I. *et al.*,** Non-T cell activation linker (NTAL): a transmembrane adaptor protein involved in immunoreceptor signaling. *J. Exp. Med.* 2002. **196:** 1617–1626.

9 **Carsetti, R.,** Characterization of B-cell maturation in the peripheral immune system. *Methods Mol. Biol.* 2004. **271:** 25–35.

10 **Lantz, O., Grandjean, I., Matzinger, P. and Di Santo, J. P.,** Gamma chain required for naive $CD4^+$ T cell survival but not for antigen proliferation. *Nat. Immunol.* 2000. **1:** 54–58.

11 **Wang, Y., Horvath, O., Hamm-Baarke, A., Richelme, M., Gregoire, C., Guinamard, R., Horejsi, V. *et al.*,** Single and combined deletions of the NTAL/LAB and LAT adaptors minimally affect B-cell development and function. *Mol. Cell. Biol.* 2005. **25:** 4455–4465.

12 **Zhu, M., Liu, Y., Koonpaew, S., Granillo, O. and Zhang, W.,** Positive and negative regulation of FcepsilonRI-mediated signaling by the adaptor protein LAB/NTAL. *J. Exp. Med.* 2004. **200:** 991–1000.

13 **Zhu, M., Koonpaew, S., Liu, Y., Shen, S., Denning, T., Dzhagalov, I., Rhee, I. and Zhang, W.,** Negative regulation of T cell activation and autoimmunity by the transmembrane adaptor protein LAB. *Immunity* 2006. **25:** 757–768.

14 **Volna, P., Lebduska, P., Draberova, L., Simova, S., Heneberg, P., Boubelik, M., Bugajev, V. *et al.*,** Negative regulation of mast cell signaling and function by the adaptor LAB/NTAL. *J. Exp. Med.* 2004. **200:** 1001–1013.

15 **Malissen, B., Aguado, E. and Malissen, M.,** Role of the LAT adaptor in T-cell development and Th2 differentiation. *Adv. Immunol.* 2005. **87:** 1–25.

16 **Malbec, O., Malissen, M., Isnardi, I., Lesourne, R., Mura, A. M., Fridman, W. H., Malissen, B. and Daeron, M.,** Linker for activation of T cells integrates positive and negative signaling in mast cells. *J. Immunol.* 2004. **173:** 5086–5094.

17 **Saitoh, S., Odom, S., Gomez, G., Sommers, C. L., Young, H. A., Rivera, J. and Samelson, L. E.,** The four distal tyrosines are required for LAT-dependent signaling in FcepsilonRI-mediated mast cell activation. *J. Exp. Med.* 2003. **198:** 831–843.

18 **Tessarz, A. S., Weiler, S., Zanzinger, K., Angelisova, P., Horejsi, V. and Cerwenka, A.,** Non-T cell activation linker (NTAL) negatively regulates TREM-1/DAP12-induced inflammatory cytokine production in myeloid cells. *J. Immunol.* 2007. **178:** 1991–1999.

19 **Dobenecker, M. W., Schmedt, C., Okada, M. and Tarakhovsky, A.,** The ubiquitously expressed Csk adaptor protein Cbp is dispensable for embryogenesis and T-cell development and function. *Mol. Cell. Biol.* 2005. **25:** 10533–10542.

20 **Xu, S., Huo, J., Tan, J. E. and Lam, K. P.,** Cbp deficiency alters Csk localization in lipid rafts but does not affect T-cell development. *Mol. Cell. Biol.* 2005. **25:** 8486–8495.

21 **Schmedt, C. and Tarakhovsky, A.,** Autonomous maturation of alpha/beta T lineage cells in the absence of COOH-terminal Src kinase (Csk). *J. Exp. Med.* 2001. **193:** 815–826.

22 **Shinkai, Y., Rathbun, G., Lam, K. P., Oltz, E. M., Stewart, V., Mendelsohn, M., Charron, J. *et al.*,** RAG-2-deficient mice lack mature lymphocytes owing to inability to initiate V(D)J rearrangement. *Cell* 1992. **68:** 855–867.

23 **Malissen, M., Gillet, A., Ardouin, L., Bouvier, G., Trucy, J., Ferrier, P., Vivier, E. and Malissen, B.,** Altered T cell development in mice with a targeted mutation of the CD3-epsilon gene. *EMBO J.* 1995. **14:** 4641–4653.

24 **Nunez-Cruz, S., Aguado, E., Richelme, S., Chetaille, B., Mura, A. M., Richelme, M., Pouyet, L. *et al.*,** LAT regulates gammadelta T cell homeostasis and differentiation. *Nat. Immunol.* 2003. **4:** 999–1008.

25 **Aguado, E., Richelme, S., Nunez-Cruz, S., Miazek, A., Mura, A.-M., Richelme, M., Guo, X.-J. *et al.*,** Induction of T helper type 2 immunity by a point mutation in the LAT adaptor. *Science* 2002. **296:** 2036–2040.

26 **Kissenpfennig, A., Henri, S., Dubois, B., Laplace-Builhe, C., Perrin, P., Romani, N., Tripp, C. H. *et al.*,** Dynamics and function of Langerhans cells *in vivo* dermal dendritic cells colonize lymph node areas distinct from slower migrating Langerhans cells. *Immunity* 2005. **22:** 643–654.

27 **Kress, C., Vandormael-Pournin, S., Baldacci, P., Cohen-Tannoudji, M. and Babinet, C.,** Nonpermissiveness for mouse embryonic stem (ES) cell derivation circumvented by a single backcross to 129/Sv strain: Establishment of ES cell lines bearing the Omd conditional lethal mutation. *Mamm. Genome* 1998. **9:** 998–1001.

28 **Scott, D., Addey, C., Ellis, P., James, E., Mitchell, M. J., Saut, N., Jurcevic, S. and Simpson, E.,** Dendritic cells permit identification of genes encoding MHC class II-restricted epitopes of transplantation antigens. *Immunity* 2000. **12:** 711–720.

29 **Genton, C., Wang, Y., Izui, S., Malissen, B., Delsol, G., Fournié, G. J., Malissen, M. and Acha-Orbea, H.,** The Th2 lymphoproliferation developing in LatY136F mutant mice triggers polyclonal B cell activation and systemic autoimmunity. *J. Immunol.* 2006. **177:** 2285–2293

30 **Sommers, C. L., Park, C. S., Lee, J., Feng, C., Fuller, C. L., Grinberg, A., Hildebrand, J. A. *et al.*,** A LAT mutation that inhibits T cell development yet induces lymphoproliferation. *Science* 2002. **296:** 2040–2043.

Appendix 11

Regulation of T-cell homeostasis by the transmembrane adaptor protein SIT

Posevitz V., Arndt B., Krieger T., Warnecke N., Schraven B., and **Simeoni L**. (2008) *J Immunol.* 180:1634-1642.

Regulation of T Cell Homeostasis by the Transmembrane Adaptor Protein SIT[1]

Vilmos Posevitz, Boerge Arndt, Tina Krieger, Nicole Warnecke, Burkhart Schraven, and Luca Simeoni[2]

The transmembrane adaptor protein SIT is a negative regulator of TCR-mediated signaling. However, little is known about the functional role of SIT in mature T cells. In this study, we show that mice deficient for SIT display a decreased number of naive $CD8^+$ T cells and a progressive accumulation of memory-like ($CD44^{high}$) $CD8^+$ T lymphocytes that resemble cells undergoing homeostatic proliferation. Indeed, when transferred into lymphopenic hosts, $SIT^{-/-}$ naive $CD8^+$ T cells undergo enhanced homeostatic proliferation and express a higher level of CD44 in comparison to wild-type T cells. By using class-I-restricted TCR transgenic models with different ligand affinity/avidity, we show that lymphopenia-induced homeostatic proliferation is more pronounced in cells carrying low-affinity TCRs. Strikingly, the loss of SIT induces homeostatic proliferation of HY TCR transgenic cells, which are normally unable to proliferate in lymphopenic mice. Collectively, these data demonstrate that SIT negatively regulates T cell homeostasis. Finally, we show that SIT-deficient T cells develop a mechanism analogous to sensory adaptation as they up-regulate CD5, down-regulate the coreceptor, and display impaired TCR-mediated ZAP-70 activation. ***The Journal of Immunology,*** **2008, 180: 1634–1642.**

The number of mature T cells is kept constant throughout the life by a tightly regulated process termed peripheral homeostasis (1). Over the past several years, studies have demonstrated that different mechanisms contribute to the maintenance of the pool of peripheral T lymphocytes. In the days following birth, the periphery is filled with naive cells emigrating from the thymus. Once these naive cells have colonized the periphery, they undergo a cell division program called homeostatic proliferation (2). Both processes, namely emigration from the thymus and expansion in the periphery, determine the initial size of the peripheral T cell pool. Prolonged survival and homeostatic proliferation of peripheral T lymphocytes allow to keep cell numbers constant during adulthood when the thymus involutes and thymic output strongly decreases. Homeostatic proliferation is also necessary to replenish the peripheral T cell pool following abnormal cell depletion caused by e.g., irradiation, chemotherapy, or infection (3–5).

Signals emanating from the TCR as well as from IL receptors (e.g., IL-7, IL-15, among others) critically regulate lymphocyte homeostasis (6–8). Several groups have addressed the role of the TCR in maintaining the peripheral T cell pool. The TCR has the ability "to sense" differences in ligand affinity and in turn is able to translate these different input signals into distinct cellular responses. The most explicit example of this phenomenon is thymic selection, where thymocytes expressing TCRs with high affinity for self-peptide/MHC complexes are negatively selected whereas those expressing TCRs with lower affinity are positively selected and mature into $CD4^+$ or $CD8^+$ cells (9, 10). Experimental evidence also suggests that interaction with self-peptide/MHC serves the additional purpose of maintaining cell survival in the periphery and of triggering homeostatic proliferation of mature T lymphocytes (11, 12). The essential role of signal strength in T cell homeostasis highlights the importance of those molecules that are able to modulate TCR-mediated signaling.

In this regard, adaptor proteins, a group of molecules that organize signaling complexes at the plasma membrane, play a pivotal role as they represent important regulators of lymphocyte homeostasis. Previously, we have shown that Src homology domain containing tyrosine phosphatase 2-interacting transmembrane adaptor protein (SIT),[3] a transmembrane adaptor strongly expressed on thymocytes and peripheral T cells, represents a multifunctional regulator of TCR-mediated signaling (13–15). The characterization of SIT-deficient mice demonstrated that SIT regulates selection processes within the thymus by setting TCR-mediated activation thresholds (13). Indeed, positive selection was partially converted to negative selection and the expression level of CD5 was strongly elevated on $SIT^{-/-}$ $CD4^+CD8^+$ immature thymocytes. CD5 is a molecule whose expression is directly proportional to the affinity of the TCR for self-peptide/MHC ligands (16). Collectively, our data had demonstrated that SIT negatively regulates TCR-mediated signal strength. As the maintenance of the peripheral T cell pool is also strictly dependent upon TCR-mediated signaling, we here investigated the role of SIT in peripheral T cell homeostasis. To date, the number of molecules that have been shown to regulate homeostatic proliferation is surprisingly limited and nothing is known about the role that transmembrane adaptor proteins play in this process.

Otto-von-Guericke University, Institute of Molecular and Clinical Immunology, Magdeburg, Germany

Received for publication June 12, 2007. Accepted for publication November 21, 2007.

The costs of publication of this article were defrayed in part by the payment of page charges. This article must therefore be hereby marked *advertisement* in accordance with 18 U.S.C. Section 1734 solely to indicate this fact.

[1] This work was supported by the Deutsche Forschungsgemeinschaft Grant FOR521, SI 861/1 and GRK-1167, and by the German Ministry of Education and Research (Bundesministerium für Bildung, Wissenschaft, Forschung und Technologie) Grant 01ZZ0407 NBL3-2.

[2] Address correspondence and reprint requests to Dr. Luca Simeoni, Institute of Molecular and Clinical Immunology, Otto-von-Guericke University, Leipziger Strasse 44, 39120 Magdeburg, Germany. E-mail address: luca.simeoni@med.ovgu.de

[3] Abbreviations used in this paper: SIT, Src homology domain containing tyrosine phosphatase 2-interacting transmembrane adaptor protein; LAT, linker for activation of T cells; WT, wild type; BTLA, B and T lymphocyte attenuator.

We report that SIT is required for proper homeostasis of peripheral T cells and negatively regulates homeostatic proliferation in lymphopenic hosts. SIT-deficient T cells further develop sensory adaptation and display impaired ZAP-70 activation. Collectively, the data shown in this study demonstrate that SIT is a critical modulator of the signaling threshold and regulates T cell development and peripheral homeostasis in a similar fashion.

Materials and Methods

Mice

$SIT^{-/-}$ mice were previously described (13). All mice used in this study were between 1 and 5 mo of age, when not otherwise indicated. OT-I TCR transgenic mice were provided by Dr. Percy Knolle, P14 by Dr. Thomas Kammerthoens, and HY TCR transgenic mice by Dr. Gary Koreztky. SIT-deficient mice carrying TCR transgenes were generated as previously described (13). All experiments involving mice were performed according to the guidelines of the State of Sachsen-Anhalt.

Flow cytometry

For FACS analysis, single cell suspensions were prepared and 1×10^6 cells were stained with indicated Abs and analyzed on a FACS Calibur using the CellQuest software (Becton Dickinson). All Abs were purchased from BD Biosciences except for HY (clone T3.70; eBioscience) as previously reported (13). For apoptosis determination, splenocytes and lymph node cells were harvested, washed, and stained with Annexin V-PE (BD Biosciences).

Intracellular staining

Intracellular Bcl-2 staining was performed by using a Bcl-2 FITC set (BD, Biosciences) according to the manufacturer's instructions.

BrdU labeling and analysis

Steady-state proliferation of T cells was measured by BrdU incorporation. Mice were fed with 0.8 mg/ml BrdU (Sigma-Aldrich) given in their drinking water. Intracellular staining for BrdU was performed by using a FITC BrdU kit (BD Biosciences) in accordance with the manufacturer's instructions.

T cell isolation

Splenic T cells were purified using a Pan T cell isolation kit (Miltenyi Biotec), while $CD4^+CD8^+$ thymocytes were enriched by using anti-FITC microbeads (Miltenyi Biotec) after staining with a FITC-labeled CD8 mAb (clone CT-CD8a, Caltag) on an AutoMACS magnetic separation system. The purity of $CD4^+CD8^+$ thymocytes was >97%. $CD8^+$ SP thymocytes were enhriched by negative selection using CD4 microbeads (Miltenyi Biotec) on an AutoMACS magnetic separation system.

Adoptive transfer

Total lymph node cells or enriched $CD8^+$ SP thymocytes were isolated from mutant and control mice, washed, counted, and resuspended at 5×10^6 cells/ml in ice cold PBS. Cells were then labeled with 0.1 μM CFSE (Molecular Probes) for 10 min at 37°C. Before i.v. injection, cells were washed with ice cold PBS containing 5% FCS and subsequently resuspended in PBS at 10×10^6/ml. Recipient B6.SJL ($CD45.1^+$) mice were irradiated (950 rad) using a BioBeam 8000 (STS Steuerungstechnik & Strahlenschutz GmbH) 1 day before adoptive transfer and injected i.v. with 200 μl (2×10^6 cells) of cell suspension. After irradiation, mice were treated with 2 mg/ml neomycin sulfate (Sigma-Aldrich). Tissues were harvested on day 3 or 7 and analyzed for the intensity of CSFE and other cell surface markers.

Immunoprecipitation, immunoblotting, in vitro kinase assay

For all biochemical analysis, lymphocytes were either left unstimulated or stimulated with 10 μg/ml biotinylated anti-CD3ε Ab (145-2C11; BD Biosciences) alone or in combination with biotinylated CD4 (GK1.5; BD Biosciences) or CD28 (37.51; BD Biosciences) followed by crosslinking with 25 μg/ml streptavidin at 37°C. Cells were lysed in lysis buffer containing 1% Nonidet P-40, 1% laurylmaltoside (N-dodecyl-β-D-maltoside), 50 mM Tris (pH 7.5), 140 mM NaCl, 10 mM EDTA, 10 mM NaF, 1 mM phenylmethylsulfonylfluorid, and 1 mM Na_3VO_4. The supernatants of the lysates were subjected to immunoblotting, or immunoprecipitated with Abs specific for linker for activation of T cells (LAT) (Transduction Laboratories), ZAP-70 (Santa Cruz Biotechnology), or TCR-ζ (Santa Cruz Biotechnology). Abs were captured using protein A-Sepharose. Proteins were separated by SDS-PAGE, electrotransferred to polyvinylidene difluoride membranes, and blotted with the following Abs: anti-phosphotyrosine (4G10), anti-ERK1/2 (Cell Signaling Technology), anti-JNK (Cell Signaling Technology), anti-p38 (Cell Signaling Technology), anti-phosphoLAT (Y171, Cell Signaling Technology; Y191, Cell Signaling Technology; Y226, Upstate Biotechnology), anti-LAT (a gift from Dr. Weiguo Zhang) anti-phosphoZAP-70 (Y319, Y493, Cell Signaling Technology), and anti-ZAP-70 (Transduction Laboratories).

For the determination of ZAP-70 kinase activity, 40×10^6 thymocytes were stimulated with 10 μg/ml biotinylated anti-CD3 (145-2C11, BD Biosciences) plus 10 μg/ml anti-CD4 Abs (GK1.5, BD Biosciences) and crosslinked with 25 μg/ml streptavidin at 37°C. Anti-ZAP-70 immunocomplexes were assayed for kinase activity as previously described (17).

Ca^{2+} flux

For Ca^{2+}-measurement, cells were incubated for 30 min with 3.75 μg/ml indo-1-AM (Molecular Probes) in phenol red-free RPMI 1640 medium (Invitrogen Life Technologies) containing 10% FCS. After washing, the cells were incubated in the presence of CD4-FITC, CD8-PE, and 10 μg/ml biotinylated CD3 (145-2C11; BD Biosciences) mAbs at 4°C. Calcium fluxes were induced by crosslinking the TCR/CD3 complex with 75 μg/ml streptavidin and were measured using a LSR flow cytometer (BD Biosciences).

Statistics

Statistical analysis were performed using GraphPad Prism (GraphPad Software). Mean values ± SEM are shown in each graph. Asterisks represent p values of an unpaired two-tailed Student's t test.

Results

$SIT^{-/-}$ mice show a reduction of $CD44^{low}$ and an accumulation of $CD44^{high}$ $CD8^+$ T cells

We have previously shown that SIT deficiency resulted in a selective decrease in the numbers of T, but not B cells in lymph nodes. This deficit seems to affect particularly the $CD8^+$ T cell pool (Fig. 1*A* and Ref. 13). To further elucidate this phenomenon, we investigated the survival rate and steady-state proliferation of peripheral T cell subpopulations. To this end, we firstly measured the expression of Bcl-2, an antiapoptotic molecule whose expression is regulated by survival signals (6, 18). Fig. 1*B* shows that intracellular expression of this protein was not affected in the absence of SIT. Furthermore, the survival rate after in vitro culture (data not shown) or Annexin V expression on ex vivo isolated $CD8^+$ T cells (Fig. 1*C*) were not altered in the absence of SIT. Hence, it appears as if loss of SIT does not affect the survival of $CD8^+$ as well as $CD4^+$ T cells (data not shown).

We next measured steady-state proliferation by determining BrdU incorporation in $CD8^+$ T cells. However, we found similar turnover rates between $SIT^{-/-}$ and wild-type (WT) mice (Fig. 1*D*).

Collectively, these data suggest that loss of SIT does not alter T cell numbers by affecting their survival or steady-state proliferation.

To shed further light onto this phenomenon, we characterized the expression of differentiation markers in lymphoid organs of SIT-deficient and WT mice by flow cytometry.

We initially assessed the expression of CD44, a cell surface marker that is generally used to distinguish between naive ($CD44^{low}$) and memory cells ($CD44^{high}$). Fig. 2*A* shows that $CD8^+$ T cells from $SIT^{-/-}$ mice display a dramatic alteration of the CD44 profile. Calculation of absolute numbers revealed a selective and marked decrease in the number of naive $CD8^+$ T cells in secondary lymphoid organs from SIT-deficient mice (Fig. 2*B*). Conversely, $CD4^+$ T cells showed only a mild alteration in the CD44 profile (Fig. 2*A*) and, accordingly, a slight reduction in the number of the naive fraction (Fig. 2*C*). The expression of the activation markers CD25 and CD69 was not altered on T cells from

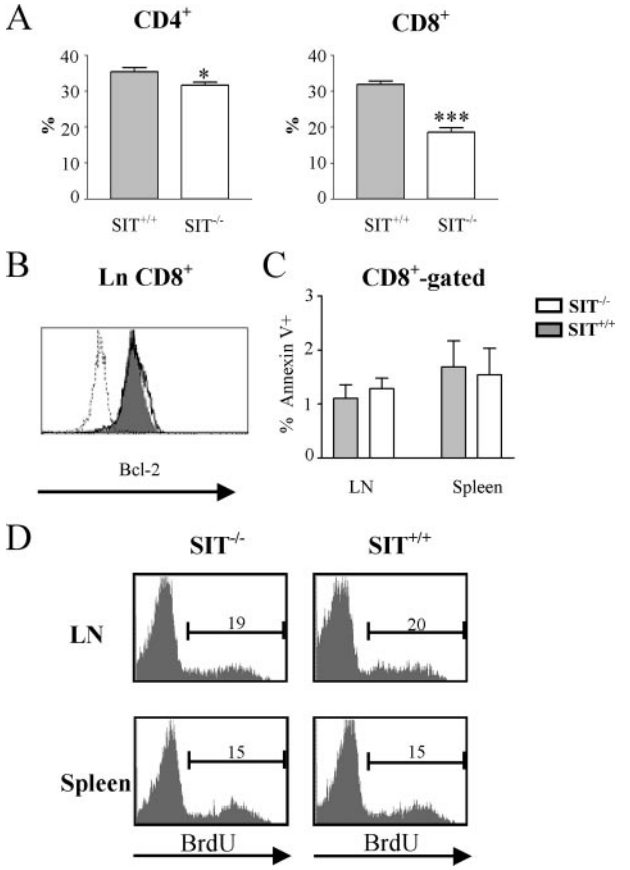

FIGURE 1. Normal survival and steady-state proliferation of $CD8^+$ T cells in $SIT^{-/-}$ mice. *A*, Lymph node cells were isolated from $SIT^{-/-}$ and $SIT^{+/+}$ mice and stained with CD4 and CD8 mAbs. Bar graphs indicate mean values ± SEM from seven $SIT^{+/+}$ and nine $SIT^{-/-}$ mice. *, $p = 0.0217$; ***, $p < 0.0001$. *B*, Intracellular Bcl-2 expression in $CD8^+$ T cells from lymph nodes of $SIT^{+/+}$ (filled histogram) and $SIT^{-/-}$ (empty histogram) mice. Isotype control is shown as dotted line. *C*, Lymph node (LN) cells and splenocytes were stained with Annexin V and CD8 mAb. The mean percentage ± SEM of Annexin V^+ within $CD8^+$ T cells from six $SIT^{+/+}$ and seven $SIT^{-/-}$ mice is shown. *D*, BrdU incorporation was measured for $CD8^+$ T cells in lymph nodes (LN) and spleen. Numbers in quadrants indicate percentages of $CD8^+$ T cells. The results shown are representative of three independent experiments.

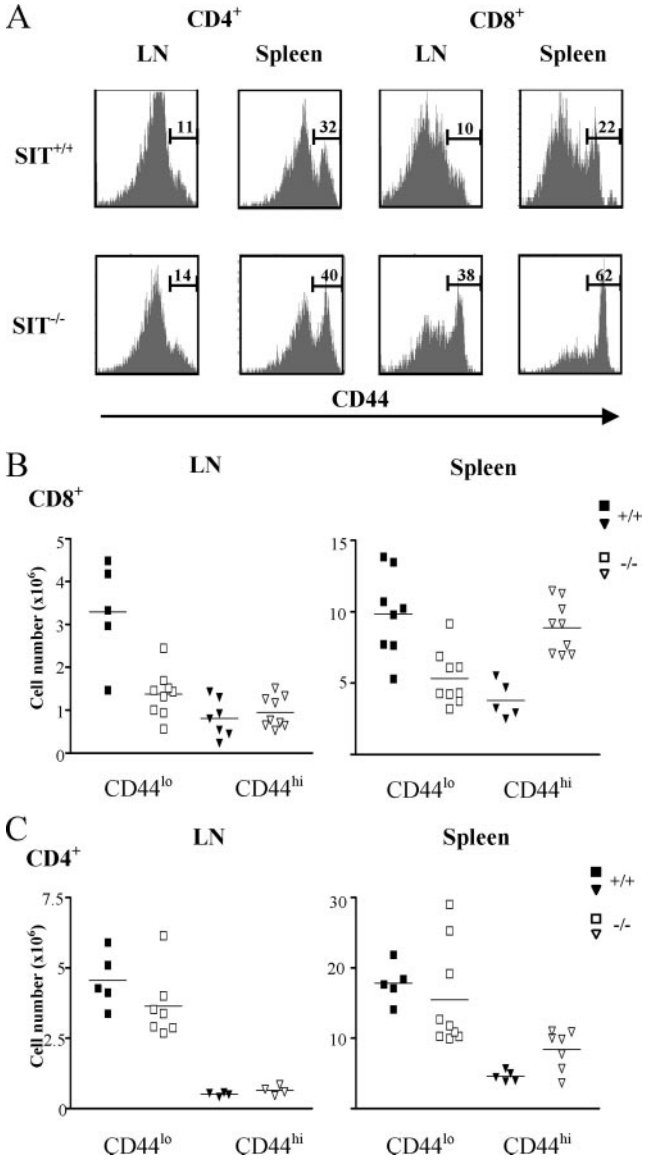

FIGURE 2. Altered distribution of $CD8^+$ T cell subsets in the periphery of $SIT^{-/-}$ mice. *A*, Representative CD44 expression profile within $CD4^+$ and $CD8^+$ T cells from lymph nodes (LN) and spleen of SIT-deficient and control mice. Absolute numbers of $CD8^+CD44^{low}$ and $CD8^+CD44^{high}$ (*B*) or $CD4^+CD44^{low}$ and $CD4^+CD44^{high}$ (*C*) T cells from spleens and lymph nodes (LN) of 5-mo-old SIT knockout and control mice were calculated. Filled squares and triangles represent $SIT^{+/+}$ mice, while empty squares and triangles represent $SIT^{-/-}$ mice.

SIT-deficient mice (data not shown), thus indicating that the activation status of the cells is normal. These results demonstrate that the paucity of mature $CD8^+$ T cells observed in the lymph nodes of $SIT^{-/-}$ mice can be exclusively attributed to the loss of the naive CD8 subset.

Furthermore, SIT-deficient mice also accumulate high numbers of $CD44^{high}$ $CD8^+$ and to a lesser extent of $CD4^+$ T lymphocytes in the spleen (Fig. 2, *B–C*).

In summary, these data show that SIT regulates the differentiation status of T cells.

We have previously shown that $SIT^{-/-}$ mice generate less $CD8^+$ SP thymocytes (13). In agreement with these data, the number of naive $CD8^+$ T cells is already severely reduced in young $SIT^{-/-}$ mice in which cells released from the thymus significantly contribute to the peripheral T cell pool (Fig. 3*A*). Moreover, we also found that the fraction of CD8 cells expressing the αE integrin (CD103) (Fig. 3*B*) and the chemokine receptor CCR9 (data not shown), which have been shown to correspond to a peripheral naive T cell subset that directly originates from recent thymic emigrants (19, 20), are severely reduced in mice lacking SIT. Thus, a decrease in the generation of thymic precursors represents a mechanism to explain the reduction of naive CD8 T cells in SIT-deficient mice.

We next investigated the mechanisms responsible for the accumulation of $CD44^{high}$ T cells in SIT-deficient mice. $CD44^{high}$ cells are usually referred to as memory cells. However, it appears that they represent a pool of cells with different origins including not only Ag-experienced T lymphocytes but also cells undergoing homeostatic proliferation. Indeed, it has been shown that during homeostatic expansion, naive T cells up-regulate CD44 and persist in the secondary lymphoid organs of adult mice, thus contributing to the $CD44^{high}$ lymphocyte pool (21). Therefore, as $CD44^{high}$ cells do not only represent memory cells, we referred to them as memory-like cells.

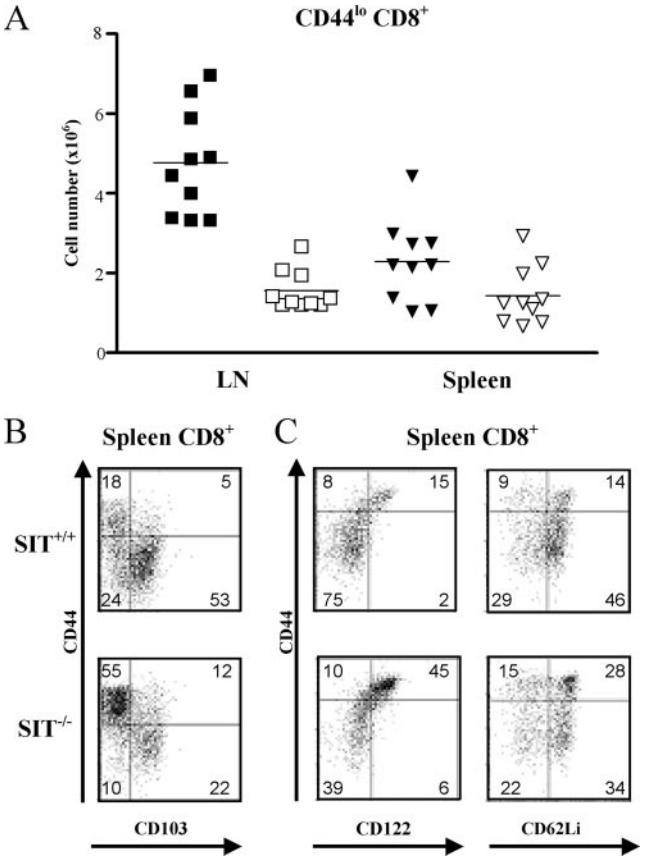

FIGURE 3. Reduced numbers of naive T cells in young $SIT^{-/-}$ mice. *A*, Number of naive $CD8^+$ T cells from lymph nodes (LN) and spleen of 1-mo-old $SIT^{+/+}$ and $SIT^{-/-}$ mice. Filled squares and triangles represent $SIT^{+/+}$ mice, while empty squares and triangles represent $SIT^{-/-}$ mice. Expression of CD44 together with CD103 (*B*), or CD122 and CD62L (*C*) is shown on $CD8^+$ splenocytes. Numbers indicate percentages of cells in each quadrant.

We focused our further investigations on $CD8^+$ T cells as they appear to be more affected by the loss of SIT than $CD4^+$ T cells. To characterize in more detail $CD8^+CD44^{high}$ T cells in SIT-deficient mice, we measured the expression of additional markers of cell differentiation. Fig. 3*C* shows that CD62L and CD122 were both highly expressed on $CD8^+CD44^{high}$ T lymphocytes thus further indicating a memory-like phenotype (Fig. 3*C*). As $CD8^+CD44^{high}CD62L^{high}CD122^{high}$ lymphocytes resemble cells undergoing homeostatic proliferation (22–24), the data shown in Fig. 3*C* suggest that homeostatic expansion is enhanced in SIT-deficient mice. To explore this possibility, we performed adoptive transfer experiments.

Loss of SIT lowers the activation threshold and enhances homeostatic proliferation of $CD8^+$ T cells

Adoptive transfer of CFSE-labeled lymph node cells into lymphopenic mice is a well-established experimental system to study homeostatic mechanisms. To investigate whether the loss of SIT resulted in enhanced T cell homeostatic proliferation, we adoptively transferred enriched $CD8^+$ SP thymocytes, as a source of naive T cells, in irradiated recipient mice. Fig. 4*A* shows that SIT-deficient $CD8^+$ T cells undergo a faster homeostatic proliferation compared with WT control T cells. As it has been shown that during homeostatic proliferation naive T cells up-regulate CD44 expression (21), we measured the level of this differentiation marker on $CD8^+$ T cells from SIT-knockout and control mice recovered after homeostatic proliferation. In agreement with the enhanced homeostatic expansion, we found that SIT-deficient naive $CD8^+$ T cells also up-regulate CD44 at a higher level than their WT counterparts (Fig. 4*B*). Fig. 4*B* also shows that the amount of CD44 expressed on $CD8^+$ SP thymocytes from knockout and WT mice before adoptive transfer is comparable. This observation indicates that the loss of SIT does not result in a general up-regulation of CD44 expression. In summary, our data demonstrate that the loss of SIT enhances both the homeostatic proliferation of naive T cells and the generation of memory-like T cells in lymphopenic mice. And, therefore, we believe that a similar mechanism is responsible for the accumulation of memory-like T cells in SIT-deficient mice.

As the TCR affinity is reported to correlate with the ability of T cells to undergo homeostatic proliferation in lymphopenic host, we performed adoptive transfer using donor cells derived from three TCR transgenic mouse lines, HY, P14, and OT-I, expressing TCRs with different affinities for self-peptides/MHC (Fig. 4*C*). This experimental design allowed us, first, to study the behavior of homogeneous naive T cell populations and, second, to grade the potential effects of SIT on TCR-mediated signal strength and in turn on homeostatic proliferation.

Because we had previously shown that signaling via the low-affinity HY TCR is particularly affected in SIT-deficient thymocytes, we performed our initial investigations using the HY TCR transgenic system (13). It has been shown that HY^+CD8^+ T cells prepared from female mice do not undergo homeostatic proliferation in lymphopenic hosts, likely because of too low TCR affinity that is not sufficient to trigger expansion of T cells in the periphery (12, 25). To assess whether loss of SIT affects the homeostatic behavior of HY^+CD8^+ T lymphocytes, CFSE-labeled lymph node cells from WT and $SIT^{-/-}$ female HY transgenic mice were adoptively transferred into irradiated female recipient animals. At day 7 after transfer, spleens were isolated and cells analyzed for the number of divisions based on CFSE content. As expected, WT HY^+CD8^+ T cells did not proliferate in lymphopenic female mice (Fig. 4*C*). In marked contrast, loss of SIT enabled HY TCR transgenic $CD8^+$ T cells to undergo vigorous homeostatic expansion (Fig. 4*C*). Similar results were obtained when we performed adoptive transfer in a second lymphopenic model, $RAG1^{-/-}$ mice (data not shown). In both systems, $SIT^{-/-}HY^+CD8^+$ T cells underwent at least two cell divisions, thus indicating that the proliferation is not a radiation-induced effect, i.e., triggered by cytokines, which are released upon irradiation (26).

The hypothesis that SIT regulates homeostasis primarily via the TCR is further supported by the fact that the in vitro response of T lymphocytes to recombinant cytokines such as IL-7 and IL-15 (which play an important role in peripheral T cell homeostasis; Refs. 7, 8, 18) was comparable in $SIT^{-/-}$ and WT $CD8^+$ T cells (data not shown).

We next tested whether SIT also exerts a negative regulatory effect on $CD8^+$ T cells carrying the P14 TCR, which possesses higher affinity than the HY TCR. Fig. 4*C* shows that, similarly to the HY TCR transgenic model, the absence of SIT enhanced the homeostatic proliferation of P14 $CD8^+$ T cells.

Finally, we investigated whether SIT has any regulatory effect on the homeostatic capability of $CD8^+$ T cells expressing a high affinity TCR, such as OT-I. In agreement with previously published data, Fig. 4*C* shows that OT-I TCR transgenic cells strongly proliferate in lymphopenic mice (25). However, Fig. 4 also demonstrates that the kinetics of homeostatic proliferation were comparable between $SIT^{-/-}$ and $SIT^{+/+}$ OT-I $CD8^+$ T cells. These data suggest that beyond a certain threshold of affinity for self-peptides/MHC complexes, SIT is dispensable for the regulation of

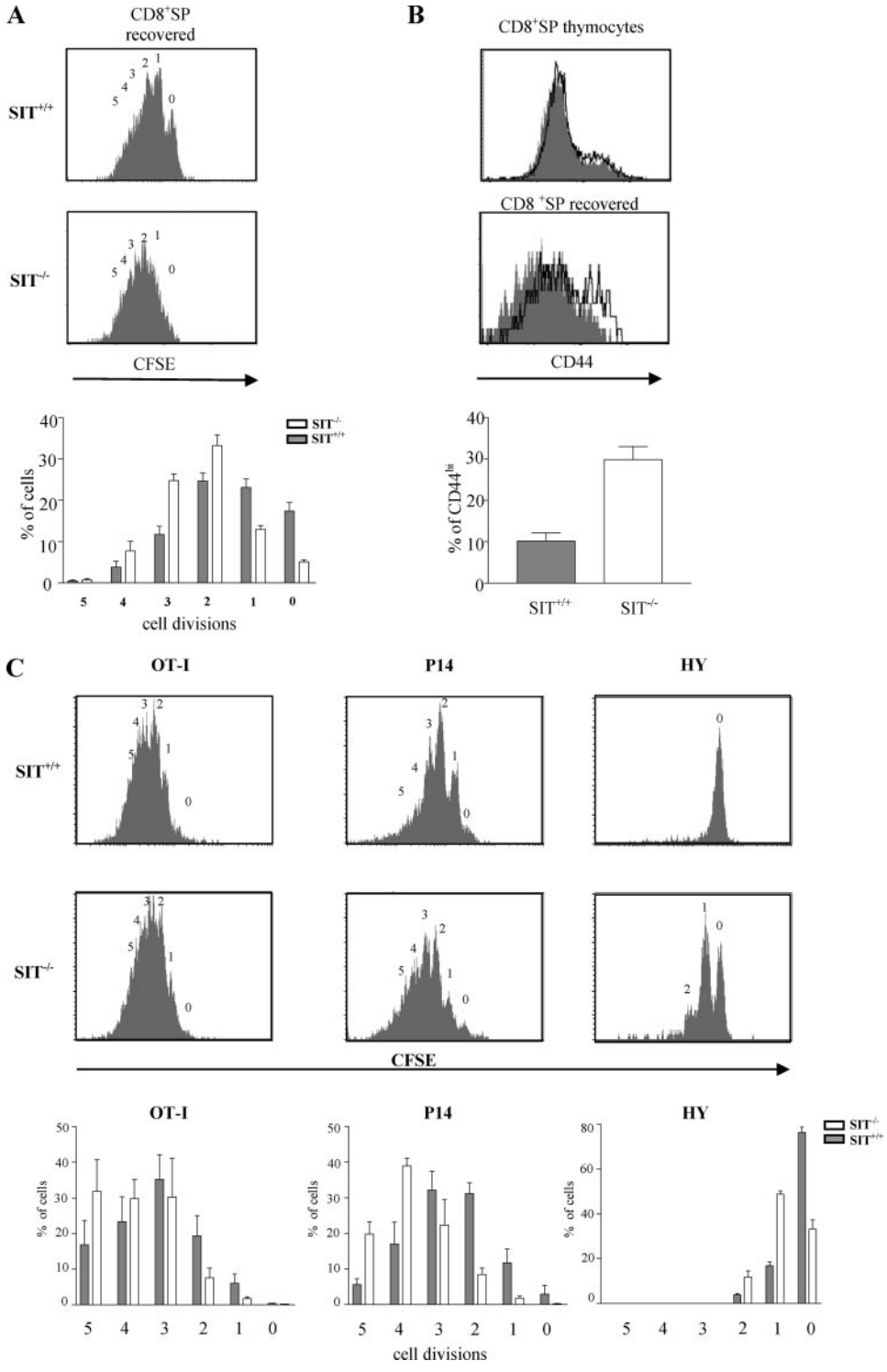

FIGURE 4. SIT negatively regulates homeostatic proliferation of $CD8^+$ T cells in lymphopenic hosts. Homeostatic proliferation of $CD8^+$ T cells after adoptive transfer in lymphopenic mice. CFSE-labeled enriched $CD8^+$ SP thymocytes (*A*) and lymph node cells carrying transgenic TCRs (HY, P14, or OT-I) (*C*) from $SIT^{+/+}$ and $SIT^{-/-}$ mice ($CD45.2^+$) were adoptively transferred into irradiated recipient mice ($CD45.1^+$). After 7 days ($CD8^+$ SP, HY, P14) or 3 days (OT-I), splenocytes were stained with CD8 and CD45.1 ($CD8^+$ SP, P14, and OT-I) or with T3.70 and CD8 (HY) mAbs. Histograms in *A* and *C* show CFSE profiles of donor derived $CD45.1^-$ $CD8^+$ ($CD8^+$ SP, P14, OT-I) or $T3.70^+$ $CD8^+$ (HY) from a representative mouse. Numbers indicate cell divisions. Bar graphs in *A* and *C* show statistical analysis of homeostatic proliferation of enriched $CD8^+$ SP thymocytes from 5 $SIT^{+/+}$ and 5 $SIT^{-/-}$ mice (*A*) and of lymph node cells from four OT-I, four P14, and six HY from WT or SIT-deficient mice (*C*). *B*, Histogram overlays compare the expression of CD44 on $CD8^+$ SP thymocytes from $SIT^{+/+}$ (filled histograms) and $SIT^{-/-}$ (empty histograms) mice before (*upper panel*) and after (*lower panel*) adoptive transfer. Statistical analysis of $CD44^{high}$ expressing $CD8^+$ SP cells from five $SIT^{+/+}$ and five $SIT^{-/-}$ mice after adoptive transfer is shown in the bar graph below.

TCR-mediated signaling. Collectively, these data demonstrate that SIT-deficiency lowers TCR-mediated activation threshold and enhances homeostatic proliferation.

Sensory adaptation of SIT-deficient T cells

Despite the lower threshold for activation, $CD8^+$ T cells from SIT-deficient mice do not display a fully activated phenotype. Therefore, it is conceivable that $SIT^{-/-}$ cells develop compensatory mechanisms to avoid improper activation. Indeed, recent observations suggest that T cells are endowed with adaptation mechanisms and may reprogram the activation threshold in reaction to strong signals (27). To assess this point, we investigated the expression of CD5, which is well established to directly correlate with the strength of TCR engagement. Moreover, the expression of CD5 is required to dampen strong TCR signaling (28). CD5 function appears to be of particular importance in $CD4^+CD8^+$ thymocytes, whose maturation critically depends upon the TCR-mediated activation threshold. In fact, we and others have previously shown that thymocytes lacking negative regulatory molecules express higher levels of CD5 as compared with WT cells (13, 29, 30). Surprisingly, we found that CD5 expression remained elevated even on peripheral $SIT^{-/-}$

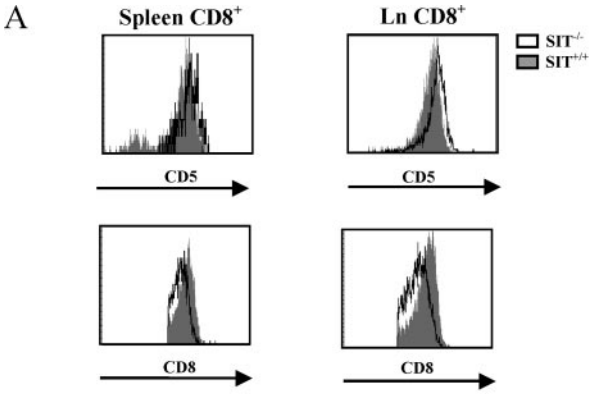

Spleen CD8+	SIT+/+	SIT-/-	
CD5 MFI	165.6 ± 4.27	230.2 ±6.86	p< 0.0001 n=8
CD8 MFI	189.8 ± 6.3	121.5 ± 6.55	p< 0.0001 n=8

Ln CD8+	SIT+/+	SIT-/-	
CD5 MFI	177.5 ±7.8	245.3 ± 7.0	p< 0.0001 n=8
CD8 MFI	166.2 ± 20.46	120.5 ± 3.41	p<0.0033 n=8

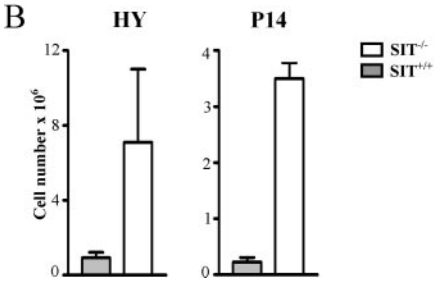

FIGURE 5. Expression of CD5 and CD8 in SIT$^{-/-}$ T cells. *A*, Histogram overlays compare the expression of CD5 and CD8 on CD8$^+$-gated splenic and lymph node T cells from SIT$^{+/+}$ (filled histograms) and SIT$^{-/-}$ (empty histograms) mice. Statistical analysis of CD5 and CD8 mean fluorescence intensity is shown below. *B*, Splenocytes from HY and P14 TCR transgenic mice were stained with CD4, CD8, and TCRα (T3.70 for HY and Vα_2 for P14) mAbs and numbers of transgenic TCRα^+CD4$^-$ CD8$^-$ were calculated. The mean ± SEM of TCRα^+CD4$^-$CD8$^-$ cells from seven SIT$^{+/+}$ and seven SIT$^{-/-}$ mice in each TCR transgenic model is shown.

CD8$^+$ T cells either in TCR transgenic or nontransgenic genetic backgrounds (Fig. 5*A* and our unpublished data). This observation corroborates the hypothesis that in addition to thymocytes, peripheral CD8$^+$ T lymphocytes receive constantly stronger signals via the TCR in the absence of SIT.

To further characterize the existence of mechanisms that would allow tuning of the activation threshold in SIT$^{-/-}$ mice, we investigated the expression of the coreceptor CD8. Recent data suggested that down-regulation of CD8 is a mechanism that allows T cells to regulate the threshold of T cell activation (31). Thus in addition to upregulating CD5, modulation of T cell responsiveness by downregulating the CD8 coreceptor represents a mechanism for sensory adaptation that prevents the activation of autoreactive T cells in the presence of persistent stimulation.

Analysis of SIT$^{-/-}$ peripheral CD8$^+$ T cells revealed significantly lower levels of CD8 expression compared with control mice (Fig. 5*A*). As CD8$^+$ single positive thymocytes express normal level of CD8 (data not shown), the down-regulation of the coreceptor in the periphery is likely induced by signals received by mature T cells. A similar coreceptor down-regulation was detected in SIT-deficient mice carrying the HY and P14 TCRs (data not shown). Moreover, HY and P14 SIT$^{-/-}$ mice also displayed unusually high numbers of transgenic TCRα^+ CD4$^-$CD8$^-$ lymphocytes in the periphery (Fig. 5*B*), thus likely indicating that a complete down-regulation of the coreceptor has occurred in some cells.

In addition to CD8$^+$ T cells, SIT-deficient CD4$^+$CD8$^+$ thymocytes show a similar phenotype and up-regulate CD5 while down-regulating CD4 (data not shown). Taken together, these observations are in line with the concept that SIT-deficient T cells counterbalance the stronger TCR-mediated stimulation by adjusting the expression of positive and negative regulatory molecules, thus reprogramming the activation threshold.

Impaired proximal signaling in SIT$^{-/-}$ T cells

The existence of compensatory mechanisms in SIT-deficient mice was further supported by the observation that thymocytes and peripheral T cells displayed impaired proximal signaling events upon in vitro stimulation with CD3 or CD3 plus CD28 Abs (Fig. 6*A* and our unpublished data). The data depicted in Fig. 6*A* show that tyrosine phosphorylation of several proteins is reduced in SIT-deficient thymocytes. In particular, we consistently observed a marked reduction of TCR-mediated tyrosine phosphorylation of LAT either assessed by global anti-phosphotyrosine immunoblotting (Fig. 6*A*), LAT immunoprecipitation, or by using phosphosite specific Abs (Fig. 6*B*).

Given the strong reduction in LAT phosphorylation it was necessary to investigate whether the activation of signaling molecules downstream of LAT is also reduced in SIT$^{-/-}$ thymocytes. Fig. 6*A* shows that TCR-mediated activation of ERK1/2 is significantly impaired in SIT-deficient mice whereas the activations of JNK/SAPK and p38 are normal. In agreement with these data, further biochemical analyses revealed that TCR-mediated phosphorylation of PLCγ1 and calcium-flux are reduced in SIT-deficient T cells (Fig. 6*C*).

ZAP-70 is believed to represent the major tyrosine kinase responsible for LAT phosphorylation (32). To assess whether the reduced levels of LAT phosphorylation in SIT-deficient mice is due to an impaired activation of ZAP-70 we investigated the phosphorylation status and the enzymatic activity of ZAP-70. In line with blunted LAT phosphorylation we found that TCR-mediated phosphorylation of two critical tyrosine residues of ZAP70, Y319, and Y493 is reduced in SIT$^{-/-}$ thymocytes (Fig. 6*D*). Similarly, in vitro kinase assays of ZAP-70 immunoprecipitates showed attenuated enzymatic activity of ZAP 70 in the absence of SIT (Fig. 6*D*).

ZAP-70 activation requires the tyrosine phosphorylation of ITAM motifs of the CD3 and TCR-ζ-chains (33). Phosphorylation of the ITAMs provides docking sites for the two SH2 domains within ZAP-70, thus positioning this kinase in the TCR/CD3 complex closed to its upstream activator Lck. Therefore, to elucidate the mechanisms responsible for impaired ZAP-70 activation in SIT-deficient T cells, we investigated TCR-ζ phosphorylation and TCR-ζ/ZAP-70 association. Fig. 6*E* shows that complete tyrosine phosphorylation of TCR-ζ upon CD3-crosslinking, which is detectable as a phospho-protein migrating at 23kDa, is comparable between SIT-deficient and WT T cells (Fig. 6*E*). Furthermore, analysis of immunoprecipitated TCR-ζ show that the association with ZAP-70 is also normal in SIT$^{-/-}$ T cells (Fig. 6*E*), thus suggesting that the phosphorylation of TCR-ζ and the recruitment of ZAP-70 to the TCR/CD3 complex are intact in SIT-deficient mice. Overall, our findings indicate the existence of a molecular mechanism that renders SIT-deficient T cells refractory to TCR-mediated stimulation by reducing ZAP-70 activation.

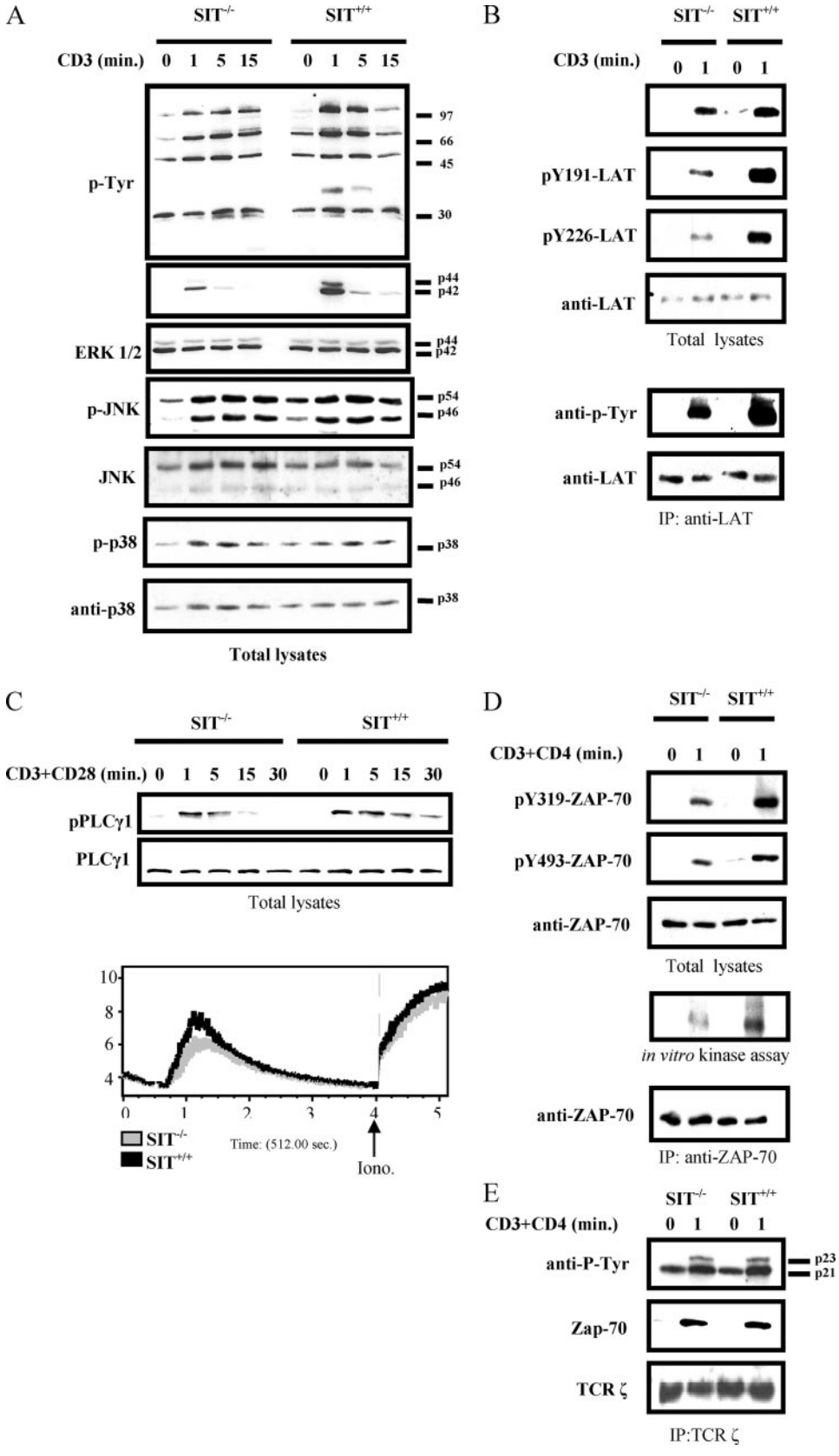

FIGURE 6. Impaired TCR-mediated signaling in SIT$^{-/-}$ T cells. *A*, Thymocytes were stimulated for the indicated times and assayed for the induction of total tyrosine phosphorylations (p-Tyr) or the activation of ERK1/2, JNK and p38. *B*, LAT phosphorylation was analyzed by blotting total cell lysates with phospho-specific Abs or by blotting anti-LAT immunoprecipitates with an anti-phosphotyrosine Ab. *C*, Purified T cells were stimulated for the indicated times and assayed for PLCγ1 phosphorylation. The panel below shows calcium flux from CD4$^+$- and CD8$^+$-gated splenocytes of SIT$^{-/-}$ and WT mice. The arrows indicate Ab crosslinking (Ab) and ionomycin (iono.), respectively. *D*, Thymocytes were stimulated and processed for immunoblotting. Phosphorylation of ZAP-70 was analyzed by immunoblotting total cell lysates directly. ZAP-70 immunoprecipitates were subjected to in vitro kinase assay. *E*, Thymocytes were stimulated and TCRζ was immunoprecipitated. Subsequently, tyrosine phosphorylation levels and association with ZAP-70 were analyzed by western blotting. Equal loading is shown by reprobing immunoblots with Abs specific for ERK1/2, JNK, and p38 (*A*), LAT (*B*), PLCγ-1 (*C*), and ZAP-70 (*D*) or TCRζ (*E*).

Discussion

The data presented in this study reveal that SIT, a nonraft-associated transmembrane adaptor, acts as a critical regulator of the peripheral T cell pool. We demonstrate that SIT contributes to the maintenance of the peripheral CD8$^+$ T cell in at least two different ways. First, by regulating the number of precursors generated within the thymus and, second, by modulating homeostatic proliferation in the periphery. Our data suggest that SIT lowers the T cell-activation threshold whereby signals that normally should promote survival may become overtly stimulatory in the absence of

SIT and may induce naive $CD8^+$ and $CD4^+$ lymphocytes to undergo a continuous slow-rate homeostatic proliferation. During this expansion, naive cells seem to progressively acquire the memory-like phenotype.

Despite the fact that SIT is expressed in both cell types, SIT-deficiency more prominently affects $CD8^+$ than $CD4^+$ T cells. Similarly, mice lacking the adaptor protein GADS, which, like SIT, is expressed in both T-lymphocyte subsets, show an impaired homeostasis in $CD4^+$ but not in $CD8^+$ T cells (34). These results are in line with the idea that homeostasis in $CD8^+$ T cells is regulated differentially than in $CD4^+$ T cells.

We propose that SIT represents a modulator of T cell homeostasis. Conversely to other molecules such as LAT or CTLA-4 that have been shown to regulate the expansion of activated T cells (35–38) SIT and the recently published human lymphocyte activation Ag 3 (39) and B and T lymphocyte attenuator (BTLA) (40) appear to be the only negative regulatory molecules known so far that selectively affect peripheral T cell homeostasis without altering the activation status of T cells.

One mechanism of action could be that SIT recruits tyrosine phosphatases such as SHP-1 and SHP-2 to the plasma membrane in a similar fashion to other negative regulatory molecules possessing ITIMs, such as CD5 (41), PD-1 (42), and BTLA (43). Indeed, SIT knockout mice share many similarities with CD5-, PD-1-, and BTLA-deficient mice. Like $SIT^{-/-}$ mice, $CD5^{-/-}$ mice also show a conversion from positive to negative selection in the HY and P14 systems (28, 44). Moreover, similar to SIT-deficient mice, $PD\text{-}1^{-/-}$ mice display increased numbers of $TCR^+CD4^-CD8^-$ peripheral T cells (45) and develop glomerulonephritis (46). Finally, both SIT and BTLA knockout mice show an increase in memory-like $CD8^+$ T cells and enhanced lymphopenia-induced homeostatic proliferation (40).

Survival and homeostatic proliferation of peripheral T cells both require the expression of self-peptide/MHC molecules (47). This requirement parallels the need for MHC restriction during Ag-specific proliferation. However, unlike Ag-induced proliferation, homeostatic proliferation does not require costimulation (23, 48) and does not result in the differentiation of effector cells (11, 23). Compelling evidences further suggest that homeostatic expansion of peripheral T cells has similarities to T cell development. Indeed, two groups have recently shown that the peptides initiating positive selection in the thymus also drive homeostatic proliferation in the periphery (11, 12). Therefore, self peptides appear to be key factors for determining cell fate. Upon TCR ligation, they rescue T lymphocytes from a default cell death pathway, thus initiating positive selection in the thymus, and, further, they induce homeostatic proliferation in the periphery. Consequently, TCR-ligand affinity plays a pivotal role in the regulation of the efficiency of these processes. In fact, transgenic T cells carrying the low affinity HY TCR undergo inefficient positive selection and show no homeostatic proliferation, whereas mice expressing TCRs with higher affinities, such as P14, 2C, and OT-I, show a more efficient positive selection and robustly proliferate in lymphopenic mice (25, 49). Thus, it is likely that thymic selection and homeostatic proliferation share similar regulatory mechanisms. How a T cell senses the degrees of TCR-ligand affinity and sorts them into specific cellular outcomes is largely unknown. However, the data presented in this study as well as our previous study on $SIT^{-/-}$ mice (13) demonstrate that SIT is an important component of the signaling machinery that translates analog inputs into digital outputs and suggest that SIT functions as a fine-tuner of the translation process. To our knowledge, SIT is the only molecule that has been shown so far to regulate both thymic development and homeostatic proliferation.

Our data suggest that SIT regulates T cell homeostasis primarily via the TCR. However, we cannot exclude the possibility that in vivo SIT could also regulate signal transduction from other receptors such as ILs receptors or even a cross-talk between the TCR and ILs receptors.

We also show that SIT-deficient T cells develop sensory adaptation, most likely in an attempt to compensate the enhanced TCR-mediated signaling. At the molecular level, $SIT^{-/-}$ T cells show an impaired ZAP-70 activity that in turn affects the activation of other downstream signaling molecules. Therefore, the perturbation of ZAP-70 activity is the most apical defect in the TCR-mediated pathway that is affected by SIT. How does loss of SIT impair ZAP-70 activation? We propose two mechanisms to answer this question. First, as SIT-deficient T cells down-regulate coreceptor expression, the amount of Lck that is activated upon TCR/coreceptor coengagement is reduced. The defective Lck activation could in turn result in a selective reduction of ZAP-70 activation. As we did not notice changes in TCR-ζ phosphorylation, it is likely that src-kinase activity associated with the TCR is not affected in SIT-deficient T cells. Alternatively, tyrosine phosphatases such as SHP-1, which are known to mediate dephosphorylation and inactivation of ZAP-70 (50) are more active in SIT-deficient T cells. In agreement with this hypothesis would be our finding that the expression of inhibitory receptors such as CD5, a molecule that down-regulates the TCR-mediated signal transduction pathway by recruiting SHP-1 to the plasma membrane (41) are enhanced in $SIT^{-/-}$ T lymphocytes.

The development of compensatory mechanisms could serve to prevent autoimmunity or chronic inflammatory processes and hence to preserve an appropriate immune competence of T cells even in the absence of SIT. Indeed, immune responses against Ags, *Toxoplasma,* and *Listeria,* as well as rejection of allograft transplantations were all normal in SIT-deficient mice (our own unpublished observations). However, despite the apparently normal immune response, it appears as if the sensory adaptation is not completely effective. In fact, we have recently shown that SIT-deficient mice spontaneously develop antinuclear Abs, glomerulonephritis, and accumulate activated CD4 T cells in secondary lymphoid organs (our unpublished results). Additionally, we showed previously that SIT-deficient mice display a more severe clinical course during Experimental autoimmune encephalomyelitis, a mouse model of multiple sclerosis (13). Individuals in which T cells undergo enhanced lymphopenia-induced homeostatic proliferation such as patients affected by immunodeficiencies (i.e., AIDS) or treated with chemo/radio therapy suffer from different autoimmune diseases (51, 52). Moreover, it has been demonstrated that T cells undergoing homeostatic expansion are more susceptible to becoming autoreactive (53). On the basis of these observations, we propose that the susceptibility of $SIT^{-/-}$ mice to develop autoimmunity is likely caused by the enhanced homeostatic proliferation of SIT-deficient T cells. In conclusion, our observations suggest that SIT plays an important role in maintaining T cell homeostasis and that alterations of SIT expression or function in humans may lead to enhanced homeostatic proliferation and to an increased susceptibility to develop autoimmune diseases.

Acknowledgments

We thank Dr. Dirk Schlüter for providing SJL mice and the employees of the animal facility for maintenance of the animals. We are grateful to Ines Meinert for excellent technical assistance, Dr. Jonathan Lindquist for critically reading the manuscript and helpful discussion, and Dr. Andrew Cope for reagents.

Disclosures

The authors have no financial conflict of interest.

References

1. Freitas, A. A., and B. Rocha. 2000. Population biology of lymphocytes: the flight for survival. *Annu. Rev. Immunol.* 18: 83–111.
2. Kelly, K. A., and R. Scollay. 1990. Analysis of recent thymic emigrants with subset- and maturity-related markers. *Int. Immunol.* 2: 419–425.
3. Margolick, J. B., and A. D. Donnenberg. 1997. T-cell homeostasis in HIV-1 infection. *Semin. Immunol.* 9: 381–388.
4. Tumpey, T. M., X. Lu, T. Morken, S. R. Zaki, and J. M. Katz. 2000. Depletion of lymphocytes and diminished cytokine production in mice infected with a highly virulent influenza A (H5N1) virus isolated from humans. *J. Virol.* 74: 6105–6116.
5. Berezne, A., W. Bono, L. Guillevin, and L. Mouthon. 2006. Diagnosis of lymphocytopenia. *Presse Med.* 35: 895–902.
6. Kirberg, J., A. Berns, and H. von Boehmer. 1997. Peripheral T cell survival requires continual ligation of the T cell receptor to major histocompatibility complex-encoded molecules. *J. Exp. Med.* 186: 1269–1275.
7. Schluns, K. S., W. C. Kieper, S. C. Jameson, and L. Lefrancois. 2000. Interleukin-7 mediates the homeostasis of naive and memory CD8 T cells in vivo. *Nat. Immunol.* 1: 426–432.
8. Tan, J. T., B. Ernst, W. C. Kieper, E. LeRoy, J. Sprent, and C. D. Surh. 2002. Interleukin (IL)-15 and IL-7 jointly regulate homeostatic proliferation of memory phenotype $CD8^+$ cells but are not required for memory phenotype $CD4^+$ cells. *J. Exp. Med.* 195: 1523–1532.
9. Starr, T. K., S. C. Jameson, and K. A. Hogquist. 2003. Positive and negative selection of T cells. *Annu. Rev. Immunol.* 21: 139–176.
10. Sebzda, E., V. A. Wallace, J. Mayer, R. S. Yeung, T. W. Mak, and P. S. Ohashi. 1994. Positive and negative thymocyte selection induced by different concentrations of a single peptide. *Science* 263: 1615–1618.
11. Goldrath, A. W., and M. J. Bevan. 1999. Low-affinity ligands for the TCR drive proliferation of mature $CD8^+$ T cells in lymphopenic hosts. *Immunity* 11: 183–190.
12. Ernst, B., D. S. Lee, J. M. Chang, J. Sprent, and C. D. Surh. 1999. The peptide ligands mediating positive selection in the thymus control T cell survival and homeostatic proliferation in the periphery. *Immunity* 11: 173–181.
13. Simeoni, L., V. Posevitz, U. Kolsch, I. Meinert, E. Bruyns, K. Pfeffer, D. Reinhold, and B. Schraven. 2005. The transmembrane adapter protein SIT regulates thymic development and peripheral T-cell functions. *Mol. Cell. Biol.* 25: 7557–7568.
14. Pfrepper, K. I., A. Marie-Cardine, L. Simeoni, Y. Kuramitsu, A. Leo, J. Spicka, I. Hilgert, J. Scherer, and B. Schraven. 2001. Structural and functional dissection of the cytoplasmic domain of the transmembrane adaptor protein SIT (SHP2-interacting transmembrane adaptor protein). *Eur. J. Immunol.* 31: 1825–1836.
15. Marie-Cardine, A., H. Kirchgessner, E. Bruyns, A. Shevchenko, M. Mann, F. Autschbach, S. Ratnofsky, S. Meuer, and B. Schraven. 1999. SHP2-interacting transmembrane adaptor protein (SIT), a novel disulfide-linked dimer regulating human T cell activation. *J. Exp. Med.* 189: 1181–1194.
16. Azzam, H. S., A. Grinberg, K. Lui, H. Shen, E. W. Shores, and P. E. Love. 1998. CD5 expression is developmentally regulated by T cell receptor (TCR) signals and TCR avidity. *J. Exp. Med.* 188: 2301–2311.
17. Schraven, B., H. Kirchgessner, B. Gaber, Y. Samstag, and S. Meuer. 1991. A functional complex is formed in human T lymphocytes between the protein tyrosine phosphatase CD45, the protein tyrosine kinase p56lck and pp32, a possible common substrate. *Eur. J. Immunol.* 21: 2469–2477.
18. Lantz, O., I. Grandjean, P. Matzinger, and J. P. Di Santo. 2000. γ-chain required for naive $CD4^+$ T cell survival but not for antigen proliferation. *Nat. Immunol.* 1: 54–58.
19. McFarland, R. D., D. C. Douek, R. A. Koup, and L. J. Picker. 2000. Identification of a human recent thymic emigrant phenotype. *Proc. Natl. Acad. Sci. USA* 97: 4215–4220.
20. Staton, T. L., B. Johnston, E. C. Butcher, and D. J. Campbell. 2004. Murine $CD8^+$ recent thymic emigrants are αE integrin-positive and CC chemokine ligand 25 responsive. *J. Immunol.* 172: 7282–7288.
21. Schuler, T., G. J. Hammerling, and B. Arnold. 2004. Cutting edge: IL-7-dependent homeostatic proliferation of $CD8^+$ T cells in neonatal mice allows the generation of long-lived natural memory T cells. *J. Immunol.* 172: 15–19.
22. Murali-Krishna, K., and R. Ahmed. 2000. Cutting edge: naive T cells masquerading as memory cells. *J. Immunol.* 165: 1733–1737.
23. Cho, B. K., V. P. Rao, Q. Ge, H. N. Eisen, and J. Chen. 2000. Homeostasis-stimulated proliferation drives naive T cells to differentiate directly into memory T cells. *J. Exp. Med.* 192: 549–556.
24. Goldrath, A. W., L. Y. Bogatzki, and M. J. Bevan. 2000. Naive T cells transiently acquire a memory-like phenotype during homeostasis-driven proliferation. *J. Exp. Med.* 192: 557–564.
25. Kieper, W. C., J. T. Burghardt, and C. D. Surh. 2004. A role for TCR affinity in regulating naive T cell homeostasis. *J. Immunol.* 172: 40–44.
26. Peterson, V. M., J. J. Adamovicz, T. B. Elliott, M. M. Moore, G. S. Madonna, W. E. Jackson, III, G. D. Ledney, and W. C. Gause. 1994. Gene expression of hematoregulatory cytokines is elevated endogenously after sublethal γ irradiation and is differentially enhanced by therapeutic administration of biologic response modifiers. *J. Immunol.* 153: 2321–2330.
27. Marquez, M. E., W. Ellmeier, V. Sanchez-Guajardo, A. A. Freitas, O. Acuto, and V. Di Bartolo. 2005. CD8 T cell sensory adaptation dependent on TCR avidity for self-antigens. *J. Immunol.* 175: 7388–7397.
28. Azzam, H. S., J. B. DeJarnette, K. Huang, R. Emmons, C. S. Park, C. L. Sommers, D. El-Khoury, E. W. Shores, and P. E. Love. 2001. Fine tuning of TCR signaling by CD5. *J. Immunol.* 166: 5464–5472.
29. Naramura, M., H. K. Kole, R. J. Hu, and H. Gu. 1998. Altered thymic positive selection and intracellular signals in Cbl-deficient mice. *Proc. Natl. Acad. Sci. USA* 95: 15547–15552.
30. Sosinowski, T., N. Killeen, and A. Weiss. 2001. The Src-like adaptor protein downregulates the T cell receptor on $CD4^+CD8^+$ thymocytes and regulates positive selection. *Immunity* 15: 457–466.
31. Maile, R., C. A. Siler, S. E. Kerry, K. E. Midkiff, E. J. Collins, and J. A. Frelinger. 2005. Peripheral "CD8 tuning" dynamically modulates the size and responsiveness of an antigen-specific T cell pool in vivo. *J. Immunol.* 174: 619–627.
32. Zhang, W., J. Sloan-Lancaster, J. Kitchen, R. P. Trible, and L. E. Samelson. 1998. LAT: the ZAP-70 tyrosine kinase substrate that links T cell receptor to cellular activation. *Cell* 92: 83–92.
33. Iwashima, M., B. A. Irving, N. S. van Oers, A. C. Chan, and A. Weiss. 1994. Sequential interactions of the TCR with two distinct cytoplasmic tyrosine kinases. *Science* 263: 1136–1139.
34. Yankee, T. M., T. J. Yun, K. E. Draves, K. Ganesh, M. J. Bevan, K. Murali-Krishna, and E. A. Clark. 2004. The Gads (GrpL) adaptor protein regulates T cell homeostasis. *J. Immunol.* 173: 1711–1720.
35. Sommers, C. L., C. S. Park, J. Lee, C. Feng, C. L. Fuller, A. Grinberg, J. A. Hildebrand, E. Lacana, R. K. Menon, E. W. Shores, et al. 2002. A LAT mutation that inhibits T cell development yet induces lymphoproliferation. *Science* 296: 2040–2043.
36. Aguado, E., S. Richelme, S. Nunez-Cruz, A. Miazek, A. M. Mura, M. Richelme, X. J. Guo, D. Sainty, H. T. He, B. Malissen, and M. Malissen. 2002. Induction of T helper type 2 immunity by a point mutation in the LAT adaptor. *Science* 296: 2036–2040.
37. Tivol, E. A., F. Borriello, A. N. Schweitzer, W. P. Lynch, J. A. Bluestone, and A. H. Sharpe. 1995. Loss of CTLA-4 leads to massive lymphoproliferation and fatal multiorgan tissue destruction, revealing a critical negative regulatory role of CTLA-4. *Immunity* 3: 541–547.
38. Waterhouse, P., J. M. Penninger, E. Timms, A. Wakeham, A. Shahinian, K. P. Lee, C. B. Thompson, H. Griesser, and T. W. Mak. 1995. Lymphoproliferative disorders with early lethality in mice deficient in Ctla-4. *Science* 270: 985–988.
39. Workman, C. J., and D. A. Vignali. 2005. Negative regulation of T cell homeostasis by lymphocyte activation gene-3 (CD223). *J. Immunol.* 174: 688–695.
40. Krieg, C., O. Boyman, Y. X. Fu, and J. Kaye. 2007. B and T lymphocyte attenuator regulates $CD8^+$ T cell-intrinsic homeostasis and memory cell generation. *Nat. Immunol.* 8: 162–171.
41. Perez-Villar, J. J., G. S. Whitney, M. A. Bowen, D. H. Hewgill, A. A. Aruffo, and S. B. Kanner. 1999. CD5 negatively regulates the T-cell antigen receptor signal transduction pathway: involvement of SH2-containing phosphotyrosine phosphatase SHP-1. *Mol. Cell. Biol.* 19: 2903–2912.
42. Chemnitz, J. M., R. V. Parry, K. E. Nichols, C. H. June, and J. L. Riley. 2004. SHP-1 and SHP-2 associate with immunoreceptor tyrosine-based switch motif of programmed death 1 upon primary human T cell stimulation, but only receptor ligation prevents T cell activation. *J. Immunol.* 173: 945–954.
43. Watanabe, N., M. Gavrieli, J. R. Sedy, J. Yang, F. Fallarino, S. K. Loftin, M. A. Hurchla, N. Zimmerman, J. Sim, X. Zang, et al. 2003. BTLA is a lymphocyte inhibitory receptor with similarities to CTLA-4 and PD-1. *Nat. Immunol.* 4: 670–679.
44. Tarakhovsky, A., S. B. Kanner, J. Hombach, J. A. Ledbetter, W. Muller, N. Killeen, and K. Rajewsky. 1995. A role for CD5 in TCR-mediated signal transduction and thymocyte selection. *Science* 269: 535–537.
45. Blank, C., I. Brown, R. Marks, H. Nishimura, T. Honjo, and T. F. Gajewski. 2003. Absence of programmed death receptor 1 alters thymic development and enhances generation of CD4/CD8 double-negative TCR-transgenic T cells. *J. Immunol.* 171: 4574–4581.
46. Nishimura, H., M. Nose, H. Hiai, N. Minato, and T. Honjo. 1999. Development of lupus-like autoimmune diseases by disruption of the PD-1 gene encoding an ITIM motif-carrying immunoreceptor. *Immunity* 11: 141–151.
47. Surh, C. D., and J. Sprent. 2000. Homeostatic T cell proliferation: how far can T cells be activated to self-ligands? *J. Exp. Med.* 192: F9–F14.
48. Prlic, M., B. R. Blazar, A. Khoruts, T. Zell, and S. C. Jameson. 2001. Homeostatic expansion occurs independently of costimulatory signals. *J. Immunol.* 167: 5664–5668.
49. Kassiotis, G., R. Zamoyska, and B. Stockinger. 2003. Involvement of avidity for major histocompatibility complex in homeostasis of naive and memory T cells. *J. Exp. Med.* 197: 1007–1016.
50. Plas, D. R., R. Johnson, J. T. Pingel, R. J. Matthews, M. Dalton, G. Roy, A. C. Chan, and M. L. Thomas. 1996. Direct regulation of ZAP-70 by SHP-1 in T cell antigen receptor signaling. *Science* 272: 1173–1176.
51. Lane, H. C. 1995. The generation of CD4 T lymphocytes in patients with HIV infection. *J. Biol. Regul. Homeostatic Agents* 9: 107–109.
52. Sasson, S. C., J. J. Zaunders, and A. D. Kelleher. 2006. The IL-7/IL-7 receptor axis: understanding its central role in T-cell homeostasis and the challenges facing its utilization as a novel therapy. *Curr. Drug Targets* 7: 1571–1582.
53. King, C., A. Ilic, K. Koelsch, and N. Sarvetnick. 2004. Homeostatic expansion of T cells during immune insufficiency generates autoimmunity. *Cell* 117: 265–277.

Appendix 12

Dynamics of proximal signaling events after TCR/CD8-mediated induction of proliferation or apoptosis in mature CD8+ T-cells

Wang X., **Simeoni L.**, Lindquist J.A., Saez-Rodriguez J., Gilles E.D., Kliche S., and Schraven B. (2008) *J Immunol.* 180:6703-6712.

Dynamics of Proximal Signaling Events after TCR/CD8-Mediated Induction of Proliferation or Apoptosis in Mature CD8$^+$ T Cells[1]

Xiaoqian Wang,* Luca Simeoni,* Jonathan A. Lindquist,* Julio Saez-Rodriguez,[‡] Andreas Ambach,[†] Ernst D. Gilles,[‡] Stefanie Kliche,[2]* and Burkhart Schraven[2]*

Engagement of the TCR can induce different functional outcomes such as activation, proliferation, survival, or apoptosis. How the TCR-mediated signaling cascades generating these distinct cellular responses are organized on the molecular level is so far not completely understood. To obtain insight into this question, we analyzed TCR/CD8-mediated signaling events in mature OT-I TCR transgenic T cells under conditions of stimulation that lead to either proliferation or apoptosis. These experiments revealed major differences in the phosphorylation dynamics of LAT, ZAP70, protein kinase B, phospholipase C-γ1, protein kinase D1, and ERK1/2. Moreover, input signals leading to apoptosis induced a strong, but transient activation of ERK1/2 mainly at sites of TCR-engagement. In contrast, stimuli promoting survival/proliferation generated a low and sustained activation of ERK1/2, which colocalizes with Ras in recycling endosomal vesicles. The transient activation of ERK1/2 under pro-apoptotic conditions of stimulation is at least partially due to the rapid polyubiquitination and subsequent degradation of ZAP70, whereas the sustained activation of ERK1/2 under survival promoting conditions is paralleled by the induction/phosphorylation of anti-apoptotic molecules such as protein kinase B and Bcl-x_L. Collectively, our data provide signaling signatures that are associated with proliferation or apoptosis of T cells. *The Journal of Immunology,* **2008, 180: 6703–6712.**

Stimulation of the TCR/CD3/ζ-complex can result in a variety of different cellular responses such as differentiation, cytokine secretion, survival, proliferation, or apoptosis. According to the currently accepted model, signaling downstream of the engaged TCR is initiated after ITAMs within the TCR-associated CD3/ζ-complex have been phosphorylated by the Src-family protein kinases Lck and Fyn (1). Phosphorylation of the ITAMs induces the recruitment of ZAP70, which is in turn phosphorylated and activated by Lck and Fyn (2). Activated ZAP70 then phosphorylates several downstream molecules, including the key adapter proteins LAT and SLP-76 (3, 4). The formation of a signalosome containing LAT and the adapter proteins Gads and SLP-76 provides a membrane-associated signaling platform that facilitates the recruitment and activation of PLC-γ1 which subsequently converts phosphatidylinositol 4,5-bisphosphate to diacylglycerol (DAG)[3] and inositol 1,4,5-trisphosphate. 1,4,5-trisphosphate mediates the release of Ca^{2+} from intracellular stores whereas DAG activates PKC as well as RasGRP, a nucleotide exchange factor for Ras (5). GTP-loaded Ras (active form) binds to and activates the serine/threonine kinase Raf-1 which subsequently activates the MEK1/2-ERK1/2 pathway (6, 7).

The kinetics of ERK1/2 activation after receptor engagement have been correlated with specific functional outcomes, including differentiation, proliferation, survival, or apoptosis (7). During thymocyte development, the fate of DP thymocytes is determined by a single receptor, which can differentially modulate ERK1/2 activity, depending on the affinity of the ligand. TCR-engagement by either positive selecting (low-affinity) peptide ligands induces a weak but sustained activation of ERK1/2 correlating with differentiation and survival of thymocytes, whereas negative selecting (high-affinity) peptides generate a strong but transient activation of ERK1/2 presumably responsible for the induction of thymocyte apoptosis (8, 9). Recently, it was shown that the different kinetics of ERK1/2 activation also correlate with distinct subcellular localization of this kinase. Thus, negative selecting ligands appear to target activated ERK1/2 to the plasma membrane whereas positive selecting ligands induce the recruitment of activated ERK1/2 to the Golgi apparatus (10). However, it is currently not clear whether different localization and/or activation kinetics of ERK1/2 are indeed directly responsible for regulating positive vs negative selection.

Abs recognizing site-specific phosphorylation motifs of key molecules have been successfully used to study the kinetics and sequence of early events leading to T cell activation. During the past years several research groups have addressed the question how the TCR regulates the activation of intracellular signaling cascades. Experimental systems included in vitro stimulation of primary T cells or Jurkat T cell lines with either soluble or immobilized Abs that recognize the TCR-associated CD3ε-chains, peptide-loaded APCs, or MHC-I/MHC-II tetramers carrying high- or low-affinity peptides. However, the number of detailed studies that

*Institute of Molecular and Clinical Immunology and [†]Department of Dermatology and Venerology, Otto-von-Guericke-University, Magdeburg; and [‡]Max-Planck-Institute for Dynamics of Complex Technical Systems, Magdeburg, Germany

Received for publication September 24, 2007. Accepted for publication March 10, 2008.

The costs of publication of this article were defrayed in part by the payment of page charges. This article must therefore be hereby marked *advertisement* in accordance with 18 U.S.C. Section 1734 solely to indicate this fact.

[1] This work was supported by grants from the German Research Foundation to B. S. and S. K. (FOR521 and GRK1167).

[2] Address correspondence and reprint requests to Dr. Burkhart Schraven and Dr. Stefanie Kliche, Institute of Molecular and Clinical Immunology, Otto-von-Guericke-University, Leipziger Strasse 44, D-39120 Magdeburg, Germany. E-mail addresses: burkhart.schraven@med.ovgu.de and stefanie.kliche@med.ovgu.de

[3] Abbreviations used in this paper: DAG, diacylglycerol; WT, wild type; tg, transgenic; p, phospho; PI, propidium iodide; PKB, protein kinase B; PKD1, protein kinase D1.

correlate phosphorylation kinetics of key molecules involved in T cell activation with different cellular responses is very low (10–12).

In the present study, we have addressed the question how different T cell responses (proliferation vs apoptosis) correlate with intracellular signaling events in mature OT-I TCR-transgenic $CD8^+$ T cells. Stimulation conditions were chosen in a way that engagement of the TCR and the CD8 coreceptor either induces proliferation/survival or cell death/apoptosis. We show that these two conditions of stimulation lead to dynamically distinct patterns of phosphorylation/activation of key molecules involved in T cell activation. Furthermore, we also demonstrate that these different cellular responses correlate with distinct subcellular localizations of ERK1/2 in peripheral T cells.

Materials and Methods

Mice, T cell purification, and activation

OT-I TCR transgenic (tg) mice were provided by Percy Knolle (University of Bonn, Bonn, Germany). Perforin knock out ($perforin^{-/-}$) mice were obtained from Jackson Laboratories. The mice were maintained in pathogen free conditions. All experiments involving mice were performed according to the guidelines of the State of Sachsen-Anhalt, Germany. Splenic $CD8^+$ T cells from OT-I TCR tg mice were purified using a pan T cell isolation kit and AutoMacs magnetic separation system (Miltenyi Biotec) according to the manufacturer's instructions. Purification of splenic $CD8^+$ T cells from wild-type (WT) or $perforin^{-/-}$ mice was performed using $CD8^+$ T cell isolation kit (Miltenyi Biotec). Cells were stimulated with biotinylated anti-mouse CD3ε (10 μg/ml) mAb and biotinylated anti-mouse CD8α (10 μg/ml) mAb (both from BD Biosciences) and cross-linked with streptavidin (50 μg/ml; Dianova). Before stimulation of cells with streptamers, either PE-conjugated or nonconjugated Strep-Tactin was incubated with recombinant monomeric biotinylated-MHC-I (1 μg/reaction) (IBA GmbH) at 4°C according to the manufacturer's instructions. Recombinant monomeric biotinylated H-$2K^b$ molecules presenting the OVA SIINFEKEL peptide specific for the OT-I-tg TCR were used in this study.

Flow cytometry and TCR internalization

$CD8^+$ T cells were stained with FITC-labeled mAbs against CD25 and CD69 (BD Biosciences). Cell-associated fluorescence was analyzed on a FACS Calibur using the Cell Quest software (BD Biosciences). To determine TCR internalization, 2×10^6 cells were either left untreated or stimulated with CD3/CD8 mAbs or OT-I-streptamers as mentioned above at 37°C for 30–120 min. Cells were stained with FITC-conjugated TCR-Vα-2 mAb (BD Biosciences) for 30 min at 4°C and analyzed by flow cytometry.

Proliferation assay

$CD8^+$ T cells were cultured in RPMI 1640 medium containing 10% FCS (PAN Biotech), 100 U/ml penicillin, 100 μg/ml streptomycin (all from Biochrom AG), and 50 μM 2-ME in 96-well plates at a concentration of 2.5×10^4 cells/well. Cells were left either unstimulated or stimulated as described above for 72 h at 37°C. Cells were then labeled with [^{3}H]thymidine (0.3 μCi/well from ICN) for 8 h, harvested onto glass fiber filter and counted with a scintillation counter (1450 MicroBeta Trilux; PerkinElmer).

Cell survival assay and caspase-3 activity

To quantify cell survival under different stimulation conditions, T cells were resuspended in RPMI 1640 containing supplements (as described above) at a density of 1×10^6 cells/ml in a 48-well tissue culture plates. Cells were stimulated with either CD3/CD8 mAbs or OT-I-streptamers (as described before) at 37°C. Cells were harvested after 8 and 24 h, respectively. The percentage of cells undergoing apoptosis was measured by flow cytometry using FITC-annexin V and propidium iodide (PI) (rh annexin V/FITC kit; Bender Medsystems) according to manufacturer's instructions. To detect activated caspase-3 in living cells, we used the caspase-3 detection kit according to the manufacturer's instructions (Calbiochem). In brief, T cells were treated as described above with OT-I-streptamers and CD3/CD8 mAbs for 8 and 24 h, respectively. Cells were washed and 1×10^6 cells were incubated with 1 μg FITC-conjugated DEVD-FMK in 30 μl PBS for 1 h at 37°C. After washing, the activated caspase-3 inside the cells was analyzed by flow cytometry.

Western blotting and immunoprecipitation

$CD8^+$ T cells were either left untreated or stimulated with CD3/CD8 mAbs or OT-I-streptamers, lysed as described in (13) and protein concentration was determined using the Roti-Nanoquant reagent (Roth) according to manufacturer's instruction. The samples were analyzed by Western blotting. Anti-phospho(p)*-ERK1/2, anti-pS^{473} protein kinase (PKB) Ab, anti-pY^{319}ZAP70, anti-pY^{171}LAT, anti-pS^{916} protein kinase D1 (PKD1) (all from Cell Signaling Technology), anti-PLC-γ1, anti-pY^{783}PLC-γ1, anti-PKD1 (all from Santa Cruz Biotechnology), anti-ZAP70 (clone 1E7.2), anti-Bcl-x_L (all from BD Biosciences), anti-pTyr* (clone 4G10) (Upstate Biotechnology), and anti-β-actin (clone AC-15) (Sigma-Aldrich) were used for Western blotting. The intensity of the detected bands was acquired using the Kodak Image station 2000R and analysis was performed using ID Image software (Kodak). To assess the ubiquitination of ZAP70, 4×10^7 T cells were either left unstimulated or treated with either CD3/CD8 mAbs or OT-I-streptamers (as mentioned before) for 3 min and resuspended in 500 μl lysis buffer. ZAP70 was immunoprecipitated using 2 μg of rabbit anti-ZAP70 Ab (Santa Cruz Biotechnology) in combination with 30 μl protein-A agarose beads (Santa Cruz Biotechnology) for 2 h at 4°C. Samples were analyzed by Western blotting using an anti-ubiquitin (Cells Signaling Technology) and anti-ZAP70 Ab (BD Biosciences).

Calcium flux

$CD8^+$ T cells (2×10^7 cells/ml) resuspended in RPMI 1640 medium (phenol-red free; Invitrogen) supplemented with 10% FCS were loaded with 3.75 μg/ml Indo-1-AM (Molecular Probes) at 37°C for 45 min. After washing, the cells were incubated in the same medium at 37°C for an additionally 45 min. The measurement was performed on a LSR flow cytometer (BD Biosciences). Cells were incubated with CD3/CD8 mAbs at 37°C for 0.5 min to establish the baseline and cross-linked with streptavidin or treated with OT-I-streptamers (as mentioned before) followed by ionomycin (10 μg/ml). Data for calcium mobilization were acquired on a LSR flow cytometer and a ratiometric analysis was performed using the Flow Jo software (BD Biosciences).

Confocal microscopy

$CD8^+$ T cells were stimulated as described above with either OT-I-streptamers or CD3/CD8 mAbs. Cells (2×10^5) were placed onto poly-L-lysine coated slides, fixed, permeablized, and blocked as described in (10). Cells were stained with anti-p*-ERK1/2, anti Rab5 mAb (BD Biosciences) or anti-pan Ras mAb (Oncogene) in combination with FITC/Cy3-conjugated goat anti-rabbit IgG, Cy3-conjugated goat anti-mouse, FITC-conjugated anti-TCR-Vα-2 mAb, or TRITC-phalloidin (Sigma-Aldrich). A minimum of 40 cells were imaged with LEICA TCS SP2 laser-scanning confocal system and analyzed with the LEICA software.

Results

The fate of mature $CD8^+$ T cells differs depending on the stimuli

The aim of this study was to assess how the TCR translates different signals into diverse cellular responses such as proliferation or apoptosis. For this purpose, we used purified $CD8^+$ T cells isolated from spleens of OT-I TCR-transgenic (tg) mice and applied two different stimuli. T cells were either activated with soluble biotinylated CD3ε mAbs in combination with biotinylated CD8α mAbs and subsequently cross-linked with strepavidin or they were incubated with biotinylated H-$2K^b$ molecules loaded with the peptide SIINFEKEL and cross-linked with Strep-Tactin (OT-I-streptamer) (14). For this study, we used 10 μg/ml each mAb or 1 μg OT-I-strepatmers to activate OT-I $CD8^+$ T cells, the binding of 1 μg OT-I- strepatmers was close to saturation under these stimulation conditions (data not shown).

To determine whether the two stimuli induce T cell proliferation we assessed [^{3}H]thymidine incorporation after 72 h of in vitro culture. Fig. 1*A* shows that $CD8^+$ T cells stimulated with CD3/CD8 mAbs did not proliferate. Importantly, stimulation of the same cells with lower doses of Abs (ranging from 10 μg/ml to 1.25 μg/ml) also did not induce proliferation (data not shown). Furthermore, preincubation of the cells with different concentration of cross-linked Abs (30 min to 2 h) followed by washing (to remove unbound antibodies) also did not result in a proliferative response

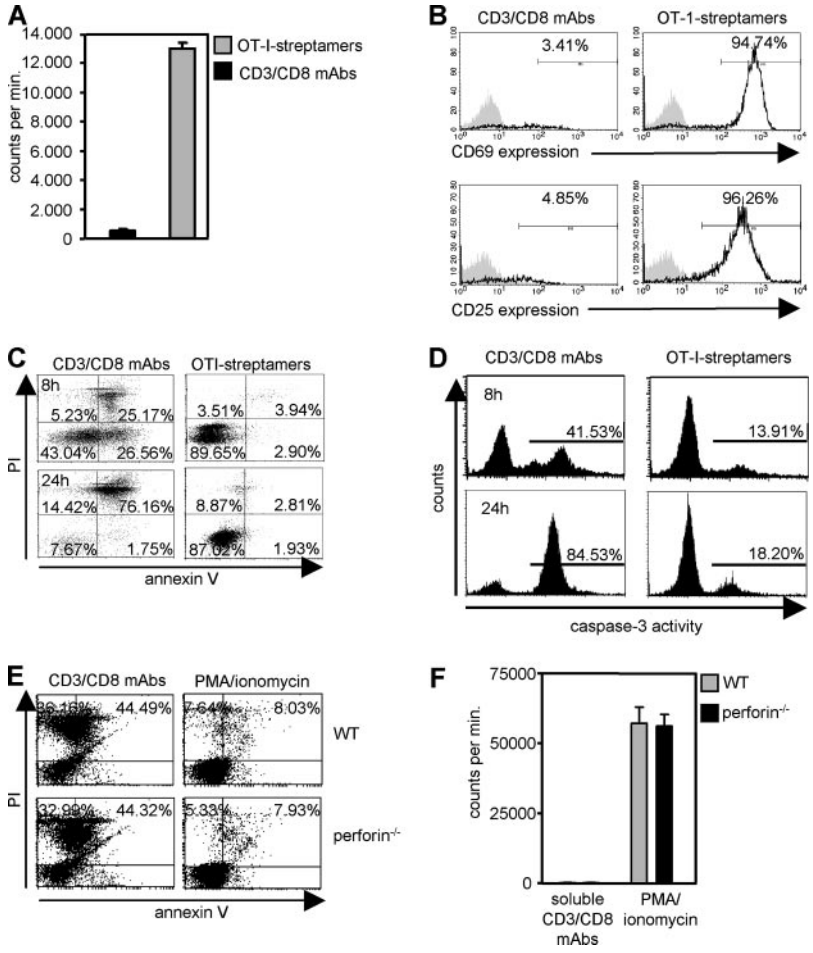

FIGURE 1. Soluble CD3/CD8 mAb treatment induces apoptosis, whereas OT-I-streptamer stimulation leads to survival and proliferation. *A*, Equal cell numbers of purified $CD8^+$ T cells were cultured with soluble CD3/CD8 mAbs or OT-I-streptamers for 72 h. Proliferation was assessed by [^{3}H]thymidine incorporation. Data represent the averages ± SEM from triplicate cultures of three individual experiments. *B*, The expression of CD69 or CD25 of untreated, OT-I-streptamer or CD3/CD8 mAb stimulated (for 24 h) cells was analyzed by flow cytometry. The histograms represent profiles of untreated (shaded) and stimulated (thick lines) cells. Data are representative of three individual experiments. *C*, $CD8^+$ T cells were stimulated with either soluble CD3/CD8 mAbs or with OT-I-streptamers for 8 and 24 h, respectively. Cell survival was assessed by FITC-annexin V and PI staining. One representative experiment of three individual experiments is shown here. *D*, $CD8^+$ T cells were stimulated with either soluble CD3/CD8 mAbs or OT-I-streptamers for 8 and 24 h, respectively and activated caspase-3 was detected using FITC-conjugated DEVD-FMK. One representative experiment of three individual experiments is shown here. *E*, Purified $CD8^+$ T cells from WT and perforin$^{-/-}$ mice were treated with soluble anti-CD3/CD8 mAbs or PMA/ionomycin for 24 h. Cell survival was assessed as described in *C*. One representative experiment of three individual experiments is shown here. *F*, T cells from WT and perforin$^{-/-}$ mice were stimulated with soluble anti-CD3/CD8 mAbs and PMA/ionomycin for 72 h. Proliferation was assessed by [^{3}H]thymidine incorporation. Data represent the averages ± SEM from triplicate cultures of three individual experiments.

(data not shown). Additionally, we excluded the possibility that sodium azide present in the Ab solution might affect proliferation (data not shown). We further examined whether the lack of proliferation under the above conditions of stimulation might be due to the fact that we used an Ab directed at the CD3ε-chain of the TCR/CD3 complex. However, identical results were obtained when cells were activated with an anti-TCRβ Ab in combination with the CD8 mAb (data not shown). CD8 is expressed as a CD8$\alpha\beta$ heterodimer on MHC I-restricted TCR$\alpha\beta$ T cells. To address whether the lack of proliferation is due to triggering of CD8α, we also stimulated the same T cells with either anti-CD3/CD8β mAbs or a combination of anti-CD3/CD8α/CD8β mAbs. Like CD3/CD8α-stimulation, no proliferation was observed under these experimental conditions (data not shown). In marked contrast to CD3/CD8 mAb stimulation, treatment of the same T cells with peptide loaded OT-I-streptamers induced robust proliferation and concomitantly led to strong expression of the activation markers CD69 and CD25 (Fig. 1*B*).

The lack of proliferation after stimulation with CD3/CD8 Abs could be due to T cell unresponsiveness or apoptosis. To distinguish between these two possibilities we assessed apoptosis of CD3/CD8 mAb- or streptamer-stimulated cells by PI and annexin V staining. The left panels of Fig. 1*C* demonstrated that already after 8 h of stimulation with CD3/CD8 Abs ~27% of the cells showed early signs of apoptosis (annexin V^+ and PI^-) and 24 h after stimulation nearly 80% of Ab-stimulated T cells stained positive for both annexin V^+ and PI^+. In contrast, only ~4% of cells were positive for annexin V^+ and PI^+ after streptamer stimulation. In line with these data, stimulation with soluble CD3/CD8 Abs, but not peptide-loaded streptamers, induced a strong activation of caspase-3 (Fig. 1*D*). Notably, treatment of these cells with lower doses of Abs (ranging from 10 μg/ml to 1.25 μg/ml) still induced apoptosis whereas increasing concentrations of streptamers did not induce cell death (data not shown). In summary, the results shown in Fig. 1 indicate that OT-I-streptamers induced proliferation and activation of peripheral T cells, whereas CD3/CD8 mAbs induced apoptosis.

Activation of $CD8^+$ T cell leads to its differentiation into CTLs. CTLs kill targeted cells mainly through the perforin/granzymes system. To assess whether Ab induced apoptosis is mediated via perforin, we stimulated purified $CD8^+$ T cells from WT and perforin$^{-/-}$ mice with soluble anti-CD3/CD8 mAbs for 24 h and assessed cell survival by propidium iodide and annexin V staining. Fig. 1*E* showed that nearly 70% of Ab-stimulated T cells from WT or perforin$^{-/-}$ mice stained positive for propidium iodide. Consistent with these data, stimulation with soluble Abs did not induce proliferation (Fig. 1*F*). These data indicated that induction of apoptosis by soluble anti-CD3/CD8 mAbs occurred independent of perforins.

OT-1-strepatmers induce sustained activation of PKB and expression of Bcl-x_L

The above system allowed us to compare signaling events leading to either T cell survival or apoptosis in more detail. We first focused on PKB (also known as Akt), a serine threonine kinase, which is critically involved in T cell survival (15). As shown in Fig. 2*A*, triggering of the TCR with CD3/CD8 Abs induced a strong, but transient phosphorylation of PKB which peaked at 3

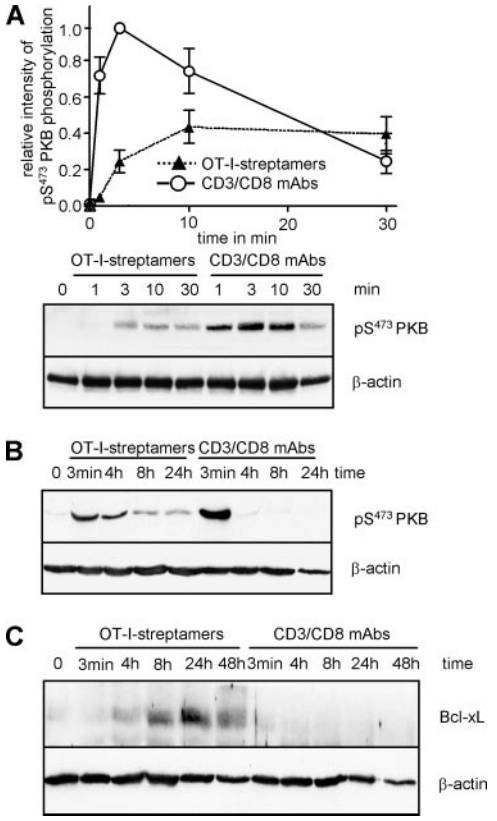

FIGURE 2. OT-I-streptamers induce sustained phosphorylation of PKB and expression of Bcl-x_L. *A*, Purified $CD8^+$ T cells were treated with soluble CD3/CD8 mAbs or OT-I-streptamers for the indicated time periods. Samples were analyzed by Western blotting using the indicated Abs. The phosphorylated PKB bands were quantified using the ImageQuant software and values were normalized to the corresponding β-actin signal. Data represent the mean ± SEM of three independent experiments. *B*, For long term stimulation, $CD8^+$ T cells were triggered with soluble Abs or OT-I-streptamers and analyzed for PKB-pS^{473} phosphorylation as described above. The data are representative of three independent experiments. Note the expression levels of PKB were not affected either in Ab- or streptamer-stimulated lymphocytes over the various time points investigated (data not shown). *C*, Purified $CD8^+$ T cells were incubated with soluble CD3/CD8 mAbs or OT-I-streptamers for the indicated periods of time. The expression of either Bcl-x_L or β-actin was assessed by Western blotting. Data are representative of three independent experiments.

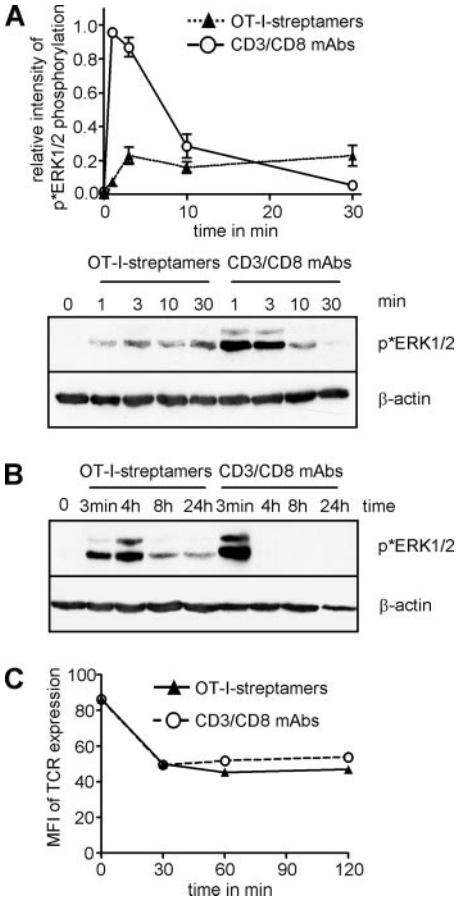

FIGURE 3. OT-I-streptamers induce sustained ERK1/2 activation. *A*, $CD8^+$ T cells were treated with soluble CD3/CD8 mAbs or with OT-I-streptamers for the indicated periods of time. Lysates were prepared and analyzed by Western blotting using the indicated Abs. The p*ERK1/2 bands were quantified using ImageQuant software and values normalized to the corresponding β-actin signal. Data represent the mean ± SEM from three independent experiments. *B*, For long term stimulation, $CD8^+$ T cells were triggered with soluble CD3/CD8 Abs or OT-I-streptamers and subsequently analyzed for ERK1/2 phosphorylation as described above. The data are representative of three independent experiments. Note the expression levels of ERK1/2 were not affected either in Ab- or streptamer-stimulated lymphocytes over the various time points investigated. Importantly, phosphorylated ERK1/2 was not detected in the absence of any stimuli after 24 h of incubation (data not shown). *C*, $CD8^+$ T cells were treated with soluble CD3/CD8 mAbs or OT-I-streptamers for the indicated times. The expression of the OT-I TCR was assessed by FITC-conjugated anti-TCR-Vα-2 mAb staining analysis by flow cytometry. Data represent the mean fluorescence intensity (MFI) of the TCR expression of three independent experiments.

min, and rapidly declined thereafter (Fig. 2*A*). In contrast, OT-I-streptamers induced a much weaker, but sustained phosphorylation of PKB that was still detectable after 24 h of stimulation (Fig. 2, *A* and *B*).

Previously, it was reported that expression of the anti-apoptotic member of the Bcl2-family, Bcl-x_L, prevents TCR-mediated apoptosis and promotes T cell survival (16). Therefore we analyzed whether OT-I-streptamers enhance the expression of Bcl-x_L. Fig. 2*C* showed that this is indeed the case. Although Bcl-x_L expression was not detectable after CD3/CD8 mAb stimulation, T cells activated with OT-I-streptamers started to express Bcl-x_L after 4 h of stimulation. Bcl-x_L expression was maximal at 24 h of stimulation and was still detectable after 48 h (Fig. 2*C*). Thus, Ab mediated T cell stimulation activates pro-apoptotic molecules, such as caspase-3 and induces apoptosis whereas peptide-loaded streptamers lead to the expression of anti-apoptotic molecules and promote cell survival. Moreover, the data shown in Figs. 1 and 2 suggest that a strong and transient activation of PKB alone is not sufficient to protect T cells from apoptosis.

OT-I-streptamers induce sustained activation of ERK1/2

The ubiquitously expressed serine/threonine kinases ERK1/2 belong to the MAPK family and are important for numerous cellular responses including proliferation and survival (7). We next investigated the kinetics of activated MAPK under survival/proliferation vs apoptosis-inducing conditions of stimulation. As shown in Fig. 3*A*, CD3/CD8 mAbs induced a strong but transient phosphorylation of ERK1/2 which peaked at 1 min, rapidly declined thereafter and was no longer detectable after 30 min of stimulation. Similar kinetics of ERK1/2 phosphorylation, but with lower maximal intensity were observed with lower doses of the stimulating Ab (data not shown), thus excluding the possibility of a concentration effect. In contrast to Ab-mediated stimulation, engagement

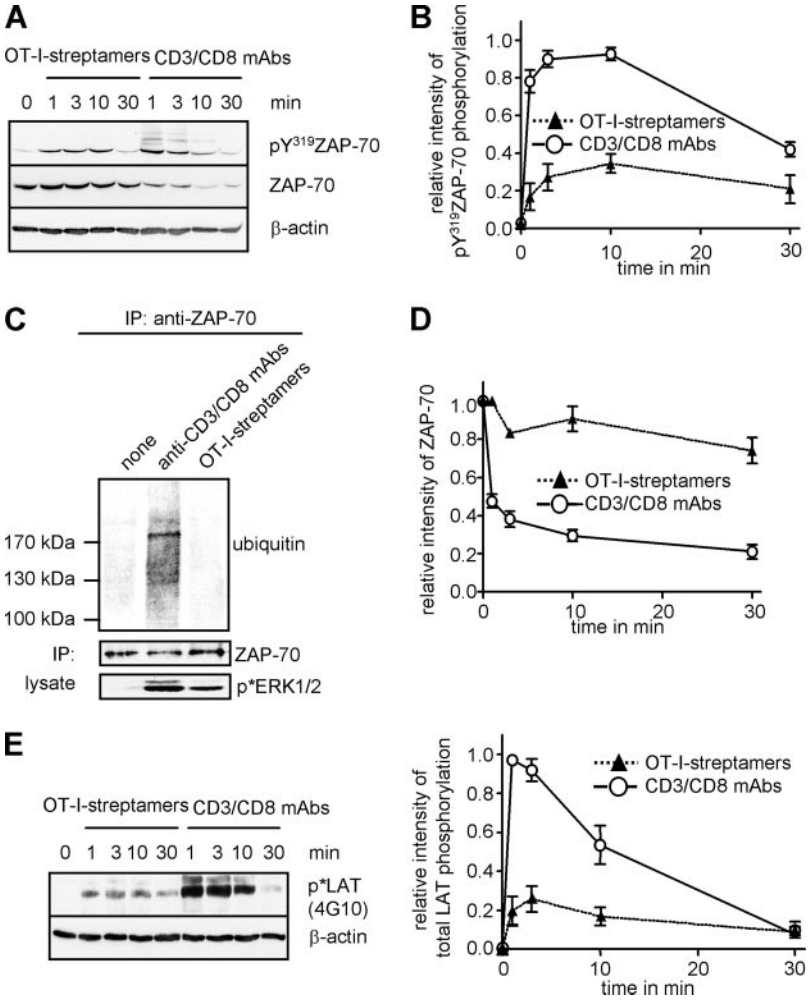

FIGURE 4. Soluble CD3/CD8 mAb stimulation induces ubiquitination and degradation of ZAP70 and transient phosphorylation of LAT. *A*, $CD8^+$ T cells were either incubated with soluble CD3/CD8 mAbs or OT-I-streptamers. The phosphorylation of pY^{319} of ZAP70, total ZAP70 along with the expression levels of β-actin, was determined by Western blotting. Data are representative of three independent experiments. *B*, Besides the main pY^{319} ZAP70 band as shown in *A*, all bands above in Ab-stimulated cells were quantified and the ratio between phosphorylated and nonphosphorylated ZAP70 was calculated for the indicated time points. Data represent the mean ± SEM from three independent experiments. *C*, Purified T cells were left untreated or incubated with soluble CD3/CD8 mAbs or OT-I-streptamers for 3 min, respectively. ZAP70 was immunoprecipitated and Western blot analysis was performed using the indicated Abs. To control successful stimulation, lysates were analyzed by Western blotting for the presence of phosphorylated ERK1/2. Data are representative of two independent experiments. *D*, The total ZAP70 *(middle panel* shown in *A*) were quantified using ImageQuant software and values normalized to the corresponding β-actin signal. Data represent the mean ± SEM from three independent experiments. *E*, $CD8^+$ T cells were incubated with soluble CD3/CD8 mAbs or OT-I-streptamers for the indicated times. Western blot analysis of cell lysates was performed using anti-phophotyrosine mAb (4G10) and the band corresponding to phosphorylated LAT was quantified as described for Fig. 2. Data represent the mean ± SEM of three independent experiments.

of the TCR/CD8 with OT-I-streptamers induced a weak, but sustained activation of ERK1/2 (Fig. 3*A*). Indeed, the level of phosphorylation after 30 min was as strong as after 3 min of stimulation. An extended kinetic analysis revealed that ERK1/2 phosphorylation was still detectable after 24 h of streptamer stimulation (Fig. 3*B*). It is important to note that in multiple experiments we observed a substantial increase in ERK1/2 phosphorylation after 4 h of streptamer stimulation. The molecular basis for the latter observation is unclear.

A rapid internalization and thus a decrease in the number of available TCR molecules on the cell surface could explain the transient activation of ERK1/2 after Ab stimulation. To assess this point, we compared the expression levels of the TCR after stimulation with either soluble CD3/CD8 mAbs or OT-I-streptamers by flow cytometry. As shown in Fig. 3*C*, treatment of T cells with either soluble Abs or OT-I-streptamers induced almost identical rates of TCR-internalization (Fig. 3*C*). Thus, differences in TCR internalization do not account for the different kinetics of ERK1/2 activation. In summary, the data shown in Fig. 3 indicate that survival and proliferation of mature T cells after streptamer stimulation correlates with a low and sustained activation of ERK1/2.

Abs induce strong activation, ubiquitination, and rapid degradation of ZAP70

Having excluded an altered rate of TCR internalization as the cause of the transient phosphorylation of ERK1/2 after Ab stimulation, we next investigated upstream signaling events involved in the activation of ERK1/2. ZAP70 activation is one of the first signaling events occurring after TCR triggering (2) and is required for the activation of ERK1/2 (17). We assessed the activation kinetics of ZAP70 after Ab vs streptamer stimulation by analyzing the phosphorylation status of pY^{319}, which appears to be required for TCR-mediated downstream signaling (17).

As shown in the upper panel of Fig. 4*A*, in terms of onset and duration, the kinetics of ZAP70 phosphorylation were comparable after CD3/CD8 mAb and streptamer-stimulation. In marked contrast to the differential activation kinetics of ERK1/2 neither of the two stimuli induced a prolonged activation of ZAP70 (data not shown). However, when normalized to the expression levels of ZAP70, Ab-mediated stimulation appeared to induce a 4- to 5-fold stronger activation of ZAP70 than streptamer-stimulation (Fig. 4*B*). In line with these data, we found a strikingly higher kinase activity of immunoprecipitated ZAP70 in Ab-stimulated T lymphocytes compared with streptamer-stimulated cells (data not shown).

The Western blot images depicted in Fig. 4*A* further showed that besides the major band corresponding to Y^{319}, additional ZAP70 bands displaying retarded migration in SDS-PAGE became visible exclusively after Ab stimulation. This observation led us to suspect that Ab stimulation not only resulted in a very strong activation of ZAP70, but also induced its ubiquitination and subsequent degradation. To address this point, T cells were stimulated for 3 min with either CD3/CD8 Abs or with streptamers. Subsequently, ZAP70 immunoprecipitates were obtained and analyzed by anti-ubiquitin or anti-ZAP70 Western blotting. Fig. 4*C* demonstrates

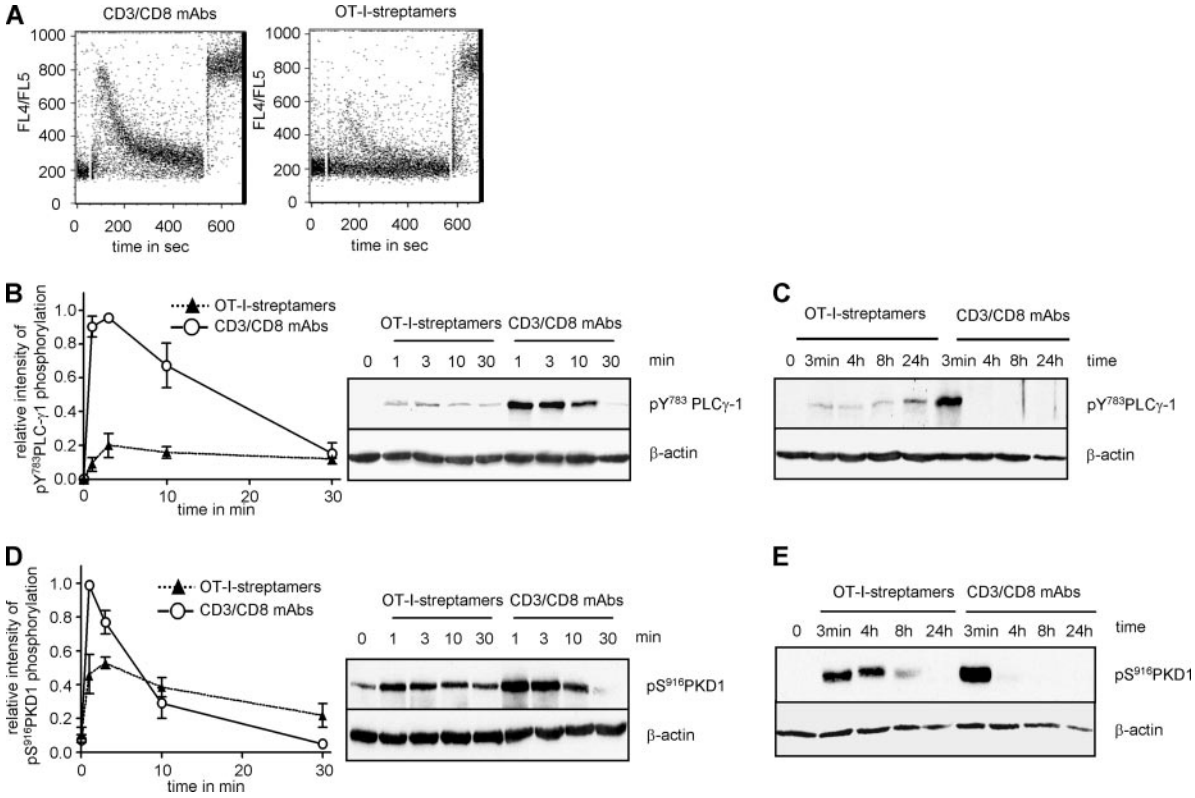

FIGURE 5. OT-I-streptamers mediate low calcium mobilization but sustained PLC-γ1 and PKD1 phosphorylation. *A*, T cells were loaded with Indo-1-AM and calcium release was triggered by soluble CD3/CD8 mAbs or OT-I-streptamers, respectively. Calcium influx was determined by cytometry based on the change in the FL4/FL5 ratio. Ionomycin was added to the end of each experiment to verify proper Indo-loading. Data are representative of three independent experiments. *B*, Purified splenic T cells were treated with soluble anti-CD3/CD8 mAbs or OT-I-streptamers, respectively. Cells were lysed and equivalent amounts of protein from whole cell extracts were analyzed for phosphorylated PLC-γ1 (pY^{783}) and were quantified using ImageQuant software. Values were normalized to the corresponding β-actin signal. Data represent the mean ± SEM of three independently performed experiments. *C*, For long term stimulation, $CD8^+$ T cells were triggered with soluble CD3/CD8 Abs or OT-I-streptamers and subsequently analyzed for PLC-γ1 phosphorylation as described above. The data are representative of three independent experiments. *D*, $CD8^+$ T cells were either incubated with soluble CD3/CD8 mAbs or OT-I-streptamers. The phosphorylation of serine 916 (S^{916}) of PKD1, along with the expression level of β-actin, was determined by Western blotting and quantified as described for Fig. 2. Data represent the mean ± SEM of three independent experiments. *E*, For long term stimulation, $CD8^+$ T cells were triggered with soluble Abs or OT-I-strepatmers and subsequently analyzed for phosphorylation of S^{916} as described above. Data are representative of three independent experiments. Note, the expression levels of PLC-γ1 or PKD1 were not affected either in Ab- or streptamer-stimulated lymphocytes over the various time points investigated. Importantly, phosphorylated PLC-γ1 or PKD1 was not detected in the absence of any stimuli after 24 h of incubation (data not shown).

that Ab-stimulation indeed induced a strong ubiquitination of ZAP70 which correlated well with the rapid loss of detectable ZAP70 protein (see Fig. 4*A, middle panels* and Fig. 4*D* for quantification). In contrast, no ubiquitination of ZAP70 was observed after streptamer-stimulation. Thus, Ab stimulation not only induces a strong activation of ZAP70, but also its ubiquitination and rapid degradation. The latter mechanism might contribute to the transient activation of ERK1/2.

We were next interested how the differential activation/expression of ZAP70 affects the phosphorylation of its substrate the transmembrane adapter protein LAT. To investigate this point, we determined the phosphorylation status of LAT by Western blotting of whole lysates using anti-phosphotyrosine Ab 4G10. Ab stimulation induced an ~5-fold stronger phosphorylation of LAT compared with streptamer stimulation (Fig. 4*E*). However, the kinetics of phosphorylation only differed slightly between the two stimuli and neither induced a sustained phosphorylation of LAT (data not shown). Note that similar results were obtained when we assessed the phosphorylation status of a specific tyrosine residue within LAT (pY^{171}; data not shown).

OT-I-streptamers mediate low calcium mobilization but sustained phophorylation of PLC-γ1

The strikingly different magnitude of LAT or ZAP70 phosphorylation after Ab vs streptamer stimulation prompted us to compare intracellular calcium flux after application of the two stimuli. As shown in Fig. 5*A*, Ab stimulation generated a strong calcium signal, whereas this signal was barely detectable after streptamer stimulation. Thus, the strong phosphorylation of LAT or ZAP70 induced by the Abs appears to correlate with a strong Ca^{2+}-response.

Upon binding to LAT PLC-γ1 becomes phosphorylated on several tyrosine residues, including Y^{783}, which is known to be vital for PLC-γ1 activity (18). To address the question whether the strong phosphorylation of LAT and the strong induction of calcium-flux that occurs after Ab-mediated stimulation correlated with the activation of PLC-γ1, we analyzed the phosphorylation status of PLC-γ1 at Y^{783} by Western blotting of whole cell lysates. As expected, CD3/CD8 mAbs induced a strong phosphorylation of PLC-γ1 whereas the signal was much weaker after streptamer stimulation (Fig. 5*B*). Surprisingly however, the activation of

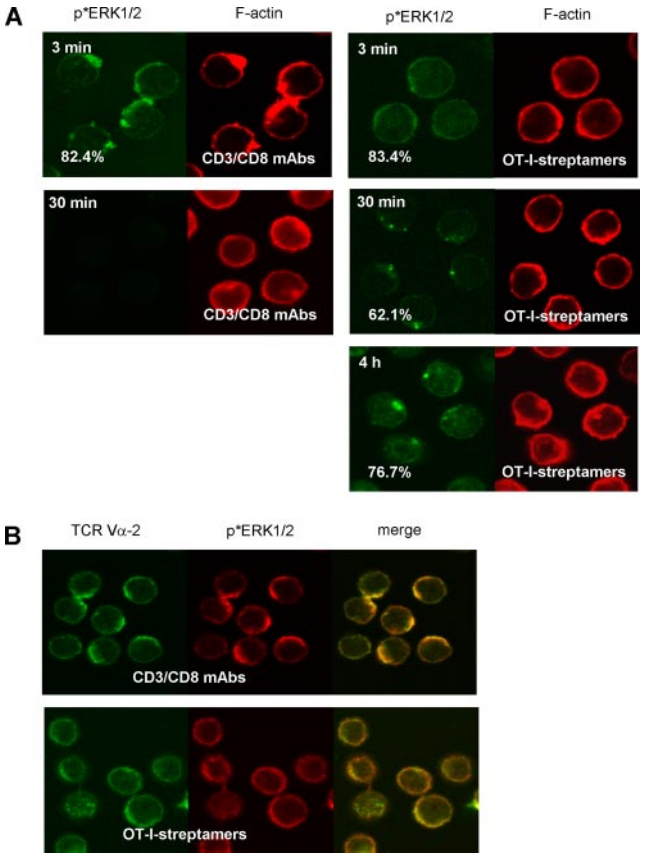

FIGURE 6. Different subcellular localization of phosphorylated ERK1/2 after OT-I-streptamer stimulation. *A*, Confocal laserscanning microscopic analysis was performed on $CD8^+$ T cells stimulated with either CD3/CD8 mAbs or OT-I-streptamers for the indicated times. Cells were permeabilized and subjected to intracellular staining to detect phosphorylated ERK1/2 (green) and F-actin (red). Cells shown in each panels are representative of at least 40 stimulated cells from two independent experiments. *B*, Cells were either left unstimulated or treated with CD3/CD8 mAb or OT-I-streptamers for 3 min and then the localization of phosphorylated ERK1/2 (red) and TCR Vα-2 (green) was assessed. The cells shown in each panels are representative of ≥40 stimulated cells from two independent experiments.

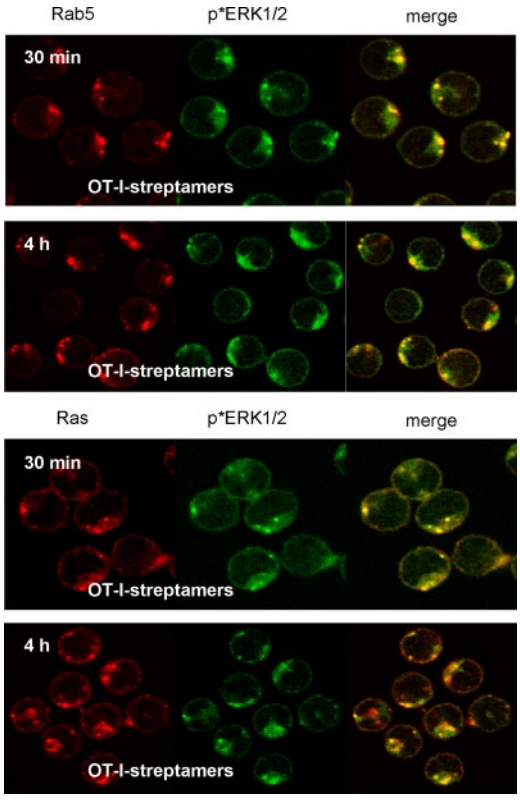

FIGURE 7. Phosphorylated ERK1/2 localizes in Rab5 and Ras containing recyling endosomale vesicles after OT-I-streptamer stimulation. Confocal laserscanning microscopic analysis was performed on $CD8^+$ T cells stimulated with OT-I-streptamers for 30 min and 4 h, respectively and cells were permeabilized and subjected to intracellular staining to detect phosphorylated ERK1/2 (green) and Rab5 or Ras (red). Cells shown in each panels are representative of ≥40 stimulated cells from two independent experiments.

PLC-γ1 appeared to be weak but sustained after streptamer-stimulation. Indeed, even after 24 h of streptamer stimulation minor phosphorylation of Y^{783} was detectable (Fig. 5*C*). Given the fact that neither Ab- nor streptamer-stimulation induced an extended activation/phosphorylation of ZAP70 and LAT, these data strongly suggest that under the experimental conditions used here, the activation kinetics of key molecules involved in the regulation of ERK1/2 activity bifurcate at the level of PLC-γ1.

The second messenger DAG is also generated by PLC-γ1 and is important to activate PKC and RasGRP, which in turn leads to activation of the Ras-ERK1/2 pathway (5). To address the question, whether the sustained activation of PLC-γ1 induced after streptamer stimulation is sufficient to produce DAG, we assessed the phosphorylation status of PKD on pS^{916}, which was previously shown to be dependent upon the production of DAG (19). Stimulation with CD3/CD8 mAbs induced a strong but transient phosphorylation of S^{916}, whereas S^{916} phosphorylation was sustained, albeit weaker, after streptamer stimulation (Fig. 5, *D* and *E*). Therefore, although OT-I-streptamers are only weak activators of PLC-γ1, they induce an extended production of DAG, which likely contributes to the sustained activation of the Ras-ERK1/2 pathway.

Distinct subcellular localizations of ERK1/2

A recent study has shown that activated ERK1/2 resides in different subcellular compartments when thymocytes undergo positive vs negative selection (10). To examine whether a similar situation also occurs in peripheral T cells undergoing apoptosis or proliferation we assessed the localization of phosphorylated ERK1/2 after Ab or streptamer-mediated T cell activation using confocal laser scanning microscopy. Fig. 6*A* demonstrates that ~80% of Ab-stimulated T cells showed an intensive localization of phosphorylated ERK1/2 close to the plasma membrane after 3 min of stimulation. Additional experiments revealed that under these conditions of stimulation activated ERK1/2 colocalized to a large extent with clustered TCR-complexes (Fig. 6*B*). In line with the quantification of the Western blot analysis shown in Fig. 3*A*, phosphorylated ERK1/2 was no longer detectable after 30 min of Ab-mediated stimulation thus confirming its transient activation under apoptosis inducing conditions of stimulation (Fig. 6*A*).

Although OT-I-streptamers induced a weaker clustering of the TCR compared with Ab-stimulation in the majority of cells, they also led to membrane targeting of phosphorylated ERK1/2 in ~80% of the cells (Fig. 6*A*). As expected from the quantification of the Western blot analysis (Fig. 3*A*) the signal was of a much lower intensity but even under these conditions phosphorylated ERK1/2 partially colocalized with the transgenic TCR (Fig. 6*B*). However, after 30 min and 4 h of stimulation in ~60–70% of streptamer-treated cells phosphorylated ERK1/2 was no longer

found at the plasma membrane but rather in small vesicular structures which were located close to the plasma membrane as well as in the cytosol.

It has been described in different cellular systems that after insulin receptor or TrkA receptor triggering, phosphorylated ERK1/2 accumulates in the recycling endosomes (20, 21). To address whether the activated ERK1/2 that we detected in vesicular structures after 30 min and 4 h OT-I-streptamer stimulation localizes to the endosomal compartment, we used Rab5 as a marker for confocal laser scanning microscopy. The upper two panels of Fig. 7 depicted that the vesicles indeed stained positive for Rab5, thus identifying them as endosomes.

Other components of the ERK1/2 signaling pathway such as the GTPase Ras have also been found in the endosomal compartment (20, 21). In line with these data we found that Ras also colocalized with phosphorylated ERK1/2 in Rab5-positive vesicles after streptamer stimulation (Fig. 7, *lower panels*). Collectively, these data indicate that under conditions promoting T cell survival and proliferation activated ERK1/2 shuttles from the plasma membrane to the recycling endosomes, whereas under conditions inducing T cell death phosphorylated ERK1/2 only transiently accumulates at sites of TCR-engagement.

Discussion

Engagement of the TCR can result in different cellular responses such as differentiation, survival, proliferation, or apoptosis. However, how the triggering of one receptor initiates different responses and how these responses are organized on the molecular level is so far not understood. To address this question we used peripheral T lymphocytes obtained from OT-I TCR-tg mice and applied two different stimuli soluble CD3/CD8 mAbs or OT-I-streptamers loaded with the agonistic OVA peptide SIINFEKL, which selectively induce either apoptosis (mAbs) or proliferation (streptamers) (Fig. 1).

Biochemical analysis of the pathways initiated by these two types of stimuli revealed that signals inducing apoptosis produce strong, rapid and transient phosphorylation/activation of key molecules involved in T cell activation including ZAP70, LAT, PKB, PLC-γ1, PKD1, and ERK1/2. In contrast to the strong and transient signals elicited by soluble mAbs, most signals that were induced by peptide loaded streptamers were of much lower intensity, but were also more sustained. This applied to the activation of ERK1/2 and of PLC-γ1, PKB, and PKD1.

Our study corroborates and extends recent experiments that had assessed selection events in OT-I TCR-tg thymocytes (10). Hence, it appears that independent of the system a strong and transient activation of ERK1/2 correlates with the induction of apoptosis, whereas a weak and sustained activation of ERK1/2 correlates with survival and proliferation of T lymphocytes.

The molecular events that translate the different activation kinetics of ERK1/2 into distinct cellular responses are still unclear. One hypothesis is that the differential localization of activated ERK1/2 within the cells contributes to these effects. Indeed, similar to the study performed by Daniels el al. (10) we also found the localization of phosphorylated (and hence activated) ERK1/2 to be markedly different under apoptosis vs proliferation inducing conditions. Thus, pro-apoptotic stimuli induced rapid targeting of activated ERK1/2 to the plasma membrane, whereas proliferation inducing stimuli led to an accumulation of activated ERK1/2 within the recycling endosomes (Fig. 6 and Fig. 7). Localization of activated ERK1/2 at the endosomes after insulin receptor or TrkA receptor stimulation is a well-documented phenomenon (20, 21). Furthermore, in insulin- or NGF-treated cells other signaling molecules required for the activation of ERK1/2 have also been described to localize in the endosomal compartment. These include Ras, Raf, MEK1, PLC-γ1, and PI3K (important for activation of PKB) (20, 21). In line with these data, we also found Ras and phosphorylated ERK1/2 in Rab5-containing vesicles after OT-I-streptamer stimulation (Fig. 7). Therefore, it is reasonable to speculate that the sustained phosphorylation kinetics of PLC-γ1 and PKB after OT-I-streptamer stimulation might also be due to targeting of these proteins to the endosomal compartment. Unfortunately, our attempts to visualize phosphorylated PLC-γ1 or PKB in Rab5-containing activated ERK1/2 vesicles by confocal laserscanning microscopy were so far not successful. This may be due to the low phosphorylation status of these proteins in streptamer-treated cells or the inaccessibility of the different phospho-specific Abs tested for immunofluoresence. Nevertheless, our data indicated that compartmentalization of ERK1/2 into the endosomes after OT-I-streptamer treatment correlates with sustained activation of this kinase. One mechanism might be that endosome-associated ERK1/2 is protected from cytoslic or membrane associated phosphatases. However, how OT-I streptamer triggering of the TCR/CD8 regulates the differential shuttling of activated ERK1/2 at the molecular level is still unclear. Experiments are currently set up in our laboratory to address this question.

Another important question that remains to be resolved is how the transient activation of ERK1/2 under apoptosis-promoting conditions is regulated on the molecular level. Here several possibilities can be envisaged. First, we observed that stimulation of T cells with CD3/CD8 mAbs results in a rapid poly-ubiquitiniation and degradation of ZAP70 (Fig. 4). Moreover, the Valitiutti group has previously demonstrated that T cell activation induces ubiquitination events at the immunological synapse (22). Thus, pro-apoptotic signals initiate a negative feedback loop that rapidly down-regulates the input signal by eliminating ZAP70. Several reports have shown that the ZAP70 related protein tyrosine kinase Syk serves as a substrate for ubiquitin-ligases (23). However, to our knowledge a TCR-mediated ubiquitination and subsequent degradation of ZAP70 has so far not been reported. Also, the enzyme(s) that is/are responsible for ZAP70 ubiquitination have yet to be determined. Obvious candidates would be members of the Cbl family which exert E3-dependent ubiquitin ligase activity and which have been shown to interact with ZAP70 (24). However, the role of Cbl in ZAP70 ubiquitination and degradation is controversial and further work is needed to address if and how Cbl contributes to ZAP70 ubiquitination.

In addition to the degradation of ZAP70, other mechanisms may also contribute to the transient activation of ERK1/2 under pro-apoptotic conditions of stimulation. One possibility would be that the strong activation of membrane proximal tyrosine kinases (e.g., ZAP70, Lck, Fyn, Itk, and Rlk) not only induces the assembly of positive-regulatory, but also of negative-regulatory signaling complexes at the plasma membrane. In this regard, it is important to mention a recent study which revealed a negative regulatory role for Lck in T cells by showing that TCR-mediated stimuli are stronger/sustained after suppression of Lck expression by siRNA in Jurkat T cells and in primary human T lymphocytes (25). Additionally, a negative regulatory role for LAT in T cell signaling has been suggested (26, 27). Thus, it is tempting to speculate that the strong phosphorylation of LAT after Ab-stimulation induces the assembly of negative regulatory complexes, which prevent a sustained activation of ERK1/2. Conversely, weaker input signals (a less strong activation of membrane proximal PTKs) would not induce the activation of these negative regulatory loops, thus allowing for a sustained activation of ERK1/2. In line with the idea that cell fate decisions are determined at the level of the LAT complex, would be our finding that the signaling molecules which

are located immediately downstream of LAT (i.e., PLC-γ1 and PKD1) already show markedly different phosphorylation kinetics in our experimental system.

Finally, ERK1/2 itself could play a major role in inhibiting its prolonged activation by inducing the phosphorylation of negative regulatory proteins close to the membrane. Indeed, recent studies (28, 29) have revealed the importance of serine phosphorylation of key molecules for T cell homeostasis (SLP-76 by HPK1). Clearly, further studies are required to elucidate the events that lead to the transient activation of ERK1/2 under apoptosis-inducing conditions of stimulation. Nevertheless, our data indicate that "optimal" membrane proximal signals, such as a strong Ca^{2+}-flux or maximal LAT phosphorylation, may not automatically be interpreted to mean that these events induce a productive T cell activation. Rather, it appears that only a detailed analysis of the dynamics of membrane proximal signaling events together with the assessment of late events of T cell activation, such as proliferation or apoptosis, allows a correct interpretation of biochemical data.

It was somewhat unexpected that soluble Abs induced a rapid apoptosis and activation of caspase-3 whereas peptide loaded streptamers induced the expression of the anti-apoptic molecule Bcl-x_L. Although the induction of Bcl-x_L expression by peptide loaded streptamers can be explained by a sustained activation of PKB (30), the induction of apoptosis by soluble Abs is more difficult to understand. Apoptotic T cell death and activation of caspase-3 can be induced via the extrinsic death-receptor-mediated pathway or through the intrinsic mitochondrial pathway (31). Currently we do not know which of the two pathways becomes activated by soluble Abs, but we clearly favor a mechanism that involves the mitochondrial pathway for the following reasons. The expression levels of CD95 were almost identical after Ab- vs streptamer-stimulation and we also could not detect enhanced expression of CD95L after either mode of stimulation (data not shown). Moreover, the time frame between the application of the death-inducing stimulus and the first signs of cell death (8 h) appears to be too short to be mediated via the CD95/CD95L-system in primary T cells. Candidate molecules that could connect the TCR to the activation of caspase-3 via the mitochondrial pathway are members of the BH3-only proteins that have been shown to promote apoptosis in T cells for example Bim (32), Bid (33), or Bad (34). Therefore, further work is needed to address which of the BH3-only proteins contribute to Ab-induced apoptosis and how these molecules organize pro-apoptotic pathways after Ab-mediated apoptosis.

In multiple experiments, we observed a substantial increase of ERK1/2 phosphorylation after 4 h of stimulation with OT-I-streptamers (Fig. 3*B*). Such a "second wave" of ERK1/2 phosphorylation has previously been observed after long-term stimulation of AND TCRtg $CD4^+$ T cells using a high-affinity peptide (35). It might be that the production and release of cytokines, such as IL-2, is responsible for the second wave of ERK1/2 phosphorylation under survival promoting conditions of stimulation. Preliminary data obtained in our laboratory indicated that IL-2 could indeed partially contribute to the second wave of ERK phosphorylation after OT-I-streptamer stimulation. Thus, in the presence of neutralizing against IL-2 Ab, the phosphorylation of ERK1/2 was reduced up to 50% after 4 h of stimulation with OT-I-streptamers (data not shown). This data indicated that not only IL-2, but also other cytokines, e.g., IL-7, may also facilitate activation, survival and proliferation of peripheral $CD8^+$ T cells (36). Therefore, we would speculate that the initial TCR-mediated signals leading to a first wave of ERK1/2 activation under survival promoting conditions are replaced at later time points by cytokine receptor-mediated signaling events. These signals may then contribute to the sustained activation of ERK1/2 and may also be involved in the sustained activation of PKB thereby supporting the expression of survival promoting molecules such as Bcl-x_L.

In summary, we have shown that triggering of the same set of receptors by different ligands can induce either survival/proliferation or apoptosis/cell death of mature $CD8^+$ T lymphocytes. We have further demonstrated that these cellular outcomes correlate with different activation/phosphorylation kinetics of key molecules involved in T cell activation which seem to bifurcate at the level of PLC-γ1. Our data corroborate and extend previous experiments (10) performed in thymocytes and suggest that the molecular mechanisms in the two systems are to a large extent comparable. How mature T cells up-regulate TCR-mediated thresholds to convert the negative selecting signal within the thymus into a proliferation-inducing signal in the periphery requires further analysis. In addition, careful kinetic and quantitative activation/phosphorylation studies are required to fully elucidate how transient vs sustained signaling events close to the membrane are converted into distinct cellular responses. Finally, these experiments will also have to take the differential compartmentalization of signaling molecules into account.

Disclosures

The authors have no financial conflict of interest.

References

1. Palacios, E. H., and A. Weiss. 2004. Function of the Src-family kinases, Lck and Fyn, in T-cell development and activation. *Oncogene* 23: 7990–8000.
2. Mustelin, T., and K. Tasken. 2003. Positive and negative regulation of T-cell activation through kinases and phosphatases. *Biochem. J.* 371: 15–27.
3. Horejsi, V., W. Zhang, and B. Schraven. 2004. Transmembrane adaptor proteins: organizers of immunoreceptor signalling. *Nat. Rev. Immunol.* 4: 603–616.
4. Wu, J. N., and G. A. Koretzky. 2004. The SLP-76 family of adapter proteins. *Semin. Immunol.* 16: 379–393.
5. Stone, J. C. 2006. Regulation of Ras in lymphocytes: get a GRP. *Biochem. Soc. Trans.* 34: 858–861.
6. Cobb, M. H. 1999. MAP kinase pathways. *Prog. Biophys. Mol. Biol.* 71: 479–500.
7. Marshall, C. J. 1995. Specificity of receptor tyrosine kinase signaling: transient versus sustained extracellular signal-regulated kinase activation. *Cell* 80: 179–185.
8. Starr, T. K., S. C. Jameson, and K. A. Hogquist. 2003. Positive and negative selection of T cells. *Annu. Rev. Immunol.* 21: 139–176.
9. Werlen, G., B. Hausmann, D. Naeher, and E. Palmer. 2003. Signaling life and death in the thymus: timing is everything. *Science* 299: 1859–1863.
10. Daniels, M. A., E. Teixeiro, J. Gill, B. Hausmann, D. Roubaty, K. Holmberg, G. Werlen, G. A. Hollander, N. R. Gascoigne, and E. Palmer. 2006. Thymic selection threshold defined by compartmentalization of Ras/MAPK signalling. *Nature* 444: 724–729.
11. Altan-Bonnet, G., and R. N. Germain. 2005. Modeling T cell antigen discrimination based on feedback control of digital ERK responses. *PLoS Biol.* 3: e356.
12. Berg, N. N., L. G. Puente, W. Dawicki, and H. L. Ostergaard. 1998. Sustained TCR signaling is required for mitogen-activated protein kinase activation and degranulation by cytotoxic T lymphocytes. *J. Immunol.* 161: 2919–2924.
13. Simeoni, L., V. Posevitz, U. Kolsch, I. Meinert, E. Bruyns, K. Pfeffer, D. Reinhold, and B. Schraven. 2005. The transmembrane adapter protein SIT regulates thymic development and peripheral T-cell functions. *Mol. Cell. Biol.* 25: 7557–7568.
14. Knabel, M., T. J. Franz, M. Schiemann, A. Wulf, B. Villmow, B. Schmidt, H. Bernhard, H. Wagner, and D. H. Busch. 2002. Reversible MHC multimer staining for functional isolation of T-cell populations and effective adoptive transfer. *Nat. Med.* 8: 631–637.
15. Song, G., G. Ouyang, and S. Bao. 2005. The activation of Akt/PKB signaling pathway and cell survival. *J. Cell. Mol. Med.* 9: 59–71.
16. Grillot, D. A., R. Merino, and G. Nunez. 1995. Bcl-XL displays restricted distribution during T cell development and inhibits multiple forms of apoptosis but not clonal deletion in transgenic mice. *J. Exp. Med.* 182: 1973–1983.
17. Williams, B. L., B. J. Irvin, S. L. Sutor, C. C. Chini, E. Yacyshyn, J. Bubeck Wardenburg, M. Dalton, A. C. Chan, and R. T. Abraham. 1999. Phosphorylation of Tyr319 in ZAP70 is required for T-cell antigen receptor-dependent phospholipase C-γ1 and Ras activation. *EMBO J.* 18: 1832–1844.
18. Poulin, B., F. Sekiya, and S. G. Rhee. 2005. Intramolecular interaction between phosphorylated tyrosine-783 and the C-terminal Src homology 2 domain activates phospholipase C-γ1. *Proc. Natl. Acad. Sci. USA* 102: 4276–4281.
19. Matthews, S. A., E. Rozengurt, and D. Cantrell. 1999. Characterization of serine 916 as an in vivo autophosphorylation site for protein kinase D/Protein kinase Cμ. *J. Biol. Chem.* 274: 26543–26549.

20. Howe, C. L., J. S. Valletta, A. S. Rusnak, and W. C. Mobley. 2001. NGF signaling from clathrin-coated vesicles: evidence that signaling endosomes serve as a platform for the Ras-MAPK pathway. *Neuron* 32: 801–814.
21. Li, H. S., D. B. Stolz, and G. Romero. 2005. Characterization of endocytic vesicles using magnetic microbeads coated with signalling ligands. *Traffic* 6: 324–334.
22. Wiedemann, A., S. Muller, B. Favier, D. Penna, M. Guiraud, C. Delmas, E. Champagne, and S. Valitutti. 2005. T-cell activation is accompanied by an ubiquitination process occurring at the immunological synapse. *Immunol. Lett.* 98: 57–61.
23. Dangelmaier, C. A., P. G. Quinter, J. Jin, A. Y. Tsygankov, S. P. Kunapuli, and J. L. Daniel. 2005. Rapid ubiquitination of Syk following GPVI activation in platelets. *Blood* 105: 3918–3924.
24. Thien, C. B., and W. Y. Langdon. 2001. Cbl: many adaptations to regulate protein tyrosine kinases. *Nat. Rev. Mol. Cell Biol.* 2: 294–307.
25. Methi, T., J. Ngai, M. Mahic, M. Amarzguioui, T. Vang, and K. Tasken. 2005. Short-interfering RNA-mediated Lck knockdown results in augmented downstream T cell responses. *J. Immunol.* 175: 7398–7406.
26. Dong, S., B. Corre, E. Foulon, E. Dufour, A. Veillette, O. Acuto, and F. Michel. 2006. T cell receptor for antigen induces linker for activation of T cell-dependent activation of a negative signaling complex involving Dok-2, SHIP-1, and Grb-2. *J. Exp. Med.* 203: 2509–2518.
27. Matsuda, S., Y. Miwa, Y. Hirata, A. Minowa, J. Tanaka, E. Nishida, and S. Koyasu. 2004. Negative feedback loop in T-cell activation through MAPK-catalyzed threonine phosphorylation of LAT. *EMBO J.* 23: 2577–2585.
28. Di Bartolo, V., B. Montagne, M. Salek, B. Jungwirth, F. Carrette, J. Fourtane, N. Sol-Foulon, F. Michel, O. Schwartz, W. D. Lehmann, and O. Acuto. 2007. A novel pathway down-modulating T cell activation involves HPK-1-dependent recruitment of 14–3-3 proteins on SLP-76. *J. Exp. Med.* 204: 681–691.
29. Shui, J. W., J. S. Boomer, J. Han, J. Xu, G. A. Dement, G. Zhou, and T. H. Tan. 2007. Hematopoietic progenitor kinase 1 negatively regulates T cell receptor signaling and T cell-mediated immune responses. *Nat. Immunol.* 8: 84–91.
30. Jones, R. G., M. Parsons, M. Bonnard, V. S. Chan, W. C. Yeh, J. R. Woodgett, and P. S. Ohashi. 2000. Protein kinase B regulates T lymphocyte survival, nuclear factor κB activation, and Bcl-X(L) levels in vivo. *J. Exp. Med.* 191: 1721–1734.
31. Willis, S. N., and J. M. Adams. 2005. Life in the balance: how BH3-only proteins induce apoptosis. *Curr. Opin. Cell Biol.* 17: 617–625.
32. Bouillet, P., J. F. Purton, D. I. Godfrey, L. C. Zhang, L. Coultas, H. Puthalakath, M. Pellegrini, S. Cory, J. M. Adams, and A. Strasser. 2002. BH3-only Bcl-2 family member Bim is required for apoptosis of autoreactive thymocytes. *Nature* 415: 922–926.
33. Bidere, N., A. L. Snow, K. Sakai, L. Zheng, and M. J. Lenardo. 2006. Caspase-8 regulation by direct interaction with TRAF6 in T cell receptor-induced NF-κB activation. *Curr. Biol.* 16: 1666–1671.
34. Villalba, M., P. Bushway, and A. Altman. 2001. Protein kinase C-θ mediates a selective T cell survival signal via phosphorylation of BAD. *J. Immunol.* 166: 5955–5963.
35. Jorritsma, P. J., J. L. Brogdon, and K. Bottomly. 2003. Role of TCR-induced extracellular signal-regulated kinase activation in the regulation of early IL-4 expression in naive $CD4^+$ T cells. *J. Immunol.* 170: 2427–2434.
36. Marrack, P., and J. Kappler. 2004. Control of T cell viability. *Annu. Rev. Immunol.* 22: 765–787.

Appendix 13

SIT and TRIM determine T-cell fate in the thymus

Kölsch U., Schraven B., and **Simeoni L.** (2008) *J Immunol.* 181:5930-5939.

SIT and TRIM Determine T Cell Fate in the Thymus[1]

Uwe Koelsch,*† Burkhart Schraven,* and Luca Simeoni[2]*

Thymic selection is a tightly regulated developmental process essential for establishing central tolerance. The intensity of TCR-mediated signaling is a key factor for determining cell fate in the thymus. It is widely accepted that low-intensity signals result in positive selection, whereas high-intensity signals induce negative selection. Transmembrane adaptor proteins have been demonstrated to be important regulators of T cell activation. However, little is known about their role during T cell development. Herein, we show that SIT (SHP2 Src homology domain containing tyrosine phosphatase 2-interacting transmembrane adaptor protein) and TRIM (TCR-interacting molecule), two structurally related transmembrane adaptors, cooperatively regulate TCR signaling potential, thereby influencing the outcome of thymic selection. Indeed, loss of both SIT and TRIM resulted in the up-regulation of CD5, CD69, and TCRβ, strong MAPK activation, and, consequently, enhanced positive selection. Moreover, by crossing SIT/TRIM double-deficient mice onto transgenic mice bearing TCRs with different avidity/affinity, we found profound alterations in T cell development. Indeed, in female HY TCR transgenic mice, positive selection was completely converted into negative selection resulting in small thymi devoided of double-positive thymocytes. More strikingly, in a nonselecting background, SIT/TRIM double-deficient single-positive T cells developed, were functional, and populated the periphery. In summary, we demonstrated that SIT and TRIM regulate cell fate of developing thymocytes, thus identifying them as essential regulators of central tolerance. ***The Journal of Immunology,*** **2008, 181: 5930–5939.**

Selection of the TCR repertoire within the thymus is a tightly regulated process that ensures development of T cell clones possessing a vigorous reactivity against foreign Ags and at the same time avoids the generation of self-reactive cells. Decisions made in the thymus are mainly dictated by signals transduced via the TCR upon binding MHC-self peptide complexes. An established model postulates that differences in the avidity/affinity are translated into distinct signaling strengths that in turn determine the developmental outcome. According to this model, strong interactions lead to apoptosis of autoreactive clones (negative selection), and intermediate or weak associations promote thymocyte survival and maturation (positive selection), whereas minimal or absent binding induces cell death (death by neglect, nonselection) (1).

The data also suggest that low-intensity signals transduced via the TCR activate the Ca^{2+}/calcineurin/NFAT and Ras/MEK/ERK pathways and lead to positive selection, whereas high-intensity signals leading to negative selection may also activate Grb2/Sos, JNK, p38, and PKC (2, 3).

Transmembrane adaptor proteins (TRAPs)[3] are integral membrane molecules participating in proximal signaling events downstream of Ag receptors (4). From their position at the plasma membrane, where signals transduced through the Ag receptor are sorted and further propagated into the cell, TRAPs may play an important role in fine-tuning TCR-mediated signal strength required to regulate positive and/or negative selection. However, with the exception of LAT (linker for activation of T cells) (5), little is known about the role of TRAPs in thymocyte development.

Previously, we showed that the Src homology domain containing tyrosine phosphatase 2-interacting transmembrane adaptor protein (SIT) regulates thymic development by setting the signaling threshold for positive selection (6), whereas mice lacking the TCR-interacting molecule (TRIM) showed normal T cell development and function (7). SIT and TRIM are structurally strongly related proteins. Indeed, they both are non-raft-associated homodimeric transmembrane adaptors and both possess several tyrosine-based signaling motifs (TBSMs) within their cytoplasmic domains, two of which are highly conserved between the two molecules (YGNL and YASV in SIT, and YGNL and YASL in TRIM) (8, 9). Interestingly, we have previously reported that the ability of SIT to modulate TCR-mediated signaling in the Jurkat T cell line is determined by these two TBSMs (10). Additionally, SIT and TRIM are both strongly expressed in thymocytes. Based on these similarities and the mild phenotype of the single knockout animals, we proposed that SIT and TRIM adaptors can largely compensate for each other when one of the molecules is lost. To assess this idea, we generated SIT/TRIM double-deficient (DKO) mice. Our data show that SIT and TRIM are indeed functionally redundant during thymic selection. We demonstrate that concomitant loss of SIT and TRIM results in an enhanced MAPK activation and in the conversion of selection processes from nonselection to positive selection or from positive selection to negative selection. Collectively, our studies identified SIT and TRIM as critical regulators of central tolerance.

Materials and Methods

Mice

$SIT^{-/-}$ (6) and $TRIM^{-/-}$ (7) mice were intercrossed to generate homozygous DKO mice. DKO mice were further interbred with TCR transgenic

*Institute of Molecular and Clinical Immunology and †Pediatric Clinic, Otto-von-Guericke University, Magdeburg, Germany

Received for publication August 29, 2007. Accepted for publication August 26, 2008.

The costs of publication of this article were defrayed in part by the payment of page charges. This article must therefore be hereby marked *advertisement* in accordance with 18 U.S.C. Section 1734 solely to indicate this fact.

[1] This work was supported by the Deutsche Forschungsgemeinschaft (DFG) (SI 861/1).

[2] Address correspondence and reprint requests to Dr. Luca Simeoni, Institute of Molecular and Clinical Immunology, Otto-von-Guericke University, Leipziger Strasse 44, 39120 Magdeburg, Germany. E-mail address: luca.simeoni@med.ovgu.de

[3] Abbreviations used in this paper: TRAP, transmembrane adaptor protein; SIT, Src homology domain containing tyrosine phosphatase 2-interacting transmembrane adaptor protein; TBSM, tyrosine-based signaling motifs; TRIM, TCR-interacting molecule; DKO, SIT/TRIM double-deficient mice; β_2m, β_2-microglobulin; DP, double positive; SP, single positive; DN, double negative.

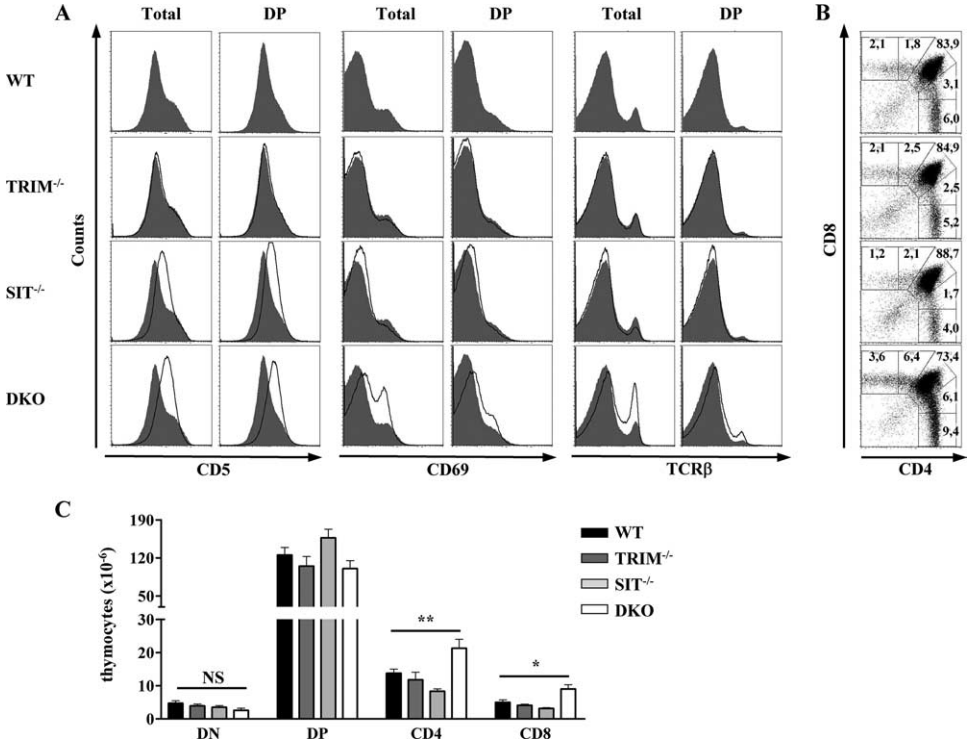

FIGURE 1. DKO thymocytes up-regulate markers of positive selection. Thymocytes isolated from control, single- and double-mutant mice were stained with Abs directed against CD4, CD5, CD8, CD69, and TCRβ and successively analyzed by flow cytometry. *A*, Histograms show expression of CD5, CD69, or TCRβ on total or $CD4^+CD8^+$ (DP) thymocytes. Expression is compared between wild-type (gray histograms) and mutant (open histograms) mice. *B*, Dot plots show CD4/CD8 staining profiles. Numbers indicate the percentage of cells in each quadrant. *C*, Absolute numbers of thymocyte subpopulations of mice of each genotype shown in *B* were calculated. Data derive from five wild-type, three $TRIM^{-/-}$, six $SIT^{-/-}$, and six DKO. **, $p < 0.005$ and *, $p < 0.05$.

mice. OT-I TCR transgenic mice were kindly provided by Dr. Percy Knolle, P14 by Dr. Thomas Kammerthoens, HY TCR transgenic mice by Dr. Gary Koreztky, and F5/β_2-microglobulin $(\beta_2m)^0$/$RAG1^0$ by Dr. Dimitris Kioussis. OT-I (11), P14 (12, 13), HY (14), and F5/β_2m^0/$RAG1^0$ (15–17) were previously described. All experiments involving mice were performed according to the guidelines of the State of Sachsen-Anhalt.

Flow cytometry

Single-cell suspensions were prepared, stained, and analyzed on a FACSCalibur using the CellQuest software (BD Biosciences) as previously reported (6). The Abs for phospho-ERK1/2, phospho-JNK, and phospho-p38 were purchased from Cell Signaling Technology. Intracellular staining was performed as previously described (6).

Proliferation assay

Lymph node cells (1×10^5 cells/well) were cultured in RPMI 1640 medium (supplemented with 10% FCS, antibiotics, 2-ME) in U-bottom 96-well plates (Costar) in the presence of plate-bound anti-mouse CD3ε (10 μg/ml, 145-2C11; BD Biosciences), anti-mouse TCRβ (10 μg/ml, H57-597; BD Biosciences), with Con A (2 μg/ml; Calbiochem) or in the presence of 2×10^5 irradiated T cell-depleted splenocytes from wild-type mice loaded with the agonist peptide NP68. Cells were pulsed with 1 μCi [^{3}H]thymidine per well during the last 8 h and harvested as previously described (6).

Statistical analysis

Statistical analyses were performed using GraphPad Prism software. Mean values ± SEM are shown in each graph. Asterisks represent *p*-values of an unpaired two-tailed Student's *t* test.

Results

Enhanced positive selection in DKO mice

Previously, we showed that loss of SIT resulted in a partial alteration of thymic selection (6), whereas the loss of TRIM had no effect upon T cell development (7). $SIT^{-/-}CD4^+CD8^+$ (double-positive, DP) thymocytes expressed higher levels of CD5 and CD69 and displayed a partial conversion from positive to negative selection in TCR transgenic mice. To explore the possibility whether SIT and TRIM, which appear to be structurally related, are functionally redundant during thymocyte selection, we bred $SIT^{-/-}$ to $TRIM^{-/-}$ mice to generate DKO mice. We initially analyzed the activation markers CD5 and CD69, whose expression was up-regulated in DP thymocytes from SIT-deficient mice (6). As shown in Fig. 1*A*, CD5 and CD69 expression was notably augmented on DP thymocytes lacking both SIT and TRIM when compared with SIT-deficient mice. Moreover, DP cells from DKO showed a marked up-regulation of TCRβ levels that was not observed in either $SIT^{-/-}$ or $TRIM^{-/-}$ mice (Fig. 1*A*). Taken together, these data suggest that SIT and TRIM may compensate for one another in lymphocyte development.

It is well established that the levels of TCRβ, CD5, and CD69 are strictly regulated during selection processes and that their expression reflects the intensity of the signal transduced via the TCR. Indeed, mice lacking negative regulators of TCR-mediated signaling such as c-Cbl (18) and SLAP (Src-like adaptor protein) (19) showed up-regulation of TCRβ, CD5, and CD69, whereas knockout mice for positive regulators of intracellular signaling pathways such as Tec-family kinases (20) or calcineurin B1 (21) show reduced levels of TCR, CD5, and CD69. Thus, on the basis of our observations, it appears as if SIT and TRIM both function as negative regulators of TCR signaling strength.

Upon TCR/MHC + self peptide interaction, immature DP thymocytes differentiate into mature $CD4^+$ or $CD8^+$ SP (single-positive) cells through a complex and ordered process that includes 1) up-regulation of TCRβ, CD5, and CD69, 2) down-regulation of one of the coreceptors, and 3) final commitment to either the CD4 or CD8 lineage (22–24).

To further investigate the effects of SIT and TRIM deficiency upon T cell development, we stained thymocyte suspensions with CD4 and CD8 mAbs. As presented in Fig. 1*B*, we found that DKO mice showed a striking difference in the distribution of thymocyte subsets in comparison to wild-type or single knockout mice. In fact, we observed an increase in the proportion of $CD4^+$ cells expressing low level of CD8 in DKO mice (Fig. 1*B*). These cells likely represent an intermediate subset of DP thymocytes that upon receiving a signal through the TCR is committed to the SP stage.

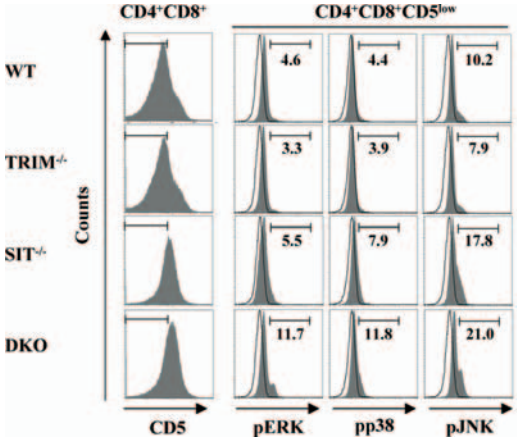

FIGURE 2. Increased MAPK activation in DKO mice. Thymocyte suspensions prepared from mice of different genotypes were rapidly fixed and stained with CD4, CD5, and CD8 mAbs and with Abs directed against the phosphorylated forms of ERK1/2, JNK/SAPK (stress-activated protein kinase), and p38 MAPKs. CD5 expression on $CD4^+CD8^+$ thymocytes is shown. Preselection thymocytes expressing low levels of CD5 were gated as indicated (*left panels*) and the intracellular levels of activated ERK1/2, JNK/SAPK, and p38 are shown (*right panels*). Open histograms represent cells stained with the secondary Ab alone. Numbers indicate the percentage of cells in each gate.

In agreement with this assumption, we also found that DKO mice display a 2-fold increase in the absolute number of SP thymocytes when compared with the other genotypes (Fig. 1*C*). Collectively, our data suggest that in the absence of both SIT and TRIM TCR-mediated signaling is considerably strengthen in DP thymocytes, resulting in a strong up-regulation of markers for positive selection and in an augmented commitment of DP thymocytes to the SP stage.

The number of early T cell precursors, defined by the lack of both CD4 and CD8 expression (double-negative (DN) cells) (Fig. 1*C*) and the differential expression of CD25 and CD44 (data not shown), are not affected in DKO mice. These data corroborate our previous observation that both SIT and TRIM are dispensable during early stages of T cell development (6, 7).

Enhanced MAPK activation in thymocytes from $SIT^{-/-}TRIM^{-/-}$ mice

It is well established that the activation of the Ras-Raf-MEK-ERK pathway is critical during positive selection (2). Therefore, we next assessed whether SIT and TRIM regulate ERK activation in thymocytes, by performing intracellular flow cytometric analyses using an Ab directed against the phosphorylated (and hence activated) forms of ERK1 and ERK2 (25). We analyzed DP thymocytes expressing low CD5 levels so that ERK activation can be solely attributed to cells that, upon TCR-MHC-self peptide engagement, are initiating thymic selection and not to postselected DP thymocytes that express CD5 at higher levels. To determine whether the magnitude of ERK phosphorylation directly correlates with positive selection, thymocyte suspensions prepared from mice of each genotype were rapidly fixed in formaldehyde to preserve the phosphorylation status of ERK. As shown in Fig. 2 and in agreement with previous observations (26), no significant ERK activity was detected in DP cells from wild-type or even single mutant mice, thus indicating that relatively few thymocytes initiate positive selection in normal mice. Conversely, we found that there was considerably more ERK phosphorylation in DP thymocytes from DKO mice (Fig. 2). These data show that the enhanced positive selection in DKO thymi correlate with an enhanced ex vivo ERK phosphorylation. Importantly, we previously showed that the more efficient positive selection/shift to negative selection observed in $SIT^{-/-}$ HY TCR transgenic female mice also correlated with stronger ex vivo ERK activity in DP thymocytes (6). Collectively, these data indicate that SIT and TRIM regulate thymic selection by modulating the degree of ERK activation.

Conversion from positive to negative selection in DKO mice

Fig. 2 also shows that DKO DP thymocytes display significantly higher levels of phosphorylated p38 and JNK when compared with single mutant and wild-type mice. Studies performed using knockout mice or specific MAPK inhibitors had suggested that JNK and p38 may be important during negative selection (2). On the basis of these observations, higher JNK and p38 activities should result in the conversion from positive to negative selection in DKO thymi. This hypothesis is also supported by our previous observation that female HY TCR transgenic $SIT^{-/-}$ mice show a partial conversion from positive to negative selection (6).

To analyze whether loss of both SIT and TRIM resulted in an enhanced conversion from positive to negative selection, we interbred DKO mice with mice expressing transgenic TCRs. Fig. 3*A* shows that the cellular pattern of positive selection in female HY DKO mice is dramatically altered and noticeably resembles that observed in HY TCR male mice where negative selection occurs (Fig. 3*A*, *upper right panel*). Indeed, thymi of DKO HY TCR transgenic female mice are completely devoid of DP cells, contain few CD8 SP thymocytes expressing lower levels of CD8 than normal HY TCR transgenic female mice, and are comprised of almost exclusively DN thymocytes (Fig. 3*A*). One result of negative selection in male HY mice is the overall reduction of thymic cellularity. Comparison of total cell numbers revealed another striking similarity between DKO HY female and HY male mice. As shown in Fig. 3*B*, DKO thymi are indeed markedly hypocellular like those of male HY mice.

These results show that the concomitant deletion of SIT and TRIM results in the complete conversion from positive to negative selection of HY TCR^+ thymocytes in female mice.

For some time, it was thought that elimination of autoreactive T cells by deletion was the main pathway for the maintenance of self-tolerance. More recent data, however, have revised this paradigm and suggested that nondeletional pathways also contribute to tolerance. For example, autoreactive T cells may escape deletion by down-regulating the coreceptor (27–30). In this way, autoreactive T cells reprogram the activation threshold and become unresponsive to self Ags. Coreceptor down-regulation has been described to take place on both thymocytes (31, 32) and peripheral mature T cells (30, 33–35) and allows the generation of large numbers of coreceptor low or DN peripheral T cells. The observation that $CD4^-CD8^{low}$ and $CD4^-CD8^-$ TCR^+ peripheral T cells are abundant in mice carrying transgenic TCRs on negatively selecting genetic background (i.e., HY TCR transgenic male mice) reinforces the idea that coreceptor down-regulation is required to maintain tolerance (14, 36, 37). However, the physiological relevance of these cells in TCR transgenic mice has been questioned due to the premature expression of the $\alpha\beta$ TCR (38).

The data shown in Fig. 3*A* indicate that the level of CD8 is reduced on thymocytes from DKO HY female mice. To investigate whether mechanisms alternative to deletion are set in motion to reprogram the activation threshold and maintain tolerance in DKO mice, we investigated CD8 expression levels in peripheral T cells. Fig. 3*C* shows that, while HY $SIT^{-/-}$ female mice display a partial down-regulation of CD8, HY DKO female mice exhibit a striking

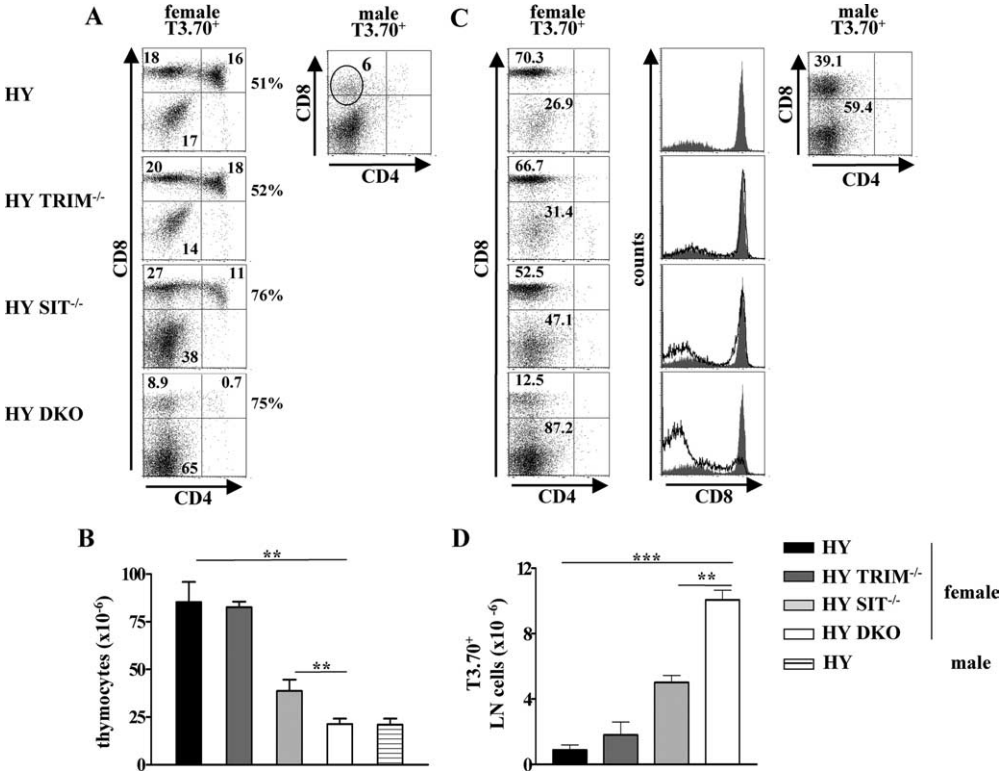

FIGURE 3. Positive selection is completely converted to negative selection in HY DKO female mice. *A*, Dot plots show CD4/CD8 staining profiles of T3.70$^+$-gated thymocytes from wild-type, single-mutant, double-mutant female HY TCR transgenic mice (*left*) or male HY TCR transgenic mice (*right*). One representative mouse of a minimum of five animals per group is shown. Numbers within the quadrants indicate the percentage of cells. The proportion of T3.70$^+$ cells in total thymocytes is indicated to the right of the dot plot profiles. *B*, Thymocyte cell numbers from the HY TCR transgenic and mutant mice shown in *A*. *C*, Two-color dot plots show CD4/CD8 staining on T3.70$^+$-gated lymph node cells. Numbers indicate the percentage of cells in that quadrant. Histograms depict the expression of CD8 on T3.70$^+$-gated lymph nodes cells in wild-type (gray histograms) and mutant (open histograms) mice. *D*, Absolute numbers of T3.70$^+$ T cells in lymph nodes were calculated. Data shown in *B* and *D* derive from at least four mice of each genotype. ***, $p = 0.0002$ and **, $p < 0.009$.

down-regulation that is even more pronounced than that seen in male HY mice (Fig. 3*C*, compare lower left and upper right dot plots), and DKO females also accumulate large numbers of T3.70$^+$ DN cells (Fig. 3*D*). These data are in agreement with our recent observation demonstrating that the loss of SIT markedly enhanced the homeostatic expansion of peripheral T3.70$^+$ T cells from HY transgenic female mice (39).

Thus, the loss of both SIT and TRIM lowers the signaling threshold in T cells and results in a massive deletion of DP cells in the thymus. Therefore, T3.70$^+$ T cells reprogram their activation

Table I. *Thymocyte subsets in TCR transgenic mice*[a]

		Vα2$^-$				Vα2$^+$				Vα2^{high}		
Genotypes	No. of Mice	CD4$^-$CD8$^-$	CD4$^+$ CD8$^+$	CD4$^+$ CD8$^-$	CD4$^-$ CD8$^+$	CD4$^-$ CD8$^-$	CD4$^+$ CD8$^+$	CD4$^+$ CD8$^-$	CD4$^-$ CD8$^+$	CD4$^+$ CD8$^+$	CD4$^+$ CD8$^-$	CD4$^-$ CD8$^+$
P14	4	1.06 ± 0.2	13.2 ± 1.6	0.6 ± 0.1	0.4 ± 0.05	1.5 ± 0.2	34.7 ± 4.3	0.2 ± 0.04	7.9 ± 1.2	5.9 ± 0.7	0.1 ± 0.01	5.6 ± 0.8
P14 TRIM$^{-/-}$	4	1.15 ± 0.2	13.2 ± 1.2	0.7 ± 0.1	0.4 ± 0.02	1.2 ± 0.2	32.3 ± 2.1	0.2 ± 0.02	7.3 ± 1.3	6.1 ± 1.8	0.1 ± 0.03	4.8 ± 1.5
P14 SIT$^{-/-}$	4	1.52 ± 0.3	17.2 ± 1.1	0.9 ± 0.1	0.9 ± 0.2	1.9 ± 0.2	22.9 ± 0.7	0.3 ± 0.01	5.4 ± 0.9	2.0 ± 0.2	0.1 ± 0.01	2.3 ± 0.1
P14 DKO	4	1.81 ± 0.3	15.8 ± 2.2	1.6 ± 0.2	1.0 ± 0.3	2.0 ± 0.9	16.5 ± 1.1	1.3 ± 0.3	5.1 ± 0.4	1.3 ± 0.04	0.4 ± 0.05	1.1 ± 0.2
p-values P14/ P14 DKO		NS	NS	0.02	NS	NS	0.007	0.02	0.02	0.0006	0.003	0.007
p-values P14 SIT$^{-/-}$/P14 DKO		NS	NS	NS	NS	NS	0.003	0.02	NS	0.04	0.002	0.008
OT-I	4	1.02 ± 0.4	14.1 ± 4.0	0.9 ± 0.2	0.8 ± 0.2	1.3 ± 0.3	23.5 ± 3.2	7.5 ± 1.7	6.9 ± 0.8	3.0 ± 0.5	1.7 ± 0.6	3.9 ± 0.6
OT-I TRIM$^{-/-}$	4	1.34 ± 0.4	18.2 ± 5.1	1.1 ± 0.3	1.1 ± 0.2	1.2 ± 0.3	22.7 ± 1.8	7.4 ± 1.7	7.2 ± 0.6	2.1 ± 0.2	1.8 ± 0.1	4.2 ± 0.6
OT-I SIT$^{-/-}$	6	1.55 ± 0.8	20.1 ± 5.2	1.1 ± 0.7	1.0 ± 0.7	1.5 ± 0.7	19.4 ± 2.7	6.6 ± 2.6	5.7 ± 1.1	1.6 ± 0.2	1.6 ± 0.2	2.2 ± 0.1
OT-I DKO	8	1.8 ± 0.4	19.5 ± 4.3	1.2 ± 0.2	1.5 ± 0.2	1.5 ± 0.3	10.1 ± 2.5	4.2 ± 1.6	1.9 ± 0.5	0.3 ± 0.07	0.8 ± 0.4	0.5 ± 0.1
p-values OT-I/ OT-I DKO		NS	NS	NS	NS	NS	0.02	0.04	0.001	0.0005	0.02	0.0001
p-values OT-I SIT$^{-/-}$/OT-I DKO		NS	NS	NS	NS	NS	0.02	NS	0.02	0.0006	0.02	0.0001

[a] All numbers are shown as × 10^6 ± SEM. Statistically significant *p*-values are indicated.

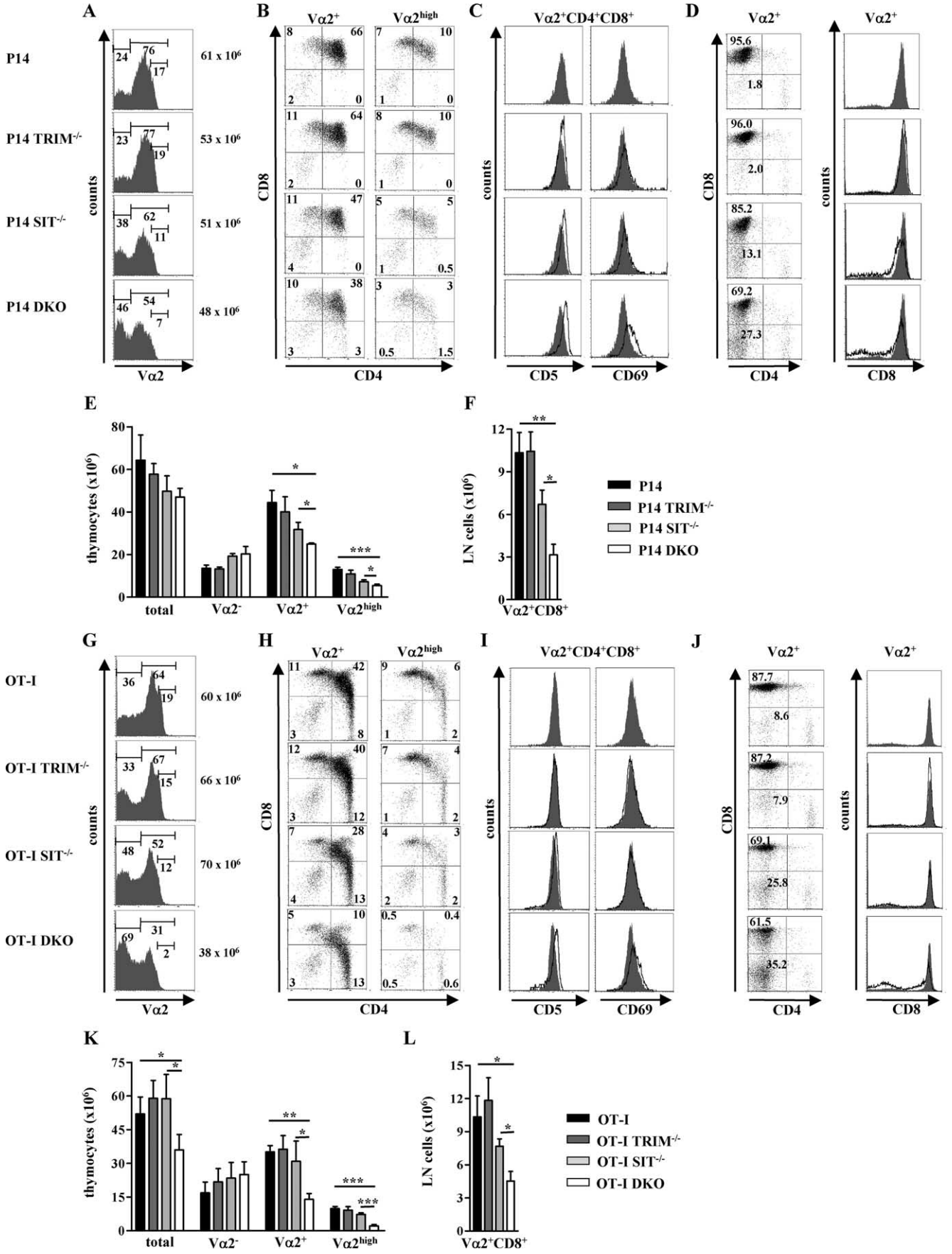

FIGURE 4. Partial conversion from positive to negative selection in P14 and OT-I DKO mice. Comparison of thymocytes and lymph node T cells from wild-type, single-mutant, or SIT and TRIM double-mutant mice expressing the P14 (*A–F*) or the OT-I (*G–L*) TCRs. *A* and *G*, Histograms show expression of the TCR transgenic α-chain (Vα2). The gates defining V$\alpha2^-$, V$\alpha2^+$, and V$\alpha2^{high}$ expressing thymocytes are indicated. The number of total thymocytes

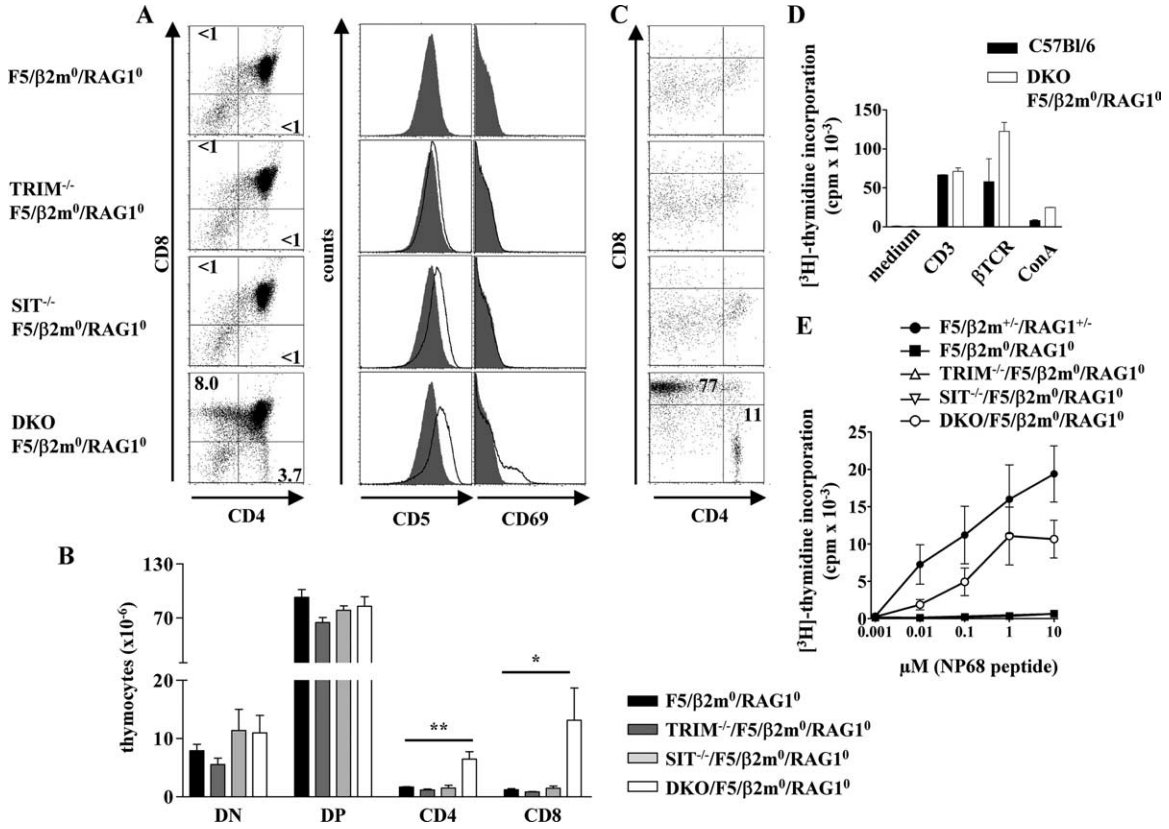

FIGURE 5. Efficient positive selection of F5 TCR transgenic T cells by low avidity TCR-MHC interactions in DKO mice. *A*, Cell suspensions from thymus were stained with CD4, CD8, CD5, and CD69 mAbs. Dot plots show CD4 and CD8 expression on thymocytes. Numbers in outlined areas represent percentage of cells. One representative mouse of at least five animals per group is shown. Histograms show the expression of CD5 and CD69 on DP thymocytes from wild-type mice (gray filled histograms) and mutant mice (solid lines). *B*, Absolute numbers of thymocyte subsets shown in *A* were calculated. Data derive from five mice of the indicated genotype. **, $p = 0.0096$ and *, $p = 0.014$. *C*, Expression of CD4 and CD8 on lymph node cells. Numbers within the quadrants indicate the percentage of cells. *D* and *E*, Lymph node cells isolated from mice of each indicated genotype were stimulated with immobilized CD3 and TCRβ mAbs or ConA (*D*) or in the presence of irradiated APCs pulsed with increasing amount of NP68 peptide (*E*). Data shown in *D* derive from three mice, whereas those presented in *E* derive from six mice of each genotype.

threshold by down-regulating CD8 expression in response to a persistent strong signal.

To further corroborate the effects of SIT and TRIM on positive selection, we used two additional TCR transgenic models expressing either the P14 or OT-I TCRs (Fig. 4). Previously, we showed that TRIM deficiency did not affect selection processes in either P14 or OT-I TCR transgenic thymocytes (7), whereas the loss of SIT modestly affected positive selection only in the P14 TCR transgenic mice (6). In agreement with our previous observations (6), the results in Fig. 4, *A* and *E*, show that P14 SIT$^{-/-}$ mice show a modest reduction in the number of total Vα2^{+} and positively selected Vα2^{high} thymocytes. Remarkably, DKO mice display a stronger decrease in the proportion and absolute numbers of thymocytes expressing the transgenic TCRα-chain (Fig. 4, *A* and *E*). In contrast, the number of nontransgenic Vα2^{-} thymocytes are not decreased but rather slightly increased, indicating that these cells may undergo expansion upon deletion of transgenic thymocytes. The decrease in the total number of clonotypic TCR^{+} thymocytes appears to be due to a reduction of both DP and CD8 SP thymocytes (Fig. 4*B* and Table I), thus indicating that, similar to the HY TCR transgenic model, positive selection is likely converted to negative selection in the absence of SIT and TRIM also in the P14 system. To further corroborate this hypothesis is the observation that thymocytes from DKO mice are hyperactivated as they up-regulate both CD5 and CD69 (Fig. 4*C*). In agreement with an altered positive selection, the number of peripheral mature Vα2^{+} T cells in lymph nodes of DKO mice are also markedly reduced in comparison to control or SIT-deficient mice (Fig. 4, *D* and *F*). These data suggest that the loss of SIT and TRIM results in an enhanced TCR-mediated signaling that converts positive to negative selection.

Subsequently, we confirmed these results and analyzed selection processes in the OT-I transgenic mice. The data presented in Fig. 4*G–L* demonstrate that loss of SIT and TRIM severely affects positive selection also in this TCR transgenic model. Indeed, DKO

from one representative mouse is indicated to the right of the histograms. *B* and *H*, Two-color dot plots show CD4/CD8 staining gated on Vα2^{+} and on Vα2^{high} thymocytes. Numbers below the gates in *A* and *G* or within the quadrants in *B* and *H* indicate the percentage of cells. *C* and *I*, Histograms show expression of CD5 and CD69 on Vα2^{+}-gated DP cells. Expression is compared between wild-type (gray histograms) and mutant (open histograms) mice. *D* and *J*, Two-color dot plots show CD4/CD8 staining on clonotype-TCR^{+} (Vα2^{+})-gated lymph node cells. Numbers indicate the percentage of cells in that quadrant. Histograms depict the expression of CD8 on Vα2^{+}-gated lymph nodes cells in wild-type (gray histograms) and mutant (open histograms) mice. *E* and *K*, Absolute numbers of total thymocytes or thymocyte subsets shown in histograms in *A* and *G* were calculated. *F* and *L*, Absolute numbers of Vα2^{+}CD8^{+} T cells in lymph nodes were calculated. Data shown derive from at least four mice per group. ***, $p < 0.0005$; **, $p < 0.005$; *, $p < 0.05$.

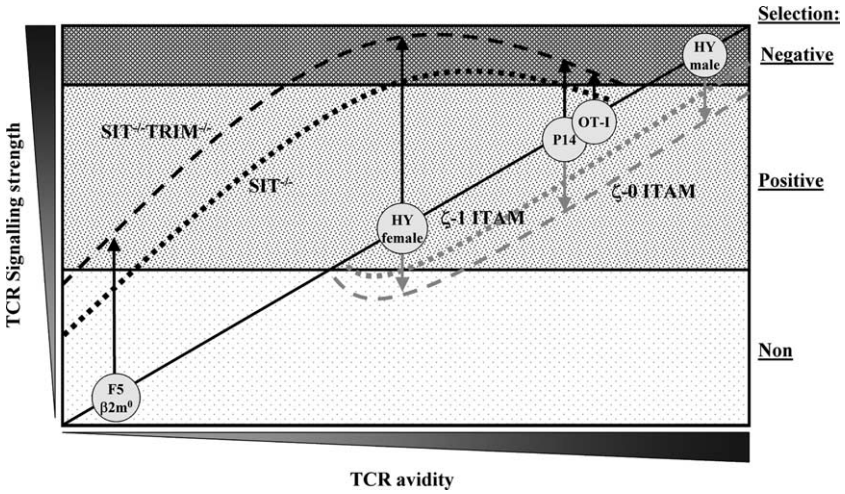

FIGURE 6. Model of thymic selection outcomes. The proposed model (summarizing our data and previously published data (Refs. 41–43) shows the effects of augmenting or diminishing signal intensity on the selection of thymocytes expressing a variety of TCRs with increasing affinity/avidity for the ligand. The effects of SIT (black dotted line) or SIT and TRIM (black dashed line) deletions on selection outcomes are compared with those obtained by TCR-ζ mutants carrying only 1 ITAM (gray dotted line) or no ITAMs (gray dashed line).

mice showed an enhanced TCR-mediated signaling in DP cells, as suggested by the higher levels of CD5 and CD69 expression (Fig. 4*I*), a marked decrease in the number of total thymocytes, total transgenic Vα2$^+$ cells, and positively selected Vα2^{high} thymocytes (Fig. 4, *G* and *K*). Moreover, DP and CD8 SP thymocytes are also markedly depleted in DKO mice (Fig. 4*H* and Table I). Finally, a reduction in mature Vα2^{high} lymph node CD8$^+$ T cells is also observed in DKO mice (Fig. 4, *J* and *L*). In agreement with our previous observations (6), the loss of SIT had only minimal affects upon positive selection. In fact, the total number of positively selected Vα2^{high} thymocytes and peripheral CD8$^+$ T cells as well as CD5 and CD69 expression are grossly unchanged in SIT$^{-/-}$ mice. Interestingly, both P14 and OT-I DKO mice down-regulate the CD8 coreceptor on peripheral TCR$^+$ cells (Fig. 4, *D* and *J*, *right panels*). Thus, in the absence of SIT and TRIM, CD8$^+$ T cells from TCR transgenic mice receive constantly stronger signals via the TCR that trigger coreceptor down-regulation.

Collectively, the data obtained from three different class I-restricted TCR transgenic lines suggest that the loss of SIT and TRIM enhances TCR-mediated signaling and converts positive into negative selection.

Conversely, when we investigated the MHC class II-restricted OT-II TCR transgenic model we did not observe any effect on positive selection (data not shown).

Finally, we investigated whether SIT and TRIM also affect negative selection. However, we found no differences in the CD4/CD8 profile or total cellularity of DKO thymocytes from male HY TCR transgenic mice (data not shown). Moreover, in vitro CD3-mediated deletion of DKO DP cells was normal (data not shown), thus suggesting that SIT and TRIM do not regulate negative selection or thymocyte survival.

In summary, these data demonstrate that SIT and TRIM cooperatively set the TCR signaling threshold for positive selection.

DKO thymocytes are efficiently positively selected by low avidity TCR-MHC interactions

The data above indicate that SIT and TRIM are critical regulators of T cell development. In all models tested, we found that positive selection is either enhanced or converted to negative selection. The enhanced MAPK activation, together with the up-regulation of CD5 and CD69, is consistent with the idea that TCR-mediated signaling is stronger in DKO mice. Therefore, we next investigated whether the loss of SIT and TRIM enables positive selection of T cells under experimental conditions in which TCR avidity is abrogated and, thus, positive selection should not occur. As a model system, we used β_2m-deficient/RAG1-deficient mice expressing the class I-restricted F5 transgenic TCR (F5/β_2m^0/RAG1^0) (17). In these mice, T cell development is blocked at the DP stage and thymic selection does not occur, as class I MHC heavy chains are expressed at extremely low levels.

To evaluate whether the loss of SIT and TRIM may alter cell fate by diverting thymocytes from nonselection to positive selection, DKO mice were bred onto F5/β_2m^0/RAG1^0 mice. As shown in Fig. 5*A*, neither the loss of SIT or TRIM alone induced the generation of mature SP thymocytes. Indeed, the CD4/CD8 profiles of single knockout mice resemble those of control F5/β_2m^0/RAG1^0 mice. Strikingly, however, significant numbers of CD8$^+$ SP thymocytes were found in F5/β_2m^0/RAG1^0 mice lacking both SIT and TRIM (Fig. 5, *A* and *B*). Analysis of the CD5 and CD69 expression levels (Fig. 5*A*) indicated that positive selection in DKO mice is likely initiated by TCR-mediated signaling, as the expression of both molecules is induced on DP thymocytes from DKO mice. Even more surprisingly, we also detected mature CD8$^+$ T cells in peripheral secondary lymphoid organs of DKO/F5/β_2m^0/RAG1^0 mice (Fig. 5*C*). However, the efficiency of positive selection remained very low, with $<$10% of the number of CD8$^+$ T cells recovered from the lymph nodes from DKO/F5/β_2m^0/RAG1^0 mice ($0.244 \times 10^6 \pm 0.021 \times 10^6$; $n = 3$ mice) as compared with F5/β_2m$^{+/-}$/RAG1$^{+/-}$ mice ($3.610 \times 10^6 \pm 0.215 \times 10^6$; $n = 3$ mice).

Therefore, it appears that the loss of SIT and TRIM likely lowers the TCR-mediated signaling threshold for positive selection, thereby enabling the maturation of T cells by TCR/low-avidity ligand-driven signals.

To test whether the loss of SIT and TRIM might have resulted in the spontaneous development of T cells in a TCR-independent manner, we investigated DKO RAG-deficient mice. RAG1^0 and DKO/RAG1^0 mice both displayed a developmental block at the DN3 stage (data not shown), thus reinforcing the idea that the loss of SIT and TRIM alone does not result in the autonomous maturation of T cells.

Unexpectedly, DKO/F5/β_2m^0/RAG1^0 mice displayed CD4$^+$ SP thymocytes (Fig. 5*A*) and peripheral CD4$^+$ T cells (Fig. 5*C*). Interestingly, also DKO mice expressing the MHC class I-restricted P14 TCR showed an increase in the number of Vα2$^+$CD4$^+$ SP thymocytes (Fig. 4*B* and Table I). Therefore, it is likely that the loss of SIT and TRIM also alters T cell lineage commitment, as the quantity of TCR-mediated signals not only influences selection processes, but also lineage commitment (40).

Having shown that DKO/F5/β_2m^0/RAG1^0 mice develop peripheral T cells, we next determined whether these T cells were also functional. Initially, total lymph node cells from wild-type C57BL6/J and DKO/F5/β_2m^0/RAG1^0 mice were stimulated in the presence of plate-bound CD3 and TCRβ mAbs or Con A. As shown in Fig. 5*D*, DKO/F5/β^2m^0/RAG1^0 cells robustly responded to all mitogenic stimuli. Finally, to determine whether DKO/F5/β_2m^0/RAG1^0 T cells specifically responded to the F5 TCR cognate peptide, lymph node cells from mice of each genotype were stimulated with irradiated APCs loaded with increasing amount of the influenza virus peptide NP68. Fig. 5*E* shows that only lymph node cells from DKO/F5/β_2m^0/RAG1^0 and from F5/$\beta_2m^{+/-}$/RAG1$^{+/-}$ control mice responded to the NP68 agonist peptide in a dose-dependent manner. Collectively, our data demonstrate that DKO F5 TCR transgenic T cells positively selected on a β_2m-deficient genetic background are functional. In summary, these results demonstrate a unique joint role for SIT and TRIM as inhibitory TRAPs that lower TCR signals, thereby directly influencing the fate of developing thymocytes.

Discussion

To date, with the exception of LAT, deletion of any other known transmembrane adaptors has had negligible effects on thymocyte development. By showing that the two related transmembrane adaptor proteins SIT and TRIM together regulate thymic selection, we revealed important insights into the role of TRAPs in T cell development and in the establishment of central tolerance. We propose that SIT and TRIM function as suppressors of signal amplification and regulate thymic selection by modulating the degree of MAPK activation. Furthermore, our data also show that SIT and TRIM function in a cooperative manner, thus indicating that TRAPs may represent a group of molecules with overlapping functions.

As summarized in Fig. 6, our data are consistent with the signaling threshold model for thymocyte selection (41). This model postulates that the TCR affinity/avidity for the selecting ligand is in a direct relationship with the strength of the TCR-mediated signaling and, in turn, with the outcome of selection. Therefore, the outcome of selection of thymocytes expressing a specific TCR can be influenced by increasing or decreasing the TCR signal potential. Indeed, as predicted by the signaling threshold model, our data show that in a TCR transgenic system where the avidity for the selecting ligand is thought to be extremely low (such as in the F5/β_2m^0/RAG1^0 system), the loss of SIT and TRIM converts nonselection into positive selection (Fig. 6). Despite the fact that loss of SIT alone is not sufficient to induce the shift into positive selection, DP thymocytes from SIT$^{-/-}$/F5/β_2m^0/RAG1^0 mice displayed enhanced CD5 levels. This observation suggests that also in SIT$^{-/-}$/F5/β_2m^0/RAG1^0 mice the TCR-mediated signaling strength is potentiated, as CD5 expression is directly regulated by TCR signal intensity (24). When we tested transgenic mice expressing a TCR with a weak ligand avidity (i.e., HY), where positive selection occurs inefficiently, the loss of SIT alone is sufficient to induce a more efficient positive selection and a partial shift to negative selection (6), whereas the loss of both SIT and TRIM results in a complete conversion to negative selection (Fig. 6). Positive selection of thymocytes expressing a TCR with a higher affinity for its selecting ligand than HY (i.e., P14) is partially converted to negative selection by the loss of SIT alone, and the additional deletion of TRIM further enhances the shift to negative selection (Fig. 6). Regardless of the outcome of selection (i.e., efficient positive selection such as in OT-I TCR transgenic mice or negative selection such as in male HY TCR transgenic mice), over a certain level of avidity and TCR signaling strength, SIT seems to be dispensable during selection processes and the further deletion of TRIM converts efficient positive selection into negative selection only in OT-I TCR transgenic mice (Fig. 6).

Models based on signal strength postulate that negative, positive, and nonselection lie on a continuum of signals emanating from the TCR and that amplification of the signals at a very proximal level determines the right signal intensity for the specific developmental outcome (40). Our data strongly support this idea and further suggest that SIT and TRIM both function as suppressors of signal amplification. Therefore, it is likely that they are located at the very apical part of the TCR signaling cascade. Interestingly, the effects of SIT/TRIM double deficiency on thymocyte development are opposite to those observed in mice carrying mutations in the TCR-associated ζ-chain, a well-known amplifier of TCR-mediated signaling. Indeed, reduction of TCR signal potential by substituting the number of ITAMs within TCR-ζ or by knocking out TCR-ζ resulted in a shift from negative to positive selection or even converted positive into nonselection (Fig. 6) (41–44).

In light of these observations, it appears that thymocytes are provided with signaling components such as the TCR ζ-chain or TRAPs such as SIT and TRIM that possess opposing regulatory functions. Therefore, signal amplification by multiple ITAMs within the TCR/CD3 complex appears to be counterregulated by an inhibitory system based on several TBSMs within transmembrane adaptors. In fact, in analogy with the effects of an incremental reduction in the number of TCR-ζ ITAMs, our data suggest that also the sequential deletion of TRAPs gradually affects selection processes. It appears that the coordinated integration of the regulatory activity of multiple positive and negative signaling motifs within membrane-associated proteins is required for shaping the T cell repertoire. As this regulatory system appears to be crucial for cell fate specifications in the thymus, it is not surprising that the molecules controlling the process are physically located at the plasma membrane as a part of, or in close proximity to, the receptor. In fact, we have shown that TRIM is an integral component of the TCR/CD3 complex (8, 45), whereas SIT was identified as a protein co-immunoprecipitating with CD3 (9).

Surprisingly, such an elaborated system for fine-tuning TCR-mediated signals does not seem to play a role during peripheral T cell activation, as mutations in the number of TCR-ζ ITAMs (41, 42) or loss of SIT and TRIM (data not shown) only minimally affect activation of mature T cells. These observations indicate that other regulatory mechanisms, such as those mediated by costimulatory molecules, are required to adjust peripheral T cell responses.

The mechanism by which SIT and TRIM regulate signaling threshold remains elusive. A major obstacle encountered in elucidating this question is the development of compensatory mechanisms in mutant mice. Indeed, we showed that thymocytes from both SIT$^{-/-}$ (6, 39) and DKO mice overexpress CD5, a negative regulator that dampens TCR-mediated signaling (24, 46–48). Changes in the level of CD5 expression is the best known example of TCR signaling tuning and hence may indicate sensory adaptation (27, 49). It is thought that CD5 expression is regulated to modulate the activation threshold in response to an altered signaling strength. In fact, cells that express a high level of CD5 display a parallel lowered responsiveness to TCR triggering (39, 47, 49). In addition to upregulating CD5, modulation of T cell responsiveness can be also achieved by down-regulating the CD8 coreceptor (29). Interestingly, T cells from SIT-deficient (39) and DKO mice also down-regulate CD8. Thus, the loss of SIT and

TRIM resulted in the development of sensory adaptation by up-regulating CD5 and down-regulating CD8.

In accordance with these observations, it is therefore not surprising that we did not observe an enhanced TCR-mediated signaling when DP thymocytes from DKO mice were stimulated with CD3 Ab in vitro (data not shown). It is likely that, in these cells, the enhanced TCR-mediated signaling caused by the loss of SIT and TRIM is counterbalanced by CD5 overexpression or perhaps even by other negative regulatory molecules. The generation of additional mouse model such as $SIT^{-/-}/TRIM^{-/-}/CD5^{-/-}$ triple knockouts is required to investigate how SIT and TRIM modulate TCR-mediated signaling when the counterbalancing effects of CD5 are no longer present.

Recent observations from our laboratory suggest that SIT and TRIM may act in concert to regulate PI3K activation. Indeed, we found that, under particular conditions of TCR stimulation, $SIT^{-/-}$ T cells showed enhanced Akt phosphorylation, a measure of PI3K activation (B. Schraven and L. Simeoni unpublished results). We have previously shown that also T cells from $TRIM^{-/-}$ mice displayed enhanced Akt phosphorylation upon TCR triggering (7). It appears that by binding the p85 regulatory subunit of PI3K, TRIM could inhibit PI3K activation, thus sequestering p85 outside of the lipid rafts. However, how SIT regulates PI3K remains as yet unknown. In fact, conversely to TRIM, SIT does not bind p85 directly. We suggest that SIT could regulate Gab association with p85 by controlling Gab phosphorylation via the tyrosine phosphatase SHP-2 (50). Interestingly, we have recently shown that SIT also shares redundant function with the third non-raft transmembrane adaptor protein LAX (linker for activation of X cells) in B1 cells and T lymphocytes (our unpublished results). Similarly to TRIM, LAX binds the p85 regulatory subunit of PI3K and the loss of LAX also resulted in an enhanced Akt phosphorylation in B and T lymphocytes (51). Based upon these data, we speculate that the non-raft adaptors SIT, TRIM, and LAX may functionally converge to regulate PI3K activation (52). Whereas SIT and TRIM appear to play a major role in thymocyte development, SIT and LAX seem to regulate B1 cell development, T cell activation, and autoimmunity. In conclusion, our studies have begun to shed light onto the redundant function of the non-raft adaptors in lymphocyte development and activation. Additional efforts are now required to reveal how these molecules regulate Ag receptor-mediated signaling in concert.

Acknowledgments

We are grateful to Vilmos Posevitz and Ines Meinert for excellent technical assistance, to Dr. Jonathan Lindquist for critically reading the manuscript and helpful discussion, and the employees of the animal facility for maintenance of the animals. We thank Dr. Dimitris Kioussis for providing $F5/\beta_2m^0/RAG1^0$ mice.

Disclosures

The authors have no financial conflicts of interest.

References

1. Sebzda, E., S. Mariathasan, T. Ohteki, R. Jones, M. F. Bachmann, and P. S. Ohashi. 1999. Selection of the T cell repertoire. *Annu. Rev. Immunol.* 17: 829–874.
2. Starr, T. K., S. C. Jameson, and K. A. Hogquist. 2003. Positive and negative selection of T cells. *Annu. Rev. Immunol.* 21: 139–176.
3. Cante-Barrett, K., E. M. Gallo, M. M. Winslow, and G. R. Crabtree. 2006. Thymocyte negative selection is mediated by protein kinase C- and Ca^{2+}-dependent transcriptional induction of bim. *J. Immunol.* 176: 2299–2306.
4. Horejsi, V., W. Zhang, and B. Schraven. 2004. Transmembrane adaptor proteins: organizers of immunoreceptor signalling. *Nat. Rev. Immunol.* 4: 603–616.
5. Malissen, B., E. Aguado, and M. Malissen. 2005. Role of the LAT adaptor in T-cell development and Th2 differentiation. *Adv. Immunol.* 87: 1–25.
6. Simeoni, L., V. Posevitz, U. Kolsch, I. Meinert, E. Bruyns, K. Pfeffer, D. Reinhold, and B. Schraven. 2005. The transmembrane adapter protein SIT regulates thymic development and peripheral T-cell functions. *Mol. Cell. Biol.* 25: 7557–7568.
7. Kolsch, U., B. Arndt, D. Reinhold, J. A. Lindquist, N. Juling, S. Kliche, K. Pfeffer, E. Bruyns, B. Schraven, and L. Simeoni. 2006. Normal T-cell development and immune functions in TRIM-deficient mice. *Mol. Cell. Biol.* 26: 3639–3648.
8. Bruyns, E., A. Marie-Cardine, H. Kirchgessner, K. Sagolla, A. Shevchenko, M. Mann, F. Autschbach, A. Bensussan, S. Meuer, and B. Schraven. 1998. T cell receptor (TCR) interacting molecule (TRIM), a novel disulfide-linked dimer associated with the TCR-CD3-ζ complex, recruits intracellular signaling proteins to the plasma membrane. *J. Exp. Med.* 188: 561–575.
9. Marie-Cardine, A., H. Kirchgessner, E. Bruyns, A. Shevchenko, M. Mann, F. Autschbach, S. Ratnofsky, S. Meuer, and B. Schraven. 1999. SHP2-interacting transmembrane adaptor protein (SIT), a novel disulfide-linked dimer regulating human T cell activation. *J. Exp. Med.* 189: 1181–1194.
10. Pfrepper, K. I., A. Marie-Cardine, L. Simeoni, Y. Kuramitsu, A. Leo, J. Spicka, I. Hilgert, J. Scherer, and B. Schraven. 2001. Structural and functional dissection of the cytoplasmic domain of the transmembrane adaptor protein SIT (SHP2-interacting transmembrane adaptor protein). *Eur. J. Immunol.* 31: 1825–1836.
11. Hogquist, K. A., S. C. Jameson, W. R. Heath, J. L. Howard, M. J. Bevan, and F. R. Carbone. 1994. T cell receptor antagonist peptides induce positive selection. *Cell* 76: 17–27.
12. Pircher, H., K. Burki, R. Lang, H. Hengartner, and R. M. Zinkernagel. 1989. Tolerance induction in double specific T-cell receptor transgenic mice varies with antigen. *Nature* 342: 559–561.
13. Pircher, H., D. Moskophidis, U. Rohrer, K. Burki, H. Hengartner, and R. M. Zinkernagel. 1990. Viral escape by selection of cytotoxic T cell-resistant virus variants in vivo. *Nature* 346: 629–633.
14. Kisielow, P., H. Bluthmann, U. D. Staerz, M. Steinmetz, and H. von Boehmer. 1988. Tolerance in T-cell-receptor transgenic mice involves deletion of nonmature $CD4^+8^+$ thymocytes. *Nature* 333: 742–746.
15. Mamalaki, C., J. Elliott, T. Norton, N. Yannoutsos, A. R. Townsend, P. Chandler, E. Simpson, and D. Kioussis. 1993. Positive and negative selection in transgenic mice expressing a T-cell receptor specific for influenza nucleoprotein and endogenous superantigen. *Dev. Immunol.* 3: 159–174.
16. Wack, A., H. M. Ladyman, O. Williams, K. Roderick, M. A. Ritter, and D. Kioussis. 1996. Direct visualization of thymocyte apoptosis in neglect, acute and steady-state negative selection. *Int. Immunol.* 8: 1537–1548.
17. Smyth, L. A., O. Williams, R. D. Huby, T. Norton, O. Acuto, S. C. Ley, and D. Kioussis. 1998. Altered peptide ligands induce quantitatively but not qualitatively different intracellular signals in primary thymocytes. *Proc. Natl. Acad. Sci. USA* 95: 8193–8198.
18. Naramura, M., H. K. Kole, R. J. Hu, and H. Gu. 1998. Altered thymic positive selection and intracellular signals in Cbl-deficient mice. *Proc. Natl. Acad. Sci. USA* 95: 15547–15552.
19. Sosinowski, T., N. Killeen, and A. Weiss. 2001. The Src-like adaptor protein downregulates the T cell receptor on $CD4^+CD8^+$ thymocytes and regulates positive selection. *Immunity* 15: 457–466.
20. Schaeffer, E. M., C. Broussard, J. Debnath, S. Anderson, D. W. McVicar, and P. L. Schwartzberg. 2000. Tec family kinases modulate thresholds for thymocyte development and selection. *J. Exp. Med.* 192: 987–1000.
21. Neilson, J. R., M. M. Winslow, E. M. Hur, and G. R. Crabtree. 2004. Calcineurin B1 is essential for positive but not negative selection during thymocyte development. *Immunity* 20: 255–266.
22. Swat, W., M. Dessing, A. Baron, P. Kisielow, and H. von Boehmer. 1992. Phenotypic changes accompanying positive selection of $CD4^+CD8^+$ thymocytes. *Eur. J. Immunol.* 22: 2367–2372.
23. Yamashita, I., T. Nagata, T. Tada, and T. Nakayama. 1993. CD69 cell surface expression identifies developing thymocytes which audition for T cell antigen receptor-mediated positive selection. *Int. Immunol.* 5: 1139–1150.
24. Azzam, H. S., A. Grinberg, K. Lui, H. Shen, E. W. Shores, and P. E. Love. 1998. CD5 expression is developmentally regulated by T cell receptor (TCR) signals and TCR avidity. *J. Exp. Med.* 188: 2301–2311.
25. Krutzik, P. O., and G. P. Nolan. 2003. Intracellular phospho-protein staining techniques for flow cytometry: monitoring single cell signaling events. *Cytometry A* 55: 61–70.
26. Priatel, J. J., S. J. Teh, N. A. Dower, J. C. Stone, and H. S. Teh. 2002. RasGRP1 transduces low-grade TCR signals which are critical for T cell development, homeostasis, and differentiation. *Immunity* 17: 617–627.
27. Marquez, M. E., W. Ellmeier, V. Sanchez-Guajardo, A. A. Freitas, O. Acuto, and V. Di Bartolo. 2005. CD8 T cell sensory adaptation dependent on TCR avidity for self-antigens. *J. Immunol.* 175: 7388–7397.
28. Illes, Z., H. Waldner, J. Reddy, A. C. Anderson, R. A. Sobel, and V. K. Kuchroo. 2007. Modulation of CD4 co-receptor limits spontaneous autoimmunity when high-affinity transgenic TCR specific for self-antigen is expressed on a genetically resistant background. *Int. Immunol.* 19: 1235–1248.
29. Maile, R., C. A. Siler, S. E. Kerry, K. E. Midkiff, E. J. Collins, and J. A. Frelinger. 2005. Peripheral "CD8 tuning" dynamically modulates the size and responsiveness of an antigen-specific T cell pool in vivo. *J. Immunol.* 174: 619–627.
30. Zhang, L., W. Fung-Leung, and R. G. Miller. 1995. Down-regulation of CD8 on mature antigen-reactive T cells as a mechanism of peripheral tolerance. *J. Immunol.* 155: 3464–3471.
31. Jameson, S. C., K. A. Hogquist, and M. J. Bevan. 1994. Specificity and flexibility in thymic selection. *Nature* 369: 750–752.
32. Wang, R., Y. Wang-Zhu, and H. Grey. 2002. Interactions between double positive thymocytes and high affinity ligands presented by cortical epithelial cells generate double negative thymocytes with T cell regulatory activity. *Proc. Natl. Acad. Sci. USA* 99: 2181–2186.

33. Rocha, B., and H. von Boehmer. 1991. Peripheral selection of the T cell repertoire. *Science* 251: 1225–1228.
34. Schonrich, G., U. Kalinke, F. Momburg, M. Malissen, A. M. Schmitt-Verhulst, B. Malissen, G. J. Hammerling, and B. Arnold. 1991. Down-regulation of T cell receptors on self-reactive T cells as a novel mechanism for extrathymic tolerance induction. *Cell* 65: 293–304.
35. Viret, C., and C. A. Janeway, Jr. 2003. Self-specific MHC class II-restricted $CD4^{-}CD8^{-}$ T cells that escape deletion and lack regulatory activity. *J. Immunol.* 170: 201–209.
36. Russell, J. H., P. Meleedy-Rey, D. E. McCulley, W. C. Sha, C. A. Nelson, and D. Y. Loh. 1990. Evidence for CD8-independent T cell maturation in transgenic mice. *J. Immunol.* 144: 3318–3325.
37. von Boehmer, H., J. Kirberg, and B. Rocha. 1991. An unusual lineage of alpha/beta T cells that contains autoreactive cells. *J. Exp. Med.* 174: 1001–1008.
38. Bruno, L., H. J. Fehling, and H. von Boehmer. 1996. The $\alpha\beta$ T cell receptor can replace the $\gamma\delta$ receptor in the development of $\gamma\delta$ lineage cells. *Immunity* 5: 343–352.
39. Posevitz, V., B. Arndt, T. Krieger, N. Warnecke, B. Schraven, and L. Simeoni. 2008. Regulation of T cell homeostasis by the transmembrane adaptor protein SIT. *J. Immunol.* 180: 1634–1642.
40. Hogquist, K. A. 2001. Signal strength in thymic selection and lineage commitment. *Curr. Opin. Immunol.* 13: 225–231.
41. Love, P. E., J. Lee, and E. W. Shores. 2000. Critical relationship between TCR signaling potential and TCR affinity during thymocyte selection. *J. Immunol.* 165: 3080–3087.
42. Shores, E. W., T. Tran, A. Grinberg, C. L. Sommers, H. Shen, and P. E. Love. 1997. Role of the multiple T cell receptor (TCR)-ζ chain signaling motifs in selection of the T cell repertoire. *J. Exp. Med.* 185: 893–900.
43. Yamazaki, T., H. Arase, S. Ono, H. Ohno, H. Watanabe, and T. Saito. 1997. A shift from negative to positive selection of autoreactive T cells by the reduced level of TCR signal in TCR-transgenic CD3 ζ-deficient mice. *J. Immunol.* 158: 1634–1640.
44. Watanabe, N., H. Arase, M. Onodera, P. S. Ohashi, and T. Saito. 2000. The quantity of TCR signal determines positive selection and lineage commitment of T cells. *J. Immunol.* 165: 6252–6261.
45. Kirchgessner, H., J. Dietrich, J. Scherer, P. Isomaki, V. Korinek, I. Hilgert, E. Bruyns, A. Leo, A. P. Cope, and B. Schraven. 2001. The transmembrane adaptor protein TRIM regulates T cell receptor (TCR) expression and TCR-mediated signaling via an association with the TCR ζ chain. *J. Exp. Med.* 193: 1269–1284.
46. Tarakhovsky, A., S. B. Kanner, J. Hombach, J. A. Ledbetter, W. Muller, N. Killeen, and K. Rajewsky. 1995. A role for CD5 in TCR-mediated signal transduction and thymocyte selection. *Science* 269: 535–537.
47. Azzam, H. S., J. B. DeJarnette, K. Huang, R. Emmons, C. S. Park, C. L. Sommers, D. El-Khoury, E. W. Shores, and P. E. Love. 2001. Fine tuning of TCR signaling by CD5. *J. Immunol.* 166: 5464–5472.
48. Bhandoola, A., R. Bosselut, Q. Yu, M. L. Cowan, L. Feigenbaum, P. E. Love, and A. Singer. 2002. CD5-mediated inhibition of TCR signaling during intrathymic selection and development does not require the CD5 extracellular domain. *Eur. J. Immunol.* 32: 1811–1817.
49. Smith, K., B. Seddon, M. A. Purbhoo, R. Zamoyska, A. G. Fisher, and M. Merkenschlager. 2001. Sensory adaptation in naive peripheral CD4 T cells. *J. Exp. Med.* 194: 1253–1261.
50. Neel, B. G., H. Gu, and L. Pao. 2003. The "Shp"ing news: SH2 domain-containing tyrosine phosphatases in cell signaling. *Trends Biochem. Sci.* 28: 284–293.
51. Zhu, M., O. Granillo, R. Wen, K. Yang, X. Dai, D. Wang, and W. Zhang. 2005. Negative regulation of lymphocyte activation by the adaptor protein LAX. *J. Immunol.* 174: 5612–5619.
52. Simeoni, L., J. A. Lindquist, M. Smida, V. Witte, B. Arndt, and B. Schraven. 2008. Control of lymphocyte development and activation by negative regulatory transmembrane adapter proteins. *Immunol. Rev.* 224: 215–228.

Appendix 14

Adenosine regulates CD8 T-cell priming by inhibition of membrane-proximal T-cell receptor signalling

Linnemann C., Schildberg F.A., Schurich A., Diehl L., Hegenbarth S.I., Endl E., Lacher S., Müller C.E., Frey J., **Simeoni L.**, Schraven B., Stabenow D., and Knolle P.A. (2009) *Immunology*. 128:e728-737.

Immunology
The Journal of cells, molecules, systems and technologies

British Society for immunology

IMMUNOLOGY ORIGINAL ARTICLE

Adenosine regulates CD8 T-cell priming by inhibition of membrane-proximal T-cell receptor signalling

Carsten Linnemann,[1,*] Frank A. Schildberg,[1,*] Anna Schurich,[1,*] Linda Diehl,[1] Silke I. Hegenbarth,[1] Elmar Endl,[1] Svenja Lacher,[2] Christa E. Müller,[2] Jürgen Frey,[3] Luca Simeoni,[4] Burkhart Schraven,[4] Dirk Stabenow[1] and Percy A. Knolle[1]

[1]*Institute for Molecular Medicine and Experimental Immunology, Friedrich-Wilhelms-University Bonn, Bonn,* [2]*Institute for Pharmaceutical Chemistry, Friedrich-Wilhelms-University Bonn, Bonn,* [3]*Biochemistry Unit II, University Bielefeld, Bielefeld and* [4]*Institute of Molecular and Clinical Immunology, Otto-von-Guericke-University, Magdeburg, Germany*

doi:10.1111/j.1365-2567.2009.03075.x
Received 11 July 2008; revised 5 November 2008; accepted 29 January 2009.
*These authors contributed equally to this work.
Correspondence: P. A. Knolle, Institute for Molecular Medicine and Experimental Immunology, Friedrich-Wilhelms-University Bonn, Sigmund-Freud-Strasse 25, 53105 Bonn, Germany.
Email: Percy.Knolle@ukb.uni-bonn.de
Senior author: Percy A. Knolle

Summary

Adenosine is a well-described anti-inflammatory modulator of immune responses within peripheral tissues. Extracellular adenosine accumulates in inflamed and damaged tissues and inhibits the effector functions of various immune cell populations, including CD8 T cells. However, it remains unclear whether extracellular adenosine also regulates the initial activation of naïve CD8 T cells by professional and semi-professional antigen-presenting cells, which determines their differentiation into effector or tolerant CD8 T cells, respectively. We show that adenosine inhibited the initial activation of murine naïve CD8 T cells after αCD3/CD28-mediated stimulation. Adenosine caused inhibition of activation, cytokine production, metabolic activity, proliferation and ultimately effector differentiation of naïve CD8 T cells. Remarkably, adenosine interfered efficiently with CD8 T-cell priming by professional antigen-presenting cells (dendritic cells) and semi-professional antigen-presenting cells (liver sinusoidal endothelial cells). Further analysis of the underlying mechanisms demonstrated that adenosine prevented rapid tyrosine phosphorylation of the key kinase ZAP-70 as well as Akt and ERK1/2 in naïve αCD3/CD28-stimulated CD8 cells. Consequently, αCD3/CD28-induced calcium-influx into CD8 cells was reduced by exposure to adenosine. Our results support the notion that extracellular adenosine controls membrane-proximal T-cell receptor signalling and thereby also differentiation of naïve CD8 T cells. These data raise the possibility that extracellular adenosine has a physiological role in the regulation of CD8 T-cell priming and differentiation in peripheral organs.

Keywords: cell activation; signal transduction; T-cell receptor; T cells

Introduction

T cells exert their effector function in peripheral tissues where they contribute to the control of viral or bacterial pathogens.[1] A balanced control of immune responses within peripheral tissues, however, is necessary to avoid over-reactive immunity that may lead to tissue damage and loss of organ function. Likewise, sufficient strength of immunity has to be maintained to contain and eliminate infectious micro-organisms. To control inflammatory reactions in peripheral tissues numerous endogenous anti-inflammatory factors have been described, such as lipocortin-1,[2] lipoxins[3] and protectins.[4] Extracellular adenosine is a further well-described inflammatory modulator of immune responses. Inflamed and damaged tissues are characterized by high extracellular adenosine levels induced by disruption of the local microcirculation and subsequent onset of hypoxia.[5] Hypoxia induces intracellular adenosine triphosphate (ATP) degradation, leading to an increase in adenosine-5′-monophosphate (AMP) and adenosine concentrations in cells.[6] The accumulation of intracellular adenosine is further increased by hypoxia-induced inhibition of adenosine kinase.[7] Accumulated adenosine is then released into the extracellular space.[8] Additionally, a hypoxia-induced increase in the expression of the membrane-bound enzymes ecto-nucleoside triphosphate diphosphohydrolase (NTPDase1, apyrase, CD39) and ecto-5′-nucleotidase (CD73) leads to dephosphorylation of adenine nucleotides to adenosine,[9,10] which further increases the extracellular adenosine concentration.

Please cite this article in press as: Linnemann C. *et al.* Adenosine regulates CD8 T-cell priming by inhibition of membrane-proximal T-cell receptor signalling, Immunology (2009) doi: 10.1111/j.1365-2567.2009.03075.x

Adenosine itself protects tissues against damage through different mechanisms initiated by inflammation.[11,12] It stimulates anti-inflammatory signalling pathways, such as activation of cyclo-oxygenase-2 (COX-2).[13,14] A direct adenosine-mediated interference with immune reactions in the tissue occurs by activation of adenosine receptors on various immune cells. Among the family of adenosine receptors, the importance of the adenosine A_{2A} receptor for the regulation of T cells has been recognized as most important. Various T-cell receptor (TCR) controlled effector functions are regulated by adenosine.[15–17] Based on these findings Sitkovsky and Ohta postulated a so-called '2-Danger-signal' model.[18] They suggested that a first signal indicates danger caused by the presence of pathogens and leads to the activation of immune cells and thereby evokes defensive effector functions. A second signal, i.e. adenosine, indicates danger from overactive immune responses and triggers down-regulation of pro-inflammatory activities of the immune system to prevent excessive collateral damage and destruction of normal tissues. These reports clearly illustrated the potent activity of adenosine to restrain the effector function of activated T cells.

It was recently reported that naïve T cells migrate through non-lymphoid organs[19] and that priming of CD8 and CD4 T-cell responses can occur outside the secondary lymphatic tissue by professional and non-professional antigen-presenting cells (APC).[20,21] Although extensive investigations on the regulation of effector or memory T-cell functions by adenosine have been published,[16,17,22] so far no clear characterization of the direct effect of adenosine on naïve murine CD8 T cells has been reported. Therefore, we characterized the influence of adenosine on naïve CD8 T-cell priming and further elucidated the molecular mechanisms underlying adenosine-induced inhibition of TCR-triggered T-cell activation.

Materials and methods

Mice and reagents

All animal experiments were performed in accordance with German law regarding the protection of animals and complied with institution guidelines and the principles of laboratory animal care (NIH publication 86-23, revised 1985). C57BL/6 mice were purchased from Elevage Janvier (Strasbourg, France). H2-$K^{bSIINFEKL}$-restricted TCR-transgenic animals (OT-I), and H2-K^{b}-restricted DesTCR mice (recognizing three endogenous peptides derived from C57BL/6 background) were bred under specific pathogen-free conditions to the FELASA guidelines in the central animal facility of the University Hospital Bonn. OT-I mice were injected with 300 μg αNK1.1 antibody (clone PK136) 2 days before killing.

Antibodies for flow cytometry and enzyme-linked immunosorbent assay (ELISA) were purchased from BD Bioscience (Heidelberg, Germany) or eBioscience (San Diego, CA). αKi67 antibody was kindly provided by Dr Elmar Endl (University Hospital, Bonn, Germany). Phospho-specific antibodies for Western blot analysis were obtained from Cell Signaling (Danvers, MA) and anti-β-actin antibody from Sigma (Deisenhofen, Germany). Adenosine, dibutyryl-cAMP and Hoechst-33258 were purchased from Sigma. 6-NBDG, Fluo-4, carboxyfluorescein succinimidyl ester (CFSE), αCD3/CD28 beads and ionomycin were obtained from Invitrogen (Karlsruhe, Germany). Streptavidin was bought at Dianova (Hamburg, Germany) and antibody-coated beads for magnetic cell separation were obtained from Miltenyi Biotec (Bergisch Gladbach, Germany). CGS21680 was provided by C. Müller (Bonn). The cAMP ELISA was purchased from R&D Systems, Minneapolis, MN and used according to the manufacturer's protocol.

Cell isolation

Highly pure liver sinusoidal endothelial cell (LSEC) isolation has been described by our group previously.[20] For separation of splenic DC, spleens were digested with 0·05% collagenase solution and $CD11c^{+}$ cells were isolated by immunomagnetic separation with αCD11c-labelled magnetic antibody cell sorting (MACS) microbeads. Splenic CD8 T cells were isolated by positive (αCD8 MACS beads) or negative selection.

Flow cytometry

Between 1×10^3 and 1×10^6 cells were stained with specific antibodies and 10 μg/ml Fc-Block (clone 2.4G2) for 15 min on ice. For staining of intracellular antigens cells were fixed with 4% [weight/volume (w/v)] paraformaldehyde in phosphate-buffered saline (PBS) for 10 min at room temperature. Afterwards cells were permeabilized with 0·5% (w/v) saponin in PBS for 15 min on ice, followed by 30 min incubation with antibody on ice and then analysed. Dead cells were excluded by Hoechst-33258 staining and total cell numbers were calculated using fluorescent labelled microbeads (BD Bioscience) as follows: $(beads_{total} \times cells_{sample})/beads_{sample}$. Acquisition and analysis was conducted with fluorescence-activated cell sorting CantoII (BD Bioscience) and FLOWJO software (Tree Star Inc, Ashland, OR). For analysis of T-cell proliferation, naïve freshly isolated CD8 T cells were labelled for 20 min with CFSE (1 μM) (Invitrogen) and washed twice with PBS. After 3 days, proliferation was assessed by flow cytometric analysis of CFSE dilution in Hoechst-$33258^{negative}$ CD8 cells. Cell division index, which indicates the average number of cell divisions undergone by the responding T cells, was calculated from $Hoechst^{negative}$

$CFSE^+$ CD8 cells using FLOWJO software according to the manufacturer's protocol.

Analysis of glucose metabolism activity

After staining of 10^6 T cells/ml with Hoechst-33258 a baseline was recorded for 10 seconds with a flow cytometer, 30 μM 6-NBDG was added and fluorescence was measured for a further 60 seconds. αCD3/CD28-stimulated CD8 T cells were activated for 24 hr, living cells were regained with gradient centrifugation (LSM 1077 Lymphocyte; PAA, Pasching, Germany) and 1×10^5 cells were seeded without stimulation in 96-well plate in RPMI-1640 medium containing 0·5% (w/v) bovine serum albumin over night. Subsequently, the supernatant was analysed for lactate levels with a 'Lac' reaction kit (Randox Laboratories, Antrim, UK) according to the manufacturer's guideline.

Western blot analysis

Negatively selected OT-I/$RAG^{-/-}$ CD8 T cells were incubated with biotinylated αCD3/CD28 antibodies and cells were activated with 40 μg/ml streptavidin, either alone or after 5 min, before incubation with 1 mM adenosine. The reaction was stopped by adding protein sample buffer [0·58 M sucrose, 4% (w/v) sodium dodecyl sulphate, 0·04% (v/v) bromphenol blue, 62·5 mM Tris–HCl pH 6·8]. Equal amounts of protein were used for sodium dodecyl sulphate–polyacrylamide gel electrophoresis (SE 600 Ruby; Amersham Biosciences, Piscataway, NJ). Proteins were blotted on a polyvinlyidene difluoride membrane (Hybond P; Amersham Biosciences) with a semi-dry transfer unit (TE77 ECL; Amersham Biosciences) and protein phosphorylation was detected with phospho-specific antibodies and horseradish peroxidase-conjugated secondary antibodies (Santa Cruz Biotechnology Inc, Santa Cruz, CA). Blots were developed using a chemiluminescent detection kit (AppliChem, Darmstadt, Germany).

Determination of calcium influx

Negatively selected CD8 T cells were incubated for 45 min at 37° with phenol-red free RPMI-1640 medium containing 10% (v/v) fetal bovine serum and 3·5 μM Fluo-4 dye. Cells were washed twice and again incubated for 45 min at 37° with phenol-red-free RPMI-1640 medium/10% (v/v) fetal bovine serum. T cells were incubated with biotinylated αCD3/CD28 antibodies for 15 min on ice, washed and baseline fluorescence was recorded. Activation was initiated by adding 40 μg/ml streptavidin immediately or after pretreatment with 1 mM adenosine. Afterwards, fluorescence intensity was recorded for a further 390 seconds. Control stimulation was performed with 1·5 μM ionomycin for each sample.

Statistics

Data are shown as mean ± standard error of the mean (SEM). For statistical analysis a Student's *t*-test was used. *P*-values $< 0{\cdot}05$ were considered significant.

Results

Adenosine inhibits αCD3/CD28-induced activation of naïve CD8 T cells

As adenosine is known to modulate the function of various immune cell populations, we used αCD3/CD28-coated microbeads as 'artificial' APC to unequivocally investigate the effects of extracellular adenosine on activation of naïve CD8 T cells. Increased expression of activation markers, such as CD25 and CD44, within 24 hr after αCD3/CD28 stimulation was prevented by incubation of naïve CD8 T cells with adenosine at high (1 mM) but not at low (0·1 mM) concentrations (Fig. 1a). As cytokine production is crucial for CD8 T-cell activation, expansion and differentiation we next examined whether adenosine influenced interleukin-2 (IL-2) and interferon-γ (IFN-γ) expression. T-cell activation in the presence of 1 mM adenosine was followed by the absence of detectable IL-2-release (Fig. 1b) and by a dramatic reduction in IFN-γ-producing T cells (Fig. 1c). Typically, T-cell activation is accompanied by increased metabolic function.[23] We observed that naïve CD8 T cells activated in the presence of adenosine showed a reduced increase in cell size compared with untreated T cells (Fig. 1d) or naïve T cells (data not shown). Furthermore, adenosine-exposed T cells also showed reduced glucose uptake and undetectable levels of lactate production over the following 24 hr (Fig. 1e,f), indicating that adenosine markedly influenced metabolic activity. It is important to mention that adenosine was removed before glucose uptake or lactate production by T cells was determined.

We analysed the influence of adenosine on consecutive events such as proliferation and expansion of T cells. A complete inhibition of T-cell proliferation after 48 hr in the presence of 1 mM adenosine during the initial αCD3/CD28-stimulation was observed (Fig. 2a). As expected the loss of proliferation correlated with a decreased percentage of divided cells as well as a reduced number of cell divisions and total cell numbers (Fig. 2b). To elucidate whether adenosine-induced inhibition of T-cell proliferation was caused by inhibition of entry into the cell cycle or by blockade within the cell cycle, we determined the intracellular levels of Ki67 in αCD3/CD28-stimulated CD8 T cells. We observed a remarkable reduction in the percentage of Ki67-positive T cells after activation in the presence of adenosine (Fig. 2c). Therefore we concluded that T cells did not enter the cell cycle. Inhibition of T-cell proliferation depended on the continuous presence

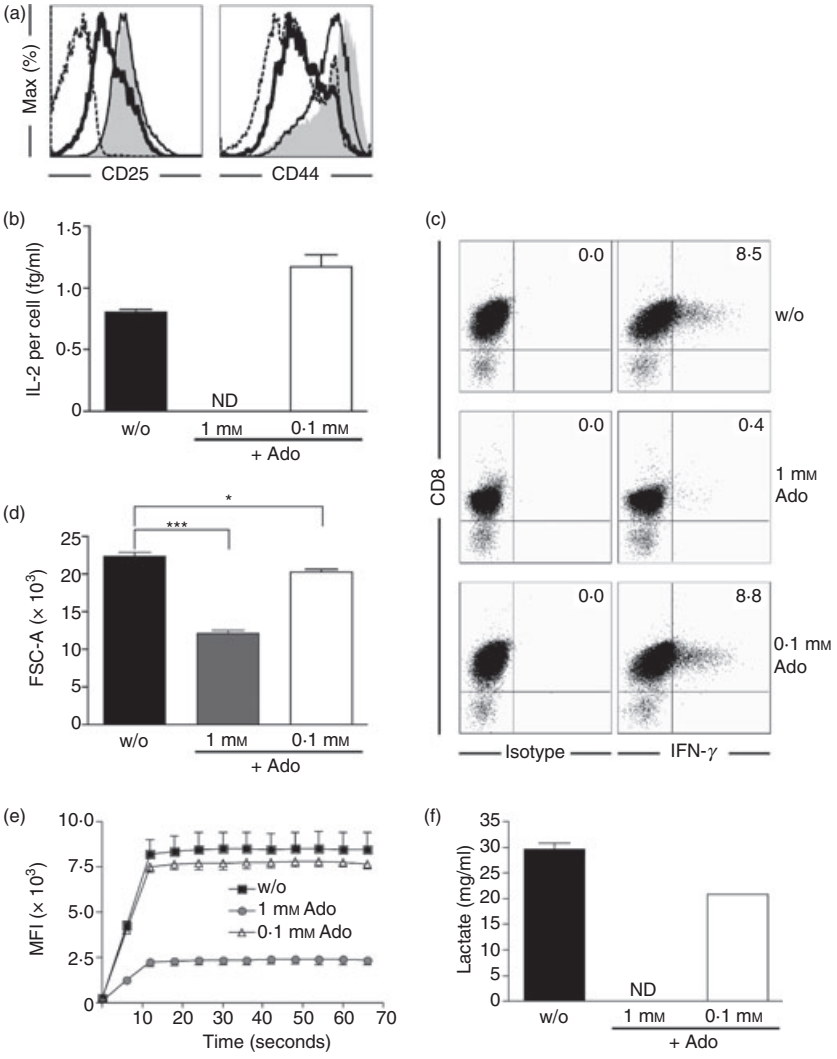

Figure 1. Adenosine inhibits early activation processes in naïve CD8 T cells after αCD3/CD28 activation. Naïve CD8 T cells were activated in the absence or presence of adenosine with αCD3/CD28 beads for 24 hr. (a) Phenotypic analysis of activation markers on CD8 T cells by flow cytometry (shaded: no adenosine; thick black line: 1 mM adenosine; black line: 0·1 mM adenosine; dashed: unstimulated). (b) Interleukin-2 (IL-2) concentration was determined in cell culture supernatants after 24 hr by enzyme-linked immunosorbent assay and calculated to the numbers of viable T cells at the end of the experiment. (c) Intracellular staining for interferon-γ (IFN-γ) in CD8 T cells after 24 hr of stimulation. (d) Flow cytometric analysis of CD8 T-cell size at 24 hr post-activation. (e) Uptake of the fluorescently labelled glucose analogue 6-NBDG (30 μM) was determined by flow cytometry in living CD8 T cells. (f) Lactate release into the cell culture supernatant over a period of 16 hr was determined from 10^5 CD8 T cells isolated at 24 hr post-activation with αCD3/CD28 beads in the absence or presence of adenosine. $^*P < 0{\cdot}05$, $^{***}P < 0{\cdot}001$.

of high concentrations of adenosine, because T cells regained the capacity to proliferate at later time-points if adenosine was not further supplemented (data not shown). The striking reduction in the absolute number of living cells in the presence of adenosine after 48 hr compared with the number initially added into the culture is probably related to increased apoptotic cell death. The induction of apoptosis is a known feature of various nucleosides including adenosine[24] and was also observed in our experiments (data not shown).

To analyse the impact of adenosine on T-cell differentiation we restimulated adenosine-exposed T cells after 72 hr of αCD3/CD28 stimulation. Notably, equal numbers of living T cells were subjected to αCD3 restimulation for 24 hr in the absence of adenosine and effector cytokine levels were determined in the cell culture supernatant by ELISA. In line with our previous observations, CD8 T cells activated in the presence of adenosine (1 mM) showed reduced capacity to produce IFN-γ and IL-2 (Fig. 2d). This indicates a failure of T-cell differentiation into effector T cells. However, CD8 T cells initially exposed to low adenosine concentrations showed a slight increase in IFN-γ production, which may be related to a less exhaustive state of the cells. Collectively, these experiments reveal a potent inhibitory function of high concentrations of adenosine on the priming and differentiation of naïve CD8 T cells.

Adenosine blocks the priming of naïve CD8 T cells by APC

Initial stimulation of naïve CD8 T cells by professional APC, such as DC, or by organ-resident APC, such as LSEC, determines differentiation into effector or tolerant CD8 T cells, respectively.[20,25] This process of tolerogenic or immunogenic stimulation of naïve CD8 T cells is driven by active signalling through either costimulatory or coinhibitory molecules. We investigated whether adenosine modulated such immunogenic as well as tolerogenic T-cell priming. We cocultured H2-K^b-restricted DesTCR

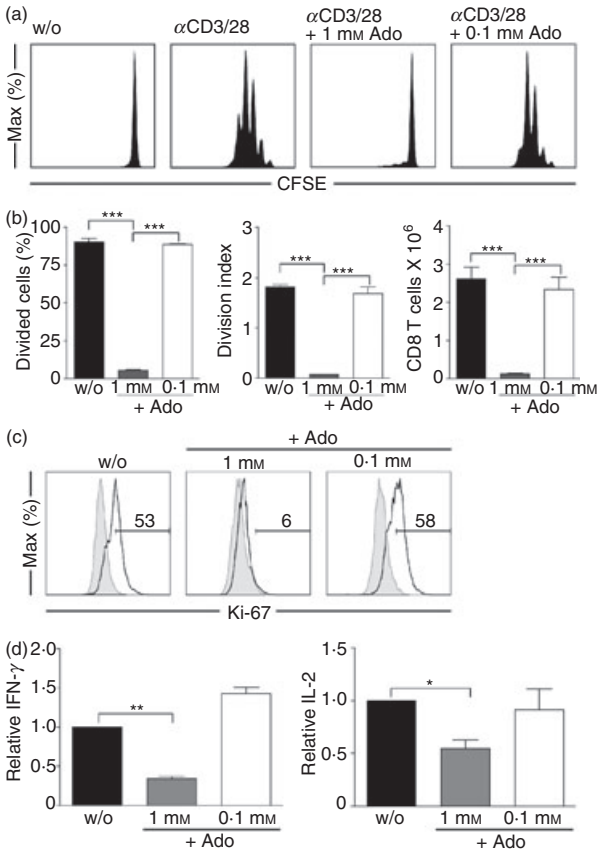

Figure 2. Adenosine inhibits expansion and effector differentiation of naïve CD8 T cells after αCD3/CD28 activation. Naïve carboxyfluorescein succinimidyl ester (CFSE)-loaded CD8 T cells were activated with αCD3/CD28 beads in the absence or presence of adenosine. (a) After 48 hr proliferation was analysed by flow cytometry. (b) Percentage of divided cells, division index and total number of living CD8 cells. (c) Intracellular staining of CD8 T cells for Ki-67 protein after stimulation with αCD3/CD28 beads in the absence or presence of adenosine for 48 hr (shaded: no adenosine; black line: 1 mM adenosine). (d) Restimulation of living CD8 T cells 72 hr post-activation with αCD3 in adenosine-free culture media. After 16 hr the cell culture supernatant was assessed for interferon-γ (IFN-γ) and interleukin-2 (IL-2) concentrations. $^{*}P < 0{\cdot}05$, $^{**}P < 0{\cdot}01$, $^{***}P < 0{\cdot}001$.

transgenic CD8 T cells with antigen-presenting splenic H2-K^{b+} DC or H2-K^{b+} LSEC in the presence or absence of adenosine. Expression of activation markers on CD8 T cells was analysed after 24 hr and proliferation after 48 hr. Similar to the results of αCD3/CD28 stimulation we observed reduced T-cell expression of CD25 and CD44 in the presence of a high concentration of adenosine after priming by antigen-presenting DC and LSEC (Fig. 3a). After 48 hr a clear reduction in APC-induced proliferation of T cells was observed in the presence of adenosine (Fig. 3b). Detailed analysis revealed that the percentage of divided cells, division index and total cell numbers of living CD8 T cells were significantly reduced after 48 hr, regardless of the stimulating APC (Fig. 3c). Compared with αCD3/CD28 stimulation, the inhibitory effects of adenosine were less pronounced, which may have been caused by more rapid degradation of adenosine by coculture of APC and T cells. We next investigated whether adenosine also affected the differentiation into effector CD8 T cells. Indeed, T cells primed by DC in the presence of high concentrations of adenosine failed to express IFN-γ after restimulation through the TCR (Fig. 3d). However, similar experiments to directly reveal adenosine-mediated inhibition of tolerance induction also demonstrated lack of IFN-γ expression (data not shown) but were not conclusive because tolerant T cells are already non-responsive to TCR stimulation.[20,26] Nevertheless, as induction of tolerance by LSEC is an active process[26] our observation that adenosine inhibited the initial tolerogenic priming of T cells indicates control of adenosine on tolerance induction. Taken together, these results support the notion that adenosine not only controlled priming by APC but also prevented effector cell differentiation in T cells.

Inhibition of membrane-proximal signalling events in TCR/CD28-induced naïve CD8 T-cell activation

It was reported that adenosine increased intracellular cAMP in T cells.[15,17] We also detected an increase in cAMP production in naïve CD8 T cells within 5 min after exposure to adenosine (Fig. 4a). To further investigate whether increased levels of cAMP influenced T-cell stimulation, we incubated αCD3/CD28-stimulated naïve CD8 T cells with a membrane-permeable cAMP analogue. The addition of dibutyryl-cAMP (db-cAMP) was associated with a decrease in CD25 and CD44 expression (Fig. 4b) and a reduction in IFN-γ expression in αCD3/CD28-stimulated naïve CD8 T cells (Fig. 4c). Moreover, in response to the addition of db-cAMP the proliferation of αCD3/CD28-stimulated naïve CD8 T cells was dramatically reduced (Fig. 4d). Consistent with a dominant effect of the A_{2A}-receptor on T-cell function and its described capacity to induce cAMP in T cells we found that the A_{2A}-receptor-specific agonist CGS21680 impeded the αCD3/CD28-induced activation of naïve CD8 T cells (Fig. 4e). These results suggested that cAMP generation induced by adenosine interfered with signalling events in T-cell activation. We therefore aimed to elucidate these events in more detail.

Naïve CD8 T-cell stimulation requires simultaneous activation of TCR- and CD28-signalling pathways to achieve full activation. We assessed classical signalling events related to TCR/CD28 signalling. As cAMP has been reported to inhibit TCR signalling already at the level of the TCR–CD3 complex,[27] we investigated the effects of adenosine on tyrosine phosphorylation of membrane-proximal signalling molecules. Adenosine treatment of

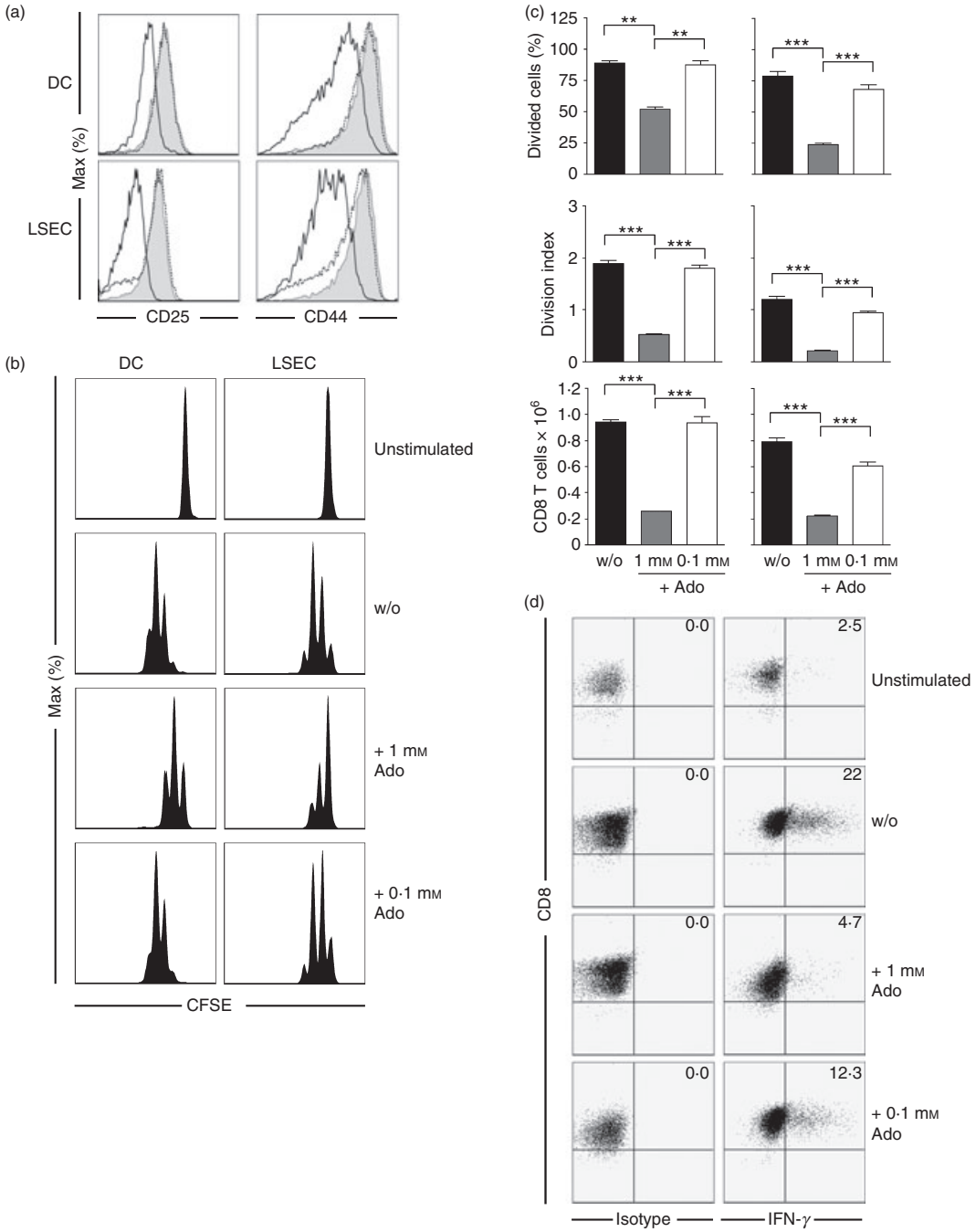

Figure 3. Adenosine blocks tolerogenic and immunogenic priming of naïve CD8 T cells. Antigen-presenting liver sinusoidal endothelial cells (LSEC; 10^6) or splenic dendritic cells (DC; 5×10^5) were cultured with 10^6 CD8 DesTCR transgenic T cells in the absence or presence of adenosine. (a) Flow cytometric analysis of activation markers after 24 hr (shaded: no adenosine; black line: 1 mM adenosine; dashed line: 0·1 mM adenosine) and (b) proliferation of DesTCR T cells after 48 hr of stimulation. (c) Percentage of divided cells, division index and total number of living DesTCR cells after 48 hr. (d) Ovalbumin (OVA) -loaded splenic DCs (5×10^5) were cultured with 10^6 CD8 OT-I T-cell receptor transgenic T cells in the absence or presence of adenosine for 48 hr. After 24 hr adenosine in indicated concentrations was added again. After 48 hr living CD8 T cells were restimulated with αCD3 in adenosine-free culture media for 4 hr and stained intracellularly for interferon-γ (IFN-γ). $^{**}P < 0{\cdot}01$, $^{***}P < 0{\cdot}001$.

naïve CD8 T cells clearly reduced tyrosine phosphorylation of ZAP-70 within 5 min after αCD3/CD28 stimulation (Fig. 5a). This is of particular relevance as ZAP-70 is a key player in TCR signalling. Reduced levels of tyrosine phosphorylation were also observed for Akt and ERK1/2 (Fig. 5a). We further confirmed the interception of

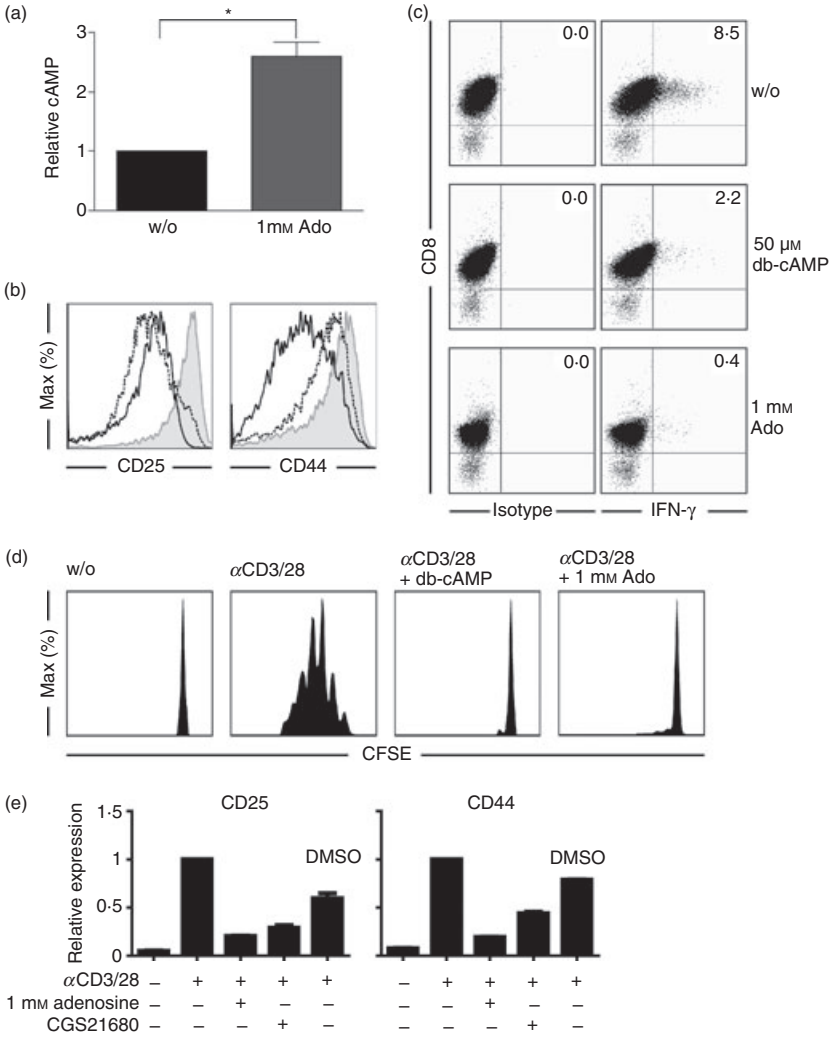

Figure 4. Increase in intracellular cAMP levels interferes with T-cell activation. (a) 4×106 naïve CD8 T cells were treated with adenosine (1 mM) for 5 min and intracellular cAMP levels were analysed. (b) T cells were activated with αCD3/CD28 beads in the absence or presence of adenosine or db-cAMP. After 24 hr, expression levels of CD25 and CD44 on living CD8 T cells were analysed by flow cytometry (shaded: no adenosine; black line: 1 mM adenosine; dashed line: 50 μM db-cAMP) (c) T cells from (b) were stained intracellularly for interferon-γ (IFN-γ). (d) Naïve carboxyfluorescein succinimidyl ester (CFSE) -loaded 10^6 CD8 T cells were activated with αCD3/CD28 beads in the presence of db-cAMP (50 μM). After 48 hr CFSE profiles of living CD8 cells were analysed by flow cytometry. (e) Naïve CD8 T cells were treated with adenosine (1 mM) or CGS21680 (100 μM) and activated with αCD3/CD28 beads for 24 hr. Activation markers (CD25, CD44 and PD1) on CD8 T cells were analysed by flow cytometry and are shown as relative expression levels compared with untreated cells. $^*P < 0{\cdot}05$.

adenosine with proximal TCR signalling by measuring calcium influx. Adenosine pre-treatment for 5 min significantly reduced calcium influx into αCD3/CD28-stimulated naïve CD8 T cells (Fig. 5b). Taken together, these results suggest that adenosine similar to cAMP interferes with membrane-proximal TCR signalling events.

Discussion

Several reports have shown, that adenosine most efficiently controls the effector functions of various immune cells including fully differentiated effector CD8 T cells.[15–17,22,28] This led to the well-established '2-Danger-signal' model of Sitkovsky and Ohta, in which adenosine acts as a modulator of immune responses in peripheral tissues.[12,18] Here, we investigate the early and membrane-proximal mechanisms mediating the effects of extracellular adenosine on the priming of naïve CD8 T cells.

We provide evidence that adenosine suppressed the activation of naïve CD8 T cells by inhibiting TCR signalling events. We observed reduced calcium influx as well as decreased tyrosine phosphorylation of signalling molecules like ERK1/2 and Akt after TCR activation. Moreover, tyrosine phosphorylation of the TCR key kinase ZAP-70 was strongly reduced in the presence of adenosine. This argues for a membrane-proximal inhibition of TCR signalling by adenosine. We assume that reduced ZAP-70 tyrosine phosphorylation is a consequence of a lack of Lck activity, which is required for recruitment of ZAP-70 to the CD3/TCR signal transduction complex.[29] Tyrosine kinase activity of Lck is under tight control of the kinase Csk.[30,31] Mustelin and Tasken have described a model for the regulation of Lck function by Csk. In this model, phosphorylation of Lck by Csk is a downstream event initiated by cAMP-dependent activation of the protein kinase A (PKA) type I.[32] Indeed, we also observed induction of increased intracellular cAMP levels in CD8 T cells after adenosine exposure. Moreover, db-cAMP treatment of naïve CD8 T cells before αCD3/CD28 stimulation also inhibited ZAP-70 phosphorylation. Therefore, our experimental data support the notion that this mechanism contributes to early adenosine-induced inhibition of

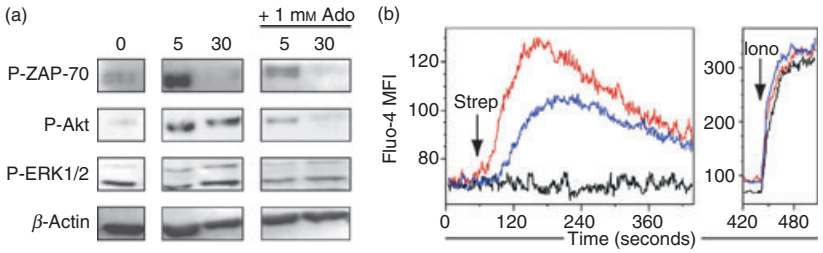

Figure 5. Adenosine-induced inhibition of membrane-proximal signalling events in T-cell receptor (TCR)/CD28-induced naïve CD8 T-cell activation. (a) Naïve OT-I/RAG$^{-/-}$ CD8 T cells were stimulated with cross-linked αCD3/CD28 antibodies for the times indicated immediately or after 5 min pre-incubation with 1 mM adenosine. Afterwards, T cells were lysed and specific protein-phosphorylation was determined. (b) Flow cytometric analysis of calcium influx in fluo-4-loaded naïve CD8 T cells after stimulation with streptavidin cross-linked αCD3/CD28 antibodies (red - line: αCD3/CD28 / no adenosine; blue line: αCD3/CD28/adenosine (1 mM); black line: isotype control). Equal loading with Fluo-4 was controlled by control stimulation with 1·5 μM ionomycin.

membrane-proximal TCR signalling. Nevertheless, it remains to be determined if other PKA-dependent mechanisms also play a role, like inhibition of Raf, phospholipase C-γ or activation of cAMP-induced transcriptional repressor ICER.[33–38] It is likely that membrane-proximal inhibition of TCR signalling by adenosine is not restricted to naïve CD8 T cells but is also operative in fully differentiated effector T cells.

We and others observed cAMP induction in CD8 T cells after adenosine exposure. Coupling to an intracellular increase in cAMP formation is a known feature of two members of the adenosine receptor family, namely adenosine A_{2A} and A_{2B} receptors.[15–17,39] Most likely, the observed cAMP induction is related to activation of the adenosine A_{2A} receptor, which has been reported to mediate the efficient regulation of T-cell functions.[15–18,40] Support for an adenosine A_{2A} receptor-dependent inhibition of T-cell activity in our experiments came from observations that the A_{2A} receptor CGS impeded activation of naïve CD8 T cells and that naïve CD8 T cells derived from adenosine A_{2B} receptor knockout mice showed similar adenosine-induced inhibition of T-cell activity after αCD3/CD28 stimulation (data not shown). Additionally, in line with previous reports, we measured reduced T-cell activation after αCD3/CD28 stimulation in the presence of 5′-(*N*-ethylcarboxamido) adenosine (NECA) (data not shown), which is a known potent agonist of adenosine A_1, A_{2A} and A_3 receptors, and a weaker agonist at the A_{2B} receptor subtype, but inactive at P2 receptor subtypes, so excluding a contribution by P2 receptors.[41,42] Inhibitory effects were observed for concentrations of 1 mM and higher (data not shown) but not of 0·1 mM adenosine. Measuring exact concentrations of adenosine in tissue is difficult so it is not known what concentrations of adenosine are actually encountered by T cells in the tissue, and hence we cannot compare these concentrations with tissue levels. However, we hypothesize that the adenosine concentrations used in our studies are likely to be present in damaged tissue *in vivo*.

Taken together, these results strongly suggest that inhibition of membrane-proximal signalling in naïve CD8 T cells was mediated through the adenosine A_{2A} receptor. The prominent role of adenosine A_{2A} receptors in controlling immune responses within peripheral tissues has been emphasized unequivocally in several *in vivo* studies using adenosine A_{2A} receptor knockout animals. In particular, adenosine A_{2A} receptors were shown to restrict anti-tumour effector functions of tumour-specific CD8 T cells giving rise to the paradox of the parallel existence of tumour and tumour-specific CD8 T cells.[39] Along the same line, A_{2A} receptor knockout animals develop uncontrolled immunity even after weak stimulation,[43,44] Furthermore, A_{2A} receptors also control IL-2 secretion and IL-2-driven expansion of effector CD8 T cells *in vivo*[45] and the colitogenic function of adoptively transferred CD45RB^{hi} T cells.[46]

Here, we report experiments suggesting that adenosine has yet another function in controlling immune responses, i.e. the prevention of priming of naïve CD8 T cells. Under defined *in vitro* conditions we observed that CD8 T-cell priming by professional antigen-presenting DC was inhibited by adenosine. While we doubt that the high concentrations of adenosine required for the inhibition of T-cell priming can be reached in secondary lymphatic tissue, we would assume that adenosine levels in peripheral tissues are sufficient to achieve regulation. Migration through non-lymphoid organs and priming of naïve CD8 T cells has been reported to occur outside the lymphatic system within the bone marrow by DC or within the liver by semi-professional LSEC or hepatocytes, giving rise to fully activated effector or tolerant CD8 T cells, respectively.[19–21,47] As tolerance induction in peripheral tissues is often associated with clonal deletion of potentially autoreactive CD8 T cells,[48] the presence of high concentrations of adenosine in peripheral tissue in response to damage or infection may prevent inadvertent deletion of rare precursor CD8 T cells with specificity for infectious micro-organisms. Moreover, adenosine-

mediated inhibition of tolerogenic T-cell-priming by antigen-presenting LSEC, which involves initial stimulation and expansion of naïve CD8 T cells,[26] may allow for the prevention of accidental tolerance induction towards circulating antigens during situations where increased adenosine concentrations are caused by local infection in the liver. Similar results were obtained recently for CD4 T cells, where adenosine was shown to promote long-term anergy and generation of regulatory T cells.[49] Furthermore, activation of A_{2A} receptors has been shown to attenuate T-cell-mediated allograft rejection *in vivo*,[50] which supports our findings that adenosine is operational in the restriction of differentiation of naïve CD8 T cells.

Taken together, our results provide evidence for the inhibition of proximal TCR signalling events by adenosine, which prevents priming and differentiation of naïve CD8 T cells and presumably is also operative in restricting effector functions of already activated CD8 T cells. Our data raise the question of the physiological relevance for inhibition of naïve CD8 T-cell activation by adenosine. Although our *in vitro* findings need to be examined in appropriate *in vivo* models, our data suggest a potential new function for adenosine in the prevention of peripheral CD8 T-cell priming in situations of local tissue damage or infection.

Acknowledgements

The authors are grateful for the technical support of the House for Experimental Therapy (HET) of the Medical Faculty of Bonn University and the Flow Cytometry Core Facility at the Institute for Molecular Medicine and Experimental Immunology. This work was supported by the DFG to P.A.K. (GRK 804, SFB 704) and the Studienstiftung des deutschen Volkes to C.L. and F.A.S.

Disclosures

None.

References

1 Harty JT, Tvinnereim AR, White DW. CD8+ T cell effector mechanisms in resistance to infection. *Annu Rev Immunol* 2000; **18**:275–308.

2 Perretti M, Flower RJ. Modulation of IL-1-induced neutrophil migration by dexamethasone and lipocortin 1. *J Immunol* 1993; **150**:992–9.

3 Ariel A, Chiang N, Arita M, Petasis NA, Serhan CN. Aspirin-triggered lipoxin A4 and B4 analogs block extracellular signal-regulated kinase-dependent TNF-alpha secretion from human T cells. *J Immunol* 2003; **170**:6266–72.

4 Ariel A, Serhan CN. Resolvins and protectins in the termination program of acute inflammation. *Trends Immunol* 2007; **28**:176–83.

5 Winn HR, Rubio R, Berne RM. Brain adenosine concentration during hypoxia in rats. *Am J Physiol* 1981; **241**:H235–42.

6 Zetterstrom T, Vernet L, Ungerstedt U, Tossman U, Jonzon B, Fredholm BB. Purine levels in the intact rat brain studies with an implanted perfused hollow fibre. *Neurosci Lett* 1982; **29**:111–5.

7 Decking UK, Schlieper G, Kroll K, Schrader J. Hypoxia-induced inhibition of adenosine kinase potentiates cardiac adenosine release. *Circ Res* 1997; **81**:154–64.

8 Pastor-Anglada M, Casado FJ, Valdes R, Mata J, Garcia-Manteiga J, Molina M. Complex regulation of nucleoside transporter expression in epithelial and immune system cells. *Mol Membr Biol* 2001; **18**:81–5.

9 Synnestvedt K, Furuta GT, Comerford KM *et al.* Ecto-5′-nucleotidase (CD73) regulation by hypoxia-inducible factor-1 mediates permeability changes in intestinal epithelia. *J Clin Invest* 2002; **110**:993–1002.

10 Deaglio S, Dwyer KM, Gao W *et al.* Adenosine generation catalyzed by CD39 and CD73 expressed on regulatory T cells mediates immune suppression. *J Exp Med* 2007; **204**:1257–65.

11 Hasko G, Cronstein BN. Adenosine: an endogenous regulator of innate immunity. *Trends Immunol* 2004; **25**:33–9.

12 Sitkovsky M, Lukashev D. Regulation of immune cells by local-tissue oxygen tension: HIF1 alpha and adenosine receptors. *Nat Rev Immunol* 2005; **5**:712–21.

13 Pouliot M, Fiset ME, Masse M, Naccache PH, Borgeat P. Adenosine up-regulates cyclooxygenase-2 in human granulocytes: impact on the balance of eicosanoid generation. *J Immunol* 2002; **169**:5279–86.

14 Gilroy DW, Colville-Nash PR, Willis D, Chivers J, Paul-Clark MJ, Willoughby DA. Inducible cyclooxygenase may have anti-inflammatory properties. *Nat Med* 1999; **5**:698–701.

15 Huang S, Apasov S, Koshiba M, Sitkovsky M. Role of A2a extracellular adenosine receptor-mediated signaling in adenosine-mediated inhibition of T-cell activation and expansion. *Blood* 1997; **90**:1600–10.

16 Lappas CM, Rieger JM, Linden J. A2A adenosine receptor induction inhibits IFN-gamma production in murine $CD4^+$ T cells. *J Immunol* 2005; **174**:1073–80.

17 Koshiba M, Kojima H, Huang S, Apasov S, Sitkovsky MV. Memory of extracellular adenosine A2A purinergic receptor-mediated signaling in murine T cells. *J Biol Chem* 1997; **272**:25881–9.

18 Sitkovsky MV, Ohta A. The 'danger' sensors that STOP the immune response: the A2 adenosine receptors? *Trends Immunol* 2005; **26**:299–304.

19 Cose S, Brammer C, Khanna KM, Masopust D, Lefrancois L. Evidence that a significant number of naive T cells enter non-lymphoid organs as part of a normal migratory pathway. *Eur J Immunol* 2006; **36**:1423–33.

20 Limmer A, Ohl J, Kurts C *et al.* Efficient presentation of exogenous antigen by liver endothelial cells to CD8+ T cells results in antigen-specific T-cell tolerance. *Nat Med* 2000; **6**:1348–54.

21 Feuerer M, Beckhove P, Garbi N *et al.* Bone marrow as a priming site for T-cell responses to blood-borne antigen. *Nat Med* 2003; **9**:1151–7.

22 Dong RP, Kameoka J, Hegen M, Tanaka T, Xu Y, Schlossman SF, Morimoto C. Characterization of adenosine deaminase binding to human CD26 on T cells and its biologic role in immune response. *J Immunol* 1996; **156**:1349–55.

23 Frauwirth KA, Riley JL, Harris MH *et al.* The CD28 signaling pathway regulates glucose metabolism. *Immunity* 2002; **16**:769–77.

24 Meisel H, Gunther S, Martin D, Schlimme E. Apoptosis induced by modified ribonucleosides in human cell culture systems. *FEBS Lett* 1998; **433**:265–8.

25 Shortman K, Naik SH. Steady-state and inflammatory dendritic-cell development. *Nat Rev Immunol* 2007; **7**:19–30.

26 Diehl L, Schurich A, Grochtmann R, Hegenbarth S, Chen L, Knolle PA. Tolerogenic maturation of liver sinusoidal endothelial cells promotes B7-homolog 1-dependent CD8+ T cell tolerance. *Hepatology (Baltimore, Md)* 2008; **47**:296–305.

27 Skalhegg BS, Tasken K, Hansson V, Huitfeldt HS, Jahnsen T, Lea T. Location of cAMP-dependent protein kinase type I with the TCR–CD3 complex. *Science* 1994; **263**:84–7.

28 Hoskin DW, Butler JJ, Drapeau D, Haeryfar SM, Blay J. Adenosine acts through an A3 receptor to prevent the induction of murine anti-CD3-activated killer T cells. *Int J Cancer* 2002; **99**:386–95.

29 Straus DB, Weiss A. Genetic evidence for the involvement of the lck tyrosine kinase in signal transduction through the T cell antigen receptor. *Cell* 1992; **70**:585–93.

30 Bergman M, Mustelin T, Oetken C *et al.* The human p50csk tyrosine kinase phosphorylates p56lck at Tyr-505 and down regulates its catalytic activity. *EMBO J* 1992; **11**:2919–24.

31 Nada S, Okada M, MacAuley A, Cooper JA, Nakagawa H. Cloning of a complementary DNA for a protein-tyrosine kinase that specifically phosphorylates a negative regulatory site of p60c-src. *Nature* 1991; **351**:69–72.

32 Mustelin T, Tasken K. Positive and negative regulation of T-cell activation through kinases and phosphatases. *Biochem J* 2003; **1**:15–27.

33 Wu J, Dent P, Jelinek T, Wolfman A, Weber MJ, Sturgill TW. Inhibition of the EGF-activated MAP kinase signaling pathway by adenosine 3′,5′-monophosphate. *Science* 1993; **262**:1065–9.

34 Hafner S, Adler HS, Mischak H *et al.* Mechanism of inhibition of Raf-1 by protein kinase A. *Mol Cell Biol* 1994; **14**:6696–703.

35 Park DJ, Min HK, Rhee SG. Inhibition of CD3-linked phospholipase C by phorbol ester and by cAMP is associated with decreased phosphotyrosine and increased phosphoserine contents of PLC-gamma 1. *J Biol Chem* 1992; **267**:1496–501.

36 Liu M, Simon MI. Regulation by cAMP-dependent protein kinase of a G-protein-mediated phospholipase C. *Nature* 1996; **382**:83–7.

37 Molina CA, Foulkes NS, Lalli E, Sassone-Corsi P. Inducibility and negative autoregulation of CREM: an alternative promoter directs the expression of ICER, an early response repressor. *Cell* 1993; **75**:875–86.

38 Bodor J, Spetz AL, Strominger JL, Habener JF. cAMP inducibility of transcriptional repressor ICER in developing mature human T lymphocytes. *Proc Natl Acad Sci USA* 1996; **93**:3536–41.

39 Ohta A, Gorelik E, Prasad SJ *et al.* A2A adenosine receptor protects tumors from antitumor T cells. *Proc Natl Acad Sci USA* 2006; **103**:13132–7.

40 Grader-Beck T, van Puijenbroek AA, Nadler LM, Boussiotis VA. cAMP inhibits both Ras and Rap1 activation in primary human T lymphocytes, but only Ras inhibition correlates with blockade of cell cycle progression. *Blood* 2003; **101**:998–1006.

41 Fredholm BB, Jzerman AP, Jacobson KA, Klotz KN, Linden J. International Union of Pharmacology XXV. Nomenclature and classification of adenosine receptors. *Pharmacol Rev* 2001; **53**:527–52.

42 Burnstock G. Purine and pyrimidine receptors. *Cell Mol Life Sci* 2007; **64**:1471–83.

43 Ohta A, Sitkovsky M. Role of G-protein-coupled adenosine receptors in downregulation of inflammation and protection from tissue damage. *Nature* 2001; **414**:916–20.

44 Sitkovsky MV, Lukashev D, Apasov S, Kojima H, Koshiba M, Caldwell C, Ohta A, Thiel M. Physiological control of immune response and inflammatory tissue damage by hypoxia-inducible factors and adenosine A2A receptors. *Annu Rev Immunol* 2004; **22**:657–82.

45 Erdmann AA, Gao ZG, Jung U, Foley J, Borenstein T, Jacobson KA, Fowler DH. Activation of Th1 and Tc1 cell adenosine A2A receptors directly inhibits IL-2 secretion *in vitro* and IL-2-driven expansion *in vivo*. *Blood* 2005; **105**:4707–14.

46 Naganuma M, Wiznerowicz EB, Lappas CM, Linden J, Worthington MT, Ernst PB. Cutting edge: critical role for A2A adenosine receptors in the T cell-mediated regulation of colitis. *J Immunol* 2006; **177**:2765–9.

47 Bowen DG, Zen M, Holz L, Davis T, McCaughan GW, Bertolino P. The site of primary T cell activation is a determinant of the balance between intrahepatic tolerance and immunity. *J Clin Invest* 2004; **114**:701–12.

48 Probst HC, McCoy K, Okazaki T, Honjo T, van den Broek M. Resting dendritic cells induce peripheral CD8+ T cell tolerance through PD-1 and CTLA-4. *Nat Immunol* 2005; **6**:280–6.

49 Zarek PE, Huang CT, Lutz ER, Kowalski J, Horton MR, Linden J, Drake CG, Powell JD. A2A receptor signaling promotes peripheral tolerance by inducing T-cell anergy and the generation of adaptive regulatory T cells. *Blood* 2008; **111**:251–9.

50 Sevigny CP, Li L, Awad AS, Huang L, McDuffie M, Linden J, Lobo PI, Okusa MD. Activation of adenosine 2A receptors attenuates allograft rejection and alloantigen recognition. *J Immunol* 2007; **178**:4240–9.

Appendix 15

Src Homology 2-Domain Containing Leukocyte-Specific Phosphoprotein of 76 kDa Is Mandatory for TCR-Mediated Inside-Out Signaling, but Dispensable for CXCR4-Mediated LFA-1 Activation, Adhesion, and Migration of T Cells

Horn J., Wang X., Reichardt P., Stradal T.E., Warnecke N., **Simeoni L.**, Gunzer M., Yablonski D., Schraven B., and Kliche S. (2009) *J Immunol.* 183:5756-5767.

Src Homology 2-Domain Containing Leukocyte-Specific Phosphoprotein of 76 kDa Is Mandatory for TCR-Mediated Inside-Out Signaling, but Dispensable for CXCR4-Mediated LFA-1 Activation, Adhesion, and Migration of T Cells[1]

Jessica Horn,[2]* Xiaoqian Wang,[2]* Peter Reichardt,* Theresia E. Stradal,† Nicole Warnecke,* Luca Simeoni,* Matthias Gunzer,* Deborah Yablonski,‡ Burkhart Schraven,[3]* and Stefanie Kliche[3]*

Engagement of the TCR or of chemokine receptors such as CXCR4 induces adhesion and migration of T cells via so-called inside-out signaling pathways. The molecular processes underlying inside-out signaling events are as yet not completely understood. In this study, we show that TCR- and CXCR4-mediated activation of integrins critically depends on the membrane recruitment of the adhesion- and degranulation-promoting adapter protein (ADAP)/Src kinase-associated phosphoprotein of 55 kDa (SKAP55)/Rap1-interacting adapter protein (RIAM)/Rap1 module. We further demonstrate that the Src homology 2 domain containing leukocyte-specific phosphoprotein of 76 kDa (SLP76) is crucial for TCR-mediated inside-out signaling and T cell/APC interaction. Besides facilitating membrane recruitment of ADAP, SKAP55, and RIAM, SLP76 regulates TCR-mediated inside-out signaling by controlling the activation of Rap1 as well as Rac-mediated actin polymerization. Surprisingly, however, SLP76 is not mandatory for CXCR4-mediated inside-out signaling. Indeed, both CXCR4-induced T cell adhesion and migration are not affected by loss of SLP76. Moreover, after CXCR4 stimulation, the ADAP/SKAP55/RIAM/Rap1 module is recruited to the plasma membrane independently of SLP76. Collectively, our data indicate a differential requirement for SLP76 in TCR- vs CXCR4-mediated inside-out signaling pathways regulating T cell adhesion and migration. *The Journal of Immunology,* **2009, 183: 5756–5767.**

Stimulation of T cells through the TCR activates a whole plethora of signaling pathways that collectively control activation, proliferation, and differentiation of T cells. One immediate consequence of TCR engagement is the formation of a multicomponent signaling complex close to the plasma membrane consisting of the Src homology 2-domain containing leukocyte-specific phosphoprotein of 76 kDa (SLP76),[4] the small adapter protein Gads, and the transmembrane adapter protein linker for activation of T cells (LAT) (1). In response to TCR engagement, LAT becomes phosphorylated on several tyrosine residues by the protein tyrosine kinase ZAP70 (1). This phosphorylation leads to recruitment of Gads. Through its constitutive association with Gads, SLP76 is also recruited to phosphorylated LAT (2). In the following, several other effector molecules assemble with the LAT/Gads/SLP76-signaling platform. These include phospholipase Cγ1 (PLCγ1), the nucleotide exchange factor Vav1, and the Tec family kinase IL-2-inducible T cell kinase (Itk) (1). Together these molecules coordinate TCR-mediated rises in intracellular calcium, up-regulation of CD69, and the activation of the Ras/ERK1/2 signaling pathway (1, 3).

The importance of SLP76 for TCR-mediated signaling events has been demonstrated in SLP76-deficient mice as well as in the SLP76-deficient Jurkat T cell line J14. Thus, loss of SLP76 in mice leads to a complete block at the double-negative 3 stage of thymic development and results in an almost complete loss of mature T cells (1). Moreover, loss of SLP76 in Jurkat T cells induces a complete failure of the TCR to induce rises in intracellular calcium, activation of the Ras/Raf/MAPK/ERK1/2 pathway, and up-regulation of CD69 expression (3).

Besides inducing the above-mentioned signaling events, TCR stimulation also leads to T cell adhesion, a process that is critical for the interaction between T cells and APCs. In T cells, the β_2 integrin LFA-1 ($\alpha_L\beta_2$) mediates adhesive events with APCs through binding to its ligand ICAM-1. LFA-1/ICAM-1 interactions are critical for T cell activation because they stabilize the interaction of T cells with APCs and the formation of the immunological synapse (IS) (4, 5).

*Institute of Molecular and Clinical Immunology, Otto-von-Guericke University, Magdeburg, Germany; †Signaling and Motility Group, Helmholtz Center for Infection Research, Braunschweig, Germany; and ‡Rappaport Faculty of Medicine and Technion-Israel Institute of Technology, Haifa, Israel

Received for publication March 3, 2009. Accepted for publication August 20, 2009.

The costs of publication of this article were defrayed in part by the payment of page charges. This article must therefore be hereby marked *advertisement* in accordance with 18 U.S.C. Section 1734 solely to indicate this fact.

[1] This work was supported by Deutsche Forschungsgemeinschaft Grants GRK1167 and KL-1295/5-1 (to B.S. and S.K.) and by German-Israeli Foundation for Scientific Research and Development Grant (to D.Y. and B.S.).

[2] J.H. and X.W. are first authors.

[3] Address correspondence and reprint requests to Drs. Stefanie Kliche or Burkhart Schraven, Institute of Molecular and Clinical Immunology, Otto-von-Guericke University, Leipziger Strasse 44, D-39120 Magdeburg, Germany. E-mail address: stefanie.kliche@med.ovgu.de

[4] Abbreviations used in this paper: SLP76, Src homology 2-domain containing leukocyte-specific phosphoprotein of 76 kDa; ADAP, adhesion- and degranulation-promoting adapter protein; IS, immunological synapse; Itk, IL-2-inducible T cell kinase; LAT, linker for activation of T cells; PFA, paraformaldehyde; PLCγ1, phospholipase Cγ1; RIAM, Rap1-interacting adapter protein; RNAi, RNA interference; SA, superantigen; sh, small hairpin RNA; siRNA, small interfering RNA; SKAP55, Src kinase-associated phosphoprotein of 55 kDa; TRITC, tetramethylrhodamine isothiocyanate.

www.jimmunol.org/cgi/doi/10.4049/jimmunol.0900649

Resting T cells are not adhesive because LFA-1 is presented in a closed, inactive conformation. Upon triggering of the TCR or of chemokine receptors (see below), a conformational change is induced within LFA-1 that augments its affinity for ICAM-1. In addition, clustering of LFA-1 molecules on the surface of T cells enhances avidity for ICAM-1 binding. The molecular events leading to integrin activation have collectively been termed inside-out signaling (6).

Gain-of-function and loss-of-function studies have demonstrated that additional signaling proteins are involved in TCR-mediated integrin activation. These include talin (6, 7), the Wiskott-Aldrich syndrome-Verprolin-homologous protein WAVE2 (8, 9), Rap1 (6, 10, 11), and its downstream targets regulator of adhesion and cell polarization enriched in lymphoid tissues or Rap1-interacting adapter protein (RIAM) (12–14), adhesion- and degranulation-promoting adapter protein (ADAP) (15, 16), and Src kinase-associated phosphoprotein of 55 kDa (SKAP55) (17, 18). Moreover, components of the LAT/Gads/SLP76 signaling platform are also critically involved in TCR-mediated activation of LFA-1. These include PLCγ1, Vav1, Itk, and ADAP (13, 19, 20). How exactly these molecules orchestrate TCR-mediated activation of integrins is not completely understood. However, we have recently shown that the formation of a signaling module consisting of ADAP/SKAP55 complex together with RIAM is required for plasma membrane targeting of Rap1 in response to TCR stimulation, and therefore for TCR-mediated activation of integrins (17, 21). In line with these data is the observation that ADAP- and SKAP55-deficient mouse T cells show a severe defect in integrin activation in response to TCR-mediated stimuli (15, 16, 18).

Currently, it is proposed that following T cell activation, tyrosine-phosphorylated ADAP binds to the Src homology 2 domain of SLP76, thereby leading to membrane recruitment of the ADAP/SKAP55/RIAM module and integrin activation. In line with this idea is the observation that disruption of the interaction between SLP76 and Gads blocks TCR-mediated adhesion to ICAM-1 (22). Furthermore, it was shown that mutation of those tyrosine residues within ADAP, which are believed to mediate the interaction between ADAP and SLP76, blocks TCR-mediated activation of LFA-1 (23). Thus, it appears as if SLP76 would also play a major role during TCR-mediated activation of integrins by facilitation membrane targeting of the ADAP/SKAP55/RIAM module. However, to date, an inducible interaction between endogenously expressed ADAP/SKAP55/RIAM module and SLP76 in response to TCR engagement has not been demonstrated biochemically. Hence, the molecular signaling events underlying the function of SLP76 for TCR-mediated integrin activation are not completely elucidated.

Importantly, integrins not only become activated after stimulation of the TCR, but also after triggering of chemokine receptors, such as CXCR4. Signaling via CXCR4 is induced by stromal cell-derived factor-1α (or CXCL12) and induces affinity and avidity regulation of LFA-1 (6). This process is important for firm T cell adhesion, T cell polarization, chemokinesis, and chemotaxis (24). Molecules involved in CXCR4-mediated integrin activation and/or chemotaxis are talin (25), Rap1 (6, 26, 27), and its downstream targets regulator of adhesion and cell polarization enriched in lymphoid tissues and *Mst*I (28–30), Itk (20), Vav1 (20, 31, 32), Rac (31), and members of the Wiskott-Aldrich syndrome protein family (33, 34). Moreover, we and others have shown that overexpression of ADAP enhances chemotaxis of T cells in response to CXCL12 (35, 36). These findings suggest an important role of ADAP for CXCR4-induced migration of T cells. However, the molecular basis of how ADAP is integrated into CXCR4 signaling is to date unclear. Based on its central role in TCR-mediated signaling processes, SLP76 would be an attractive candidate that could facilitate membrane targeting of ADAP after CXCR4 stimulation. Indeed, it was shown recently that SLP76 regulates CXCR4-induced Ca^{2+} flux and ERK1/2 phosphorylation (31). Conversely, we had demonstrated that disruption of the SLP76/Gads association, albeit impairing TCR-mediated signaling processes, does not affect CXCR4-induced Ca^{2+} flux and chemotaxis (22). Thus, it is unclear whether SLP76 is also important for CXCR4-mediated activation of integrins and chemotaxis.

In this study, we have addressed critical questions regarding the function of SLP76 during TCR vs CXCR4-mediated signaling. We show that SLP76 is indeed a critical regulator of TCR-mediated inside-out signaling events in T cells, and we demonstrate that SLP76 is mandatory for induction of TCR-mediated adhesion, affinity/avidity regulation of LFA-1, and the interaction between T cells and B cells. Furthermore, we show that SLP76 is required for TCR-induced Rap1 activation, Rac-mediated actin dynamics, and recruitment of both talin and the ADAP/SKAP55/RIAM/Rap1 module to the plasma membrane and to the IS. Surprisingly, however, SLP76 is not mandatory for CXCR4-mediated activation of LFA-1. In addition, SLP76 is dispensable for adhesion and migration of T cells in response to CXCL12. Finally, we demonstrate that the ADAP/SKAP55/RIAM/Rap1 module is crucial for T cell adhesion and migration in response to CXCR4 triggering, but is recruited to the plasma membrane independently of SLP76. Our findings show that SLP76 acts as a key player during TCR-mediated inside-out signaling, whereas the adapter protein appears to be dispensable for chemokine-dependent processes that regulate adhesion and migration of T cells.

Materials and Methods

Reagents and Abs

All tissue culture reagents were from Biochrom, and all chemicals were from Roth, unless mentioned otherwise. Staphylococcal enterotoxin B, D, and E were purchased from Toxin Technology, respectively. Indo-1 AM, Blue-7-amino-4-chloromethylcoumarin, DDAO-SE, and Alexa Fluor 633-phalloidin were bought from Molecular Probes. FITC or tetramethylrhodamine isothiocyanate (TRITC) phalloidin was from Sigma-Aldrich. PMA was purchased from Calbiochem. Glutathione-Sepharose beads were bought from Pharmacia. Protein A- and protein G-agarose beads were from Santa Cruz Biotechnology. The chemokine CXCL12 was bought from Tebu-bio, and the human Fc-tagged ICAM-1 was from R&D Systems. The anti-RIAM rat mAbs were raised against the bacterially expressed GST-tagged fragment of RIAM (1–420 aa), as previously described (37). Supernatants of secreting hybridomas were screened by Western blotting, immunofluorescence, and intracellular flow cytometry (FACS), and among the various clones tested, the mAb RIAM15B7E8 was selected. The mouse anti-CD3 mAb C305 (IgM) (38), OKT3 (ATCC), biotinylated UCHT-1 (NatuTec), or MEM92 (provided by V. Horejsi, Academy of Sciences of the Czech Republic, Czech Republic) was used for TCR stimulation of Jurkat T cells or human T cells. For protein surface expression analysis by FACS, the following mAbs were used: CD18 (MEM48), CD29 (MEM101A; both provided by V. Horejsi), CD184 (CXCR4; clone 12G5; BD Biosciences), MHC class I (clone W6/32; ATCC), KIM127 (provided by N. Hogg, Cancer Research U.K. London Research Institute, London, U.K.), APC-conjugated anti-CD69 (BD Bioscience), or FITC-conjugated MEM48 (Immunotools). The anti-SLP76 and anti-preimmune sheep serum (39), anti-SKAP55 rabbit serum (40), or anti-Gads rabbit serum (Upstate Biotechnology) was used for immunoprecipitation studies. The following Abs were used for immunoblot analysis and/or immunofluorescence in this study: anti-SKAP55 rat mAb (SK13B6) (17), anti-GST rat mAb (provided by C. Erk, Helmholtz-Zentrum für Infektionsforschung, Braunschweig, Germany), anti-β-actin mAb (Sigma-Aldrich), anti-phospho-ERK1/2 (T^{202}, Y^{204}) rabbit serum and anti-Vav rabbit serum (both from Cell Signaling Technology), anti-SLP76 mAb (Santa Cruz Biotechnology), anti-LAT mAb (BD Biosciences), anti-ADAP sheep serum (41), anti-phospho-SLP76 mAb (pY145; BD Biosiences), anti-phospho-LAT (pY171) rabbit serum and anti-phospho-ZAP70 (pY319) rabbit serum (both from Cell

Signaling Technology), anti-Rap1 rabbit serum (Santa Cruz Biotechnology), anti-Rap1 mAb and anti-Rac mAb (both from BD Biosciences), and anti-talin mAb (clone 8D4; Sigma-Aldrich). The following Abs were used for phospho-epitope staining by FACS: anti-phospho-ZAP70 (pY319)-Alexa Fluor 647, anti-phospho-PLCγ1 (pY783)-Alexa Fluor 647 (both from BD Biosciences), and anti-phospho-ERK1/2 (pT202, pY204; clone E10; Cell Signaling Technology). Streptavidin, HRP-labeled secondary Abs, and FITC-, Cy3-, APC-, and Cy5-conjugated secondary Abs were purchased from Dianova.

RNA interference (RNAi) of SLP76, ADAP, SKAP55, or RIAM and cDNA constructs

For small hairpin RNA (shRNA) of SLP76, the following oligonucleotides, shC (CCAAGTAATGTAGGATCAA; *Renilla*) and shSLP76 (CGAAGA GAGGAGGAGCATC; shSLP76), were cloned into pSuper (provided by T. Seufferlein (Universitätsklinik und Poliklinik für Innere Medizin I, Halle, Germany) and pCMS3-EGFP vector (provided by D. Billadeau (Mayo Clinic, Rochester, MN). For shRNA of ADAP and RIAM, the previously published oligonucleotides were cloned into the pCMS3 vector (12, 42). The pCMS3-EGFF construct for silencing of SKAP55 has been described (17). The pGEX PAK-PBD was provided by T. Seufferlein. The pGEX RalGDS-RBD was provided by J. Bos (University Medical Center, Utrecht, The Netherlands), and the pmCherry-C1 vector was purchased from BD Clontech.

Cell culture and transfection

Jurkat T cells (ATCC), B cells (Raji; ATCC), and SLP76-deficient/reconstituted Jurkat T cells (J14, J14-76-11, and J14-76-18) (3) were maintained in RPMI 1640 medium supplemented with 10% FBS (PAN) and stable L-glutamine at 37°C with 5% CO_2. Jurkat T cells (2×10^7) were transfected by electroporation, as previously described (17). Transfection with the pCMS3-EGFP vector into Jurkat T cells consistently yielded in an average of >80% GFP-expressing cell population. Primary human T cells were prepared from healthy donors by standard separation methods using AutoMACS (Miltenyi Biotec) maintained in RPMI 1640 medium containing 10% FBS, stable L-glutamine, and 1000 U/ml penicillin/streptomycin. Approval for these studies was obtained from the Ethics Committee of the Medical Faculty at the Otto-von-Guericke University. Informed consent was obtained in accordance with the Declaration of Helsinki. For electroporation of small interfering RNA (siRNA), human peripheral T cells (8×10^6) were washed in PBS containing Ca^{2+}/Mg^{2+} and resuspended in 200 μl of Opti-MEM (Invitrogen). siRNA smart pool against SLP76, ADAP (Dharmacon smart pools for SLP76 or ADAP), control siRNA (si*CONTROL* nontargeting smart pool from Dharmacon), Vav1.3 (31), siRNA for SLP76, or control siRNA *Renilla* (see above; all purchased from Invitrogen) was added, and after 3 min cells were transfected by electroporation (square-wave pulse, 1000 V, 0.5 ms, 2 pulses (pulse interval 5 s); Bio-Rad X-cell). The cells were then added to prewarmed cell culture medium, as described above, and cultured for 72 h before use. The knockdown efficiency of SLP76, ADAP, SKAP55, RIAM, or Vav1 was evaluated either by Western blotting or on a single-cell basis by intracellular flow cytometry.

Immunoprecipitation, Western blot analysis, isolation of cytosolic and plasma membrane fractions, and GTPase assays

Cell lysis and immunoprecipitation were performed, as previously described (17, 21). Equivalent amounts of protein (determined by Bradford assay (Roth)) were used in precipitation studies (500 μg of total protein from either Jurkat T cells or human primary T cells). Cell lysates (50 μg of total protein) or immune complexes were separated by SDS-PAGE and transferred to nitrocellulose. Western blots were conducted with the indicated Abs and developed with the appropriate HRP-conjugated secondary Abs and the Luminol detection system (Roth). Isolation of cytosolic and plasma membrane fractions has been described previously (17). GTPase activity of Rap1 or Rac activity was assessed, as previously described (17). Briefly, Jurkat T cells were either left untreated or stimulated for various time points with anti-CD3 mAb C305 or CXCL12 (100 ng/ml) and lysed. An aliquot of the lysate (10%) was used as loading control. Activated GTPases were precipitated using either glutathione-Sepharose conjugated with the GST-RalGDS fusion protein for Rap1 (RBD) or glutathione-Sepharose coupled with the GST fusion protein of the p21-binding domain of Pak (PBD) for Rac. Bound GTPases were quantified by Western blotting.

Flow cytometry, calcium release, and CD69 up-regulation

To analyze the cell surface expression of β_1 or β_2 integrin, CXCR4, TCR, and MHCI, cells were stained with the indicated Abs in combination with APC-conjugated goat anti-mouse IgG and analyzed using a FACSCalibur flow cytometer and CellQuestPro software (BD Biosciences). Soluble Fc-ICAM-1 binding of T cells after various stimuli was assessed, as previously described (43). Briefly, T cells suspended in binding puffer (HBSS containing 2% FBS) were either left untreated or stimulated with anti-CD3 mAb, CXCL12, or Mg^{2+}/EDTA for 5 min in the presence of 20 μg/ml human rFc-ICAM-1, and bound Fc-ICAM-1 was detected by flow cytometry. Intracellular staining by flow cytometry for SLP76, ADAP, SKAP55, or RIAM was performed, as previously described (44). The specificity of the staining for each serum or mAb was assessed using either SLP76-deficient/reconstituted Jurkat T cells or after loss of ADAP, SKAP55, or RIAM expression by vector-based shRNA in Jurkat T cells (please see supplemental Fig. 1).[5] To assess the F-actin content, T cells (1×10^5) were left untreated or stimulated with anti-CD3 mAbs or CXCL12, and reactions were stopped by adding PBS containing 4% paraformaldehyde (PFA), 2 μg/ml FITC- or Alexa Fluor 633-phalloidin, and 0.2% Triton X-100. After 15 min, cells were washed with 1% PFA in PBS and analyzed by flow cytometry. Measurement of TCR-induced calcium release and CD69 up-regulation have been previously described (17). Analysis of protein phosphorylation with phospho-specific Abs by flow cytometry was performed, as described (45).

Conjugate formation, adhesion, migration, and motility assays

Conjugate assays were performed, as described (21). Briefly, superantigen (SA) mixture of staphylococcal enterotoxin B-, D-, and E-pulsed and DDAO-SE-labeled Raji B cells were incubated with an equal number of Jurkat T cells or CFSE-loaded human T cells for 30 min at 37°C. Nonspecific aggregates were disrupted; cells were fixed with 1% PFA, and then analyzed by flow cytometry. The percentage of conjugates was defined as the number of double-positive events in the upper right quadrant. Adhesion assays were performed, as previously described (17). Briefly, Jurkat T cells or peripheral human T cells were stimulated with OKT3, PMA, or $MnCl_2$ for 30 min at 37°C before adhesion on Fc-ICAM-1-coated dishes. The bound total or GFP-expressing cell fraction was determined by counting four independent fields by microscopy using an ocular counting reticule. To assess CXCR4-mediated adhesion, peripheral human T cells were incubated for 10 min at 37°C on Fc-ICAM-1-coated dishes coimmobilized with or without CXCL12; subsequently, nonbound cells were removed by washing with HBSS and bound cells were counted, as described above. Chemotaxis assays were performed, as previously described, using Transwells (Costar) coated with fibronectin (35). After 2 h, the number of migrated cells into the lower chamber was counted and the percentage of GFP-expressing Jurkat T cells was determined by flow cytometry. For live cell imaging of either random or CXCL12-induced motility of T cells on Fc-ICAM-1, self-constructed imaging chambers (46) were coated with Fc-ICAM-1 in PBS at 4°C overnight. Immediately before imaging, cells were left untreated or stimulated with CXCL12 (100 ng/ml), and imaging was performed on a CellR imaging workstation (Olympus) using an upright microscope stage (BX61) with a ×20 lens. Using an automated X-Y-Z stage, at least two optical fields were chosen for each culture condition. Images were taken every 15–60 s for 2 h. At least 30 cells per observation field were analyzed. Tracking analysis of migrating cells to determine the velocity was done by computer-assisted cell tracking using the Software CellTracker (46).

Immunofluorescence microscopy

For B cell/T cell conjugates, SA- and Blue-7-amino-4-chloromethylcoumarin-loaded Raji B cells were incubated for 30 min at 37°C with human T cells on poly(L-lysine)-coated coverslips and fixed with 3.5% PFA in PBS for 10 min. Cells were permeabilized with 0.1% Triton X-100 in PBS, blocked with 5% horse serum in PBS, and incubated with the indicated Abs or phalloidin. Coverslips were mounted in Mowiol 488 and imaged with a LEICA TCS SP2 laser-scanning confocal system (Leica Microsystems) using a plan apochromatic oil emerging ×63 objective (NA 1.4). Figure constructions of images were performed in COREL Photopaint. For quantification of recruitment of proteins and F-actin at the contact zone or at the uropod, line scans (1 μm) were obtained. Fluorescence intensity was plotted as function of distance along this line, and the integrated areas under the curves representing the fluorescence intensity were calculated as ratio between the immunological synapse vs the uropod. Thirty conjugates were analyzed per experiment. To assess TCR-induced clustering of LFA-1, Jurkat T cells were incubated with biotinylated anti-UCHT-1 in the presence of streptavidin at 4°C. After washing, the cells were stimulated at 37°C for 30 min on poly(L-lysine)-coated slides, fixed with 3.5% PFA in PBS, and then blocked with 5% horse serum in PBS. The cells were stained

[5] The online version of this article contains supplemental material.

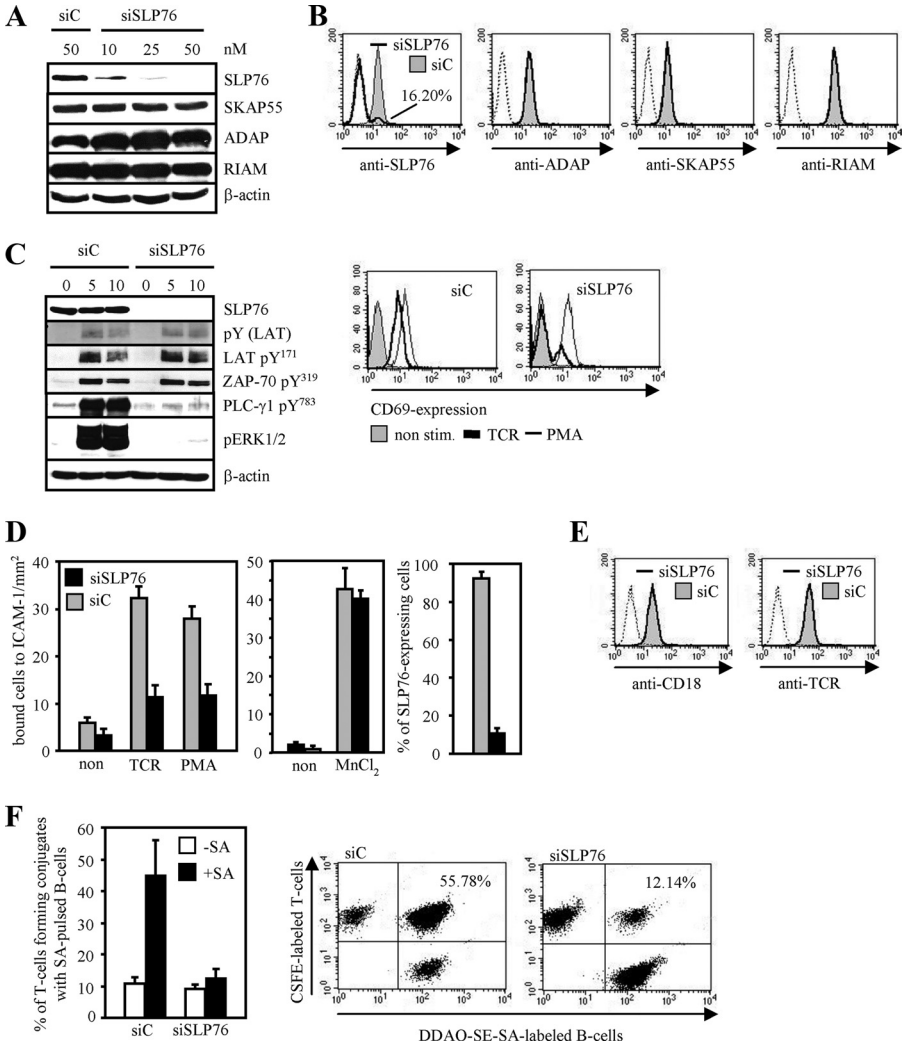

FIGURE 1. SLP76 is crucial for TCR-induced adhesion to ICAM-1 and conjugate formation. *A*, Purified human T cells were transfected with control siRNA (siC) or the indicated concentrations of siRNAs against SLP76 (siSLP76). After 72 h, whole-cell extracts were analyzed by Western blotting with the indicated Abs. *B*, In parallel, cells transfected with 50 nM siC or siSLP76 were analyzed by flow cytometry for the intracellular expression of SLP76, ADAP, SKAP55, and RIAM (black line). The preimmune sheep serum and the anti-GST mAb were used as isotype controls (dashed line). *C*, Human T cells transfected as described in *A* were left untreated or stimulated with anti-CD3 mAbs (TCR) for the indicated period of time. Lysates were analyzed by Western blotting using the indicated Abs. Moreover, the same transfectants were cultured on plate-bound anti-CD3 mAbs (TCR) or in the presence of PMA for 18 h, stained with anti-CD69 mAbs, and analyzed by flow cytometry. Data are representative of three individual experiments. Note that the total expression of LAT, ZAP70, PLCγ1, or ERK1/2 was not affected (data not shown). *D*, Human T cells transfected as described above were left untreated or stimulated with anti-CD3 mAb (TCR), PMA, or $MnCl_2$ for 30 min, and subsequently analyzed for their ability to adhere to Fc-ICAM-1. Suppression of SLP76 expression for each experiment was assessed by flow cytometry, and the percentage of SLP76-expressing cells was calculated. Data represent the mean and SE of three independently performed experiments. *E*, In parallel, transfectants were analyzed for the surface expression of CD18 or the TCR (black line), and control IgG were used as isotype controls (dashed line). One representative experiment of three is shown. *F*, Equal numbers of the same cells as described in *A* were stained with CFSE and incubated for 30 min without SA (−SA) or with SA-pulsed (+SA) DDAO-SE-labeled B cells. The percentage of conjugate formation was assessed by flow cytometry. Data represent the mean and SE of three independently performed experiments. Representative histograms of SA-pulsed DDAO-SE B cells conjugated with CFSE-stained T cells in the presence or absence of SLP76 are shown.

with FITC-conjugated anti-MEM48 and imaged, as described above. For each experiment, a minimum of at least 40 cells with LFA-1 polarized to one side of the cell was regarded as polarized, whereas those cells showing equal distribution of LFA-1 were considered not to be polarized. The percentage of polarized cells in each field was determined.

Results

Loss of SLP-76 impairs TCR-mediated activation of LFA-1 and T cell-APC conjugation

By using a small peptide that disrupts the constitutive interaction between SLP76 and Gads, we recently provided evidence that formation of the LAT/Gads/SLP76 signaling platform at the plasma membrane is required for TCR-mediated integrin activation (22). However, we formally could not exclude the possibility that the functional effects exerted by the Gads-binding fragment were not due to targeting the SLP76/Gads complex, but rather to disruption of a distinct signaling pathway that regulates intergrin activation in response to TCR stimulation. To assess this point more specifically, we reduced the expression of SLP76 in primary human T cells by RNAi. As shown in Fig. 1, *A* and *B*, SLP76 siRNA treatment lowered the expression levels of endogenous SLP76 up to 80%, whereas the expression levels of ADAP, SKAP55, and RIAM remained unaffected.

Previously, it had been reported that SLP76 is required for phosphorylation of PLCγ1, activation of ERK1/2, as well as for expression of CD69 upon TCR stimulation. To first address whether loss of SLP76 interferes with these SLP76-mediated functions also in primary human T cells, we analyzed the ability of SLP76-deficient human T cells to activate PLCγ1 and ERK1/2 in response to TCR stimulation by Western blotting and to up-regulate CD69 expression by flow cytometry. As shown in Fig. 1*C*, loss of SLP76 strongly attenuated TCR-mediated phosphorylation of PLCγ1 at Y^{783}, activation of ERK1/2, and up-regulation of CD69. As expected, more proximal signaling events such as the phosphorylation of ZAP70 at Y^{319} or tyrosine phosphorylation of LAT (either global or at Y^{171}) were not affected in the absence of SLP76 (Fig. 1*C*). Note that similar data were obtained, when we suppressed the expression of SLP76 by shRNA in Jurkat T cells (supplemental Fig. 2). Thus, with regard to well-established SLP76-regulated signaling processes, SLP76-deficient primary human T cells behave like their corresponding Jurkat T cell counterparts (3).

Using the siRNA approach, we next analyzed the capability of T cells to adhere to ICAM-1-coated dishes in response to various stimuli. As shown in Fig. 1*D* and supplemental Fig. 3*A*, control transfected human T cells and Jurkat T cells readily adhered to ICAM-1 upon TCR or PMA treatment. In contrast, loss of SLP76 substantially attenuated both PMA- and TCR-induced adhesion to ICAM-1 (*left panel*), whereas the cells showed no defect in their adhesiveness in response to Mn^{2+} (*middle panel*). The defect in TCR- or PMA-induced adhesion to ICAM-1 was not due to an altered expression of the β_2 integrin (or the TCR) as determined by flow cytometry (Fig. 1*E* and supplemental Fig. 3*B*).

Because the interaction of LFA-1 with ICAM-1 is important for the establishment and maintenance of T cell/APC interactions (5), we next analyzed whether SLP76 is required for conjugate formation between human T cells and SA-loaded B cells. Fig. 1*F* shows that in contrast to control transfected T cells, loss of SLP76 substantially blunted conjugate formation. Similarly, $SLP76^{low}$ Jurkat T cells failed to interact with SA-loaded B cells (supplemental Fig. 3*C*). Collectively, the experiments shown in Fig. 1 indicate that SLP76 is mandatory for both TCR-mediated adhesion to ICAM-1 and conjugate formation.

Loss of SLP76 attenuates TCR-mediated affinity/avidity regulation of LFA-1

TCR-mediated inside-out signaling alters both LFA-1 affinity (conformation) and avidity (clustering) (6). To determine the role of SLP76 for LFA-1 affinity modulation, we assessed the ability of soluble Fc-ICAM-1 to bind to SLP76-proficient and SLP76-deficient T cells after TCR stimulation by means of flow cytometry. Fig. 2*A* shows that knockdown of SLP76 in human T cells abrogates binding of soluble Fc-ICAM-1 after TCR stimulation (for Jurkat T cells, please see supplemental Fig. 3*D*). In contrast, both transfectants were able to bind similar amounts of Fc-ICAM-1 after treatment with Mg^{2+}/EDTA, which directly induces the high-affinity conformation of LFA-1.

Next, we investigated avidity regulation of LFA-1 by analyzing clustering of CD18 (the β2 chain of LFA-1) to the IS in response to TCR stimulation. Fig. 2*B* shows that localization of CD18 to the IS occurred readily in SLP76-expressing T cells after incubation with SA-pulsed B cells, whereas it was severely impaired in $SLP76^{low}$ T cells. In line with these data, $SLP76^{low}$ Jurkat T cells also displayed no typical clustering of CD18 upon cross-linking of the TCR (supplemental Fig. 3*E*). Taken together, SLP76 is required for both affinity and avidity regulation of LFA-1 after stimulation of the TCR.

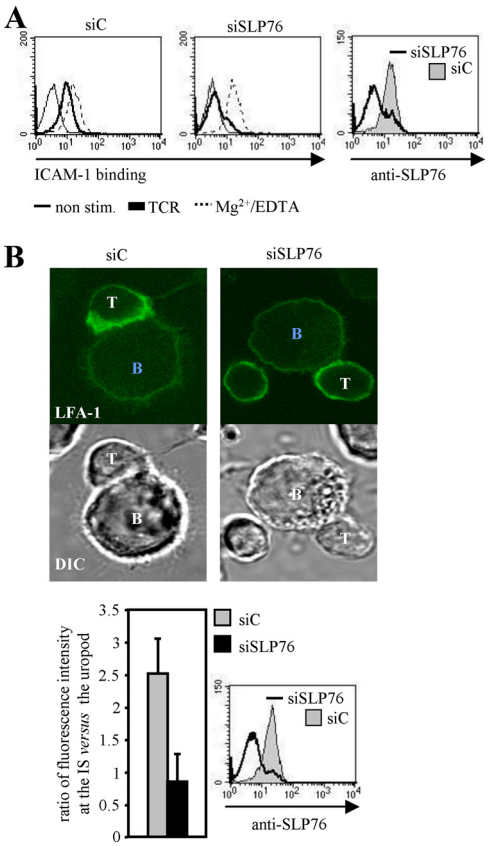

FIGURE 2. TCR-induced affinity/avidity regulation of LFA-1 depends on SLP76. *A*, Human T cells were transfected with either 50 nM control siRNA (siC) or siRNAs against SLP76 (siSLP76). After 72 h, cells were analyzed for their ability to bind soluble Fc-ICAM-1 in response to anti-CD3 mAb (TCR) or Mg^{2+}/EDTA stimulation for 5 min. Suppression of SLP76 expression was evaluated by flow cytometry. One representative experiment of three is shown. *B*, Human T cells transfected as described in *A* were allowed to form conjugates with SA-pulsed B cells for 30 min. Fixed cells were stained for the β2 subunit of LFA-1 (green) to determine IS localization of LFA-1. Fluorescence intensity of LFA-1 at the contact zone or the uropod was quantified and calculated as ratio of intensity at the IS vs the uropod. Knockdown efficiency of SLP76 expression was assessed by flow cytometry. Data present the average of three independently performed experiments.

TCR-mediated activation of Rac and actin dynamics require SLP76

Reorganization of the actin cytoskeleton is required for TCR-mediated integrin activation and conjugate formation (33, 34), and the small GTPase Rac is a major regulator regulating this process. In T cells, activation of Rac is mediated via the nucleotide exchange factor Vav1, which is recruited to and activated by SLP76 upon T cell activation (32). Therefore, it seemed likely that loss of SLP76 also leads to alterations in actin dynamics upon TCR stimulation. As depicted in Fig. 3, this is indeed the case. TCR-mediated activation of Rac (Fig. 3*A*), formation of F-actin (Fig. 3*B*), as well as accumulation of F-actin at the IS (Fig. 3*C*, *upper right panel*) are severely impaired in SLP76-deficient T cells. Note that similar data were obtained when the F-actin content after TCR triggering was assessed in $SLP76^{low}$ Jurkat T cells (data not shown). Hence, loss of SLP76 induces a failure to activate Rac and a defect in F-actin remodeling upon TCR stimulation.

Because the scaffolding protein talin links newly synthesized F-actin branches to LFA-1 and, hence, stabilizes the position of LFA-1 in the IS (7, 47), we also investigated whether SLP76 is required for targeting of talin to the IS after TCR stimulation.

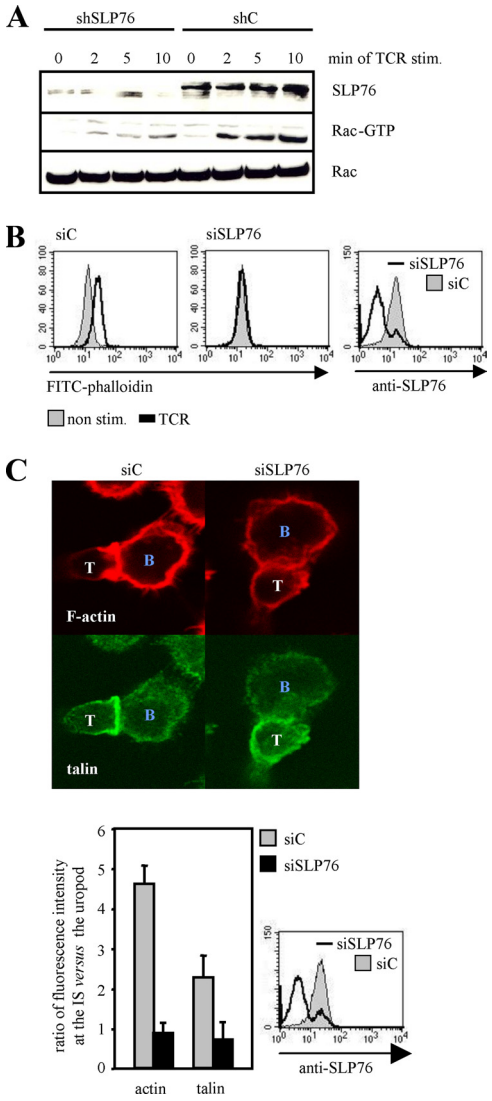

FIGURE 3. TCR-mediated actin remodeling, Rac activation, and recruitment of talin to the IS require the presence of SLP76. *A*, Jurkat T cells were transfected with either control vector (shC) or SLP76-suppression vector (shSLP76). After 48 h, cells were either left untreated or stimulated with anti-CD3 mAbs (TCR) for the indicated periods of time. GTP-loaded Rac was precipitated using the GST-PBD fusion protein. Precipitates and aliquots of whole-cell extracts were analyzed using the indicated Abs by means of Western blotting. One representative experiment of two is shown. *B*, Purified human T cells were transfected with either control siRNA (siC) or siRNA against SLP76 (siSLP76). After 72 h, cells were left untreated or stimulated with anti-CD3 mAbs (TCR) for 5 min and stained with FITC-coupled phalloidin. Reduction of SLP76 expression in human T cells was assessed by flow cytometry. Data are representative of three individual experiments. *C*, Human T cells transfected as described above were allowed to form conjugates with SA-loaded B cells for 30 min. Cells were fixed, permeabilized, and stained with TRITC-phalloidin (red) or talin (green). Fluorescence intensity of F-actin and talin at IS or uropod was quantified and calculated as ratio of intensity for the individual molecules at the IS vs the uropod. The knockdown efficiency of SLP76 was evaluated by flow cytometry. Data present the average results of three independent experiments.

Fig. 3*C* (*lower right panel*) shows that SLP76^{low} T cells also fail to target talin to the IS upon incubation with SA-pulsed B cells. Thus, SLP76 appears to also regulate LFA-1-dependent adhesion processes in activated T cells through its ability to recruit talin to the IS.

Activation of Rap1 and localization of the SKAP55/RIAM module to the IS depend on SLP76

Both the activation and the transport of Rap1 to the plasma membrane are known to regulate LFA-1 activation (6, 17, 48). Therefore, we next investigated whether loss of SLP76 affects TCR-mediated activation of Rap1. Fig. 4*A* demonstrates that control transfected cells exhibited strong activation of Rap1 within 2–10 min after TCR stimulation, whereas in SLP76^{low} Jurkat T cells, TCR-induced Rap1 was strongly suppressed. These results demonstrate that SLP76 is critically involved in Rap1 activation in response to TCR triggering.

We have recently shown that formation and membrane recruitment of a signaling module consisting of the cytosolic adapter proteins ADAP and SKAP55 and the Rap1 effector molecule RIAM (ADAP/SKAP55/RIAM module) regulate TCR-mediated LFA-1 activation through recruitment of Rap1 to the plasma membrane (17, 21). Moreover, an inducible association between SLP76 and ADAP following TCR stimulation had been suggested in several previous studies, but the question of whether SLP76 links the TCR via the ADAP/SKAP55/RIAM module to integrin activation has to date not been addressed directly. To clarify this point, we immunoprecipitated SLP76 from resting or TCR-stimulated T cells and subsequently analyzed the precipitates for coprecipitation of ADAP, SKAP55, RIAM, and Rap1 by means of Western blotting. Fig. 4*B* depicts that SLP76 inducibly associates with both the ADAP/SKAP55/RIAM complex and Rap1 upon TCR stimulation of Jurkat T cells (Fig. 4*B*, *left panel*) as well as of primary T cells (Fig. 4*B*, *right panel*). Analysis of SKAP55 immunoprecipitates that were prepared from either SLP76-proficient or SLP76-deficient T cells further revealed that Rap1 only associates with the ADAP/SKPAP55//RIAM module if SLP76 is present (Fig. 4*C*). Because only active Rap1 can interact with RIAM (12), this finding is most likely due to the attenuated activation of Rap1 in the absence of SLP76 (see Fig. 4*A*).

The immunoprecipitation data shown in Fig. 4, *B* and *C*, were further substantiated by cellular subfractionation experiments that showed that TCR-mediated plasma membrane recruitment of ADAP, SKAP55, RIAM, and Rap1 (Fig. 4*D*) and, consequently, targeting of SKAP55, RIAM, and Rap1 to the IS (Fig. 4*E*) were strongly impaired in SLP76^{low} T cells. In summary, the data shown in Fig. 4 indicate that SLP76 is required for both activation and plasma membrane/IS targeting through the ADAP/SKAP55/RIAM/Rap1 module of Rap1 after TCR triggering.

SLP76 is dispensable for CXCR4-mediated adhesion to ICAM-1 and affinity regulation of LFA-1

Similar to the TCR, triggering of the chemokine receptor CXCR4 leads to activation of LFA-1 and T cell adhesion to ICAM-1 (6). Above we have shown that SLP76 is mandatory for TCR-mediated integrin activation (Figs. 1 and 2). Therefore, we were interested to investigate whether SLP76 is also required for CXCR4-mediated adhesion. To assess this point, we down-regulated SLP76 expression by siRNA and subsequently analyzed the capability of SLP76^{low} T cells to adhere to ICAM-1 in response to CXCL12 in an adhesion assay. Surprisingly, these experiments revealed that SLP76^{low} T cells were as capable to adhere to Fc-ICAM-1 in response to CXCL12 as their SLP76^{high} counterparts (Fig. 5*A*). Similarly, neither the binding of soluble Fc-ICAM-1 (Fig. 5*B*) nor of the conformation-sensitive anti-LFA-1 mAb KIM127 (data not shown) was altered in SLP76^{low} T cells. Hence, we conclude that, in contrast to TCR stimulation, the presence of SLP76 is dispensable for T cell adhesion and affinity regulation in response to CXCL12 stimulation.

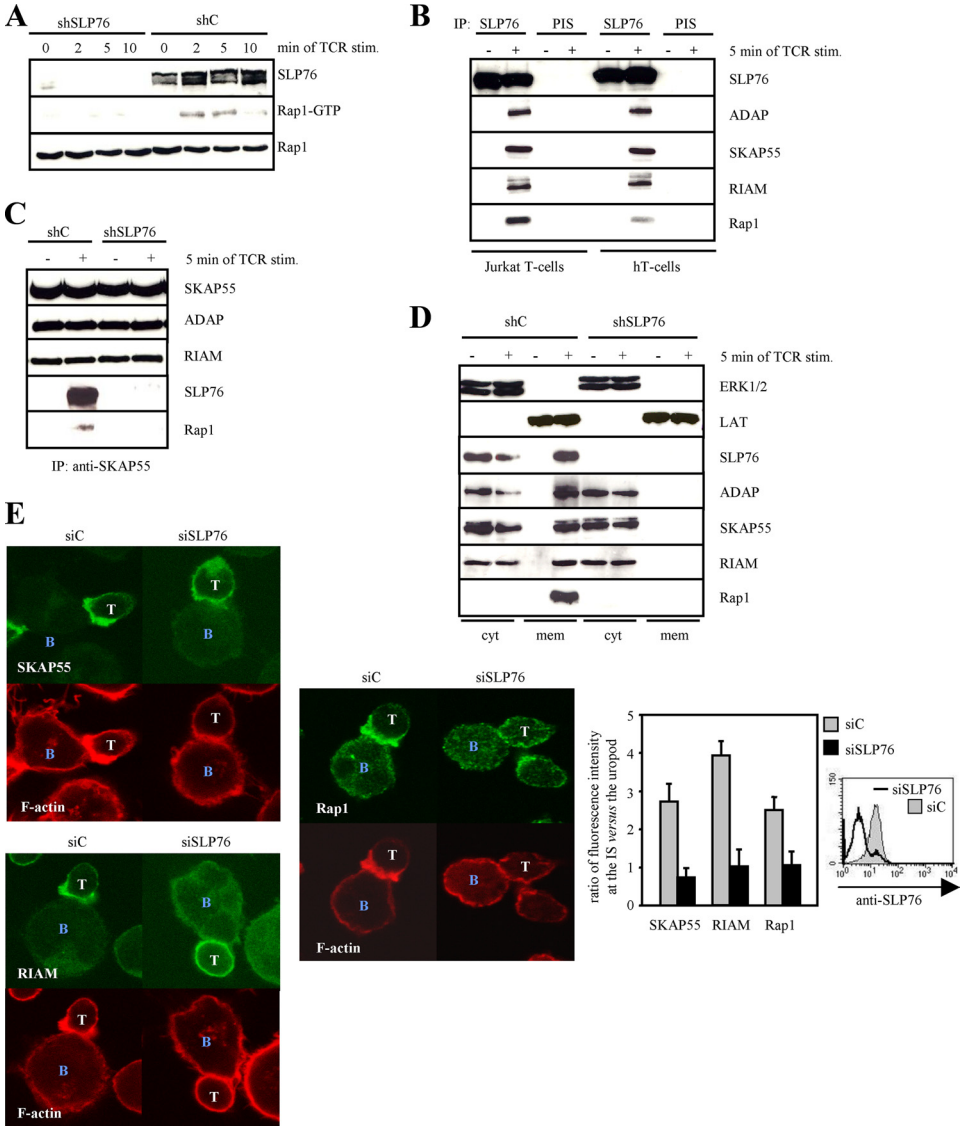

FIGURE 4. The inducible interaction between ADAP and SLP-76 is mandatory for the recruitment of SKAP55, RIAM, and Rap1 to the plasma membrane. *A*, Jurkat T cells were transfected with either control vector (shC) or SLP76-suppression vector (shSLP76). After 48 h, cells were either left untreated or stimulated with anti-CD3 mAbs (TCR) for the indicated periods of time. GTP-loaded Rap1 was precipitated using the GST-RalGDS-RBD fusion protein. Precipitates and aliquots of whole-cell extracts were analyzed with the indicated Abs by Western blotting. One representative experiment of three is shown. *B*, Jurkat T cells or human T cells (hT-cells) were left untreated or stimulated with anti-CD3 mAbs (+). Immunoprecipitations were performed using anti-SLP76 or preimmune sheep serum (anti-PIS), and precipitates were analyzed by Western blotting with the indicated Abs. One representative experiment of two is shown. *C*, Jurkat T cells were transfected as described in *A*. SKAP55 was immunoprecipitated from untreated or stimulated cells, and proteins interacting with SKAP55 were detected by Western blotting using the indicated Abs. Data are representative for two individual experiments. *D*, Jurkat T cells were transfected as described in *A*, and plasma membrane or cytosolic fractions were prepared from untreated (−) or TCR-stimulated cells (+). The individual fractions were analyzed by Western blotting using the indicated Abs. Fractionation efficiency was assessed by Western blotting using anti-LAT (plasma membrane) or anti-ERK1/2 (cytosol) Abs, respectively. One representative experiment of two is shown. *E*, Human T cells transfected with control siRNA (siC) or siRNA against SLP76 (siSLP76) were allowed to form conjugates with SA-loaded B cells for 30 min. Fixed and permeabilized cells were stained with mAbs to SKAP55, RIAM, or Rap1 (green) and TRITC-phalloidin (red). Fluorescence intensity of SKAP55, RIAM, or Rap1 at IS or uropod was quantified and calculated as ratio of intensity for the individual protein at the IS vs the uropod. Loss of SLP76 expression for each experiment was analyzed by flow cytometry. Data present the average results of three independently performed experiments.

SLP76 is dispensable for CXCR4-mediated Rac activation, actin dynamics, and migration

Similar to TCR stimulation, remodeling of the actin cytoskeleton through Rac is crucial for inducing T cell adhesion, polarization, and chemotaxis following CXCR4 stimulation (33). Our above findings led us to ask whether the presence of SLP76 might be dispensable for Rac activation in response to CXCL12 triggering. As shown in Fig. 6*A*, SLP76^{low} Jurkat T cells indeed display no obvious defect in CXCL12-mediated activation of Rac. Moreover, both SLP76^{high} and SLP76^{low} T cells revealed comparable levels of F-actin formation in response to CXCL12 (Fig. 6*B*). These data strongly suggest that SLP76 is indeed dispensable for signaling events that are critically involved in CXCR4-mediated activation of Rac and actin polymerization.

To prove whether expression of SLP76 is required for CXCR4-induced T cell chemokinesis, we determined the lateral locomotion of T cells by live cell imaging on Fc-ICAM-1-coated coverslips. As shown in Fig. 6*C*, both SLP76^{high} and SLP76^{low} T cells showed comparable basal and CXCL12-induced velocities. In contrast, and in line with previously published data (31), Vav1-deficient T cells displayed

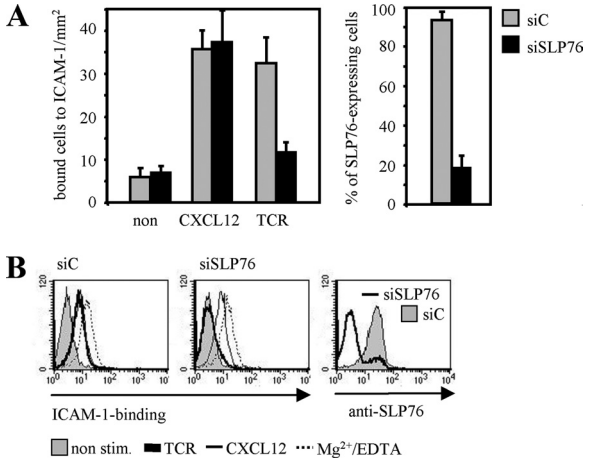

FIGURE 5. SLP76 is dispensable for CXCL12-mediated adhesion to ICAM-1, affinity maturation of LFA-1. *A*, Human T cells were transfected with control siRNA (siC) or siRNAs against SLP76 (siSLP76). Cells were left untreated or stimulated with immobilized CXCL12 (10 min) or anti-CD3 mAbs (TCR) for 30 min. Subsequently, cells were analyzed for their ability to adhere to Fc-ICAM-1. Suppression of SLP76 expression was assessed by flow cytometry, and the percentage of SLP76-expressing cells was calculated. Data represent the mean and SE of three independently performed experiments. *B*, Human T cells transfected as described in *A* were analyzed for their ability to bind soluble Fc-ICAM-1 upon anti-CD3 (TCR), CXCL12, or Mg^{2+}/EGTA (positive control) treatment for 5 min. Suppression of SLP76 expression was evaluated by flow cytometry. One individual experiment of three is shown.

a strongly reduced motility upon CXCR4 triggering (Fig. 6*C*). It is also important to note that nearly all $SPL76^{low}$ T cells displayed a polarized phenotype upon chemokine stimulation, whereas the majority of Vav1-depleted T cells remained a round, nonpolarized shape (Fig. 6*C*). Fig. 6*D* further demonstrates that the absence of SLP76 does not alter CXCR4-induced chemotaxis of human primary T cells in response to a CXCL12 gradient in vitro. In summary, it appears as if SLP76 is not mandatory for migratory steps triggered by CXCL12.

The ADAP/SKAP55/RIAM module is recruited to the plasma membrane independently of SLP76

Upon T cell activation, the Gads/SLP76 complex is recruited to phosphorylated LAT, thereby coupling the TCR to the intracellular signaling machinery (2, 49). Given the above data, we next investigated whether the LAT/Gads/SLP76 signaling platform would be assembled after CXCR4 stimulation. To test this, we stimulated human T cells for various periods of time with CXCL12 and subsequently analyzed global tyrosine phosphorylation of LAT by Western blotting. In contrast to TCR stimulation, phosphorylation of LAT was only very weakly induced upon CXCR4 triggering (Fig. 7*A*). Similar results were obtained when the phosphorylation status of LAT at Y^{171} (which is important for Gads binding) was assessed (Fig. 7*A*). These data suggested that the Gads/SLP76 complex might not associate with LAT following CXCR4 triggering. To investigate this point in more detail, we immunoprecipitated the Gads/SLP76 complex from untreated, TCR-stimulated, or CXCR4-triggered T cells. Fig. 7*B* shows that an inducible interaction among Gads/SLP76, LAT, and Vav1 was readily detectable after TCR stimulation. In contrast, neither LAT nor Vav1 was found to be associated with the Gads/SLP76 complex in

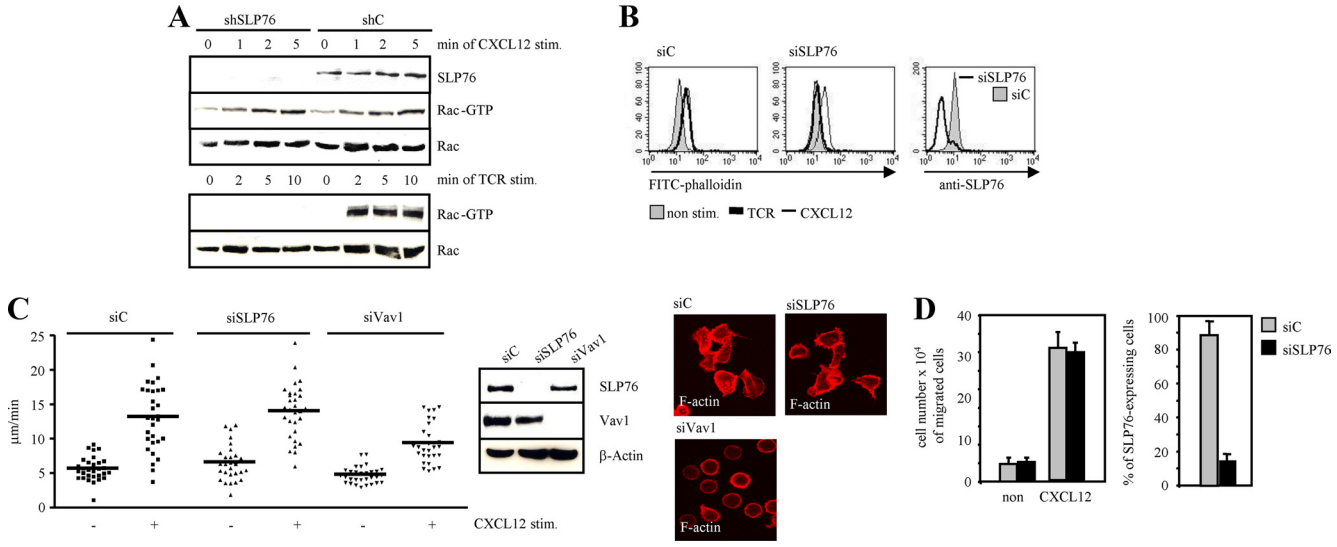

FIGURE 6. The presence of SLP76 is not required for Rac activation, actin polymerization, motility, and chemotaxis in response to CXCL12. *A*, Jurkat T cells were transfected with either control vector (shC) or SLP76-suppression vector (shSLP76). After 48 h, cells were either left untreated, or stimulated with CXCL12 or anti-CD3 mAbs (TCR) for the indicated time points. Activated Rac was precipitated using the GST-PBD fusion protein. Precipitates and aliquots of whole-cell extracts were analyzed by Western blotting using the indicated Abs. One representative experiment of three is shown. *B*, Human T cells were transfected with control siRNA (siC) or siRNA against SLP76 (siSLP76). After 72 h, cells were left untreated, stimulated with anti-CD3 mAbs (TCR, for 5 min) or CXCL12 for 1 min, and stained with FITC-coupled phalloidin. Reduction of SLP76 expression in human T cells was assessed by flow cytometry. Data are representative of three independent experiments. *C*, Human T cells were transfected with control siRNA (siC), siRNA against SLP76 (siSLP76), or siRNA against Vav1 (siVav1). After 72 h, motility of T cells in the absence or presence of CXCL12 was determined on Fc-ICAM-1-coated coverslips, as described in *Materials and Methods*. In parallel, transfectants were stimulated on Fc-ICAM-1-coated coverslips with CXCL12 for 30 min. Cells were fixed, permeabilized, and stained with TRITC-phalloidin. Whole-cell extracts were analyzed by Western blotting for the expression of SLP76, Vav1, and β-actin. One individual experiment of three is shown. *D*, Chemotaxis of human T cells transfected as described in *A* was addressed using a Transwell assay, as described in *Materials and Methods*. After 2 h, the number of migrated cells into the lower chamber was counted. Suppression of SLP76 expression was assessed by flow cytometry, and the percentage of SLP76-expressing cells was calculated. Data represent the mean and SE of three independently performed experiments.

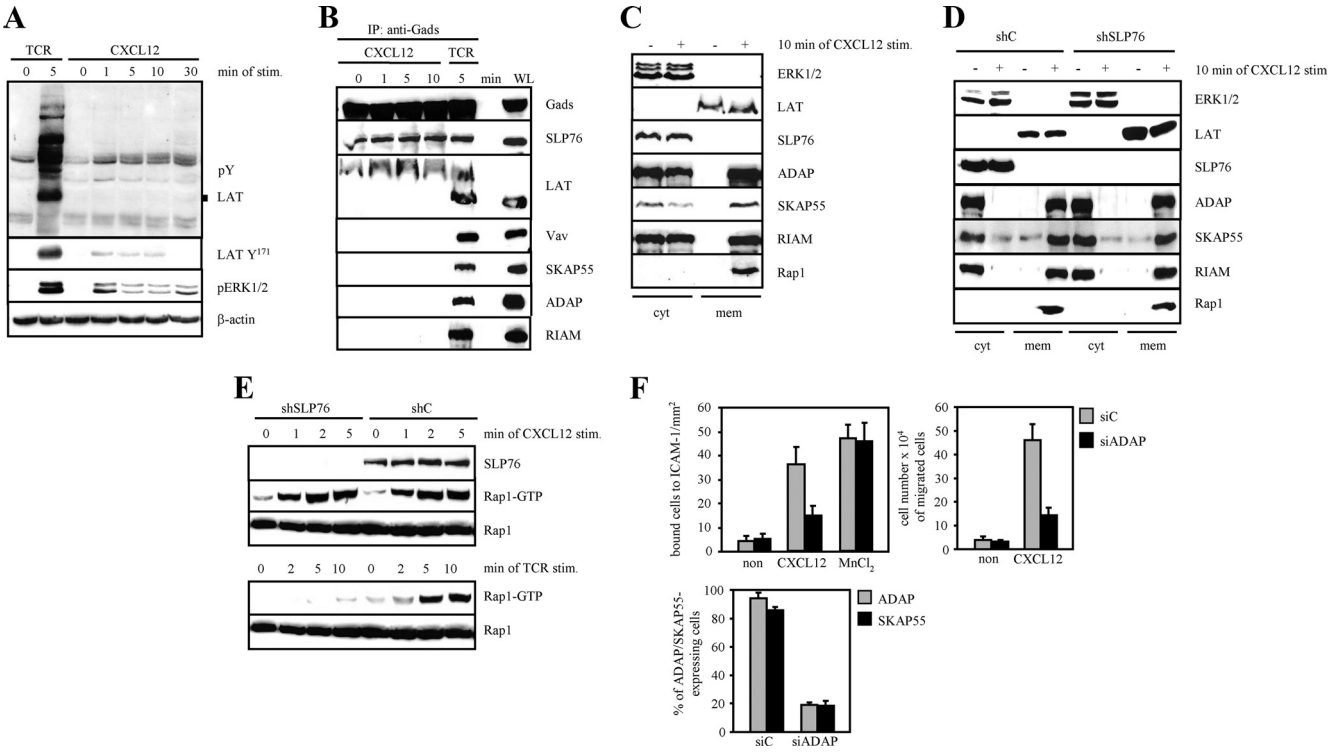

FIGURE 7. The SLP76/Gads complex is not associated with LAT or transported to the plasma membrane upon CXC12 stimulation. *A*, Human T cells were either left untreated, or stimulated with anti-CD3 mAbs (TCR) or CXCL12 for the indicated periods of time. Lysates were analyzed by Western blotting using the indicated Abs. *B*, The cell extracts as described in *A* were used for immunoprecipitation using anti-Gads Ab. Precipitates were analyzed by Western blotting using the indicated Abs. *C*, Plasma membrane or cytosolic fractions were prepared from untreated (−) or CXCR4-stimulated human T cells (+). The individual fractions were analyzed by Western blotting using the indicated Abs. Fractionation efficiency was assessed by Western blotting using anti-LAT (plasma membrane) or anti-ERK1/2 (cytosol) Abs, respectively. One representative experiment of two is shown. *D*, Jurkat T cells were transfected with either control vector (shC) or SLP76-suppression vector (shSLP76). After 48 h, plasma membrane or cytosolic fractions were prepared from untreated (−) or CXCR4-stimulated cells (+). The individual fractions were analyzed by Western blotting using the indicated Abs. Fractionation efficiency was assessed by Western blotting using anti-LAT (plasma membrane) or anti-ERK1/2 (cytosol) Abs, respectively. One representative experiment of two is shown. *E*, Jurkat T cells were transfected with either control vector (shC) or SLP76-suppression vector (shSLP76). After 48 h, cells were either left untreated, or stimulated with CXCL12 or anti-CD3 mAbs (TCR) for the indicated time points. GTP-loaded Rap1 was precipitated using the GST-RalGDS-RBD fusion protein. Precipitates and aliquots of whole-cell extracts were analyzed by Western blotting using the indicated Abs. One representative experiment of three is shown. *F*, Human T cells were transfected with control siRNA (siC) or siRNA against ADAP (siADAP). After 72 h, transfectants were left untreated or stimulated with CXCL12 (for 10 min) or $MnCl_2$ (for 30 min) and subsequently analyzed for their ability to adhere to Fc-ICAM-1. Chemotaxis of the same cells was analyzed using a Transwell assay, as described in *Materials and Methods*. After 2 h, the number of migrated cells into the lower chamber was determined. Suppression of ADAP and SKAP55 expression was determined by flow cytometry, and the percentage of ADAP/SKAP55-expressing cells was calculated. Note that loss of ADAP abrogates SKAP55 expression (17). Data represent the mean and SE of three independently performed experiments.

response to CXCL12 stimulation (Fig. 7*B*). These experiments indicate that the LAT/Gads/SLP76 signaling platform is not assembled in response to CXCL12 in T cells.

Above we have shown that the ADAP/SKAP55/RIAM module inducibly interacts with SLP76 upon TCR-mediated T cell activation, and that SLP76 is mandatory for membrane targeting of the ADAP/SKAP55/RIAM module and for activation of Rap1 (Fig. 4). In marked contrast, CXCL12 stimulation of T cells did not lead to an inducible interaction between the LAT/Gads/SLP76 complex and the ADAP/SKAP55/RIAM module (Fig. 7*B*). However, the ADAP/SKAP55/RIAM module (and also Rap1) was properly recruited to the plasma membrane in response to CXCR4 stimulation in both SLP76-proficient and -deficient T cells (Fig. 7, *C* and *D*). Moreover, $SLP76^{low}$ Jurkat T cells displayed no obvious defect in CXCL12-mediated activation of Rap1 (Fig. 7*E*). These data suggest that SLP76 is not required for CXCR4-mediated Rap1 activation and plasma membrane targeting of ADAP, SKAP55, RIAM, and Rap1.

To exclude the possibility that ADAP and SKAP55 themselves are dispensable for CXCR4-regulated adhesion and migration, we down-regulated ADAP expression in human T cells by siRNA and subsequently assessed both the adhesiveness and migratory capacity of these cells in response to CXCL12. Fig. 7*F* shows that loss of ADAP strongly attenuated CXCR4-induced adhesion and chemotaxis in human T cells. Similar data were obtained when we assessed CXCR4-induced migration of $ADAP^{low}$ Jurkat T cells or of T cells obtained from ADAP-deficient mice (data not shown). In summary, our data show that in contrast to TCR stimulation, SLP76 is not involved in membrane recruitment of the ADAP/SKAP55/RIAM module, the activation of Rac or Rap1, and the induction of adhesion or migration in response to CXCR4 stimulation.

Discussion

Together with the transmembrane adapter protein LAT, the cytosolic adapter protein SLP76 facilitates the formation of a signaling platform (LAT/Gads/SLP76) following TCR stimulation that leads to the activation of multiple intracellular signaling pathways (49). Our previous data suggested that the signaling pathways controlled by the Gads/SLP76 complex also include those regulating adhesion processes (22). In this study, we confirm this hypothesis by showing that suppression of SLP76 expression by RNAi in human T cells or the

Jurkat T cell line abrogates TCR-mediated conjugate formation, adhesion to ICAM-1, and affinity/avidity maturation of LFA-1. Consistent with previously published data (50, 51), we also found that loss of SLP76 attenuates adhesion to fibronectin (the ligand of β_1 integrins; VLA-4) in response to TCR stimulation (J. Horn and S. Kliche, unpublished data). Thus, SLP76 regulates TCR-induced inside-out signaling, leading to the activation of β_1 and β_2 integrins.

Reorganization of the actin cytoskeleton is critically involved in TCR-mediated integrin activation (33, 34). Moreover, it has previously been demonstrated that overexpression of SLP76 enhances F-actin formation in response to TCR stimulation (52). In addition to these overexpression data, we show in this study that loss of SLP76 attenuates TCR-mediated polymerization of F-actin. Together these findings suggest that SLP76 is one of the (if not the) central molecule that links the TCR to remodeling of the actin cytoskeleton.

The defect in actin dynamics most likely results from an abrogated activation of the small GTPase Rac. Activation of Rac depends on membrane recruitment and activation of the GEF Vav1 and the Tec kinase Itk (20, 32). Both Vav1 and Itk associate with SLP76 upon TCR stimulation, and both molecules are required for F-actin formation at the IS, activation of Rac, clustering of LFA-1, adhesion to ICAM-1, and conjugate formation (20, 32). In this scenario, the role of Vav1 is to generate sufficient pools of activated Rac to promote F-actin polymerization through activation of proteins of the Wiskott-Aldrich syndrome protein/Wiskott-Aldrich syndrome-Verprolin-homologues protein family (33, 34). Our data showing attenuated actin reorganization in SLP76^{low} cells are in line with a model in which loss of SLP76 blocks activation of Rac (and consequently signaling events downstream of Rac) by impairing the functions of Vav1 and Itk.

We are, however, aware that another group recently reported that TCR-mediated actin remodeling is not attenuated in the SLP76-deficient Jurkat T cell line J14 (53). In addition, no defect in Rac activation upon TCR stimulation was observed in this Jurkat variant (54). The reasons for these discrepant findings in SLP76-deficient Jurkat T cells vs SLP76^{low} human T cells are unclear at present. A possible explanation may come from compensatory mechanisms that developed in line J14 to escape the selection pressure that cannot develop in short-term manipulated T cells.

Besides the reorganization of the actin cytoskeleton, one critical regulator of TCR-mediated conjugate formation and inside-out signaling is the small GTPase Rap1 (6). Several studies have reported that Rap1 activation critically depends on the expression of PLCγ1 (13, 26, 55). PLCγ1 signaling to Rap1 occurs via the nucleotide exchange factor calcium and diacylglycerol-regulated guanine nucleotide exchange factor I that is activated by the second messengers calcium and diacylglycerol (which both are generated following phosphatidylinositol 4,5-bisphosphate hydrolysis by PLCγ1). Thus, a defect in PLCγ1 activation in SLP76-suppressed T cells (see Fig. 1*C* and supplemental Fig. 2, *C* and *D*) and consequently a failure to activate CalDAG-GEFI might be largely responsible for the attenuated activation of Rap1 after TCR triggering in the absence of SLP76. However, additional mechanisms controlled by SLP76 may also contribute to the block in Rap1 activation. For example, SLP76 is mandatory for activation and membrane targeting of protein kinase Cθ, which has recently been identified to control TCR-induced Rap1 activity by phosphorylation of Rap1-GEF2 (56, 57). Hence, loss of SLP76 might affect several signaling pathways that are critical for TCR-induced activation of Rap1.

We had previously shown that the ADAP/SKAP55/RIAM complex is required for plasma membrane targeting of Rap1. Moreover, we had demonstrated that this event is crucial for inside-out signaling and for the activation of integrins in response to TCR stimulation. However, loss of ADAP and/or SKAP55 selectively abrogated plasma membrane recruitment of Rap1, although TCR-mediated activation of Rap1 was not affected (17, 21). In contrast, the data presented in this study show that SLP76 is mandatory for both membrane targeting and activation of Rap1 after TCR triggering. The former event most likely involves the ADAP/SKAP55/RIAM module, whereas the activation of Rap1 might be regulated through the PLCγ1- or the protein kinase Cθ-signaling pathways that were discussed above. Hence, our data support a model in which plasma membrane targeting and activation of Rap1 are two interrelated, but distinctly controlled signaling events that are organized at the level of SLP76.

The activation of Rap1 and Rac as well as changes in F-actin dynamics are also mandatory for affinity modulation of LFA-1, T cell adhesion, and migration in response to CXCR4 stimulation (6, 58). Given the central role of SLP76 in TCR-mediated signaling, it was totally unexpected for us to find that loss of SLP76 did not affect these events after CXCR4 stimulation and that the SLP76/Gads complex was not recruited to LAT in response to CXCR4 stimulation. The latter observation is probably due to the fact that the tyrosine residue within LAT that is responsible for recruiting the Gads/SLP76 complex (Y^{171}) is not phosphorylated in response to CXCL12 triggering.

Our data also showed that SLP76 is not involved in the recruitment (and consequently the activation) of downstream effector molecules (e.g., Vav1) that are important for mediating adhesion and migration processes of T cells in response to CXCL12 triggering (58). Indeed, whereas Vav1-deficient T cells failed to polarize in response to CXCL12 stimulation, SLP76^{low} T cells showed no defect in this process. Moreover, CXCL12-induced lateral migration velocity and chemotaxis were unaffected in SLP76^{low} T cells. Hence, it appears as if SLP76 is dispensable for both adhesive and migratory processes in response to CXCL12 stimulation.

In line with the functional data, we found that membrane recruitment of the ADAP/SKAP55/RIAM module that is critical for CXCR4-mediated adhesion and migration of T cells was not affected by loss of SLP76. Although this finding strongly supports our above discussed hypothesis that membrane targeting of Rap1 and activation of this GTPase are distinct processes that are individually regulated by different signaling receptors, it opens the question as to which signaling molecule provides the molecular link between CXCR4 and the ADAP/SKAP55/RIAM module.

In this regard, it has recently been shown that the cytosolic adapter protein Shc is phosphorylated upon CXCR4 stimulation and assembles into a complex that includes Lck, ZAP70, Vav1, and LAT (59). Moreover, Shc-deficient Jurkat T cells show an attenuated migratory capacity and impaired F-actin dynamics upon CXCR4 stimulation, and mutation of critical tyrosine residues of Shc ($YY^{238/240}$ or Y^{317}) results in defective phosphorylation of Vav1 and Itk (59). Thus, Shc might be an attractive candidate to connect CXCR4 with the Vav1-Itk-dependent pathway of F-actin polymerization and T cell migration (59). It will be important to assess the role of Shc in CXCR4-induced inside-out signaling, adhesion, and Rap1 activation in future studies. Similarly, it needs to be analyzed whether, and if so how, LAT is involved in this process. Experiments are currently set up in our laboratory to assess these points. Nevertheless, our data collectively and surprisingly indicate that, in contrast to TCR signaling, SLP76 is not a key component connecting the chemokine receptor CXCR4 with the activation of integrins and the induction of T cell adhesion and migration.

Acknowledgments

We thank A. Weiss, V. Horejsi, J. Bos, T. Seufferlein, D. D. Billadeau, G. A. Koretzky, and N. Hogg for providing reagents, and K.-D. Fischer for critical reading of this manuscript. We are thankful to A. Ramonat, J. Hoppe, S. Holze, and N. Jüling for excellent technical assistance.

Disclosures

The authors have no financial conflict of interest.

References

1. Koretzky, G. A., F. Abtahian, and M. A. Silverman. 2006. SLP76 and SLP65: complex regulation of signalling in lymphocytes and beyond. *Nat. Rev. Immunol.* 6: 67–78.
2. Liu, S. K., N. Fang, G. A. Koretzky, and C. J. McGlade. 1999. The hematopoietic-specific adaptor protein gads functions in T-cell signaling via interactions with the SLP-76 and LAT adaptors. *Curr. Biol.* 9: 67–75.
3. Yablonski, D., M. R. Kuhne, T. Kadlecek, and A. Weiss. 1998. Uncoupling of nonreceptor tyrosine kinases from PLC-γ1 in an SLP-76-deficient T cell. *Science* 281: 413–416.
4. Grakoui, A., S. K. Bromley, C. Sumen, M. M. Davis, A. S. Shaw, P. M. Allen, and M. L. Dustin. 1999. The immunological synapse: a molecular machine controlling T cell activation. *Science* 285: 221–227.
5. Gunzer, M., C. Weishaupt, A. Hillmer, Y. Basoglu, P. Friedl, K. E. Dittmar, W. Kolanus, G. Varga, and S. Grabbe. 2004. A spectrum of biophysical interaction modes between T cells and different antigen-presenting cells during priming in 3-D collagen and in vivo. *Blood* 104: 2801–2809.
6. Kinashi, T. 2005. Intracellular signalling controlling integrin activation in lymphocytes. *Nat. Rev. Immunol.* 5: 546–559.
7. Kim, M., C. V. Carman, and T. A. Springer. 2003. Bidirectional transmembrane signaling by cytoplasmic domain separation in integrins. *Science* 301: 1720–1725.
8. Nolz, J. C., R. B. Medeiros, J. S. Mitchell, P. Zhu, B. D. Freedman, Y. Shimizu, and D. D. Billadeau. 2007. WAVE2 regulates high-affinity integrin binding by recruiting vinculin and talin to the immunological synapse. *Mol. Cell. Biol.* 27: 5986–6000.
9. Nolz, J. C., L. P. Nacusi, C. M. Segovis, R. B. Medeiros, J. S. Mitchell, Y. Shimizu, and D. D. Billadeau. 2008. The WAVE2 complex regulates T cell receptor signaling to integrins via Abl- and CrkL-C3G-mediated activation of Rap1. *J. Cell Biol.* 182: 1231–1244.
10. Duchniewicz, M., T. Zemojtel, M. Kolanczyk, S. Grossmann, J. S. Scheele, and F. J. Zwartkruis. 2006. Rap1A-deficient T and B cells show impaired integrin-mediated cell adhesion. *Mol. Cell. Biol.* 26: 643–653.
11. Sebzda, E., M. Bracke, T. Tugal, N. Hogg, and D. A. Cantrell. 2002. Rap1A positively regulates T cells via integrin activation rather than inhibiting lymphocyte signaling. *Nat. Immunol.* 3: 251–258.
12. Lafuente, E. M., A. A. van Puijenbroek, M. Krause, C. V. Carman, G. J. Freeman, A. Berezovskaya, E. Constantine, T. A. Springer, F. B. Gertler, and V. A. Boussiotis. 2004. RIAM, an Ena/VASP and Profilin ligand, interacts with Rap1-GTP and mediates Rap1-induced adhesion. *Dev. Cell* 7: 585–595.
13. Katagiri, K., M. Shimonaka, and T. Kinashi. 2004. Rap1-mediated lymphocyte function-associated antigen-1 activation by the T cell antigen receptor is dependent on phospholipase C-γ1. *J. Biol. Chem.* 279: 11875–11881.
14. Katagiri, K., M. Imamura, and T. Kinashi. 2006. Spatiotemporal regulation of the kinase Mst1 by binding protein RAPL is critical for lymphocyte polarity and adhesion. *Nat. Immunol.* 7: 919–928.
15. Griffiths, E. K., C. Krawczyk, Y. Y. Kong, M. Raab, S. J. Hyduk, D. Bouchard, V. S. Chan, I. Kozieradzki, A. J. Oliveira-Dos-Santos, A. Wakeham, et al. 2001. Positive regulation of T cell activation and integrin adhesion by the adapter Fyb/Slap. *Science* 293: 2260–2263.
16. Peterson, E. J., M. L. Woods, S. A. Dmowski, G. Derimanov, M. S. Jordan, J. N. Wu, P. S. Myung, Q. H. Liu, J. T. Pribila, B. D. Freedman, et al. 2001. Coupling of the TCR to integrin activation by Slap-130/Fyb. *Science* 293: 2263–2265.
17. Kliche, S., D. Breitling, M. Togni, R. Pusch, K. Heuer, X. Wang, C. Freund, A. Kasirer-Friede, G. Menasche, G. A. Koretzky, and B. Schraven. 2006. The ADAP/SKAP55 signaling module regulates T-cell receptor-mediated integrin activation through plasma membrane targeting of Rap1. *Mol. Cell. Biol.* 26: 7130–4144.
18. Wang, H., H. Liu, Y. Lu, M. Lovatt, B. Wei, and C. E. Rudd. 2007. Functional defects of SKAP-55-deficient T cells identify a regulatory role for the adaptor in LFA-1 adhesion. *Mol. Cell. Biol.* 27: 6863–6875.
19. Bezman, N. A., L. Lian, C. S. Abrams, L. F. Brass, M. L. Kahn, M. S. Jordan, and G. A. Koretzky. 2008. Requirements of SLP76 tyrosines in ITAM and integrin receptor signaling and in platelet function in vivo. *J. Exp. Med.* 205: 1775–1788.
20. Gomez-Rodriguez, J., J. A. Readinger, I. C. Viorritto, K. L. Mueller, R. A. Houghtling, and P. L. Schwartzberg. 2007. Tec kinases, actin, and cell adhesion. *Immunol. Rev.* 218: 45–64.
21. Menasche, G., S. Kliche, E. J. Chen, T. E. Stradal, B. Schraven, and G. Koretzky. 2007. RIAM links the ADAP/SKAP-55 signaling module to Rap1, facilitating T-cell-receptor-mediated integrin activation. *Mol. Cell. Biol.* 27: 4070–4081.
22. Jordan, M. S., J. S. Maltzman, S. Kliche, J. Shabason, J. E. Smith, A. Obstfeld, B. Schraven, and G. A. Koretzky. 2007. In vivo disruption of T cell development by expression of a dominant-negative polypeptide designed to abolish the SLP-76/Gads interaction. *Eur. J. Immunol.* 37: 2961–2972.
23. Wang, H., F. E. McCann, J. D. Gordan, X. Wu, M. Raab, T. H. Malik, D. M. Davis, and C. E. Rudd. 2004. ADAP-SLP-76 binding differentially regulates supramolecular activation cluster (SMAC) formation relative to T cell-APC conjugation. *J. Exp. Med.* 200: 1063–1074.
24. Campbell, D. J., C. H. Kim, and E. C. Butcher. 2003. Chemokines in the systemic organization of immunity. *Immunol. Rev.* 195: 58–71.
25. Smith, A., Y. R. Carrasco, P. Stanley, N. Kieffer, F. D. Batista, and N. Hogg. 2005. A talin-dependent LFA-1 focal zone is formed by rapidly migrating T lymphocytes. *J. Cell Biol.* 170: 141–151.
26. Ghandour, H., X. Cullere, A. Alvarez, F. W. Luscinskas, and T. N. Mayadas. 2007. Essential role for Rap1 GTPase and its guanine exchange factor CalDAG-GEFI in LFA-1 but not VLA-4 integrin mediated human T-cell adhesion. *Blood* 110: 3682–3690.
27. Shimonaka, M., K. Katagiri, T. Nakayama, N. Fujita, T. Tsuruo, O. Yoshie, and T. Kinashi. 2003. Rap1 translates chemokine signals to integrin activation, cell polarization, and motility across vascular endothelium under flow. *J. Cell Biol.* 161: 417–427.
28. Katagiri, K., T. Katakai, Y. Ebisuno, Y. Ueda, T. Okada, and T. Kinashi. 2009. Mst1 controls lymphocyte trafficking and interstitial motility within lymph nodes. *EMBO J.* 28: 1319–1331.
29. Katagiri, K., N. Ohnishi, K. Kabashima, T. Iyoda, N. Takeda, Y. Shinkai, K. Inaba, and T. Kinashi. 2004. Crucial functions of the Rap1 effector molecule RAPL in lymphocyte and dendritic cell trafficking. *Nat. Immunol.* 5: 1045–1051.
30. Miertzschke, M., P. Stanley, T. D. Bunney, F. Rodrigues-Lima, N. Hogg, and M. Katan. 2007. Characterization of interactions of adapter protein RAPL/Nore1B with RAP GTPases and their role in T cell migration. *J. Biol. Chem.* 282: 30629–30642.
31. Garcia-Bernal, D., N. Wright, E. Sotillo-Mallo, C. Nombela-Arrieta, J. V. Stein, X. R. Bustelo, and J. Teixido. 2005. Vav1 and Rac control chemokine-promoted T lymphocyte adhesion mediated by the integrin $\alpha_4\beta_1$. *Mol. Biol. Cell* 16: 3223–3235.
32. Tybulewicz, V. L. 2005. Vav-family proteins in T-cell signalling. *Curr. Opin. Immunol.* 17: 267–274.
33. Burkhardt, J. K., E. Carrizosa, and M. H. Shaffer. 2008. The actin cytoskeleton in T cell activation. *Annu. Rev. Immunol.* 26: 233–259.
34. Billadeau, D. D., J. C. Nolz, and T. S. Gomez. 2007. Regulation of T-cell activation by the cytoskeleton. *Nat. Rev. Immunol.* 7: 131–143.
35. Heuer, K., M. Sylvester, S. Kliche, R. Pusch, K. Thiemke, B. Schraven, and C. Freund. 2006. Lipid-binding hSH3 domains in immune cell adapter proteins. *J. Mol. Biol.* 361: 94–104.
36. Hunter, A. J., N. Ottoson, N. Boerth, G. A. Koretzky, and Y. Shimizu. 2000. Cutting edge: a novel function for the SLAP-130/FYB adapter protein in β_1 integrin signaling and T lymphocyte migration. *J. Immunol.* 164: 1143–1147.
37. Jenzora, A., B. Behrendt, J. V. Small, J. Wehland, and T. E. Stradal. 2005. PREL1 provides a link from Ras signalling to the actin cytoskeleton via Ena/VASP proteins. *FEBS Lett.* 579: 455–463.
38. Weiss, A., and J. D. Stobo. 1984. Requirement for the coexpression of T3 and the T cell antigen receptor on a malignant human T cell line. *J. Exp. Med.* 160: 1284–1299.
39. Motto, D. G., S. E. Ross, J. Wu, L. R. Hendricks-Taylor, and G. A. Koretzky. 1996. Implication of the GRB2-associated phosphoprotein SLP-76 in T cell receptor-mediated interleukin 2 production. *J. Exp. Med.* 183: 1937–1943.
40. Marie-Cardine, A., L. R. Hendricks-Taylor, N. J. Boerth, H. Zhao, B. Schraven, and G. A. Koretzky. 1998. Molecular interaction between the Fyn-associated protein SKAP55 and the SLP-76-associated phosphoprotein SLAP-130. *J. Biol. Chem.* 273: 25789–25795.
41. Musci, M. A., L. R. Hendricks-Taylor, D. G. Motto, M. Paskind, J. Kamens, C. W. Turck, and G. A. Koretzky. 1997. Molecular cloning of SLAP-130, an SLP-76-associated substrate of the T cell antigen receptor-stimulated protein tyrosine kinases. *J. Biol. Chem.* 272: 11674–11677.
42. Huang, Y., D. D. Norton, P. Precht, J. L. Martindale, J. K. Burkhardt, and R. L. Wange. 2005. Deficiency of ADAP/Fyb/SLAP-130 destabilizes SKAP55 in Jurkat T cells. *J. Biol. Chem.* 280: 23576–23583.
43. Li, Y. F., R. H. Tang, K. J. Puan, S. K. Law, and S. M. Tan. 2007. The cytosolic protein talin induces an intermediate affinity integrin $\alpha_L\beta_2$. *J. Biol. Chem.* 282: 24310–24319.
44. Dluzniewska, J., L. Zou, I. R. Harmon, M. T. Ellingson, and E. J. Peterson. 2007. Immature hematopoietic cells display selective requirements for adhesion- and degranulation-promoting adaptor protein in development and homeostasis. *Eur. J. Immunol.* 37: 3208–3219.
45. Krutzik, P. O., and G. P. Nolan. 2003. Intracellular phospho-protein staining techniques for flow cytometry: monitoring single cell signaling events. *Cytometry A* 55: 61–70.
46. Reichardt, P., F. Gunzer, and M. Gunzer. 2007. Analyzing the physicodynamics of immune cells in a three-dimensional collagen matrix. *Methods Mol. Biol.* 380: 253–269.
47. Liu, S., D. A. Calderwood, and M. H. Ginsberg. 2000. Integrin cytoplasmic domain-binding proteins. *J. Cell Sci.* 113: 3563–3571.
48. Bivona, T. G., H. H. Wiener, I. M. Ahearn, J. Silletti, V. K. Chiu, and M. R. Philips. 2004. Rap1 up-regulation and activation on plasma membrane regulates T cell adhesion. *J. Cell Biol.* 164: 461–470.
49. Singer, A. L., S. C. Bunnell, A. E. Obstfeld, M. S. Jordan, J. N. Wu, P. S. Myung, L. E. Samelson, and G. A. Koretzky. 2004. Roles of the proline-rich domain in SLP-76 subcellular localization and T cell function. *J. Biol. Chem.* 279: 15481–15490.

50. Epler, J. A., R. Liu, H. Chung, N. C. Ottoson, and Y. Shimizu. 2000. Regulation of β_1 integrin-mediated adhesion by T cell receptor signaling involves ZAP-70 but differs from signaling events that regulate transcriptional activity. *J. Immunol.* 165: 4941–4949.
51. Nguyen, K., N. R. Sylvain, and S. C. Bunnell. 2008. T cell costimulation via the integrin VLA-4 inhibits the actin-dependent centralization of signaling microclusters containing the adaptor SLP-76. *Immunity* 28: 810–821.
52. Bubeck Wardenburg, J., R. Pappu, J. Y. Bu, B. Mayer, J. Chernoff, D. Straus, and A. C. Chan. 1998. Regulation of PAK activation and the T cell cytoskeleton by the linker protein SLP-76. *Immunity* 9: 607–616.
53. Barda-Saad, M., A. Braiman, R. Titerence, S. C. Bunnell, V. A. Barr, and L. E. Samelson. 2005. Dynamic molecular interactions linking the T cell antigen receptor to the actin cytoskeleton. *Nat. Immunol.* 6: 80–89.
54. Ku, G. M., D. Yablonski, E. Manser, L. Lim, and A. Weiss. 2001. A PAK1-PIX-PKL complex is activated by the T-cell receptor independent of Nck, Slp-76 and LAT. *EMBO J.* 20: 457–465.
55. Peak, J. C., N. P. Jones, S. Hobbs, M. Katan, and S. A. Eccles. 2008. Phospholipase Cγ1 regulates the Rap GEF1-Rap1 signalling axis in the control of human prostate carcinoma cell adhesion. *Oncogene* 27: 2823–2832.
56. Herndon, T. M., X. C. Shan, G. C. Tsokos, and R. L. Wange. 2001. ZAP-70 and SLP-76 regulate protein kinase C-θ and NF-κB activation in response to engagement of CD3 and CD28. *J. Immunol.* 166: 5654–5664.
57. Letschka, T., V. Kollmann, C. Pfeifhofer-Obermair, C. Lutz-Nicoladoni, G. J. Obermair, F. Fresser, M. Leitges, N. Hermann-Kleiter, S. Kaminski, and G. Baier. 2008. PKC-θ selectively controls the adhesion-stimulating molecule Rap1. *Blood* 112: 4617–4627.
58. Patrussi, L., and C. T. Baldari. 2008. Intracellular mediators of CXCR4-dependent signaling in T cells. *Immunol. Lett.* 115: 75–82.
59. Patrussi, L., C. Ulivieri, O. M. Lucherini, S. R. Paccani, A. Gamberucci, L. Lanfrancone, P. G. Pelicci, and C. T. Baldari. 2007. p52Shc is required for CXCR4-dependent signaling and chemotaxis in T cells. *Blood* 110: 1730–1738.

Appendix 16

The transmembrane adaptor protein SIT inhibits TCR-mediated signaling

Arndt B., Krieger T., Kalinski T., Thielitz A., Reinhold D., Rössner A., Schraven B., and **Simeoni L.** (2011) *PLosONE*, 6: e23761. doi:10.1371/journal.pone.0023761.

OPEN ACCESS Freely available online

PLoS one

The Transmembrane Adaptor Protein SIT Inhibits TCR-Mediated Signaling

Börge Arndt[1¤], Tina Krieger[1], Thomas Kalinski[2], Anja Thielitz[3], Dirk Reinhold[1], Albert Roessner[2], Burkhart Schraven[1], Luca Simeoni[1]*

1 Institute of Molecular and Clinical Immunology, Otto-von-Guericke University Magdeburg, Magdeburg, Germany, **2** Institute of Pathology, Otto-von-Guericke University Magdeburg, Magdeburg, Germany, **3** Clinic of Dermatology and Venerology, Otto-von-Guericke University Magdeburg, Magdeburg, Germany

Abstract

Transmembrane adaptor proteins (TRAPs) organize signaling complexes at the plasma membrane, and thus function as critical linkers and integrators of signaling cascades downstream of antigen receptors. We have previously shown that the transmembrane adaptor protein SIT regulates the threshold for thymocyte selection. Moreover, T cells from SIT-deficient mice are hyperresponsive to CD3 stimulation and undergo enhanced lymphopenia-induced homeostatic proliferation, thus indicating that SIT inhibits TCR-mediated signaling. Here, we have further addressed how SIT regulates signaling cascades in T cells. We demonstrate that the loss of SIT enhances TCR-mediated Akt activation and increased phosphorylation/inactivation of Foxo1, a transcription factor of the Forkhead family that inhibits cell cycle progression and regulates T-cell homeostasis. We have also shown that $CD4^+$ T cells from SIT-deficient mice display increased CD69 and CD40L expression indicating an altered activation status. Additional biochemical analyses further revealed that suppression of SIT expression by RNAi in human T cells resulted in an enhanced proximal TCR signaling. In summary, the data identify SIT as an important modulator of TCR-mediated signaling that regulates T-cell activation, homeostasis and tolerance.

Citation: Arndt B, Krieger T, Kalinski T, Thielitz A, Reinhold D, et al. (2011) The Transmembrane Adaptor Protein SIT Inhibits TCR-Mediated Signaling. PLoS ONE 6(9): e23761. doi:10.1371/journal.pone.0023761

Editor: Jose Alberola-Ila, Oklahoma Medical Research Foundation, United States of America

Received December 20, 2010; **Accepted** July 25, 2011; **Published** September 21, 2011

Funding: The work was supported by grants from the German Research Foundation (DFG), FOR-521 [SI861/1], GRK-1167 [TP12] and SFB-854 [TP19] to BS and LS. The funders had no role in study design, data collection and analysis, decision to publish, or preparation of the manuscript.

Competing Interests: The authors have declared that no competing interests exist.

* E-mail: luca.simeoni@med.ovgu.de

¤ Current address: Department of Medicine Innenstadt, Diabetes Centre, Ludwig-Maximilian University, Munich, Germany

Introduction

Transmembrane adaptor proteins (TRAPs) are a group of molecules involved in immune cell activation [1]. Among these, LAT, PAG/Cbp, NTAL/LAB and LIME are mainly localized in the lipid rafts; while TRIM, SIT and LAX are excluded from the raft fraction of the plasma membrane (reviewed in 1).

The common characteristic of TRAPs is the presence of several tyrosine-based signaling motifs (TBSMs) within their cytoplasmic tails. These are phosphorylated by protein tyrosine kinases of the Src and Syk families, thereby, enabling the TRAPs to recruit SH2-containing cytoplasmic signaling and/or effector proteins to the plasma membrane. Thus, TRAPs function as important regulators of signal transduction, connecting signal transducing cell-surface receptors with downstream cellular signaling pathways [1].

During the last years, several groups have generated knockout mice to investigate the *in vivo* function of these molecules. The data demonstrate that TRAPs play an important role in the regulation of immune-cell homeostasis. For example, LAT-deficient mice display a severe alteration of the immune system and T-cell development is completely blocked at the DN3 stage [2]. NTAL-deficient mice develop a spontaneous autoimmune disease characterized by splenomegaly, elevated levels of anti-double-stranded DNA autoantibodies, and deposition of immune complexes within the glomeruli [3]. Moreover, LAX-deficient mice display hyperactive T, B and mast cells [4,5].

We have shown that SIT-deficient mice have altered thymic selection and decreased numbers of peripheral naïve T cells [6–8]. Moreover, T cells from $SIT^{-/-}$ mice also display hyperresponsiveness to CD3 stimulation and undergo enhanced lymphopenia-induced expansion [6,7]. Finally, we showed that the clinical course of experimental autoimmune encephalomyelitis (EAE) is more severe in $SIT^{-/-}$ mice [6]. Thus, these data suggest that SIT plays an important role in T-cell homeostasis and in the establishment of tolerance.

In the present study, we extended our previous investigations on the function of SIT. We focused particularly on how SIT regulates signaling in T cells. We provide further evidence that SIT negatively regulates proximal TCR signaling and TCR-mediated phosphorylation of Akt *in vitro*. We additionally show that the phosphorylation/inactivation of Foxo1, a transcription factor downstream of Akt that inhibits cell cycle progression and regulates T-cell homeostasis [9,10], is significantly enhanced in $SIT^{-/-}$ T cells. Moreover, $CD4^+$ T cells within the secondary lymphoid organs of $SIT^{-/-}$ mice show signs of mild hyperactivation. In summary, our studies demonstrate that SIT is an important inhibitory molecule of T-cell activation.

Methods

Human Ethics

Approval for these studies involving the analysis of TCR-mediated signaling in human T cells was obtained from the Ethics

Committee of the Medical Faculty at the Otto-von-Guericke University, Magdeburg, Germany with the permission number [107/09]. Informed consent was obtained in writing in accordance with the Declaration of Helsinki.

Animal Ethics

All experiments were performed with samples taken from euthanized animals in accordance with the German National Guidelines for the Use of Experimental Animals (Animal Protection Act, Tierschutzgesetz, TierSchG). Animals were handled in accordance with the European Communities Council Directive 86/609/EEC. All possible efforts were made to minimize animal suffering and the number of animals used.

Mice

$SIT^{-/-}$ mice were previously described [6]. The mice were maintained in a pathogen free condition.

Flow cytometry

Single cell suspensions were prepared from spleen. Subsequently, 1×10^6 cells were stained with different monoclonal antibodies for 15 min at 4°C, washed and then analyzed on a FACSCalibur using the CellQuest software (Becton Dickinson). Antibodies were purchased from BD Pharmingen. Anti-CD40L (MR1) Abs was from eBioscience.

The analysis of Annexin V, Bcl-2, and BrdU was performed as previously described [7].

Cell culture

Peripheral blood mononuclear cells were isolated by Ficoll gradient (Biochrom) centrifugation of heparinized blood collected from healthy volunteers. Human T cells were further purified by non-T cell depletion using the Pan T cell isolation kit II (Miltenyi Biotec). The purity of T cells, determined by flow cytometry, was usually more then 96%. Cells were maintained in RPMI 1640 medium containing 10% FBS, stable L-glutamine, and 1000 U/ml penicillin/streptomycin at 37°C with 5% CO_2 over night before transfection. Jurkat T cells (ATCC) were maintained in RPMI 1640 medium supplemented with 10% FBS (PAN) and stable L-glutamine at 37°C with 5% CO_2.

RNA interference, plasmids and cell transfection

The following SIT siRNA duplex containing 25 nucleotides were purchased from Invitrogen: 5′-GGC UGC AGA GGA GGU GAU GUG CUA U-3′, 5′-GGG CUG UGA CGC UGC UAU UUC UCA U-3′ and 5′-GCC AGA CCA GCA GGA UCC AAC UCU U-3′. As negative control we used a Renilla Luciferase siRNA duplex from Invitrogen. To achieve efficient SIT downregulation, primary human T cells (3×10^6) were transfected with a mix of siRNA (120 nM for each duplex) using the Nucleofection Kit (Amaxa) according to the manufacturer's instruction or the Gene Pulser Xcell (Bio-Rad) as previously described [11]. Cells were harvested 72 h after electroporation. 20×10^6 Jurkat T cells were resuspended in 0.4 ml of PBS containing Ca^{2+} and Mg^{2+} and incubated with a mix of siRNA (200 nM for each duplex). Cells were transfected using Gene Pulser II (Bio-Rad) set at 230 mV, 950 µF. Cells were cultured for 48 h after electroporation.

Cell stimulation, Immunoblotting, and immunoprecipitation

Purified mouse $CD4^+$ T cells were stimulated at 37°C with 5 µg/ml soluble anti-mouse CD3ε (145-2C11; BD Biosciences) without cross-linking for the indicated time points. Human T cells were stimulated at 37°C by using OKT3 mAb without cross-linking for the indicated time points. Cell lysates were prepared and analyzed as previously described [12]. Anti-pS^{473}Akt (PKB), anti-pY^{319}ZAP70, anti-pY^{191}LAT, anti-pS^{256}Foxo1, (all from Cell Signaling Technology), anti-pY^{783}PLCγ-1, CD3ε (Santa Cruz Biotechnology), anti-pY^{145}SLP-76 (BD Biosciences), anti-β-actin (clone AC-15) (Sigma-Aldrich), anti-p-Tyr (4G10) (Upstate Biotechnology), anti-ZAP-70 (Transduction Laboratories), and anti-SIT [13] antibodies were used for Western blotting. The intensity of the detected bands was acquired using the Kodak Image station 2000R and analysis was performed using ID Image software (Kodak).

In immunoprecipitation experiments, 10×10^6 Jurkat T cells were either left unstimulated or stimulated with 5 µg/ml purified OKT3 mAb without cross-linking for 5 min at 37°C. Cell lysates were immunoprecipitated with agarose-conjugated CD3ζ (Santa Cruz Biotechnology) (Santa Cruz Biotechnology) antibody followed by recombinant protein G-Sepharose 4B (Zymed Laboratories Inc.) at 4°C overnight. After washing, CD3ζ immunoprecipitates were resolved by SDS-PAGE, transferred to a membrane, and analyzed by immunoblotting with the indicated antibodies.

Statistics

Statistical analyses were performed using GraphPad Prism (GraphPad Software Inc., San Diego, CA). p values were determined by an unpaired two-tailed Student's t test.

Results

Loss of SIT results in an enhanced activation of the TCR-mediated Akt-Foxo pathway

Recently, we have shown that SIT is an important modulator of T-lymphocyte functions. SIT negatively regulates selection processes within the thymus, peripheral T-cell activation and T-cell homeostasis [6–8]. Moreover, SIT-deficient mice are more susceptible to the development of EAE, a mouse model of Multiple Sclerosis [6]. As the data suggest that SIT plays an inhibitory role in T cells, we have next attempted to investigate whether SIT influences TCR-mediated signaling. However, we have found that SIT-deficient T cells develop sensory adaptation and are refractory to stimulation upon extensive crosslinking of the TCR/CD3 complex [7], Therefore, we used an alternative stimulation condition that induces only a minimal crosslinking of the antigen receptor on T cells, thus better mimicking the physiological situation. Under these conditions of stimulation, we found that SIT-deficient T cells show enhanced Akt phosphorylation (figure 1). We next investigated which intracellular signaling pathways might be affected by the augmented Akt activation in SIT-deficient T cells. We have shown that the loss of SIT results in an enhanced T-cell proliferation [6,7]. Therefore, as a putative target of Akt, we chose Foxo1, a member of the Forkhead family of transcription factors, which is implicated in cell cycle regulation [9]. One of the known functions of Foxo is to activate the transcription of the cell cycle inhibitor $p27^{kip1}$. Members of the Foxo family are phosphorylated by Akt. Phosphorylation by Akt results in the sequestration of Foxo1 into the cytosol, thus preventing $p27^{kip1}$ transcription and cell cycle inhibition. Although well characterized in other cellular systems, it is poorly understood how the Akt-Foxo pathway is activated in T cells. Recently, it has been shown in T cells that Vav1 activates the PI3K-Akt-Foxo1 pathway, thus regulating cell cycle progression [14]. Loss of Vav1 resulted in reduced activation of Akt, blunted Foxo1 phosphorylation, and cell cycle arrest. Conversely to $Vav1^{-/-}$ T cells, SIT-

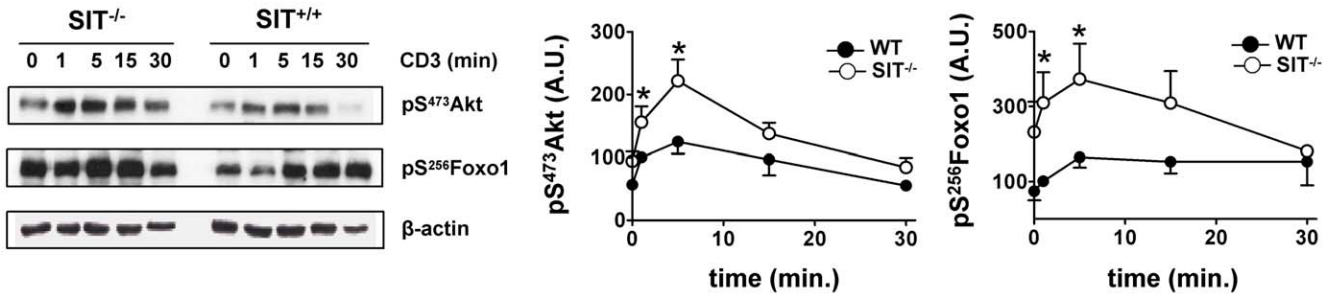

Figure 1. Enhanced phosphorylation of Akt and Foxo1 in SIT$^{-/-}$ CD4^{+} T cells. Purified splenic CD4^{+} T cells from 3–4 month-old SIT$^{-/-}$ or WT mice were stimulated with non-crosslinked CD3 (clone 145-2C11) mAb for the indicated times. Samples were analyzed by Western blotting using the indicated Abs. The phosphorylated Akt and Foxo1 bands were quantified using the ImageQuant software and values were normalized to the corresponding β-actin signal. Graphs show the phosphorylation levels of Akt and Foxo1 shown as of arbitrary units ± SEM of at least 3 independent experiments. Statistical significance * $p<0.05$.
doi:10.1371/journal.pone.0023761.g001

deficient T cells are hyperproliferative and display enhanced Akt activation. Thus, we expected to observe an enhanced phosphorylation of Foxo1 in SIT$^{-/-}$ T cells. As shown in figure 1, we found that the level of phospho-Foxo1 is indeed higher in lysates from SIT-deficient CD4^{+} T cells than in wild type cells. These results suggest that SIT inhibits TCR-mediated Akt activation and Foxo1 phosphorylation, thus likely negatively regulating T-cell proliferation.

Suppression of SIT expression enhanced proximal TCR signaling

As mentioned above, SIT-deficient mouse T cells develop compensatory mechanisms that alter proximal TCR signaling [7]. Therefore, the enhanced phosphorylation of Akt observed in SIT-deficient T cells could be due to the altered status of SIT-deficient mouse T cells. To confirm that SIT regulates Akt activation, we

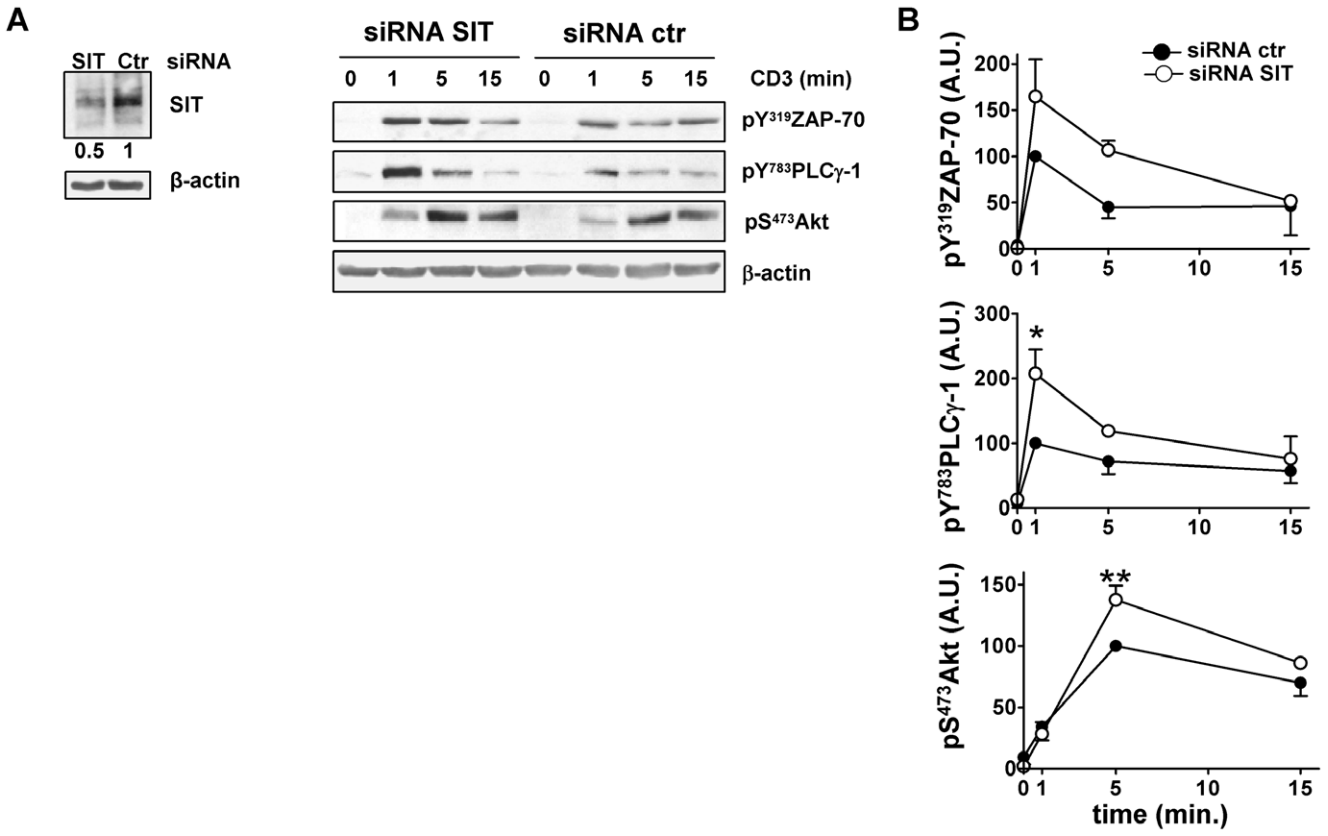

Figure 2. Downregulation of SIT results in an enhanced TCR-mediated signaling in primary human T cells. A) Primary human T cells were transfected with control or SIT-specific siRNA and 72 h later were stimulated with non-crosslinked CD3 (clone OKT3) mAb for the indicated times. Cell lysates were analyzed by immunoblotting using phosphospecific antibodies for ZAP-70, PLCγ-1, and Akt. Immunoblots verifying SIT downregulation are shown. B) Phosphorylated bands were quantified using the ImageQuant software and values were normalized to the corresponding β-actin signal. Graphs show the phosphorylation levels of ZAP-70, PLCγ-1, and Akt shown as of arbitrary units ± SEM of 2, 4, and 6 independent experiments, respectively. Statistical significance in B) * $p<0.05$ and ** $p<0.01$.
doi:10.1371/journal.pone.0023761.g002

performed RNA interference in primary human T cells. The results shown in figure 2 demonstrate that, similar to mouse T cells, downregulation of SIT in human primary T cells results in an enhanced TCR-mediated Akt phosphorylation.

Collectively, these data suggest that SIT regulates T-cell activation likely by inhibiting proximal TCR signaling events leading to Akt activation. Therefore, we next analyzed proximal TCR signaling in primary human T cells upon downregulation of

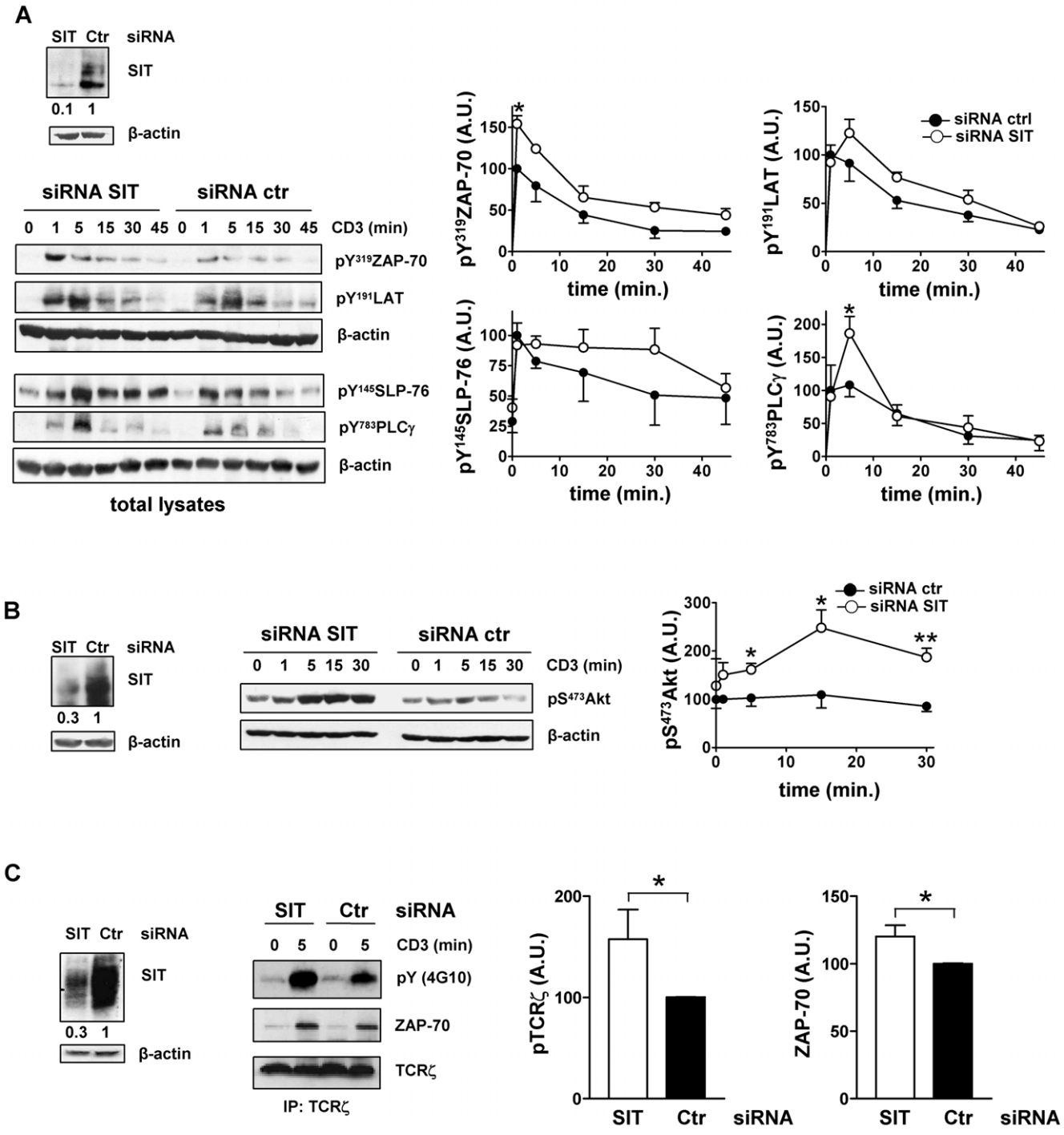

Figure 3. Suppression of SIT expression results in an enhanced proximal TCR signaling. siRNA duplex for SIT or control were introduced in Jurkat T cells by electroporation. Cells were stimulated 48 h after transfection with non-cross-linked CD3 Ab for the indicated times. Total cell lysates (A–B) or TCRζ immunoprecipitates (C) were prepared and analyzed by Western blotting using the indicated Abs. The data are representative of at least 3 independent experiments. Immunoblots verifying SIT downregulation are shown. Equal loading is shown by reprobing immunoblots with antibodies specific for β-actin (A–B) or TCRζ (C). The phosphorylated bands were quantified using ImageQuant software and values were normalized to the corresponding β-actin signal. Graphs show the phosphorylation levels shown as of arbitrary units ± SEM of at least 3 independent experiments. Statistical significance * $p<0.05$ and ** $p<0.01$.
doi:10.1371/journal.pone.0023761.g003

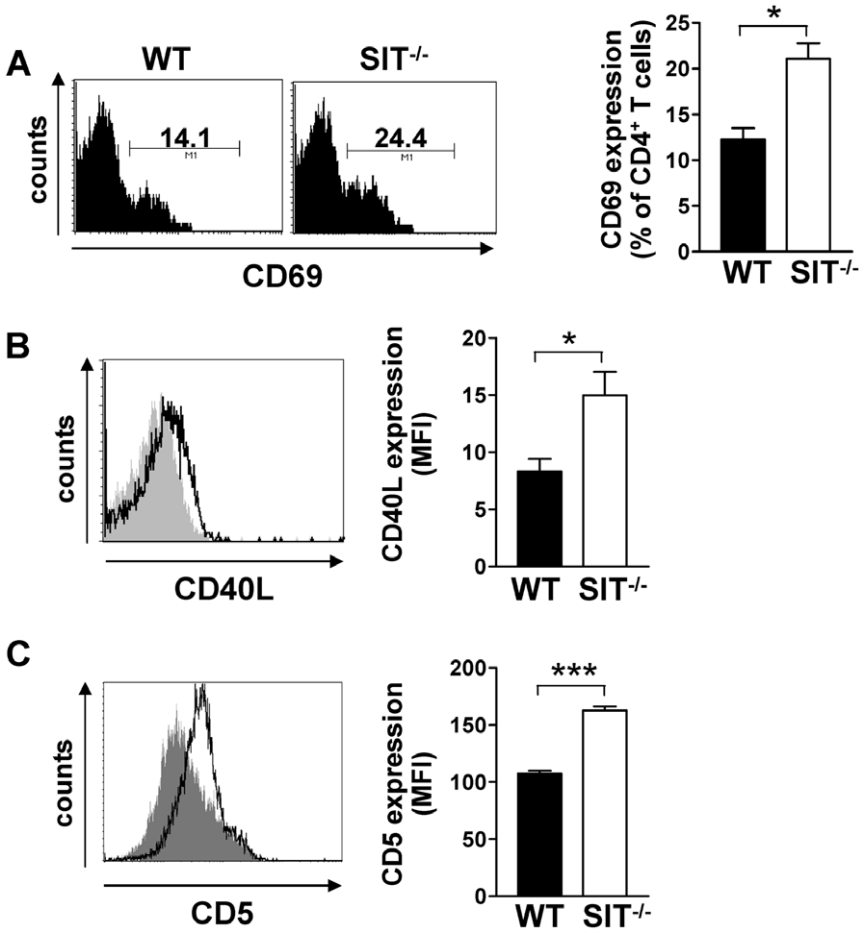

Figure 4. Analysis of activation markers in SIT$^{-/-}$ mice. A) Splenic CD4$^+$ T cells from 1 year-old SIT-deficient and wild-type mice were analyzed for CD69 expression. Numbers within histograms indicate the percentage of cells. One representative profile per group is shown. B) Comparison of CD40L expression on CD4$^+$ T cells isolated from SIT-deficient (empty histogram) and wild-type (filled histogram) mice. Mean fluorescent intensity (MFI) from one representative mouse per group is indicated. C) Comparison of CD5 expression on CD4$^+$ T cells isolated from SIT-deficient (empty histogram) and wild-type (filled histogram) mice. Bar graphs in A), B), and C) represent statistical analyses of CD69, CD40L, and CD5 expression, respectively. Data derive from at least 5 mice per group. Statistical significance * $p<0.05$ and ***$p<0.0001$.
doi:10.1371/journal.pone.0023761.g004

SIT. As shown in figure 2, we found that the phosphorylation of both ZAP-70 and PLCγ-1 was enhanced. Thus, it appears that SIT suppresses proximal TCR signaling.

In primary human T cells, the downregulation efficiency of SIT is approximately 50% (figure 2A). In order to obtain a more efficient suppression of SIT, we used the Jurkat T-cell line. As shown in figure 3, we were able to downregulate up to 70–90% of SIT in Jurkat T cells. Therefore, we used this well-characterized T-cell line to further analyze the role of SIT on proximal TCR signaling. The data presented in figure 3A show that, similar to the downregulation of SIT in primary human T cells, also suppression of SIT in Jurkat T cells results in an enhanced proximal TCR signaling. SIT-depleted Jurkat T cells showed an augmented TCR-mediated phosphorylation of ZAP-70, LAT, SLP-76 and PLCγ-1 (figure 3A). We additionally found that suppression of SIT strongly enhanced Akt phosphorylation upon CD3 stimulation even in a system where Akt is already constitutively activated (figure 3B) [15,16].

To further elucidate the mechanism responsible for the enhanced proximal TCR signaling, we investigated TCRζ phosphorylation and TCRζ/ZAP-70 association. In agreement with the enhanced phosphorylation of ZAP-70, LAT, SLP-76, and PLCγ-1, the phosphorylation of TCRζ was also enhanced upon suppression of SIT expression (figure 3C). Additionally, analysis of

Table 1. T-cell subsets in lymph nodes.

Genotype	βTCR$^+$CD45RB$^+$	βTCR$^+$CD62L$^+$	CD4$^+$CD25$^+$	CD4$^+$CD103$^+$
SIT$^{+/+}$	32.8±3.5 (n = 6)	66.3±7.0 (n = 4)	7.5±0.2 (n = 3)	2.8±0.5 (n = 10)
SIT$^{-/-}$	27.2±1.8 (n = 6)	60.3±7.5 (n = 4)	7.6±0.6 (n = 3)	2.8±0.4 (n = 10)

% of lymph node cells ± SEM. n = number of examined mice.
doi:10.1371/journal.pone.0023761.t001

Table 2. T-cell subpopulations in the spleen.

Genotype	Splenocytes	$CD4^+$	$CD4^+CD44^{hi}CD62^{lo}$
$SIT^{+/+}$ (n = 8)	111.3±24.6	19.6±6.5	8.64±3.8
$SIT^{-/-}$ (n = 8)	98.8±26.1	19.6±4.1	11.44±2.5

Number of cells in the spleen ($\times 10^6$) ± SEM. n = number of examined mice.
doi:10.1371/journal.pone.0023761.t002

immunoprecipitated TCRζ showed that the association with ZAP-70 was also increased in SIT dim T cells (figure 3C). Thus, these data suggest that suppression of SIT expression enhanced proximal TCR signaling at the level of TCRζ phosphorylation.

Increased proportion of activated $CD4^+$ T cells in aged SIT-deficient mice

The PI3K-Akt pathway regulates a variety of cellular processes including proliferation and apoptosis. Therefore, we next investigated whether $SIT^{-/-}$ mice developed any dysfunction within the lymphocyte compartment. We found that $CD4^+$ T cells from aged $SIT^{-/-}$ mice showed a modest but consistent increase in the expression of CD69 and CD40L (figure 4A, 4B). Moreover, these cells also express increased levels of CD5 (figure 4C), which we have previously shown to be altered also in thymocytes and $CD8^+$ T cells [6,7]. We additionally analyzed the expression of a variety of other surface markers, including CD3, CD4, CD25, CD44, CD45RB, CD62L, and CD103, but we did not observe significant differences between WT and SIT-deficient mice ([6,7], table 1, and table 2). We also did not observe significant differences in the size of secondary lymphoid organs. In fact, the numbers of total splenocytes, total splenic $CD4^+$ T cells, and effector/memory $CD4^+$ T cells in the spleen were not affected (table 2). We found only a modest decrease in the number of $CD4^+$ T cells in lymph nodes [6]. Finally, we also did not observe significant differences in BrdU incorporation (figure 5A), in the intracellular expression of the antiapoptotic molecules Bcl-2 (figure 5B), and in Annexin V expression (figure 5C) on *ex vivo* isolated $CD4^+$ T cells from SIT-deficient mice. Thus, these data indicate that loss of SIT results in a partial alteration of the activation status of $CD4^+$ T cells without affecting their steady-state proliferation or apoptosis. We hypothesize that the compensatory mechanism displayed by SIT-deficient mice may prevent the development of a more severe hyperactivation of T cells and lymphoproliferative diseases.

Discussion

In this study, we provide new insights into the function of the transmembrane adaptor protein SIT. We show that SIT inhibits TCR-mediated signaling. This is an important finding as the mechanism by which SIT inhibits T-cell activation was not clear. We have previously shown that overexpression of SIT suppressed transcription of an NFAT-driven reporter gene in the Jurkat T-cell line [13]. However, we did not find obvious alterations of more proximal TCR signaling events in this T-cell line upon strong stimulation of the antigen receptor. Here, we now show that SIT negatively regulates the phosphorylation/activation of crucial signaling molecules such as ZAP-70, LAT, PLCγ-1, and Akt upon weak T-cell stimulation. Potential clues to the mechanisms underlying the inhibitory effect of SIT on TCR-mediated signaling may be provided by recent unexpected observations suggesting that Grb2 amplifies TCR signaling by regulating Lck activation [17]. SIT possesses two Grb2 consensus binding motifs and indeed inducibly binds Grb2 upon TCR stimulation [13,18]. It has been suggested that non-raft TRAPs inhibit antigen-receptor-mediated signaling by sequestering signaling molecules away from the lipid rafts [1]. Thus, we propose a scenario whereby SIT, by functioning as a dosage regulator of Grb2 at the plasma membrane, may in turn dampen proximal TCR signaling.

We have additionally uncovered a link between the transmembrane adaptor SIT and the Akt-Foxo1 pathway. Whether SIT inhibits the phosphorylation of Akt-Foxo1 directly or indirectly (i.e. by negatively regulating proximal signaling) requires further investigation. Nevertheless, our study adds new insights into the regulation of Foxo1 in T cells. We show that low affinity ligands induced Foxo1 phosphorylation/inactivation in mouse T cells and that the loss of SIT enhances the TCR-mediated inactivation of Foxo1. Thus, SIT could modulate cell cycle progression (e.g. triggered by low affinity ligands) via Foxo1. Intriguingly, similar to $SIT^{-/-}$ mice [6,7] $Foxo1^{-/-}$ mice display reduced numbers of naïve cells and an accumulation of $CD44^{hi}$ memory-like T cells [10]. It will be interesting to determine whether SIT is involved in the regulation of other members of the Foxo family such as Foxo4 and Foxo3a. In fact, the characterization of Foxo3a-deficient mice revealed a phenotype resembling that of SIT-deficient mice, such as T-cell hyperactivation, enhanced production of IL-2 and Th1 and Th2 cytokines [19].

We have previously shown that SIT regulates thymocyte selection [6,8]. It is tempting to speculate that an altered Foxo-mediated pathway also accounts for the defects in thymic development in SIT-deficient mice. Indeed, it has been recently

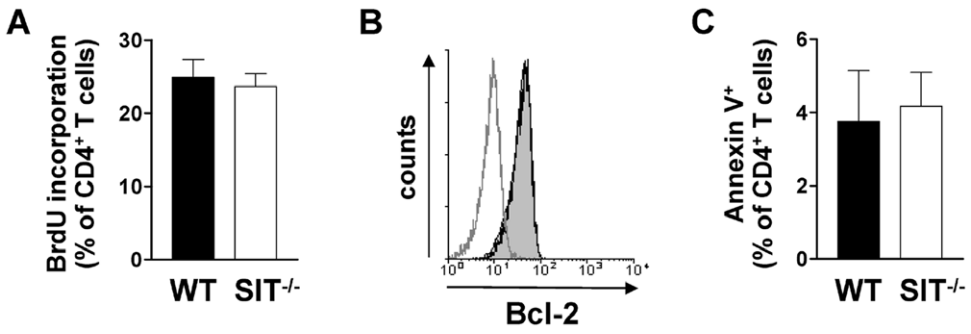

Figure 5. Normal survival and steady-state proliferation of SIT-deficient $CD4^+$ T cells. Lymph node cells were isolated and stained with CD4 and CD8 mAbs. A) BrdU incorporation was measured for $CD4^+$ T cells. Bar graphs indicate mean values ± SEM from 3 $SIT^{-}/^{-}$ and 5 $SIT^{+}/^{+}$ mice. B) Intracellular Bcl-2 expression in $CD4^+$ T cells from $SIT^{-}/^{-}$ (empty histogram) and $SIT^{+}/^{+}$ (filled histogram) mice. Isotype control is shown as a gray line. C) Annexin V expression on $CD4^+$ T cells. Bar graphs indicate mean values ± SEM from 3 $SIT^{-}/^{-}$ and 3 $SIT^{+}/^{+}$ mice.
doi:10.1371/journal.pone.0023761.g005

shown that the adaptor protein SLP-65 regulates B-cell development via Akt-Foxo3a [20]. How Foxo family members regulate lymphocyte development is not yet clear. They may be involved in the regulation of transcriptional activation of genes required in developmental processes.

Our data suggest that the loss of SIT also results in an altered function of $CD4^+$ T cells. In fact, both TCR-mediated signaling and the expression levels of CD69 and CD40L are augmented. Moreover, we have previously shown that SIT-deficient T cells were hyperresponsive to CD3 stimulation, produced higher amount of cytokines *in vitro*, and more importantly, displayed a more severe clinical course of the experimentally induced autoimmunity EAE [6]. Thus, it appears that the loss of SIT generally enhances the activation status of T lymphocytes. Despite the fact that T cells are hyperactivated, SIT-deficient mice do not develop signs of chronic inflammation or lymphoproliferation. We propose that the development of compensatory mechanisms in SIT-deficient mice [7] could serve to prevent autoimmunity or chronic inflammatory processes, thus preserving immune functions. However, whether sensory adaptation is completely effective is currently under investigations. In fact, we have recently found that SIT-deficient mice spontaneously develop anti-nuclear antibodies and glomerulonephritis (Arndt and Simeoni, unpublished observations).

In summary, the data presented here together with previous studies demonstrate a critical function for SIT in fine-tuning signals emanating from the TCR leading to proliferation, differentiation and tolerance and further emphasize the important role that TRAPs play in regulating homeostasis within the immune system.

Acknowledgments

We are grateful to Dr Jonathan Lindquist for critically reading the manuscript and helpful discussion and to Ines Meinert, Marita Lotzing and Britta Bogel for excellent technical assistance.

Author Contributions

Conceived and designed the experiments: BA AR BS LS. Performed the experiments: BA T. Krieger T. Kalinski AT DR. Analyzed the data: BA T. Krieger DR LS. Wrote the paper: LS.

References

1. Horejsi V, Zhang W, Schraven B (2004) Transmembrane adaptor proteins: organizers of immunoreceptor signalling. Nat Rev Immunol 4: 603–616.
2. Zhang W, Sommers CL, Burshtyn DN, Stebbins CC, DeJarnette JB, et al. (1999) Essential role of LAT in T cell development. Immunity 10: 323–332.
3. Zhu M, Koonpaew S, Liu Y, Shen S, Denning T, et al. (2006) Negative regulation of T cell activation and autoimmunity by the transmembrane adaptor protein LAB. Immunity 25: 757–768.
4. Zhu M, Granillo O, Wen R, Yang K, Dai X, et al. (2005) Negative regulation of lymphocyte activation by the adaptor protein LAX. J Immunol 174: 5612–5619.
5. Zhu M, Rhee I, Liu Y, Zhang W (2006) Negative regulation of Fc epsilonRI-mediated signaling and mast cell function by the adaptor protein LAX. J Biol Chem 281: 18408–18413.
6. Simeoni L, Posevitz V, Kolsch U, Meinert I, Bruyns E, et al. (2005) The transmembrane adapter protein SIT regulates thymic development and peripheral T-cell functions. Mol Cell Biol 25: 7557–7568.
7. Posevitz V, Arndt B, Krieger T, Warnecke N, Schraven B, et al. (2008) Regulation of T Cell Homeostasis by the Transmembrane Adaptor Protein SIT. J Immunol 180: 1634–1642.
8. Koelsch U, Schraven B, Simeoni L (2008) SIT and TRIM determine T cell fate in the thymus. J Immunol 181: 5930–5939.
9. Birkenkamp KU, Coffer PJ (2003) FOXO transcription factors as regulators of immune homeostasis: molecules to die for? J Immunol 171: 1623–1629.
10. Kerdiles YM, Beisner DR, Tinoco R, Dejean AS, Castrillon DH, et al. (2009) Foxo1 links homing and survival of naive T cells by regulating L-selectin, CCR7 and interleukin 7 receptor. Nat Immunol 10: 176–184.
11. Horn J, Wang X, Reichardt P, Stradal TE, Warnecke N, et al. (2009) Src homology 2-domain containing leukocyte-specific phosphoprotein of 76 kDa is mandatory for TCR-mediated inside-out signaling, but dispensable for CXCR4-mediated LFA-1 activation, adhesion, and migration of T cells. J Immunol 183: 5756–5767.
12. Kolsch U, Arndt B, Reinhold D, Lindquist JA, Juling N, et al. (2006) Normal T-cell development and immune functions in TRIM-deficient mice. Mol Cell Biol 26: 3639–3648.
13. Marie-Cardine A, Kirchgessner H, Bruyns E, Shevchenko A, Mann M, et al. (1999) SHP2-interacting transmembrane adaptor protein (SIT), a novel disulfide-linked dimer regulating human T cell activation. J Exp Med 189: 1181–1194.
14. Charvet C, Canonigo AJ, Becart S, Maurer U, Miletic AV, et al. (2006) Vav1 promotes T cell cycle progression by linking TCR/CD28 costimulation to FOXO1 and p27kip1 expression. J Immunol 177: 5024–5031.
15. Freeburn RW, Wright KL, Burgess SJ, Astoul E, Cantrell DA, et al. (2002) Evidence that SHIP-1 contributes to phosphatidylinositol 3,4,5-trisphosphate metabolism in T lymphocytes and can regulate novel phosphoinositide 3-kinase effectors. J Immunol 169: 5441–5450.
16. Shan X, Czar MJ, Bunnell SC, Liu P, Liu Y, et al. (2000) Deficiency of PTEN in Jurkat T cells causes constitutive localization of Itk to the plasma membrane and hyperresponsiveness to CD3 stimulation. Mol Cell Biol 20: 6945–6957.
17. Jang IK, Zhang J, Chiang YJ, Kole HK, Cronshaw DG, et al. (2010) Grb2 functions at the top of the T-cell antigen receptor-induced tyrosine kinase cascade to control thymic selection. Proc Natl Acad Sci U S A 107: 10620–10625.
18. Pfrepper KI, Marie-Cardine A, Simeoni L, Kuramitsu Y, Leo A, et al. (2001) Structural and functional dissection of the cytoplasmic domain of the transmembrane adaptor protein SIT (SHP2-interacting transmembrane adaptor protein). Eur J Immunol 31: 1825–1836.
19. Lin L, Hron JD, Peng SL (2004) Regulation of NF-kappaB, Th activation, and autoinflammation by the forkhead transcription factor Foxo3a. Immunity 21: 203–213.
20. Herzog S, Hug E, Meixlsperger S, Paik JH, DePinho RA, et al. (2008) SLP-65 regulates immunoglobulin light chain gene recombination through the PI(3)K-PKB-Foxo pathway. Nat Immunol 9: 623–631.

Appendix 17

TCR-mediated Erk activation does not depend on Sos and Grb2 in peripheral human T cells

Warnecke N., Poltorak M., Kowtharapu B.S., Arndt B., Stone J.C., Schraven B., and **Simeoni L.** (2012) *EMBO Rep*, doi: 10.1038/embor.2012.17.

EMBO reports

scientific report

TCR-mediated Erk activation does not depend on Sos and Grb2 in peripheral human T cells

Nicole Warnecke[1], Mateusz Poltorak[1]*, Bhavani S. Kowtharapu[1], Boerge Arndt[1†], James C. Stone[2], Burkhart Schraven[1,3] & Luca Simeoni[1+]*

[1]Institute of Molecular and Clinical Immunology, Otto-von-Guericke University, Magdeburg, Germany, [2]Department of Biochemistry, University of Alberta, Edmonton, Alberta, Canada and [3]Department of Immune Control, Helmholtz Centre for Infection Research, Braunschweig, Germany

Sos proteins are ubiquitously expressed activators of Ras. Lymphoid cells also express RasGRP1, another Ras activator. Sos and RasGRP1 are thought to cooperatively control full Ras activation upon T-cell receptor triggering. Using RNA interference, we evaluated whether this mechanism operates in primary human T cells. We found that T-cell antigen receptor (TCR)-mediated Erk activation requires RasGRP1, but not Grb2/Sos. Conversely, Grb2/Sos—but not RasGRP1—are required for IL2-mediated Erk activation. Thus, RasGRP1 and Grb2/Sos are insulators of signals that lead to Ras activation induced by different stimuli, rather than cooperating downstream of the TCR.

Keywords: T cells; Sos; Grb2; RasGRP1; Erk

EMBO *reports* advance online publication 17 February 2012; doi:10.1038/embor.2012.17

INTRODUCTION

Signalling via the Erk cascade is essential for cell-fate decisions in many cell types including T lymphocytes [1]. On ligation of the T-cell antigen receptor (TCR), the activation of the Erk cascade is thought to occur through the action of two distinct GEFs, RasGRP1 and the ubiquitously expressed Sos proteins [2]. The activation of both RasGRP1 and Sos depends on the transmembrane adaptor linker for activation of T cells (LAT), which might therefore activate Ras via two distinct pathways: (i) PLCγ1-DAG-RasGRP1 and (ii) Grb2-Sos.

A key finding on Ras-Erk regulation in T cells came from recent studies based on lymphoid cell lines, thymocytes and *in silico* simulations showing that Ras activation is further controlled by an unusual interplay between RasGRP1 and Sos [3,4]. This model has important implications for T-cell function, as it helps to explain how antigenic peptide/major histocompatibility complexes, which are usually rare during *in vivo* infections, induce productive T-cell activation [4]. These studies propose that, on initial receptor triggering, Ras is exclusively activated by RasGRP1. Successively, RasGTP will prime Sos thereby activating a positive feedback loop and allowing full T-cell activation [4].

Thus, the current model postulates that the coordinated action of RasGRP1 and Sos regulates the magnitude of Ras-Erk activation. However, it has not yet been demonstrated whether this model for TCR-mediated Ras-Erk is also valid in primary human T cells. Given the central role of Erk activation in cell-fate specification processes induced by TCR triggering, we have examined the molecular events leading to Erk activation in peripheral human T cells in more detail.

Surprisingly, we found that Sos proteins and Grb2 are not limiting for full Erk activation upon TCR stimulation in primary human T cells. Thus, this study shows that the contribution of Sos to the regulation of the magnitude of Erk activation in primary human T cells is considerably different from that predicted by the current model.

RESULTS

Sos and Grb2 are not limiting for Erk activation

On the basis of overexpression experiments in Jurkat T cells and computer simulations, it has been postulated that Sos is important in inducing robust Ras signalling in T cells [3,4]. To evaluate whether Sos also has a similar role in primary T cells, we performed short interfering RNA (siRNA)-mediated downregulation of Sos. We initially evaluated the role of Sos1. As shown in Fig 1A, transfection with RNA duplex efficiently suppressed Sos1 expression in peripheral human T cells. Next, human T cells were treated with two different CD3ε monoclonal antibodies, MEM92 or OKT3. As expected, suppression of Sos1 did not alter the activation status of the upstream signalling molecules LAT, PLCγ1 and ZAP-70 (data not shown). However, when we analysed Erk activation we surprisingly found that Erk phosphorylation was not reduced upon TCR stimulation in primary T lymphocytes (Fig 1A). In the case of stimulation with MEM92, Erk phosphorylation was even slightly enhanced (Fig 1A).

[1]Institute of Molecular and Clinical Immunology, Otto-von-Guericke University, Leipziger Strasse 44, Magdeburg 39120, Germany
[2]Department of Biochemistry, University of Alberta, Edmonton, Alberta, Canada T6G 2H7
[3]Department of Immune Control, Helmholtz Centre for Infection Research, Inhoffenstrasse 7, Braunschweig 38124, Germany
*These authors contributed equally to this work
[†]Present address: Diabetes Centre, Department of Medicine-Innenstadt, Ludwig-Maximilian University, Munich 80336, Germany
[+]Corresponding author. Tel: +49 391 6717894; Fax: +49 391 6715852; E-mail: luca.simeoni@med.ovgu.de

Received 28 July 2011; revised 20 January 2012; accepted 23 January 2012; published online 17 February 2012

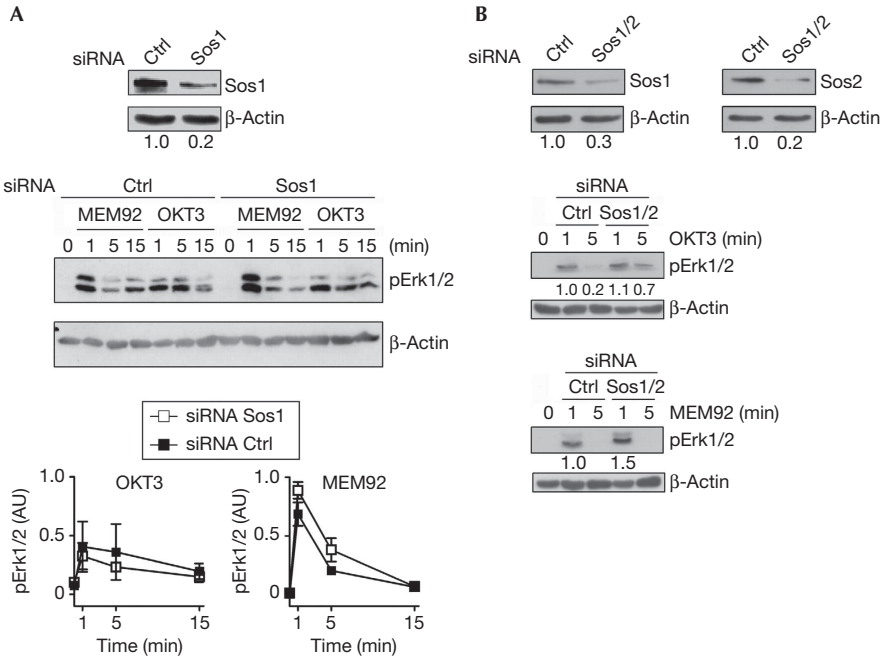

Fig 1 | TCR-mediated activation of Erk does not depend on Sos in primary T cells. Peripheral human T cells were transfected with Ctrl, Sos1-specific (**A**) or Sos1/Sos2 (**B**) siRNA and cultured for 72 h. Cells were stimulated with CD3 mAbs (clone OKT3 or MEM92) for the indicated times. Cell lysates were analysed by immunoblotting using the indicated Abs. Immunoblots verifying Sos1 and Sos2 downregulation are shown. Bands in **A** were quantified using the ImageQuant software and values were normalized to the corresponding β-actin signal. Graph in **A** show the phosphorylation levels of Erk1/2 as arbitrary units ± s.e.m. of six experiments. One representative experiment out of four is shown in **B**. Numbers below the band indicate expression levels or fold induction of phosphorylation compared with Ctrls. Ab, antibody; Ctrl, control; mAb, monoclonal antibody; siRNA, short interfering RNA; TCR, T-cell antigen receptor.

To check whether the highly homologous Sos2 might compensate for Sos1, we suppressed both Sos1 and Sos2 expression. As shown in Fig 1B, downregulation of both Sos proteins also did not affect but rather slightly enhanced Erk activation. Similar results were obtained by analysing the level of phosphorylated Erk by flow cytometry (supplementary Fig S1 online). Thus, these data indicate that, in contrast to the proposed model, Sos proteins are not limiting for full Ras-Erk activation in primary human T lymphocytes.

Sos constitutively binds the adaptor protein Grb2 by its two SH3 domains [5]. It is well established that, during T-cell activation, this constitutive interaction recruits Sos to the plasma membrane upon binding of the Grb2-SH2 domain to phosphorylated LAT [6]. The interaction between Sos and Grb2 is also required to activate the Ras-Erk cascade by binding of the Grb2-SH2 domain to phosphorylated Shc, an adaptor protein that directly binds to phosphorylated TCR-ζ immunoreceptor tyrosine-based activation motifs [7]. In addition to Sos, Grb2 could regulate Erk activation via Themis [8]. Hence, given the crucial role of Grb2 in regulating the activation of Ras, we evaluated whether suppression of Grb2 expression in primary human T cells would result in defective Erk activation. The results presented in Fig 2 show that, similarly to Sos, the downregulation of Grb2 did not reduce Erk activation. Rather, Erk activation was slightly enhanced on strong TCR stimulation. Similar results were obtained by using another set of siRNA duplex targeting another region of Grb2 mRNA (data not shown).

To evaluate whether residual expression of Grb2 and Sos might still be sufficient to activate Erk, we simultaneously downregulated Sos1, Sos2 and Grb2. Also under this condition we did not observe a reduction in Erk activation (supplementary Fig S2 online). In addition, we tested the hypothesis that Grb2 and Sos might have a role in Ras activation in different T-cell subsets. To assess this possibility, the expression of Grb2 and Sos1/Sos2 was suppressed in $CD4^+$ naive (supplementary Fig S3 online) and memory T cells (supplementary Fig S4 online). Also in these cells the downregulation of Grb2 and Sos1/Sos2 did not reduce Erk activation.

As our data showed that Sos1 and Grb2 are not crucial for the activation of Erk in primary human T cells, we next analysed whether they might have a role in the activation of other mitogen-activated protein kinases (MAPK). These investigations were motivated by the observation that $Grb2^{-/-}$ thymocytes [9] and thymocytes with Grb2 haploid insufficiency clearly showed weakened TCR-mediated JNK and p38, but normal Erk activation [10]. Therefore, Grb2 and Sos1 might be required for JNK or p38 activation rather than for Erk upon TCR stimulation. However, we found that both molecules also do not influence the activation of JNK and p38 in primary human T cells (supplementary Fig S5 online).

According to the proposed model, Sos1 might function as an amplifier of the Ras-Erk cascade in Jurkat T cells. Therefore, to further test the validity of our approach, we suppressed the expression of Sos1 and Grb2 in Jurkat T cells in an attempt to recapitulate the current model. In marked contrast to primary T cells, we found that downregulation of Sos1 (supplementary Fig S6A online) or Grb2 (supplementary Fig S6B online) resulted in a reduction of Erk activation on both strong and weak TCR

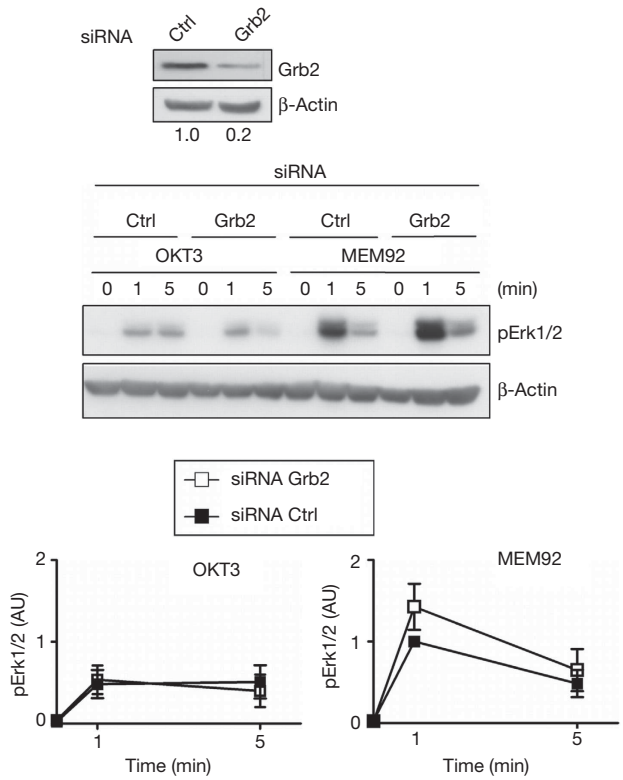

Fig 2 | Knockdown of Grb2 does not reduce Erk phosphorylation in primary T cells. Peripheral human T cells transfected with siRNA duplex for Grb2 or Ctrl were stimulated with CD3 mAb (clone OKT3 or MEM92) for the indicated times. Total cell lysates were prepared and analysed as in Fig 1. Graphs show the phosphorylation levels of Erk1/2 as arbitrary units ± s.e.m. of at least three independent experiments. Ctrl, control; mAb, monoclonal antibody; siRNA, short interfering RNA.

stimulation in Jurkat T cells, thus confirmed that the prediction made by the model are valid in the Jurkat T cell line.

Altogether, our data demonstrate that, conversely to Jurkat T cells, Sos and Grb2 do not significantly contribute to full TCR-mediated Ras-Erk activation in primary human T cells. Surprisingly, both Sos and Grb2 seem to have a modest inhibitory effect on Erk phosphorylation.

RasGRP1 regulates TCR-mediated Erk activation

To assess how Erk is activated on TCR triggering in primary human T cells, we next investigated the role of another important Ras activator, RasGRP1. To this end, we suppressed RasGRP1 expression by RNA-mediated interference. The data shown in Fig 3A indicate that knockdown of RasGRP1 results in a severe reduction of Erk phosphorylation, but not of another MAPK, p38 upon TCR stimulation (data not shown). The analysis of the intracellular levels of phospho-Erk by flow cytometry confirmed this result (supplementary Fig S1 online). Thus, in addition to be involved in Erk activation in murine thymocytes [11], peripheral $CD8^+$ [12,13] and Jurkat T cells [3,14], RasGRP1 is also an important regulator of Ras-Erk activation on TCR stimulation in primary human T lymphocytes.

Interestingly, we found that Erk activation on CD3xCD28 stimulation is less dependent on RasGRP1, as suppression of RasGRP1 only modestly affected Erk phosphorylation (Supplementary Fig S7 online). This indicates that CD28 costimulation either triggers RasGRP1-independent pathways to activate Erk (for example, by activating a PKC-Raf axis) or that it enhances the activation of the residual RasGRP1.

It has been proposed that, to be activated, Sos requires a priming by active Ras produced by RasGRP1 [3]. Therefore, it is possible that Sos function is masked by the dominant action of RasGRP1 in primary human T cells, and hence, the effect of Sos on Ras-Erk activation cannot be detected when sufficient amount of RasGRP1 are expressed. To address this possibility, we simultaneously suppressed both Sos1 and RasGRP1. If Sos1 and RasGRP1 cooperate to regulate Ras activation, the suppression of both Sos1 and RasGRP1 should affect Erk activation in a more pronounced manner compared with RasGRP1 alone. Surprisingly, we found that the further suppression of Sos1 neutralizes the effect seen with RasGRP1 (Fig 3B). Similar results were obtained when we suppressed both Grb2 and RasGRP1 (supplementary Fig S8 online). Thus, these results suggest that rather than cooperatively, Sos1 and RasGRP1 antagonize one another to regulate Ras activation.

Sos and Grb2 regulate IL-2R-mediated Erk activation

As our data show that Sos and Grb2 are not crucial for TCR-mediated Erk activation in primary human T cells, we next analysed whether they have a role in the activation of Erk downstream of other receptors such as the IL-2R, which is also essential for T-cell activation. Therefore, we generated T-cell blasts in which the expression of Grb2, Sos1/Sos2 and RasGRP1 was suppressed by RNA-mediated interference. Erk activation was analysed on IL-2 stimulation. As shown in Fig 4A,B,D, suppression of Grb2 and Sos1/Sos2 expression significantly reduced IL-2-mediated Erk phosphorylation. Consistent with previously published data [13], we found that the downregulation of RasGRP1 did not affect IL-2-mediated Erk activation (Fig 4C,D). The data in Fig 4 also show that the phosphorylation of STAT3, which does not depend on Grb2/Sos, is not affected.

Collectively, these results show that Grb2/Sos and RasGRP1 are involved in the activation of the Ras-Erk cascade downstream of different receptors. Whereas Grb2/Sos are required for IL2- but not TCR-mediated Erk activation, RasGRP1 is an activator of Ras downstream of the TCR, but it is not required for IL2 receptor signalling.

Finally, we tested whether suppression of Grb2, Sos1/Sos2 and RasGRP1 affect T-cell activation. In agreement with previously published data [12], we found that suppression of RasGRP1 expression markedly reduced CD3-mediated proliferation (Fig 5). Similarly, also the suppression of Grb2 and Sos1/Sos2 reduced proliferation. However, the effect of Sos1/Sos2 was more pronounced than that of Grb2. It is possible that during proliferation T cells might compensate the loss of Grb2 by other adaptor molecules. In summary, the data indicate that both Grb2/Sos and RasGRP1 are required for T-cell activation, albeit downstream of different receptors.

DISCUSSION

Erk functions as a hub that directs signals coming from different cell-surface receptors (for example, growth factor, chemokine, cytokine and antigen receptors) towards the receptor-specific

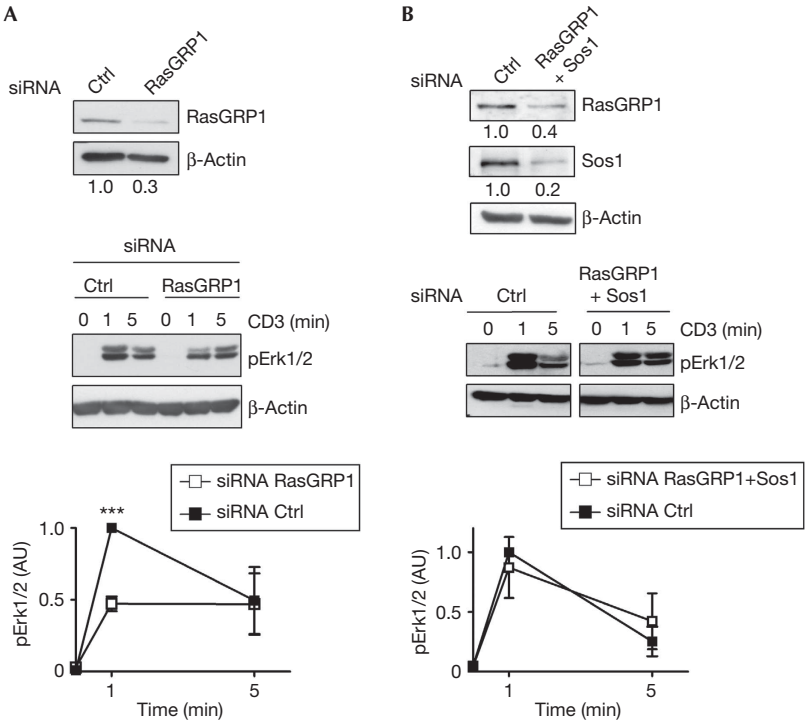

Fig 3 | RasGRP1 is required for full Erk activation in primary T cells. Peripheral human T cells transfected with siRNA duplex for RasGRP1 (**A**) or RasGRP1 and Sos1 (**B**) and were stimulated as indicated with CD3 mAbs (clone MEM92). Total cell lysates were prepared and analysed as in Fig 1. Graphs show the phosphorylation levels of Erk1/2 as arbitrary units ± s.e.m. of at least three independent experiments. Statistical significance ***$P<0.001$. mAb, monoclonal antibody; siRNA, short interfering RNA.

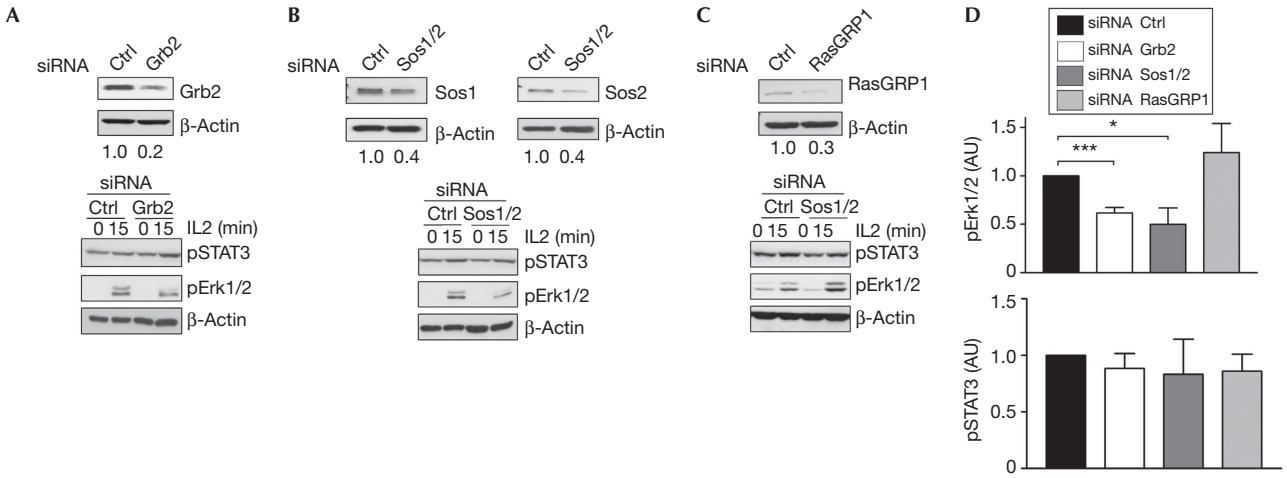

Fig 4 | Sos and Grb2 regulate IL2-mediated Erk activation. T-cell blasts were generated, transfected with siRNA duplex for Grb2 (**A**), Sos1/Sos2 (**B**) or RasGRP1 (**C**), and stimulated with IL2 as indicated. Total cell lysates were prepared and analysed as in Fig 1. Graphs in **D** present the mean of the phosphorylation levels as arbitrary units ± s.e.m. of four independent experiments. Statistical significance ***$P<0.001$, *$P<0.05$. siRNA, short interfering RNA.

cellular response. How Erk performs its function has now begun to be understood. It seems that signalling through the Erk module is controlled by several upstream regulators that determine the duration, the magnitude and the compartmentalization of Erk activation [15]. Thus, by eliciting different modes of Erk activation, the generation of a receptor- or ligand-specific cellular outcome is ensured.

By using lymphoid cell lines and *in silico* simulations, it has recently been proposed that RasGRP1 and Sos synergistically function as upstream activators of the Ras-Erk cascade and

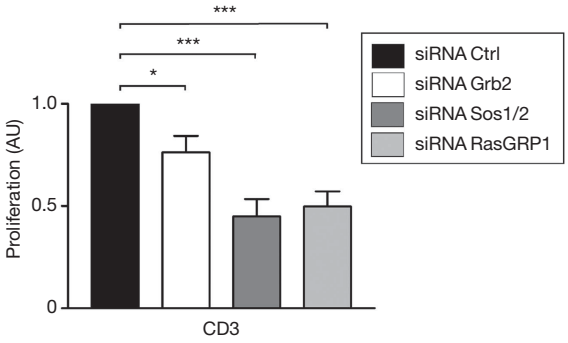

Fig 5 | Grb2/Sos and RasGRP1 are required for T-cell activation. Peripheral human T cells were transfected with siRNA duplex for Grb2, Sos1/Sos2, RasGRP1 or siRNA Ctrl. Subsequently, cells were stimulated with plate-bound CD3 for 2 days, pulsed with [^{3}H]-thymidine and processed for standard scintillation counting. Graphs show proliferation expressed as arbitrary units ± s.e.m. of Grb2-, Sos1/Sos2- and RasGRP1-low T cells compared with Ctrls. Results are from at least three independent experiments. Statistical significance ***$P<0.001$, *$P<0.05$. Ctrl, control; siRNA, short interfering RNA.

cooperatively regulate the magnitude of Erk activation on TCR stimulation [3,4,16]. The mechanism described by this model might have important consequences for our understanding of how T cells are selected in the thymus and how they are activated during an immune response. Recently, conditional Grb2$^{-/-}$ [9] and Sos1$^{-/-}$ [17] mice have been generated. The data suggest that both Grb2 and Sos1 are required at different stages during thymocyte development. However, whereas Sos1 contributes to TCR-mediated Erk activation in immature T cells, Grb2 seems to be dispensable.

Here, we have assessed the role of Sos and Grb2 in TCR-mediated Erk activation in mature human T cells isolated from peripheral blood. We found that the Grb2/Sos signalling module does not appear essential for full Erk activation on TCR stimulation in primary human T cells. Our data corroborate recent observations showing that CD4$^+$ peripheral T cells from conditional Sos1$^{-/-}$ mice also display normal TCR-mediated Erk activation [17].

In addition, we show that Sos1 and Grb2 are required for Erk activation in Jurkat T cells. Thus, our data demonstrate that the prediction made by the current model of Ras-Erk activation is valid for Jurkat, but not in primary human T cells. The reason for the differential requirement of Grb2/Sos in primary versus Jurkat T cells is not yet clear. Jurkat T cells seem to have the characteristic of immature double-negative thymocytes. It is possible that the requirement of Sos to activate Ras might differ in immature versus mature T cells. This hypothesis seems to be in line with recent observations by Kortum *et al* [17] suggesting that immature T cells require Sos1 to activate Erk, whereas mature T cells are largely Sos1 independent. However, it should also be kept in mind that, although being the best characterized model system to study TCR-mediated signalling, Jurkat are a transformed T-cell line that are known to carry mutations in different genes which could account for the observed differences to primary T cells.

Whereas RasGRP1 is the major activator of Ras in immature CD4$^+$CD8$^+$ thymocytes [11,12], it seems that mature T cells use both RasGRP1-dependent and -independent pathways to activate Erk. In fact, despite the strong depletion (80%) of RasGRP1 that we were able to archive in our experiments, Erk phosphorylation was reduced by only about 50%. In line with our findings, recent data show that RasGRP1 deficiency partially affects, but does not completely abrogate TCR-mediated Erk activation, CD69 and CD25 upregulation in peripheral mouse T lymphocytes [12,13].

One of the RasGRP1-independent pathways could be mediated by RasGRF2. However, recent data suggest that loss of RasGRF2 induces no major changes in Erk activation in TCR-stimulated splenic T cells [18]. Thus, it is currently not clear which RasGRP1-independent signalling pathways contribute to Erk activation in primary T lymphocytes.

Our experiments also show that, in addition to being not crucial for TCR-mediated Ras-Erk activation, Sos1 and Grb2 are not limiting for TCR-mediated JNK or p38 activation in primary human T cells. These results were unexpected in light of recent data demonstrating defective TCR-mediated JNK and p38 activation in Grb2$^{-/-}$ [9] and Grb2$^{+/-}$ [10] thymocytes. This once again indicates that thymocytes and peripheral T cells differentially use signalling pathways to activate MAPKs upon TCR stimulation.

Another surprising observation of our study was that down-regulation of Grb2 or Sos slightly enhanced TCR-mediated activation of Erk. This suggests that Grb2 and Sos might function as inhibitory signalling molecules in primary human T cells. In line with this assumption, it has been proposed that Grb2 is required for the assembly of an inhibitory signalling complex in T cells with the lipid phosphatase SHIP1 and the adaptor protein Dok2, which might inhibit Ras upon binding to RasGAP [19]. We have found that the inhibitory effect on TCR-mediated Erk activation was more evident on Grb2 knockdown compared with Sos1 or Sos1/Sos2 suppression. Thus, it is likely that Grb2 performs parts of its inhibitory signalling functions independently of Sos proteins.

An important question arising from our study is whether Sos activity is required for the activation of Ras in mature T cells. We explored the possibility that Sos1 and/or Sos2 regulates Ras activation in signalling pathways mediated by other receptors, such as the IL-2R. This hypothesis is in line with the observation that cytokine receptors can also activate Ras-Erk on recruitment of the Grb2/Sos complex to the phosphorylated receptor by the adaptor protein Shc [20]. We found that Grb2/Sos is indeed required to regulate IL-2-mediated Erk activation, whereas RasGRP1 appears to be dispensable, which in line with recently published data [13]. Thus, RasGRP1 and Grb2/Sos do not function as integrators, but they might rather function as insulators allowing the cells to distinguish the source of the input. Understanding the spatio-temporal contribution of signals from different receptors such as the TCR, the IL-2R and perhaps also by costimulatory molecules, such as integrins, is essential to predict cellular behaviour in a physiological context [21].

METHODS

Approval for these studies was obtained from the Ethics Committee of the Medical Faculty at the Otto-von-Guericke University, Magdeburg, Germany. Informed consent was obtained in accordance with the Declaration of Helsinki Principles.

Cell culture. Peripheral blood T cells were isolated as previously described [22]. T-cell blasts were generated as previously described [21].

siRNA duplex and transfection. siRNA duplex containing 19 nucleotides with 2 thymidine 3′ overhangs were purchase from

Invitrogen. The sequences were as follow: for Sos1: 5′-UUGCCC AUUUAUCAAUUGGTT-3′, for Grb2: 5′-CAUGUUUCCCCGCA AUUAUTT-3′, for RasGRP1: 5′-GGGUGAGGAGUUACAUUG CTT-3′, and as negative control we used a Renilla luciferase siRNA duplex 5′-CCAAGUAAUGUAGGAUCAATT-3′. For Sos2 downregulation, a STEALTH pool of three siRNAs (Invitrogen) was used. To achieve efficient downregulation, primary human T cells or T-cell blasts were transfected with siRNA duplex using either the Nucleofection Kit (Amaxa) according to the manufacturer's instruction or the Gene Pulser Xcell (Bio-Rad) as previously described [22]. Cells were collected 72 h after electroporation.

Cell stimulation and western blot analysis. Cell stimulations and cell lysates were prepared as previously described [22]. Anti-CD3 OKT3 (ATCC) and anti-CD3 MEM92 (kindly provided by V. Horejsi, Academy of Sciences of the Czech Republic, Czech Republic) were used for stimulation as hybridoma supernatants. Before experiments, hybridoma supernatants were titrated by two-fold dilution (from 1:1 to 1:64) to determine the appropriate monoclonal antibody concentration resulting in optimal T-cell stimulation (judged by phosphorylated Erk staining). T-cell blasts were stimulated as previously described [21]. Human recombinant IL-2 (Peprotech) was used at 100 U/ml. Western blots were conducted with the following antibodies: anti-phosphospecific antibodies (all from Cell Signaling Technology), anti-β-actin (clone AC-15; Sigma-Aldrich), anti-RasGRP1 [23], anti-Sos1 (C-23), anti-Sos2 and anti-Grb2 (C-23; Santa Cruz Biotechnology). Membranes were probed with the appropriate horseradish peroxidase-conjugated secondary antibodies and developed using the ECL detection system (Amersham Pharmacia).

Proliferation assay. To assess the proliferative capacity, cells were transfected with siRNA duplex as described above, rested overnight and stimulated in 96-well round-bottomed tissue culture plates (Costar; Corning Life Sciences, Acton, MA) coated with CD3 monoclonal antibody (MEM92). Cells were plated at 5×10^4 cells per well in quadruplicates and cultured for 2 days. [^{3}H]-Thymidine (0.3 μCi per well; specific activity, 50 Ci/mmol) was added for the last 8 h, and the plates were collected using a PHD cell harvester (Inotech AG, Basel, Switzerland). Thymidine incorporation was measured by liquid scintillation counting.

Statistics. Statistical analyses were performed using GraphPad Prism (GraphPad Software Inc., San Diego, CA). *P*-values were determined by an unpaired two-tailed Student's *t*-test. Statistical significance is indicated by asterisks.

Supplementary information is available at EMBO *reports* online (http://www.emboreports.org).

ACKNOWLEDGEMENTS

We are grateful to Jonathan Lindquist and Tilo Beyer for critically reading the manuscript and helpful discussion and to Nicole Jueling and Ines Meinert for excellent technical assistance. This work was supported by grants from the German Research Foundation (DFG), FOR-521 [SI861/1], GRK-1167 [TP12] and SFB-854 [TP19].

Author contributions: N.W., M.P. and B.S.K. performed research and analysed data; B.A. and B.S. designed research; J.C.S. contributed vital new reagents; L.S. analysed data, designed research and wrote the paper.

CONFLICT OF INTEREST

The authors declare that they have no conflict of interest.

REFERENCES

1. Yasuda T, Kurosaki T (2008) Regulation of lymphocyte fate by Ras/ERK signals. *Cell Cycle* **7:** 3634–3640
2. Roose J, Weiss A (2000) T cells: getting a GRP on Ras. *Nat Immunol* **1:** 275–276
3. Roose JP, Mollenauer M, Ho M, Kurosaki T, Weiss A (2007) Unusual interplay of two types of Ras activators, RasGRP and SOS, establishes sensitive and robust Ras activation in lymphocytes. *Mol Cell Biol* **27:** 2732–2745
4. Das J, Ho M, Zikherman J, Govern C, Yang M, Weiss A, Chakraborty AK, Roose JP (2009) Digital signaling and hysteresis characterize ras activation in lymphoid cells. *Cell* **136:** 337–351
5. Buday L, Downward J (1993) Epidermal growth factor regulates p21ras through the formation of a complex of receptor, Grb2 adapter protein, and Sos nucleotide exchange factor. *Cell* **73:** 611–620
6. Buday L, Egan SE, Rodriguez Viciana P, Cantrell DA, Downward J (1994) A complex of Grb2 adaptor protein, Sos exchange factor, and a 36-kDa membrane-bound tyrosine phosphoprotein is implicated in ras activation in T cells. *J Biol Chem* **269:** 9019–9023
7. Zhang L, Lorenz U, Ravichandran KS (2003) Role of Shc in T-cell development and function. *Immunol Rev* **191:** 183–195
8. Brockmeyer C *et al* (2011) T cell receptor (TCR)-induced tyrosine phosphorylation dynamics identifies THEMIS as a new TCR signalosome component. *J Biol Chem* **286:** 7535–7547
9. Jang IK, Zhang J, Chiang YJ, Kole HK, Cronshaw DG, Zou Y, Gu H (2010) Grb2 functions at the top of the T-cell antigen receptor-induced tyrosine kinase cascade to control thymic selection. *Proc Natl Acad Sci USA* **107:** 10620–10625
10. Gong Q, Cheng AM, Akk AM, Alberola-Ila J, Gong G, Pawson T, Chan AC (2001) Disruption of T cell signaling networks and development by Grb2 haploid insufficiency. *Nat Immunol* **2:** 29–36
11. Dower NA, Stang SL, Bottorff DA, Ebinu JO, Dickie P, Ostergaard HL, Stone JC (2000) RasGRP is essential for mouse thymocyte differentiation and TCR signaling. *Nat Immunol* **1:** 317–321
12. Priatel JJ, Teh SJ, Dower NA, Stone JC, Teh HS (2002) RasGRP1 transduces low-grade TCR signals which are critical for T cell development, homeostasis, and differentiation. *Immunity* **17:** 617–627
13. Priatel JJ *et al* (2010) RasGRP1 regulates antigen-induced developmental programming by naive CD8 T cells. *J Immunol* **184:** 666–676
14. Roose JP, Mollenauer M, Gupta VA, Stone J, Weiss A (2005) A diacylglycerol-protein kinase C-RasGRP1 pathway directs Ras activation upon antigen receptor stimulation of T cells. *Mol Cell Biol* **25:** 4426–4441
15. Ebisuya M, Kondoh K, Nishida E (2005) The duration, magnitude and compartmentalization of ERK MAP kinase activity: mechanisms for providing signaling specificity. *J Cell Sci* **118:** 2997–3002
16. Prasad A, Zikherman J, Das J, Roose JP, Weiss A, Chakraborty AK (2009) Origin of the sharp boundary that discriminates positive and negative selection of thymocytes. *Proc Natl Acad Sci USA* **106:** 528–533
17. Kortum RL, Sommers CL, Alexander CP, Pinski JM, Li W, Grinberg A, Lee J, Love PE, Samelson LE (2011) Targeted Sos1 deletion reveals its critical role in early T-cell development. *Proc Natl Acad Sci USA* **108:** 12407–12412
18. Ruiz S, Santos E, Bustelo XR (2007) RasGRF2, a guanosine nucleotide exchange factor for Ras GTPases, participates in T-cell signaling responses. *Mol Cell Biol* **27:** 8127–8142
19. Acuto O, Di Bartolo V, Micheli F (2008) Tailoring T-cell receptor signals by proximal negative feedback mechanisms. *Nat Rev Immunol* **8:** 699–712
20. Ravichandran KS, Igras V, Shoelson SE, Fesik SW, Burakoff SJ (1996) Evidence for a role for the phosphotyrosine-binding domain of Shc in interleukin 2 signaling. *Proc Natl Acad Sci USA* **93:** 5275–5280
21. Beyer T *et al* (2011) Integrating signals from the T-cell receptor and the interleukin-2 receptor. *PLoS Comput Biol* **7:** e1002121
22. Arndt B, Krieger T, Kalinski T, Thielitz A, Reinhold D, Roessner A, Schraven B, Simeoni L (2011) The transmembrane adaptor protein SIT inhibits TCR-mediated signaling. *PLoS ONE* **6:** e23761
23. Ebinu JO *et al* (2000) RasGRP links T-cell receptor signaling to Ras. *Blood* **95:** 3199–3203

Appendix 18

Analysis of TCR activation kinetics and feedback regulation in primary human T cells upon focal or soluble stimulation

Arndt B., Kowtharapu B.S., Wang X., Lindquist J.A., Schraven B., and **Simeoni L.** J Immunol., in revision

Analysis of TCR activation kinetics and feedback regulation in primary human T cells upon focal or soluble stimulation

Running title: TCR activation kinetics

Boerge Arndt[*,3,5], Bhavani S. Kowtharapu[*,4,5], Mateusz Poltorak[*], Xiaoqian Wang[*], Jonathan A. Lindquist[*,†], Burkhart Schraven[*,†] and Luca Simeoni[*,2]

Address: [*]Otto-von-Guericke University, Institute of Molecular and Clinical Immunology, Leipziger Str. 44, 39120 Magdeburg, Germany; [†]MaCS, Magdeburg Center for Systems Biology, and the SYBILLA Consortium.

[2]**Address correspondence to**:
Luca Simeoni, Institute of Molecular and Clinical Immunology, Otto-von-Guericke University,
Leipziger Str. 44, 39120 Magdeburg, Germany
Tel. +49 391 67 17894,
Fax +49 391 6715852
e-mail: luca.simeoni@med.ovgu.de

Keywords: Human, T cells, T cell receptors, cell activation, signal transduction.

Abstract

Signaling through the TCR is crucial for the generation of different cellular responses including proliferation, differentiation, and apoptosis. A growing body of evidence indicates that differences in the magnitude and the duration of the signal are critical determinants in eliciting cellular responses. Here, we have analyzed signaling dynamics induced upon TCR/CD28 ligation in primary human T cells. We used CD3xCD28 antibodies either cross-linked in solution (sAbs) or immobilized on microbeads (iAbs), two widely employed methods to stimulate T cells *in vitro*. It is well-established that sAbs induce only a transient signal but no productive T-cell responses (unresponsiveness). Conversely, iAbs induce T-cell activation and proliferation. A comparative analysis of the signaling properties of iAbs and sAbs revealed that, under proliferation-inducing conditions, feedback regulation is markedly different from that leading to an unresponsive state. In fact, whereas TCR-mediated signaling is prolonged by a positive feedback loop involving Erk upon iAbs stimulation, sAbs strongly activate inhibitory molecules that likely terminate signaling. In summary, our analysis documents TCR signaling kinetics and feedback regulation under proliferation-inducing conditions. As iAbs appear to mimic signaling dynamics triggered by antigen specific systems, we propose that iAbs are better suited for studying TCR-mediated signaling.

Introduction

Triggering of the T cell receptor (TCR) by pathogens activates an intricate network of signaling cascades that are both temporally and spatially regulated. These signaling events will lead to transcriptional activation, proliferation, and differentiation of T cells that will ultimately culminate in an immune response. Defects in signal transduction may lead to either T-cell hyperresponsiveness or impaired T-cell activation, which result in autoimmunity or immunodeficiency, respectively. Thus, the study of how TCR signaling is initiated, propagated, and translated into a cellular response is important for the understanding not only of physiological processes, but also of the molecular mechanisms underlying human diseases.

To reproduce *in vitro* the signaling events occurring during physiological T-cell activation, immunologists need to pay particular attention in the choice of an appropriate stimulus. *In vivo*, T cells are activated upon contact with APCs expressing the agonistic peptide in the context of MHC-molecules. Therefore, the ideal method to activate T cells *in vitro* e.g. for biochemical analyses should mimic these conditions. Antigen-based systems, however, can only be used for the *in vitro* stimulation of monoclonal T-cell populations expressing a specific TCR, usually expressed on transgenic T cells, and are thus limited to mouse models. Alternative methods such as artificial antigen-presenting systems employing both cell-based and acellular technologies have been developed and are now being used to different extents in immunotherapy (1). However, to assess biochemical events during T-cell activation, soluble polyclonal stimuli such as agonistic antibodies against the TCR/CD3 complex, the coreceptors and/or the costimulatory molecule CD28 are still largely used. For more than 30 years, this method has been extensively employed and indeed, has provided significant insight into the molecular events occurring during T-cell activation. However, stimulations with soluble ligands have clear limitations, as they fail to reproduce the extra dimension of a cell-cell contact and, more importantly, they do not induce T-cell responses (2, 3). Thus, it is

questionable whether TCR signaling induced upon stimulation with soluble Abs mirrors the physiologic signaling cascade leading to productive T-cell responses. Moreover, it appears somehow surprising that, despite the availability of tools that trigger T-cell activation, mimic APCs, and induce proliferation, the analyses of intracellular signaling pathways are still mainly performed by applying soluble ligands.

Microbeads coated with functional antibodies, such as CD3 and CD28, are an efficient tool that can be used to expand T cells *ex vivo* especially for immunotherapeutic applications (4-6). To date, there are no studies that directly compare the signaling properties and the functional effects of conventional stimuli such as CD3xCD28 Abs cross-linked in solution (sAbs), to those of attractive alternative systems that might more closely mimic cell-cell contact such as CD3xCD28 Abs immobilized on microbeads (iAbs). Therefore, we performed a systematic analysis of the signaling signatures induced by CD3xCD28 Abs either cross-linked in solution or immobilized on microbeads.

Our studies show that, conversely to sAbs that induce transient signaling, but not proliferation, iAbs trigger sustained TCR-mediated signaling, activate a positive regulatory circuit involving Erk phosphorylation of Lck, resulting in proliferation. Most importantly, signaling features of iAbs appear similar to those of antigen-driven systems. Our analysis document signaling kinetics and feedback regulation of iAbs and show that they are better suited than sAbs for studying TCR-mediated signaling.

Materials and Methods

Human Ethics. Approval for these studies involving the analysis of TCR-mediated signaling in human T cells was obtained from the Ethics Committee of the Medical Faculty at the Otto-von-Guericke University, Magdeburg, Germany with the permission number [107/09]. Informed consent was obtained in writing in accordance with the Declaration of Helsinki.

T-cell purification. Peripheral blood mononuclear cells were isolated by Ficoll gradient (Biochrom) centrifugation of heparinized blood collected from healthy volunteers. Human T cells were further purified by non-T cell depletion using T cell isolation kits (Miltenyi Biotec). The purity of T cells, determined by flow cytometry, was usually more then 96%.

T-cell stimulation. After isolation, T cells were cultured overnight in RPMI 1640 medium containing 10% FCS (PAN Biotech), 100 U/ml penicillin, 100 µg/ml streptomycin (all from Biochrom AG). Successively, T cells were stimulated with either soluble or immobilized CD3xCD28 mAbs as follow. For soluble Ab stimulation, $2x10^6$ cells were loaded with 10 µg/ml biotinylated anti-human CD3 (clone UCHT1, eBioscience) and 10 µg/ml biotinylated anti-human CD28 (clone CD28.2, eBioscience) mAbs in 100 µl RPMI 1640 and incubated for 10 min on ice. After washing, receptors were cross-linked by adding 25 µg/ml NeutraAvidin™ (Pierce). For microbead stimulation, SuperAvidin™-coated polystyrene microspheres (Ø=10.48 µm, 1.566e+7/ml density, Bangs laboratories, Inc./Polysciences Europe) were coated with biotinylated CD3 and CD28 mAbs (10 µg/ml each) for 30 min at 37 °C in PBS. Antibody-coated microbeads were washed twice with PBS, resuspended in RPMI 1640 and incubated with T cells in a 1:1 ratio. Stimulation of T cells was facilitated and synchronized by centrifugating samples for about 5 sec at 1000 rpm.

Biotinylated IgG2a and IgG1 mouse immunoglobulins (eBioscience) were used as a control.

Stimulations in the presence of either the MEK1/2 inhibitor, UO126 (Cell Signaling Technology) or DMSO (Sigma-Aldrich) were performed by pre-incubating T-cells for 30 min with 10μM of the compounds before stimulation with soluble Abs. For microbead stimulation, 10μM of either UO126 or DMSO were added 30 min after stimulation.

Western blotting. T cells were lysed in buffer containing 1% lauryl maltoside (N-dodecyl β-maltoside), 1% NP-40, 1 mM Na_3VO_4, 1 mM PMSF, 10 mM NaF, 10 mM EDTA, 50 mM Tris pH 7.5, and 150 mM NaCl. Postnuclear lysates were separated by SDS-PAGE and transferred onto nitrocellulose membranes. Membranes were probed with the indicated primary antibodies and the appropriate HRP-conjugated secondary antibodies (Dianova) and developed using the ECL detection system (Amersham Pharmacia). The following antibodies were used for Western blotting in this study: anti-phospho(p)-T^{202}/Y^{204} ERK1/2, anti-pS^{473}Akt, anti-pY^{319}ZAP-70, anti-pY^{171}LAT, anti-pY^{783}PLC-γ1, anti-pS^{9}GSK-3β, anti-pS^{338}-c-Raf, anti-$pS^{217/221}$MEK1/2, anti-pS^{380}p90RSK, anti-pY^{731}-c-Cbl, anti-pY^{351}-p56Dok-2 (all from Cell Signaling Technology), anti-Lck (from BD Transduction laboratories), anti-ZAP70 (Santa Cruz Biotechnology), anti-pTyr (clone 4G10)-HRP conjugate (Millipore), and anti-β-actin (clone AC-15) (Sigma-Aldrich). For quantifications of the Western blots, the intensity of the detected bands was acquired using the Kodak Image Station 2000R and analysis was performed using 1D ImageQuant software (Kodak).

***In vitro* assays.** Proliferation experiments were carried out in 96-well plates (Costar). Purified human T cells were labelled with 0,1 μM CFSE (Molecular Probes) for 10 min at 37°C. After washing, 2 x 10^5 cells were seeded in a total volume of 200 μl to each well and cultured in RPMI (supplemented with 10% FCS, antibiotics and β-Mercaptoethanol). T cells were either left unstimulated or were stimulated with soluble or immobilized CD3xCD28 mAbs as indicated above (see T-cell stimulation). For stimulation with plate-bound mAbs, 10μg/ml CD3 and 10μg/ml CD28 mAbs were incubated overnight in 96-well plates (Costar). T cells

were cultured for 72 h at 37°C, 5% CO_2. Proliferation was assessed by CFSE dilution using a FACS-Calibur and the CellQuest software (BD, Biosciences).

To determine T-cell activation, T cells were stimulated as described above. After 24h, T cells were stained with either FITC- or PE-labelled mAbs against CD25 and CD69 (BD, Biosciences), respectively. Cell associated fluorescence was analysed by flow cytometry.

To quantify cell survival under different stimulation conditions, T cells were stimulated with either soluble or immobilized mAbs as described above, and resuspended in RPMI supplemented with 10% FCS at a density of $1x10^6$ cells/ml in a 24-well tissue culture plate. Cells were harvested after 24 h and the percentage of cells undergoing apoptosis was measured by flow cytometry using FITC-annexin V and propidium iodide (PI) (rh annexin V/FITC kit; Bender MedSystems) according to manufacturer's instructions. Cell-associated fluorescence was acquired using a FACS Calibur and the data was analyzed using the CellQuest software (BD Biosciences).

TCR internalization. To determine TCR internalization, $1x10^6$ cells were stimulated with sAbs or iAbs as mentioned above at 37°C for 0–60 min. Cells were stained with PE-conjugated TCRαβ mAb (BD Biosciences) for 15 min at 4°C and analyzed by flow cytometry.

Results

iAbs induce activation and proliferation, whereas, sAbs result in T-cell unresponsiveness.

It is generally accepted that soluble antibodies cannot induce productive T-cell responses. Indeed, we and others have demonstrated that OT-I transgenic T cells and cytotoxic T-lymphocyte clones are not activated and do not differentiate upon stimulation with antibodies cross-linked in suspension (2, 3). Here, we have stimulated primary human T cells with either sAbs or iAbs and analyzed their functional responses. Figure 1A-B (middle panels) shows that treatment of T cells with iAbs led to a rapid expression of CD25 and CD69 and to a strong proliferative response. Conversely, treatment with sAbs failed to induce T-cell activation as indicated by the absence of CD69 and CD25 expression (Fig. 1A). In agreement with these data, proliferation assays revealed that T cells stimulated with sAbs also did not proliferate (Figure 1B). In contrast to sAbs, when CD3 (either OKT3, UCHT-1, or MEM92) mAbs were immobilized on plastic together with CD28, T-cell activation and proliferation were observed (Fig. 1A-B and data not shown).

Finally, similar to human T cells, also the stimulation of mouse T cells with TCRβxCD28 mAbs either immobilized on microbeads or on a plastic surface resulted in proliferation, whereas, stimulation with the same antibodies cross-linked in suspension did not induce proliferation (Supplementary Fig.1A).

We have previously shown that cross-linked soluble CD3xCD8 antibodies induce apoptosis rather than proliferation in OT-I TCR transgenic $CD8^+$ mouse T cells (2). To analyze whether stimulation of human T cells with sAbs may also induce apoptosis, peripheral T cells were stimulated overnight and assayed for annexin V expression. Figure 1C shows that, in contrast to mouse, stimulation of human T cells with sAbs did not induce apoptosis.

Thus, despite the fact that sAbs are commonly used to activate proximal and distal TCR-mediated signaling pathways, they are unable to induce productive T-cell activation and proliferation.

CD3xCD28 antibodies immobilized on microbeads efficiently stimulate T cells.

To date, little is known about the signaling properties of CD3xCD28 mAbs coated to microbeads. Therefore, we systematically compared proximal TCR signaling induced by either sAbs or iAbs. We initially established a protocol to efficiently stimulate T cells with iAbs. For stimulation, we employed 10μm microbeads that were coated with supravidine. This gives the possibility to bind any biotin-labeled antibody or recombinant protein on the surface of the microbeads. For this investigation, we used biotinylated CD3ε and CD28 mAbs unless indicated otherwise. Microbeads were coated with 10 μg/ml biotinylated CD3 and CD28 mAbs. Microbeads loaded with non-relevant antibodies of the same isotype were used as control. To induce rapid and synchronous cell contact with the beads, we performed a brief centrifugation (5 seconds at 1000 rpm) in a small volume (100 μl). Aliquots of the samples were taken at regular time intervals and analyzed on a FACS Calibur. Supplementary Figure 2A shows that T cells and microbeads have clearly different physical parameters and can be easily visualized in FSC/SSC dot plots. The data also demonstrate that a significant number of cells associated with microbeads coated with CD3xCD28 Abs and appeared as a new population indicated in the gate R_{Tc+m} (Supplementary Fig. 2B). Conversely, in the control samples the emergence of a new population in the R_{Tc+m} gate is not detected (Supplementary Fig. 2B, upper panels), thus indicating that microbeads loaded with isotype controls do not bind to T cells. Successively, to quantify T cell-microbead association, we calculated the ratio R_a of the number of T cell/microbead conjugates (events in the R_{Tc+m} gate) to the total number of T cells (events in the R_{Tc} gate). We found that a high fraction of the cells was in contact with microbeads already after 5 min incubation, with R_a approximately 0.2 (Supplementary

Fig. 2C). After 15 min incubation, the proportion of T cells in contact with microbeads increased up to 50% (R_a=0.5). Afterwards, the R_a slightly decreased and stabilized at values close to 0.3. A similar association rate between Jurkat T cells and CD3-coated micrometric particles has been recently described (7). To further address this issue and to check whether mechanical stress during flow cytometry measurements resulted in the disruption of T cell/bead conjugates, we performed additional analyses. We initially assessed cell/bead conjugates using light microscopy (Supplementary Fig. 2D). We found that a high number of T cells rapidly established contact with iAbs. We next quantified cell/bead conjugates by manual counting in a haemocytometer. The data depicted in supplementary Figure 2E show that around 50-70 % of the cells conjugate with beads. As the proportion of T cell/microbead conjugates were slightly higher than those presented in supplementary Figure 2C, this suggests that some contacts with beads were lost during flow cytometry. Collectively, these data demonstrate that a very high number of iAbs interact with T cells, thus ensuring a focal stimulation.

We next quantified the effectiveness of the stimulation by analyzing the proportion of cells displaying phosphorylated Erk1/2. The data presented in supplementary Figure 2F confirmed that the cell/bead contact indeed resulted in T-cell stimulation as the proportions of T cells in contact with beads and those displaying intracellular phospho-Erk1/2 were similar. Similar proportions of activated T cells were also obtained upon stimulation with sAbs (Supplementary Fig. 2G). Thus, the efficiency of iAbs and sAbs in stimulating T cells appears to be comparable.

Sustained versus transient activation kinetics in TCR-mediated signaling induced by iAbs and sAbs, respectively.

As sAbs and iAbs induce markedly different cellular outcomes, we next performed a comparative analysis of their signaling signatures in primary human T cells. In agreement

with the current knowledge, Figure 2 shows that stimulation with sAbs resulted in a strong and transient induction not only of global tyrosine phosphorylation (Fig. 2A), but also of ZAP-70, LAT, and PLCγ-1 (Fig. 2B, 2E). In contrast, when primary human T cells were treated with iAbs, global tyrosine phosphorylation (Fig. 2A) as well as the phosphorylation of ZAP70, LAT and PLCγ-1 (Fig. 2B, 2E) were very weak, but sustained. Thus, despite the fact that both iAbs and sAbs displayed efficient activation of downstream signaling molecules such as Erk (Supplementary Fig. 2F-G), focal stimulation of primary human T cells by iAbs resulted in a weak but sustained activation of proximal TCR signaling.

We next analyzed signaling kinetics of more distal pathways. Surprisingly, we found that AKT- (Fig. 2C, 2F) and Erk1/2-mediated pathways (Fig. 2D, 2G) were very strongly activated under both conditions of stimulation. However, the activation induced by iAbs was sustained and lasted up to 90 minutes. An extended kinetic analysis revealed that Erk1/2 phosphorylation was still detectable after 12h of iAbs stimulation (data not shown). Thus, despite the weak activation of proximal signaling molecules, iAbs are capable of inducing strong and prolonged activation of downstream signaling pathways. Conversely, the activation kinetics of the AKT- (Fig. 2C, 2F) and Erk1/2- mediated pathways (Fig. 2D, 2G) upon stimulation with sAbs were transient, peaked at 5-10 minutes, and rapidly declined thereafter. Cells that were treated with microbeads loaded with isotype controls failed to induce any detectable activation of TCR-mediated signaling, thus demonstrating that microbeads alone or irrelevant antibodies do not stimulate human T cells (Supplementary Fig. 2F).

Next, we compared activation kinetics of purified naïve and memory $CD4^+$ T cells upon stimulation with sAbs and iAbs. Similar to unfractionated T cells, both $CD4^+$ T-cell subsets displayed a transient activation upon sAbs stimulation, but sustained signaling upon treatment with iAbs (Fig. 3). Thus, it appears that the signaling signatures of sAbs and iAbs are independent of the differentiation status of the cells.

Moreover, similar activation kinetics were also observed when purified mouse splenic T cells were stimulated with TCRβxCD28 Abs immobilized on microbeads or cross-linked in solution (Supplementary Fig. 1B-C), suggesting that TCR-mediated signaling induced by antibodies immobilized on beads are not dependent on the antibody clones used for stimulation.

We next analyzed the signaling kinetics induced by physiological stimuli. We used $CD4^+$ T cells isolated from OT-II transgenic mice that were stimulated with APCs alone as control or with APCs loaded with the $OVA_{323–339}$ peptide. Supplementary Figure 3 shows that only stimulation with peptide loaded APCs, but not with control APCs induces phosphorylation of Erk1/2 in OT-II transgenic T cells. More importantly, phosphorylation of Erk1/2 seems to be weak, but sustained upon physiological stimulation. These data further corroborate our previous observations showing that the stimulation of $CD8^+$ T cells from OT-I transgenic mice with physiological ligands also induced weak and sustained phosphorylation of signaling molecules such as Erk, PLCγ-1, and Akt (2). It is important to note that, similar to iAbs, physiological stimulation of OT-II and OT-I transgenic T cells also induces T-cell responses (data not shown and (2)).

Finally, we analyzed the signaling signatures induced by plate-bound antibodies (Supplementary Fig. 4), which also induce T-cell activation and proliferation (Fig. 1 A-B, lower panels). As shown in Supplementary Figure 4, we found that plate-bound Abs have signaling kinetics similar to iAbs.

Collectively, these data show that stimulation of human T cells with immobilized Abs induce activation kinetics similar to those induced by physiological ligands in mouse TCR transgenic systems and that sustained activation of TCR signaling correlates with proliferation.

Feedback regulation of TCR-mediated signaling is markedly different upon stimulation with iAbs versus sAbs.

The data presented above, show that sAbs induced a rapid, but transient TCR-mediated signaling kinetics, whereas stimulation with iAbs resulted in a sustained activation of a variety of signaling molecules. We next investigated how TCR-mediated signaling is differentially regulated under the two conditions of stimulation. We hypothesized that a fast internalization of the available TCR molecules upon stimulation with sAbs could provide an explanation for the rapid termination of TCR-mediated signaling. Therefore, we compared the expression levels of the TCR after stimulation with either sAbs or iAbs by flow cytometry. The data presented in Figure 4A show that stimulation with iAbs does not reduce, but rather slightly increases TCR levels. This is likely due to the fact that Abs bound to a solid matrix limit TCR internalization, but do not interfere with TCR expression. On the other hand, Figure 4A shows that sAbs induce a slow rate of TCR downregulation, which became evident after 30 minutes of stimulation. It is important to note that the majority of the signaling molecules that we have tested reverted to the dephosphorylated/inactive state already 15 minutes after sAbs stimulation (Fig. 2). Therefore, termination of TCR-mediated signaling occurs before TCR internalization. Moreover, we have previously shown that sustained TCR-mediated signaling and proliferation can occur under conditions of stimulation inducing TCR downregulation (2). Thus, on the basis of these observations, we exclude that TCR internalization induced by sAbs is the cause of transient signaling.

Having ruled out this possibility, we next focused on the analysis of feedback regulation events, which have been shown to play a crucial role in T-cell activation (8-10). Proximal negative feedback loops can be activated by the TCR signalosome and can regulate the amplitude, the duration, and the specificity of the signal (reviewed in Acuto et al. (10)). We asked the question of whether the stimulation with sAbs induced the activation of negative

regulatory molecules that may terminate signaling, thus resulting in the transient signal observed above. Among the many inhibitory molecules organizing inhibitory regulatory circuits, we decided to focus on c-Cbl, an E3 ubiquitin ligase belonging to the CBL family, and the adaptor protein DOK2, which regulate TCR-mediated signaling through two different mechanisms. Whereas members of the CBL family are involved in the down-regulation of signaling molecules via ubiquitination (11), DOK2 and its homolog DOK1 inhibit the activation of signaling pathways by competing for binding to SH2 domains or by recruiting other negative regulators such as SHIP1 or RasGAP to the TCR signalosome (12). The activity of both c-Cbl and DOK2 has been reported to be regulated by tyrosine phosphorylation (12-14) and can be easily monitored by using anti-c-Cbl and anti-DOK2 phosphospecific antibodies, respectively. Figure 4A and B shows that upon sAbs stimulation, T cells very rapidly and strongly phosphorylated both c-Cbl and DOK2, whereas, treatment of human T cells with iAbs resulted only in a very weak phosphorylation of both molecules.

c-Cbl targets many signaling molecules for degradation, including ZAP-70 (15). Thus, we next tested whether sAbs in addition to inducing strong c-Cbl phosphorylation would also induce ZAP-70 ubiquitination and degradation, as we have previously shown in mouse OT-I T cells that ubiquitination of ZAP-70 results in the appearance of ZAP-70 bands displaying retarded migration in SDS-PAGE (2). We checked whether stimulation with soluble CD3xCD28 Abs also resulted in the appearance of ZAP-70 bands running at a higher molecular weight in primary human T cells and we found that activation/phosphorylation of c-Cbl upon stimulation with sAbs indeed correlates with retarded ZAP-70 migration (Fig. 4C). Additionally, the data presented in Figure 4C suggest that stimulation with sAbs also induced ZAP-70 degradation. Conversely, stimulation with iAbs did not significantly induce either c-Cbl phosphorylation or retarded migration and degradation of ZAP-70 (Fig. 4B, 4C). Thus, it appears that stimulation with sAbs activates inhibitory feedback loops that may be responsible for terminating TCR-mediated signaling.

We next investigated whether positive feedback loops may be triggered by iAbs, thus leading to sustained activation of TCR-mediated signaling. In particular, we explored the regulatory circuit involving Lck phosphorylation by activated Erk (8). This model is based on observations showing that the Erk-mediated phosphorylation of Lck on serine 59 alters the ability of the SH2 domain of Lck to bind phosphotyrosines (16). Stefanova et al. further demonstrated that Erk-mediated phosphorylation of Lck prevents SHP-1 binding, thus interfering with SHP-1-mediated Lck inactivation (8). According to this model, active Erk would feedback to Lck to sustain signaling. To assess whether stimulation with iAbs triggers this Erk-mediated positive feedback loop, T cells were stimulated with iAbs and sAbs and the phosphorylation of Lck on S^{59} was detected by the appearance of a new Lck band running at 59 kDa by Western blot (8). As shown in Figure 5A, stimulation of T cells with iAbs clearly resulted in the formation of p59 Lck whereas this shift in the molecular weight of Lck was only barely detectable upon sAbs treatment. Quantification of the proportion of p56 and p59 Lck revealed that the majority of Lck is serine phosphorylated upon iAbs stimulation (Fig. 5B). To demonstrate that the appearance of p59 Lck indeed depends on Erk-mediated phosphorylation, T cells were stimulated with iAbs for 30 min to allow Erk to become activated and subsequently incubated with UO126, an inhibitor of the Erk activator MEK. This treatment has previously been shown to abolish the conversion of Lck to the p59 form (8). In agreement with these observations, we also found that treatment of iAbs-stimulated T cells with UO126 completely abolished both Erk activation and the shift of Lck to the p59 form (Fig. 5C-D). To check whether the inhibition of Erk-mediated Lck phosphorylation also resulted in a reduction of its activity, we investigated phosphorylation levels of downstream signaling molecules that are substrate of Lck, such as the tyrosine kinase ZAP-70, and the adaptor protein LAT whose phosphorylation depends on ZAP-70. The data presented in Figure 5C-D show that the phosphorylation of both ZAP-70 and LAT is reduced upon MEK inhibition, thus indicating that Erk-mediated Lck phosphorylation may enhance its response.

Conversely, preincubation of sAbs-stimulated T cells with the MEK inhibitor reduced Erk phosphorylation, as expected, but not ZAP-70 or LAT phosphorylation (Fig. 5E-F).

Collectively, these data suggest that only stimulation with iAbs activates an Erk-mediated positive feedback loop. Importantly, the regulatory circuit induced by iAbs seems to mimic a previously described mechanism that is induced in T cells upon physiological stimulation (8).

Discussion

Current stimulation protocols to study T-cell signaling are mainly based on agonistic antibodies cross-linked in solution. This method has several advantages such as low costs, easy handling, high reproducibility, effective activation of signaling molecules, polyclonal activity and, most of all, it is well-characterized. However, despite its routine use to study signaling during T-cell activation, it is known that sAbs induce only a transient activation signal that results in an abortive response. Moreover, soluble antibodies do not reproduce the cell-cell contact induced by an APC and therefore fail to mimic at least one crucial event occurring during T-cell activation.

Here, we have analyzed whether Abs immobilized on microbeads, which mimic APCs and induce proliferation, represent an alternative and more suitable method to sAbs for the stimulation of T cells for signaling studies. We further compared the kinetics of central signaling events induced by CD3xCD28 Abs immobilized on microbeads to those generated by CD3xCD28 Abs cross-linked in solution. We document profound signaling differences between these methods of stimulation.

One of the most important findings is that the sustained activation and feedback regulation induced by iAbs recapitulated signaling events observed in antigen-specific systems. In fact, we have previously shown that H-2K^{b} molecules loaded with the SIINFEKEL peptide triggered prolonged activation of ZAP-70, LAT, PLCγ-1, Erk1/2, and Akt and also induced proliferation in OT-I transgenic T cells (2). Further, Stefanova et al. had demonstrated that the sustained signaling, which is necessary for transcriptional activation triggered upon stimulation with agonist peptides, is supported by a positive feedback loop involving phosphorylation of Lck by activated Erk in 5C.C7 transgenic T cells (8).

In addition to the immobilization on beads, Abs can also be bound to cell culture plates. Similarly to iAbs, also plate-bound antibodies induce functional responses. Previous studies

have shown that plate-bound, but not soluble CD3 Abs induce sustained TCR-mediated tyrosine phosphorylation and MAPK activation in murine CTL clones (3, 17, 18). However, the relevance of these studies is limited. First, they utilize $CD8^+$ T-cell clones, which were expanded in the presence of IL-2 and were stimulated with CD3 Abs alone in the absence of costimulation. Therefore, it is questionable whether these data also apply to primary human T cells. Second, the authors do not provide insight into the mechanisms regulating the different activation kinetics. Conversely, in our studies we have provided an extensive biochemical characterization of signaling networks upon stimulation with either sAbs or iAbs in total human peripheral T cells as well as in naïve and memory $CD4^+$ T cells. To our knowledge similar studies describing the signaling properties of Abs immobilized either on beads or cell culture plates have not been performed. Despite the fact that both iAbs and plate-bound antibodies induce functional responses and likely similar signaling kinetics, antibodies immobilized on microbeads allow an easier handling of the samples during stimulation compared to plate-bound antibodies. Therefore, we believe that iAbs are a valid method of stimulation that allows easy and large scale biochemical analyses of TCR-mediated signaling events.

The availability of a method that mimic antigen-specific systems is of particular importance to study primary human T-cells, which can not be stimulated on a large scale by antigen-specific systems. Data from primary human T cells are still scarce and the bulk of our knowledge on signaling in human T cells is based upon data obtained from the analysis of lymphoid cell lines that were stimulated with cross-linked soluble mAbs. Experiments employing primary human cells stimulated with more physiological systems are necessary not only to study the basis of T-cell function, but are also essential to understand the molecular basis of human diseases such as autoimmunity and cancerogenesis.

We have further shown that iAbs allowed the analysis of the dynamics and feedback control of signaling cascades that correlate with a productive response in primary human T cells. As an example, we analyzed the regulation of the Erk signaling pathway, which has been demonstrated to be crucial for the translation of input signals into specific cellular responses in different cell types (19, 20). We have found major differences in the regulation of Erk activation between sAbs and iAbs. TCR-mediated Erk activation upon stimulation with iAbs appears to be not only quantitatively, but also qualitatively different from that induced by sAbs. It has been shown that Erk activation in cytotoxic mouse T lymphocytes after stimulation with immobilized antibodies depends on nPKCs, whereas, sAbs stimulation activates Erk also via cPKCs (18). Thus, it will be important in the future to investigate whether other qualitative and also quantitative differences in TCR-mediated signaling exist between iAbs and sAbs. This may lead to a substantial revision of the current knowledge on signaling in human T cells. We also believe that the data presented here may also help to explain why *in vitro* biochemical data, which are usually obtained by employing sAbs that may trigger pathways not active under physiological conditions, do not always correlate with functional responses.

In summary, our studies clearly show that iAbs are a valid alternative to sAbs for stimulation of T cells for signaling analysis. First, iAbs are easy and ready-to use. Second, iAbs trigger signaling pathways correlating with T-cell activation and proliferation. Third, we show that TCR signaling kinetics and feedback regulation under proliferation-inducing conditions (iAbs) are markedly different from those leading to unresponsiveness (sAbs).

Acknowledgements:

We are grateful to Tilo Bayer for critically reading the manuscript and helpful discussion and to Nicole Jüling and Ines Meinert for excellent technical assistance.

References

1. **Kim, J. V., J. B. Latouche, I. Riviere, and M. Sadelain. 2004. The ABCs of artificial antigen presentation.** ***Nat Biotechnol 22:403-410*****.**
2. **Wang, X., L. Simeoni, J. A. Lindquist, J. Saez-Rodriguez, A. Ambach, E. D. Gilles, S. Kliche, and B. Schraven. 2008. Dynamics of Proximal Signaling Events after TCR/CD8-Mediated Induction of Proliferation or Apoptosis in Mature CD8+ T Cells.** ***J Immunol 180:6703-6712*****.**
3. **Berg, N. N., L. G. Puente, W. Dawicki, and H. L. Ostergaard. 1998. Sustained TCR signaling is required for mitogen-activated protein kinase activation and degranulation by cytotoxic T lymphocytes.** ***J Immunol 161:2919-2924*****.**
4. **Levine, B. L., W. B. Bernstein, M. Connors, N. Craighead, T. Lindsten, C. B. Thompson, and C. H. June. 1997. Effects of CD28 costimulation on long-term proliferation of CD4+ T cells in the absence of exogenous feeder cells.** ***J Immunol 159:5921-5930*****.**
5. **Garlie, N. K., A. V. LeFever, R. E. Siebenlist, B. L. Levine, C. H. June, and L. G. Lum. 1999. T cells coactivated with immobilized anti-CD3 and anti-CD28 as potential immunotherapy for cancer.** ***J Immunother 22:336-345*****.**
6. **Trickett, A., and Y. L. Kwan. 2003. T cell stimulation and expansion using anti-CD3/CD28 beads.** ***J Immunol Methods 275:251-255*****.**
7. **Carpentier, B., P. Pierobon, C. Hivroz, and N. Henry. 2009. T-cell artificial focal triggering tools: linking surface interactions with cell response.** ***PLoS One 4:e4784*****.**
8. **Stefanova, I., B. Hemmer, M. Vergelli, R. Martin, W. E. Biddison, and R. N. Germain. 2003. TCR ligand discrimination is enforced by competing ERK positive and SHP-1 negative feedback pathways.** ***Nat Immunol 4:248-254*****.**

9. Altan-Bonnet, G., and R. N. Germain. 2005. Modeling T cell antigen discrimination based on feedback control of digital ERK responses. *PLoS Biol 3:e356*.

10. Acuto, O., V. Di Bartolo, and F. Micheli. 2008. Tailoring T-cell receptor signals by proximal negative feedback mechanisms. *Nat Rev Immunol 8:699-712*.

11. Loeser, S., and J. M. Penninger. 2007. Regulation of peripheral T cell tolerance by the E3 ubiquitin ligase Cbl-b. *Semin Immunol 19:206-214*.

12. Dong, S., B. Corre, E. Foulon, E. Dufour, A. Veillette, O. Acuto, and F. Michel. 2006. T cell receptor for antigen induces linker for activation of T cell-dependent activation of a negative signaling complex involving Dok-2, SHIP-1, and Grb-2. *J Exp Med 203:2509-2518*.

13. Levkowitz, G., H. Waterman, S. A. Ettenberg, M. Katz, A. Y. Tsygankov, I. Alroy, S. Lavi, K. Iwai, Y. Reiss, A. Ciechanover, S. Lipkowitz, and Y. Yarden. 1999. Ubiquitin ligase activity and tyrosine phosphorylation underlie suppression of growth factor signaling by c-Cbl/Sli-1. *Mol Cell 4:1029-1040*.

14. Kassenbrock, C. K., and S. M. Anderson. 2004. Regulation of ubiquitin protein ligase activity in c-Cbl by phosphorylation-induced conformational change and constitutive activation by tyrosine to glutamate point mutations. *J Biol Chem 279:28017-28027*.

15. Wang, H. Y., Y. Altman, D. Fang, C. Elly, Y. Dai, Y. Shao, and Y. C. Liu. 2001. Cbl promotes ubiquitination of the T cell receptor zeta through an adaptor function of Zap-70. *J Biol Chem 276:26004-26011*.

16. Joung, I., T. Kim, L. A. Stolz, G. Payne, D. G. Winkler, C. T. Walsh, J. L. Strominger, and J. Shin. 1995. Modification of Ser59 in the unique N-terminal region of tyrosine kinase p56lck regulates specificity of its Src homology 2 domain. *Proc Natl Acad Sci U S A 92:5778-5782*.

17. **Puente, L. G., J. C. Stone, and H. L. Ostergaard. 2000. Evidence for protein kinase C-dependent and -independent activation of mitogen-activated protein kinase in T cells: potential role of additional diacylglycerol binding proteins.** ***J Immunol 165:6865-6871*****.**

18. **Puente, L. G., J. S. He, and H. L. Ostergaard. 2006. A novel PKC regulates ERK activation and degranulation of cytotoxic T lymphocytes: Plasticity in PKC regulation of ERK.** ***Eur J Immunol 36:1009-1018*****.**

19. **Daniels, M. A., E. Teixeiro, J. Gill, B. Hausmann, D. Roubaty, K. Holmberg, G. Werlen, G. A. Hollander, N. R. Gascoigne, and E. Palmer. 2006. Thymic selection threshold defined by compartmentalization of Ras/MAPK signalling.** ***Nature 444:724-729*****.**

20. **Marshall, C. J. 1995. Specificity of receptor tyrosine kinase signaling: transient versus sustained extracellular signal-regulated kinase activation.** ***Cell 80:179-185*****.**

Footnotes

[1] The work was supported by grants from the German Research Foundation (DFG), FOR-521 [SI861/1], GRK-1167 [TP12] and SFB-854 [TP19].

[3] Present address, Diabetes Centre, Department of Medicine Innenstadt, Ludwig-Maximilian University, 80336 Munich, Germany.

[4] Present address, Vectorology and Experimental Gene Therapy, University of Rostock, 18057 Rostock, Germany.

[5] B.A. and B.S.K. contributed equally to this work.

Legends to the figures

Figure 1. Analysis of the functional effects of sAbs and iAbs.

Purified human T cells were treated as indicated. A) 24h after stimulation, the activation of T cells was analyzed by staining with CD25 and CD69 and flow cytometry. B) T cells were labeled with CFSE and stimulated as indicated. Proliferation was assed after 72h by analyzing CFSE content on a FACS Calibur. C) T cells were stimulated as indicated for 24h. Cell survival was assessed by FITC-annexin V and PI staining. One representative experiment of at least three independent experiments is shown here.

Figure 2. sAbs induce transient, whereas, iAbs induce sustained signaling.

A-D) Purified human T cells were treated with either soluble (sAbs) or immobilized (iAbs) CD3xCD28 mAbs for the indicated time periods. Samples were analyzed by Western blotting using the Abs indicated. One representative immunoblot is shown. Phosphorylated bands in B, C, and D were quantified using the ImageQuant software and values were normalized to the corresponding β-actin signal. Data in E-G represent the mean of the phosphorylation levels shown as arbitrary units ± SEM of 5 independent experiments.

Figure 3. sAbs induce transient, whereas, iAbs induce sustained signaling in human naïve and memory $CD4^+$ T cells.

Human naïve A-B) and memory C-D) $CD4^+$ T cells were treated with either soluble (sAbs) or immobilized (iAbs) CD3xCD28 mAbs for the indicated time points. Samples were analyzed by Western blotting using the indicated Abs. One representative immunoblot is shown. Phosphorylated bands in A) and C) were quantified as described in Figure 2 and data are shown in B) and D), respectively. Graphs show the mean of the phosphorylation levels shown as arbitrary units ± SEM from 1 to 5 experiments.

Figure 4. sAbs, but not iAbs, induce strong activation of negative regulatory molecules and ZAP-70 degradation.

Purified human T cells were treated with either soluble (sAbs) or immobilized (iAbs) CD3xCD28 mAbs for the indicated time points. A) Measurement of TCR internalization. The expression of the TCR was assessed by PE-conjugated anti-TCRαβ mAb staining analysis by flow cytometry. Data represent the % of the mean fluorescence intensity (MFI) of the TCR expression relative to time 0 of 4 independent experiments. B) The phosphorylation of c-Cbl on Y^{731} and Dok2 on Y^{351} was determined by Western blotting. The phosphorylated c-Cbl and Dok2 bands were quantified using the ImageQuant software and the values normalized to the corresponding β-actin signal. Data represent the mean of the phosphorylation levels shown as arbitrary units ± SEM of at least 4 independent experiments. C) The expression of ZAP-70 was determined by Western blotting. Equal loading is shown by reprobing immunoblots with antibodies specific for β-actin. ZAP-70 bands were quantified as above. Data represent the mean of the expression levels shown as arbitrary units ± SEM of 6 independent experiments.

Figure 5. iAbs induce an Erk-mediated positive feedback loop.

A) Purified human T cells were treated with either soluble (sAbs) or immobilized (iAbs) CD3xCD28 mAbs for the indicated time points. Lck expression was detected in cell lysates by anti-Lck immunoblotting. B) Bands corresponding to p56 or p59 Lck were quantified as described in Figure 3. Data represent the mean of the levels of p56, p59 and total (p56+p59) Lck shown as arbitrary units ± SEM of 5 independent experiments. C) Purified human T cells were treated with iAbs alone for 30 min and then either DMSO or the MEK inhibitor UO126 was added and incubated for an additional 30 to 60 min. Samples were analyzed by Western blotting using the indicated Abs. D) Bands in C) were quantified and the values normalized as

described. Graphs show the mean of the phosphorylation levels of Erk1/2, ZAP-70, and LAT or the level of p59 Lck as arbitrary units ± SEM of 4 independent experiments. E) Purified human T cells were preincubated either in the presence of DMSO or the MEK inhibitor UO126 and successively stimulated with sAbs for the indicated time points. Sample were analyzed by Western blotting using the indicated Abs. F) Bands in E) were quantified as described above and the data from two independent experiments are shown.

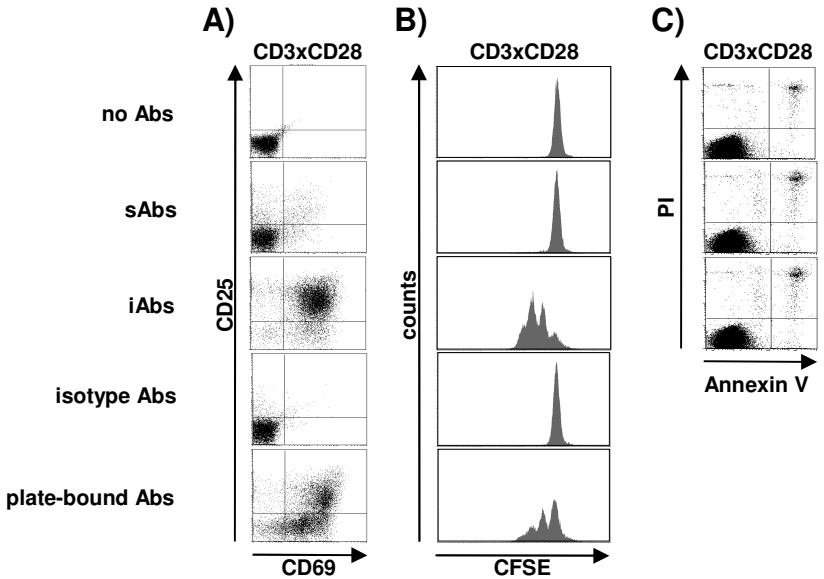
A)
CD3xCD28
no Abs
sAbs
iAbs
isotype Abs
plate-bound Abs
CD25
CD69
B)
CD3xCD28
counts
CFSE
C)
CD3xCD28
PI
Annexin V

Figure 1

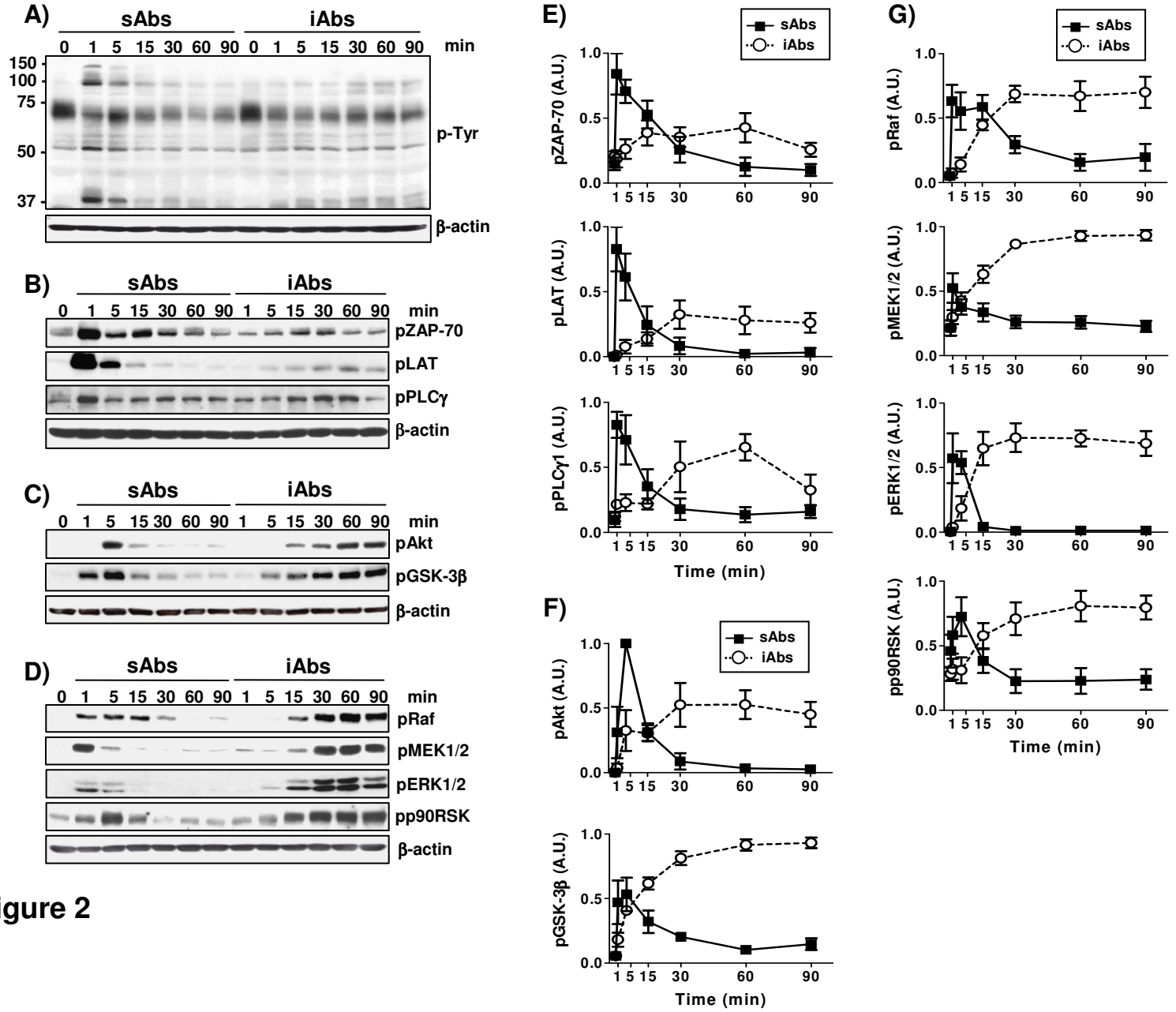
A)
sAbs
iAbs
0 1 5 15 30 60 90 0 1 5 15 30 60 90 min
150
100
75
50
37
p-Tyr
β-actin
B)
sAbs
iAbs
0 1 5 15 30 60 90 1 5 15 30 60 90 min
pZAP-70
pLAT
pPLCγ
β-actin
C)
sAbs
iAbs
0 1 5 15 30 60 90 1 5 15 30 60 90 min
pAkt
pGSK-3β
β-actin
D)
sAbs
iAbs
0 1 5 15 30 60 90 1 5 15 30 60 90 min
pRaf
pMEK1/2
pERK1/2
pp90RSK
β-actin
E)
sAbs
iAbs
pZAP-70 (A.U.)
pLAT (A.U.)
pPLCγ1 (A.U.)
1.0
0.5
0.0
1 5 15 30 60 90
Time (min)
F)
sAbs
iAbs
pAkt (A.U.)
pGSK-3β (A.U.)
1.0
0.5
0.0
1 5 15 30 60 90
Time (min)
G)
sAbs
iAbs
pRaf (A.U.)
pMEK1/2 (A.U.)
pERK1/2 (A.U.)
pp90RSK (A.U.)
1.0
0.5
0.0
1 5 15 30 60 90
Time (min)

Figure 2

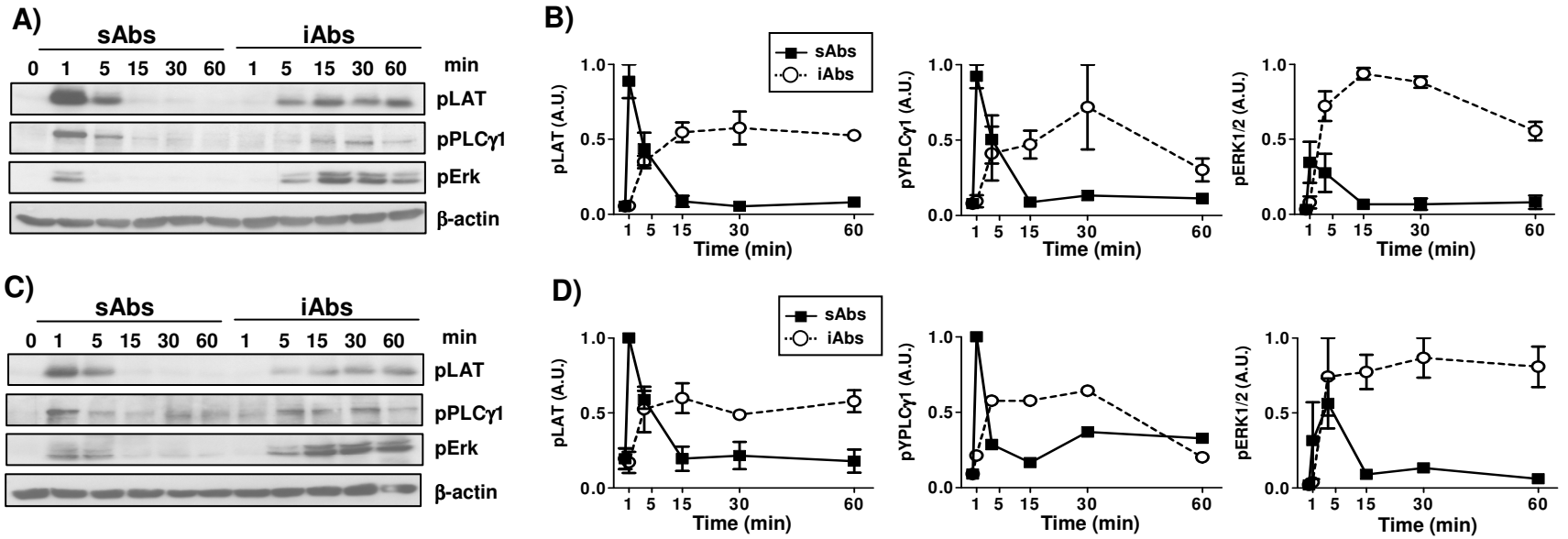
A)
sAbs
iAbs
0 1 5 15 30 60 1 5 15 30 60
min
pLAT
pPLCγ1
pErk
β-actin
B)
sAbs
iAbs
pLAT (A.U.)
pYPLCγ1 (A.U.)
pERK1/2 (A.U.)
Time (min)
C)
sAbs
iAbs
0 1 5 15 30 60 1 5 15 30 60
min
pLAT
pPLCγ1
pErk
β-actin
D)
sAbs
iAbs
pLAT (A.U.)
pYPLCγ1 (A.U.)
pERK1/2 (A.U.)
Time (min)

Figure 3

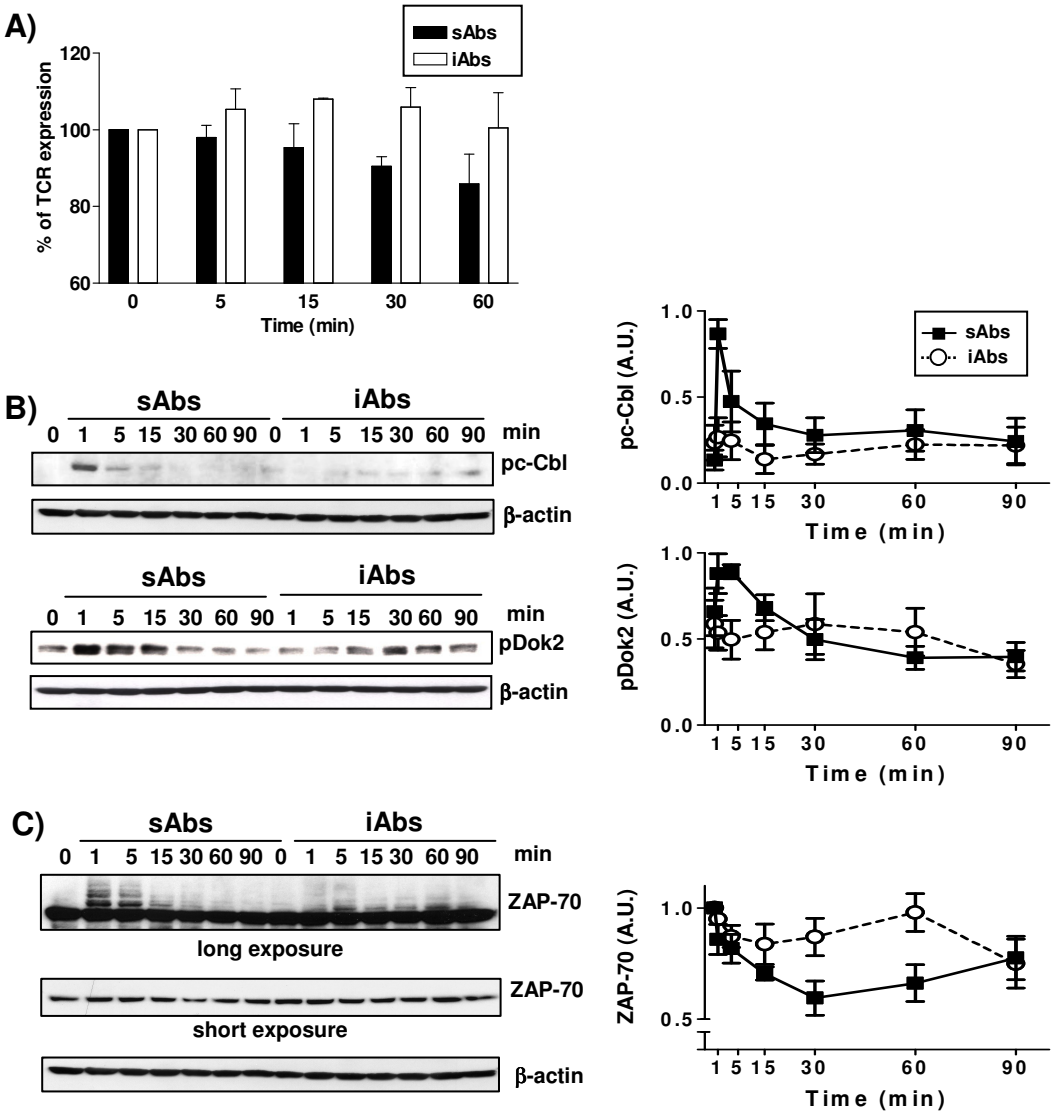
A)
sAbs
iAbs
% of TCR expression
120
100
80
60
0
5
15
30
60
Time (min)
B)
sAbs
iAbs
0 1 5 15 30 60 90 0 1 5 15 30 60 90
min
pc-Cbl
β-actin
sAbs
iAbs
0 1 5 15 30 60 90 1 5 15 30 60 90
min
pDok2
β-actin
pc-Cbl (A.U.)
1.0
0.5
0.0
1 5 15 30 60 90
Time (min)
sAbs
iAbs
pDok2 (A.U.)
1.0
0.5
0.0
1 5 15 30 60 90
Time (min)
C)
sAbs
iAbs
0 1 5 15 30 60 90 0 1 5 15 30 60 90
min
ZAP-70
long exposure
ZAP-70
short exposure
β-actin
ZAP-70 (A.U.)
1.0
0.5
1 5 15 30 60 90
Time (min)

Figure 4

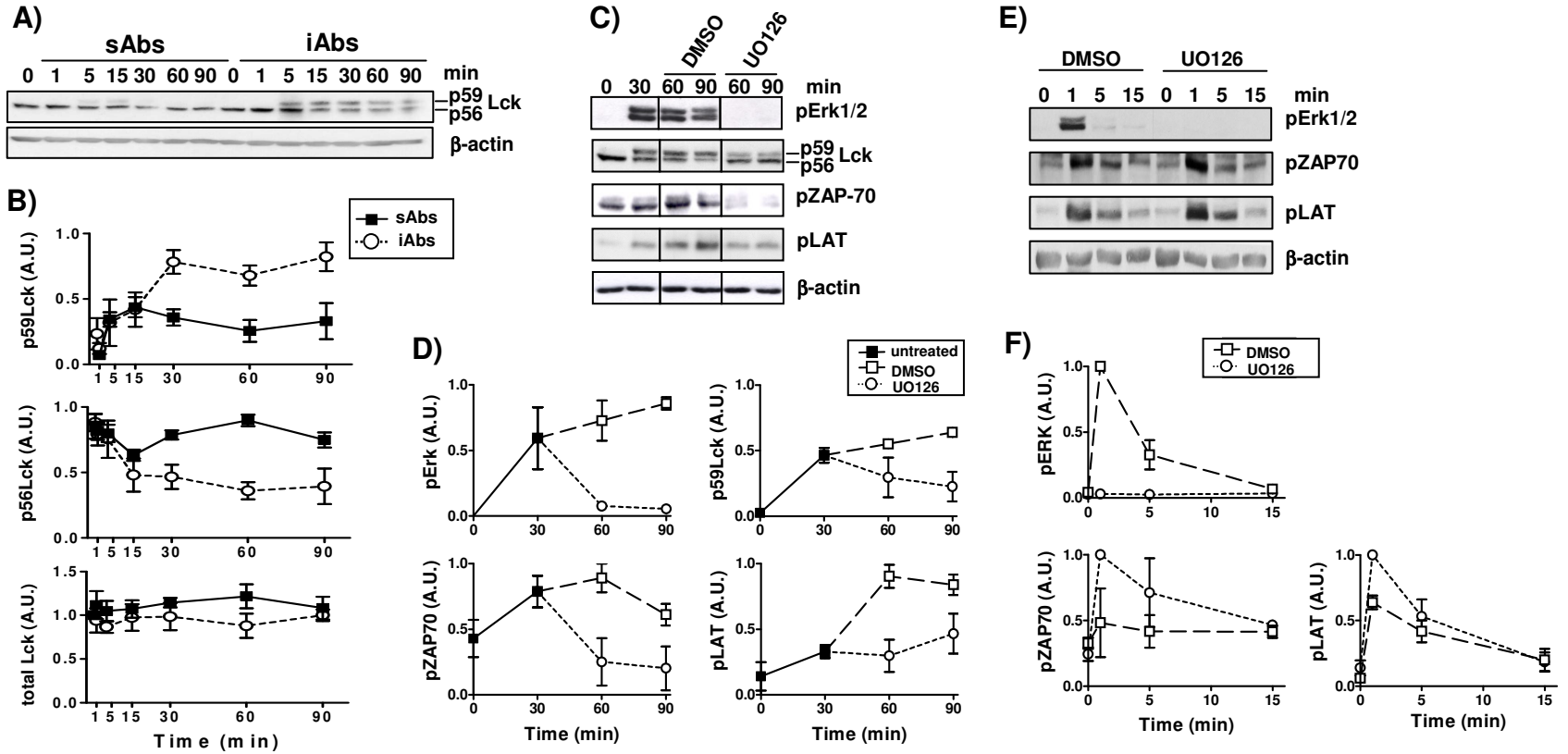
A)
sAbs
iAbs
0 1 5 15 30 60 90 0 1 5 15 30 60 90 min
p59
p56 Lck
β-actin
B)
sAbs
iAbs
p59Lck (A.U.)
p56Lck (A.U.)
total Lck (A.U.)
Time (min)
C)
DMSO
UO126
0 30 60 90 60 90 min
pErk1/2
p59
p56 Lck
pZAP-70
pLAT
β-actin
D)
untreated
DMSO
UO126
pErk (A.U.)
p59Lck (A.U.)
pZAP70 (A.U.)
pLAT (A.U.)
Time (min)
E)
DMSO
UO126
0 1 5 15 0 1 5 15 min
pErk1/2
pZAP70
pLAT
β-actin
F)
DMSO
UO126
pERK (A.U.)
pZAP70 (A.U.)
pLAT (A.U.)
Time (min)

Figure 5

Legends to the Supplementary Figures

Supplementary Figure 1. Analysis of the biochemical and functional effects of sAbs and iAbs in mouse splenic T cells.

Purified mouse splenic T cells were treated as indicated. A) Proliferation was assed after 72h by analyzing CFSE content on a FACS Calibur. One representative experiment of three independent experiments is shown here. B) Samples were analyzed by Western blotting using the indicated Abs. One representative immunoblots is shown. C) Phosphorylated bands in B) were quantified as described in Figure 2. Data represent the mean of the phosphorylation levels shown as arbitrary units ± SEM from 5 independent experiments.

Supplementary Figure 2. Analyses of the binding and stimulation efficiency of Tcell/microbead.

A) T cells and microbeads alone were analyzed by side scattering versus forward scattering dot plots. B) Subsequently, T cells and microbeads loaded either with isotype controls (isotypes, upper panels) or CD3xCD28 mAbs (iAbs, lower panels) were brought into contact for the indicated time periods. T cell/microbeads conjugates (R_{Tc+m}) are clearly distinct from free T cells (R_{Tc}) and microbeads (R_m). C) Statistical analysis of the ratio (R_a) between the numbers of T cell/microbead conjugates (events in the R_{Tc+m} gate) to the total number of T cells (events in the R_{Tc} gate) is presented. D) Transmission light images of T cells incubated with microbeads loaded either with isotype controls (isotypes, upper panels) or CD3xCD28 mAbs (iAbs, lower panels) are shown. E) T cell/microbeads conjugates were diluted and manually counted in a haemocytometer. The graph shows statistical analysis of the ratio (R_a) between the numbers of T cell/microbead conjugates to the total number of T cells from three independent experiments. F) Human T cells were purified and stimulated with beads loaded either with CD3xCD28 mAbs (iAbs) or isotype control (isotypes) for the indicated time

points. The level of pErk1/2 as marker of activation was measured by intracellular staining. Data represent the mean proportions of pErk1/2 positive cells ± SEM of 3 independent experiments. G) Human T cells were purified and either left unstimulated (medium) or were treated with CD3xCD28 mAbs cross-linked in solution (sAbs) for 2 min. The graph shows the mean proportions of pErk1/2 positive cells ± SEM from 3 independent experiments.

Supplementary Figure 3. Stimulation of OT-II transgenic T cells with APCs loaded with the agonist peptide $OVA_{323–339}$ induces sustained Erk1/2 activation.

Purified mouse splenic OT-II transgenic T cells were stimulated with APCs either left unloaded or loaded with the agonist peptide $OVA_{323–339}$ for the indicated time points. Samples were analyzed by Western blotting using the indicated Abs. One representative immunoblot is shown.

Supplementary Figure 4. Stimulation of primary human T cells with plate-bound CD3xCD28 Abs induces sustained signaling.

Purified human peripheral T cells were stimulated with plate-bound CD3xCD28 Abs for the indicated time points. Samples were analyzed by Western blotting using the indicated Abs. One representative immunoblot is shown.

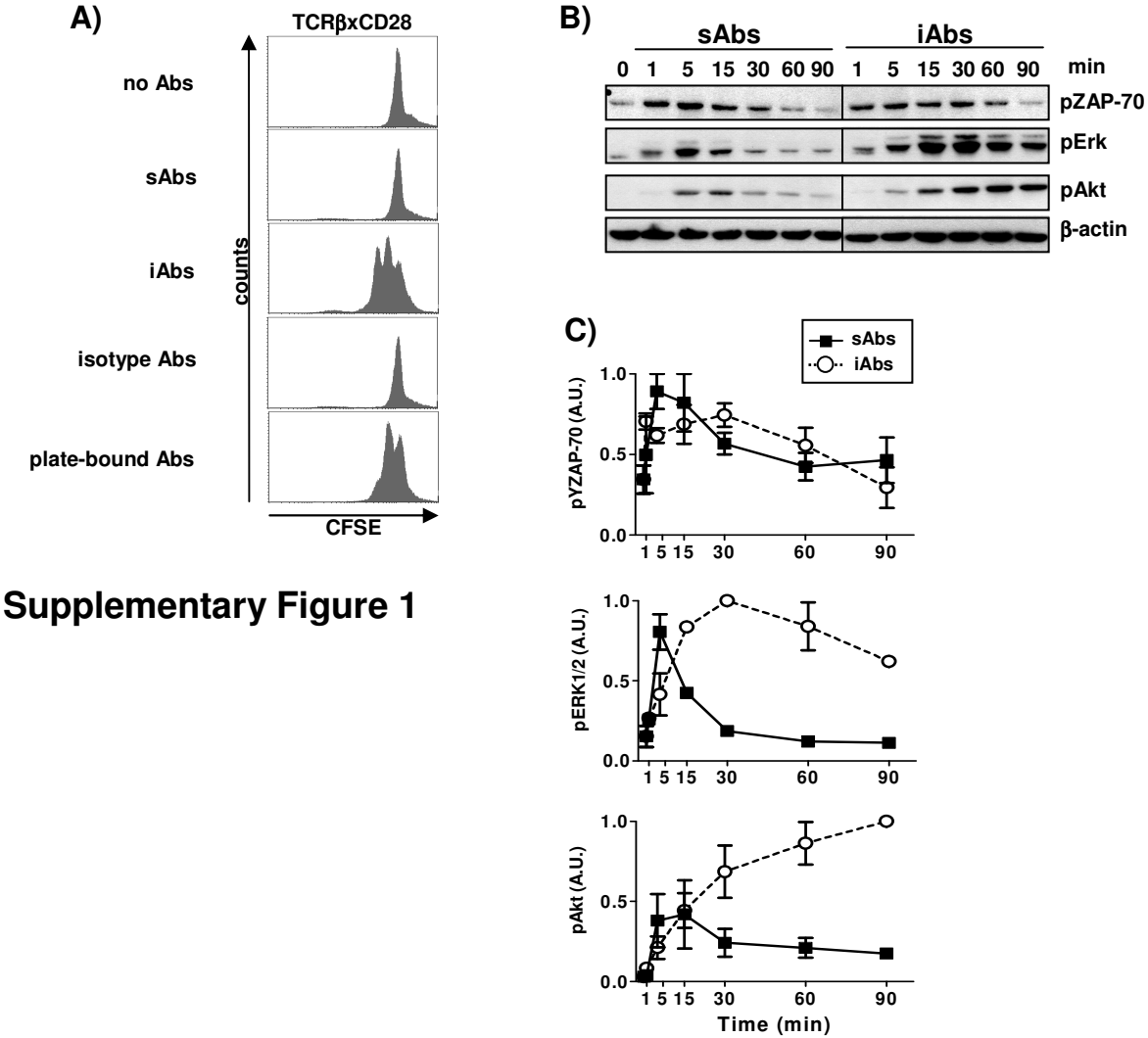

Supplementary Figure 1

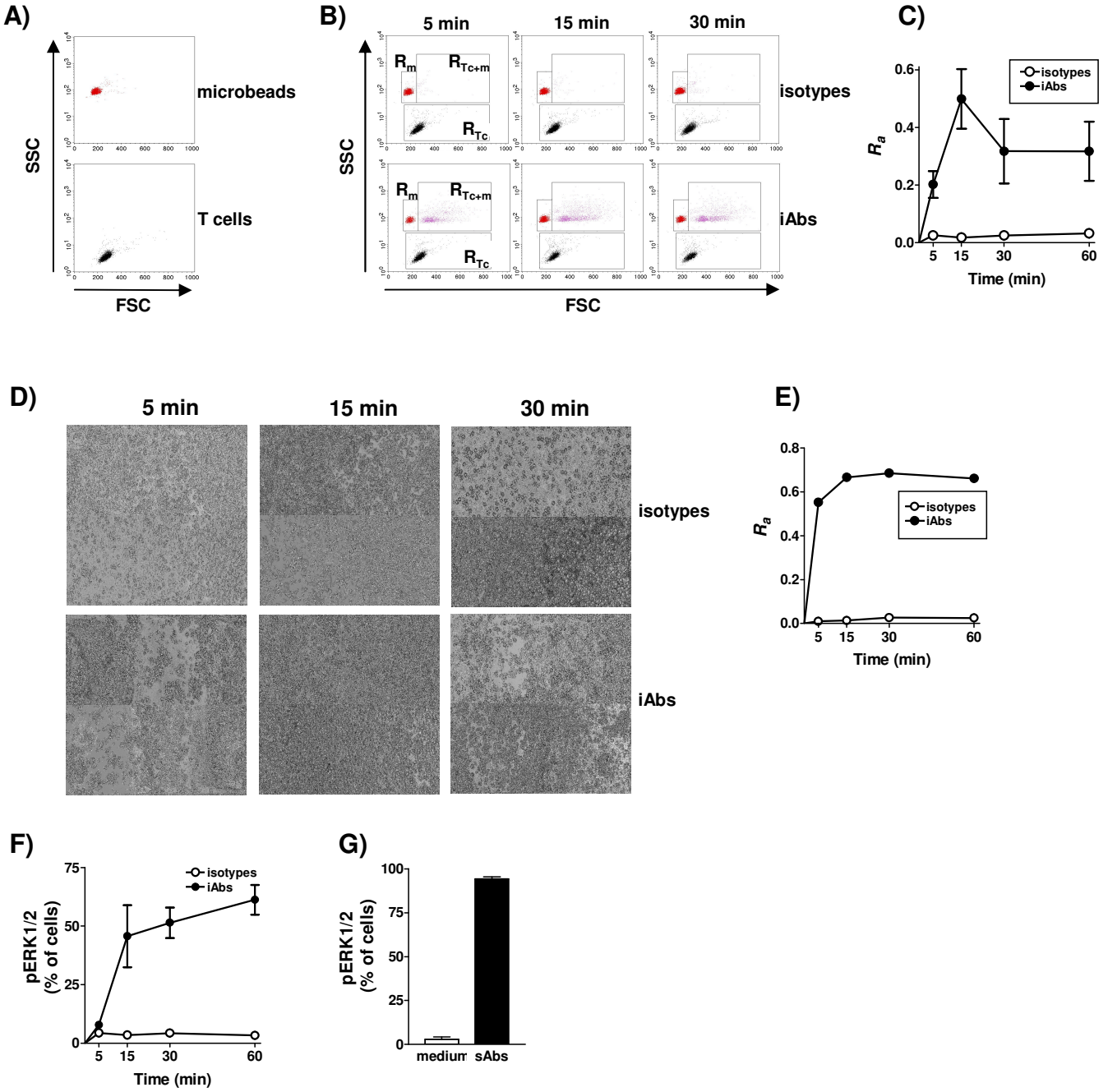

Supplementary Figure 2

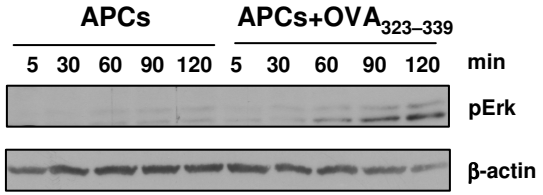

Supplementary Figure 3

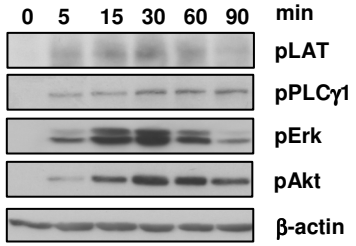

Supplementary Figure 4

Appendix 19

Cooperative immunoregulatory function of the transmembrane adaptor proteins SIT and LAX

Arndt B., Kalinski T., Reinhold D., Thielitz A., Rössner A., Schraven B., and **Simeoni L.** Submitted

Cooperative immunoregulatory function of the transmembrane adaptor proteins SIT and LAX*.

Börge Arndt[*,§,1], Thomas Kalinski[†], Dirk Reinhold[*], Anja Thielitz[‡], Albert Roessner[†], Burkhart Schraven[*] and Luca Simeoni[*]

Addresses: Otto-von-Guericke University Magdeburg, [*]Institute of Molecular and Clinical Immunology, [†]Institute of Pathology, [‡]Clinic of Dermatology and Venerology, Leipziger Str. 44, 39120 Magdeburg, Germany

[§] present address: Medizinische Klinik und Poliklinik IV, Klinikum der LMU, Ziemssenstr. 1, 80336 München, Germany

[1]**Address correspondence to:** Börge Arndt, Medizinische Klinik und Poliklinik IV, Klinikum der LMU, Ziemssenstr. 1, 80336 München, Germany Tel. +49 89 5160 2111, Fax +49 89 5160 4911, e-mail: Boerge.Arndt@med.uni-muenchen.de

Summary sentence: SIT and LAX, two transmembrane adaptor molecules, cooperatively regulate immune functions and limit autoimmunity.

Short running title: SIT and LAX negatively regulate immune responses

Word count (summary sentence): 25

Word count (Abstract): 244

Total character count (text): 22353

Total number of figures: 7

Total number of coloured figures: 1

Total number of references: 36

Key words: Transmembrane adaptor molecules, T cells, B-1 cells, autoimmunity, cell activation, transgenic/knockout mice.

Abbreviations:

ANAs: Antinuclear antibodies

BCR: B cell receptor

DKO: Double-knockout mice

DNP-KLH: Dinitrophenyl keyhole limpet hemocyanin

LAT: Linker for activation of T cells

LAX: Linker for activation of X cells

LIME: LCK-interacting molecule

LPS: Lipopolysaccharide

NTAL: Non-T cell activation linker

PAG: Phosphoprotein associated with GEMs

PMA: Phorbol 12-myristate13-acetate

SIT: SHP-2-interacting transmembrane adaptor protein

TBSM: Tyrosine-based signaling motif

TCR: T cell receptor

TD: Thymus dependent

TI: Thymus independent

TNP-LPS: Trinitrophenyl lipopolysaccharide

TRAP(s): Transmembrane adaptor protein(s)

TRIM: TCR-interacting molecule

WT: Wild type

Abstract

Lymphocyte activation is crucial for the generation of immune responses. *In vitro* studies have demonstrated that transmembrane adaptor proteins (TRAPs) are critical regulators of lymphocyte activation. However, more recent *in vivo* studies have demonstrated that, with the exception of LAT, TRAPs such as SIT, NTAL, and LAX only minimally affect immune cell function. Additional studies have suggested that the mild or the apparent lack of a phenotype displayed by most TRAP knockout mice may be explained by the existence of functional redundancy among this family of adaptors. In fact, it has been shown that the phenotype of NTAL/LAT or SIT/TRIM double-deficient mice is more severe than that of the single knockouts. Here, we have evaluated whether SIT and the related transmembrane adaptor LAX have overlapping functions by generating SIT/LAX double-knockout (DKO) mice. We show that DKO, in contrast to single-knockout mice, accumulate large numbers of activated $CD4^+$ T cells in the spleen. Moreover, conventional B cells from DKO mice are hyperproliferative upon CD40 stimulation. Additionally, we found that DKO mice displayed an expansion of the B1 cell pool in the peritoneal cavity, hypergammaglobulinaemia, and an enhanced immune response to the T1-independent antigen TNP-LPS. Finally, we demonstrate that SIT/LAX double deficiency resulted in a more pronounced breakdown of peripheral tolerance and the development of autoimmunity characterized by antinuclear antibodies (ANAs), and renal disease (glomerulonephritis and proteinuria). Collectively, our data indicate that SIT and LAX are important negative regulators of immune responses that functionally cooperate.

Introduction

Transmembrane adaptor proteins (TRAPs) represent a family of molecules that organize membrane-proximal signaling. To date, seven TRAPs have been identified. Among these, LAT, PAG/Cbp, NTAL/LAB and LIME are mainly localized in the lipid rafts, while TRIM, SIT, and LAX are excluded from the raft fraction of the plasma membrane (reviewed in 1).

The common features of all known transmembrane adapters are the presence of a short extracellular domain, a single membrane-spanning region, and multiple tyrosine-based signaling motifs (TBSMs) within the cytoplasmatic tail [1, 2]. These TBSMs become phosphorylated after antigen receptor engagement and allow inducible protein-protein interactions. Therefore, by recruiting other signal transducing molecules, TRAPs represent important regulators of signaling cascades that are required for the propagation and fine-tuning of the signal from the antigen receptor.

During the last years, the physiological role of TRAPs has been highlighted in studies using cell lines and knockout mice. The generation of $LAT^{-/-}$ mice revealed its essential role in T-cell development. LAT-deficient mice lack peripheral T cells, whereas the generation of B cells and NK cells was not altered [3]. In addition to LAT, other TRAPs are also important for proper immune function. However, loss of these adaptors only modestly affects immune functions. For example, NTAL-deficient mice developed an autoimmune disease with age [4], whereas LAX-deficient mice show abnormally activated lymphocytes, spontaneous germinal center formation in the spleen of unimmunized mice, hypergammaglobulinemia, and hyperreactive mast cells [5, 6]. Moreover, we have shown that SIT-deficient mice displayed an enhanced positive selection in the thymus, hyperactivated peripheral T cells, and an increased homeostatic proliferation. [7-9]. Conversely, mice lacking TRIM [10], PAG [11, 12], and LIME [13] have no significant alteration of the immune system.

The observation that TBSMs are highly conserved among transmembrane adaptors and that knockout mice have no phenotype or only a mild alteration of the immune system has led to the hypothesis that TRAPs are functionally redundant [1]. Indeed, by generating SIT/TRIM double-deficient mice, we have shown that SIT and TRIM (which share the two TBSMs: YGNL and YASV/L, respectively) modulate T-cell development by setting the threshold for thymocyte activation [14]. In addition, the analysis of LAT/NTAL double-deficient mast cells revealed that they display a more severe defect in FcεRI-mediated activation than mast cells lacking LAT alone, thus demonstrating that LAT and NTAL function in a complementary manner [15, 16].

In the present study, we have evaluated whether SIT and LAX cooperate during lymphocyte development and activation by generating SIT/LAX double-knockout (DKO). The rational basis for this approach was given by several structural and functional similarities between the two adaptors: (i) SIT and LAX are both non-raft associated TRAPs (ii) they both negatively regulate antigen receptor mediated signaling, (iii) they share canonical Grb2-binding motifs (YxN) and associate with Grb2 upon antigen receptor stimulation, and finally, (iv) they possess an overlapping tissue distribution in lymphocytes [4, 7-9, 17, 18].

We show that aged DKO mice accumulated larger numbers of activated $CD4^+$ T cells in the spleen. In addition, we also demonstrated that, despite the fact that SIT and LAX do not overlap during thymic selection and during the development of conventional B cells, they cooperatively regulate the generation of B1 B cells and immune functions, such as basal serum immunoglobulin levels and T-I immune responses. Finally, we found that DKO mice develop elevated levels of anti-nuclear antibodies (ANAs) in the sera and further develop glomerulonephritis and proteinuria. This lupus-like disease appears to be more severe than in age-matched SIT- or LAX-single knockout mice.

In summary, our studies shed further light on the role of non-raft transmembrane adaptors in lymphocytes and demonstrate that SIT and LAX are important regulators of immune function that partially overlap.

Material and methods

Animal Ethics. All experiments were performed with samples taken from euthanized animals in accordance with the German National Guidelines for the Use of Experimental Animals (Animal Protection Act, Tierschutzgesetz, TierSchG). Animals were handled in accordance with the European Communities Council Directive 86/609/EEC. All possible efforts were made to minimize animal suffering and the number of animals used.

Mice. $SIT^{-/-}$ and $LAX^{-/-}$ mice were previously described [5, 7]. $LAX^{-/-}$ mice were kindly provided by W. Zhang. $SIT^{-/-}$ mice were mated with $LAX^{-/-}$ to generate $SIT^{+/-}LAX^{+/-}$ mice, which were then crossed to generate $SIT^{-/-}LAX^{-/-}$ double-deficient (DKO) mice. Mice were genotyped for SIT and LAX mutations as previously described [5, 7]. All mice used in this study were between 4 and 10 weeks of age, when not otherwise indicated.

Flow cytometry. Single cell suspensions were prepared from thymus, spleen, lymph nodes, bone marrow, and peritoneal cavity. Subsequently, $1x10^6$ cells were stained with different monoclonal antibodies for 15 min at 4°C, washed, and then analyzed on a FACS Calibur using the CellQuest software (Becton Dickinson). Antibodies against CD3ε (145-2C11); CD4 (RM4-5); CD5 (53-7.3); CD8 (53-6.7); CD21 (7G6); CD23 (B3B4); CD25 (7D4); CD40 (3/23); CD44 (IM7); CD62L (MEL-14); CD69 (H1.2F3); CD86 (GL1); β-TCR (H57-597); B220 (RA3-6B2); IgM (11/41); IgD (11-26c.2a); MAC-1 (M1/70); were purchased from BD Bioscience. CD40L (MR1) were purchased from eBioscience.

Proliferation assay. Splenic B lymphocytes or $CD4^+$ cells were purified using a B-cell isolation kit or a $CD4^+$ isolation kit (Miltenyi Biotech) on an AutoMACS magnetic separation system. The purity that we obtained during the isolation process was usually >94% and was confirmed by flow cytometry. Purified B cells ($5x10^4$ cells/well) and purified $CD4^+$ cells ($2x10^5$ cells/well) were cultured in RPMI medium (supplemented with 10% fetal calf serum,

antibiotics, and β-mercaptoethanol) and either left unstimulated or activated with the following mitogens: anti-IgM F(ab)'2 fragment, CD40, LPS, CD3 and PMI and Ionomycin. Anti-IgM F(ab)'2 was added in solution, whereas CD40 and CD3 were coated to the plate. LPS was used at 1 μg/ml. Cells were cultured for 72 hours at 37°C with 5% CO2. During the last 8 hours, cells were pulsed with 0.5μCi/well of [^{3}H]-thymidine. Subsequently, cells were harvested and [^{3}H]-thymidine incorporation was measured by using the microplate liquid scintillation counter Wallac MicroBeta® TriLux from Perkin Elmer.

Mouse immunization and ELISA. For T-independent (TI) immune responses, mice were immunized intraperitoneally with 50μg TNP-LPS (Sigma). Sera were collected before immunization and at day 10 after immunization. Immunoglobulin levels were determined as previously described [19]. Basal IgE levels were determined by using a Mouse-IgE Quantitation-Kit (Bethyl-Laboratories).

Anti-nuclear antibody (ANA) production. The presence of anti-nuclear antibodies was analyzed by using a 12-well microscope slide (Innogenetics) covered with human HEp-2 cells. HEp-2 cells were blocked and then incubated with the indicated mouse serum dilutions for 30 min. Successively, the slides were washed and incubated for additional 30 min with a FITC-labeled goat anti-mouse IgM antibody (Sigma) or donkey anti-mouse IgG antibody (Dianova). Slides were analyzed by fluorescence microscopy.

Histology. Kidneys from 12 month old C57BL/6 wild-type and mutant mice were fixed in formalin and embedded in paraffin for histological studies. Sections were stained with hematoxylin and eosin (H&E) and additionally with periodic acid-Schiff (PAS). Slides were analyzed by light microscopy in a blinded fashion.

Immunofluorescence. For immunohistochemistry, kidneys were quickly frozen in liquid nitrogen. Sections were stained with FITC-conjugated goat anti-mouse IgG and analyzed by fluorescence microscopy.

Proteinuria. Proteinuria was measured by using urine analysis sticks (Bayer).

Statistics. Statistical analyses were performed using GraphPad Prism (GraphPad Software Inc., San Diego, CA). *p* values were determined by an unpaired two-tailed Student's *t* test.

Results

Accumulation of activated $CD4^+$ T cells in DKO mice.

Recently, it has been shown that SIT and LAX are important negative regulators of lymphocyte activation [5, 7, 9]. As $SIT^{-/-}$ and $LAX^{-/-}$ mice display only a mild alteration in immune function, we have investigated whether the loss of both SIT or LAX results in a more severe phenotype. To assess this issue, we generated $SIT^{-/-}/LAX^{-/-}$ double-knockout mice (DKO). We have previously shown that loss of SIT altered thymic selection. Conversely, LAX is dispensable for lymphocyte development [5]. To assess whether the concomitant ablation of LAX further aggravates the defective thymic development of SIT-deficient mice, we analyzed primary and secondary lymphoid organs from $SIT^{-/-}$, $LAX^{-/-}$, and DKO mice. The numbers as well as the CD4/CD8 profiles of thymocytes from DKO were comparable to those of SIT-deficient mice (data not shown). Moreover, detailed analyses of both positive and negative selection in TCR transgenic models also revealed no difference between SIT-deficient and DKO mice (data not shown). Thus, it appears that SIT and LAX do not overlap during T-cell development. Also the size of the spleen and lymph nodes were comparable between mutant and wild type mice, thus indicating that DKO, similar to single mutant mice, do not develop lymphopenia or lymphoproliferative disease (data not shown). However, a detailed analysis of lymphocyte subsets revealed that aged, but not young, DKO mice have clearly elevated numbers of $CD4^+$ T cells in the spleen (Table 1). The expansion of $CD4^+$ T cells was not detected in either $LAX^{-/-}$ or $SIT^{-/-}$ mice. Successively, we examined whether $CD4^+$ T cells from aged DKO mice showed additional abnormalities. FACS analyses revealed that $CD4^+$ T cells from DKO mice express a significantly higher level of CD69 compared to the single mutant mice (Figure 1A). In contrast to $CD4^+$ T cells from $LAX^{-/-}$ and $SIT^{-/-}$ mice, those from DKO also displayed elevated expression levels of the IL-2 receptor alpha chain CD25 (Figure 1A). Moreover, aged DKO mice, but not single mutant mice, also displayed a

striking increase in the numbers of $CD4^+$ T cells that express high levels of CD44 and low levels of CD62L corresponding to activated/effector T cells (Figure 1B and Table 1). We additionally investigated a variety of surface markers and found that $CD4^+$ T cells of all mutant mice express higher amounts of CD40L compared to WT mice (Figure 1C). Conversely to CD69 and CD25, we did not find any enhancement of SIT/LAX double-deficiency on CD40L expression.

Given the fact that T cells from aged DKO and $SIT^{-/-}$ appear to be expanded *in vivo*, we investigated their proliferative capability *in vitro*. As shown in Figure 2 and in agreement with our previously published data [7], loss of SIT enhanced CD3-mediated proliferation. Moreover, the data presented in Figure 2 also suggest that $CD4^+$ T cells from 12 month-old DKO mice proliferate stronger in response to the applied stimuli in comparison to cells from either single knockout mice or WT controls. Taken together, it appears that SIT and LAX synergize to regulate the activation status of $CD4^+$ T cells.

Normal development of conventional B cells but increased numbers of B1 B cells in SIT/LAX double-deficient mice.

We next evaluated the role of SIT and LAX in the B-cell compartment. We found that the development of conventional B cells is not affected by either single or double deletion of the two transmembrane adaptors (data not shown). In agreement with this observation, we found normal B-cell numbers in all mutant mice (data not shown). To assess whether other B-cell subsets, such as B1 cells that appear to have a distinct origin than conventional B cells [20], were affected by the loss of SIT and LAX, B1 cells were prepared from the spleen and peritoneal lavages, stained with IgM and CD5 Abs and analyzed by flow cytometry. As shown in Figure 3A-B, DKO mice possess a two-fold higher proportion of B1 cells compared to wild type mice both in the peritoneal cavity and the spleen. It is important to note that the proportion of B1 cells is normal in both SIT and LAX single-knockout mice. Thus, our data

reveal that, although SIT and LAX do not possess redundant function during the development of conventional B lymphocytes, they collaborate in regulating the size of the peripheral B1-cell pool.

B cells from DKO mice express higher levels of CD40 and are hyperproliferative upon CD40 stimulation

We next investigated the function of the peripheral B-cell pool. We found that splenic B cells from all mutant mice displayed normal expression of the activation markers CD69 and CD86 (Figure 4A and 4B). Figure 4C and D show that $SIT^{-/-}$ and $LAX^{-/-}$ mice also display normal levels of CD40 expression, while in contrast, splenic B cells from DKO mice have a marked increase in CD40 expression. CD40 is constitutively expressed on B cells. Crosslinking of CD40 initiates proliferation, differentiation, and Ig production.

Next, we wanted to investigate whether SIT and LAX regulate the proliferative capability of B cells *in vitro*. Freshly purified splenic B cells were cultured and stimulated with different concentrations of anti-IgM F[ab']2, CD40, and LPS. B cells from DKO mice displayed an equal proliferation potential compared to single knock-out mice upon anti-IgM F[ab']2 stimulation (data not shown). In contrast, upon stimulation with anti-CD40, B cells from DKO mice proliferated strongly (Figure 5). Taken together, these results demonstrate that SIT and LAX alone do not regulate proliferative response *in vitro* upon antigen receptor stimulation in B cells. In contrast, both adaptors together appear to regulate CD40 expression and hence proliferation upon CD40 stimulation in B cells in a redundant manner.

SIT/LAX double-deficient mice display hypergammaglobulinemia and enhanced TI immune responses.

Having demonstrated that SIT and LAX cooperatively regulate the activation status of $CD4^{+}$ T cells and the number of B1 B cells, we wanted to evaluate whether the absence of both SIT and LAX also affects the immune response *in vivo*. We have previously shown that the

absence of SIT does not alter the basal serum immunoglobulin levels. Moreover, T-dependent (TD) and T-independent (TI) responses were also normal in $SIT^{-/-}$ mice [7]. Conversely to $SIT^{-/-}$ mice, LAX-deficient mice have been reported to possess elevated levels of basal immunoglobulins [5]. In agreement with these data, we found that $SIT^{-/-}$ mice possess normal levels of serum immunoglobulins, whereas LAX-deficient mice display higher levels of IgG1, IgG3, IgM, and IgE (Figure 6A). When we investigated the immunoglobulin levels in the sera of DKO mice, we observed that the production of IgG3, IgE, and particularly IgM is further enhanced in the DKOs compared to $LAX^{-/-}$ mice (Figure 6A). As SIT-deficient mice possess normal levels of immunoglobulins, the augmented concentration of IgG3, IgE, and IgM in the sera of DKO mice appears to indicate that SIT and LAX function in a cooperative manner in regulating immunoglobulin production *in vivo*.

The augmented basal immunoglobulin levels observed in DKO mice prompted us to examine the humoral immune responses in these mice. To address this point, mice were immunized with the T-dependent antigen DNP-KLH and the T-independent antigen TNP-LPS. The concentration of anti-hapten antibodies after primary and secondary immunization with the DNP-KLH antigen was indistinguishable among SIT-, LAX-deficient, SIT/LAX double-deficient, and wild type mice (data not shown). These observations confirm previous data and demonstrate that SIT and LAX are dispensable for TD immune responses [5, 7]. However, when mice were immunized with the TI-1 antigen TNP-LPS DKO mice showed a slight, but significant enhancement of the antibody titer (Figure 6B). Conversely, single mutant mice generated a normal antibody response against the TI-1 antigen TNP-LPS (Figure 6B). Collectively, these data suggest that SIT and LAX cooperatively regulate TI antibody production.

SIT and LAX cooperate to limit autoimmunity.

The data presented above indicate that T and B cells from DKO have an altered function. We next analyzed whether our mutant mice spontaneously develop autoimmune diseases. We initially determined the constitutive production of autoantibodies by analyzing sera from aged $SIT^{-/-}$, $LAX^{-/-}$, DKO mice, and wild type littermates for the presence of antinuclear antibodies (ANAs). HEp-2 epithelial cells were permeabilized and incubated with sera from mutant and control mice. The immunofluorescence data presented in Figure 7A show that sera collected from 12 month-old $SIT^{-/-}$ and $LAX^{-/-}$ mice display an homogeneous antinuclear staining similar to what is observed in human Systemic Lupus Erythematosus (SLE) [21]. We next determined the ANA titer in $SIT^{-/-}$ and $LAX^{-/-}$ mice through serial dilution of the serum and found a titer of 247.3 ± 53.3 in $SIT^{-/-}$ and 221.8 ± 55.9 in $LAX^{-/-}$ mice whereas the mean of ANA titer in control mice was only 16.7 ± 9.1 (Figure 7B). On the other hand, DKO mice also showed an homogeneous antinuclear staining (Figure 7A) and displayed an antibody titer that was approximately two fold higher than in either single knockout (480 ± 97) (Figure 7B). Kidneys from DKO mice were markedly abnormal and displayed a more severe glomerulonephritis and an augmented IgG deposition compared to single knockout mice (Figure 7C). Moreover, glomeruli showing pathological signs were more frequent in DKO mice (data not shown). Additionally, DKO mice also displayed significantly enhanced proteinuria compared to single-mutant mice (Figure 7D). Thus, it appears that DKO mice suffer from a more severe disease than the single-knockout mice, as they display higher ANA titers and a more severe kidney disease. However, this seems to be an additive effect of the two phenotypes observed in single knockout mice. Thus, we propose that SIT and LAX cooperate to limit autoimmunity.

Discussion

SIT and LAX possess similar structure, function, tissue distribution, and membrane localization. Here, we have investigated whether these two TRAPs also share overlapping functions in lymphocytes. The principal finding of our study is that SIT and LAX negatively regulate several aspects of the immune system in a cooperative manner. First, SIT and LAX appear to cooperate to limit autoimmunity. The clinical features of the lupus-like disease in our mice are similar to those seen in knockout mice for other adaptor molecules such as NTAL and TSAd [4, 22], as the disease is late in onset and does not affect mortality/morbidity. In NTAL- and TSAd-deficient mice the disease appears to be triggered by an abnormal T-cell function. However, in the case of $SIT^{-/-}$, $LAX^{-/-}$, and DKO mice, it is not clear whether T cells play a major role in the development of the lupus-like disease. We favor the hypothesis that an altered T-cell function is responsible for the development of autoantibodies. In fact, it has been shown that both SIT- and LAX-deficient T cells are hyperactive [5, 7, 9]. Here, we additionally show that LAX-deficient T cells display enhanced CD69 and CD40L expression. The intensity of CD40L expression seems to correlate with the susceptibility of the mice to develop Systemic Lupus Erythematosus. In fact, increased expression of CD40L was found on $CD4^+$ T cells from lupus patients [23, 24]. Moreover, crossing MRL/lpr mice onto CD40L-deficient mice resulted in a decreased level of IgG autoantibodies, and a less severe renal disease [25]. Additionally, in SWR × NZB F1 mice, another murine lupus model, the administration of antibodies against CD40L (CD154) delayed the onset of the disease [26].

Thus, it may be that the increased CD40L expression observed in $SIT^{-/-}$, $LAX^{-/-}$, and DKO mice also contributes to the autoimmune syndrome, e.g. by supporting the production of high affinity IgG autoantibodies. Nevertheless, as SIT and LAX are also expressed in B cells, it is possible that B cells could also contribute to the development of the disease. Indeed, B-cell

functions are markedly altered in LAX-deficient mice [5]. Here, we have shown that DKO mice have enhanced TI-1 immune responses and display more B1 cells. However, additional experiments are required to asses the contribution of T and B cells to the development of the lupus-like disease in these mice.

Second, our data suggest that SIT and LAX synergistically regulate the development of B-1 cells, a peculiar subset of B lymphocytes. B1 cells express different surface markers (e.g. CD5) and also have different functions compared to conventional B2 cells [27]. In fact, B1 cells are resistant to anti-IgM induced proliferation and apoptosis, produce low affinity antibodies with a broad specificity, and mediate mainly T-independent immune responses [27]. The importance of B1 cells is emphasized by the discovery that this lymphocyte subpopulation is implicated in the pathogenesis of many human diseases, such as autoimmunity and malignant transformation [20, 28].The origin of B1 cells is still under debate, but several studies indicate that the development of B1 cells appears to be critically dependent upon BCR signal strength. Disruption of genes that decrease BCR-mediated signaling results in a reduction of B-1 cells, whereas mutations that enhance BCR-mediated signal strength results in an expansion of B-1 cells [29]. Thus, mice lacking or carrying mutations in negative regulators of BCR-mediated signaling such as CD22, Lyn, PD-1, and SHP-1 show increased numbers of B1 cells. As SIT and LAX also represent negative regulators of antigen receptor-mediated signaling, the observation that B1-cell numbers are increased in DKO mice is in line with the idea that signals emanating from the BCR critically regulate B1 cell numbers. Our data further corroborate the hypothesis that the lack of negative regulators of BCR-mediated signaling leads to the expansion of the B-1 cell pool.

How could SIT and LAX regulate the expansion of B1 cells? It has been shown that the development of B-1 cells depends critically on the transcription factor NFAT [30]. Indeed, the absence of NFATc1 resulted in a severe depletion of B1 cells by more than seven fold.

Berland and Wortis also demonstrated that B1 cells express five times more NFATc1 than conventional B2 cells [30]. Interestingly, both SIT and LAX were shown to regulate NFAT activity in Jurkat T cells in a dose-dependent manner [18, 31].

Third, we have shown that together SIT and LAX regulate basal Ig levels and TI-1 immune responses. It is possible that the increased levels of IgM and IgG3 in DKO may be due to the increased number of B1 cells in these mice. In fact, B1 cells are believed to be the primary source of natural IgM and IgG3 [32, 33]. These natural antibodies react weakly with self antigens, but strongly with many common pathogen-associated carbohydrate antigens. Almost all of the natural antibodies that react with LPS are produced by B1 cells [34]. These antibodies are very important for the clearance of LPS and, therefore, for protection against endotoxin-mediated sepsis. Thus, these data suggest that also the elevated antibody titer to TNP-LPS immunization in DKO mice may be due to the expanded B1-cell population.

Despite the fact that our *in vivo* data suggest that SIT and LAX are important regulators of lymphocyte function, how SIT and LAX together fine-tune antigen receptor signaling is not yet clear. Previously published biochemical studies have revealed that LAX negatively regulates antigen receptor signaling by inhibiting PI3K signaling [5]. More recently, we have shown that SIT inhibits TCR-ζ phosphorylation, thus affecting proximal TCR signaling [9]. However, our extensive biochemical analysis of both T and B cells did not reveal any additional effect in DKO mice compared to the single mutants (data not shown). As both adaptors do not associate with membrane rafts, where signaling complexes are organized, we suggest that SIT and LAX may regulate the availability of cytoplasmic adaptors and effector molecules by sequestering them into the non-raft compartment. By acting as dosage-dependent regulators of signaling pathways, SIT and LAX could control signals that are not only transduced via antigen receptors, but also through other surface receptors and could therefore modulate the general activation threshold of lymphocytes.

Collectively, our data suggest that lymphocytes are endowed with a set of TRAPs that exert subtle effects in regulating antigen receptor-mediated signaling. Thus, the question arises why lymphocytes need to express several TRAPs. Our data suggest that it is not the action of a single TRAP, but rather the coordinated action of multiple TRAPs that finely tunes the immune response. This regulation seems to be important not only for peripheral immune functions, but also for lymphocyte development. Indeed, we show here that SIT and LAX regulate the number of peripheral B1 cells and additional data from our laboratory suggest that the two transmembrane adaptor molecules SIT and TRIM concomitantly regulate T-cell development [14]. As suggested by studies demonstrating that NTAL and LAT function in a complementary manner to regulate FcεRI-mediated signaling in mast cells, it thus appears as if TRAPs possess a redundant role not only in lymphocytes, but also in other cell types within the immune system [16, 35].

It is tempting to speculate that functional redundancy is not only limited to the adaptor pairs SIT/LAX, NTAL/LAT, and SIT/TRIM, but indeed might apply to all TRAPs. In fact, the structural similarities between LAX and TRIM (note that both molecules are capable of binding PI3K and are strongly expressed in $CD4^+$ T cells) or between NTAL and LAX (which both carry several Grb2-binding site and both are expressed in B cells and mast cells) are suggestive of the existence of sophisticated and redundant mechanisms that regulate antigen receptor-mediated signaling. Interestingly, it has been published that aged NTAL-deficient mice show hyperactivation of $CD4^+$ T cells, anti-nuclear antibodies and develop a lupus-like autoimmune disease [4]. This phenotype strikingly resembles the alteration of the immune system that we observe in the SIT/LAX double-deficient mice. It will now be important to assess whether SIT/LAX/NTAL-triple deficient mice show an even more aggravated autoimmune phenotype. Similarly, the generation of additional double or even triple knockout

mice will help to assess how TRAPs control the intricate signal transduction network within immune cells.

Nevertheless, it is striking to note that NTAL, SIT, TRIM, and LAX all appear to primarily exert negative regulatory signaling functions within the immune system. Similarly, although PAG/Cbp-deficient mice do not show an obvious phenotype [11, 12], siRNA studies demonstrate that PAG is an important negative regulatory protein in T cells [36]. Thus, it appears as if the strong positive regulatory function of LAT is balanced by a plethora of negative regulatory TRAPs that help to maintain homeostasis within the immune system.

Acknowledgements:

We are grateful to Dr Jonathan Lindquist and Tilo Beyer for critically reading the manuscript and helpful discussion and to Ines Meinert, Marita Lotzing and Britta Bogel for excellent technical assistance. We thank Dr Weiguo Zhang for providing $LAX^{-/-}$ mice and the employees of the animal facility for maintenance of the animals.

Disclosures

We declare that we, the authors, have no conflicting interest.

The work was supported by grants from the German Research Foundation (DFG), FOR-521 [SI861/1], GRK-1167 [TP12] and SFB-854 [TP19].

Authorship:

Principle investigator: L. Simeoni

Co-principle investigator and corresponding author: B. Arndt

Co-investigators: T. Kalinski, D. Reinhold, A. Thielitz, A. Roessner, B. Schraven

References:

1. **Horejsi, V., Zhang, W., Schraven, B. (2004) Transmembrane adaptor proteins: organizers of immunoreceptor signalling. *Nat Rev Immunol* 4, 603-16.**
2. **Simeoni, L., Kliche, S., Lindquist, J., Schraven, B. (2004) Adaptors and linkers in T and B cells. *Curr Opin Immunol* 16, 304-13.**
3. **Zhang, W., Sommers, C.L., Burshtyn, D.N., Stebbins, C.C., DeJarnette, J.B., Trible, R.P., Grinberg, A., Tsay, H.C., Jacobs, H.M., Kessler, C.M., Long, E.O., Love, P.E., Samelson, L.E. (1999) Essential role of LAT in T cell development. *Immunity* 10, 323-32.**
4. **Zhu, M., Koonpaew, S., Liu, Y., Shen, S., Denning, T., Dzhagalov, I., Rhee, I., Zhang, W. (2006) Negative regulation of T cell activation and autoimmunity by the transmembrane adaptor protein LAB. *Immunity* 25, 757-68.**
5. **Zhu, M., Granillo, O., Wen, R., Yang, K., Dai, X., Wang, D., Zhang, W. (2005) Negative regulation of lymphocyte activation by the adaptor protein LAX. *J Immunol* 174, 5612-9.**
6. **Zhu, M., Rhee, I., Liu, Y., Zhang, W. (2006) Negative regulation of Fc epsilonRI-mediated signaling and mast cell function by the adaptor protein LAX. *J Biol Chem* 281, 18408-13.**
7. **Simeoni, L., Posevitz, V., Kolsch, U., Meinert, I., Bruyns, E., Pfeffer, K., Reinhold, D., Schraven, B. (2005) The transmembrane adapter protein SIT regulates thymic development and peripheral T-cell functions. *Mol Cell Biol* 25, 7557-68.**
8. **Posevitz, V., Arndt, B., Krieger, T., Warnecke, N., Schraven, B., Simeoni, L. (2008) Regulation of T Cell Homeostasis by the Transmembrane Adaptor Protein SIT. *J Immunol* 180, 1634-42.**

9. Arndt, B., Krieger, T., Kalinski, T., Thielitz, A., Reinhold, D., Roessner, A., Schraven, B., Simeoni, L. The Transmembrane Adaptor Protein SIT Inhibits TCR-Mediated Signaling. *PLoS One* 6, e23761.

10. Kolsch, U., Arndt, B., Reinhold, D., Lindquist, J.A., Juling, N., Kliche, S., Pfeffer, K., Bruyns, E., Schraven, B., Simeoni, L. (2006) Normal T-cell development and immune functions in TRIM-deficient mice. *Mol Cell Biol* 26, 3639-48.

11. Xu, S., Huo, J., Tan, J.E., Lam, K.P. (2005) Cbp deficiency alters Csk localization in lipid rafts but does not affect T-cell development. *Mol Cell Biol* 25, 8486-95.

12. Dobenecker, M.W., Schmedt, C., Okada, M., Tarakhovsky, A. (2005) The ubiquitously expressed Csk adaptor protein Cbp is dispensable for embryogenesis and T-cell development and function. *Mol Cell Biol* 25, 10533-42.

13. Gregoire, C., Simova, S., Wang, Y., Sansoni, A., Richelme, S., Schmidt-Giese, A., Simeoni, L., Angelisova, P., Reinhold, D., Schraven, B., Horejsi, V., Malissen, B., Malissen, M. (2007) Deletion of the LIME adaptor protein minimally affects T and B cell development and function. *Eur J Immunol* 37, 3259-69.

14. Koelsch, U., Schraven, B., Simeoni, L. (2008) SIT and TRIM determine T cell fate in the thymus. *J Immunol* 181, 5930-9.

15. Zhu, M., Liu, Y., Koonpaew, S., Granillo, O., Zhang, W. (2004) Positive and negative regulation of FcepsilonRI-mediated signaling by the adaptor protein LAB/NTAL. *J Exp Med* 200, 991-1000.

16. Volna, P., Lebduska, P., Draberova, L., Simova, S., Heneberg, P., Boubelik, M., Bugajev, V., Malissen, B., Wilson, B.S., Horejsi, V., Malissen, M., Draber, P. (2004) Negative regulation of mast cell signaling and function by the adaptor LAB/NTAL. *J Exp Med* 200, 1001-13.

17. Pfrepper, K.I., Marie-Cardine, A., Simeoni, L., Kuramitsu, Y., Leo, A., Spicka, J., Hilgert, I., Scherer, J., Schraven, B. (2001) Structural and functional

dissection of the cytoplasmic domain of the transmembrane adaptor protein SIT (SHP2-interacting transmembrane adaptor protein). ***Eur J Immunol*** **31, 1825-36.**

18. Zhu, M., Janssen, E., Leung, K., Zhang, W. (2002) Molecular cloning of a novel gene encoding a membrane-associated adaptor protein (LAX) in lymphocyte signaling. ***J Biol Chem*** **277, 46151-8.**

19. Togni, M., Swanson, K.D., Reimann, S., Kliche, S., Pearce, A.C., Simeoni, L., Reinhold, D., Wienands, J., Neel, B.G., Schraven, B., Gerber, A. (2005) Regulation of in vitro and in vivo immune functions by the cytosolic adaptor protein SKAP-HOM. ***Mol Cell Biol*** **25, 8052-63.**

20. Kantor, A.B., Herzenberg, L.A. (1993) Origin of murine B cell lineages. ***Annu Rev Immunol*** **11, 501-38.**

21. Tan, E.M., Chan, E.K., Sullivan, K.F., Rubin, R.L. (1988) Antinuclear antibodies (ANAs): diagnostically specific immune markers and clues toward the understanding of systemic autoimmunity. ***Clin Immunol Immunopathol*** **47, 121-41.**

22. Drappa, J., Kamen, L.A., Chan, E., Georgiev, M., Ashany, D., Marti, F., King, P.D. (2003) Impaired T cell death and lupus-like autoimmunity in T cell-specific adapter protein-deficient mice. ***J Exp Med*** **198, 809-21.**

23. Yellin, M.J., Thienel, U. (2000) T cells in the pathogenesis of systemic lupus erythematosus: potential roles of CD154-CD40 interactions and costimulatory molecules. ***Curr Rheumatol Rep*** **2, 24-31.**

24. Grammer, A.C., Slota, R., Fischer, R., Gur, H., Girschick, H., Yarboro, C., Illei, G.G., Lipsky, P.E. (2003) Abnormal germinal center reactions in systemic lupus erythematosus demonstrated by blockade of CD154-CD40 interactions. ***J Clin Invest*** **112, 1506-20.**

25. Ma, J., Xu, J., Madaio, M.P., Peng, Q., Zhang, J., Grewal, I.S., Flavell, R.A., Craft, J. (1996) Autoimmune lpr/lpr mice deficient in CD40 ligand: spontaneous Ig class switching with dichotomy of autoantibody responses. *J Immunol* 157, 417-26.

26. Mohan, C., Shi, Y., Laman, J.D., Datta, S.K. (1995) Interaction between CD40 and its ligand gp39 in the development of murine lupus nephritis. *J Immunol* 154, 1470-80.

27. Rothstein, T.L. (2002) Cutting edge commentary: two B-1 or not to be one. *J Immunol* 168, 4257-61.

28. Kasaian, M.T., Casali, P. (1993) Autoimmunity-prone B-1 (CD5 B) cells, natural antibodies and self recognition. *Autoimmunity* 15, 315-29.

29. Hardy, R.R., Hayakawa, K. (2001) B cell development pathways. *Annu Rev Immunol* 19, 595-621.

30. Berland, R., Wortis, H.H. (2003) Normal B-1a cell development requires B cell-intrinsic NFATc1 activity. *Proc Natl Acad Sci U S A* 100, 13459-64.

31. Marie-Cardine, A., Kirchgessner, H., Bruyns, E., Shevchenko, A., Mann, M., Autschbach, F., Ratnofsky, S., Meuer, S., Schraven, B. (1999) SHP2-interacting transmembrane adaptor protein (SIT), a novel disulfide-linked dimer regulating human T cell activation. *J Exp Med* 189, 1181-94.

32. Forster, I., Rajewsky, K. (1987) Expansion and functional activity of Ly-1+ B cells upon transfer of peritoneal cells into allotype-congenic, newborn mice. *Eur J Immunol* 17, 521-8.

33. Herzenberg, L.A., Stall, A.M., Lalor, P.A., Sidman, C., Moore, W.A., Parks, D.R., Herzenberg, L.A. (1986) The Ly-1 B cell lineage. *Immunol Rev* 93, 81-102.

34. Su, S.D., Ward, M.M., Apicella, M.A., Ward, R.E. (1991) The primary B cell response to the O/core region of bacterial lipopolysaccharide is restricted to the Ly-1 lineage. *J Immunol* 146, 327-31.

35. Janssen, E., Zhu, M., Craven, B., Zhang, W. (2004) Linker for activation of B cells: a functional equivalent of a mutant linker for activation of T cells deficient in phospholipase C-gamma1 binding. *J Immunol* 172, 6810-9.

36. Smida, M., Posevitz-Fejfar, A., Horejsi, V., Schraven, B., Lindquist, J.A. (2007) A novel negative regulatory function of the phosphoprotein associated with glycosphingolipid-enriched microdomains: blocking Ras activation. *Blood* 110, 596-615.

Legend to figures.

Figure 1. Analysis of T-cell activation markers

A) Histograms show the expression of the activation markers CD69 or CD25. Numbers within the histograms indicate the percentage of $CD4^+$ T cells that express CD69 or CD25. Graphs show statistical analyses of CD69 and CD25 expression. Bars represent the mean ± SEM from four mice. Statistical significance is indicated (* p<0,05). B) $CD4^+$ T cells were analyzed for the expression of CD44 and CD62L. Numbers indicate the percentage of cells in the region. C) Histograms compare the expression of CD40L on $CD4^+$ T cells from WT (shaded) and mutant mice (black line). Left panel: comparison between WT and $SIT^{-/-}$ mice; middle panel: comparison between WT and $LAX^{-/-}$ mice; right panel: comparison between WT and DKO mice. Bar graphs on the right represent statistical analysis from five mice. Statistical significance is indicated (* p<0,05).

Figure 2. T cells from DKO mice are hyperactivated

Purified splenic $CD4^+$ T cells from aged mutant and control mice were stimulated in a 96-well plate with the indicated doses of coated CD3 or PMA plus ionomycin (P&I) (2 ng/ml PMA and 0,5 µg/ml Ionomycin) for 72 hours. Cells were pulsed with [^{3}H]-thymidine and processed for standard scintillation counting. Data represent mean counts per minute (cpm) ± SEM from five mice. * $p < 0.05$; ** $p < 0.01$; *** $p < 0.0001$; ns=not significant.

Figure 3. Increased numbers of B1 cells in DKO mice

A) Peritoneal cells were stained with mAbs against CD5 and IgM. B1 cells were defined as IgM^{hi} and $CD5^+$. Numbers indicate the percentages of living cells that reside in the corresponding gate. One representative mouse out of ten per each group is shown. B) Bar graphs show the absolute numbers of B1 cells in the peritoneal cavity (left) and spleen (right). * $p < 0.05$; ** $p < 0.01$.

Figure 4. Analysis of B-cell activation markers in aged mice.

A) Histograms display the expression of the activation marker CD69 on $B220^+$-gated cells from aged DKO, $SIT^{-/-}$ or $LAX^{-/-}$ and WT mice. Numbers indicate the percentage of living cells that express CD69. B and C) $B220^+$-gated splenic cells were analyzed for the expression of CD86 and of CD40. One representative mouse of four is shown. D) Statistical analysis of CD40 expression. Data show the MFI ± SEM from four mice. *** $p < 0.001$.

Figure 5: Hyperproliferation of B cells from DKO mice upon CD40 stimulation

Purified splenic B cells from aged mutant and control mice were stimulated with the indicated concentrations of plate-bound CD40 mAb or LPS in a 96-well plate for 72 hours. Proliferation was assessed by $[H^3]$-thymidine incorporation for the last 6-8 hours. Data represent mean counts per minute (cpm) ± SEM from triplicate cultures of four mice per each group. Statistical significance is indicated * $p < 0.05$; ** $p < 0.01$.

Figure 6. Hypergammaglobulinemia in DKO mice

A) Basal immunoglobulin levels in the sera from ten DKO, $SIT^{-/-}$, $LAX^{-/-}$ and WT mice were determined by ELISA. (B) T cell-independent immune response. Mice were immunized with 50µg TNP-LPS, sera were collected before (Day 0) and after (Day 10) immunization and analyzed for TNP-specific antibodies. A total of 11 mice per group were analyzed. Asterisks indicate the statistical significance * $p < 0.05$; ** $p < 0.01$; *** $p < 0.0001$.

Figure 7. Development of ANAs and glomerulonephritis in DKO, $SIT^{-/-}$ and $LAX^{-/-}$ mice

A) The presence of autoantibodies (ANAs) in sera from aged mutant and WT mice was determined by immunofluorescent staining of HEp-2 epithelial cells. The pattern of nuclear staining of HEp-2 cells using 1:80 dilution is shown. ANAs were detected with FITC-conjugated secondary antibody against mouse IgG. B) Statistical analysis of ANA titer in

mutant and wild type mice. The bars represent the mean values of ANA titers. C) Kidney sections from 1 year-old mutant and wild type mice were stained with periodic acid-Schiff (PAS), hematoxylin and eosin (H&E) or with FITC-conjugated goat anti-mouse IgG. Sections were analyzed in a blinded fashion by light microscopy and scored for mesangial cellularity, increased mesangial matrix, infiltration of inflammatory cells and thickness of basal membranes or capillary walls. Representative glomeruli from control and mutant mice are shown (1 x 400). Kidney cryosections were also stained with FITC-conjugated goat anti-mouse IgG and the presence of immune complexes was visualized by fluorescence microscopy. D) Statistical analysis of proteinuria in mutant and wild type mice. The bars represent the mean values of proteinuria. Proteinuria was measured by using urine analysis sticks and graded according to the following scale: negative, 0 mg/dl; 1, < 30mg/dl; 2, < 100mg/dl and 3, > 100mg/dl. Asterisks in B) and D) indicate statistical significance (* $p<0,05$; ** $p<0.01$; *** $p<0.0001$).

Table 1: Cellularity of peripheral T-cell subsets from aged mutant and wild type mice. The numbers of lymphocyte subsets were determined on the basis of the total cell numbers and flow cytometric analysis. Data represent means ± standard errors (SD) of the mean.

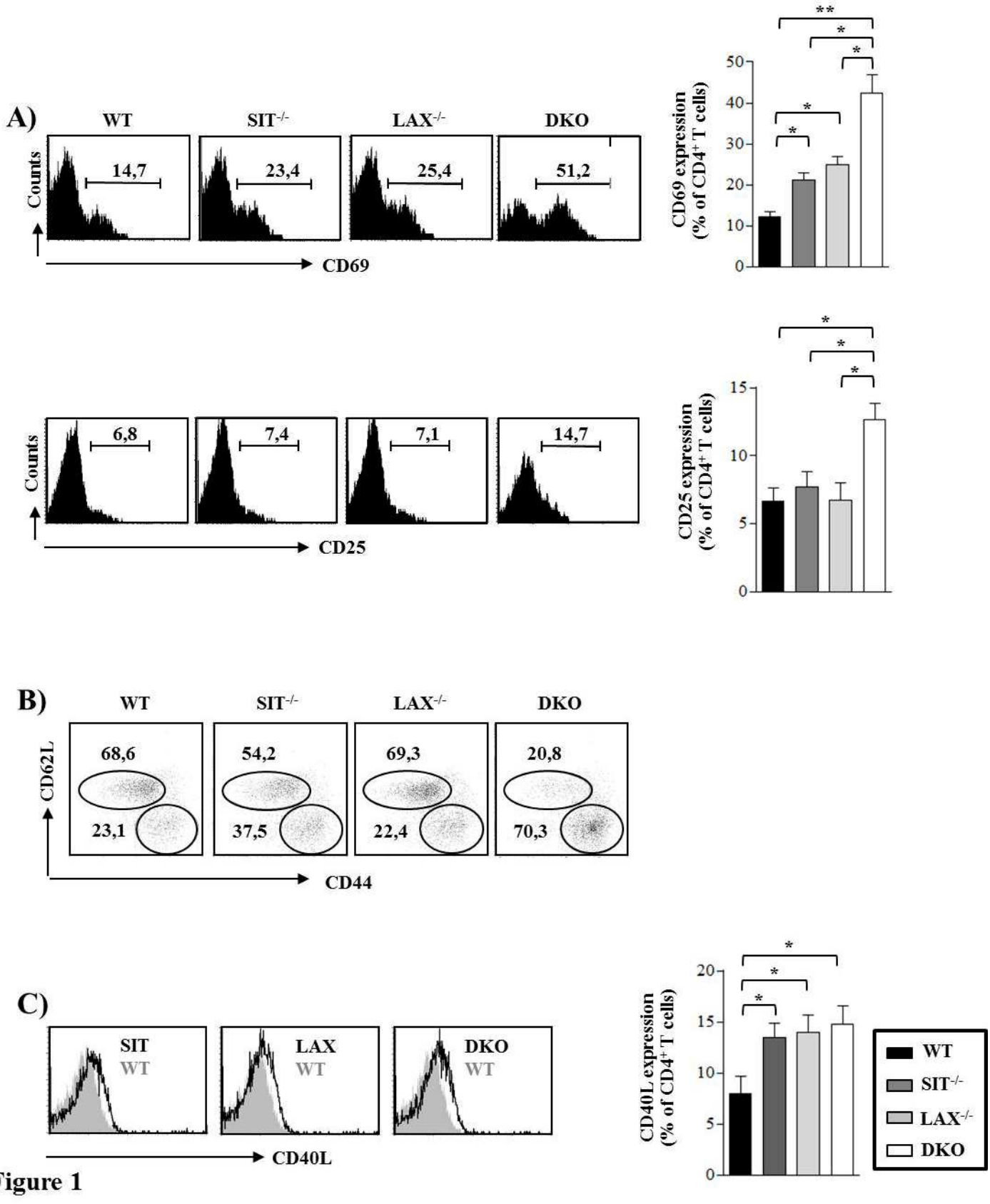
A)
WT
SIT-/-
LAX-/-
DKO
Counts
14,7
23,4
25,4
51,2
CD69
CD69 expression (% of CD4+ T cells)
6,8
7,4
7,1
14,7
CD25
CD25 expression (% of CD4+ T cells)
B)
CD62L
68,6
23,1
54,2
37,5
69,3
22,4
20,8
70,3
CD44
C)
SIT
WT
LAX
WT
DKO
WT
CD40L
CD40L expression (% of CD4+ T cells)
WT
SIT-/-
LAX-/-
DKO

Figure 1

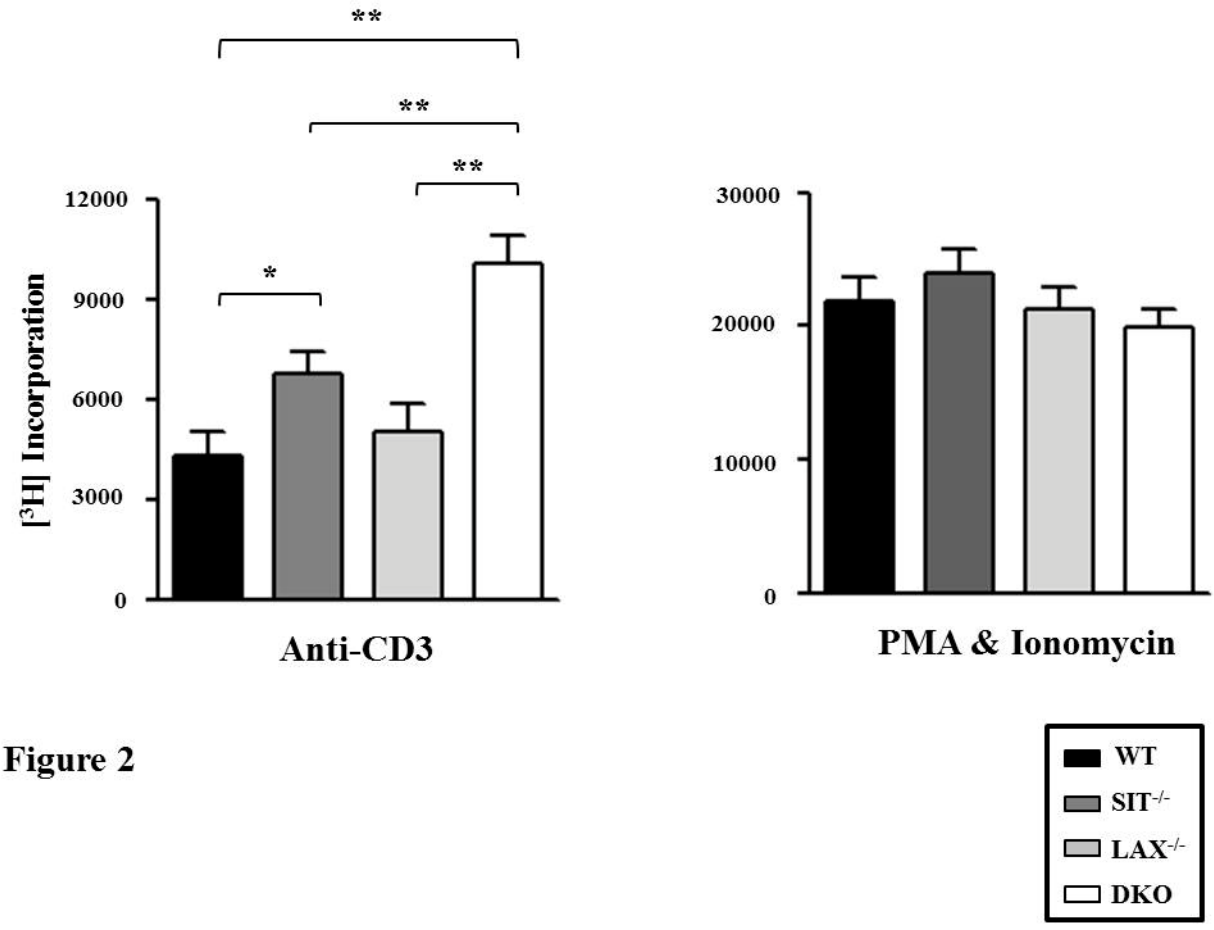
**
**
**
*
12000
9000
6000
3000
0
[3H] Incorporation
Anti-CD3
30000
20000
10000
0
PMA & Ionomycin
WT
SIT-/-
LAX-/-
DKO

Figure 2

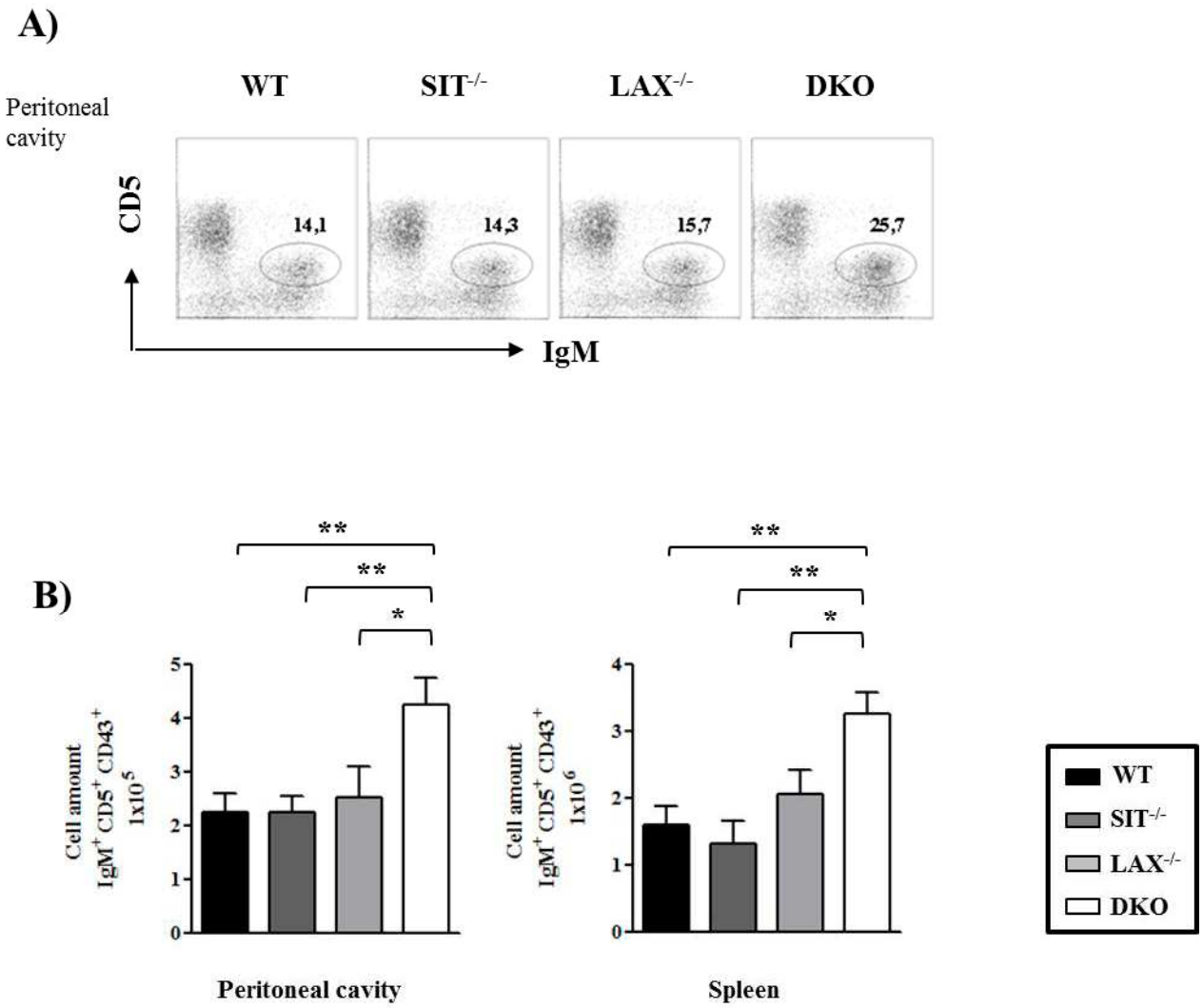
A)
WT
SIT-/-
LAX-/-
DKO
Peritoneal cavity
CD5
14,1
14,3
15,7
25,7
IgM
B)
**
**
*
Cell amount IgM+ CD5+ CD43+ 1x10^5
Peritoneal cavity
Cell amount IgM+ CD5+ CD43+ 1x10^6
Spleen
WT
SIT-/-
LAX-/-
DKO

Figure 3

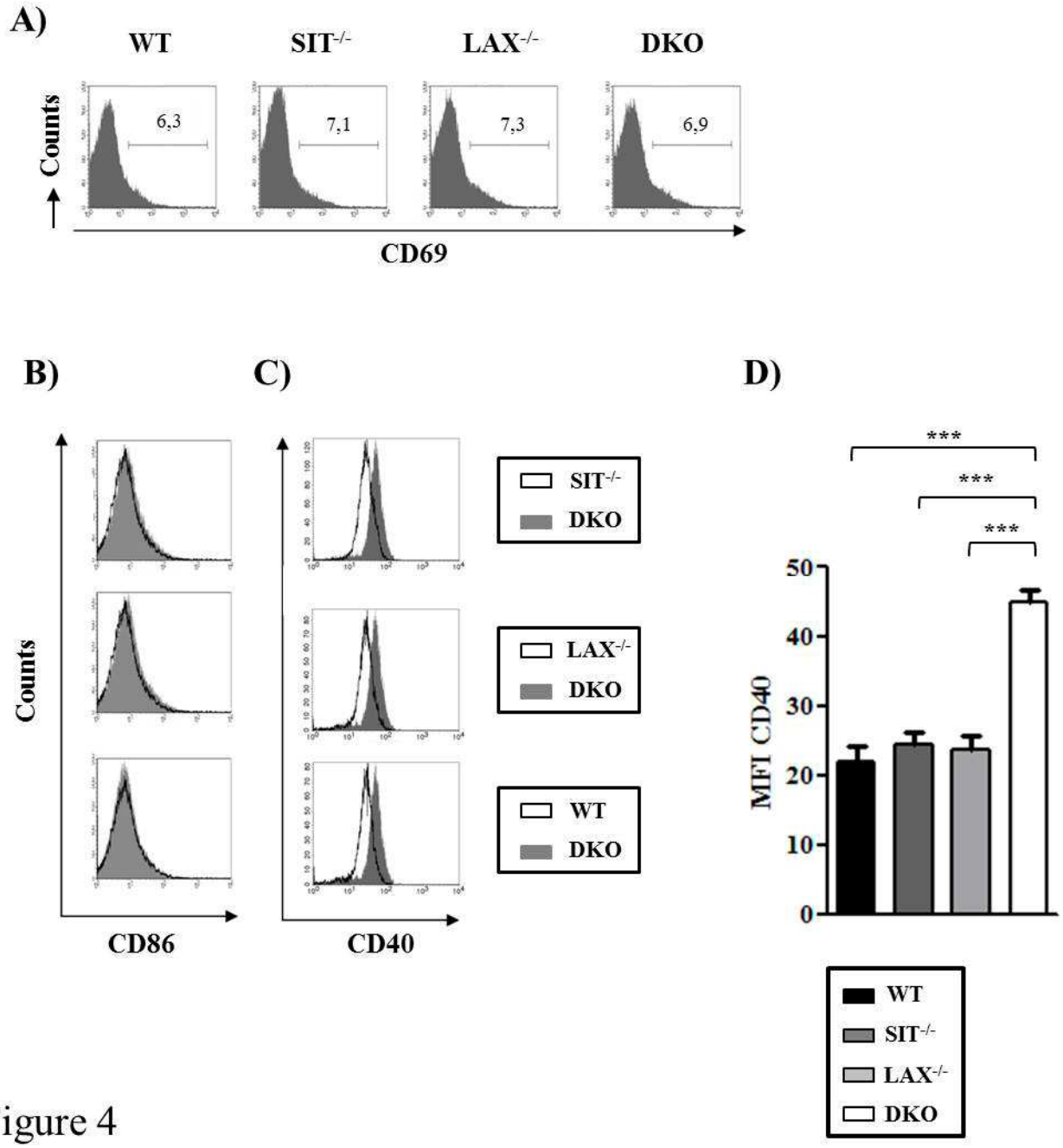
A)
WT
SIT-/-
LAX-/-
DKO
Counts
6,3
7,1
7,3
6,9
CD69
B)
C)
D)
SIT-/-
DKO
LAX-/-
DKO
WT
DKO
Counts
CD86
CD40
***
***
***
MFI CD40
50
40
30
20
10
0
WT
SIT-/-
LAX-/-
DKO

Figure 4

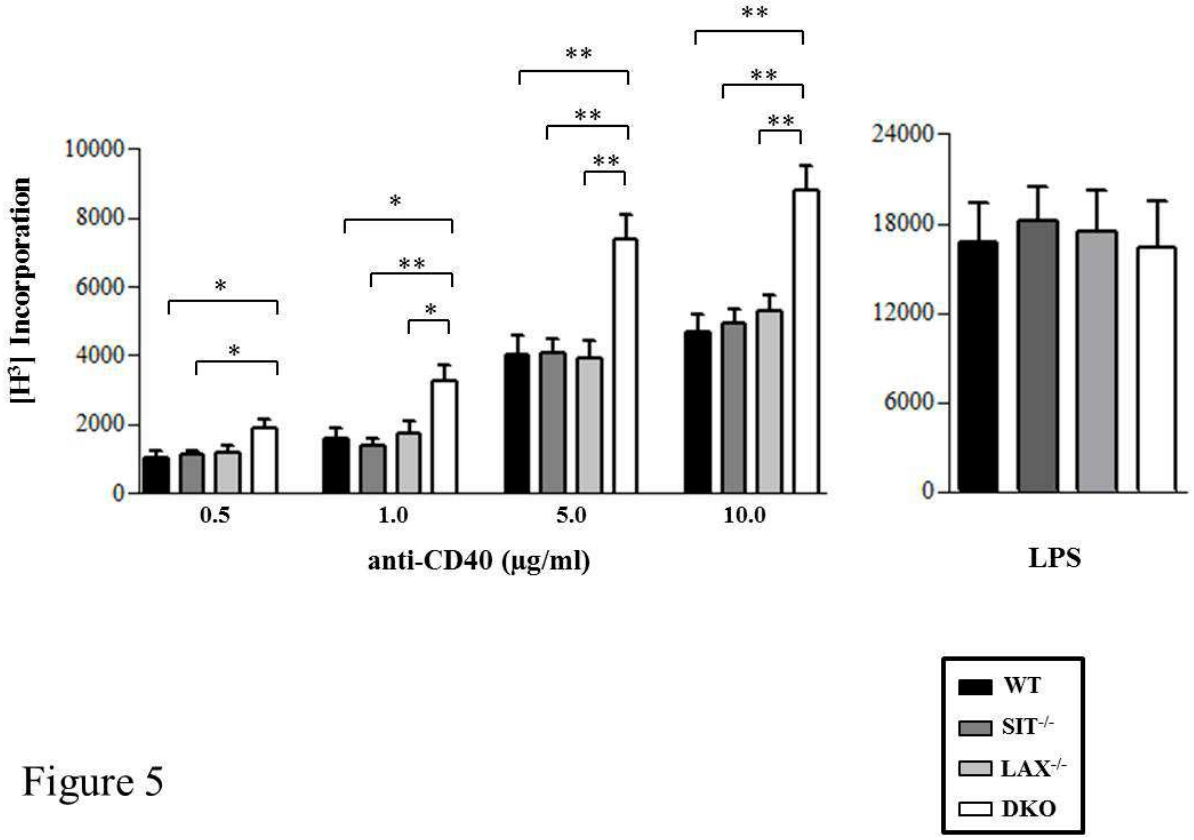
[H3] Incorporation
10000
8000
6000
4000
2000
0
0.5
1.0
5.0
10.0
anti-CD40 (µg/ml)
24000
18000
12000
6000
0
LPS
WT
SIT-/-
LAX-/-
DKO

Figure 5

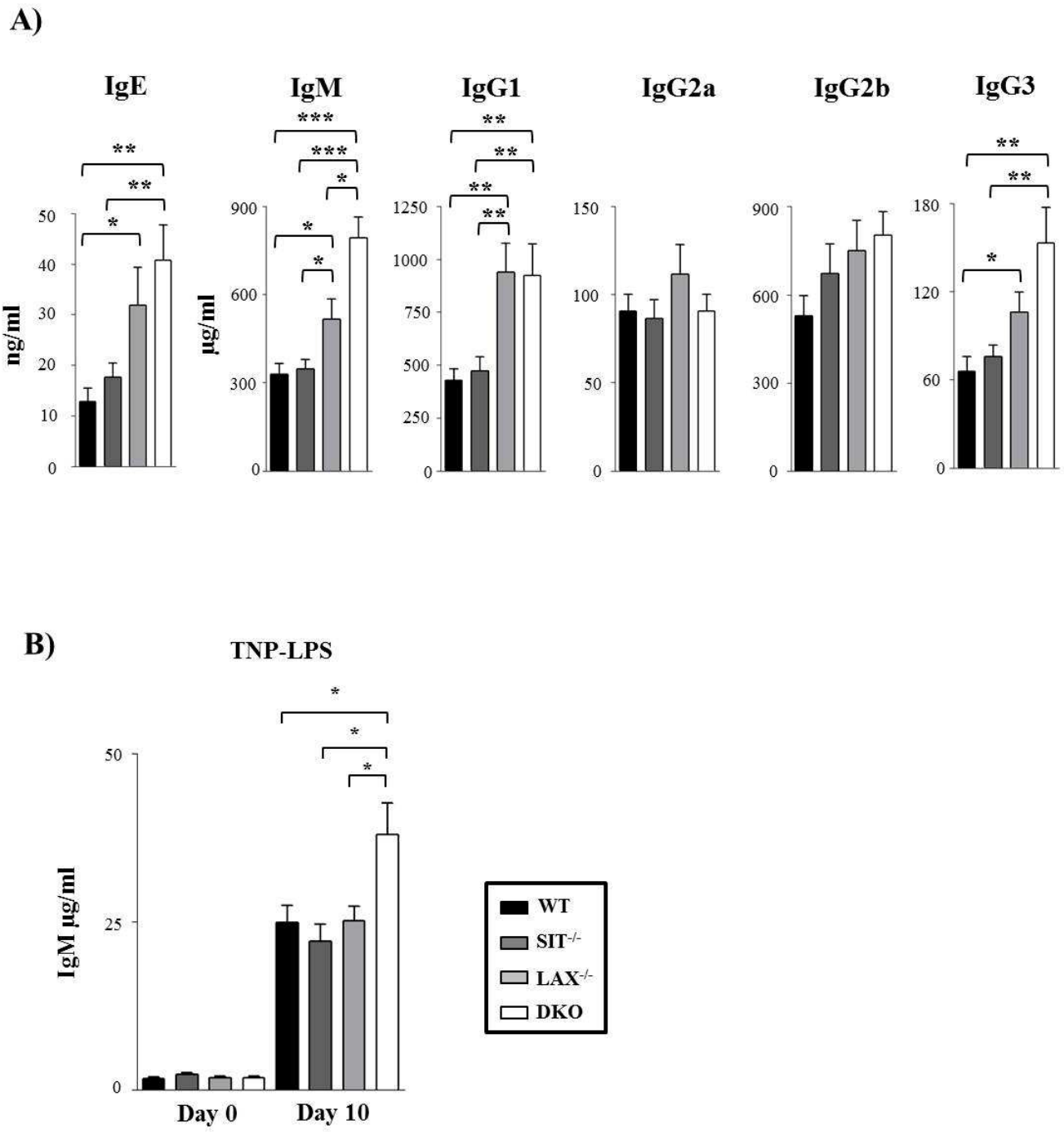
A)
IgE
IgM
IgG1
IgG2a
IgG2b
IgG3
ng/ml
µg/ml
B)
TNP-LPS
IgM µg/ml
Day 0
Day 10
WT
SIT-/-
LAX-/-
DKO

Figure 6

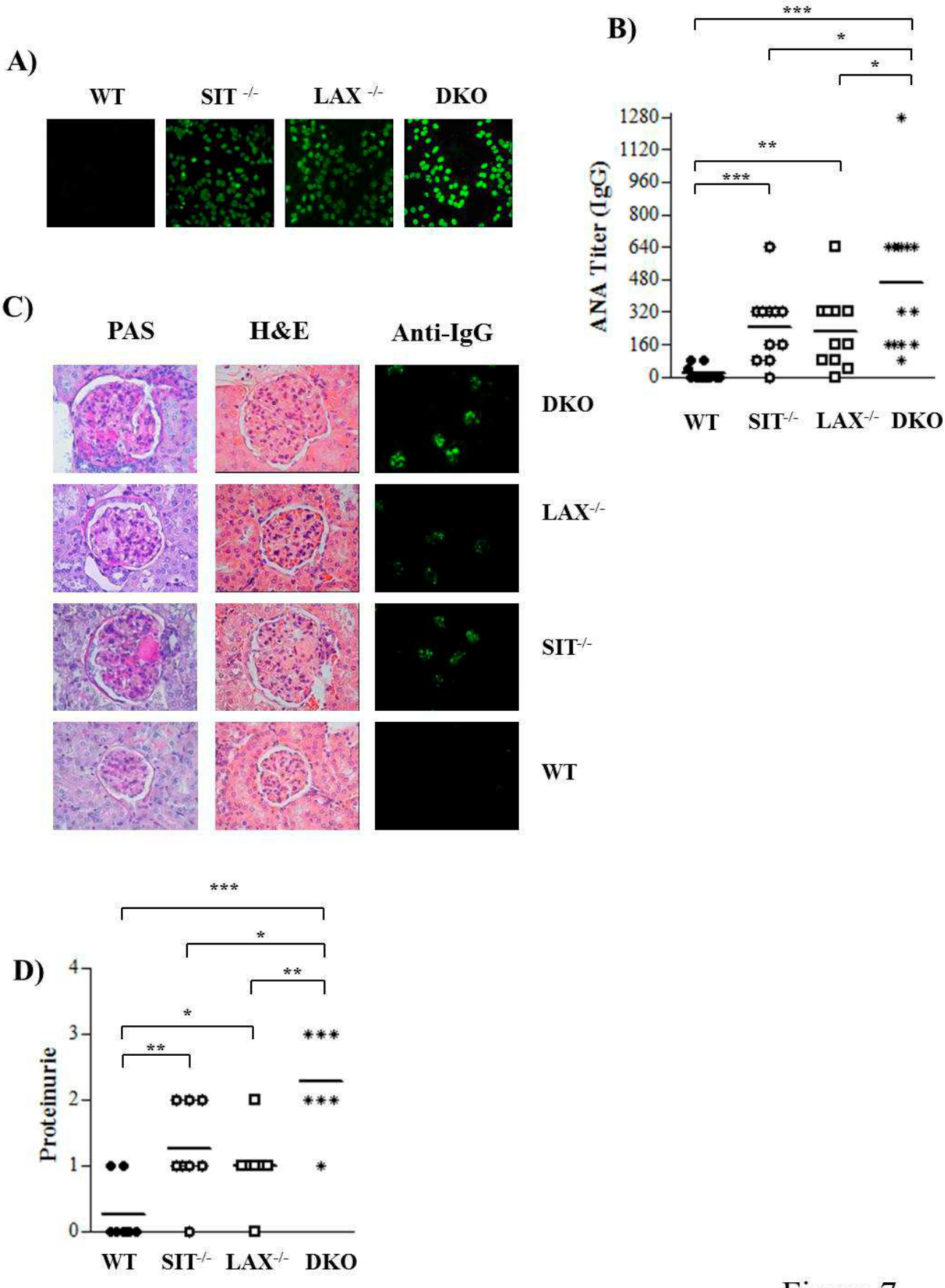
A)
WT
SIT -/-
LAX -/-
DKO
B)
ANA Titer (IgG)
1280
1120
960
800
640
480
320
160
0
WT
SIT-/-
LAX-/-
DKO
C)
PAS
H&E
Anti-IgG
DKO
LAX-/-
SIT-/-
WT
D)
Proteinurie
4
3
2
1
0
WT
SIT-/-
LAX-/-
DKO

Figure 7

Genotype	**Number of examined mice**	**Number ($1x10^6$) of Spleenocytes ±SD**			
		Total	$CD4^+$	$CD4^+$ $CD44^{hi}$ $CD62^{low}$	$CD8^+$
DKO	12	113.3±29.0	27.3±6.9	19.2±5.2	8.2±2.8
$LAX^{-/-}$	6	109.5±22.0	20.6±5.6	10.1±2.5	12.1±4.8
$SIT^{-/-}$	6	98.8±26.1	19.6±4.1	11.4±2.0	8.5±1.8
WT	8	111.3±24.6	19.6±6.5	8.6±3.8	13.0±3.5
p values			DKO vs LAX **0.04** DKO vs SIT **0.01** DKO vs WT **0.01**	DKO vs LAX **0.0008** DKO vs SIT **0.0034** DKO vs WT **0.0001**	DKO vs LAX 0.11 DKO vs SIT 0.87 DKO vs WT **0.02**

Table 1